The role of the Smc5/6 complex in meiosis

Sonya Newcombe

Thesis qualification for DPhil

University of Sussex

May 2017

Acknowledgements

Firstly I would like to thank Eva Hoffmann for her guidance throughout my PhD. Eva has helped me to greatly develop as both a scientist and an individual. I would also like to thank all of the members of the Hoffmann lab for their support and advice during my PhD. Specifically I would like to thank Louise Newnham for her unwavering support, guidance and friendship. I will always remember our 'Team Egg' visits to Rome. I would also like to thank my co-supervisor Alan Lehmann for all of his help and advice throughout my PhD. Thanks is also owed to my colleagues at the GDSC many of whom have provided me with help and advice and kept me happy even when experiments failed.

I also want to thank the medical research council for funding my PhD. Without funding I would not have been able to undertake this PhD. I would also like to thank my family for their support over the years, especially when things have been tough. I would not have got this far without their love and their belief in me. Finally I would like to say a very special thank you to my husband Adam who has been my rock and supported me from the beginning of my PhD, even though it meant not living in the same city. Adam has kept me smiling and laughing through all of the highs and lows and for this I am eternally grateful.

Declaration

I hereby declare that this thesis was composed by me, and the research presented is my own, unless otherwise stated.

Sonya Newcombe

May 2017

University of Sussex

DPhil. Biochemistry

The role of the Smc5/6 complex in meiosis

Meiosis is a specialised cell division that results in the production of haploid gametes. Errors in meiotic chromosome transmission can lead to chromosomally imbalanced embryos which lead to miscarriage or if the offspring survive to term congenital birth defects.

SMC proteins are well known to have roles in regulating chromosome segregation, condensation and repair. The roles of cohesin and condensin in chromosome cohesion and condensation are well characterised. Much less is known about the third SMC complex, the Smc5/6 complex. The Smc5/6 complex is known to have roles in both DNA repair and cohesin regulation during mitosis. The work outlined here demonstrates that the Smc5/6 complex also has important roles in both *Saccharomyces cerevisiae* and mouse female meiosis. Live cell imaging in *Saccharomyces cerevisiae* demonstrated that the Smc5/6 complex is required for meiotic chromosome segregation and cohesin regulation. To investigate if the Smc5/6 complex also played a similar role in mammalian meiosis, oocytes from *Smc6*$^{GT/+}$ mice were analysed. *Smc6*$^{GT/GT}$ mice are embryonic lethal. Contrastingly *Smc6*$^{GT/+}$ mice are relatively unaffected. The only phenotype observed in *Smc6*$^{GT/+}$ mice was reduced litter sizes. Interestingly analysis of the lost embryos, from *Smc6*$^{GT/+}$ mouse crosses, found that they were not lost because they were homozygous for *Smc6*$^{GT/GT}$. The lost embryos were either wild type or *Smc6*$^{GT/+}$ (Ju et al, 2013). The work outlined here indicates it is likely that the embryos were lost due to aneuploidy in the oocytes from the *Smc6*$^{GT/+}$ mother. Many of the metaphase II oocytes from the *Smc6*$^{GT/+}$ mother were found to be aneuploid. Subsequent analysis of metaphase I oocytes from the *Smc6*$^{GT/+}$ mother indicated that the aneuploidy was due to weakened cohesion, as demonstrated by the increased numbers of separated homologous chromosomes in the MI oocytes from the *Smc6*$^{GT/+}$ mother and the overall reduced levels of acetylated Smc3 staining. It was also observed that chromosome condensation

was affected in the oocytes from the *Smc6*$^{GT/+}$ mother. This indicates that the Smc5/6 complex plays an important role in promoting accurate chromosome segregation in mammalian meiosis alongside both cohesin and condensin.

Table of contents

Chapter 1. Introduction

Chapter 2. Materials and Methods

Chapter 3. SMC5/6 promotes chromosome resolution in meiosis

Chapter 4. Investigating the effect of the haploinsufficiency of SMC6 on mammalian meiosis

Chapter 5. Analysis of the SMC protein levels in the *Smc6*$^{+/GT}$ mouse

Chapter 6. Discussion

Chapter 7. Bibliography

Chapter 8. Appendix

Figure list

Supplementary figure 5. mFISH on bunched MII oocyte spread

Supplementary figure 6. Live cell imaging of oocytes from both wildtype and *Smc6*$^{+/GT}$ mice

Supplementary figure 7. Centromeric SMC6 signal varies with CREST signal

Supplementary figure 8. CREST fluorescence does not vary with total SMC6 fluorescence

Supplementary figure 9. Total SMC6 signal does not vary with DAPI signal

Supplementary figure 10. Oocytes with reduced levels of centromeric SMC6 do not have larger chromosomes

Supplementary figure 11. Low SMC6 staining does not correlate with chromosome fraying

Supplementary figure 12. Low levels of SMC6 fluorescence do not correlate with an increased chance of the spread displaying distal chromosomes

Supplementary figure 13. Low levels of SMC6 staining do not correlate with reduced acetylated SMC3 staining

Supplementary figure 14. Low levels of SMC6 staining do not correlate with increased inter-kinetochore distances

List of abbreviations

- APC – Anaphase promoting complex
- ATP – Adenosine triphosphate
- CdLS - Cornelia de Lange syndrome
- ChIP – Chromatin immunoprecipitation
- Cy5 – Cyanine 5
- DNA - Deoxyribonucleic acid
- DAPI – 4', 6-diamidino-2-phenylindole
- dHJ – Double Holliday junction
- DSB – Double strand break
- DTT – Dithiothreitol
- EDTA – Ethylenediaminetetraacetic acid
- FITC – Flourescein isothiocyanate
- FISH - Fluorescence in *situ* hybridisation
- g – Gram
- HR – Homologous recombination
- HU – Hydroxyurea
- LH - Luteinizing hormone
- mg – Miligram
- ml – Mililitre
- mM – Milimolar
- mmol – Milimole
- mFISH – Multi-colour fluorescence in *situ* hybridisation
- MI – Meiosis I
- MII – Meiosis II
- NCO – Non-crossover recombinant
- NDJ – Non-dysjunction
- PBS – Phosphate buffered saline
- PCR – Polymeraise chain reaction
- PGC - Primordial germ cells
- RNA – Ribonucleic acid
- rDNA – Ribosomal deoxyribonucleic acid

- SAC – Spindle assembly checkpoint
- SC – Synaptonemal complex
- SCI – Sister chromatid interwinnings
- SEI – Single end invasion
- SMC – Structural maintainance of chromosomes
- SUMO – Small ubiquitin-like modifier
- TIRF - Total internal reflection fluorescence
- YEPD – Yeast extract, Peptone, Dextrose
- μl – Microlitre
- μg – Microgram
- μm - Micromolar

Introduction

1.1 Overview of meiosis

Meiosis is a specialized form of cell division, required for sexual reproduction, that results in the production of gametes (Figure 1.1A). Unlike the daughter cells produced in mitosis (Figure 1.1B) these gametes only contain half of the chromosome complement so that when two fuse, one from the mother and one from the father, the original diploid chromosome complement is restored. At the beginning of meiosis the DNA replicates, which acts to produce two identical sister chromatids. DNA replication is followed by two successive rounds of DNA segregation. In the first cellular division the homologous chromosomes segregate to opposite poles, referred to as the reductional division. In the second cellular division the sister chromatids segregate to opposite poles, analogous to mitosis, referred to as the equational division. In yeast and mammalian spermatogenesis this results in the production of four haploid gametes. Contrastingly in mammalian oocytes only one haploid gamete is produced (explained in more detail in Section 1.13).

The process of meiosis is complex and highly regulated at each stage to ensure that the chromosomes segregate accurately. Errors in chromosome segregation during meiosis can have serious consequences. In humans defects in chromosome segregation are the leading cause of miscarriage and birth defects (Hassold and Hunt, 2001). Despite the prevalence of chromosome mis-segregation in humans little is known about its causes. In the last decade a large amount of research has been carried out in order to attempt to decipher the factors that are required for accurate chromosome segregation in meiosis. Research has found that the SMC proteins are important for most DNA-based processes that take place within the cell (reviewed in Uhlmann, 2016). This indicates that defects in these proteins could contribute to problems in chromosome segregation in human meiosis (Murdoch et al, 2013; Hodges et al, 2005).

1.2 Overview of meiotic prophase

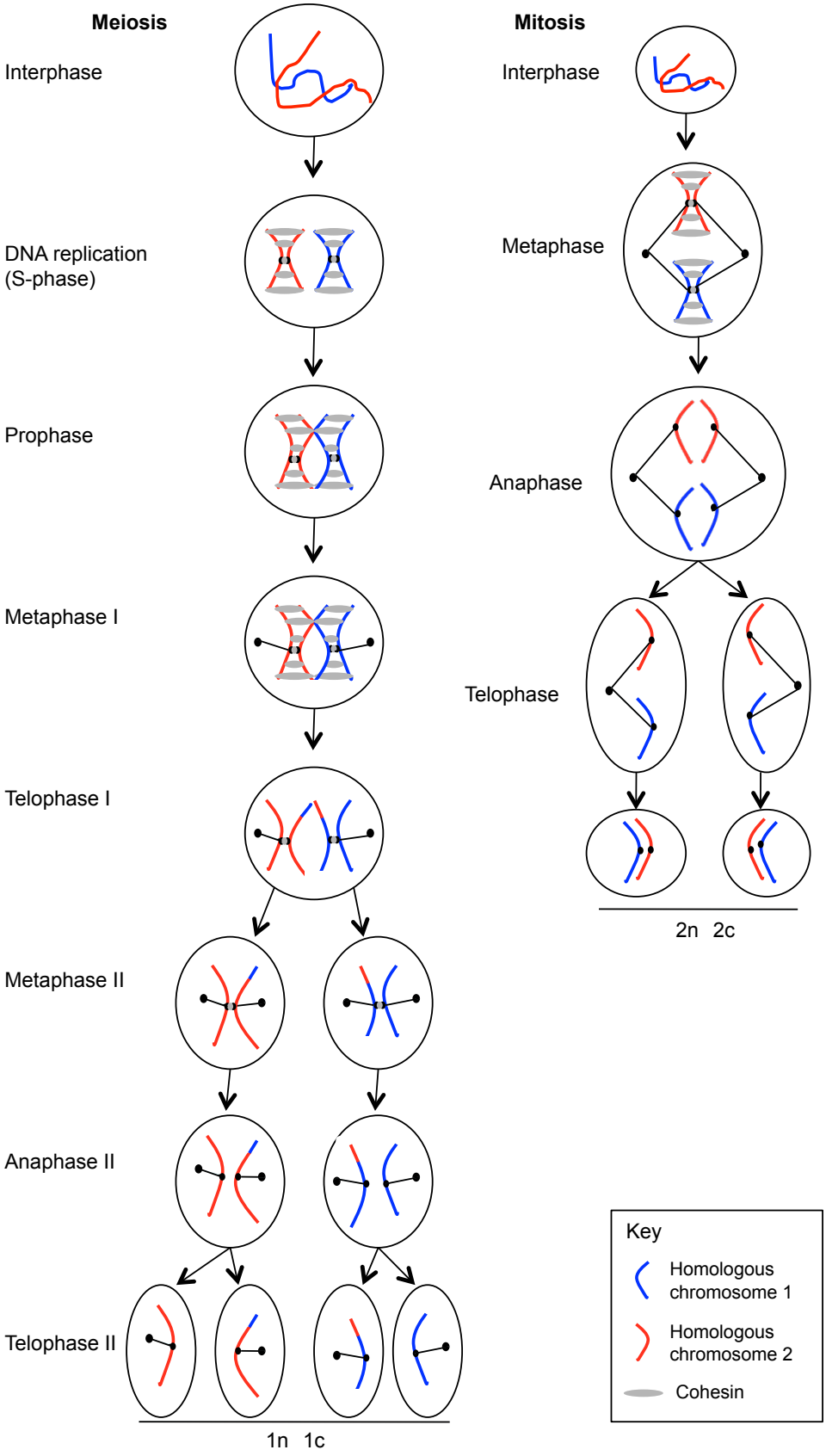
Meiosis
Interphase
DNA replication
(S-phase)
Prophase
Metaphase I
Telophase I
Metaphase II
Anaphase II
Telophase II
1n 1c
Mitosis
Interphase
Metaphase
Anaphase
Telophase
2n 2c
Key
Homologous chromosome 1
Homologous chromosome 2
Cohesin

Figure 1.1 – Meiosis and mitosis in yeast

Diagram of meiosis (left) and mitosis (right). Meiosis begins with as single round of DNA replication followed by two cell divisions. At the beginning of meiosis, after DNA replication, the homologous chromosomes (shown in blue and red) pair and cross over. (Here only a single chromosome pair is shown for clarity.) Cohesin (shown in grey) is removed from the chromosome arms and the homologous chromosomes segregate to opposite daughter cells. This is known as a "reductional division". In meiosis II, centromeric cohesin is cleaved and the sister chromatids segregate into separate daughter cells. This is known as a "equatorial division". The four daughter cells produced only contain half of the number of chromosomes of the original parent cell. Mitosis also begins with DNA replication which generates sister chromatids. The chromosomes align along the spindle equator and once aligned cohesin between the sister chromatids is cleaved. This is followed by a cell division where the sister chromatids are partitioned into opposite daughter cells. The two daughter cells produced in mitosis are genetically identical to one another and the original parent cell.

Once the cells have duplicated their DNA they enter prophase. During prophase the homologous chromosomes (maternal and paternal chromosomes) pair, the synaptonemal complex forms and the homologous chromosomes recombine. Prophase can be divided into several separate sub stages (Figure 1.2). The first stage, leptotene, is characterised by dynamic chromosome moments, which act to facilitate the pairing of the homologous chromosomes (Section 1.3). During leptotene meiotic recombination also begins (Section 1.4). This is catalyzed by Spo11, a topoisomeraise II like protein (Bergerat et al, 1997). In the next stage of prophase, zygotene, the homologous chromosomes pair and repair of the programmed double strand breaks (DSBs) induced previously begins (Section 1.4.2). Zygotene is also characterized by the formation of the synaptonemal complex between the homologous chromosomes (Section 1.5). This is a proteinaceous structure that when fully formed synapses the homologous chromosomes together along their entire length (MacQueen et al, 2002; Page and Hawkley et al, 2004). The synaptonemal complex is fully formed at pachytene. At diplotene the spindle pole bodies separate, the synaptonemal complex disassembles and there is resolution of the dHJ into crossovers or non-crossovers (Allers and Lichten, 2001). In the final stage of prophase, diakinesis, there is recondensation of the chromosomes. At this stage the chromosomes can be observed as two individual threads joint at the centromere. Each of these stages are explained in detail below.

1.3 Chromosome pairing

In order for chromosomes to accurately segregate in meiosis I the homologous chromosomes must be paired. We only know how chromosomes pair in a small number of organisms and interestingly the method by which chromosomes pair has been found to vary from organism to organism. Recombination plays a central role in chromosome pairing in many species including animals, plants and some fungi. This is known as the “canonical” program. Several organisms also use recombination independent pairing of the telomeres in early prophase. This is known as the “non-canonical” program. In *S. pombe* and *Aspergillus ridulans*

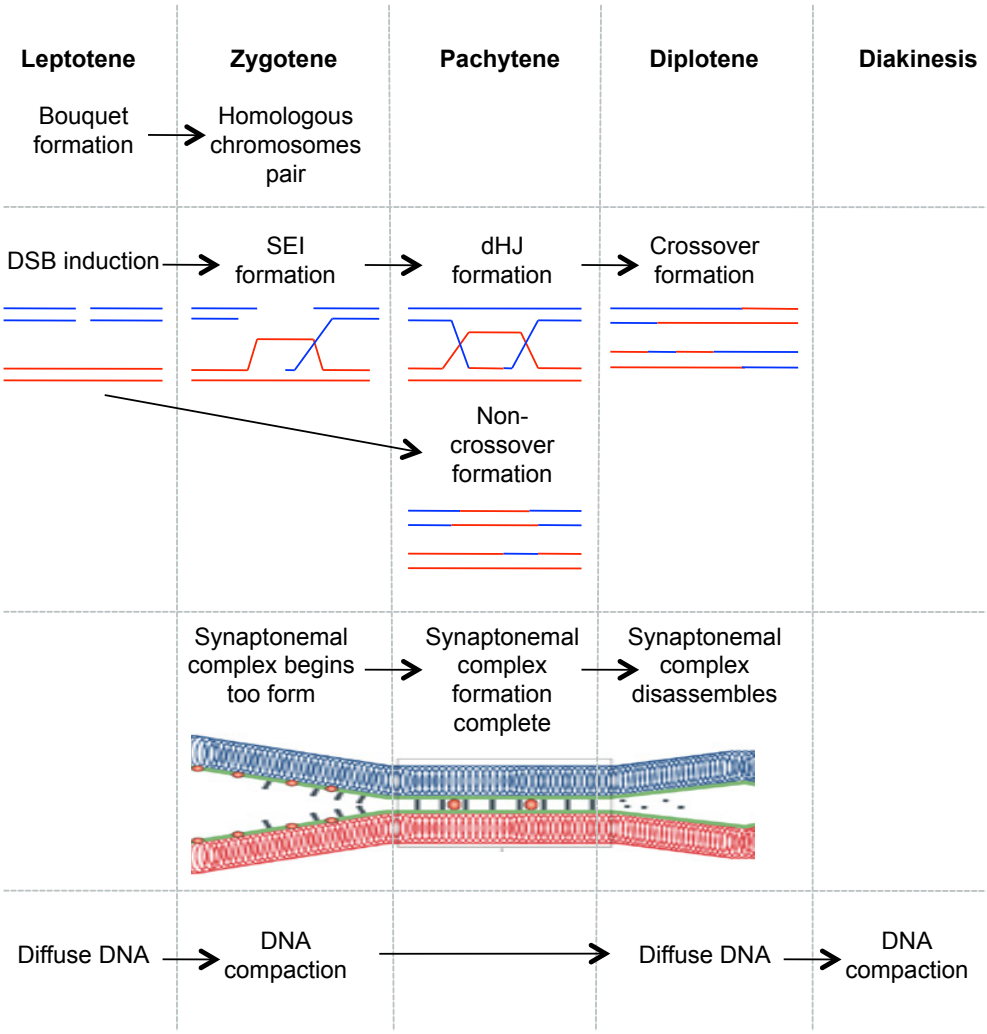

Figure 1.2 – Stages of Prophase

Prophase consists of five separate sub-stages: Leptotene, Zygotene, Pachytene, Diplotene and Diakinesis. In Leptotene bouquet formation takes place which aids chromosome pairing in Zygotene. During Leptotene double strand break (DSB) induction also takes place. DSBs are resolved into crossovers or non-crossovers. In the crossover pathway the DSBs are converted to stables single end invasions (SEI) at Zygotene and subsequently double Holliday junctions (dHJ) at Pachytene. Double Holliday junctions are resolved to form crossover products at Diplotene. In the non-crossover pathway DSBs produced at Leptotene are converted into non-crossover products at Pachytene. During Zygotene the Synaptonemal complex begins to form. It synapses the full length of the chromosomes at Pachytene. It then disassembles at Diplotene. (Image taken from Burgoyne et al (2009).)The DNA goes through two stages of compaction throughout Prophase. At Leptotene the DNA is diffuse. DNA compaction occurs at Zygotene. At the time of synaptonemal complex dissolution, Diplotene, the DNA again becomes diffuse. DNA recompaction takes place at Diakinesis.

(filamentous fungi) both recombination dependent and recombination independent pairing occurs (Bahler et al, 1993; Egel-Mitani et al, 1982). Contrastingly in *C.elegans* homologue pairing, via the pairing centres, can take place in the absence of either recombination or synapsis (MacQueen et al, 2005). In *Drosophila* it was observed that pairing and synapsis are independent of recombination (Lake and Hawley, 2012). Interestingly in both *C. elegans* and *Drosophila* the number of DSB induced is significantly lower than the number of DSB observed in organisms that use the "canonical" method of pairing. This is predicted to be because here the DSB are not required to facilitate pairing (Zickler and Kleckner, 2015).

Both the "canonical" and "non-canonical" methods of pairing use the well conserved "bouquet formation". At the beginning of prophase the chromosomes organise so that the telomeres are clustered in the vicinity of the centrosome/spindle pole body in order to form the "bouquet formation" (Zickler and Kleckner, 1998). This acts to bring the chromosomes into close proximity. Previously this was thought to facilitate a comparison of chromosome homology, therefore enabling homologous chromosomes to pair (Zickler and Kleckner, 1998). The exact mechanisms of pairing are still not clear, as pairing, recombination and synapsis all appear to take place simultaneously. However an insight has been obtained from work in *C.elegans* in which specific "pairing centers" initially pair and only once they have paired does recombination and synapsis take place (MacQueen et al, 2005).

1.4 Meiotic recombination

A unique feature of meiosis is the induction of hundreds of double strand breaks during early Prophase. In meiosis the chromosomes are arranged in loops linked to a proteinaceous axis (Zickler and Kleckner, 1999). DSB are made in the chromosome loops and these are brought down to the chromosome axis so DNA repair via homologous recombination can take place (Blat et al, 2002; Panizza et al, 2011). Recombination is extremely important in meiosis, not only because it introduces genetic variation but also because it acts, alongside cohesin, to form an

essential connection between the homologous chromosomes (chiasmata). Chiasmata promote the proper orientation of the chromosomes at metaphase, therefore aiding accurate chromosomes segregation. Cells that lack chiasmata and centromeric cohesin protection (by Shugoshin, Section 1.7) display high levels of sister chromatid bipolar attachment at anaphase (Hirose et al, 2011).

The pathways for DSB repair are commonly studied in yeast as yeast is easy to manipulate and is able to survive in a large range of environmental conditions. Work in other organisms indicates that the pathways for DSB repair are conserved (Berchowitz et al, 2007; Holloway et al, 2008). The process of meiotic recombination begins with the initial induction of hundreds of DSBs, which are subsequently processed into crossovers or non-crossovers. DSBs formation requires many different genes. These include Spo11, MEI1, Rec102, Rec104, Rec114, Mer2, RAD50, XRS2 and MRE11 (Ajimura et al, 1992; Alani et al, 1990; Bullard et al, 1996; Cao et al, 1990; Ivanov et al, 1992; Menees et al, 1992; Rockmill et al; 1995). If the cell is depleted of any of these proteins, DSB formation is blocked and chromosome non-disjunction is observed during meiosis. Further work has found that these proteins group together to form sub-complexes, which work together to promote DSB formation. The sub-complexes observed are Rec102-Rec104, Mre11-Rad50-Xrs2 (MRX), Rec114-Mei4-Mer2 and Ski8-Spo11 (Arora et al, 2004; Jiao et al, 2003; Kee et al, 2004; Maleki et al, 2007; Ohta et al, 1998). Spo11 is responsible for the induction of DSBs throughout the genome (Bergerat et al, 1997; Keeney et al, 1997). It requires Ski8 for its association with the chromatin (Arora et al, 2004). Exactly how the other sub-complexes facilitate DSB formation is not known. Cells deficient in the MRX complex have been found to display an altered chromosomes structure. This indicates that the MRX complex may alter the chromosome structure so that it can be accessed or processed (Ohta et al, 1998).

1.4.2 Spo11 DSB induction

The central protein involved in the induction of meiotic recombination is Spo11. Most of our knowledge about the function of Spo11 is based on research carried

out in yeast. Cytological and genetic data however support that Spo11 and its mechanisms of action are conserved in worms, plants and mammals (Baudat et al, 2000; Dernberg et al, 1998; Grelon et al, 2001; Keeney et al, 1997). Interestingly it has been found that some organisms that do not carry out meiosis also have functional orthologues of Spo11. This may be linked to the finding that Spo11 (but not its catalytic activity) is required for the pairing of homologous chromosomes (Boateng et al, 2013).

Spo11 is a topoisomeraise II like protein responsible for the induction of hundreds of programmed DSBs (Bergerat et al, 1997; Keeney et al, 1997). Spo11 functions via a transferase reaction (Keeney et al, 1997). In this reaction the tyrosine (Y153) on Spo11 attacks the phosphodiester backbone of the DNA. This acts to form a phosphodiester linkage between Spo11 and the DNA at the 5' terminus of the newly broken strand. Spo11 monomers act in pairs to generate nicks simultaneously on both the DNA strands, therefore producing a symmetrical DSB (Keeney et al 1997). Once the DSB has formed Spo11 is removed via an endonucleolytic reaction (Neale et al, 2005). This endonucleolytic cleavage is facilitated by Sae2 and the MRX complex (Neale et al, 2005; Prinz et al, 1997; Usui et al, 1998).

The first signal of DSB formation, in Leptonema, is the appearance of phosphorylation of the histone variant of H2AX (Mahadevaiah et al, 2001). This phosphorylation is carried out by ATM and ATR kinases and has been found to trigger DSB repair responses (Bellani et al, 2005; Jackson and Bartek, 2009). When Spo11 is removed from the DNA it leaves extended 5' single stranded overhangs either side of the DSB. Resection occurs at the 5' termini by Exo1 and Mre11 to form 3' single stranded overhangs (average length 440bp) (Mimitou et al, 2008; Niccolette et al, 2010; Sun et al. 1991). Dmc1 and Rad51 bind the single stranded overhangs, which act to facilitate a homology search in the homologous chromosome (Bishop et al, 1992; Shinohara et al, 1997). Rad51 has been found to be involved in homologous recombination in both mitotic and meiotic cells (Shinohara et al, 1997). Dmc1 however is meiosis-specific (Bishop et al, 1992). It is thought to promote inter-homologue recombination and prevent inter-sister

recombination during meiosis (Niu et al, 2009). The joint molecule forming functions of Rad51 are not essential for meiotic recombination. Contrastingly loss of Dmc1s joint molecule forming function leads to severe recombination defects. Biochemical experiments indicate that Rad51 acts as an accessory factor of Dmc1 indicating that Rad51 directly catalyses recombination in mitosis and indirectly catalyses recombination in meiosis (Cloud et al, 2012). As both Rad51 and Dmc1 have been found to localize at the chromosome axis this supports that DSB repair takes place at the chromosome axis (Barlow et al, 1997; Moens et al, 2002).

The loading of the strand exchange proteins, Rad51 and Dmc1, are dependent on Breast Cancer 2 Protein (Brac2) in mammals (Sharan et al, 2004). It is likely that Breast Cancer 1 Protein (Brac1) also has a role in the loading of the strand exchange proteins as it has such a large role in the repair of DSBs in mammalian somatic cells. Currently a meiotic role is yet to be elucidated (Xu et al, 2003). The activities of both Rad51 and Dmc1 are regulated by several mediators including homologous-pairing protein 2 homologue (Hop2) and meiotic nuclear division protein 1 homologue (Mnd1) (Chi et al, 2007; Petukhova et al, 2005). In yeast mutation of *HOP2* or *MND1* leads to synaptonamal complex formation between non-homologous chromosomes indicating that Hop2 and Mnd1 are required to prevent inappropriate synapsis or incorrect chromosome pairing (Leu et al, 1998; Tsubouchi and Roeder, 2002). Hop2 deficient mice display wildtype levels of DSBs and localisation of both Dmc1 and Rad51. They however have been found to be sterile due to a defect in the repair of the DSBs. This indicates that Hop2 promotes the function but not binding of the strand exchange proteins (Petukhova et al, 2003).

Rad52 has been found to catalyse the Rad51-mediated strand invasion of the broken 3' strand into its undamaged homologue, therefore producing a single end invasion (SEI) intermediate (Figure 1.3) (Shinohara and Ogawa, 1998). Extension of the invading 3' end then takes place using the undamaged strand as a template. The extension of the 3' of the invading strand acts to displace one of the DNA strands of the undamaged homologue leading to the formation of a D-loop (Hunter and Kleckner, 2001). In the non-crossover pathway, there is only a

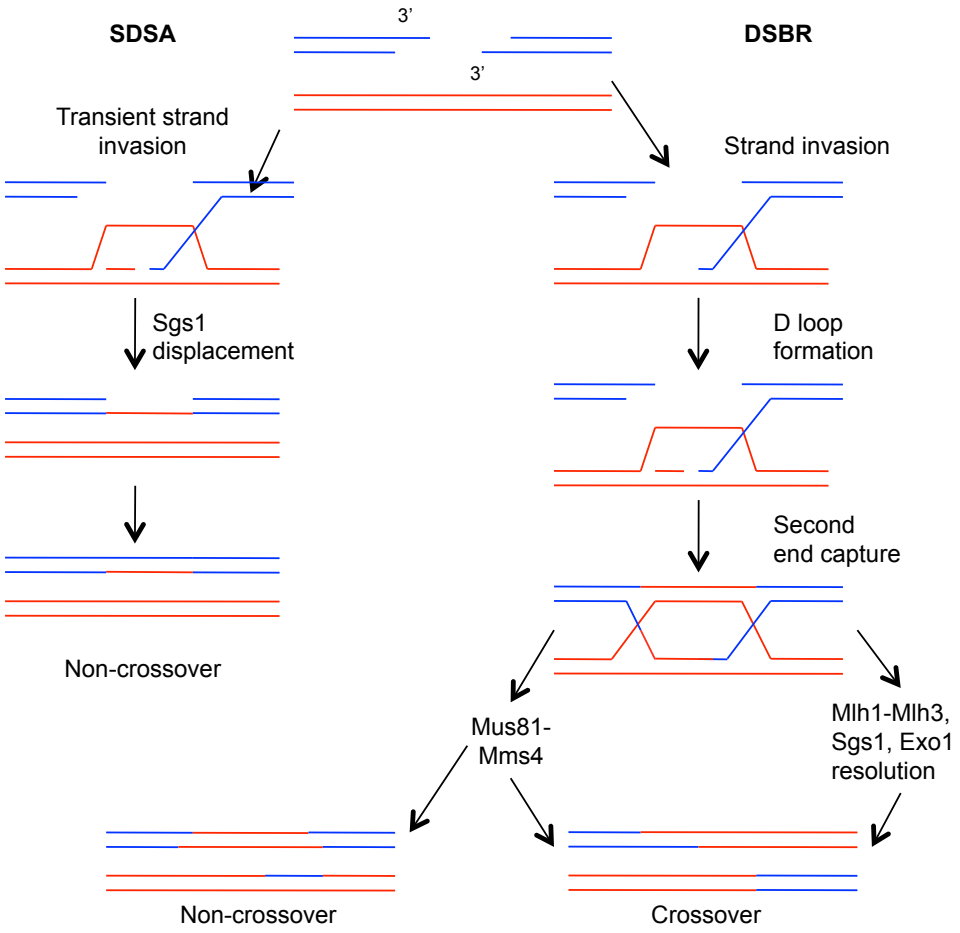

Figure 1.3 – Meiotic Recombination

Diagram demonstrating the DSB pathways in *S.cerevisiae.* For clarity only a single chromatid from each chromosome is shown. There are two major forms of homologous recombination: double strand break repair (DSBR) and synthesis dependent strand annealing (SDSA) Both pathways begin similarly but differ in their resolution. After formation of a DSB there is resection to produce 3' overhangs. This then invades into the homologous DNA duplex, here coloured red. The 3' end is extended resulting in the formation of a D-loop. In SDSA repair once the 3' end has been sufficiently extended the strand is displaced. It then anneals to the other 3' overhang resulting in a non-crossover product. In DSBR the 3' end anneals to the other end of the break in a process know as 'second end capture'. The second 3' end can also be repaired using the D-loop as a template. This leads to the formation of a double 'holliday junction'. Cleavage of the double holiday junction leads to the formation of a crossover product. This is form of DSBR is known as the ZMM pathway. A small amount of the joint molecules escape this processing and are resolved by the Mus81 pathway. This can result in the formation of either a crossover or a non-crossover product.

transient Rad52 independent SEI intermediate. Once the invading strand is sufficiently elongated, the invading strand is displaced and forms an interaction with the other broken strand from the DSB (Figure 1.3; SDSA). In the crossover pathway the second end captures the protruding D-loop in a process known as second end capture (Figure 1.3; Lao et al, 2008). The 3' end of the broken strand is then extended using the D-loop as a template resulting in the formation of a double 'Holliday Junction' (Schwacha and Kleckner, 1995; Szostak et al, 1983). In the crossover pathways, crossovers are produced by resolution of the Holliday junctions. The specific structure of the joint molecule determines exactly how the joint molecule needs to be resolved. Some need a DNA helicase, an endonuclease or a topoisomeraise and some need a combination of all three enzymes. Displacement loops for example can be unwound using a helicase whereas Holliday junctions require resolution by endonucleases.

In *S.cerevisiae* two different crossover pathways have been identified, the ZMM pathway and the Mus81-Mms4 pathway. The ZMM pathway is subject to positive crossover interference, which means the presence of a crossover reduces the likelihood of a crossover forming nearby (Section 1.4.3; Fung et al, 2004; Novak et al 2001; Sym and Roeder, 1994). This ensures that crossovers are evenly spaced along the entire length of the chromosomes. The ZMM pathway also carries out cross over assurance. This ensures that each pair of homologous chromosomes forms at least one crossover (Section 1.4.3; Shinohara et al, 2008).

The ZMM pathway is present in yeast, mice and most likely humans (Borner et al, 2004; Edelmann et al, 1999; Kneitz et al, 2000). The proteins involved in co-coordinating the ZMM pathway are the ZMM proteins Zip1, Zip2, Zip3, Zip4, Spo16, Pph3, Mer3, Msh4 and Msh5 (Borner et al, 2004; Shinohara et al, 2008). The synaptonemal complex proteins (Zip1, Zip2, Zip3, Zip4, Spo16) form a structure, the synaptonemal complex, which acts to facilitate meiotic recombination (Section 1.5). Mer3 is a DNA helicase used to unwind the DNA in order to enable joint molecule (JM) processing and Msh4-Msh5 (the MutSγ complex) binds directly to the JM therby stabilising the JM (Borner et al, 2004; Snowden et al, 2004). Once the joint molecule is stablised, MutSγ then interacts

with Mlh1-Mlh3 (MutLγ) and Exo1 to resolve the double Holliday junction into a crossover (Hunter, 2011; Kolas et al, 2005; Kolas and Cohen, 2004; Zakharyevich et al, 2010). Sgs1 is also required for resolution with MutLγ (Amin et al, 2010; Zackharyevich et al, 2012). Previously it was thought that Sgs1 solely had an anti-recombination activity (Jessop et al, 2006). More recent research indicates that Sgs1 also regulates which recombination pathway is chosen during meiosis. Sgs1 is thought to disassemble unprotected recombination intermediates and direct their resolution towards the non-crossover pathway or towards protection by the ZMM proteins. Joint molecules that are protected by the ZMM proteins undergo subsequent resolution into crossovers (De Muty et al, 2012).

The ZMM proteins have been found to impact crossover levels but not DSB repair when depleted. From this it has been hypothesized that they act to stabilize the SEI and promote the formation of the dHJ (Borner et al, 2004; Lynn et al, 2007; Zakharyevich et al, 2010). A small amount of joint molecules are not stabilized in this manner. These are processed in the Mus81-Mms4 pathway (Zakhareyvich et al, 2012). This pathway is a non-interfering crossover pathway that produces non-crossovers and about 10% of all crossovers (Holloway et al, 2008). Three different endonucleases have been identified in the Mus81-Mms4 pathway that can resolve joint molecules *in vitro* and *in vivo*, Mus81-Mms4, Slx1-Slx4 and Yen1 (Zackhareyvich et al, 2012). Mus81 is an XPF-family endonuclease. It is the central resolvase required for the resolution of joint molecule's that have evaded resolution by Mlh1-Mlh3. Mus81 forms a complex with Mms4 in yeast and Eme1 in humans (Ciccia et al, 2008). It is able to cleave a range of structures including D-loops, nicked Holliday junctions and 3' flaps (Schwartz and Heyer, 2011). Slx1 is from the URI-YIG family of endonucleases (Dunin-Horkawicz et al, 2006). Its nuclease activity has been found to be dependent on an interaction with Slx4. The Slx1-Slx4 complex has been found to be capable of cleaving Holliday junctions and 5'-flaps. It is also able to resolve joint molecules when Sgs1 is not present (Munoz et al, 2009; Svendsen et al, 2009; Zakharyevich et al, 2012). Gen1/Yen1 is a member of the XPG endonuclease family. It works by carrying out symmetrical cleavage of the Holliday junction, similar to the archetypical prokaryotic RuvC resolvase (Ip et al, 2008; Rass et al, 2010). Yen1 does not play an essential role in

the resolution of recombination intermediates. When cells are depleted of Yen1 they display little, if any, meiotic defect. Interestingly Yen1s activity been found to partially suppress the recombination phenotype of cells depleted of Mus81 (Agmon et al, 2011). However when Mus81 is depleted, even though Yen1 is present, cells still display defects in joint molecule processing (De Los Santos et al, 2003; Matos et al, 2011). This indicates that Yen1 is able to resolve some, but not all of the joint molecules that would normally be resolved by Mus81. Recent work has found that Yen1 is only activated at meiosis II (Matos et al, 2011). From this it has been hypothesised that Mus81 resolves the majority of unresolved joint molecules in meiosis I and that Yen1 acts to resolve any remaining joint molecules in meiosis II.

The role of the different factors involved in joint molecule resolution differs from organism to organism. Joint molecule resolution in budding yeast however seems to be most similar to the situation in mammals. In both *Arabidopsis* and mouse, like budding yeast, the majority of crossovers are resolved by Mlh1-Mlh3 (MutLγ) and the remaining crossovers are resolved by Mus81-Mms4 (Berchowitz et al, 2007; Higgins et al, 2008; Holloway et al, 2008). Furthermore joint molecule resolution in mice, like in budding yeast, becomes dysregulated when BLM (an orthologue of Sgs1) is depleted (Holloway et al, 2010; Oh et al, 2007). Holloway *et al* (2010) saw high levels of multi chromatid joint molecules when BLM was depleted reminiscient of what is seen in budding yeast when Sgs1 is depleted (Oh et al, 2007). In contrast to what is observed in mammals and budding yeast, fission yeast solely rely on Mus81-Eme1 for joint molecule resolution. They do not have ZMM proteins or Yen1 (Cromie et al, 2006; Smith et al, 2003). However like in budding yeast, fission yeast also require their Sgs1 orthologue, Rqh1, for both non-crossover and crossover formation (Cromie et al, 2008). Sgs1 orthologues in both *Drosophila* (MUS309) and *C. elegans* (HIM-6) also appear to have a role in the production of crossovers indicating that Sgs1 has a central role in crossover formation from yeast to mammals (McVey et al, 2007; Zetka and Rose, 1995).

Non-crossovers are made through synthesis dependent strand annealing (SDSA) (Figure 1.3; Allers and Lichten, 2001; McMahill et al, 2007). In SDSA, 'nascent'

strand invasion of only one of the broken chromosome arms occurs. DNA synthesis takes place and the newly synthesized strand is displaced from the template strand and annealed back to its original strand (Paques and Haber, 1999). Sgs1 is important for the unwinding of the D-loop thereby aiding in the strand displacement (Bachrati et al, 2006). In mitosis Sgs1 also acts, alongside Srs2, to suppress crossover formation (Ira et al, 2003). This indicates that Sgs1 works in concert with helicases involved in non-crossovers formation such as Srs2 and Mph1 (Ira et al, 2003; Prakash et al, 2009).

1.4.3 DSB regulation

The induction of DSBs throughout the genome is an inherently dangerous but essential process in meiosis. If recombination fails to take place properly this affects chromosomes segregation and therefore gamete formation (Petronczki et al, 2003). Failure of chromosomes to recombine has been found to be a major cause of miscarriage in humans (Nagaoka et al, 2012). Because of potential dangers associated with the induction of hundreds of DSB throughout the genome, the process must be highly regulated. DSBs must only be induced once DNA replication is complete and when cohesin has been loaded onto the chromosomes. In *S. cerevisiae* DSB formation generally occurs about 90 minutes after replication (Borde et al, 2000). DDK (Cdc7-Dbf4) and S-CDK (Cdc28, alongside either of its cyclin partners Clb5 or Clb6) initiate DSB formation (Hardy et al, 1997). DDK and CDK-S are also required for replication and cellular divisions (Schild and Byers, 1978; Valentin et al, 2006; Wan et al, 2006). The levels of both of these kinase raises gradually throughout meiosis indicating that there may be a threshold level for replication and then a later, higher threshold level for DSB induction (Henderson et al, 2006; Wan et al, 2006).

It is likely that other pathways also act to ensure that DSB induction occurs at the correct stage of the cell cycle. The transcription of many proteins involved in DSB formation are carefully regulated throughout the cell cycle. This acts to ensure that cells are only capable of forming DSBs at a specific stage of the cell cycle (Murakami and Keeney, 2008). Furthermore once the synaptonamal complex is

fully formed DSBs are no longer induced (Thacker et al, 2014). Exit from Pachytene is also highly regulated. NDT80, the transcription factor, only promotes the expression of genes required for exit from pachytene when all of the DSBs within the cell have been repaired (Chu and Herskowitz, 1998; Sourirajan and Lichten, 2008).

Both DDK and CDK-S phosphorylate Mer2, one of the nine known proteins found to be required for DSB induction (Henderson et al, 2006; Wan et al, 2008). CDK-S and DDK phosphorylation of Mer2 is required to promote Spo11 recruitment (Henderson et al, 2006; Sasanuma et al, 2008). Interestingly CDK-S and DDK phosphorylate separate phosphorylation sites on Mer2 independently of one another (Sasannuma et al, 2008, Wan et al, 2008). Two replisome associated factors, Tof1 and Csm3, associate with DDK in order to recruit it to the replisome where it phosphorylates Mer2. This may be in order to temporally and spatially co-ordinate replication and DSB induction (Murakami and Keeney, 2014). Mer2 has also been found to associate with the chromosomes independently of phosphorylation. However only when Mer2 is phosphorylated is there the recruitment of the other proteins involved in DSB induction to the chromatin (Henderson et al, 2006; Panizza et al, 2011; Sasanuma et al, 2008). Work by Panizza et al (2011) found that the phosphorylation of Mer2 by CDK-S and DDK acts to modulate Mer2's interactions with DSB proteins such as Mei4 and Rec114. Interestingly in a Mer2 mutant that contains mimics of phosphorylation at all of the sites identified to be phosphorylated by DDK and CDK-S, both CDK-S and DDK have been found to be required for the induction of DSB. (Wan et al, 2008). This either indicates that there are more phosphorylation sites that have not yet been identified or that DDK and CDK-S are also involved in phosphorylating other substrates. It is unlikely that phosphorylation of Mer2 alone is sufficient to induce DSB

DSB are highly regulated and do not occur at random as demonstrated by through the use of genome wide DSB maps (Baudat et al, 2007; Lichten et al, 2011; Smagulova et al, 2011). When analysed on a fine scale it has been observed that DSB are induced at discrete, non-randomly distributed regions described as DSB

hotspots. Analysis in *S.cerevisiae* found that there were periodic peaks and troughs of recombination potential throughout the yeast genome (Pan et al, 2011). Roughly 3600 hotspots have been identified in budding yeast and between 10,000 – 40,000 have been identified in mammals (Khil et al, 2012; Pan et al, 2011; Pratto et al, 2014; Smagulova et al, 2011). In budding yeast the DSB tend to be concentrated within the promoter regions and at GC enriched regions (Gerton et al, 2000). Contrastingly in mice it has been found that recombination takes place away from transcription start sites (Brick et al, 2012). Interestingly work has found that hotspots tend to be located at the loop of the DNA (Blat et al, 2002). This was first thought to be counter intuitive as the machinery required for the induction and regulation of DSB is found at the chromosome axis. However in attempt to explain this the tethered-loop axis model was proposed. This details that Spp1 binds to both the chromosome axis and H3K4me3 (which is enriched at hotspots in *S.cerevisiae*) therefore acting as a linker between the axis and the loop enabling DSB formation (Acquaviva et al, 2013; Borde et al, 2009; Sommermeyer et al, 2013; Tischfield et al, 2012).

In some mammals (*M.musculus* and *H.sapiens*) a single protein, PRDM9, directs hotspot designation (Baudat et al, 2010). PRDM9 deposits H3K4me3 marks onto the chromatin and it is hypothesized that these markers are responsible for the recruitment of Spo11 machinery (Grey et al, 2011; Smagulova et al, 2011). It has been found that hotspot placement is not random. The spatial regulation of DSBs is known as DSB interference. DSB interference acts to reduce the frequency of DSB in any given region below that predicted by chance. Tel1^{ATM}, the DNA damage response (DDR) kinase, exerts a localized suppressive effect, which acts to prevent any two DSBs from forming within roughly 70-150kb of one another (Garcia et al, 2015). This is known as cis interference. Tel1^{ATM} alongside Mec1^{ATR}, a further DDR kinase, has been found to function in another form of spatial regulation, trans interference. Here the presence of a DSB on one sister chromatid suppresses the formation of a DSB in the same locus on its sister chromatid or homologue likely through modulation of the chromosome structure (Zhang et al, 2011). This ensures there is always an undamaged repair template. Cis and trans interference work together to ensure that recombination events are equally

spaced along the chromosomes and that induced recombination can be accurately repaired. There is also a third layer of spatial regulation known as DSB competition. It is proposed that only a relatively low number of DSBs form as only limited amounts of pro-recombination factors such as the RMM complex (comprising of Rec114, Mei2 and Mei4) are present within the cell at any one time (Cooper et al, 2016; Panizza et al, 2011; Robine et al, 2007). These forms of interference have currently only been found in *S.cerevisiae*. It is yet to be determined if they also exist in higher organisms.

1.5 Synaptonemal complex

The synaptonemal complex (SC) is important for chromosome synapsis, meiotic recombination and homologous chromosome segregation (Zickler and Kleckner, 2015). Once the chromosomes pair the synaptonemal complex forms between them along their entire length (Sym and Roeder, 1995). This acts to tightly associate the homologous chromosomes. The structure of the SC was first determined through the use of electron microscopy. This found that the synaptonemal complex has a tripartite, ribbon like structure (Fawcett and Moses, 1956). The SC consists of lateral elements joined by perpendicularly orientated central elements, leading to the formation of an overall 'ladder like' structure (Reviewed in Hawley, 2011).

At the beginning of prophase, during leptotene, the axial elements form between the sister chromatids of each of the homologous chromosomes (von Wettstein, 1984). Specifically the axial elements form along the axis of the sister chromatids. At this stage the chromatin of the meiotic chromosomes is mainly found as loops with only their bases joined to the synaptonemal complex (Costa et al, 2005). During zygotene the axial elements come into close proximity and become termed the lateral elements (Sym and Roeder, 1995). A central element then joins the two lateral elements, thereby bringing the homologous chromosomes into close proximity (Wettstein and Sotelo, 1971). Synapsis at zygotene has been found to begin from several different initiation sites, such as the designated recombination sites and the centromeres, and spread in both directions in a 'zipper like' fashion

(Henderson and Keeney, 2004; Tsubouchi et al, 2008). At pachynema the SC is fully formed. From this stage it acts to hold the homologous chromosomes together until it disassembles at diplotene (von Wettstein, 1984). This occurs at the same time as the resolution of double Holliday junctions into crossovers. This is thought to be because *NDT80* expression triggers both double Holliday Junction resolution and SC disassembly (Allers and Lichten, 2001). Once the SC disassembles, the homologous chromosomes remain held together by cohesion and chiasmata.

The synaptonemal complex is conserved from yeast to mammals (Westergaard and Von Wettstein, 1972; Zickler and Kleckner, 1999). In yeast five proteins, Red1, Hop1, $Smt3^{SUMO}$ and Zip1, have been identified as major components of the synaptonemal complex. Red1, Hop1 and $Smt3^{SUMO}$ form the lateral elements of the SC and Zip1 forms the central element (Carballo et al, 2008; Cheng et al, 2006; Lin et al, 2010; Sym et al, 1993). Emc11-Gmc2 promotes central element formation (Humphreys et al, 2013). Cohesin has also found to be important in the formation of the lateral elements (Klein et al, 1999; Prieto et al, 2001). In mammals seven proteins have been identified as major components of the synaptonemal complex. SYCP1 forms the central element and SYCP2 and SYCP3 form the lateral elements (Meuwissen et al, 1992; Offenberg et al, 1998; Schalk et al, 1998). Additionally four other proteins have been identified that also form part of the central element, Tex12, SYCE1, SYCE2 and SYCE3 (Costa et al, 2005; Hamer et al, 2006; Schramm et al, 2011). As well as being essential for chromosome synapsis, the synaptonemal complex also has a central role in DSB repair. If the synaptonemal complex is depleted in mouse oocytes, through the depletion of both SYCP3 and SYCP1, no MLH1 foci are observed and correspondingly very low levels of chiasmata are found. This then leads to subsequent defects in chromosome segregation (Kouznetsova et al, 2011).

1.6 Kinetochore structure

At metaphase the chromosome-microtubule interactions are mediated by kinetochores. These are proteinaceous structures that form at the centromere of

each chromosome which become the sites where microtubules attach to the centromeres (Cheeseman and Desai, 2008; Santaguida and Musacchio, 2009). Kinetochores act to control the movement of the chromosomes at metaphase in both meiosis and mitosis in order to ensure that there is accurate chromosome segregation. A lot of what we know about the assembly, composition and functions of the kinetochore has been learnt from yeast. The kinetochore is made up of several different layers; an outer layer that associates with the microtubules, an inner layer that connects to the centromere and a central layer that connects the outer layer to the inner layer (Cheeseman and Desai, 2008). More than 50 proteins are required to make up the kinetochores, many of which are very well conserved among eukaryotes (Westermann and Schleiffer, 2013). The centromeric DNA, onto which the kinetochore binds, varies greatly in sequence between different organisms and even between the two yeasts (Chikashige et al, 1989; Clarke and Carbon, 1980; Cleveland et al, 2003). It has however been found that many centromeric nucleosomes contain a histone H3 variant (CENP-A, Cse4, Cnp1)(reviewed in Black and Bassett, 2008). The histone H3 variant is an essential part of the inner kinetochore and has therefore been identified as an epigenetic marker for kinetochore assembly (Barnhart et al, 2011; Mendiburo et al, 2011). CENP-T/Cnp20/Cnn1 and CENP-C are other essential inner kinetochore protein (Foltz et al, 2006; Screpanti et al, 2011). CENP-T has been found to be required for the binding of Ndc80, an outer kinetochore protein important for microtubule attachment (Powers et al, 2009). The interaction between Ndc80 and the microtubules is regulated by a conserved kinase, Ipl1/Aurora B. When erroneous attachments occur between the microtubules and the kinetochores Aurora B phosphorylates Ndc80, which causes it to detach from the microtubules. This is an essential process for correction of erroneous attachments (Cheeseman et al, 2006; Deluca et al, 2006). KNL1/Scp7/Spc105 also has a microtubule binding activity that is regulated by phosphorylation by Aurora B, indicating that Aurora B has an essential role in promoting faithful chromosome segregation in both mitosis and meiosis (Cheeseman et al, 2006).

It has been proposed that Aurora B can differentiate between correct and erroneous microtubule attachments by assessing the tension between the sister

kinetochores. Aurora B localizes between the sister kinetochores as part of the chromosomal passenger complex (CPC) (Ruchaud et al, 2007). When the kinetochores are correctly attached to the microtubules, tension is generated between the kinetochores. In erroneous attachments sufficient tension is not generated and the erroneous attachments become closer to the inner centromere, where the CPC is located. When this happens Aurora B phosphorylates attachments at these sites, which acts to destabilize the microtubule-kinetochore attachments (Liu et al, 2009). When the kinetochores attach correctly to the microtubules the distance between the kinetochore substrates and Aurora B increases. When this occurs the kinetochore substrates are de-phosphorylated by PPI phosphatase, which acts to stabilize the attachment (Liu et al, 2009)

The kinetochores also form a platform for the activation of the spindle assembly checkpoint (SAC). The SAC acts to delay the onset of anaphase until the chromosomes are properly aligned. It does this by inhibiting the Anaphase Promoting Complex (APC) (Musacchio and Salmon, 2007; Rudner and Murray, 1996). Unattached kinetochores are detected by the SAC components (Mad1, Mad2, Mad3/BubR1, Mps1/Mph1, Bub1, Bub3). These accumulate on the kinetochores of unattached chromosomes and inactivate Cdc20 (an activator of the APC) therefore delaying anaphase onset (Hwang et al, 1998; Kim et al, 1998; Li and Murray, 1991; Taylor et al, 1998). Only once the chromosomes are properly aligned is the APC activated which, degrades securin (an inhibitor of separase) therefore activating separase (Cohen-Fix et al, 1996; Funabiki et al, 1996).

1.7 Shugoshin

In *S.cerevisiae* meiosis cohesin is lost from the chromosomes in a two-step process. At metaphase I cohesin is lost from the chromosome arms. Cohesin is retained at the centromeres until metaphase II in order to ensure that the sister chromatids do not separate until meiosis II. Shugoshin (SGO which is Japanese for guardian spirit) is the protein responsible for protection of cohesin at the centromeres. Shugoshin was first discovered in *Drosophila melanogaster.*

Goldstein (1980) found that the MEI-S332 mutant displayed precocious sister chromatid separation. A later genome-wide screen in budding yeast, by Kitajima et al (2004), looking for mutants that when over-expressed maintained cohesin at the chromosomes identified Shugoshin 1 (Sgo1). Subsequent homology searches indicated that Sgo1 is a distant relative of MEI-S332 (Rabitsch et al, 2004). Analysis found that cells depleted of Sgo1 displayed precocious loss of centromeric Rec8 in meiosis I, which led to chromosome mis-segregation in meiosis II (Katis et al, 2004; Marston et al, 2004). Genome-wide localisation analysis found that Sgo1 localises at cohesin associated regions at the centromere until metaphase II, the time at which centromeric cohesin is also lost (Kiburz et al, 2005; Klein et al, 1999).

Shugoshin is conserved from yeast to mammals (Hamant et al, 2005; Katis et al, 2004; Lee et al, 2008; Llano et al, 2008). Shugoshin consists of three key components, a central domain that has been found to bind to SA3/Scc3, a C terminal domain that is responsible for its recruitment to the centromeres and its N terminal domain that facilitates binding to PP2A via its B regulatory subunit (Hara et al, 2014; Xu et al, 2009). It is still not clear exactly how Shugoshin is recruited to the centromeres. Work has shown that the recruitment is dependent on Bub1 (budding uninhibited by benzimidazoles 1), a central component of the SAC, and its kinase activity (Perera and Taylor, 2010). Specifically data indicates that the recruitment of Sgo1 is dependent on the phosphorylation of histone H2A at S121 by Bub1 (Kawashima et al, 2010). Recent work by Nerusheva et al (2014) however found that S121 is not the sole residue on Bub1 responsible for Sgo1 recruitment. They found that Sgo1s recruitment is dependent on Bub1, even when S121 is replaced with aspartic acid.

Both *S.cerevisiae* and *D.melanogaster* only have a single Shugoshin protein. Plants, fission yeast and mammals however all have two Shugoshin-like proteins, Sgol1 and Sgol2. In these organisms Sgol1 is required in order to protect mitotic centromeric cohesin from the prophase pathway and Sgol2 is required to protect meiotic centromeric cohesin from the separase-dependent pathway in meiosis I (Lee et al, 2008; Llano et al, 2008; Salic et al, 2004). Sgol2 has also been found

have a role in aligning the chromosomes at metaphase, silencing the spindle assembly checkpoint (by binding Mad2 and PP2A) and regulating several enzymes involved in this process including MCAK (microtubule depolymerizing kinesin) and Mad2 (an essential component of the mitotic checkpoint complex) (Huang et al, 2007; Rattani et al, 2013). Shugoshins have also been implicated in the recruitment of Aurora B kinase to the kinetochores (Tsukahara et al, 2010).

In yeast and humans, in order for Shugoshin to protect centromeric Rec8 it must recruit PP2A (Kitajima et al, 2006; Riedel et al., 2006). Shugoshin interacts with PP2A via its regulatory subunit Rts1 (Kitajima et al, 2006; Riedel et al, 2006). Inactivation of PP2A causes loss of centromeric Rec8 (Riedel et al., 2006). It is still unknown if PP2A protects cohesin by inhibiting separase, by removing Rec8 phosphorylation or by direct binding to Rec8 (Holland et al, 2007; Katis et al, 2010). Ipl1 (the yeast homologoue of Aurora B) is required in order to maintain PP2A at the centromeres (Yu and Koshland, 2007). It has been found that tethering of PP2A to the centromere is sufficient to maintain cohesin at the centromeres indicating that the main role of Shugoshin is to recruit PP2A (Kitajima et al., 2006). This idea is supported by work in budding yeast, which found if the localisation of PP2A to the centromeres is abolished; Sgo1 was not sufficient to maintain centromeric cohesin (Xu et al, 2009).

Shugoshin also has a central role in bi-orientation in budding yeast. It promotes bi-orientation through two separate mechanims (Verzijlbergen et al, 2014). Shugoshin retains Ipl1 at kinetochores that are not under tension. This acts to promote the recruitment of error correction machinery. Shugoshin also plays a role in the recruitment of condensin to the kinetochores. This in turn biases sister kinetochores to attach to microtubules from opposite poles of the cell (Verzijlbergen et al, 2014).

1.8 Mono-orientation of sister chromatids in meiosis I

In mitosis the DNA is initially replicated so each chromosome consists of two sister chromatids. At metaphase the sister chromatids are bi-orientated (i.e.

where the kinetochores from the sister chromatids attach to spindles from opposite poles) so that they are segregated into opposite daughter cells (reductional division). This acts to ensure that the daughter cells are genetically identical to the parent cells. In meiosis I the sister chromatids are mono-orientated (i.e. where both kinetochores from the sister chromatids attach to microtubules from the same pole) to ensure that the homologous chromosomes separate away from one another but that the sister chromatids remain together. In meiosis II the sister chromatids are bi-orientated, so they segregate away from one another, as in mitosis.

Most of what is known about the mechanisms of mono-orientation has been learnt from *S.cerevisiae*. A key component in sister kinetochore mono-orientation has been identified to be Monopolin. Monopolin is made up for four different subunits, Csm1 (chromosome segregation in meiosis protein I), Hrr25 kinase, Lrs4 (Loss of rDNA silencing protein 4) and Mam1 (monopole microtubule attachment during meiosis protein I)(Petronczki et al, 2006; Rabitsch et al, 2003; Toth et al, 2000). Csm1, Hrr25 and Lrs4 have all been identified in both meiosis and mitosis. Mam1 contrastingly is only present within the cell during meiosis I (Toth et al, 2000). In mitosis both Lrs4 and Csm1 form a complex that localizes to the rDNA at the nucleolus (Huang et al, 2006). Here the complex has been found to recruit condensin to replication fork barriers and to prevent unequal crossovers within the rDNA repeats (Joshua and Horiatis, 2009). The Lrs4-Csm1 complex also localizes to the nucleolus during meiosis, where it is proposed to carry out the same role. During prophase of meiosis I Cdc5 promotes release of the Lrs4-Csm1 complex from the nucleolus (Clyne et al, 2003; Lee and Amon, 2003; Rabitsch et al, 2003). Cdc5, Spo13 and Cdc7 then all work together to carry out phosphorylation of Lrs4, which acts to promote its recruitment to the kinetochores (Kiburz et al, 2005; Matos et al, 2008). At the kinetochores the Lrs4-Csm1 complex binds to Mam1, which promotes the recruitment of HRR25 completing the monopolin complex (Rabitsch et al, 2003; Petronczki et al, 2006).

Mam1 was first identified in a screen by Toth *et al* (2000) in which they aimed to identify genes involved in chromosome mis-segregation. They found Mam1

depletion reduced spore viability to 5%. Further analysis found that the low viability observed was due to high levels of chromosome mis-segregation (Toth et al, 2000). Analysis of the cells depleted of Mam1 found that the cells only displayed one round of chromosome segregation during meiosis. They failed to undergo meiosis I and only underwent a single round of chromosomes segregation in which all of the sister kinetochores were segregated from one another. This produced two diploid cells, rather than the 4 haploid cells usually observed at the end of meiosis (Toth et al, 2000). From this Toth *et al* (2000) hypothesised that mono-orientation of the sister chromatids fails to take place when Mam1 is not present. The sister chromatids are instead bi-orientated at meiosis I (as in mitosis). Just under half of the sister chromatids were not observed to separate in meiosis I due to the presence of centromeric cohesin. Only once the centromeric cohesin was lost, in meiosis II, could the sister chromatids separate (Katis et al, 2004). Further analysis found that Csm1, Lrs4 and Hrr25 are also important for the mono-orientation of the sister chromatids indicating that the monopolin complex as a whole is required for mono-orientation (Petronczki et al, 2006; Rabitsch et al, 2003).

Analysis of the Mam1 protein localisation further supports that Mam1 has a role in mono-orientation of the chromosome at meiosis I. Mam1 is recruited and potentially stabilized at the centromeres by Spo13 (sporulation specific protein 13) and Cdc5 at pachytene (Katis et al, 2004; Matos et al, 2008). By co-staining with NDC10 it was identified that Mam1 specifically associates with the kinetochores (Katis et al, 2004). Mam1 is then retained at the centromeres until the anaphase I. At the onset of anaphase the APC (anaphase promoting complex) breaks Spo13 down (Sullivan and Morgan, 2007). It is likely that this is the reason that monopolin is only functional during meiosis I. However it is likely there are other mechanisms that are responsible for the breakdown/loss of function of monopolin as even when the cell contains a non-degradable version of Spo13, monopolin is not active in meiosis II (Sullivan and Morgan, 2007).

Mam1 is poorly conserved between different species. It is likely that similar molecules may exist in higher eukaryotes, but that they are not conserved to a

level that can be recognized using bio-informatics. Homologoues of Csm1 and Lrs4 (Pcs1 and Mde4) have been identified in fission yeast. Interestingly, in fission yeast, they have been found to have different roles than in budding yeast. In fission yeast Pcs1 and Mde4 are required in order to prevent merotelic attachment of kinetochores in mitosis (Gregan et al, 2007). It is likely that Pcs1 and Mde4 work via the same mechanism in both species of yeast. In budding yeast each kinetochore only contains one microtubule-binding site (Winey et al, 1995). In fission yeast however each kinetochore contains several microtubule-binding sites (Ding et al, 1993). It is predicted that Csm1 and Lrs4 act to clamp adjacent microtubule binding sites, in both species of yeast, in order to promote accurate chromosome segregation. In budding yeast the complex acts to join microtubule binding sites of sister chromatids whereas in fission yeast the complex acts to bind the multiple microtubule binding sites at each kinetochore.

A large amount of research has gone into how monopolin functions to promote the mono-orientation of the sister chromatids at meiosis I. Crystal structures indicate that Csm1 dimerises to form a short coiled-coil and a globular domain. Lrs4 also dimerises to produce a C-terminal globular domain and an N-terminal coiled coil domain. Both Lrs4 and Csm1 interact with one another to form an overall V shaped structure made up of two molecules of Lrs4 and four molecules of Csm1 (Corbett et al, 2010). Mam1 then acts to tie the whole complex together. The globular domains of Csm1 interact with the C-terminal domain of Mam1 and the N-terminal domain of Mam1 interacts with Hrr25 therefore forming the monopolin complex (Corbett and Harrison, 2012). The monopolin complex contains two sites that are capable of binding at DSN1s, an MIND kinetochore complex component, Csm1 interacting domain. This indicated that the monopolin complex may crosslink the MIND complexes of the sister kinetochores thereby tying the sister kinetochores together (Corbett et al, 2010; Sarkar et al, 2013). Alternatively as there are many copies of DSN1 in each kinetochore, both copies of Mam1 may bind to the same kinetochore and the other kinetochore is shut off (Monje-Casas et al, 2007; Winey et al, 2005). Work by Sarangapani et al (2014) indicated that co-segregation of sister chromatid is due to sister kinetochore fusion. They found that monopolin, at meiosis I, produces kinetochores of a

greater strength and with more microtubule binding sites than kinetochores isolated from either cells at either meiosis II or mitosis. It is unknown how monopolin complexes can differentiate MIND complexes from different kinetochores as each kinetochore contains many different copies of the MIND complex. It is also unknown how monopolin can differentiate between soluble MIND complexes and those bound to the kinetochores. Alternatively it is possible that Csm1-Lrs4 complex does not cross-link the kinetochores. Instead it might act to recruit Hrr25, which may promote mono-orientation through its kinase activity. A further possibility is that mono-orientation involves both of these models. It is possible that the Lrs4-Csm1 complex acts to crosslink the kinetochores and that the kinase activity of Hrr25 acts to modify the kinetochores in some way (Nasmyth, 2015).

Moa1 is also a meiosis specific protein that is required for monopolar attachment. It was first identified in a screen looking for factors that promoted reductional segregation during meiosis I in *S.pombe* (Yokobayashi and Watanabe, 2005). Moa1 binds to the kinetochore via Cnp3/CENP-C. If Moa1 is depleted this disrupts centromeric cohesion which in turn disrupts sister kinetochore mono-orientation (Yokobayashi and Watanabe, 2005). Meikin (meiosis-specific kinetochore protein) has also recently been identified to be important for monopolar attachment (Kim et al, 2015). Like Monopolin, Meikin is only present in meiosis I, not in meiosis II or mitosis. However, unlike Monopolin, Meikin is conserved from yeast (Spo13) to humans. Meikin binds to the kinetochores at prophase I and is lost at anaphase I (Kim et al, 2015). This observation led to the proposal that Meikin has a role in regulating the maintenance of cohesin at the centromeres. This is supported by the finding that mice depleted of Meikin display increased levels of split kinetochores at pro-metaphase I (Kim et al, 2015). Clear mono-orientation defects, in Meikin mutants, were not observed until Mlh1 was also depleted (meaning crossovers were not produced). This indicated it is unlikely that Meikin alone promotes mono-orientation. Instead it is likely that Meikin promotes mono-orientation alongside centromeric cohesin. Kim *et al* (2015) found that Meikin$^{-/-}$ mutants displayed diminished levels of Shugoshin 2 (Sgo2) indicating Meikin has a role in stablising Sgo2 at the centromeres of the meiotic

chromosomes. As the protection of centromeric cohesin is not totally abolished in Meikin$^{-/-}$ mice this indicates that Meikin may function in the pathway that promotes the shugoshin dependent protection of centromeric cohesin rather than itself being a protector of centromeric cohesin.

It is possible that other proteins/complexes also have a role in regulating mono-orientation in other organisms. A potential candidate is Rec8. Rec8 has been found to have a role in mono-orientation in fission yeast (Petronczki et al, 2006). In fission yeast deletion of Rec8 causes the chromosomes to segregate equatorially rather than reductionally in meiosis I, indicating that cohesion at the core centromeres of the sister chromatids is responsible for mono-orientation (Watanabe et al, 2001). Disruption or premature cleavage of the kleisin subunit of cohesin also causes bi-orientation in meiosis I in plants and in mouse oocytes (Chelysheva et al, 2005; Tachibana-Konwalski et al, 2013). Chiasmata, held in place by cohesin, between the homologous chromosomes are also important for the mono-orientation of the sister chromatids. They act to form a physical linkage between the homologous chromosomes and are required for the accurate binding of microtubules from opposite poles to the homologous chromosomes.

1.9 SMC proteins

DNA molecules make up the genome in all living organisms. These are generally significantly longer in length than the organism themselves. Because of this the cell has specialized mechanisms in order to pack the DNA into the nuclei of every cell i.e. through the use histones. During meiosis and mitosis the chromatin is further compacted in order for the chromosomes to accurately segregate. The proteins that are responsible for reshaping the chromosomes and ordering the DNA so that it can be accurately segregated are the Structural Maintenance of Chromosomes (SMC) complexes. These act to regulate high order chromosome structure. There are three SMC complexes, Cohesin, Condensin and the Smc5/6 complex (Figure 1.4). All of the SMC complexes associate with the chromosomes genome wide and are evolutionarily conserved from bacteria to humans. Cohesin is required for chromosome cohesion (Figure 1.4A; explained in more detail in

Section 1.10). As the name suggests Condensin is required for chromosome condensation (Figure 1.4B; explained in more detail in Section 1.11). Significantly less is known about the Smc5/6 complex. The Smc5/6 complex was initially identified as having a role in DNA repair (Nasim and Smith, 1975). Recent research has also implicated that it may also be involved in several other cellular processes (Figure 1.4C; explained in more detail in Section 1.12).

All the SMC complexes adopt ring-shaped structures. They each consist of a heterodimers of two SMC proteins joint by a kleisin (Figure 1.3; Haering et al, 2002; Schleiffer et al, 2003). The SMC proteins consist of two coiled coil domains each flanked by either a globular N or C terminal domain (Michaelis et al, 1997). They also have a hinge at the centre so they can fold back on themselves causing their N and C globular domains to interact, therefore forming long anti-parallel coiled coils. (Haering et al, 2002). The N and C globular domains contain Walker A and Walker B motifs that form an ATPase domain (ATP binding cassette) when they associate (Lowe et al, 2001). The SMC complexes have all been found to associate with the DNA regardless of the presence of ATP. It however has been found that they require the activity of ATP in order to become intramolecular or intermolecular DNA linkers (Cobbe and Heck, 2006; Hirano, 2006; Kanno et al, 2015; Kimura and Hirano, 1997; Kimura et al, 1999; Losada and Hirano, 2001; Murayama and Uhlmann, 2015; Wilhelm et al, 2015).

1.10 Cohesin

The most well understood SMC complex is Cohesin (Figure 1.4A). Cohesin was first identified in budding yeast (Michaelis et al, 1997). Michaelis *et al* (1997) found that cells were not capable of holding their sister chromatids together during metaphase if cohesin was not present. Further research in eukaryotic cells found that mitotic and meiotic chromosome segregation was impaired if cohesin was not present. If cohesin was depleted precocious sister chromatid separation, inefficient bi-orientation and problems in chromosome alignment were observed (Britton et al, 1998; Hoque et al, 2002; Sonoda et al, 2001). Further research also found that cohesin has roles in synaptonemal complex formation (Section 1.5),

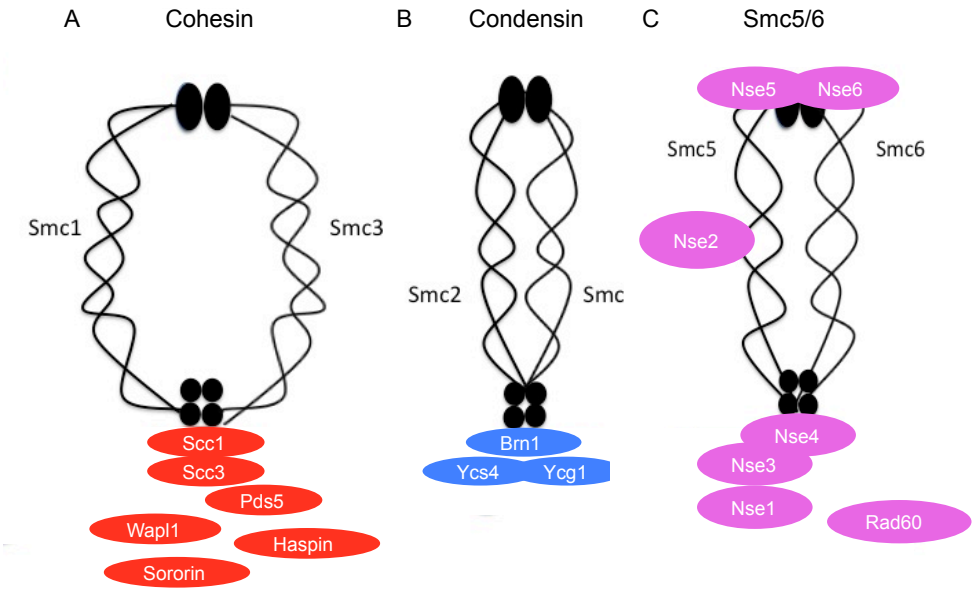

Figure 1.4 –Structure of Smc5/6, Cohesin and Condensin in *S.cerevisiae*

The central part of each of the complexes consists of a dimer of two SMC proteins. Each SMC protein consists of a long coiled coil domain, broken up by the hinge that can fold back on itself so that its N and C termini interact. These contain Walker A and B motifs respectively and when they come together they form a functional ATP-ase active site. The two ATPase domains are bridged by a kleisin subunit. This gives the complexes overall ring shaped structure.. Cohesins two central SMC proteins are Smc1 and Smc3 (A) (Haering et al, 2002; Haering et al, 2004). They are bridged by the kleisin Scc1 and Scc3 at the head domain (Losada et al, 2000; Roig et al, 2014). In meiosis Scc1 is replaced by the meiosis specific kleisin Rec8. Pds5 also associates with the cohesin complex (Chan et al, 2013; Muir et al, 2016; Panizza et al, 2000). There are also several accessory proteins associated with the cohesin complex. Wapl1, Sororin and Haspin (Dai et al, 2006; Gandhi et al, 2006; Hartman et al, 2000; Panizza et al, 2000; Rankin et al, 2005). Condensins two central SMC proteins are Smc2 and Smc4 (Hirano et al, 1997; Sutani et al, 1999) (B). These are bridged at their base by Brn1 (Onn et al, 2007). Brn1 is related to kleisins, but is not cleaved. The Ycs4 and Ycg1 subunits associate via Brn1 subunit and contain HEAT repeats (Hirano, 2012). There are 8 components in the Smc5/6 complex (C). The two central SMC proteins are Smc5 and Smc6. They are joint by a Nse4 (Palecek et al, 2006). Nse2, a sumo ligase, binds to the middle of the coiled coil region in Smc5 (McDonald et al, 2003). Nse5 and Nse6 bind at the hinge domain and Nse1 and Nse3 interact to form a unbiquitin ligase which binds to Nse4 (Fujioka et al 2002; McDonald et al 2003; Perbernard et al, 2004; Doyle et al, 2010; Perbernard et al, 2006). Rad60 is essential for the function of the complex (Morikawa et al, 2004; Novatchkova et al, 2005)

double strand break (DSB) repair (Section 1.4) and mono-orientation (Section 1.8) (Agostinho et al, 2016; Gyuricza et al, 2016; Klein et al, 1999; Petronczki et al, 2006; Pidoux et al, 2004; Revenkova and Jessberger, 2006; Sjögren and Nasmyth, 2001; Strom et al, 2004).

The central ring of cohesin consists of Smc1 and Smc3 joined by the kleisin Scc1 in mitosis (or Rec8/Rad21L in meiosis) (Haering et al, 2002; Haering et al, 2004). The kleisin is bound at its C-terminus by Scc3, a HEAT-repeat domain protein and Scc1 (Losada et al, 2000; Roig et al, 2014). Scc3 is required for cohesion establishment and cohesion maintenance (Roig et al, 2014; Toth et al, 1999). Another HEAT-repeat protein, Pds5, also associates with the cohesin complex (via Scc1) but not as strongly as the other proteins (Chan et al, 2013; Muir et al, 2016; Panizza et al, 2000). Like Scc3, Pds5 is required for cohesion maintainance and establishment (Carretero et al, 2013; Chan et al, 2013; Hartman et al, 2000; Vaur et al, 2012). The cohesin complex is conserved from yeast to humans (Table1) (Losada et al, 1998; Pasierbek et al, 2001; Sonoda et al, 2001). Mammals have several homologues of many of the cohesin subunits. Mammals have three homologues of Scc3 (STAG1/SA1, STAG2/SA2 and STAG3/SA3). STAG1 and STAG2 are both present in mitosis. STAG3 however is present in meiosis only (Carramolino et al, 1997; Losada et al, 2000; Sumara et al, 2000). Mammals also have two homologues of Smc1, Smc1α and Smc1β. Smc1α is found in meiosis and mitosis whereas Smc1β is found in meiosis only (Revenkova et al, 2004). Mammals also have several kleisin subunits, Rad21, Rad12L and Rec8. Rad21 is present in mitosis whereas both Rad21L and Rec8 are meiosis specific. As mammals have a variety of different cohesin subunits a large range of cohesin complexes varying in composition can be formed.

Cohesin is believed to be loaded onto the DNA by the Scc2/4 complex before S phase (Ciosk et al, 2000). The Scc2/4 loading sites differ from the localisation of cohesin observed later in mitosis (Lengronne et al, 2004). From this it was predicted that the cohesin is initially loaded at the Scc2/4 association sites and that it translocates along the DNA away from these sites (Lengronne et al, 2004). Cohesin loading has been proposed to occur by the replication fork passing

through the cohesin rings (Haering et al, 2002). Recently however this theory has been put into question as it has been found, through the use of TIRF (total internal reflection fluorescence) microscopy, that the cohesin rings pore size is much smaller than was originally thought. Initially it was believed, from electron microscopy studies, that the cohesin complex had a diameter of 40 nm (Hearing et al, 2002). The results from TIRF microscopy studies however indicate that the cohesin pore size significantly smaller, roughly 11 nm in size (Stigler at el, 2016). As replisomes have been found to be roughly 20 nm in size, this raises the question of whether cohesin is in fact loaded when the replication fork passes through the cohesin ring (Sun et al, 2015).

In order to determine the mechanism of how the cohesin ring binds to the DNA experiments have been carried out using engineered versions of the cohesin ring in which specific proteins have been fused or where the ring can be artificially locked closed (Buheitel and Stemmann, 2013). Using this technique Buheitel and Stemmann (2013) found that cohesin is loaded onto the chromosomes via opening of the Smc1-Smc3 hinge region in human cells. This supports previous results obtained in *S.cerevisiae* indicating that this is a universal entry gate for cohesin loading (Gruber et al, 2006). Work by Hu et al (2011) found that cohesin, which is able to engage the nucleotide binding domains of Smc1 and Smc3 but is unable to hydrolyse ATP, is still able to associate with the chromatin. It however does not bind stably (Hu et al, 2011). This indicates that ATP binding is required for cohesin ring closure.

It is still not well understood exactly how cohesin associates with the DNA, as it is currently not possible to visualize the cohesin/DNA interactions in a native environment. Several different models have been proposed describing how the cohesin complex holds the sister chromatids together (Figure 1.5). Initially it was proposed that the ring like structure of cohesin entraps both of the sister chromatids following DNA replication (Figure 1.5B). This is known as the 'embrace' model (Haering et al, 2002). This model is still currently favored among the field as it can explain why cohesin is readily released once Scc1 is cleaved (Losada et al, 2001; Uhlmann et al, 1999). An alternative method for how cohesin

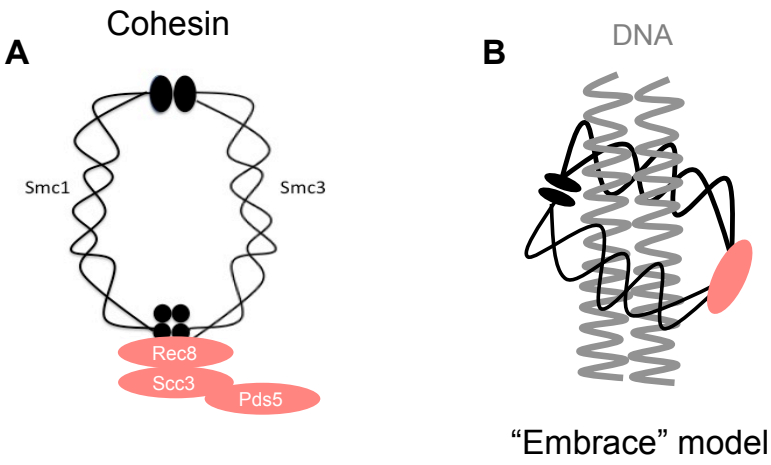
A
Cohesin
Smc1
Smc3
Rec8
Scc3
Pds5
B
DNA
"Embrace" model
C
"Handcuff" model
D
"Non-embracing" model

Figure 1.5 – Proposed methods in which cohesin facilitates sister chromatid cohesion

A Structure of the cohesin complex. The central ring of cohesin consists of Smc1 and Smc3 joint by the klesin Rec8 in meiosis. Rec8 is bound at its C-termius by Scc3, a HEAT-repeat domain protein (Haering et al, 2002). Pds5 also associates with the cohesin complex but not as strongly as the other proteins (Panizza et al, 2000).

B Diagram demonstrating the most commonly accepted 'Embrace' model. In this model it is predicted that the sister chromatids are entrapped within the cohesin complex and that they are only released when the ring is opened (Haering et al, 2002).

C Diagram demonstrating the alternative 'Handcuff' model. Here each sister chromatid is entrapped within a single cohesin ring and that the two rings topologically interact therefore holding the sister chromatids together (Zhang et al, 2008).

D Diagram demonstrating the 'Non-embracing' model. Here the cohesin rings do not entrap the sister chromatids, instead the DNA binds to the SMC dimer (Huang et al, 2005).

holds the sister chromatids together is the 'handcuff' model (Figure 1.5C; Zhang et al, 2008). This model suggests that each sister chromatid is entrapped within a single cohesin ring and that the two rings topologically interact therefore holding the sister chromatids together. A final model, the 'non-embracing' or 'oligomerisation' model, proposes that the cohesin rings do not entrap the sister chromatids at all (Figure 1.5D). Instead the DNA is thought to bind to the SMC dimer via the head domains (Huang et al, 2005).

Currently a large proportion of research supports the 'embrace' model. Biochemical isolation of cohesin has not found significant levels of oligomerisation (Haering et al, 2002; Hauf et al, 2005; Gruber et al, 2003). These results however have been challenged, as in these extractions the DNA must initially be solubilized before the cohesin can be extracted. Furthermore recent work by Gligoris *et al* (2014) found evidence, through the use of thiol specific cross-linking, that sister chromatids were entrapped within a single cohesin ring *in vivo*. Work looking at condensin and its bacterial homologoue Smc–ScpAB in yeast and bacteria indicate that condensin binds the chromosomes using the same topological method (Cuylen et al, 2011; Wilhelm et al, 2015). This indicates it is possible that there is a universal method of entrapment used by all of the SMC complexes.

Contrastingly the finding that there is a loss of chromosome cohesion but not chromosome-associated cohesin when Pds5 is depleted supports the 'handcuff' or 'non-embracing' model. When Pds5 was depleted, from budding yeast, cohesin was found to remain associated with both of the sister chromatids (Kulemzina et al, 2012). An alternative hypothesis is that cohesin works differently in different situations or that the cell organizes the DNA using more than one method. It is possible that cohesin only oligomerises when it is required to carry out long-range interactions (Eng et al, 2015).

1.10.2 Cohesin regulation

Cohesin is believed to be loaded onto the DNA at S phase through the action of Scc2-Scc4 complex (Ciosk et al, 2000; Watrin et al, 2006). It is loaded along the length of the chromosomes and is enriched at the pericentromeres, the region around the centromere (Blat and Kleckner 1999; Megee et al, 1999; Tanaka et al, 1999). Cohesin still binds to the DNA in the absence of Scc2-Scc4. It however does not bind stably (Stigler et al, 2016). From this it has been proposed that, as well as loading the cohesin onto the chromosomes; Scc2-Scc4 acts to arrange cohesin into the correct conformation so that it can stably bind to the DNA. It has been hypothesized that cohesin's interaction with Scc2-Scc4 causes a structural rearrangement within cohesin, which acts to expose cohesin's DNA binding region (Murayama and Uhlmann, 2014).

Cohesin loaded along the chromosome arms must be modified in order to make it cohesive. The protein found to be responsible for this is Eco1/Ctf7, an acetyl transferase (Ben-Shahar et al, 2008; Toth et al, 1999). Mutants lacking Eco1 load cohesin normally but the sister chromatids are not cohesed, as indicated by a significant increase in the number of separated sister chromatids (Toth et al, 1999). Smc3 has been identified as the substrate of Eco1. This is acetylated, by Eco1, at residues K112 and K113 (Ben-shahar et al, 2008; Rowland et al, 2009; Sutani et al, 2009; Unal et al, 2008; Zhang et al, 2008). Recent work has found that the acetylation of Smc3, by Eco1, only takes place if Eco1 is associated with the replication machinery (Song et al, 2012). This indicates that cohesion is established as soon as the sister chromatids form. It is still unknown if Eco1 also moves along with the replication fork. There are two homologoues of Eco1 in mammals, Esco1 and Esco2. Interestingly they acetylate Smc3 through different mechanisms and only Esco2 interacts with Smc3 during DNA replication (Minamino et al, 2015). This indicates that only Esco2 functions during DNA replication. Eco1 has also been found to be required for cohesion establishment in response to the induction of DSBs at G2/M (Unal et al, 2007). Several other factors have also been identified that are important for cohesion establishment. These include components of the replication machinery such as Ctf18 and Ctf4 which all act closely with the replication fork (Bermudez et al, 2003; Bylund et al, 2005; Hanna et al, 2001; Mayer et al, 2001).

There are also several accessory proteins that are involved in the regulation of cohesin association with the chromosomes. These include Pds5, Scc3, Wapl1, Sororin and Haspin (Dai et al, 2006; Gandhi et al, 2006; Hartman et al, 2000; Panizza et al, 2000; Rankin et al, 2005). The role of Pds5 has been found to vary from organism to organism. In *S.cerevisiae* Pds5 is required to promote chromsome cohesion by maintaining actylation of Smc3 (Chan et al, 2013). Pds5 also plays an important role in sister chromatid cohesion in both *C.elegans* and Xenopus. In *C.elegans* Pds5 is important for chromosome cohesion in both meiosis and mitosis and in Xenoupus, depletion of the two vertebrate forms of Pds5, Pds5A and Pds5B leads to sister chromatid cohesion defects (Losada et al, 2005). In contrast in mammals depletion of PDS5A or PDS5B has not been found to lead to any defects in sister chromatid cohesion (Zhang et al, 2009). Interestingly alongside its role in cohesin establishment Pds5 also has a role in cohesin destablisation. In *S.pombe* lethality caused by Eco1 deletion can be suppressed by disruption of Pds5, indicating that Pds5 has a negative effect on cohesin establishment (Ben-Shahar et al, 2008; Tanaka et al, 2001). Pds5 forms a complex with Wpl1 and Scc3 that associates with the cohesin complex. Work in budding yeast has found that mutations in Pds5, Scc3 or Wpl1 are able to suppress the lethality of Eco1 disruption indicating that all these proteins have anti-establishment functions (Rowland et al. 2009). Wpl1 regulates the dissociation of cohesin from the chromosomes at anaphase in humans (Chan et al, 2012; Gandhi et al, 2006; Kueng et al, 2006). It is thought to do this by targeting the interface between Scc1 and Smc3, the “exit gate” of cohesin (Beckouet et al, 2016). Acetylation of Smc3 by Eco1 is proposed lock the “exit gate,” meaning it cannot be opened by Wpl1 (Chan et al, 2012). It is proposed that Pds5 and Scc3 allow Wapl1 to access the cohesin (Rowland et al, 2009). In order to ensure that cohesin is not lost prematurely Eco1 acts to antagonize Wpl1. It does this by acetylating Smc3, which acts to maintain cohesion (Sutani et al, 2009). *In vitro* data has found that Eco1 acts to block the ATPase dependent opening of the Scc1-Smc3 DNA exit gate (Murayama and Uhlmann, 2014). This has led to the overall model that when DNA interacts with the cohesin ring it may stimulate the ATPase activity which causes the ring to open, therefore allowing the entry of the DNA into the ring. It is then

predicted that the acetylation of Smc3 by Eco1 acts to block the interaction of the DNA with Smc3 therefore closing the ring (Rankin and Dawson, 2016). Chromosome cohesion as well as being regulated by Smc3 actylation is regulated by Sororin. Soroin acts to displace Wapl1 from Pds5 therfore preventing Wapl1s activity (Nishiyama et al, 2010).

1.10.3 Cohesin in meiosis

In meiosis the homologous chromosomes must remain held together throughout G2 and meiosis, until the metaphase-anaphase transition. At anaphase the homologous chromosomes segregate but the sister chromatids remain held together. They remain together until they segregate at metaphase II. The accurate segregation of the chromosomes is the most important event in the cell cycle. Defects in DNA segregation led to aneuploidy in the daughter cells and therefore must be carefully regulated. There are two processes that act to ensure that the chromosomes segregate accurately in meiosis. These are the step-wise loss of sister chromatid cohesion and meiotic recombination (Section 1.4).

Cohesin between the sister chromatids and the chiasmata between the homologous chromosomes act to hold the sister chromatids together until anaphase I. In metaphase I the spindle attaches to the chromosomes and acts to pull the homologous chromosomes to opposite poles of the cell. The presence of cohesin and chiasmata mean that tension is generated between the kinetochores and the microtubules when both the maternal and paternal homologues attach to microtubules from the opposite poles of the cell. Only once sufficient tension has been generated is cohesin lost along the chromosomes arms (Ulhmann et al, 1999). The loss of cohesin along the chromosomes arms, alongside the resolution of chiasmata, mean that the homologous chromosomes can separate. The sister chromatids however remain attached, due to retention of Rec8 at the centromeres, and therefore segregate together (Klein et al, 1999). The centromeric Rec8 is retained until metaphase II in order to ensure that there is bipolar attachment of the sister kinetochores in meiosis II.

The protease responsible for removing cohesin from the chromosomes at the metaphase/anaphase transition is known as Esp1 in budding yeast (seperase in mammals). Esp1 removes cohesin from the chromosomes via proteolytic cleavage of the kleisin subunit, Rec8 in meiosis (Uhlmann et al, 2000; Ciosk et al, 1998; Buonomo et al, 2000). Once cleaved the cohesin dissociates from the chromosome arms therefore enabling the homologous chromosomes to segregate in meiosis I. The spindle checkpoint acts to prevent the removal of cohesin until the chromosomes are accurately aligned along the spindle equator. It does this by preventing the activation of the anaphase-promoting complex (APC) until the kinetochore-spindle tension is generated (Tanaka et al, 2000). The activity of Esp1 is regulated by Pds1 (securin in mammals) which itself is regulated by the APC (Ciosk et al, 1998; Nakajima et al, 2007; Tinker-Kulberg and Morgan, 1999). Pds1 acts to repress the activity of Esp1. Only when the chromosomes are properly aligned is the APC activated, which in turn ubiquitinates Pds1 therefore targeting it for destruction (Cohen-Fix et al, 1996; Zachariae and Naysmyth, 1999). As Pds1 is no longer present this means that the activity of Esp1 is no longer repressed. Esp1 then proceeds to cleave Rec8, which promotes the release of cohesin from the chromosomes, meaning homologous chromosomes can segregate to opposite poles. The removal of cohesin also promotes the resolution of the chiasmata joining the homologous chromosomes (Buonomo et al, 2000).

Cdc5 phosphorylation of Scc1 has been found to promote Scc1 cleavage in mitosis (Alexandru et al, 2001). Contrastingly Cdc5 is not required for Rec8 cleavage in meiosis. When all of the residues of Rec8 known to be phosphorylated by Cdc5 were mutated cohesin removal in meiosis I still occurred (Brar et al, 2006). Casein kinase 1δ/ε (CDK1, HRR25 in yeast) and Dbf4-dependent Cdc7 (DDK) are instead required for Rec8 cleavage along the chromosome arms in meiosis I (Katis et al, 2010). Rec8 at the centromeres is retained until metaphase of meiosis II. This is predicted to be due to dephosphorylation of cohesin at the centromeres by the Sgo1-PP2A complex, which acts to protect it from removal by separase (Kitajima et al, 2006; Riedel et al, 2006). This idea however has been challenged in work by Liu *et al* (2013) in which they observed that cohesin (SA2) is phosphorylated at the kinetochores bound by SGO1-PP2A. This indicates that the Sgo1-PP2A

complex may protect centromeric cohesin through alternative mechanisms. It is possible that the presence of the Sgo1-PP2A complex at the centromeres sterically antagonizes the binding of Wapl1. In support of this model Lui *et al* (2013) found that mutated versions of SA2 that are not able to bind Wapl1 do not require Sgo1.

In all lower eukaryotes cohesin is removed from the chromosomes arms at metaphase-anaphase in one step, through the action of separase (Uhlmann et al, 1999). Contrastingly in vertebrates cohesin is lost in two steps. During prophase a large bulk of the cohesin from the cohesin arms is lost during the prophase pathway (Waizenegger et al, 2000). The remaining cohesin is then removed via the separase dependent pathway at the metaphase-anaphase transition (Riedel et al, 2006; Sumara et al, 2000). The prophase pathway is regulated through phosphorylation of SA2/STAG2 by PLK1 (Polo-like kinase 1) and Aurora B and is mediated through the action of the Wapl1, Scc3, Pds5 subcomplex (Alexandru et al, 2001; Gandhi et al, 2006; Gimenez-Abian et al, 2004; Hauf et al, 2005; Kueng et al, 2006; Ouyang et al, 2013; Rowland et al, 2009; Sumara et al, 2002). This begins when the chromosomes start to condense and bi-orientate along the spindle.

1.10.4 Cohesin in mouse meiosis

Research *in vivo* also supports that cohesin has a central role in meiosis. Mice defective in Smc1B are sterile. Analysis found these mice displayed precocious loss of sister chromatid cohesion and defects in synaptonemal complex formation (Revenkova et al, 2004). Mice depleted of Rec8, the kleisin subunit of cohesin, also displayed defects in synaptonemal complex formation. Interestingly in Rec8 mutants the synaptonemal complexes formed between the sister chromatids rather than the homologous chromosomes (Xu et al, 2005). Expression of Rec8 that is poorly cleaved (Rec8-N) *in vivo* causes sterility in male mice. Contrastingly expression of Rec8-N in female mice does not greatly affect fertility (Kudo et al, 2009). This difference is likely to be due to differences in the ways in which oocytes and sperm respond to delayed chiasmata resolution. Importantly this demonstrates that Rec8 cleavage promotes chiasmata resolution as it does in other organisms. Rad21L deficient mice also show defects in synaptonemal

complex formation. In males this led to a zygotene-like arrest. In females however the deficiency does not cause an arrest. Instead the mice display an age dependent sterility (Herran et al, 2011). This reflects clear differences in tolerance of damage between males and females in meiosis (Section 1.15). Stag3 mutants display notably more severe defects than observed in any of the other cohesin single mutants. The meiotic defects observed include disrupted synapsis, aberrant DNA repair and disrupted centromeric cohesin. These led to an overall prophase arrest and apoptosis of both the male and female germ cells (Hopkins et al, 2014).

1.10.5 Cohesin and recombination

There are two populations of cohesin, those that are loaded onto the DNA at S phase and those that are loaded in response to DNA damage at the site of the DSB break (Strom et al, 2004; Unal et al, 2004). After DNA damage cohesin is recruited to a ~100kb domain around the damaged site (Unal et al, 2004). DNA damage also causes genome wide establishment of cohesin in G2/M (Unal et al, 2007). If cohesin is prevented from binding to the DNA after DNA damage then DNA repair does not take place (Strom et al, 2004). Cohesin is recruited to DSB through the DNA damage response pathway. It acts to promote repair of the DSBs via the homologous chromosome in meiosis (explained in section 1.4) and via the sister chromatid in mitosis (Sjogren et al, 2001). Suppressing recombination between homologous chromosomes during mitosis is very important in order to prevent chromosome instability. Contrastingly promoting recombination between homologous chromosomes in meiosis is important in order to promote accurate chromosome segregation and to generate genetic diversity. Cohesin previously loaded in S-phase is removed upon DNA damage. This is may happen in order to allow the repair factors to access the DNA (McAleenan et al, 2013). Removal of cohesin after DNA damage takes place via separase-mediated cleavage of Scc1 (McAleenan et al, 2013). Separase mediated cohesin removal is globally prevented until the metaphase/anaphase transition. This indicates that separase must also be regulated locally to remove cohesin from sites of damage.

1.10.6 Cohesinopathies

There are several known human diseases that are caused by mutations in subunits of the cohesin complex. These are termed cohesinopathies and include Cornelia de Lange (CdLS), Roberts syndrome and Warsaw breakage syndrome. Patients carrying these mutations do not display defects in DNA repair or chromosome segregation seen in mice depleted in the cohesin subunits. This is likely to be because null mutations are lethal. Most patients who have cohesinopathies instead display developmental defects such as growth and intellectual disability, craniofacial abnormalities and limb deformations. Patients with Cornelia de Lange (CdLS) for instance display growth and cognitive disability, cardiac defects and gastrointestinal abnormalities due to small insertions/deletions or point mutations in Scc2, Smc1 or Smc3 (Krantz et al, 2004; Tonkin et al, 2004; Musio et al, 2006; Deardorff et al, 2007). Patients with Roberts syndrome display multi-system disorders involving neurocognitive disjunction and systemic abnormalities due to a homozygous mutation in Esco2 (Eco1 in yeast) (Vega et al, 2005). These phenotypes likely correspond to a role of cohesin in gene expression during embryonic development (Brooker and Berkowitz, 2014).

Analysis of the binding profile of cohesin, mapped using chromatin immunoprecipitation, indicates that cohesin has a role in regulating gene expression. In metazoans both Scc2 and cohesin have been found to colocalise with RNA polymerase II at the sites of transcribed genes (Misulovin et al, 2008). Furthermore the depletion of cohesin has been found to lead to changes in gene expression (Kagey et al, 2010; Wendt et al, 2008). Genetic studies in Drosophila have also found that when the levels of the cohesin-loading factor are reduced, the expression of specific genes is altered during development (Rollins et al, 1999; Fay et al, 2011; Wu et al, 2015). Interestingly studies on patients with Cornelia de Lange syndrome found they frequently carry heterozygous mutations in the cohesin loader Scc2-Scc4 (Krantz et al, 2004; Mannini et al, 2013; Tonkin et al, 2004; Zuin et al, 2014). As patients with Cornelia de Lange syndrome do not display defects in the segregation of their chromosomes it is predicted that the syndrome is instead caused by defects in transcriptional regulation. In flies and

yeast it has been found that a small reduction in the levels of cohesin effects gene expression. Only when there is a significant loss of cohesin (>85%) are defects in chromosome segregation and cohesion observed (Heidinger-Pauli et al, 2010; Schaaf et al, 2009). In humans it has been proposed that cohesin uses a different molecular mechanisms in cohesion and transcription.

1.11 Condensin

In order for chromosomes to accurately segregate in meiosis and mitosis the DNA must be packed into DNA fibers. The chromatin must metamorphose from a diffuse chromatin at interphase to structured chromatids in order to do this (Cremer et al, 1988). The complex responsible for this structural change is condensin (Figure 1.4B). Condensin has been found to be required to promote chromosome condensation and also to promote disentanglement of sister chromatids (Losada and Hirano, 2001; Kimura and Hirano, 1997; Kimura et al, 1999). If condensin is defective, chromosome compaction is reduced and this leads to problems in DNA segregation (Freeman et al, 2000; Lavoie et al, 2004). Condensin was first isolated over two decades ago, in cell-free extracts of *Xenoupus laevis* eggs, and was identified to be important for both the formation and maintenance of chromosomes (Hirano et al, 1997; Hirano and Mitchison, 1994). Like both the other SMC complexes, Condensin is made up of two SMC proteins, Smc2 and Smc4, and several non-SMC proteins (Figure 1.3B; Hirano et al, 1997; Sutani et al, 1999). In yeast there is only one type of condesin complex, condensin I. In *D.melanogaster* and vertebrates there are two types of condensin complex, condensin I and condensin II, which differ only by their kleisin. *C. elegans* has also been found to contain two forms of condensin. They contain condensin II and a condensin I like complex, condensin IDC, instead of condensin I (Csankovszki et al, 2009). It is believed that higher organisms may have gained condensin II during evolution (Hirano et al, 2012).

The most prominent phenotype observed by mutation of the core subunits of condensin in budding yeast, fission yeast, flies, worms and chicken cells is sister chromatid entanglement in mitosis leading to defects in chromosome segregation

(Bhalla et al, 2002; Bhat et al, 1996; Hagstrom et al, 2002; Hudson et al, 2003; Lavoie et al, 2000; Lieb et al, 1998; Saka et al, 1994; Steffensen et al, 2001; Strunnikov et al, 1995; Sutani et al, 1999; Vagnarelli et al, 2006). Chromosome bridges, during anaphase, are also commonly seen in condensin mutants. These are further indicative of defects in chromosome segregation (Saka et al, 1994; Strunnikov et al, 1995). In order to look at the role of condensin in mammalian meiosis Houlard *et al* (2015) deleted floxed alleles of Ncaph1 or Ncaph2 in mouse oocytes, which in turn caused the depletion of condensin I or condensin II. This method allowed the researchers to inactivate condensin I, condensin II or both condensin I and condensin II during the long dictyate arrest in the mouse oocytes. This allowed analysis of condensins role in meiosis and in the longitudinal rigidity of the chromosomes. Using this system Houlard *et al* (2015) found thread-like sister chromatid formation, in meiosis, is disrupted when condensin II is depleted, consistent with what has been previously observed in *Xenoupus* egg cell free extracts (Shintomi and Hirano, 2011). Condensin II was found to be essential for meiosis. Contrastingly condensin I was not (Houlard et al, 2015). When condensin I was depleted, chromosomes were observed to be slightly shorter and wider than observed in wild type. When condensin II was not present condensin I was the main protein responsible for chromosome compaction (Houlard et al, 2015). This indicates that condensin I is able to partially compensate for condensin II loss. This is in contrast to what is seen in mitosis. In mitosis depletion of condensin I causes a delay in mitotic progression (Nishide and Hirano, 2014). The difference in the condensin requirements in both mitosis and meiosis is likely to be linked to differences in the regions at which spindle tension is applied. In meiosis spindle tension is applied along the chromosome arms whereas in mitosis tension is applied at the inner centromere (Lee et al, 2011). This idea is supported by the finding that condensin I and condensin II have different localizations along the chromosomes (Ono et al, 2004).

In the study by Houlard *et al* (2015) it was noted that there was still some chromatin compaction when Ncaph1 and Ncaph2 were deleted. This indicated that there might be other condensin independent processes that contribute to chromosome compaction. Alternatively it is possible that the condensin

complexes were incompletely depleted in the study by Houlard *et al* (2015). Furthermore it is possible that condensin protein turnover is slow, meaning that residual protein was present in the oocytes. Complete depletion of condensin may abolish chromosome compaction. It is possible that the defects in thread formation were not observed previously, when Smc2 transcription was turned off or condensin is depleted using RNA interference, because the cells entered mitosis with a level of condensin sufficient to in order to promote accurate thread formation (Hirota et al, 2004; Hudson et al, 2003).

Condensin has also been found to regulate the rigidity of the chromosomes. When condensin is depleted sister chromatids are observed to be further apart. This indicates that it is possible that condensin is required in order to regulate the function or alter the distribution of proteins involved in sister chromatid cohesion (Gerlich et al, 2006; Oliveira et al, 2005; Ribeiro et al, 2009). Analysis of chromosome extension of both newt and human chromosomes have indicated that condensin association may make chromosomes more rigid, compared to when chromosomes are associated with histones alone (Almagro et al, 2004). It is still unknown if a single activity of condensin is responsible for chromosome compaction, chromosome rigidly and chromosome disentanglement. It has been hypothesized that condensin may promote chromosome compaction by attaching to the chromatin loops, and enlarging the loops until they can approach adjacent complexes at the base of the loops (Nasmyth et al, 2002). Condensin is also thought to induce positive supercoils, which act to drive chromosome compaction, indicating that condensin may function enzymatically (Baxter and Aragon, 2012; St-Pierre et al, 2009). Furthermore condensin has been found to promote the function of Top2 (Baxter et al, 2011). Top2 functions by inducing transient DNA breaks which mean that the sister chromatids can disentangle from one another. Top2 is then able to catalyse the resolution of both positive and negative supercoils by promoting the passage of DNA double helixes through one another (Wang et al, 2002). This indicates that it is likely that condensin carries out its roles through several different methods.

1.12 Smc5/6 complex

A large amount is known about the two well-known SMC complexes, Cohesin (Section 1.10) and Condensin (Section 1.11). Considerably less is known about the third SMC complex, Smc5/6. Smc6 (previously known as Rad18) was first identified in a fission yeast screen for radiation sensitive mutants (Nasim and Smith, 1975). Because of this many labs initially looked into its roles in DNA repair. The Smc5/6 complex since has been found to have a major role in the regulation of factors involved in restart of stalled replication forks, chromosome topology, homologous recombination and maintenance of heterochromatin, telomeres and rDNA (Branzei et al, 2006; Chiolo et al, 2011; De Piccoli et al, 2006; Lehmann et al, 1995; Potts et al, 2009; Tapia-Alveal et al, 2010; Torres-Rosell et al, 2007). This indicates that the Smc5/6 complex is responsible for chromatin changes throughout mitosis. Recent studies have begun to indicate that it also has an important role in meiosis.

The structure of the Smc5/6 complex was identified from purification of the subunits from *S.pombe* (Fousteri and Lehmann, 2000; Sergeant et al, 2005). Like cohesin and condensin, the Smc5/6 complex has a ring like structure made up of two central SMC proteins (Smc5 and Smc6) and several non-SMC elements (Nse1-4) all of which are conserved from yeast to mammals. (Figure 1.3A) (De piccoli et al, 2009; Duan et al, 2009; Fujioka et al, 2002; Hu et al, 2005; McDonald et al, 2003; Pebernard et al 2004; Sergeant et al, 2005; Taylor et al, 2008; Zhoa and Blobel, 2005). The similar structure of the three SMC proteins indicates that the SMC complexes may share a common mode of action. Throughout the subunits of the Smc5/6 complex will be referred to using yeast nomenclature unless a specific organism is being referred to (in which case the nomenclature for that organism will be used). Smc5 and Smc6 interact with one another through their hinge domains and with the kleisin Nse4 at their heads (Palecek et al, 2006). The kleisin Nse4 also forms a subcomplex with Nse1 and Nse3 (Duan et al, 2009; Palecek et al, 2006; Pebernard et al, 2008). The subcomplex, Nse1-Nse3-Nse4, has been found to bind to the double stranded DNA and single stranded DNA with no preference for recombination/replication intermediates. From this it was

proposed that this subcomplex is important for the loading of the Smc5/6 complex onto the chromosomes (Pebernard et al, 2008; Zabrady et al, 2016).

The Smc5/6 complex, unlike the other SMC complexes, contains two catalytic subunits. These potentially enable the Smc5/6 complex to modify target proteins (as well as itself) and regulate their function. Nse1 contains a ring finger domain commonly found in E3 ubiquitin ligases and Nse3 contains a melanoma-associated antigen gene domain (Fujioka et al 2002; McDonald et al 2003; Perbernard et al, 2004). When Nse3 binds to Nse1 it has been found to enhance the E3 ubiquitin ligases activity of Nse1 (Doyle et al, 2010). Nse2 (Mms21) interacts with Smc5 (McDonald et al, 2003). It contains a SP-RING domain and acts as a small unbiquitin-related modifier (SUMO) ligase (McDonald et al, 2003; Zhao and Blobel, 2005). Potential targets of Nse2 include Scc1, Smc5 and Ndc10 (Wu et al, 2012; Yong-Gonzales et al, 2012; Zhao and Blobel, 2005). Nse5 and Nse6 also form part of the Smc5/6 complex (Sergeant et al, 2005). Interestingly Nse5 and Nse6 are only essential in *S.cerevisiae* and not *S.pombe* (Pebernard et al 2006; Zhao and Blobel, 2005). Furthermore they associate at different regions of the Smc5/6 complex in budding and fission yeast. In budding yeast the Nse5-Nse6 sub-complex associates with the hinge region and in fission yeast the Nse5-Nse6 sub-complex associates with the head domains, which has been proposed to enhance the stability of the complex (Figure 1.6A & 1.6B; Duan et al, 2009; Perbernard et al, 2006). Orthologues of Nse5 and Nse6 have not been found in any other organisms. Rad60, a protein part of the RENi family, also physically interacts with Smc5/6 complex, but much more loosely than the other subunits (Morikawa et al, 2004; Novatchkova et al, 2005). It is essential for the DNA repair functions of the Smc5/6 complex (Morishita et al, 2002).

The Smc5/6 complex is present on the chromosomes at S-phase in both yeast and humans (Gallego-Paez et al, 2014; Kegel et al, 2011). It can be loaded onto the chromosomes in both an Scc2 (sister chromatid cohesion protein-2) dependent or an Scc2 independent manner (Copsey et al, 2013; Lindroos et al, 2006; Xaver et al, 2013). As Scc2/4 has a role in the loading of both Smc5/6 and cohesin onto the chromosomes it is unsurprising that many of the Smc5/6 interaction sites overlap

with those of cohesin (Lindroos et al, 2006). Like cohesin, the Smc5/6 complex has been found to bind along the chromosome arms and at the rDNA, centromeres and telomeres (Lindroos et al, 2006; Torres-Rosell et al, 2005). Furthermore research indicates that both the Smc5/6 complex and cohesin are recruited to the sites of DSB in order to promote DSB repair (Copsey et al, 2013; De piccoli et al, 2006; Lindroos et al, 2006; Potts et al, 2006; Strom et al, 2004; Unal et al, 2004; Wu and Yu, 2012; Xaver et al, 2013). As the Smc5/6 complex shares the same ring like structure as cohesin the Smc5/6 complex may also binds to the DNA in a similar way to cohesin, through ATP-regulated topological entrapment. This is supported by the finding that hypomorphic Smc5/6 mutants that cannot carry out ATP hydrolysis, cannot interact with the DNA (Kanno et al, 2015).

1.12.2 Smc5/6 in homologous recombination

The DNA repair functions of the Smc5/6 complex have been analysed using several viable hypomorphic yeast mutants. Many of the hypomorphic yeast mutants tested displayed unrepaired chromosomes after treatment with ionizing radiation indicating that these mutants were defective in homologous recombination (Lehmann et al, 1995; Lindroos et al, 2006; Morikawa et al, 2004; Verkade et al, 1999). Furthermore it was found that these mutants also failed to accurately segregate their chromosomes in mitosis after DNA damage (Ampatzidou et al, 2006; Miyabe et al, 2006; Verkade et al, 1999). Interestingly the problems in chromosome segregation were alleviated if homologous recombination was also inhibited, indicating that defects in the Smc5/6 complex are unlikely to cause problems in the early stages of homologous recombination such as strand exchange and ligation (Ampatzidou et al, 2006; Miyabe et al, 2006). It is instead likely that the mutants are defective in joint molecule resolution.

In fission yeast, budding yeast, mammals and plants the Smc5/6 complex has a role in facilitating homologous recombination (Ampatzidou et al, 2006; Cost and Cozzarelli, 2006; Lehmann et al, 1995; McDonald et al 2003, Mengiste et al, 1999; Perbernard et al, 2006; Stephan et al, 2011; Torres-Rosell et al, 2005; Watanabe et al, 2009). Depletion of the subunits of the Smc5/6 complex has been found to

led to an accumulation of joint molecules supporting the idea that the Smc5/6 complex specifically has a role in joint molecule resolution. If these joint molecules are not removed prior to anaphase then they can lead to chromosome mis-segregation. Interestingly if Nse2's SUMO ligase activity is removed in yeast, cells are viable but have an intermediate homologous recombination defect (Andrews et al, 2005; Zhao et al, 2005;Xaver et al, 2013). The same results have been found through siRNA knock down experiments in human cells (Potts et al, 2005). Further work by Bermudez-Lopez *et al* (2010) indicates that the SUMO ligase activity of Nse2 is required for dissolution of physical connections between the sister chromatids in mitosis. It is therefore likely that the SUMO ligase of Nse2 sumoylates an unknown substrate which promotes joint molecule resolution. The SUMO ligase activity of Nse2 has also been implicated to have a role in telomere maintenance. Potts *et al* (2007) found that there was a reduction in homologous recombination dependent telomere elongation when the SUMO ligase activity of Nse2 is compromised. This indicates that the Smc5/6 complex has a role in coordinating HR in several different contexts.

Smc5/6 is also has several roles at stalled replication forks. It is required to maintain replication fork stability, to prevent recombination at replication forks and for the restart of stalled replication forks (Irmisch et al, 2009; Murray and Carr, 2008). When Nse2 or Smc6 are depleted in budding yeast this results in an accumulation of Rad51 dependent X-shaped intermediates at stalled replication forks and subsequent chromosome segregation defects (Ampatzidou et al, 2006; Branzei et al, 2006). Later work by Irmisch *et al* (2009) found that the Smc5/6 complex has a role in loading Rad52 and RPA onto collapsed or stalled replication forks so that the replication forks are maintained in a recombination-competent conformation. It has further been proposed that Smc5/6 may be required to orient the replication forks in a configuration that can be processed by Mus81 (Irmisch et al, 2009; Roy et al, 2011). This hypothesis is supported by the finding that that Smc5/6 mutants demonstrate similar levels of joint molecules intermediates to those found in Mus81 mutants (Wehrkamp-Richter et al, 2012).

Overexpression of BRC1 in Smc6 hypomorphic mutants suppresses the defects observed in Smc5/6 mutants (Lee et al, 2007; Sheedy et al, 2005; Verkade et al, 1999). Brc1 forms foci on the DNA in response to DNA damage (MMS) and has been found to bind to many different repair proteins. From this it is hypothesised that BRC1 binds to the DNA damage and acts to recruit other repair factors (Roberts et al, 2006). This indicates that the overexpression of BRC1 can bypass the defects observed in the Smc5/6 mutants by promoting an alternative repair process through the recruitment of other repair factors such as Slx4 (Roberts et al, 2006). From this it was proposed that the Smc5/6 complex has a regulatory role in coordinating DNA repair after DNA damage.

Sgs1 alongside both Rmil and Top3 forms a complex called STR (Sgs1-Top3_Rmil) (Ashton & Hickson, 2010; Bennett et al, 2000; Chang et al, 2005; Gangloff et al, 1994; Mullen et al, 2005; Oakley et al, 2002). The STR complex has been found to have a role in the 5'-to-3' DNA resection at DSB and for D-loop dissolution (Bachrati et al, 2006; van Brabant et al, 2000). The STR complex has also been found to be involved in the resolution of dHJ and Sgs1 is specifically well known to have a role in the dissolution of stalled replication forks (Cejka et al, 2010; Liberi et al, 2005). Phenotypes caused by the inactivation of Sgs1 are similar to what is observed when the Smc5/6 complex is depleted (Bermudez-Lopez et al, 2016; Branzei et al, 2006). Bermudez-Lopez *et al* (2016) found that Sgs1 and subunits of the Smc5/6 complex are substrates of Nse2 (Mms21) indicating that the Smc5/6 complex is involved in the regulation of STR's recombinogenic activity. They further identified that the Smc5/6 complex has two roles in Sgs1 regulation (Bermudez-Lopez et al, 2016). The Smc5/6 complex is required for the recruitment of Sgs1 to the chromatin and for the pro-recombinogenic activity of Sgs1. They also found that there is hyper-SUMOylation of many of the subunits of the Smc5/6 complex (Smc5, Smc6, Nse3, Nse4) by Nse2 when the Smc5/6 complex is required to carry out HR-dependent repair (Bermudez-Lopez et al, 2016). Sgs1 localises to DNA damage sites via recognition of the hyper-SUMOylated Smc5/6 complex. This is due Sgs1's two SIM's (SUMO interacting motifs), which are able to recognize hyper-SUMOylated Smc5/6 complex (Bermudez-Lopez et al, 2016).

Bermudez-Lopez *et al* (2016) also found that SUMO compromised Sgs1 (Sgs1-K621R) can localize to DNA damage but is not functional. SUMO dead alleles of Sgs1 and Sgs1-SIMΔ display severe defects in DNA end resection and high levels of unprocessed damaged replication forks. This indicates that Sgs1 must be sumoylated in order to carry out its pro-recombinogenic activity and that the Smc5/6 complex must be hyper-SUMOylated for its recruitment (Bermudez-Lopez et al, 2016). Top3 has also been found to be sumoylated by Nse2. Its sumoylation is also required for the function of the STR (Bermudez-Lopez et al, 2016). The Smc5/6 complex has been found to be involved in regulating the activity of Mph1 helicase, human FANCM orthologue. It has been found to restrain its replication fork regression in order to allow replication fork repair (Xue et al, 2014). It is possible that this is also through sumoylation by Nse2.

The Smc5/6 complex has also been implicated to have a role in the resolution of topological stress (Carter and Sjogren, 2012; Jeppsson et al, 2014). When the Smc5/6 complex is depleted an accumulation of intertwining sister chromatid DNA is observed (as demonstrated by the presence of anaphase bridges). These phenotypes are reminiscent of seen when TopoII is depleted (Spence et al, 2007). Because of this it was questioned if the Smc5/6 complex has a role in regulating the activity of TopoII (Gomez et al, 2013). TopoII induces DSB at sites of DNA topological constraints, which acts to decatenate the DNA (Nitiss et al, 2009). In wild type cells, TopoII is enriched at the centromeres but is also present at a lower level along the chromosome arms. When Smc5 or Smc6 is depleted, in humans, the localisation of TopoII changes. TopoII is found to accumulate at the distal arm regions and less is observed at the centromeres indicating that the Smc5/6 complex is important for topoisomeraise IIα localisation (Gallego-Paez et al, 2014). Chromatin immuno precipitation analysis indicated that the redistribution of topoisomeraise IIα from the interphase binding sites to the centromeres at mitosis is blocked in the Smc5/6 complex mutants (Gallego-Paez et al, 2014).

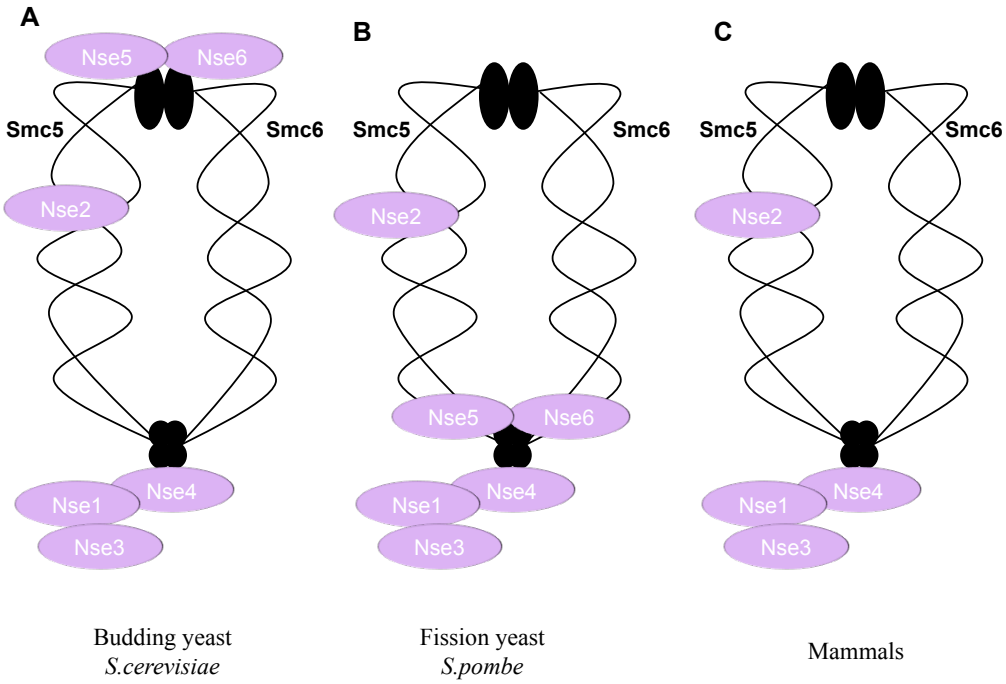

Figure 1.6 – SMC5/6 complex in *S.cerevisiae*, *S.pombe* and mammals

A, the structure of the Smc5/6 complex in *S.cerevisiae* B, the structure of the Smc5/6 complex in *S.pombe* C, the structure of the Smc5/6 complex in mammals. The Smc5/6 complex has two central SMC proteins, Smc5 and Smc6 and several non-SMC elements. Only Nse1-4 have been found to be conserved from yeast to mammals. Homologues of Nse5 and Nse6 have not been identified in mammals. The complexes in yeast also differ in the location of the Nse5 and Nse6 proteins. In *S.cerevisiae* they are located at the head domains and in *S.pombe* they are located at the hinge domains (Verver et al, 2016).

As well as recruiting TopoII to the chromosomes it as been found that the Smc5/6 complex may partially compensate for TopoII in cells where TopoII is depleted. The Smc5/6 complex is enriched at the centromeres and in TopoII inhibiting conditions along the chromosome arms. Furthermore the Smc5/6 complex has been found to be responsible for the resolution of sister chromatid interwinings (SCIs) when Top2 is inhibited (Jeppsson et al, 2014). It is proposed to carry this out by promoting replication fork rotation (Kegel et al, 2011).

1.12.3 Smc5/6 in meiosis

Recently it has become clear that the Smc5/6 complex also plays an important role in meiosis. At the beginning of meiosis Smc6 localises at the nucleolus (Farmer at el, 2011; Lilienthal et al, 2013). Once the chromosome axes have formed and DSB induction is initiated, Smc6 and Smc5 appear as foci along the length of the chromosome axis in both yeast and mice (Copsey et al, 2013; Farmer et al, 2011; Gomez et al, 2013; Lilienthal et al, 2013; Xaver et al, 2013). The localisation of Smc6 was found not to be dependent on the formation of DSBs (Copsey et al, 2013; Farmer et al; 2011). Nsmce1, Smc5 and Smc6 were found to localize to the pericentromeric heterochromatin throughout the whole of meiosis in both mouse and human spermatocytes. The localisation was only observed to disappear when the sister chromatids began to elongate (Gomez et al, 2013; Verver et al, 2013).

Smc6 has also been found to co-localise with Rad51 indicating that the Smc5/6 complex may have a role in strand invasion during meiotic recombination (Copsey et al, 2013; Xaver et al, 2013). As synapsis occurs Smc5/6 staining along the chromosomes becomes more profuse (Copsey et al, 2013; Lilienthal et al, 2013; Xaver et al, 2013). In some mouse reports, and in budding yeast, Smc6 is observed to be retained at the centromeres until late anaphase (Gomez at al, 2013; Lindroos et al, 2006). Contrastingly in human studies and several studies in mice it was found that the Smc5/6 complex was lost from the chromosomes by metaphase (Gallego-Paez et al, 2014; Taylor et al, 2001; Verver et al, 2013 & 2014). These differences could real or may instead be due to differences in the

antibodies or chromosome spread preparation, which could affect the sensitivity of the antibodies.

Lilienthal *et al* (2013) found that the binding of Smc6 at the chromatin was dependent on Rec8. Contrastingly Copsey *et al* (2013) and Hwang *et al* (2017) found that the localisation of Smc5 and Smc6 was not affected in the absence of Rec8. Differences have also been observed in the localisation of the Smc5/6 complex during late prophase. Xaver *et al* (2013) found that Smc6 localises to the chromosomes during both meiotic divisions. Copsey *et al* (2013) and Lilienthal *et al* (2013) however found that the amount of Smc5 and Smc6 are reduced at late prophase and are absent at early metaphase. It is possible that differences are due to differences in the spread preparation or accessibility of the antibody to its corresponding epitope.

1.12.3.2 Smc5/6 in meiotic recombination

Unresolved joint molecules can impede chromosome segregation in meiosis if left unresolved (Copsey et al, 2013; Jessop and Lichten et al; 2008; Matos et al, 2008; Xaver et al 2013). The Smc5/6 complex has been found to prevent the accumulation of joint molecules in two ways. The first is by facilitating joint molecule resolution (Copsey et al, 2013; Lilienthal et al, 2013; Xaver et al, 2013). The second is through destabilization of the non-ZMM SEI intermediates (Xaver et al, 2013). The Smc5/6 complex destabilizes the SEI intermediates using the SUMO E3 ligase of Nse2 (Xaver et al, 2013). Interestingly the SUMO E3 ligase of Nse2 does not have a role in the Smc5/6 mediated resolution of joint molecules (Xaver et al, 2013). During meiotic recombination, in fission yeast, the single Holliday junction intermediates formed are resolved by the Mus81-Eme1 complex (Boddy et al, 2001; Cromie et al, 2006; Osman et al, 2003). It has been proposed that the Smc5/6 complex regulates the recruitment of the structure specific endonucleases (Slx1-Slx4, Mus81-Mms4 and Yen1) in order to promote joint molecule resolution in budding yeast (Copsey et al, 2013; Xaver et al, 2013). This hypothesis is supported by the finding that the Smc5/6 complex is required for the association of Mus81 to the meiotic chromosomes (Copsey et al, 2013). In

C.elegans depletion of the Smc5/6 complex led to an increased number of Rad51 foci along the chromosomes during meiosis I and increased levels of chromosome fragmentation (Bickel et al, 2010). Furthermore it was found that *mus-81* mutants displayed the same phenotype as both *smc5* and *smc6* mutants. This indicates that, like in yeast, the Smc5/6 complex is required for Holliday Junction resolution in *C.elegans* (O'Neil et al, 2013).

Sgs1 has been found to limit the number of multi-chromatid joint molecules formed in meiosis (Chen et al, 2010; Fabre et al, 2002; Jessop and Lichten 2008; Sugawara et al, 2004). In *C.elegans* it has been proposed that the Smc5/6 complex works with Sgs1 in order to process recombination intermediates, to carry cross over regulation and bivalent maturation and to regulate chromosome structure (Hong et al, 2016). Furthermore, in budding yeast, results indicate that the Smc5/6 complex acts to co-ordinate helicases, such as Sgs1, and resolvases at D-Loops and Holliday junctions (Xaver et al, 2013). The finding that *smc5 sgs1* or *nse4 sgs1* double mutants display significantly increased levels of joint molecules than observed in *smc5* or *nse4* single mutants indicates that the Smc5/6 complex and Sgs1 function in different pathways. *sgs1*, *smc5* and *nse4* individual mutants respectively exhibited 0.6%, 1.5% and 13% joint molecules on completion of meiosis. *smc5 sgs1* and *nse4 sgs1* repectively exhibited 14% and 20% joint molecules on completion of meiosis (Copsey et al, 2013).

1.12.3.3 Smc5/6 and chromosome synapsis

Smc5 and Smc6 localize at the central region of the synaptonemal complex from zygotene to diplotene in both mice and humans spermatocytes (Gomez et al, 2013; Verver et al, 2014). In mice Smc6 staining only co-localised with TEX12 and SYCP1 (synaptonemal complex central elements) indicating that the Smc5/6 complex only binds to synapsed chromosomes in mice (Gomez et al, 2013). Loading of the Smc5/6 complex was independent of SMC1β and REC8 indicating that the association of the Smc5/6 complex could be related to chromosome structure (Gomez et al, 2013; Jeppsson et al, 2014).

During prophase any unsynapsed chromosomes are silenced through MSUC (meiotic silencing of unsynapsed chromosomes). Specific silencing of the unsynapsed X and Y chromosomes is called MSCI (meiotic sex chromosome inactivation). This takes place via the formation of the XY body (Ichijima et al, 2012). In mice Smc5, Smc6 and Nsmce1 were found to localize to the chromatin of the XY body indicating that the Smc5/6 complex may be carrying out meiotic sex chromosome inactivation at the XY body (Gomez et al, 2013). Verver *et al* (2014) contrastingly found that Smc6 only localizes to the unsynapsed X and Y-chromosomes in human spermatocytes. This indicates that the Smc5/6 complex may have a role in double strand break repair at the X and Y chromosomes (Verver et al, 2014). This is supported by the observation that Rad51 and Smc6 localised to unsynapsed autosomes (Verver et al, 2014). As it is known that Spo11 creates DSB even in the absence of synapsis (including in the unsynapsed regions of the sex chromosomes) these studies indicate that the Smc5/6 complex may have a role in repairing DSB at unsynapsed regions of the meiotic chromosomes (Kauppi et al, 2013).

1.12.4 Smc5/6 complex and Topoisomeraise II

The Smc5/6 complex is essential for cell viability. However spores produced from diploids homozygous null for components of the Smc5/6 complex often do not die during their first mitosis. Many are able to propagate for 2-3 cell cycles (Harvey et al, 2004; Verkade et al, 1999). After 2-3 cell cycles null diploids then display the "cut" phenotype (where the chromatin fails to separate and the division septum forms). Contrastingly if the spores are exposed to DNA damaging agents they die in their first mitosis due to defects in chromosome segregation. Verkade *et al* (1999) also found that Smc5/6 mutants were synthetically lethal in combination with a temperature sensitive allele of Topoisomeraise II (*top2-191*). Because of this finding it was assumed that the *top2-191* mutant has a low level of DNA damage, which the cell is able to tolerate alone, as demonstrated by its normal growth, but that the cell cannot tolerate in combination with Smc6 mutants including *smc6-74* (A151T). It was therefore proposed that defects in

chromosome segregation, observed in the double mutant, were due to incomplete repair of the sister chromatids.

In order to test this Outwin *et al* (2009) inhibited cytokinesis in the *smc6-74 top2-191* double mutants. This acted to provide the cells with an increased amount of time in order to accurately repair the sister chromatids. Analysis found that, even after the delay, the sister chromatids were still unable to accurately segregate in *smc6-74 top2-191* double mutants. Interestingly the cells were observed to undergo another round of DNA replication, which would not occur if unrepaired DNA was present (due to activation of the cell cycle checkpoint arrest). This, alongside pulse field gel analysis, indicated that there was something other than unrepaired DNA damage which was preventing the sister chromatids from segregating (Outwin et al, 2009). Cellular analysis using integrated LacO arrays and GFP LacI fusion proteins and ChIP (Chromatin Immunoprecipitation) found, in *smc6-74 top2-191* double mutants, *smc6-74* after HU treatment and *smc6-74* after UV-C treatment, that the sister kinetochores separated on time but that the chromosome arms remained joined (Outwin et al, 2009; Tapia-Alveal et al, 2010). In order to determine what was holding the chromosome arms together Outwin *et al* (2009) carried out a screen for high-copy suppressors of the defects caused in the *smc6-74 top2-191* double mutants. They identified that over-expression of Cut1 (the *S.pombe* homologue of separase) rescued the lethality of the *smc6-74 top2-191* double mutants and *smc6-74* mutants after HU treatment. The overexpression of Cut1 was not able to rescue the lethality of *smc6-74* mutants after UV-C treatment likely due to the high level of recombination intermediates (that were not observed in the *smc6-74 top2-191* double mutants) (Outwin et al, 2009; Tapia-Alveal et al, 2010). This further indicated that the lethality of the *smc6-74 top2-191* double mutants and *smc6-74* mutants after HU treatment were not due to an accumulation of recombination intermediates. These results instead suggested that the lethality is caused by retention of cohesin, which prevents chromosome arm segregation. It is likely that this defect was previously obscured by the well-characterised homologous recombination defects.

In *S.pombe* a large amount of the cohesin from the chromosome arms is lost in a separase-independent pathway before anaphase known as the prophase pathway. As cohesin is lost from the kinetochores with normal timing but retained along the chromosome arms this indicates that the *smc6-74* mutants after HU treatment or coupled with *top2-191* have defects in their separase-independent removal of cohesin (Outwin et al, 2009). Interestingly the lethality of the *smc6-74 top2-191* double mutants was rescued after the expression of catalytic dead TopII (Y835F) indicating that an incorrect chromosome structure may mean that proteins involved in cohesin disassembly cannot properly access the chromosomes (Outwin et al, 2009). This hypothesis is supported by work by Kegel *et al* (2011) whose results indicate that the Smc5/6 complex functionally interacts with topisomeraises in order to regulate the topology of longer chromosomes in *S.cerevisiae*. Furthermore human cells depleted of the Smc5/6 complex have been observed to display disrupted structures, which also led to defects in chromosome segregation. Analysis of chromosomes from cells depleted of the Smc5/6 complex found that these defects were accompanied by an altered distribution of both condensin and TopoIIα further indicating that TopoIIα and the Smc5/6 complex functionally interact (Gallego-Paez et al, 2014).

Interestingly a further screen, by Tapia-Alveal *et al* (2014), looking for suppressors of the mitotic defects caused in the *nse1-C216S top2-191* double mutants found that loss of H2A.Z (a histone variant) allowed mitosis to take place. Further analysis found that loss of H2A.Z is required for the removal of cohesin from the chromosomal arms, but not the centromeres, and that its loss was also able to suppress the mitotic defect in *smc6-74 top2-191* double mutants (Tapia-Alveal et al, 2014). H2A.Z, as well as promoting cohesin loading and maintenance at the chromosomes, behaves as a condensin chromosomal receptor, promoting the recruitment of condensin to the chromosomes (Tada et al, 2011). This led to the idea that that the SMC complex dynamics may be regulated by the histone code. Alternatively it is possible that H2A.Z acts to locally regulate chromosome topology in order to promote accurate chromosome segregation (Tapia-Alveal et al, 2014). Recent work by Lin *et al* (2016) found that the retention of cohesin in *smc6-74* mutants after HU treatment is also suppressed in *S.pombe* by Eso1

inactivation (eso1-H17) (orthologue of *S.cerevisiae* Eco1). This is proposed to be via Psm3 (orthologue of *S.cerevisiae* Smc3) hypoacteylation (Lin et al, 2016). They also found that the cohesin that is retained, along the chromosome arms, is from the existing pool of cohesin rather than newly recruited cohesin to sites of DNA damage (Lin et al, 2016). Interestingly the role of the Smc5/6 complex in cohesin removal has not been observed in *S.cerevisiae* mitosis (Jeppsson et al, 2014). This is proposed to be because cohesin is removed in one step in *S.cerevisiae* mitosis, as the separase-independent pathway does not exist.

1.12.5 Smc5/6 at the heterochromatin

The rDNA consists of 100-200 identical repeats on chromosome XII that code for ribosomal DNA. This is found within the nucleolus (Oakes et al 2006). As the rDNA is highly repetitive, homologous recombination must be suppressed in order to prevent unequal sister chromatid exchange (Eckert-Boulet and Lisby, 2009). The Smc5/6 complex has been found to localize to the rDNA and the telomeres during meiotic prophase I in both budding and fission yeast (Ampatzidou et al, 2006; Farmer et al, 2011; Lilienthal et al, 2013; Torres-Rosell et al, 2005; Xaver et al, 2013). Because of this it was hypothesised that it may have a role in suppressing homologous recombination within the heterochromatin. When the Smc5/6 complex is depleted, regions of the DNA containing highly repetitive sequences become unstable, supporting the idea that the Smc5/6 complex has an anti-recombinogenic role at the heterochromatin (Goodarzi and Jeggo, 2012; Torres-Rosell et al, 2005 and 2007). When the Smc5/6 complex is depleted an increased number of DSBs were observed within the nucleolus (Torres-Rosell et al, 2005). Because of this Torres-Rosell *et al* (2005) hypothesised that the Smc5/6 complex has a role in moving any DSB generated within the rDNA outside the nucleolus for repair (Torres-Rosell et al 2005 and 2007). Similar results were observed in *Drosophila melanogaster* by Chiolo *et al* (2011). They also found that homologous recombination within the heterochromatin is suppressed until the DSB is moved outside the nucleolus (Chiolo et al, 2011). It is however possible that increased numbers of DSBs observed within the nucleolus, when the Smc5/6 complex was depleted, were

instead due to problems in repair of DSB when the Smc5/6 complex is not present. It was also found, by Torres-Rosell *et al* (2005), that rDNA segregation is defective when the Smc5/6 complex is depleted. It has been proposed that when the function of the Smc5/6 complex is compromised, rDNA replication is incomplete which in turn causes the defects in segregation.

Both the rDNA and the telomeres are replicated unidirectionally. This is to make sure that replication and transcription do not clash (Kobayashi et al, 2005). In the rDNA unidirectional replication is due to the activity of Fob1, which prevents forks traveling in the left direction. When Fob1 is deleted, in Smc6 mutants, this results in a decrease in rDNA missegregation (Torres-Rosell et al, 2007). The decrease in mis-segregation observed is likely to be due to the DNA being replicated bidirectionally, which means that converging forks can recover stalled forks. When a fork stalls in the rDNA or at the telomeres this can normally only be resolved using recombination based replication or restart. This therefore indicates that it is likely that the global defects seen in Smc5/6 mutants are accentuated at the telomeres and rDNA because the stalled forks that form within the telomeres and rDNA cannot be recovered due to the unidirectional nature of the replication.

The Smc5/6 complex has also been proposed to have a role in preventing homologous recombination at the pericentromeric heterochromatin. Pericentromeric heterochromatin is made up of densely packed repetitive sequences and because of this recombination is generally repressed in these regions (Lynn et al, 2004). In mice a lack of Rad51 or YH2AX staining specifically at the pericentromere was observed alongside an enrichment of Smc6 staining at the pericentromere. This indicates that the Smc5/6 complex has a role in preventing recombination at the pericentromere in mice (Verver et al, 2013). In drosophila and budding yeast the Smc5/6 complex has been found to localize at the pericentromeres indicating it has a role in prevent HR at the pericentromeres (Chiolo et al 2011; Lindroos et al, 2006). Contrastingly however the Smc5/6 complex was not observed to localize to the pericentromeric heterochromatin in human spermatocytes (Verver et al, 2014). This difference could be due to

differences in spread preparation or antibodies used. It is also however possible that the Smc5/6 complex is not required for suppression of recombination at the heterochromatin in humans.

1.12.6 Smc5/6 and condensin

The Smc5/6 complex has been found to have a role in regulating chromosome structure in mitosis. Sister chromatids become curly along the chromosome arms and hypocondensed at the centromeres when the Smc5/6 complex is depleted. This is predicted to be due to the role of the Smc5/6 complex in regulating chromatin organisation during DNA replication (Gallego-Paez et al, 2014). The Smc5/6 complex is required for condensin localisation to the mitotic chromosomes in humans. When Smc5 or Smc6 are depleted in mammalian cells, perturbation in the localisation of Condensin was observed (Gallego-Paez et al, 2014; Pryzhkova and Jordan, 2016; Hwang et al, 2017). Furthermore in human cells depleted of Smc5 or Smc6 perturbations in the localisation of TopoII was also observed (Gallego-Paez et al, 2014). In wildtype, during propmetaphase, condensin is localized along the chromosome arms and enriched at the pericentromeres. In mESC's (mouse embryonic stem cells) depleted of Smc5, decreased levels of condensin were observed at the pericentromere and increased levels were observed along the chromosome arms (Pryzhkova and Jordan, 2016). Furthermore Pryzhkova and Jordan (2016) observed that the levels of PLK1 were reduced at the pericentromeres and that the levels of Aurora B were increased along the chromosome arms. Cdk1, Aurora B kinase and PLk1 act to phosphorylate condensin in order to induce efficient chromosome formation (Abe et al, 2011; Lipp et al, 2007; Tada et al, 2011). Phosphorylation of condensin specifically by Aurora B regulates the association of condensin with the chromatin (Lipp et al, 2007; Tada et al, 2011). As it was observed there was an enrichment of both Aurora B and condensin along the chromosome arms when the Smc5/6 complex was depleted this indicates that the Smc5/6 complex may have a role in promoting the release of Aurora B from the chromatin once condensin has been loaded, potentially through ubiquitin or SUMO modification of Aurora B. It is

possible that condensin along the chromosome arms can only redistribute once Aurora B is removed.

1.12.7 Patients with defects in the Smc5/6 complex

Mutations in subunits of the Smc5/6 complex have been indentified in several different patients. Van der Crabben *et al* (2016) identified two sets of young patients with missense mutations in Nsmce3 (a homologue of yeast Nse3). The patients displayed chromosome breakage syndrome, which correlated with severe lung disease early in life (lung disease immunodeficiency and chromosome breakage syndrome (LICS)). The patients also displayed chromosome rearrangements, sensitivity to replication stress, defective homologous recombination and defects in their T and B cell functions. All patients displaying missense mutations in Nsmce3 died very early in childhood. Analysis found that the Nsmce3 mis-sense mutations that the patients displayed disrupted Nsmce3's interactions with the rest of the Smc5/6 complex, therefore destabilising the complex (Van der Crabben et al, 2016). Patients carrying mutations in Nsmce2 have also been identified. Payne *et al* (2014) identified two patients with frameshift mutations in Nsmce2, which led to decreased levels of Nsmce2 expression. These patients displayed insulin resistance, primordial dwarfism, gonadal failure and difficulties in recovery from replication stress (Payne et al, 2014). Here the phenotypes observed were not as severe as seen in the patients with defects in Nsmce3 (Van der Crabben et al, 2016). This is likely to be because the SUMO ligase activity of Nse2 is not required for all of the functions of the Smc5/6 complex. It could also be linked to differences in the level of protein present in each of the patients.

1.13 Oogenesis

Most of what we know about oogenesis in mammals comes from the mouse model. This has provided information that could not be obtained from humans for ethical reasons. Oogenesis is a form of gametogenesis, in mammalian females, in which a diploid cell, the oogonium, divides to form a haploid egg cell, known as

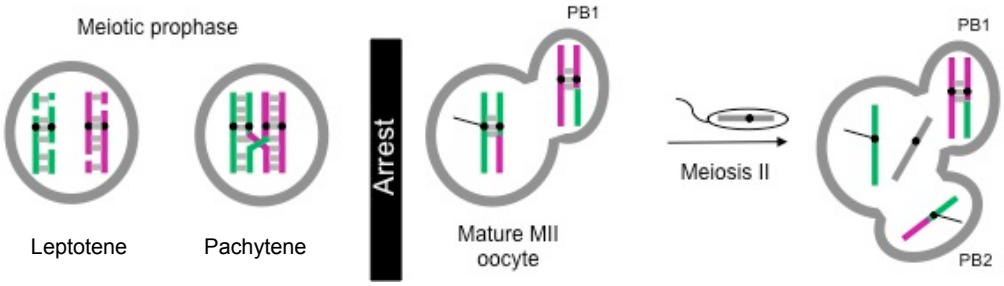

Figure 1.7 – Stages of oogenisis

The oocytes progress through meiosis until they reach diplotene. The oocytes then enter an arrest known as the dictyate arrest and remain in this arrest until ovulation (Hunt and Hassold, 2008). At ovulation an oocyte is released from the dictyate arrest and carries out the first meiotic division. The homologous chromosomes segregate and two daughter cells are produced, one small daughter cell that contains only a very small amount of cytoplasm (the polar body) and one significantly larger metaphase II cell containing the majority of the cytoplasm (the secondary oocyte) (Petronczki et al, 2003). Only when the sperm comes into contact with the secondary oocyte is the second meiotic division triggered which is also characterised by unequal cytokinesis.

the oocyte. Contrastingly to the situation in yeast, mammalian oogenesis only results in the production of a single germ cell. Oogonia are derived from primordial germ cells (PGCs) (Lawson and Hage, 1994). In mice, at day 10.5, the PGCs migrate towards the genital ridge. Here they proliferate, via mitosis, to produce oogonia. During this time sex determination starts (Bowles and Koopman, 2010). At day E13.5 PGCs undergo a further round of mitosis but here there is incomplete cytokinesis leading to the formation of germ cell nests (Pepling, 2006). From this point the oogonia no longer divide mitotically, instead the germ cells initiate meiosis (and become known as primary oocytes) (Ginsberg et al, 1990).

The oocytes progress through meiosis (as described above in yeast) until they reach diplotene (Figure 1.7). The oocytes then enter an arrest known as the dictyate arrest (Hunt and Hassold, 2008). Meiosis up until dictyate arrest occurs before birth in female mammals (Pepling, 2006). The oocytes remain in the dictyate arrest until ovulation. This means that, in some cases, oocytes are held at this arrest stage for up to 50 years in humans. At ovulation luteinizing hormone (LH) releases an oocyte from the arrest and induces the final stage of oocyte maturation. The ovulated primary oocyte then carries out the first meiotic division. The germinal vesicle (nucleus) breaks down and the chromosomes segregate (metaphase I) to produce two daughter cells, one small daughter cell that contains only a very small amount of cytoplasm (the polar body) and one significantly larger metaphase II cell containing the majority of the cytoplasm (the secondary oocyte) (Petronczki et al, 2003).

Only when the sperm comes into contact with the secondary oocyte is the second meiotic division triggered. Here again there is an unequal cytokinesis. The ovum retains most of the cytoplasm as this contains all the nutrients and substances required for early development. The ova greatly increase in size during oogenesis (approximately 35-120 μm in humans and 20-80 μm in mouse) (Eppig and O'Brien, 1996; Picton et al, 1998). During this growth period the ova synthesise proteins and RNA required for their growth and development into an embryo (Bachvarova, 1985; Moore and Lintern-Moore, 1978). In early development the

synthesis of transcripts is very high. However at the time of oocyte maturation there is silencing of the transcriptional activity and some of the mRNA is degraded (Bachvarova et al, 1985; De la Fuente et al, 2004).

Gametogenisis occurs very differently in males. In males meiosis begins at puberty and after puberty continually takes place throughout their lifetime. Furthermore, contrastingly to what is observed in oogenesis, during spermatogenisis four sperm are produced in each round of meiosis. This means that men can produce millions of sperm throughout their lifetime.

1.14 Chromosome mis-segregation

During meiosis I the homologous chromosomes segregate away from one another to opposite spindle poles and therefore end up in separate daughter cells (Figure 1.8Ai). In order to ensure that the homologous chromosomes rather than the sister chromatids segregate at meiosis I the cells uses several unique chromosome behaviors. These include homologous chromosome pairing, chromosome mono-orientation and regulated removal of sister chromatid cohesin. In a small number of cases however the homologous chromosomes do not segregate properly. This could be due to homologous chromosome non-disjunction. This results in one of the daughter cells containing both of the homologs and the other will contain none (Figure 1.8Aii). Additionally premature sister chromatid separation can occur. This leads to the production of one daughter cell containing one chromatid and another daughter cell containing the other 3 chromatids (Figure 1.8Aiii). In around 50% of cases the chromosome mis-segregation that occurs in meiosis I will be corrected in meiosis II. A large proportion of meiotic errors occur in meiosis I. Errors also occur during meiosis II (Hassold et al, 1996). For example, during meiosis II, both the sister chromatids can be pulled to one pole of the cell meaning that one daughter cells ends up with both the chromatids and the other ends up with none (figure 1.8Bii). Recently a new form of chromosome segregation, reverse segregation, has been identified in humans (Ottolini et al, 2015). In reverse segregation the homologoues equatorially segregate at meiosis I, resulting in two daughter cells each containing two non-sister chromatids

(A)

(i) Accurate MI chromosome segregation

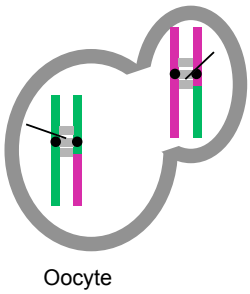

(ii) Homologous chromosome non-disjunction

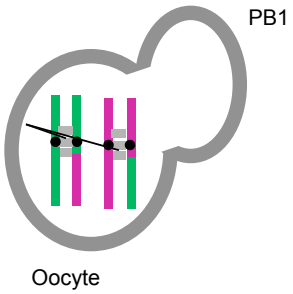

(iii) Precocious sister chromatid separation

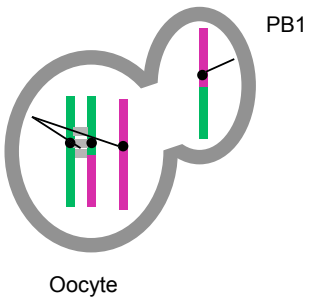

(iv) Reverse segregation

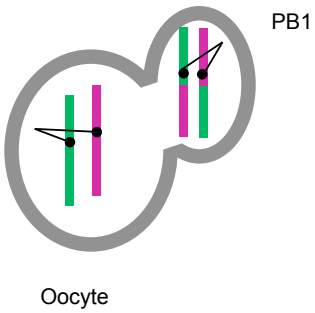

(B)

(i) Accurate MII chromosome segregation

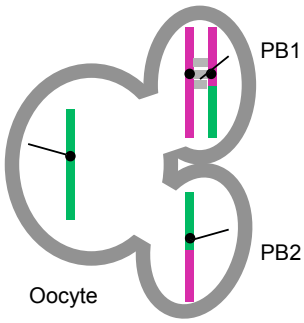

(ii) Meiosis non-disjunction

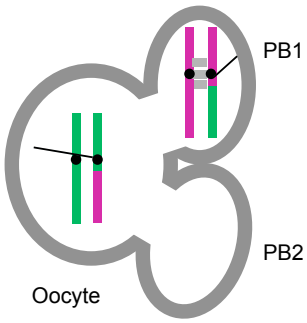

Figure 1.8 – Normal and abnormal chromosome segregation at meiosis I

A. Diagrams demonstrating the different types of chromosome segregation that can take place at anaphase of meiosis I. If the chromosomes segregate accurately then one of the homologous chromosomes will be lost to the polar body and the other will remain in the secondary oocyte (i). Sometimes the homologous chromosomes do not segregate and so both end up in either the polar or the secondary oocyte (ii). This is known as homologous chromosome non- disjunction or meiosis I non-dysjunction. There can also be precocious sister chromatid separation (iii). Here the sister chromatids prematurely separate and so one is lost to the polar body and the other remains in the secondary oocyte. Recently it has been discovered, in humans that the homologoues can segregate equatorially at meiosis I, resulting in two daughter cells each containing two non-sister chromatids (iv). This is known as reverse segregation.

B. Diagrams demonstrating the different types of chromosome segregation that can take place at anaphase of meiosis II. If the chromosomes segregate accurately then one of the sister chromatids will be lost to the second polar body and the other will remain in the secondary oocyte (i). Sometimes the sister chromatids do not segregate and so both end up in either the polar body or the secondary oocyte (ii).

(Figure 1.8Aiv). This is similar to 'inverted meiosis' seen in organisms that have holocentric chromosomes (Heckmann et al, 2014).

Aneuploidy is the main cause of miscarriage, birth defects and mental retardation. The level of aneuploidy in human pregnancies has been found to be extremely high. 10-30% of clinically recognized pregnancies are aneuploid (Hassold and Hunt, 2001). As this value only includes clinically recognized pregnancies and does not include pregnancies that are lost by spontaneous abortion, it is likely to be an underestimate. A large majority of aneuploid embryos are predicted to be lost through spontaneous abortions. 4% however led to stillbirths and 0.3% to live birth (Hassold et al, 1996). Interestingly the levels of aneuploidy in humans have been found to be significantly higher than observed in other organisms such as *Saccharomyces cerevisiae* (<0.0001%) or *Drosophila melanogaster* (0.1%) indicating that humans are particularly susceptible to meiotic errors (Hassold et al, 1995; Kota and Feil, 2010). Despite the prevalence of aneuploidy in humans we know very little about its genetic basis. Only recently is research beginning to give us an insight into the potential causes of aneuploidy in humans (Holubcová et al, 2015; Ottolini et al, 2015).

Monosomies (where the fetus only has a single copy of a chromosome, inherited from either the father or the mother) of most the chromosomes are not tolerated in the fetus. The only known monosomy that is tolerated and that leads to a live birth is monosomy of the X chromosome (Jacobs, 1992). Patients whose cells only contain a single copy of the X chromosome are said to have Turner syndrome and generally display severe developmental disabilities. Some trisomies' are tolerated in the fetus and mean the fetus will survive to term. Patients with trisomies generally display mental retardation and developmental disabilities. These can range in severity depending on the specific chromosome that the patient is aneuploid for. The most common syndromes associated with trisomy of specific chromosomes are Down's syndrome (trisomy of chromosome 21) and syndromes caused by trisomies of the sex chromosomes (Klinefelter syndrome 47 XYY, XXY syndrome 47 XXY and triple X syndrome 47 XXX) (Hassold and Jacobs, 1984). Most of the known cases of trisomy 21 are caused by errors in chromosome

segregation during meiosis known as chromosome nondisjunction (caused by a failure to resolve chiasmata between the homologous chromosomes meaning that both homologues segregate together) (Hassold and Hunt, 2001). Trisomies can also be caused by a failure to establish chiasmata or premature resolution of chiasmata. This results in independent segregation of the homologues at meiosis I (achaismate nondisjunction) or precocious sister chromatid separation (Hassold and Hunt, 2001).

1.15 Sex specific differences

Aneuploidy can result from both paternal and maternal meiotic errors. Early studies demonstrated that the majority of meiotic errors (95%) arise during female meiosis and that aneuploidy increased with increased maternal age (Hassold and Hunt, 2001). Analysis using FISH indicated that ~2% of sperm are aneuploid (Hassold, 1998). Maternally derived aneuploidy was contrastingly found to be as high as 20-25% (Jacobs, 1992; Volarcik et al, 1998). This difference is likely to be due to the protracted dictyate arrest in females. It is known that chromosomes that fail to recombine or have sub-optimally placed crossovers contribute to human aneuploidy (Hassold and Hunt, 2001). Meiotic recombination takes place very early on in the female's life, in the fetal ovary before the dictyate arrest, and therefore must be maintained for the duration of the arrest. Because of this it was questioned if oocytes displayed high levels of chromosomes that had failed to combine. Interestingly the frequency of human oocytes that contain at least one chromosome pair lacking a crossover was found to be over 10% (Cheng et al, 2009; Gruhn et al, 2013). Contrastingly a analysis of chromosome orientation in human spermatocytes, by Lynn *et al* (2002), found that the majority of the homologous chromosomes were joined by one or more crossovers. This indicates that vulnerable chromosome configurations are established during prophase.

In mitotic cells, before the cells can enter anaphase, each of the chromosomes must form a bipolar attachment and align along the spindle equator. In spermatocytes if even one chromosome is misaligned then this means that the

spindle assembly checkpoint will be activated which acts to delay the onset of anaphase (Musacchio and Salmon, 2007). Interestingly the situation is not the same in oocytes. In oocytes it has been found that the presence of one or even several univalents does not led to a cell cycle delay (Kouznetsova et al, 2007). It is predicted that univalents, in oocytes, are able to satisfy the SAC by forming bipolar attachments before the cell reaches anaphase (Kouznetsova et al, 2007).

Two major factors have been identified to affect mis-segregation rates in oocytes. These are meiotic recombination and maternal age. Altered rates of recombination are directly linked with human aneuploidy (Hassold and Hunt, 2001; Ottolini et al, 2015). Analysis of crossover placement along chromosome 21 found that most normally disjoining chromosomes have a meiotic exchange at the centre of chromosome 21 (Lamb et al, 2005). The presence of a crossover near the centromere is linked to an increased likelihood of an MII nondisjunction and the presence of a crossover near the telomere has been linked to an increased risk of an MI mis-segregation (Lamb et al, 1997; Orr-Weaver, 1996). It has been found that the location of the meiotic exchange differs with maternal age. Older women have an enrichment of pericentromeric exchanges (Oliver et al, 2008). It is possible the presence of a pericentromeric exchange leads to a conformation that is more susceptible to the effect of other risk factors associated with increased maternal age. For instance the presence of a pericentromeric exchange may exacerbate the loss of centromeric cohesion with age.

Non-recombinant chromatids have also been to be linked to an increased risk of chromosome mis-segregation. From this is proposed that non-recombinant chromatids may have an increased chance of dissociating from their bivalent during the dictyate arrest (Ottolini et al, 2015). Furthermore it has been identified that non-recombinant chromatids are around twice as likely to end up in polar body two rather than the secondary oocyte. This is known as a chromosomal or meiotic drive (Ottolini et al, 2015).

In 1933 it was first correlated that there was an increased chance of having a child with Downs syndrome with increased maternal age (Penrose, 1933). More

recently Hassold and Chiu (1985) found that the probability of a woman having an aneuploid pregnancy dramatically increased after the age of 35. The probability of a woman under 25 having an aneuploid pregnancy is around 2%. This increases to 35% in women over the age of 40 (Erickson, 1978; Hassold and Chiu, 1985). As this data was only based on clinically recognized pregnancies and it is known that a large amount of chromosomally abnormal embryos are lost early in pregnancy this indicates that these numbers are likely to be an under estimate. This indicates that there is a clear age dependent increase in aneuploidy pregnancies indicating that the oocytes become unstable during the long pachytene arrest.

The main factor identified thought to contribute to the maternal age effect is the loss of cohesin with increased maternal age. Cohesin holds homologous chromosomes together along their entire length and is important for accurate chromosome segregation (Section 1.10). When cohesin is lost or mutated the inter-kinetochore distances increase and in some cases the bivalents will break down (Hodges et al, 2005; Lister et al, 2010). Research in mice has shown that there is no turnover of cohesin proteins during meiosis (Renenkova et al, 2010; Tachiban-Konwalski et al, 2010). If the situation is the same in humans then this means that cohesin must be maintained along the chromosome arms during the dictyate arrest (up to 50 years in some cases). Work using *drosophilla* provided the first evidence that cohesion weakened with age and that this led to meiotic nondisjunction (Jeffreys et al, 2003). Subsequently several mouse models have found that this is a loss of cohesin with increased maternal age (Chiang et al, 2010; Lister et al, 2010; Liu and Keefe, 2008). (These results however should be treated with caution as they were obtained from mice that were reproductively senescent.) It has been proposed that the situation is the same in humans (Tsutsumi et al, 2014; Zielinska et al, 2015).

Interestingly it has been found that different chromosomes have different probabilities of becoming aneuploid. Large (chromosomes 2 and 4) and medium (chromosomes 8, 9 and 10) sized chromosomes generally display lower levels of mis-segregation after the age of 30 compared to the smaller chromosomes (Risch

et al, 1986; Hassold et al, 1996). This however has not found to be true for all chromosomes. Chromosome 16 shows a linear increase in aneuploidy rate from puberty, which is quite different to other chromosomes of the similar size (Hassold et al, 1996). This indicates that there may be other factors that contribute to the maternal age effect, as it does not appear that a single non-disjunction mechanism applies to all chromosomes. The chromosome specific differences are likely to be due to differences in recombination placement and recombination levels, as well as cohesin. Furthermore it has also been identified that there are several environmental factors that may contribute towards aneuploidy. These include alcohol, smoking, endocrine disrupting hormones (BPA) and radiation exposure (Hassold and Jacobs, 1984; Pacchierotti et al, 2007).

1.16 Aims and objectives

The main aim of this thesis was to determine the role of the Smc5/6 complex in meiosis. Initially I aimed to investigate the role of the Smc5/6 complex, specifically in chromosome segregation and cohesin regulation, using yeast as a model system. In order to do this a mixture of live cell imaging and chromosome spreads were used. I then aimed to investigate the role of the Smc5/6 complex in mammalian meiosis using a mouse strain with reduced levels of SMC6 ($Smc6^{+/GT}$). Here I initially aimed to examine chromosome segregation and chromosome structure in the oocytes from the $Smc6^{+/GT}$ mouse. I then aimed to examine if SMC protein levels varied in oocytes from the $Smc6^{+/GT}$ mouse.

2 Materials and methods

2.1 Materials

2.1.1 Yeast media

All yeast cells were grown in YPD (Yeast extract, peptone, dextrose medium, Table 2.1). To make solid media for use in plates 2% w/v agar was added before the media was autoclaved. Yeast were grown on YEPEG (Yeast extract, peptone, ethanol, glycerol medium) so cells with functional mitochondria could be selected for. In order to determine the mating type of the haploids dissected from yeast crosses, cells were grown on minimal media and then replica plated onto complete media. To assess whether colonies from the crosses contained the correct markers the dissected cells were replica plated onto drop out plates. These are the same as the complete media plates but have specific amino acids omitted from the added nutrient mix.

Table 2.1 Yeast and *E. coli* media

Solution	Concentration in media
YPD	1% w/v Yeast extract 2% w/v Bacto Peptone 2% w/v Dextrose 3% w/v Powdered adenine pH 6-6.5 using HCL
YEPEG	1% w/v Succinic acid 1% w/v Yeast extract 2% w/v Bacto Peptone 2% w/v Glycerol 0.073g Adenine 2% v/v Ethanol

	pH 5.5 using 10M NaOH
SPS	0.625% w/v Yeast extract 1.25% w/v Peptone 0.2125% w/v Yeast and nitrogen base (without amino acids and ammonium sulphate) 1.25% w/v Potassium acetate 0.625% w/v Ammonium sulphate 1.275% Potassium hydrogen phthalate
Complete media	0.17% w/v Yeast nitrogen base 2% w/v D-glucose 0.087% w/v nutrient mix 0.05% ammonium sulphate pH 7.25 using HCL
Minimal media	0.17% w/v Yeast nitrogen base 2% w/v D-glucose 0.05% ammonium sulphate pH 7.25 using HCL
KAc- with added amino acids	1% w/v Potassium acetate 0.02% w/v Raffinose 0.02% v/v Histidine 0.04% v/v Lysine 0.02% v/v Arginine 0.12% v/v leucine 0.1% v/v Uracil
KAc-COM	2% w/v Pottasium acetate 0.05% w/v Dextrose 0.0875% w/v COM drop out powder pH 7 using 1M HCL

Luria Broth (LB)	1% w/v bactotryptone 0.5% w/v yeast extract 0.5% NaCl pH 7 using 1M HCL

Table 2.2 Amino acids included in the nutrient mix

Amino acid	Concentration in media (% w/v)
Adenine	0.003
L-arginine	0.003
L-aspartic acid	0.016
L-histidine	0.003
L-leucine	0.003
L-lysine	0.005
L-methionine	0.003
L-phenylalanine	0.007
L-threonine	0.0032
L-tryptophan	0.003
L-tyrosine	0.005
Uracil	0.003

2.1.2 Buffers

Table 2.3 List of all the solutions used in this work

Solution	Composition
PBS	137 mM NaCl 4.3 mM Na2PO4·7H2O 2.7 mM KCl 1.4 mM KH_2PO_4
Dissecting buffer	10 mM EDTA 1 M Sorbital 10 mM NaH_2PO_4

SSC	3 M NaCl 300 mM $Na_3C_3H_5O_7$
TE	10 mM Tris-Cl 1 mM EDTA pH 8.0

2.1.3 Drugs and antibiotics

Table 2.4 List of all the drugs and anti-biotics used in this work		
Drug	Supplier	Stock concentration
G418	Invitrogen	400 μg/ml
Ampicillin	Sigma	100 μg/ml
Hygromycin B	Invitrogen	300 μg/ml

2.1.4 Enzymes

Table 2.5 List of all the enzymes used in this work	
Enzyme	Supplier
RNAse	Sigma
Taq DNA polymeraise	Thermo scientific
Primestar DNA polymeraise	Clontech
DNArelease	ThermoFisher
Zymolyase (100T)	Seikagaku Corporations
Zymolyase (20T)	Seikagaku Corporations

2.1.5 Oligos

Table 2.5 List of all the Oligos used in this work			
Oligo	Name	Sequence (5'-3')	Application
01483	SGO1_F2	GGTAAGGCAGTGA AACATCAACCAAA AACATATCGCACC AAAAAATACGCTG	Forward primer for C-terminal tagging of Sgo1

		CAGGTCGACGG	
01484	SGO1_R1	AAATATAGAAATTATTAAGGAACACCAGGGCAAAAAGACTATATAGAATTCGAGCTCGTTTAAAC	Reverse primer for C-terminal tagging of Sgo1
01521	SGO1_C	AAATTCTACTTACGCGACCC	Forward primer 500bp from the end of *SGO1* ORF
01552	SGO1_D	CCAGAAATCCAAGACCATTCCCG	Reverse primer 500bp from the end of *SGO1* ORF
02038	MAM1_MXF	TAGCAAAAGCATTTTCAGAGAATTTTTTTGTTTCCTGAAAAAAAACGTACGCTGCAGGTC	Forward primer to replace the *MAM1* ORF
02039	MAM1_MXR	TGAGTCGCCGTTTTAACCGGTGGTAATGTGCAGACAATACTTTCAATCGATGAATTCGAG	Reverse primer to replace the MAM1 ORF
02085	MAM1_Z	CTCCAGACGTTCATGGAAAG	Forward primer 500bp from the end of the MAM1 ORF
02086	MAM1_E	GTTCTTTTGGAGAGAATAGG	Reverse primer 500bp from the end of the MAM1 ORF
01885	MAM1_F2	ATCATAGGTGCTTTGGAAAGAAAGCTACATATAGATGAAAATCAACGGATCCCCGGGTTAATTAA	Forward primer for C-terminal tagging of MAM1

01886	MAM1_R2	TGAGTCGCCGTTT TAACCGGTGGTAA TGTGCAGACAATA CTTTCAGAATTCG AGCTCGTTTAAAC	Reverse primer for C-terminal tagging of Mam1
01275	MAM1_C	CCTTGGAAGTGGT TCCCAA	Forward primer 500bp from the end of the Sgo1 ORF
01276	MAM1_D	GTCGCCGTTTTAA CCGGTGG	Reverse primer 500bp from the end of the SGO1 ORF
02150	Smc6 Exon6 Fwd	CCGTGGTTTCTAC TAGGAAAAGA	Forward primer for *SMC6* mouse genotyping
02151	Beta-geo rev2	GGATAGGTTACGT TGGTGTAGATG	Reverse primer used to detect the presence of the β-geo insertion in *SMC6* exon 5
02152	Smc6 intron 6 rev	CCACAGTTTGTCTC TTGAGTAGTC	Reverse primer used to check PCR is working during mouse experiments

2.1.6 Plasmids

Table 2.6 List of all the plasmids used in this work

pEH plasmid No.	Alternative names	Description	Plasmid source
pEH 90	pRED460	For amplification of the HYG cassette	Yeast 15: 1541-1553
pEH95	pRED518	For amplification of GFP for C-terminal tagging	Yeast 14. 953-961 Longtine et al., 1998

2.1.7 Yeast strains

Table 2.7 List of all the strains used in this work			
EH strain No.	Strain background	Ploidy	Genotype
3606	SK1	2N	*HTB1*-mCherry-*NATMX4*, *PDS1-tdTomato-KITRP1*, *his3::HIS3p-GFP-TUB1-HIS3*
3627	SK1	2N	*KANMX6-pCLB2-3HA-SMC5, HTB1*-mCherry-*NATMX4*, *PDS1-tdTomato-KITRP1*, *his3::HIS3p-GFP-TUB1-HIS3*
3630	SK1	2N	*HYG-pCLB2-3HA-NSE4, HTB1*-mCherry-*NATMX4*, *PDS1-tdTomato-KITRP1*, *his3::HIS3p-GFP-TUB1-HIS3*
3887	SK1	2N	*HTB1*-mCherry-*NATMX4, his3::HIS3p-GFP-TUB1-HIS3, CDC14-GFP-LEU2*
3890	SK1	2N	*KANMX6-pCLB2-3HA-SMC5, Htb1*-mCherry-*NATMX4, his3::HIS3p-GFP-TUB1-HIS3, CDC14-GFP-LEU2*
3893	SK1	2N	*HYG-PCLB2-3HA-NSE4, Htb1*-mCherry-*NATMX4, his3::HIS3p-GFP-TUB1-HIS3, CDC14-GFP-LEU2*
2333	SK1	1N	*spo11-Y135F-HA-URA3*
5614	SK1	2N	*Htb1*-mCherry-*NATMX4, PDS1-tdTomato-KITRP1, his3::HIS3p-GFP-TUB1-HIS3, spo11-Y135F-HA-URA3*
5617	SK1	2N	*KANMX6-pCLB2-3HA-SMC5, Htb1*-mCherry-*NATMX4, PDS1-tdTomato_KITRP1, his3::HIS3p-GFP-TUB1-HIS3, spo11-Y135F-HA-URA3*
5620	SK1	2N	*HYG-pCLB2-3HA-NSE4, Htb1*-mCherry-*NATMX4, PDS1-tdTomato_KITRP1, his3::HIS3p-GFP-TUB1-HIS3, spo11-Y135F-*

			HA-URA3
2572	SK1	2N	*REC8-GFP-URA3, PDS1-tdTomato-KITRP1(HOMO), CNM67-3mCherry-NATMX(HOMO)*
2673	SK1	2N	*KANMX6-pCLB2-3HA-SMC5, REC8-GFP-URA3, PDS1-tdTomato-KITRP1, CNM67-*3mCherry-*NATMX*
3047	SK1	2N	*KANMX6-pCLB2-3HA-NSE4, REC8-GFP-URA3, PDS1-tdTomato-KITRP1, CNM67-*3mCherry-*NATMX*
4441	SK1	2N	*MTW1*-mCherry*::HPHMX4, pCLB2-3HA-NSE4::KANMX6*
4458	SK1	1N	*PDS1-tdTomato-KITRP1, SGO1-GFP-HIS3*
4480	SK1	1N	*PDS1-tdTomato-KITRP1, SGO1-GFP-HIS3, MTW1*-mCherry*::HPHMX4, pCLB2-3HA-NSE4(KANMX6)*
1586	SK1	1N	*EstrogenReceptor-GAL4TF(URA3), proGAL1-NDT80(TRP1)*
4836	SK1	2N	*PDS1-tdTomato-KITRP1, SGO1-GFP-HIS3, MTW1*-mCherry*::HPHMX4, EstrogenReceptor-GAL4TF(URA3), proGAL-NDT80(TRP1)*
4837	SK1	2N	*KANMX6-pCLB2-3HA-NSE4, PDS1-tdTomato-KITRP1, SGO1-GFP-HIS3, MTW1*-mCherry*::HPHMX4, EstrogenReceptor-GAL4TF(URA3), proGAL-NDT80(TRP1)*
5378	SK1	1N	*PDS1-tdTomato_KTRP1, CNM67-*3mCherry-*NATMX4*
3412	SK1	1N	*CNM67*-3mCherry-*NATMX4, leu2::promURA3::TetR::GFP::LEU2, tetOx224-HIS3*

5379	SK1	1N	*PDS1-tdTomato-KTRP1, CNM67-*3mCherry-*NATMX4, leu2::promURA3::TetR::GFP::LEU2, tetOx224-HIS3*
5398	SK1	2N	*PDS1-tdTomato-KTRP1, CNM67-*3mCherry-*NATMX4, leu2::promURA3::TetR::GFP::LEU2, tetOx224-HIS3(hetero)*
5419	SK1	2N	*KANMX6-pCLB2-3HA-SMC5, PDS1-tdTomato-KTRP1, CNM67-*3mCherry-*NATMX4, leu2::promURA3::TetR::GFP::LEU2, tetOx224-HIS3(hetero)*
5399	SK1	2N	*KANMX6-pCLB2-3HA-NSE4, PDS1-tdTomato-KTRP1, CNM67-*3mCherry-*NATMX4, leu2::promURA3::TetR::GFP::LEU2, tetOx224-HIS3(hetero)*
5671	SK1	2N	*mam1::TRYP1, PDS1-tdTomato-KTRP1, CNM67-*3mCherry-*NATMX4, leu2::promURA3::TetR::GFP::LEU2, tetOx224-HIS3(hetero)*
5665	SK1	2N	*KANMX6-pCLB2-3HA-NSE4, mam1::TRYP1, PDS1-tdTomato-KTRP1, CNM67-*3mCherry-*NATMX4, leu2::promURA3::TetR::GFP::LEU2*, tetOx224-HIS3(hetero)
5306	SK1	2N	*CNM67-*3mCherry-*NATMX4, MAM1-yeGFP*
5451	SK1	2N	*pCLB2-3HA-SMC5(KANMX6), CNM67-*3mCherry-*NATMX4, MAM1-yeGFP*
5607	SK1	2N	pCLB2-3HA-NSE4(HYG/HPHMX), CNM67-*3mCherry-NATMX4, MAM1-yeGFP*

2.1.8. Antibodies

Table 2.8 List of all the antibodies used in this work			
Antibody name	Dilution	Supplier	Catalog number
Donkey anti rabbit FITC	1:200	Jackson Immunofluorescence	711-095-152
Donkey anti-rabbit TR	1:200	Jackson Immunofluorescence	711-165-152
Donkey anti-rabbit CY5	1:200	Jackson Immunofluorescence	711-175-152
Donkey anti-mouse FITC	1:200	Jackson Immunofluorescence	715-545-151
Donkey anti-mouse TR	1:200	Jackson Immunofluorescence	715-585-150
Donkey anti-mouse CY5	1:200	Jackson Immunofluorescence	715-175-151
Goat anti-GFP	1:200	Abcam	ab6673
Rabbit anti-Zip1	1:200	Hoffmann lab	Jordan et al, 2009
Donkey anti-goat FITC	1:200	Jackson Immunofluorescence	705-546-147
Human anti-centromere	1:200	Antibodies Incorporated	15-234-0001
Donkey anti-human FITC	1:200	Jackson Immunofluorescence	709-546-098
Donkey anti-human TR	1:200	Jackson Immunofluorescence	709-166-098
Donkey anti-human CY5	1:200	Jackson Immunofluorescence	709-606-098

Rabbit anti-Rec8	1:200	Garcia-Cruz lab	Garcia-Cruz et al, 2010
Mouse anti-Smc3-acetyl	1:200	Shiranhige lab	Beckouet et al, 2010
Mouse anti-SCP3	1:300	Santa Cruz	sc-74569
Rabbit anti-SMC4	1:200	Novus biologicals	NB100-374
Rabbit anti-SMC6L	1:200	Lehmann Lab	Gomez et al, 2013
Mouse anti-MLH1	1:200	BD Pharmingen	G168-728

2.2. Methods

2.2.1 Bacterial methods

2.2.1.1 Bacterial Growth

Bacterial cells were grown in LB at 37 °C overnight (Table 2.1). Plasmid selection was carried out using antibiotics specific to the plasmid (Table 2.4).

2.2.1.2 Plasmid extraction

Plasmid extraction was carried out using a QIAprep spin miniprep kit according to the manufacturers instructions.

2.2.2 SK1 Growth conditions

2.2.2.1 Vegetative growth conditions

Cells were taken up from the -80 °C freezer, streaked onto a YEPEG plate (see Table 2.1) and incubated at 30 °C for two days to in order to obtain single colonies. Three single colonies were added to a green topped tube containing 5 mls of YPD and the tube was placed into a 30 °C shaking incubator until the cells had reached an OD_{600} of 1.2-1.4 (~16 hours). For growth on solid media, cells are patched onto YPD plates and incubated at 30 °C overnight.

2.2.2.2 Sporulation conditions

A solution containing 50 mls of YPD and 50 µl of ampicillin was prepared in a Falcon tube. 1ml of this solution was transferred to an Eppendorf tube. Three single smooth colonies from the YEPEG plate were selected and added to the Eppendorf tube. This alongside the remaining solution from the Falcon tube was added to a 50 ml flask and placed in a shaker set at 30 °C and 200 rpm overnight.

24 hours after inoculation the OD_{600} of the cells was analysed. In the microbial hood four solutions containing 50 mls of SPS and 25 µl of Ampicillin were made up. The cells were inoculated in the SPS solution at an OD_{600} of around 0.15, 0.2, 0.25 and 0.3. The flasks were then placed in the shaker overnight at 30°C and 200rpm.

Once the cells had reached an OD_{600} of 1.2-1.4 (around 16 hours after the cells had been added to SPS) a 5 µl sample was taken for analysis under the light microscope to check if the cells were healthy and to check the percentage of cells that were budding. Healthy samples with the lowest percentage of budding cells were selected. The cells of the chosen samples were centrifuged in a benchtop centrifuge (Eppendorf 5810R) at 3000 rpm for 5 minutes. They were then washed in pre-warmed (30 °C) KAc. 50 mls of warm 30 °C KAc were then added to the final pellet and this solution was transferred to a 500 ml flask. This was placed in the shaking incubator at 30 °C and 200 rpm.

For strains, which contained *NDT80* placed under the *GAL1* promoter (which acted to arrest the cells at pachytene), 1 μM β-estradiol was added to the spourilation media at 6 hours to induce the cells to resume meiosis. Samples for live cell imaging were taken 30 minutes after the addition of β-estradiol.

2.2.3 Yeast strain generation

2.2.3.1 Genetic crosses

Genetic crosses were made by mixing two haploid strains on a YPD plate using a wooden dowel. The plate was then placed in a 30 °C incubator for 5 hours so that the cells could mate. The YPD plate was then replica plated onto a KAc-COM plate and placed in a 30 °C incubator for three days (Table 2.1). After three days the sporulation of the cells was checked under a light microscope. If the cells has successfully mated a small amount of the cells were taken from the plate using a wooden dowel and placed in an Eppendorf tube containing 100 μl of dissecting buffer (Table 2.3) and 5 μl of zymolyase (20T, 10 mg/ml). The cells were incubated for 30 minutes at 37 °C and then 400 μl of dissecting buffer. Digestion of the cells was analysed using a light microscope in order to check that the cells were adequately digested.

A strip was cut along the centre of a YPD plate and a wooden dowel used to add some of the digested cells to the strip. A Nikon Eclipse 50i microscope was then used to carry out the tetrad dissection. The plates containing the dissected cells were placed in the 30 °C incubator for 2-3 days. Once the haploids had grown up the YPD plates were replica plated onto plates containing media with the appropriate selection markers.

2.2.3.2 Diploid generation

In order to make diploids two haploids were mated on an YPD plate for 4-24 hours. Some of the cells were then selected using a wooden dowel and streaked across a fresh YPD plate in order to obtain single yeast colonies. After 2-3 days

several single smooth colonies (diploid) were selected and re-patched onto a new YPD plate for screening. This plate was then placed in the 30 °C incubator to grow over night.

2.2.3.3 Yeast transformation

Transformation was carried out using the lithium acetate protocol (Gietz et al, 1995). The cells for transformation were grown up overnight in 5 mls of YPD. The following morning the cells were diluted 1 in 25 in fresh YPD. Cells were grown in fresh YPD for three hours and then harvested via centrifugation for three minutes at 2000 rpm. The pellet of cells obtained were then washed in 5 mls of 100 mM LiAc twice and the final pellet was resuspended in 1 ml of LiAc and transferred to a 1.5 ml Eppendorf tube. Cells were again centrifuged in a bench-top centrifuge (Eppendorf 5415D) for 30 seconds at 13,00 rpm. The obtained pellet was resuspended in 250 μl of LiAc and 50 ml was aliquotted into two new 1.5 ml eppendorf tubes (one for transformation and one for the control – the number of tubes was increased depending on the number of transformations carried out). Each of the tubes were centrifuged in a bench top centrifuge for 30 seconds at 13,000 rpm. The supernatant was removed and 240 μl of 50% PEG-3500, 36 μl of 1M LiAc, 50 μl of salmon sperm DNA (boiled) and 2 μl of DNA (or 2 μl of water to the control) were added to the pellet (in the listed order). The mixture was thoroughly mixed using a sterile wooden toothpick and placed at 30 °C for 30 minutes. The tubes were then transferred to a 42 °C water bath for 20 minutes. 1 ml of sterile water was then added to the tube and the cells were centrifuged gently in a bench centrifuge at 4000 rpm. If the cells were to be selected by drug resistance, the pellet was resuspended in YPD and placed in the shaking incubator at 30 °C for 3 hours. The cells were then gently centrifuged in a bench top centrifuge (Eppendorf 5415D) at 4000 rpm and resuspended in 500 μl of distilled water. 250 μl of the solution was then added to plates that contained the drug selection required. The plates were then placed in the 30 °C incubator for 3 days for the transformants to grow up. When selecting for prototrophy cells were instead spun down in a bench top centrifuge (Eppendorf 5415D) for 30

seconds at 4000 rpm and then resuspended in 500 µl of distilled water. 250 µl was then added to the appropriate drop-out plates. The plates were then incubated for 3 days at 30 °C. Transformants were then checked by PCR.

2.2.3.4 Gene deletion via PCR

Gene deletion cassettes were made via the Longtine method (Longtine et al., 1998). Primers were designed so that they had ~45 bp homology to both the site of integration and the cassette to be integrated (*HYGMX4* was used in this work.) The amplified PCR fragment was then added to the chosen base strain via transformation. Integration at the correct location was assessed by PCR using primers upstream and downstream to the site of integration and within the gene deletion cassette.

2.2.3.5 C-terminal tagging via PCR

Primers were designed so that they had ~45 bp homology to both the site of integration and the cassette to be integrated (Longtine et al, 1998). Here primers were designed so that the cassette would be integrated just upstream of the stop codon of the gene being tagged. The amplified PCR fragment was then added to the chosen base strain via transformation. Here correct integration was checked by using primers upstream of the integration site and within the added cassette.

2.2.3.6 -80 °C storage of yeast strains

The strain to be frozen was patched onto a YPD plate using a wooden dowel and placed in a 30 °C incubator overnight to grow up. The cells were then removed from the plate and placed in a 1.5 ml tube containing 30% glycerol. The tubes were frozen at -80 °C.

2.2.3.7. Oocyte collection

Mice 4 weeks of age were given a peritoneal injection of 5-10 IU pregnant mares serum gonadatrophin (Sigma G4527). The ovaries were then transferred to pre-warmed (37°C) pH buffered media, containing serum albumin (G-MOPS 10130; Vitro life) for dissection. The oocyte-cumulus complexes were released from the ovarian follicles using a 0.5 mm × 16 mm needle. The cumulus cells were then removed from the oocytes using a glass pipette linked to a mouth aspirator. The GV oocytes were then added to one of several drops of mouse collection media (made up of 1 part fetal bovine serum (25 μg/ml) and 9 parts Waymouth media pre-equilibrated to 5% CO_2 and 37°C) overlaid with mineral oil. In order to wash the oocytes, they were moved to a fresh drop of mouse collection media. The oocytes were then cultured for four hours in order for them to reach metaphase I or 16 hours in order for them to reach metaphase II.

2.2.4 Cytological methods

2.2.4.1 Sporulation analysis

In order to assess sporulation 5-10 μl of cells at the 24-hour time point were added to a glass microscope slide and covered with a small 22x22 mm cover slip. Cells were then analysed using a light microscope. ~100 cells were scored as being tetrads, dyads or singles.

2.2.4.2 Immunofluorescence of fixed yeast cells

At the time point of interest 8mls of sample were collected from the 2% KAc culture and added to a 15 ml falcon tube. 4% formaldehyde was added and the cells were left at room temperature for 1 hour. After an hour 2 mls of SKP (1.2 M sorbital, 50 mM KPO_4, pH 7) was added to the cells and the solution mixed. Cells were then centrifuged for 3 minutes at 3500 rpm. This was repeated two more times. After the final centrifugation the pellet was resuspended in 100 μl of SKP and the solution transferred to a 1.5 ml Eppendorf tube. 10 μl of Zymolyase (10 mg/ml – 100T) and 2 μl of 1 M DTT were added to the Eppendorf tube and the tubes were incubated at 37°C for 30 minutes. The cells were then checked to

ensure that the spheroblasting was sufficient by adding 5 μl of cellular suspension and 5 μl of water to a microscope slide (covered with a 22x22 mm coverslip) and analyzing it under a light microscope. If some of the cells appeared to have burst and many appeared to have swelled up then it was judged that the spheroblasting was sufficient. 100 μl of PBS was then added to the cells and the cells were gently centrifuged in a bench top centrifuge at 4000 rpm for 1 minute. The obtained pellets were then resuspended in 1ml of a stock solution containing of 67 μl of PBS and 0.1% NP40 and were left for 30 minutes at room temperature. 33 μl of fetal bovine serum containing the chosen antibodies (2.1.8) were added to the cellular suspension and then the cells were incubated overnight at 4 °C.

The next day the cells were washed three times with PBS. After the final wash the cells were resuspended in 100 μl of a solution containing 4% BSA in PBS and the chosen secondary antibodies (Section 2.1.8). The cells were incubated at room temperature (in the dark) for 2-3 hours. The cells were then washed three times in PBS. After the final wash the pellet was resuspended in 50 μl of Vectasheild™ and 20 μl added to a Superfrost™ microscope slide. A 22x50 cover slip was placed on the slide and the slide sealed using clear nail varnish.

2.2.4.3 Yeast chromosome spreads

1.5 ml of cells were taken from the KAc culture at the chosen time point and the cells collected in a 2 ml round bottomed Eppendorf in a tabletop centrifuge (Eppendorf 5415D) at 13000 rpm for a minute. The pellet was then resuspended in 0.5 mls of KAc-SORB (2% KAc, 1M Sorbital, pH 7) and supplemented with 5 μl of 1M DTT and 10 μl of zymolyase (100T 10 mg/ml). The solution was mixed and placed in a rollerdrum at 30 °C for 10-20 minutes. Over this time the level of spheroblasting was monitored by adding a small amount of the cells to water and examining the level of burst cells under a light microscope. During assessment of the spheroblasting level the samples were kept on ice.

Once the spheroblasting was complete 2 mls of cold MES-Sorbital (0.1M MES, 1 mM EDTA, 0.5mM $MgCl_2$, 1M sorbitol) was added to the cells. Then the cells were gently spun in a tabletop centrifuge (Eppendorf 5415D) at 4000 rpm for 1.5 minutes. The liquid was then gently decanted from the Eppendorf. Then the Eppendorf was tipped on its side and 50 µl of MES-EDTA_$MgCl_2$ (0.1M MES, 1mM EDTA, 0.5mM $MgCl_2$, pH 6.4) was added. This was then tapped down onto the cells and allowed to mix for 10 seconds. Then 50 µl of 3% formaldehyde and 50 µl of lipsol were added to the cellular suspension. 50 µl of the cellular suspension was then added to a Superfrost™ microscope slide. The mixture was then spread across the slide using a pipette tip and then the slide was left to dry. Once dry the slides were washed with 0.4% Photoflo (KODAK) and allowed to dry once more.

50 µl of a solution of 1 part FBS and two parts PBS-4% BSA supplemented with the chosen primary antibodies was then added to the slides (Section 2.1.8). The slides were placed in a humid chamber and incubated at 4 °C overnight. The next mornings the slides were washed in PBS for 5 minutes. (This was carried out by placing the slides in a coplin jar.) This was repeated three times. 50 µl of a solution of PBS-4% BSA supplemented with the chosen secondary antibodies was then added to each of the slides. The slides were then covered with a coverslip, placed in a humid chamber and incubated at room temperature in the dark for 2-3 hours. The coverslips were gently removed and the slides were washed in PBS for 5 minutes. Again this was repeated three times. The slides were then stained with Vectasheild™, covered with a 22 x 50 mm^2 coverslip and then sealed using clear nail varnish.

2.2.4.4. Live-cell imaging sample preparation

20 µl of cells to be imaged were added to a Y04D CellASIC plate (CellASIC ONIX microfluidic perfusion system) and imaged inside an environmental chamber set at 30 °C. CellAsics microfluidics were chosen as they can be set to add fresh media to the cells over time and they allow a large amount of cells to be imaged at any one time (when compared to trials with the Labtech alternative). This was desirable, as a large number of cells need to be imaged from each strain for

statistical analysis. A flow rate of 8 psi was used to load the cells and a steady-state flow rate of 2 psi was used to supplement the cells with 2% KAc for the duration of the imaging. In order to visualise single cells from prophase to anaphase II imaging was carried out for 2-3 hours (to take into account that the mutants take longer to progress through the cell cycle and that the cells are not completely synchronous).

2.2.4.5 Mouse chromosome spreads

Oocytes were collected from the female mice by Dr. L Newnham. Oocytes were the spread using a variation of the protocol in Hodges and Hunt (2002). Using a micropipette the MI or MII oocytes were transferred into a 50 μl drop of Tyrode's solution (Sigma) on the lid of a culture dish in order to remove the zona pellucida. The eggs were the watched under a stereomicroscope until it appeared that the zona had loosened. Once the zona has loosened the oocytes were moved to a drop containing 0.9% sodium citrate solution. The oocytes were left in the 0.9% sodium citrate solution for 1 minute in order for them to swell. A slide was taken out of the coplin jar containing 1% PFA (1% paraformaldehyde, Triton X-100, DTT) and the majority of the formaldehyde tapped off onto a paper towel. The oocytes were then transferred onto the slide into a pre marked circle in the centre of the slide and the slide placed in a humid chamber. The slides were left in a humid chamber for 2 hours to gradually dry. After this the slides were placed in a coplin jar containing Photoflo™ for 2 minutes and then left to dry.

Slides were blocked in ADB solution (3% w/v BSA, 10% v/v donkey serum, 1.1% v/v triton (X-100) and 85.9% PBS) for 30 minutes to reduce non-specific binding. 50μl of ADB solution supplemented with the chosen primary antibodies (Section 2.1.8) were then added to the slides. The slides were covered with 50 x 22 coverslips and placed back in the humid chamber. The slides were then incubated overnight at 4 °C. The next day the slides were washed in PBS for five minutes. This was repeated three times. Then 50 μl of ADB supplemented with the chosen secondary antibodies was then added to the slides. The slides were covered with 22 x 50 mm^2 coverslips, placed back in the humid chamber and incubated at

room temperature for 2-3 hours. The slides were again washed in PBS for five minutes three times. A drop of VECTASHEILD antifade mounting media was then added to the slides, they were covered with a 22 x 50 coverslip and sealed with nail polish.

2.2.4.6 Pachytene oocyte spreads

Pachytene spreads from fetal oocytes were prepared by Dr J Gruhn. Before staining the slides were blocked in 1 × ADB (detailed in 2.2.4.5). 60 μl of ADB solution supplemented with the chosen primary antibodies (Section 2.1.8) was then added to the tip of the slides and gently spread over the slides using a rocking motion. The slides were the covered with parafilm and placed in a humid chamber at 37 °C for 2 hours. The parafilm was removed and the slides were washed in 1 × ADB for 30 minutes and then again for 1 hour in order to remove any unbound antibody. 60 μl of ADB solution supplemented with the chosen secondary antibodies (Section 2.1.8) was then added to the tip of the slides and gently spread over the slides using a rocking motion. The slides were covered with parafilm and placed in a humid chamber at 37 °C overnight. The parafilm was removed and the slides were washed in 1 × ADB for 30 minutes and then again for 1 hour. Any excess ADB was drained off onto a paper towel and a drop of VECTASHEILD antifade mounting media was added to the slides. Slides were covered with a 24 × 50 coverslip and the edges were sealed with clear nail varnish.

2.2.4.7 mFISH probe staining

The slides to be probed were immersed in 2 × SCC (Saline-Sodium Citrate buffer – Table 2.3) for two minutes at room temperature. The slides were then dehydrated through an ethanol series (70%, 85% and 100% ethanol – two minutes in each) and left to dry. 10 μl of probe (21X mouse mFISH probe – Metasystems) was then added to each of the slides and the probed area covered with a 22 × 22 mm^2 coverslip and sealed using nail varnish. The samples and

probe were then placed on a 75 °C heat block to denature and then placed in a humid chamber for 2 days at 37 °C. After two days the coverslips were carefully removed and the slides placed in 72 °C SCC for two minutes. The slides were then added to 2 x SSCT (Saline-Sodium Citrate buffer + Tween 20) for two minutes and then washed in distilled water. The slides were left to dry, DAPI added to the slide and then the slides were sealed using clear nail varnish. The slides were then visualised using the Leica SP8.

2.2.5 Image acquisition and processing

2.2.5.1 Fixed cell image acquisition

Imaging was carried out on the DeltaVision IX70 (Applied Precision) using the associated proprietary software (SoftWoRx software; version 4.0.0, Applied Precision). Images were captured using an Olympus Plan Apo 100× lens with a numerical aperture of 1.4. The excitation ranges for each of the filters were DAPI (ex 350 nm, em 460 nm), FITC (ex 490 nm – em 525 nm), Texas red (ex 572 nm, em 630 nm) and Cy5 (ex 655 nm, em 710 nm). The camera used for the image aqusition was a 12-bit CoolSnap CCD camera.

2.2.5.2 Live-cell image acquisition

Time-lapse microscopy was carried out on a Personal DeltaVision (Applied Precision) with xenon or solid-state illumination, using associated proprietary software (SoftWoRx software; version 4.0.0, Applied Precision). Images were captured using an UPLS Apochromat 1.4 numerical aperture, x100 magnification oil immersion objective (Olympus), standard DeltaVision filter sets FITC (ex 490 nm, em 525 nm) and TRIC (ex 555, nm em 605 nm), yielding approximate resolutions (Rayleigh's d) of ~229 nm and 264 nm in the xy, respectively, whereas axial resolutions were approximately 811 nm and 935 nm. Photon detection was carried out using a Cascade2 1K EMCCD camera (Photometrics) using a gain of 4.00 and no binning. Effective pixel size was ~0.0645 μm in the xy. Reference images and final images of sporulation were carried out with DIC, 32%

transmission and 0.08 sec. exposure. When Nyquist sampling was required (e.g. for accurate spindle measurements), 25-30 z-stacks of 0.3 μm thickness were taken of each cell. When Nyquist sampling was not required 7-8 z-stacks of 1 μm thickness were taken of each cell. Around 12 hours after imaging the sporulation of the cells at each point of imaging was assessed and compared to the sporulation found of the corresponding cells from a shaking incubator.

2.2.5.3 Live-cell imaging optimisation

To understand the defect in chromosome resolution caused by the induction of meiotic DSBs, strains containing GFP -tagged Tub1 and mCherry-labeled H2B were imaged via live cell imaging. This system allows the DNA segregation to be visualised alongside the spindle elongation meaning any defects during metaphase-anaphase transition can be identified.

The initial aim of imaging optimisation was to image the cells at Nyquist sampling while maintaining the viability of the cells. Imaging was first optimised with the aim of visualizing the spindle dynamics in meiosis I and II (Table 2.9 - Stage 1, Y3606). Analysis of the images found that some of the spindles elongated out of the defined Z-region and that the DNA appeared very bright. Therefore the z-region was increased to 10.4 μm and the TRITC excitation was reduced (Stage 2, Y3606). Analysis of the images produced again found that some of the spindles moved out of the defined z-region and so this was further increased (Stage 3, Y3606). In the images produced it was found that the ends of the spindles were unclear in some places and so in order to obtain accurate spindle lengths the FITC exposure was increased (Stage 4, Y3606). Under these conditions it was found that the length of the spindle could be accurately measured. However many of the cells did not spourulate well under this level of light exposure.

The addition of LEDs to the personal Delta Vision (to replace the xenon bulb) meant that the cells could be imaged at much lower exposures while still obtaining sufficient resolution for accurate spindle measurement. This is because the LED's provide better illumination at all wavelengths compared to the xenon

bulb, which has maxima and minima all across the spectrum. The light levels used previously were greatly reduced and it was found that the spindle elongation and chromosome segregation could clearly be observed (Stage 5, Y3606). Under these imaging conditions it was found that the cells sporulated well and the whole length of the spindle could be accurately measured. (Figure 3.3)

To assess spindle dynamics in the *smc5/6* mutants (as seen in some of the initial imaging of Y3606 under high exposures), GFP-Cdc14 was incorporated into the strain containing GFP-Tub1 and mCherry-H2B. Cdc14, a protein phosphatase, is released from the nucleolus at early anaphase and can therefore be used as a marker of the metaphase-anaphase transition. This allowed the time of the first spindle elongation to be accurately identified. As Cdc14 needed to be clearly visualised at the same time as the spindle a higher exposure was required than used previously. In order to minimize damage to the cells a lower TRITC exposure was used as previously the DNA still appeared relatively bright. Initially it was observed that some of the cells did not segregate well likely due to the high FITC exposure used (Stage 1, Y3887). Some cells survive better when longer exposures and lower light transmissions are used rather than short exposures at higher light levels (Swedlow and Andrews, 2005), therefore the transmission was greatly reduced and the exposure increased (Stage 2, Y3887). Under these conditions the cells were found to complete both meiotic divisions and CDC14 and the spindle could be clearly seen. (Figure 3.4)

Table 2.9 Optimisation of live cell imaging for strains Y3606, Y3887, Y2572, Y4151, Y4836 and Y5398.

Strain	Stage 1	Stage 2	Stage 3	Stage 4	Stage 5
Y3606 (GFP-Tub and mCherry H2B)	FITC: 32% T, 0.4 E TRITC: 32% T, 0.08E Z-stack: 21 (8.4 μm)	FITC: 32% T, 0.4 E TRITC: 10% T, 0.05E Z-stack: 26 (10.4 μm)	FITC: 32% T, 0.4 E TRITC: 10% T, 0.08E Z-stack: 30 (12 μm)	FITC: 32% T, 0.5 E TRITC: 10% T,0.08 E Z-stack: 30 (12 μm)	*FITC: 10% T, 0.05 E TRITC:10% T, 0.025E Z-stack:35 (10.5 μm)
Y3887 (GFP-tubulin, GFP, CDC14 and mCherry H2B)	FITC: 32% T, 0.025E TRITC: 5% T, 0.025E Z-stack: 27 (8.1 μm)	*FITC: 7% T, 0.4 E TRITC: 2% T, 0.2 E Z-stack: 27 (8.1 μm)			
Y2572 (GFP-Rec8, mCherry CNM67, td-tomato Pds1)	FITC: 50% T, 0.2 E TRITC: 32% T, 0.4 E Z-stack: 25 (10 μm)	FITC: 32% T, 0.3 E TRITC: 32% T, 0.3 E Z-stack: 25 (10 μm)	FITC: 32% T, 0.4 E TRITC: 50% T, 0.3 E Z-stack: 25 (10 μm)	*FITC: 32% T, 0.025E TRITC: 32% T, 0.1 E Z-stack: 10 (10 μm)	
Y4151 (GFP-Mam1, mCherry- CNM67)	FITC: 32% T, 0.1 E TRITC: 32% T, 0.15E Z-stack: 17 (6.8 μm)	FITC: 32% T, 0.1 E TRITC: 32% T, 0.15E Z-stack: 8 (8 μm)	*FITC: 14% T, 0.065E TRITC: 14% T, 0.065E Z-stack: 8 (8 μm)		
Y4836 (GFP-Sgo1, mCherry- CNM67, td-tomato Pds1)	FITC: 32% T, 0.08 E TRITC: 10% T, 0.15E Z-stack: 8 (8 μm)	FITC: 32% T, 0.05 E TRITC: 32% T, 0.15E Z-stack: 7 (7 μm)			
Y5398 (TetR-GFP, mCherry- CNM67, td-tomato Pds1)	FITC: 25% T, 0.10 E TRITC: 35% T, 0.16E Z-stack: 8 (8 μm)	FITC: 25% T, 0.7 E TRITC: 40% T, 0.2 E Z-stack: 8 (8 μm)	*FITC: 7% T, 0.025 E TRITC: 20% T, 0.075E Z-stack: 8 (8 μm)		

*T refers to transmission and E refers to exposure. * Indicates images taken using a LED light source rather than a xenon bulb.*

To examine if there were defects in cohesin regulation in the *smc5/6* mutants imaging was then optimised so that cohesin (Rec8 tagged with GFP) could be visualised in single cells from prophase to anaphase II (staged using Cnm67 and Pds1). Different imaging conditions were required than those used to analyse the spindle dynamics as Pds1 has a very dim fluorescence and so requires a much greater TRITC exposure than was required to image m-cherry labeled H2B (Table 2.9).

Analysis of the initial images produced found that there was some bleaching of the Rec8 signal (Stage 1, Y2572) and so the FITC transmission was reduced to 32% (Stage 2, Y2572). From analysis of these images it was found that there was no longer any bleaching of Rec8. However it was found that it was very difficult to judge the time of Pds1 disappearance (important for distinguishing the beginning of anaphase) and so the TRITC transmission was increased (Stage 3, Y2572). Analysis of the images found that Pds1 disappearance could be accurately visualized. However the sporulation was only around 50%. As it was decided measurements were not required from these images, Nyquist sampling was not required. Therefore the number of z-sections was reduced to 10 and they were spaced 1 μm apart. The addition of LED's to the microscope at this stage meant that much lower exposures could be used (Stage 4, Y2572). Under the optimised conditions it was observed that Rec8 and Cnm67 localisation and Pds1 presence could accurately be assessed. The cells were also found to sporulate well under these conditions. (Figure 3.5)

To investigate if there were defects in the kinetics of monopolin assembly and disassembly imaging was optimised so that GFP-tagged Mam1 (a component of monopolin) could be visualized from its localisation at the kinetochores during prophase I until anaphase I, when it is lost (Petronczki et al., 2006; Matos et al, 2008). As it was decided that a high z-resolution was not required in this experiment, as no accurate measurements were required, the number of z-sections used were greatly reduced. 8 z-sections with a distance of 1 μm, as used by Matos et al (2008) were used. The length

of imaging was also extended to allow the capture of a larger number of cells displaying Mam1. (Images were taken every 15 minutes for 4 hours - Stage 2, Y4151). Here it was found that some of the cells did not sporulate well. Again the addition of LED's meant that that much lower exposures could be used (Stage 3, Y4151). Under these conditions mam1 could be clearly seen and the cells were found to sporulate well. (Figure 3.7)

To examine if there were defects in Shugoshin in the *smc5/6* mutants imaging was optimised so that Shugoshin assembly at pachytene to its disassembly at anaphase could be visualised. Similar imaging conditions to those used to image GFP-Mam1 were then applied to the imaging of GFP-Sgo1 (Stage 1, Y4836). Here the cells were initially arrested using an Ndt80 block to hold the cells at pachytene to synchronize the cells. This was required so that Sgo1 could be visualised in the majority of the cells so that it could be accurately determined if there was any loss of shugoshin in the *smc5/6* mutants. Analysis of the initial images found that the loss of Pds1 could not be accurately judged so the TRITC exposure was increased. The GFP exposure however was reduced slightly as the Sgo1 foci appeared quite bright. (Stage 2, Y4836) Under these conditions it was found that Sgo1 could be clearly seen from pachytene to its loss at anaphase. (Figure 3.9)

In order to further investigate if there was precocious sister chromatid separation in the *smc5/6* mutants strains were used containing TetO-CEN5, TetR-GFP. Segregation of one copy of chromosome *V* was followed through the incorporation of tetracycline repressor protein fused with GFP (TetR-GFP). These bind to tandem repeats of *Tet* operators that are integrated at the *URA3* locus, 35kb from the centromere of chromosome *V* (Michaelis et al., 1997). Here only one copy of chromosome V carried TetO-CEN5 so that precocious sister chromatid separation could clearly be observed. Analysis of the initial images produced found that Pds1 loss could not be clearly seen and that the GFP was very bright (Stage 1, Y5398). Therefore the TRITC exposure was increased and the FITC exposure was reduced (Stage 2, Y5398) Again it was found it was hard to clearly stage the loss of Pds1 and so

the TRITC exposure was again increased (Stage 3, Y5398). Under these conditions it was found that CNM67, Pds1 and the TetR-GFP foci could be clearly visualised. (Figure 3.12)

2.2.5.4 Optimisation of mFISH probe visualization

The Leica SP8 was used to image the mFISH samples as it has narrow emission windows, which could be adjusted so that the correct number of chromosomes could be observed in each channel (meaning that each of the chromosomes in the chromosome spread could be identified using the table provided from MetaSystems). DEAC could not be clearly visualised using the SP8 so was imaged on the pDV using a DEAC filter (ex 436 nm, em 480 nm). Spreads were imaged using an HC Plan Apo CS2, 1.4 numerical aperture, 63× magnification oil immersion objective (Leica). The 488 nm laser was used to visulaise FITC, Spectrum orange and TRITC and the 633 nm laser was used to visulaise Cy5. The emission windows were adjusted to 502-551 nm to see FITC, 566-600 nm to visualise Spectrum orange, 619-639 nm to visualise TRITC and 641-692 nm to visualise Cy5. Photon detection was carried out using a gain of 446 and no binning. The effective pixel size was ~0.0743 µm in the xy.

2.2.5.5 Image analysis & manipulation

Images were deconvolved using SoftWoRx software (3 iterations) or using Huygens. When using Huygens to carry out deconvolution, the lens oil refractive index was set to 1.52 and the medium was selected to be water and the refractive index set as 1.338. The final output of deconvolution was compared to the original image to make sure that the deconvolution had not introduced any imaging artifacts. Subsequent 3D analysis to measure spindle length was carried out using Imaris (version 7.0.0, Bitplane).

3D images are presented as maximum projections, rendered in Softworx or Imaris. Some images were manipulated in Adobe Photoshop CS5.1 using the

following procedure. Images were converted to .psd files from *Softworx* files before being opened in Adobe Photoshop. Only the max/min input levels of each channels were adjusted manually to adjust differences in the imaging intensities. Images were cropped preserving the relative ratios, and the size bar copied to a second layer of the image.

2.2.5.6 Statistical analysis

Statistical tests were used to determine if different data sets produced were significantly different from one another. The t-test was used when the results were hypothesized to follow a normal distribution. This works by comparing the means of the different datasets. The Kruskal-Wallis test was used when the results were hypothesized not to follow a normal distribution. This compares the medians of the different data sets.

2.2.6 DNA methods

2.2.6.1 ABgene DNA Taq PCR

PCR was used in order to verify that an added cassette had been incorporated into the correct position in the genome or to amplify a cassette for gene deletion or gene tagging (2.2.3.4 & 2.2.3.5). In order to tell if a cassette had incorporated into the correct position or for any PCR reaction where strict proofreading was not required ABgene DNA Taq polymerase was used. This was used with the accompanying 10× buffer. Primers were diluted 1:100 to a concentration of 1μM. Template DNA was adjusted to a concentration of 100-250ng. The final volume of the PCR reaction was 20μl. PCR was carried out on an Eppendorf Mastercycler using the program below:

1. 95°C for 3 minutes
2. 35 cycles of 95°C for 30 seconds, 50-60°C for 30 seconds (depending on the T_m of the primer pair used), 72°C for 1 minute/kb
3. 72°C for 10 minutes

4. Hold at 14°C

2.2.6.2 DreamTaq DNA polymeraise PCR

DreamTaq DNA polymeraise was used when stringent proofreading activity was required such as when creating a cassette for use in transformation. This was used with the accompanying 10×Taq buffer. Primers were diluted 1:100 to a concentration of 1 μM. Template DNA was adjusted to a concentration of 100-250 ng. The final volume of the PCR reaction was 20 μl. PCR was carried out on an Eppendorf Mastercycler using the program below:

1. 95 °C for 3 minutes
2. 30 cycles of 95 °C for 30 seconds, 94 °C for 30 seconds, 45 °C for 30 seconds (depending on T_m of primer pair used) 72 °C for 1 minute/kb
3. 72 °C for 10 minutes
4. Hold at 14 °C

2.2.6.3 Phire animal tissue PCR

In order to determine the genotype of the mouse tails the Phire animal tissue direct PCR kit was used. Here PCR was performed according to manufacturers instructions.

2.2.6.4 Genomic DNA extraction from yeast

Cells containing the DNA of interest were grown overnight in 5mls of YPD in green-capped glass tubes. The cells were spun down for 3 minutes at 3500 rpm and the pellets resuspended in 1ml of distilled water. The cellular solution was then transferred to a 1.5 ml Eppendorf and the solution spun down in a bench top centrifuge for 1 minute at 13,000 rpm. The supernatant was removed and the pellet was resuspended in 500 μl of 1 M sorbitol. In order to digest the cells 8 μl of Zymolyase and 15 μl of 1 M DTT were added

to the cellular solution and placed in a 37 °C incubator for one hour. Then 70 µl of 10 % SDS and 200 µl of TE were added to the cellular suspension and the tube was placed in a water bath at 65 °C for 10 minutes. 320 µl of 5 M KAc was then added to the cellular suspension, the tube inverted six times and then left on ice for 30 minutes. The sample was then spun in a bench top centrifuge for six minutes at 13,000 rpm. 650 µl of the supernatant produced was added to a 2 ml Eppendorf containing 200 µl of 5 M ammonium acetate and 1 ml of isopropanol. The tube was inverted six times and then the solution was spun down in a bench top centrifuge for one minute at 4000 rpm. The supernatant was removed and the pellet left to dry in the vaccum hood. Once dry, 300 µl of TE and 10 µl of RNAse (10 mg/ml) was added to the pellet. The tube was then placed in a water bath at 37 °C for 30 minutes and the concentration of the DNA quantified using the Nanodrop™.

2.2.7 Computational tools

2.2.7.1 Software used

Table 2.10 List of software used in this work

Software	Supplier/Reference
SoftWorX Deltavision	GE Healthcare life sciences
Huygens	Scientific Volume Imaging
Imaris	Bitplane
Image J	National Institute of Health https://imagej.nih.gov/ij/
Adobe photoshop	Adobe
R	https://www.r-project.org/

2.2.5.2 Websites used

Table 2.11 List of websites used in this work

Website name	Website address	Description of use

BLAST	https://blast.ncbi.nlm.nih.gov/Blast.cgi	Used to determine areas of similarity in nucleotide sequences
Saccharomyces Genome Database	http://www.yeastgenome.org/	Used to obtain biological information about the budding yeast genome
Reverse compliment	http://www.bioinformatics.org/sms	Use to determine reverse compliments of DNA sequences for primer generation

Chapter 3: SMC5/6 promotes chromosome resolution in meiosis

3.1 Introduction

In meiosis cell cycle progression has to be carefully coordinated with chromosome segregation in order to ensure the accurate division of the genetic material. In meiosis I the homologous chromosomes must be separated to opposite poles. In order to ensure this occurs faithfully the homologous chromosomes are paired via meiotic recombination. This is initiated through the induction of 100s of DSBs by the Spo11 endonuclease (Keeney and Neale, 2006). At midprophase I these DSBs are repaired to produce joint molecules (the precursors to crossovers) or non-crossover (NCO) recombinants (Bishop and Zickler, 2004). A majority of the joint molecules are then resolved into crossovers upon pachytene exit (Allers and Lichten, 2001). These crossovers act to ensure genetic diversity and alongside cohesion between sister chromatids ensure accurate biorientation of homologs at meiosis I (Petronczki et al, 2003).

The cell has specialised checkpoint systems that monitor meiotic recombination to ensure that recombination is efficiently processed by the end of prophase (Roeder and Bailis, 2000). The transcription factor Ndt80 is a major target of the checkpoint systems (Tung et al, 2000). Ndt80 promotes the expression of over 200 genes during mid-meiosis (Chu and Herskowitz, 1998). Two central targets of Ndt80 are the cell cycle kinases, Cdc5, the sole yeast orthologue of Polo-like kinase (PLK), and cyclin-dependent kinase (CDK) (Clyne et al, 2003; Xu et al, 1995). Work by Sourirajan and Lichten (2008) demonstrates that Cdc5 is the main protein involved in promoting pachytene exit. It is important for both synaptonemal complex disassembly and the resolution of joint molecule intermediates (Sourirajan and Lichten, 2008). Cdc5 promotes joint molecule resolution through the activation Mus81, by phosphorylating the interacting protein, Mms4 (Matos et al, 2011). This happens in concert with the chromosomes going into their diffuse stage (at exit from pachytene) where the DNA becomes diffuse after being highly compact (Sourirajan and Lichten, 2008).

The release of chromosome compaction has been proposed to allow enzymatic access of proteins to the joint molecules.

It has previously been identified, in budding yeast meiosis, that *smc5* and *nse4* have poor DNA encapsulation into their spores indicative of problems in chromosome resolution (Figure 3.1A, Copsey et al, 2013; Farmer et al, 2011). Results from work by Farmer et al, (2011) indicated that the DNA-separation defects observed in the *smc5/6* mutants were due to S-phase problems. Findings from three different labs, however, indicated that the DNA separation defects were instead due to unresolved meiotic recombination (Copsey et al, 2013; Xaver et al, 2013; Lilenthal et al, 2013). This was tested using strains containing a mutation within Spo11's catalytic domain (*spo11-Y135F*), which renders Spo11 incapable of inducing meiotic DSBs (Cha et al, 2000). As DSBs were not present, meiotic recombination could not take place and therefore recombination-dependent linkages were not formed between the homologous chromosomes. If the chromosome segregation defects were only due to problems within pre-meiotic S-phase then the *spo11-Y135F* mutation should not affect the chromosome segregation in *smc5/6* mutants. It was found in a range of *smc5/6* mutants that the chromosome segregation defects were rescued when the *spo11-Y135F* mutation was introduced (Figure 3.1B, Copsey et al, 2013; Xaver et al, 2013; Lilenthal et al, 2013). This indicated that Smc5/6 has a major role in the resolution of meiotic recombination, supporting results previously observed in *S. pombe* (Wehrkamp-Richter et al, 2012).

It is likely that different results were obtained by Farmer *et al* (2011) due to the use of temperature sensitive mutants in their study. When using temperature sensitive mutants, the shift to non-permissive temperatures cannot be controlled tightly with regards to the specific stage of the meiotic cell cycle. It is possible, when temperature sensitive mutants are used, that the proteins can be depleted too early. Thus severe segregation defects due to replication problems would obscure any further defects induced by meiotic recombination. This could lead to the difference in phenotypes observed. In Copsey *et al* (2013) (Figure 3.1C) and in some of the work by Xaver *et al* (2013) and Lilenthal *et al* (2013) components

(A)

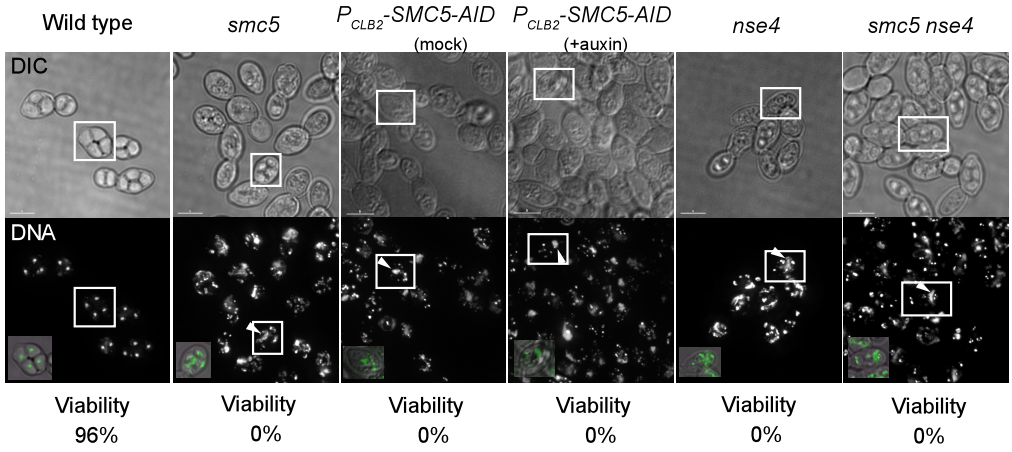

(B)

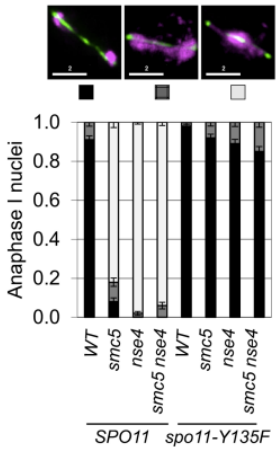

(C)

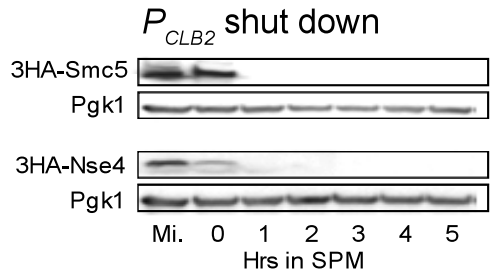

(Copsey et al, 2013)

Figure 3.1 – *smc5* and *nse4* mutants demonstrate DNA encapsulation defects during meiosis that are Spo11 dependent

A. Panel demonstrating DNA encapsulation defects observed in each of the mutants compared to wild type. The upper panel contains representative DIC images and the lower panel contains the corresponding DAPI images. An asci has been boxed from each strain so specific asci in the DIC images can easily be compared with the DAPI images (here DAPI has been pseudo coloured green) (Figure by Chi-ho Chan).

B. Introduction of *spo11-Y135F* mutation removes nuclear separation defects from *smc5, nse4* and *smc5 nse4*. (n >100 cells) Strain used: WT(Y1381), *smc5* (Y2705), *nse4* (Y2704), *smc5 nse4* (Y3185), *spo11-Y135F* (Y3147), *spo11-Y135F smc5* (Y3150), *spo11-Y135F nse4* (Y3153), *spo11-Y135F smc5 nse4* (Y4202) (Figure by Chi-ho Chan).

C. A western blot demonstrating the depletion of 3HA-Smc5 (Y491) and 3HA-Nse4 (Y492) protein levels when placed under the P_{CLB2} promoter (Blot by Phil Jordan).

of the Smc5/6 complex were depleted by placing them under the *CLB2* promoter, which is strongly repressed in meiosis (Chu et al, 1998). This ensured that the protein of interest was knocked down in meiosis only. Furthermore in order to determine if the segregation defects, observed in the *smc5/6* mutants, were due to independent sister chromatid entanglements both Spo13 and Spo11 were deleted from the strains containing *nse4* and *smc5*. This acted to de-protect centromeric cohesin and abolish meiotic recombination therefore converting their meiosis I to a 'mitotic like' division. In both these strains no problems were observed and viable dyads were formed (Figure 3.2A & 3.2B). This indicated that the sister chromatids in *smc5* and *nse4* were able to separate in the absence of recombination (Copsey et al, 2013).

Further research into the recombination defects that cause the segregation failure in the *smc5/6* mutants revealed that there is an accumulation of unresolved joint molecules (including multi-chromatid joint molecules, double Holliday junctions and single-end invasions between both the homologues and the sister chromatids) when the Smc5/6 complex is depleted in meiosis (Copsey et al, 2013; Xaver et al, 2013; Lilenthal et al, 2013). If these joint molecules are left unresolved they can block chromosome segregation (Jessop and Lichten, 2008). Resection and the appearance and disappearance of DSBs occurred with wild type kinetics in both *smc5* and *nse4* indicating that the Smc5/6 complex does not have a role in the initiation of recombination. This instead indicated that the Smc5/6 complex is specifically required for the formation and resolution of the joint molecules (Copsey et al, 2013). The Smc5/6 complex has been found to prevent the accumulation of joint molecules by destabilizing the SEIs via Nse2's SUMO ligase and by facilitating joint molecule resolution (Copsey et al, 2013; Xaver et al, 2013; Lilenthal et al, 2013). Specifically research indicates that the Smc5/6 complex is required for the resolution of joint molecules processed by the structure-specific endonucleases Mus81-Mms4, Slx1-Slx4 and Yen1 (Copsey at al, 2013; Xaver et al, 2013; Lilenthal et al, 2013; Zakharyevich et al., 2012). Consistent with this, the Smc5/6 complex is required for the localisation of Mus81-Mms4 to meiotic chromosomes in *S. cerevisiae* (Copsey et al., 2013). This indicates that, like in *S.pombe*, the Smc5/6 complex in *S.cerevisiae* is involved in

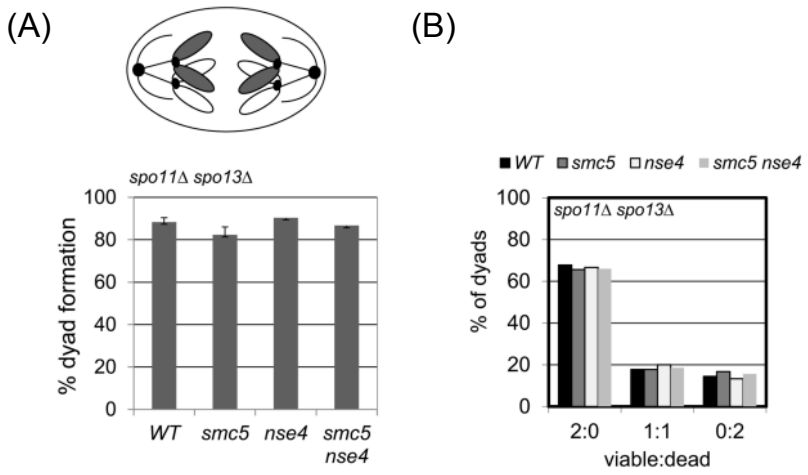

(Copsey et al 2013)

Figure 3.2 – *smc5* and *nse4* meiotic specific defects are Spo11 dependent

A. Cartoon demonstrating chromosome segregation at meiosis I in *spo11*Δ *spo13* Δ mutants. Graph demonstrating dyad formation in *Smc5/6* mutants also containing *spo11*Δ *spo13*Δ after 24 hours in sporulation medium. Strains used: *spo11*Δ *spo13*Δ (Y2816), *spo11*Δ *spo13*Δ *smc5* (Y2846) and *spo11*Δ *spo13*Δ *nse4* (Y2848) (Figure by Chi-ho Chan).

B. Dyad formation compared to viability after 24 hours in sporulation medium in wild type, *smc5, nse4* and *smc5 nse4* (Figure by Chi-ho Chan).

joint molecule resolution mediated by the Mus81-Mms4 endonuclease (Wehrkamp-Richter et al, 2012). The Smc5/6 complex is either required for the recruitment of Mus81 or to stabilize recombination intermediates so that they can be resolved by Mus81 (Copsey et al, 2013).

Another factor that is known to affect chromosome segregation when mis-regulated is cohesin. Cohesin must be cleaved along the chromosome arms so that the homologous chromosomes can segregate in meiosis I (Buonomo et al, 2000). It must be retained at the centromeres until meiosis II to ensure accurate sister chromatid separation (Buonomo et al, 2000). Three studies from mitosis in *S. pombe* have reported mis-regulation of cohesin in *smc5/6* mutants (Outwin et al, 2009; Tapia-Alveal et al, 2014; Lin et al, 2016). Outwin *et al* (2009) initially observed cohesin retention in *smc6-74* following HU treatment or when Top2 was inactivated (*top2-191*). Interestingly they found that separase overexpression rescued the observed segregation defects observed (Outwin et al, 2009). Work by Lin *et al* (2016) found that the retention of cohesin in *smc6-74* after HU treatment could be suppressed by Eso1 inactivation (*eso1-H17*) (orthologue of *S. cerevisiae* Eco1). This is proposed to be via $Psm3^{SMC3}$ hypoacetylation. Tapia-Alveal *et al* (2014) found that the observed segregation defects due to cohesin retention, in *smc6-74 top2-191* double mutants, could be suppressed through the loss of H2A.Z, a histone variant required for removal of cohesin from the chromosome arms. These studies all indicate that cohesin retention is the major factor preventing the chromosome segregation in *smc6-74 mutants* after HU treatment or combined with Top2 inactivation (*top2-191*). This led me to investigate whether cohesin defects in the *smc5* and *nse4* depletion mutants contributed towards the meiotic catastrophe observed.

3.2 Materials and methods

3.2.1 Time-lapse imaging

Previous observations showed that Smc5/6 inactivation leads to stretched nuclei due to an accumulation of joint molecules (Copsey et al., 2013; Xaver et al., 2013;

Lilenthal et al., 2013). To understand how meiosis and its progression is affected by the accumulation of joint molecules in these strains, time-lapse imaging was used to monitor spindle and chromatin dynamics. Live cell imaging was selected over fixed cell analysis as it allows the visualization of the dynamics and kinetics of biological processes on a single cell basis over real time. Due to the problems of toxicity and photobleaching associated with live cell imaging the conditions of imaging needed to be optimised.

Time-lapse imaging to investigate spindle elongation and Rec8 localisation in *S.cerevisiae* has been carried out in other studies. However, in these cases imaging was carried out at a low spatial resolution, well below Nyquist sampling (8 z-sections, 1 μm apart) (Matos et al, 2008). This provided important temporal markers, however the conditions that they used would not provide great enough resolution to look at dynamics and kinetics being investigated in this study. In this study five live cell imaging systems were used. These were to examine the distribution and localisation of Rec8, Mam1 and Sgo1 (in each case the protein of interest was GFP-tagged), to carry out analysis of spindle dynamics and the DNA segregation (through the use of GFP tagged Tub1 and mCherry tagged H2B) and to investigate sister chromatid segregation (through the use of the tetO-*CEN5,* tetR-GFP system) in wild type compared to *smc5* and *nse4*. Imaging conditions were carefully optimised for each of the imaging systems in order to ensure that the components of interest could be clearly visualised whilst maintaining the viability of the cells (Section 2.2.5.3 of Materials and Methods).

To analyse how protein localisation, spindle dynamics and chromosome segregation was affected in *smc5/6* mutants two strains were used in which either Smc5 or Nse4 were depleted by placing the protein of interest under a *CLB2* promoter, which is strongly repressed in meiosis (Chu et al, 1998). Analysis of the protein levels on a Western blot confirmed their knockdown in meiosis only (Figure 3.1C). The knockdown was further verified through the assessment of spore encapsulation in each of the strains compared to wild type (Figure 3.1A) (Copsey et al, 2013).

3.3 Results

3.3.1 Defects in DNA separation and spindle dynamics in *smc5* and *nse4* mutants.

To understand the defect in chromosome resolution caused by induction of meiotic DSBs, strains containing GFP tagged Tub1 and mCherry labeled H2B were imaged in real time. In the wild type, spindle elongation occurred continuously and there was clear nuclear separation at anaphase I. Anaphase II was detected by the presence of two concomitant spindles and the end of meiosis was confirmed by the formation of four distinct nuclei (Figure 3.3A & 3.3B, Wild type). In order to visualise the cells through the whole of meiosis imaging was carried out for 3 hours. In the *smc5* and *nse4* mutants defects could be seen by anaphase I (Figure 3.3B). In the *smc5* mutants there was much greater stretching of the DNA than observed in the *nse4* mutants and occasionally some separation of the DNA was observed (Figure 3.3B, *smc5*- upper panel, 0:20 min). However at the end of meiosis the DNA generally collapsed back to form an individual mass (Figure 3.3B *smc5*- upper panel, 0:30 min). Occasionally the DNA remained separated as can be seen in Figure 3.3B (*smc5*-lower panel). Fragmented nuclei were also often observed in both *smc5* and *nse4* (as distinguished by the black arrows Figure 3.3B). These were also seen *Drosophila* embryos depleted of the Smc5/6 complex and are likely to be due to the aberrant chromosome morphology of the chromosomes in *smc5/6* mutants (Tran et al, 2016).

It is predicted that the differences observed in the Smc5-depleted cells may be due to intercellular differences in the level of Smc5 depletion. No clear nuclear separation was seen in the *nse4* mutant and the DNA was observed to stretch to a much lesser extent than observed in the cells depleted of Smc5, indicating that the defect is considerably more severe. This is consistent with defects observed in recombination. In the *smc5* mutant, joint molecules accumulated to 4.7% of the DNA signal and in *nse4* they were found to accumulate to 10% of the DNA signal, compared to 3% seen in wild type (Copsey et al, 2013). The differences are likely to be due to less efficient depletion of Smc5. When Smc5 is further depleted,

(A)

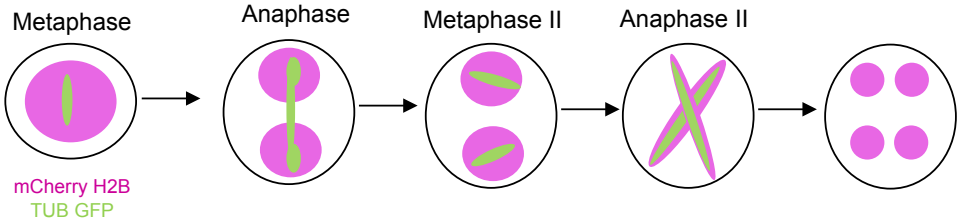
Metaphase
Anaphase
Metaphase II
Anaphase II
mCherry H2B
TUB GFP

(B)

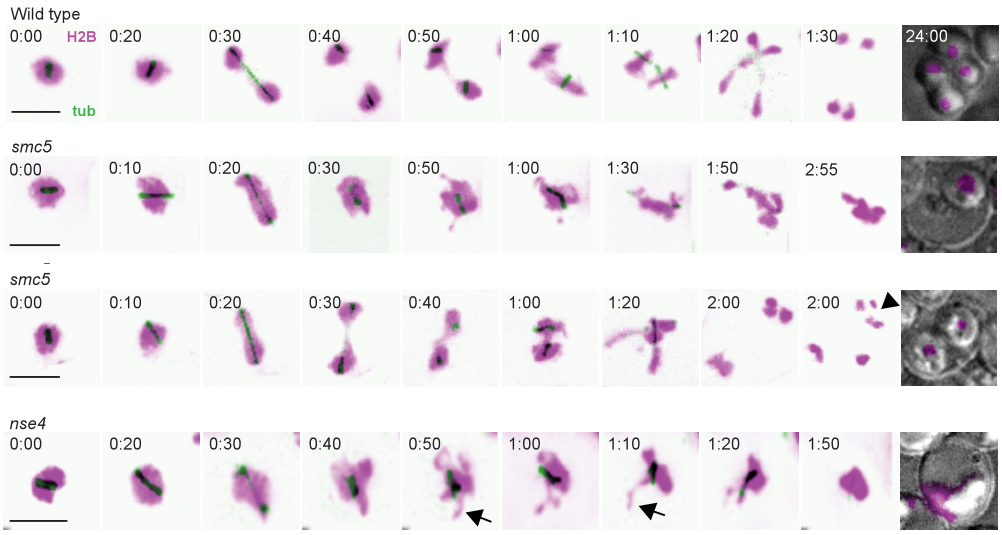
Wild type
0:00 H2B
tub
0:20
0:30
0:40
0:50
1:00
1:10
1:20
1:30
24:00
smc5
0:00
0:10
0:20
0:30
0:50
1:00
1:30
1:50
2:55
smc5
0:00
0:10
0:20
0:30
0:40
1:00
1:20
2:00
2:00
nse4
0:00
0:20
0:30
0:40
0:50
1:00
1:10
1:20
1:50

(C)

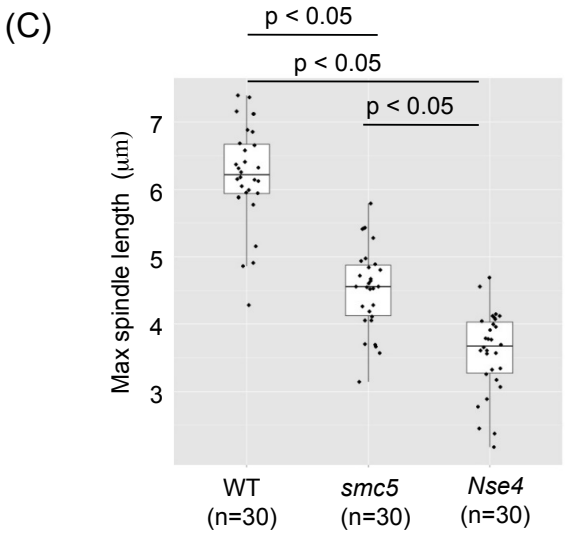
p < 0.05
p < 0.05
p < 0.05
Max spindle length (µm)
7
6
5
4
3
WT
(n=30)
smc5
(n=30)
Nse4
(n=30)

Figure 3.3 – Spindle elongation is reduced in *smc5* and *nse4* mutants

A. Spindle elongation and nuclear divisions were assessed in strains containing tubulin tagged with GFP and H2B tagged with mCherry. In wild type spindles reach their maximum length and the chromatin divides into two equal masses at anaphase I. At metaphase II spindles begin to form in each of the chromatin masses. At anaphase II these spindles reach their maximum length and the chromatin masses again divide producing a total of 4 chromatin masses.

B. Live cell imaging montage of strains containing GFP tagged Tub1 and mCherry tagged H2B. Wild type (Y3606), *smc5* (Y3627) and *nse4* (Y3630). Imaging was carried out using FITC (10% transmission, 0.05 second exposure) and TRITC (10% transmission, 0.025 second exposure). Images were taken every 5 minutes, using a z-stack containing 32 slices, 0.3 μm microns apart (12 μm in total). The scale bar corresponds to 5 μm. Arrows label chromatin spikes. (Data published in Copsey et al, 2013) Experiments 52 and 57.

C. Maximum spindle lengths in wild type (average 6.2 μm), *smc5* (average 4.5 μm) and *nse4* (average 3.6 μm). The maximum spindle lengths measured in each of the mutants were significantly smaller than those measured in wild type ($P < 0.05$)

through the use of an auxin-inducible degron fusion (P_{CLB2}-*SMC5-AID*), the defects in chromosome segregation more closely reflect the defects seen in *nse4* (Copsey et al, 2013; Nishimura et al, 2009). I conclude that *smc5* and *nse4* have severe chromosome separation defects.

The maximum spindle length was significantly reduced in both *nse4* (n=30, average 3.6 ± 0.7 μm) and *smc5* (n=30, average 4.5 ± 0.6 μm) compared to wild type (n=30, average 6.2 ± 0.6 μm; Figure 3.3C, Kruskal-Wallis test, $P<0.05$ for both pairwise comparisons). However, as the spindles were observed to only elongate slightly in *nse4*, it was sometimes difficult to determine the exact time of anaphase. In order to accurately stage anaphase, GFP-Cdc14 was incorporated into the strains (Figure 3.4A). Cdc14 is a protein phosphatase that is released from the nucleolus at early anaphase. The maximum spindle lengths measured, where Cdc14-GFP was used to time the onset of anaphase I, were very similar to what was found previously. The maximum spindle length was reduced significantly in both *nse4* (n=23, average 3.4 μm ± 0.9 μm) and *smc5* (n=25, average 4.6 ± 0.9 μm) compared to wild type (n=26, average 6.2 ± 1.3 μm; Figure 3.4C; Kruskal-Wallis test – $P<0.05$ in both cases). Again it was observed that the maximum spindle length was significantly shorter in *nse4* compared to *smc5* (Kruskal-Wallis $P<0.05$). The more severe defects in chromatin segregation and spindle elongation in the *nse4* compared to the *smc5* mutant are consistent with the more complete depletion of Nse4, although it cannot be ruled out that Nse4 has roles independent of the Smc5/6 complex (Copsey et al. 2013; Palecek et al, 2006).

3.3.2 Abolition of Spo11 activity rescues spindle elongation defects in *smc5/6* mutants

The defects in spindle elongation could be due to defects in the resolution of joint molecules, which are known to impede chromosome segregation and could therefore counteract the pulling forces of the microtubules. To determine whether the spindle elongation defect was due to problems in meiotic recombination, the *spo11-Y135F* mutation was incorporated into the strains

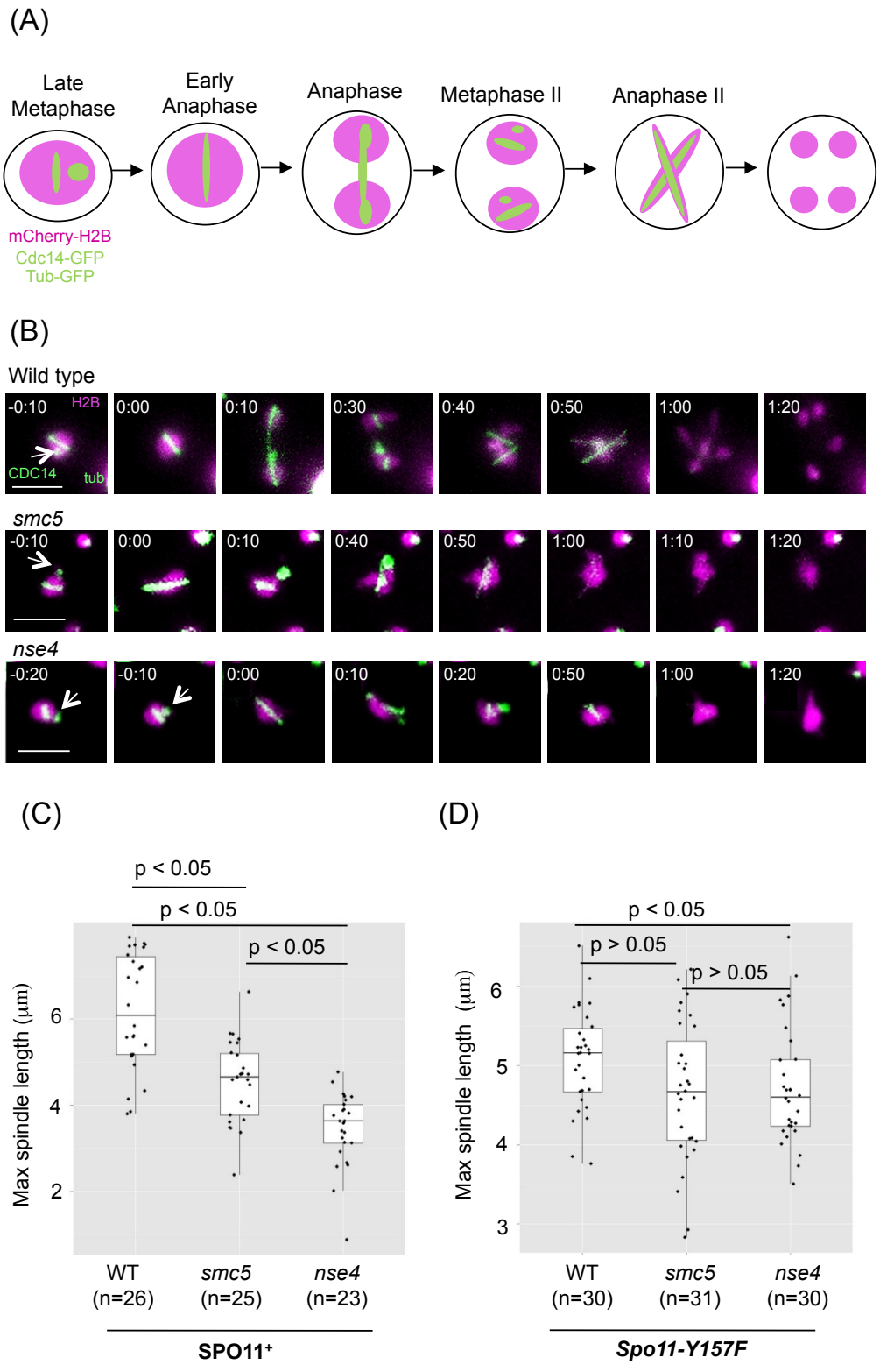
(A)
Late Metaphase
Early Anaphase
Anaphase
Metaphase II
Anaphase II
mCherry-H2B
Cdc14-GFP
Tub-GFP
(B)
Wild type
-0:10
H2B
CDC14
tub
0:00
0:10
0:30
0:40
0:50
1:00
1:20
smc5
-0:10
0:00
0:10
0:40
0:50
1:00
1:10
1:20
nse4
-0:20
-0:10
0:00
0:10
0:20
0:50
1:00
1:20
(C)
p < 0.05
p < 0.05
p < 0.05
Max spindle length (μm)
6
4
2
WT (n=26)
smc5 (n=25)
nse4 (n=23)
SPO11+
(D)
p < 0.05
p > 0.05
p > 0.05
Max spindle length (μm)
6
5
4
3
WT (n=30)
smc5 (n=31)
nse4 (n=30)
Spo11-Y157F

Figure 3.4 – Spindle elongation is reduced in *smc5* and *nse4* mutants (part two)

A. To assess the spindle elongation and nuclear divisions strains were used containing tubulin and CDC14 tagged with GFP and H2B tagged with mCherry. In wild type, at anaphase onset, CDC14 disappears from the nucleolus, spindles elongate and the chromatin divides into two equal masses. At metaphase II spindles begin to form in each of the chromatin masses. At anaphase II these spindles reach their maximum elongation and the chromatin masses again divide producing a total of four chromatin masses.

B. Live cell imaging montage of strains containing GFP tagged Tub1 and Cdc14 and mCherry-tagged H2B. Arrows indicate the location of Cdc14. Wild type (Y3887), *smc5* (Y3890) and *nse4* (Y3893). Imaging was carried out using FITC (7% transmission, 40 ms exposure) and TRITC (2 % transmission, 40 ms exposure). Images were taken every 10 minutes, using a z-stack containing 27 slices, 0.3 microns apart (8.1 μm in total). The scale bar corresponds to 5 μm. Experiments 184, 186, 187, 188, 189, 193.

C. Maximum spindle lengths in wild type (Y3887, average 6.2 μm), *smc5* (Y3890, average 4.6 μm) and *nse4* (Y3893, average 3.4 μm). The maximum spindle lengths measured in each of the mutants were significantly smaller than those measured in wild type ($P < 0.05$).

D. Maximum spindle lengths in strains containing *spo11*. Wild type (Y5614, average 5.1 μm), *smc5* (Y5617, average 4.7 μm) and *nse4* (Y5620, average 4.7 μm).

containing tagged H2B, tubulin and Cdc14. The *spo11-Y135F* mutation abolishes the catalytic activity of Spo11, thus if joint molecules impede spindle elongation, then we predict that spindle elongation should be restored to wild type levels if the strains contain *spo11-Y135F*. In the *spo11-Y135F* mutant background the spindle elongation defect was rescued in the *smc5* and *nse4* mutant, since the maximum lengths obtained were not dissimilar from wild type (WT - average 5.1 ± 0.6 μm, *smc5* - average 4.7 ± 0.9 μm and *nse4* - average 4.7 ± 0.7 μm; Figure 3.4D). This indicated that the spindle elongation defect is dependent on the induction of meiotic recombination. The maximum spindle lengths observed in *smc5* were not significantly different to wild type (Kruskal-Wallis test $P>0.05$). The maximum spindle lengths in *nse4 spo11-Y135F* were however found to be significantly different to *spo11-Y135F* (Kruskal-Wallis $P<0.05$). This potentially indicates recombination-independent roles of the Smc5/6 complex. Furthermore the maximum spindle lengths of *spo11-Y135F* were found to be significantly shorter than observed in wild type (Kruskal-Wallis test $P>0.05$). This may indicate that the spindle needs to elongate to a lesser extent, when chiasmata are not present, in order to segregate the DNA.

3.3.3 Cohesin mis-regulation in *smc5* and *nse4* mutants

In meiosis, cohesin is lost in a stepwise manner to ensure that the homologous chromosomes segregate at anaphase I but that the sister chromatids remain together until metaphase II (Buonomo et al, 2000). Smc5/6 mutants, in mitosis, have been found to display problems segregating their DNA at anaphase due to a retention of cohesin along their chromosome arms (Outwin et al, 2009; Tapia-Alveal et al, 2014; Lin et al, 2016). To address whether cohesin defects in *smc5* and *nse4* contribute towards the observed meiotic catastrophe, the bulk cohesin levels in wild type and each of the mutants were initially analysed on a Western blot. No differences were observed (Dr. A. Copsey, Supplementary figure 1). It is however unlikely that a Western blot would be able to detect small changes in the levels of chromosomally-bound cohesin. I therefore employed live cell imaging to enable visualization of the levels of cohesin and the kinetics of cohesin loss on a single cell basis. To this end, I first optimized the time-lapse imaging of

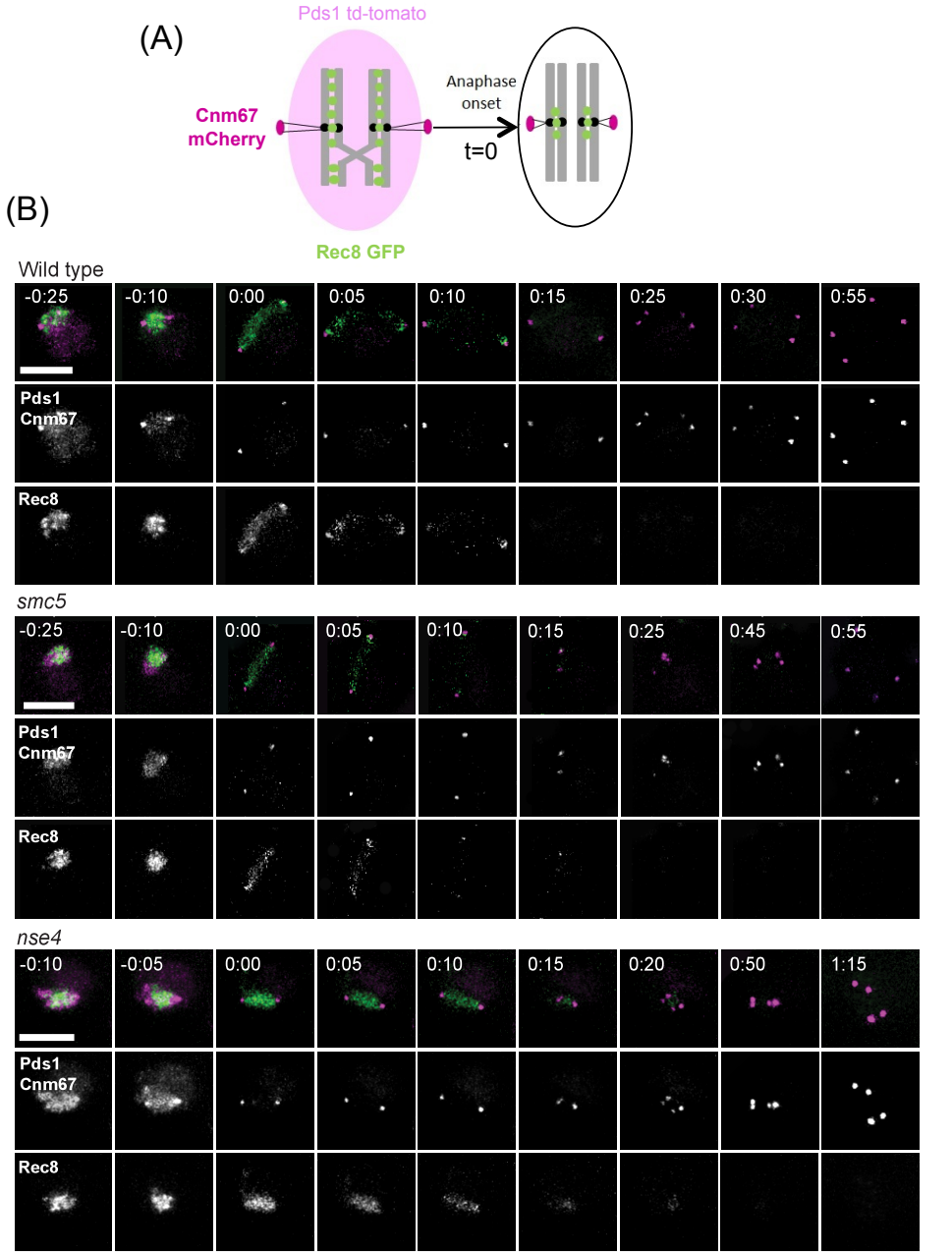

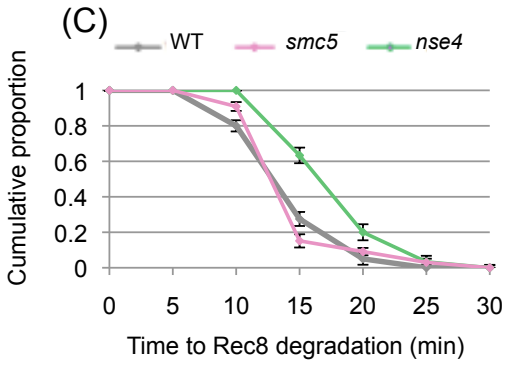

(D) Centromeric cohesin at anaphase I

		WT	*smc5*	*nse4*
Centromeric	SPB Rec8	93	65	31
Loss of cohesin		7	19	51
Non determinable		0	16	19
Total (n=)		100	68	75

Figure 3.5 - Cohesin misregulation in *smc5/6* mutants (low resolution)

A. To assess the cohesin levels strains were used containing Rec8 tagged with GFP. The time of anaphase onset was determined by Pds1 (tagged with td-tomato) degradation and an increase in the distance between the Cnm67 foci (tagged with mCherry). In wild type Rec8 is lost from the arm region at anaphase I and is retained at the centromeres until metaphase II.

B. Examples of time lapse imaging from wild type (Y2572), *smc5* (Y2673) and *nse4* (Y3047). Scale bars correspond to 4 μm. Images were acquired every 5 minutes for the first 90 minutes, every 20 minutes for the next 80 minutes and then every 45 minutes for the last 90 minutes. 10 z-sections covering a distance of 10 μm were used. (Published in Copsey et al, 2013) Experiment 30 and 52.

C. Graph demonstrating the time from anaphase onset (Pds1 loss, indicated as 0:00 in A) to arm cohesin degradation. Cases where cohesin loss was could not be determined were excluded. The Kruskal-Wallis test ($p<0.05$) demonstrated cohesin loss was delayed in *nse4* compared to both wild type and *smc5.* (Published in Copsey et al, 2013) Error bars correspond to standard error.

D. Comparison of centromeric cohesin presence in wild type, *smc5* and *nse4* from time-lapse imaging. Three categories were observed. Centromeric cohesin present, centromeric cohesin absent and non-determinable (when the Cnm67 foci came back together such that the remaining cohesin could not be classified as centromeric or arm cohesin). (Published in Copsey et al, 2013)

strains containing Rec8-GFP and then conducted experiments in order to assess real-time dissociation of cohesin from meiotic chromosomes in the presence or absence of the Smc5/6 complex.

To investigate if there was a delay in the removal of cohesin after the induction of meiotic recombination in *smc5* and *nse4* mutants, the meiotic kleisin, Rec8, was tagged with GFP. To determine the time of both prophase and anaphase cells were staged using Pds1 tagged with td-tomato and Cnm67 tagged with m-cherry (Figure 3.5A, Matos et al, 2008). Pds1 (securin) is degraded in early anaphase. Cnm67 is a component of the spindle pole bodies. The spindle pole body separates to two at early metaphase and these reach their maximum separation at anaphase (Xu et al, 1995). At metaphase II four spindle pole bodies are seen (Figure 3.5A). In wild type, Rec8 and presumably meiotic cohesin is initially evenly distributed between the elongated Cnm67 foci (Figure 3.5B wild type t=0). As the Cnm67 reach their maximum separation the Rec8 signal splits into two, indicative of the DNA separating. The cohesin signal is then slowly lost over 5 to 25 min. until it is only seen at the centromeres (Figure 3.5B). Centromeric cohesin is then lost from the centromeres at anaphase II.

3.3.3.2 Smc5/6 mutants show retention of arm region Rec8

To investigate cohesin regulation in the Smc5/6 mutants I first assessed the time taken to remove cohesin from the chromosome arms at anaphase I onset. I used two different conditions for imaging cohesin, referred to as low and high resolution (Section 2.2.5.3). In the lower resolution imaging of wild type cells, the average removal time was 15.6 (±4.0) minutes after the onset of anaphase I. A similar average retention time was seen in *smc5* (16 ± 4.1 minutes). The average retention time was increased in *nse4* mutant with Rec8-GFP being retained for on average 19.8 (±4.7) minutes. This was significantly increased compared to wild type (Kruskal-Wallis test $p<0.05$; Figure 3.5C). In the higher resolution imaging the difference was more pronounced (Figure 3.6C). In wild type, the average retention time was 14.2 (±5.7) minutes. This was significantly increased in each of the mutants, where the retention times were 23.5 (±11.1)

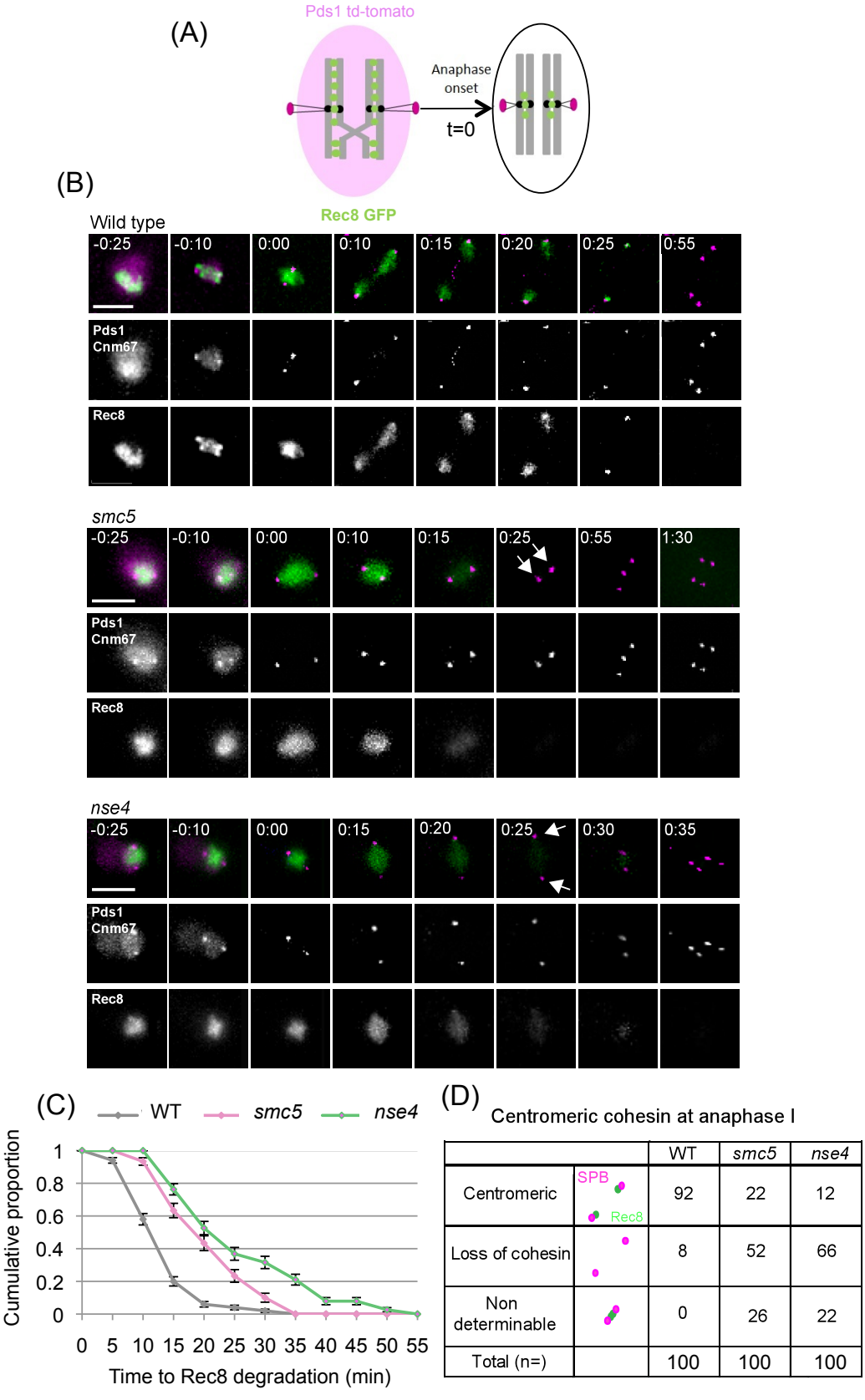
(A)
Pds1 td-tomato
Anaphase onset
t=0
Rec8 GFP
(B)
Wild type
-0:25
-0:10
0:00
0:10
0:15
0:20
0:25
0:55
Pds1 Cnm67
Rec8
smc5
-0:25
-0:10
0:00
0:10
0:15
0:25
0:55
1:30
Pds1 Cnm67
Rec8
nse4
-0:25
-0:10
0:00
0:15
0:20
0:25
0:30
0:35
Pds1 Cnm67
Rec8
(C)
WT
smc5
nse4
Cumulative proportion
1
0.8
0.6
0.4
0.2
0
0 5 10 15 20 25 30 35 40 45 50 55
Time to Rec8 degradation (min)
(D)
Centromeric cohesin at anaphase I
WT
smc5
nse4
Centromeric
SPB
Rec8
92
22
12
Loss of cohesin
8
52
66
Non determinable
0
26
22
Total (n=)
100
100
100

Figure 3.6 - Cohesin misregulation in *smc5/6* mutants (high resolution)

A. To assess the cohesin levels strains were used containing Rec8 tagged with GFP. The time of anaphase onset was determined by Pds1 (tagged with td-tomato) degradation and an increase in the distance between the Cnm67 foci (tagged with mCherry). In wild type Rec8 is lost from the arm region and is retained at the centromeres until metaphase II.

B. Examples of time lapse imaging from wild type (Y2572), *smc5* (Y2673) and *nse4* (Y3047). Scale bars correspond to 4 μm. Images were acquired every 5 minutes for a total of 3 hours. 25 z-sections covering a distance of 10 μm were used. Arrows indicate Cnm67 foci. Experiments 3, 7, 8 12, 41 and 45.

C. Graph demonstrating the time from anaphase onset (Pds1 loss, indicated as 0:00 in A) to arm cohesin degradation. Cases where cohesin loss was classified as non-determinable were excluded. The Kruskal-Wallis test ($p<0.05$) demonstrated cohesin loss was delayed in *nse4* and *smc5* compared to wildtype. Error bars correspond to standard error.

D. Comparison of centromeric cohesin presence in wild type, *smc5* and *nse4* from time-lapse imaging. Three categories were observed. Centromeric cohesin present, centromeric cohesin absent and non-determinable (when the Cnm67 foci came back together such that the remaining cohesin could not be classified as centromeric or arm cohesin).

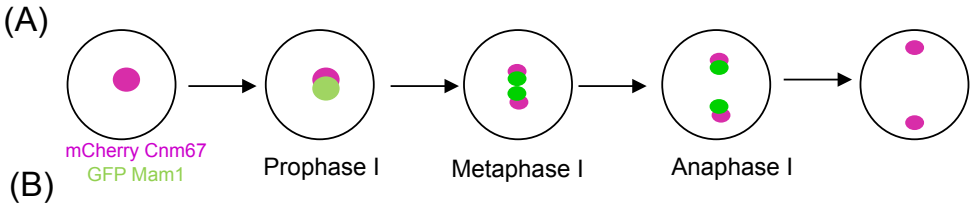
(A)
mCherry Cnm67
GFP Mam1
Prophase I
Metaphase I
Anaphase I

(B)

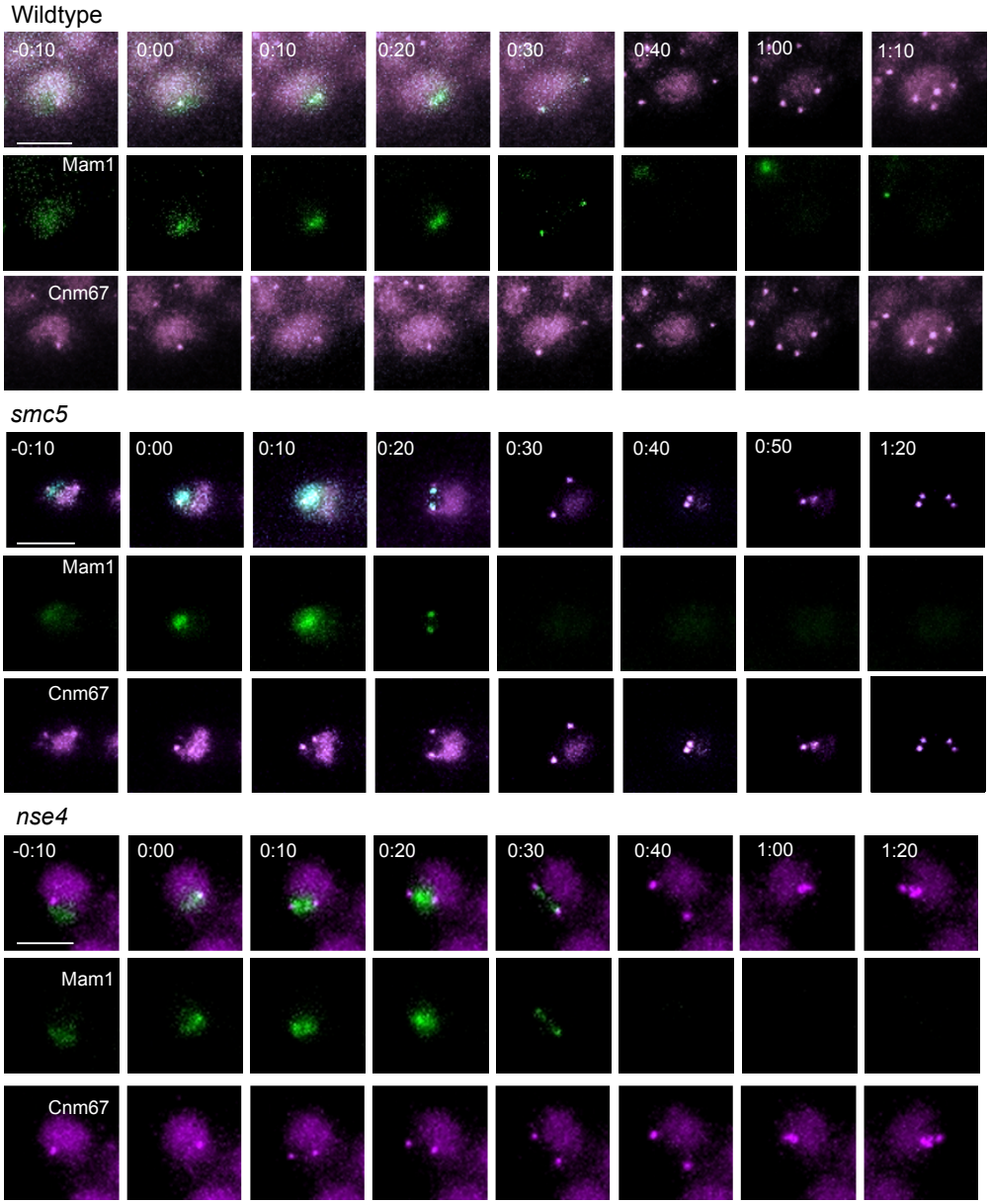
Wildtype
-0:10
0:00
0:10
0:20
0:30
0:40
1:00
1:10
Mam1
Cnm67
smc5
-0:10
0:00
0:10
0:20
0:30
0:40
0:50
1:20
Mam1
Cnm67
nse4
-0:10
0:00
0:10
0:20
0:30
0:40
1:00
1:20
Mam1
Cnm67

Figure 3.7 – Mam1 localisation is unaffected in both *smc5* and *nse4* mutants

A. Cartoon demonstrating the kinetics of Mam1 in a wild type situation. To assess the Mam1 association strains were used containing GFP tagged Mam1. The time of anaphase onset was determined by the separation of the Cnm67 foci (td-tomato tagged). In wild type Mam1 is loaded at the centromeres at prophase and lost at late anaphase.

B. Live cell imaging montage of wild type (Y5306), *smc5* (Y5451) and *nse4* (Y5607) strains containing GFP tagged Mam1, mCherry tagged Cnm67 and td-tomato tagged Pds1. Scale bar 5 μm. Experiments 173, 204, 220.

minutes in *smc5* and 28.4 (±13.3) minutes in *nse4* (Kruskal-Wallis test $p<0.05$). The difference in retention times between the high and low resolution imaging is likely to be due to the photodamage induced in the higher resolution imaging, evidenced by poor sporulation rates in the higher resolution imaging. This suggests that Smc5/6 may have a role in the removal of cohesin at anaphase.

3.3.3.3 Smc5/6 mutants are deficient in the retention of centromeric Rec8

In the previous live cell imaging I observed retention of centromeric cohesin lasting several frames in the majority of wild-type cells. Centromeric cohesin was observed in 93% of wild type cells (n=100) in the low-resolution imaging and 92% of wild type cells (n=100) in the high-resolution imaging (Figure 3.5D and 3.6D). Despite the retention of cohesin in a subset of cells, I also observed the precocious depletion of the centromeric Rec8-GFP signal, prior to metaphase II, in both of the *smc5* and the *nse4* mutants (Figure 3.5D and 3.6D). In the *smc5* mutant, 19% of cells (n=68) in the low-resolution imaging and 52% of cells (n=100) in the high-resolution imaging displayed a loss of centromeric Rec8 prior to metaphase II ($P<0.05$ in the low and high resolution imaging). This was increased in the *nse4* mutant to 51% (n=75) in the low-resolution imaging and 68% (n=100) in the high-resolution imaging (Figure 3.5D and 3.6D) ($P<0.05$ in both cases). This indicates that there is significant loss of centromeric Rec8 in the Smc5/6 mutants prior to the onset of anaphase II. It is likely that the differences observed between the low and high-resolution imaging are due to photobleaching of the centromeric Rec8-GFP. Regardless of these differences, the data suggest that Smc5/6 is important for the retention of centromeric Rec8.

3.3.4 Smc5/6 mutants display a metaphase I - anaphase I delay

As I observed that a delay in the removal of cohesin from the chromosome arms in both *smc5* and *nse4*, I investigated if this was in fact a delay in the removal of cohesin or if the mutants were instead progressing through the cell cycle more slowly than wild type. To do this, I monitored Cnm67-mCherry and Mam1-GFP using time-lapse imaging (Figure 3.7A & 3.7B). Mam1 is a central component of

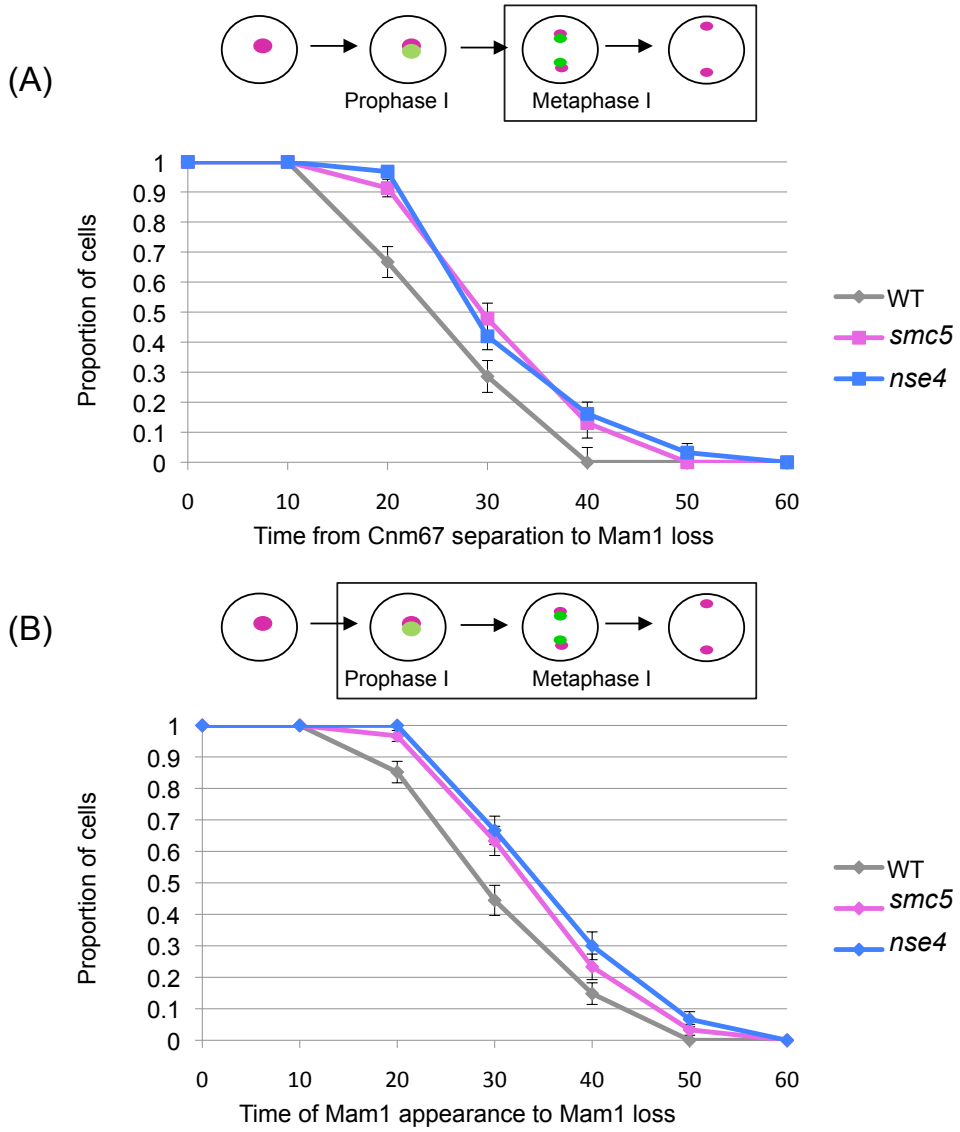

Figure 3.8 – Live cell imaging of strains containing GFP-Mam1 indicate that Mam1 is retained for slightly longer in both *smc5* and *nse4* mutants

A. Retention time of Mam1 from Cnm67 separation to Mam1 loss (Strains - Wild type (Y5306, n=21), *smc5* (Y5451, n=23) and *nse4* (Y5607, n=31))

B. Retention time of Mam1 from Mam1 appearance to Mam1 loss (Strains - Wild type (Y5306, n=30), *smc5* (Y5451, n=27) and *nse4* (Y5607, n=30))

the monopolin complex, which is required for mono-orientation of the sister chromatids at metaphase I (Toth et al, 2000, Section 2.2.5.3). It was chosen as it associates with the kinetochores at pachynema and is retained until anaphase I (Katis et al, 2004; Matos et al, 2008).

Initially the time from metaphase (Cnm67-mCherry separation) to anaphase I (Mam1 loss) was assessed (Figure 3.8A). As quite a high level of light was required to clearly visualise Mam1 appearance and disappearance, imaging could not be carried out every five minutes. Imaging was instead carried out every ten minutes. I found that there was a significant delay in the time from metaphase I to early anaphase I onset in both *smc5* (average time 35.2 ± 8.5 min, Kruskal-Wallis test $p<0.05$) and *nse4* (average time 35.8 ± 8.9 min, Kruskal-Wallis test $p<0.05$) compared to wild type (average time 29.5 ± 8 min).

The time from pachynema (Mam1 appearance) to anaphase (Mam1 loss) was also assessed. As shown in Figure 3.8B, I found a slight delay in the loss of Mam1 signal in *smc5* (average time 38.6 ± 9 min) compared to wild type (average time 34.4 ± 9.3 min, Kruskal-Wallis test $p>0.05$) and a significant delay in *nse4* compared to wild type (average time 40.3 ± 9.3 min, Kruskal-Wallis $p<0.05$). These results indicate that there is a significant delay in the metaphase to anaphase transition in both *smc5* and *nse4* and a significant delay in the pachynema to anaphase transition in *nse4*.

3.3.5 Shugoshin loading is normal in *smc5* and *nse4* mutants

Shugoshin has the central role in protecting centromeric cohesin from removal until anaphase II (Section 1.11, Katis et al, 2004; Marston et al, 2004). If Shugoshin is depleted the percentage of cells displaying centromeric Rec8 at anaphase drops to 16% (Katis et al, 2004). Because of the precocious depletion of centromeric Rec8 in *smc5/6* mutants, I investigated whether defects in Shugoshin may be responsible for the precocious loss of centromeric Rec8. To analyse Shugoshin loading, I tagged the single Shugoshin in budding yeast, Sgo1, with GFP, and used Cnm67-mCherry and Pds1-tdTomato to stage the cell cycle

(A)

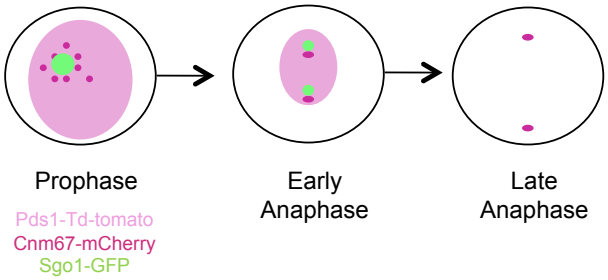
Prophase
Early Anaphase
Late Anaphase
Pds1-Td-tomato
Cnm67-mCherry
Sgo1-GFP

(B)

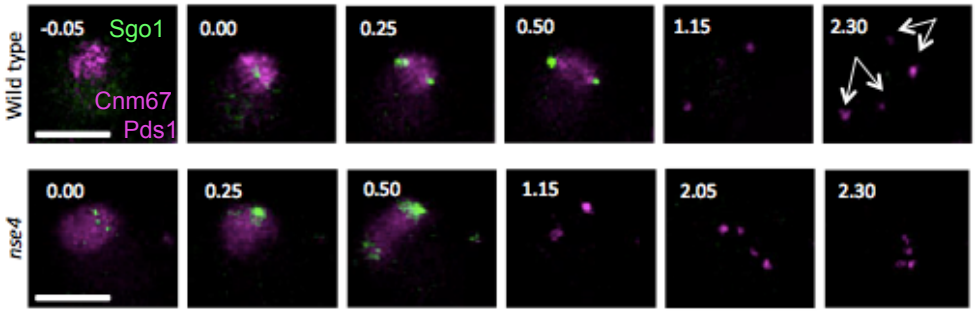
Wild type
-0.05
Sgo1
Cnm67
Pds1
0.00
0.25
0.50
1.15
2.30
nse4
0.00
0.25
0.50
1.15
2.05
2.30

(C)

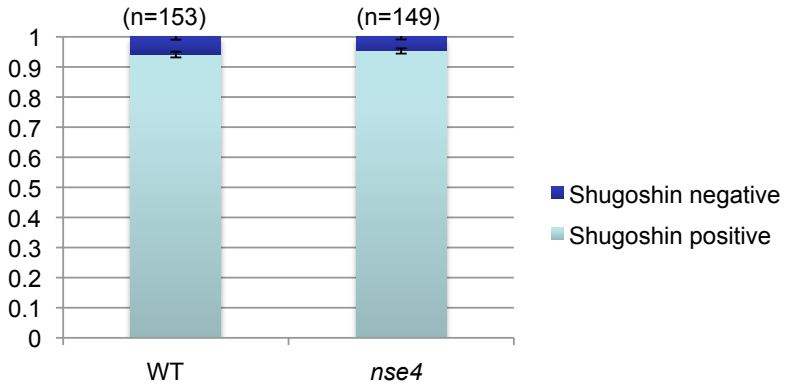
(n=153)
(n=149)
1
0.9
0.8
0.7
0.6
0.5
0.4
0.3
0.2
0.1
0
WT
nse4
Shugoshin negative
Shugoshin positive

Figure 3.9 - Shugoshin1 is not affected in *smc5* and *nse4* mutants in meiosis I

A. Cartoon demonstrating the kinetics of Shugoshin in a wild type situation. To assess the Shugoshin association in wild type and each of the mutant's, strains were used containing GFP tagged Shugoshin. The time of anaphase onset was determined by the loss of Pds1 (mCherry tagged) and separation of the Cnm67 foci (td-tomato tagged). In wild type Shugoshin is lost from the centromeric region at late anaphase.

B. Live cell imaging montage of wild type (Y4836) and *nse4* (4837) strains containing GFP tagged Shugoshin and mCherry tagged Mtw1 and Pds1. Scale bar 5 micron. Arrows are used to distinguish the 4 spindle pole bodies in the top panel. Experiments 103 and 104.

C. Bar graph demonstrating the percentage of cells that were either Shugoshin positive or Shugoshin negative in wild type and *nse4* at prophase. In wild type Shugoshin was observed in 94% of cells analysed and in *nse4* Shugoshin was observed in 95% of cells analysed (T-test $p>0.05$).

(Figure 3.9A). The cells were initially arrested using the *NDT80-IN* promoter, which synchronises cells in pachynema until the addition of β-estradiol. This allows the loading of Sgo1-GFP in late prophase I to be visualised across the whole population of cells. If Sgo1-GFP misregulation causes the precocious loss of Rec8 in *smc5/6* mutants, then Sgo1-GFP may either fail to localize or be maintained at centromeres. I hypothesized that successful Shugoshin loading or maintenance of Shugoshin would be observed in a smaller population of cells in each of the mutants compared to wild type. After release from *ndt80* arrest, however, Sgo1-GFP was observed to load in 94% of wild type cells (n=153) and 95% of *nse4* cells (n=149;Figure 3.9C; Section 2.2.5.3). Shugoshin was then lost at anaphase I in both wild type and *nse4*. This indicated that defects in Shugoshin localization were not responsible for the precocious loss of centromeric Rec8.

3.3.6 Low levels of sister kinetochore separation were observed in fixed cells from *smc5* and *nse4* mutants

Time-lapse imaging indicated a significant precocious loss of centromeric cohesin in both *smc5* and *nse4*. If centromeric cohesin is lost prior to anaphase this would act to promote precocious sister chromatid separation (separation of sister chromatids at meiosis I instead of meiosis II). To address whether the loss of centromeric cohesin led to precocious separation of sister kinetochores, sister kinetochore separation at anaphase I was assessed. This was carried out using the TetO-TetR system. Segregation of one copy of chromosome *V* was followed through the incorporation of tetracycline repressor protein fused with GFP (TetR-GFP). These bind to tandem repeats of *Tet* operators that are integrated at the *URA3* locus, 1.5 kb from the centromere of chromosome *V* (Michaelis et al., 1997). In the wild type, the sister chromatids remain together in meiosis I (seen as a single GFP foci at one end of the spindle) and then segregate from one another in meiosis II (seen as two GFP foci at opposite ends of the spindle; Figure 3.10 A).

To analyse the level of sister chromatid separation in the *smc5/6* mutants, initially cells were spread at anaphase (staged by assessment of the spindle

(A)

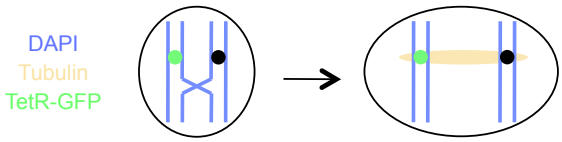
DAPI
Tubulin
TetR-GFP

(B)

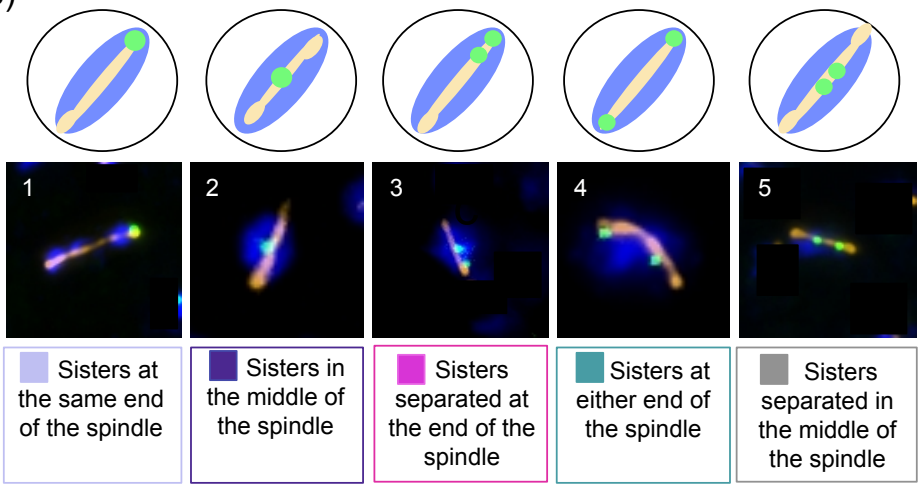
1
2
3
4
5
Sisters at the same end of the spindle
Sisters in the middle of the spindle
Sisters separated at the end of the spindle
Sisters at either end of the spindle
Sisters separated in the middle of the spindle

(C)

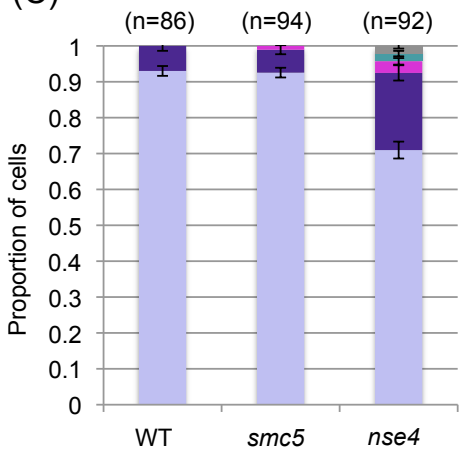
(n=86)
(n=94)
(n=92)
Proportion of cells
1
0.9
0.8
0.7
0.6
0.5
0.4
0.3
0.2
0.1
0
WT
smc5
nse4

Figure 3.10 – Precocious sister chromatid separation is increased in *smc5* and *nse4* mutants (fixed cell analysis)

A. Cartoon demonstrating chromosome segregation in a wild type strain containing TetR-GFP. Spreads were also stained with an antibody against tubulin and DAPI. Tubulin was used to roughly determine when the cells were at anaphase.

B. Example of sister chromatid behavior in fixed cells. In (1) both of the sister chromatids have gone to the same end of the spindle, in (2) there has been no separation and both sister chromatids have remained in the centre of the spindle, in (3) the sister chromatids have become separated at one end of the spindle, in (4) the sister chromatids have gone to opposite ends of the spindle and in (5) the sister chromatids have become separated in the middle of the spindle. Strains used were wild type (Y5398), *smc5* (Y5419) and *nse4* (Y5399). Experiments 175, 176 and 183.

C. Proportion of cells that display the variety of forms of sister chromatid segregation displayed in B at anaphase I. (n = No. of cells) Only spindles that were longer than 2.5 μm were analysed. In wild type the sister chromatids were found at the same end of the spindle in 93% of cells analysed and in the middle of the spindle in 7% of cells analysed. In *smc5* the sister chromatids were found at the same end of the spindle in 93% of cells analysed ($p > 0.05$), in the middle of the spindle in 6% of cells analysed ($p > 0.05$) and at opposite ends of the spindle in 1% of cells analysed ($p > 0.05$). In the *nse4* mutant sister chromatids were found at the same end of the spindle in 71% of the cells analysed ($p < 0.05$), in the middle of the spindle in 4% of the cells ($p > 0.05$), at the same end of the spindle in 2% of cells ($p > 0.05$) and at either end of the spindle in 4% of cells ($p > 0.05$).

length) and the sister chromatid separation was classified (Figure 3.10B). Spindle length was used as a rough guide of the cell stage. Cdc14 was not used, as it could not be visualised in the spreads. I observed in wild type that 93% of the cells displayed sister chromatids at the same end of the spindle at anaphase (n=86). This was reduced slightly in *smc5* (92% - n=94, t-test $p>0.05$) but more significantly in *nse4* (71% n=92, t-test $p<0.05$). The proportion of cells displaying sister chromatids joined in the middle of the spindle was significantly lower in wild type (7%) compared to *nse4* (21%, t-test $p<0.05$). I did not detect any sister chromatids that were separated in the wild type (n = 86). 1% of the *smc5* cells displayed separated sister chromatids at one end of the spindle. This was increased in *nse4* with 8% of the cells displaying separated sister chromatids (3% separated sister chromatids at one end of the spindle, 2% sister chromatids at either end of the spindle, 2% sister chromatids separated in the middle of the spindle) (t-test $p<0.05$). This indicates that precocious sister chromatid separation is significantly increased in *nse4* compared to wild type but not detectably changed in *smc5* compared to wild type.

3.3.6.2 Low levels of sister kinetochore separation were observed in live cells from *smc5* and *nse4* mutants

As fixed cells only show a snapshot, time-lapse imaging was used to examine sister kinetochore separation in *nse4* compared to wild type. To do this Cnm67-mCherry and Pds1-tdTomato were incorporated into the TetO-TetR strain used previously to monitor cell cycle progression (Section 2.2.5.3). Using the time of Pds1-tdTomato loss and Cnm67-mCherry maximum elongation, the time of anaphase could be accurately determined. TetR-GFP association with the Cnm67 foci was used to determine sister chromatid segregation at meiosis I (Figure 3.11). If only one GFP focus was observed and it was found at the same pole as one of the Cnm67 foci at anaphase then this indicated that the sisters had segregated together (Figure 3.11A). If only one GFP focus was observed in the centre of the separated Cnm67 foci this indicated that sister chromatids had remained together and not segregated during anaphase (Figure 3.11B). If two GFP foci were observed at the same pole as one of the Cnm67 foci then this

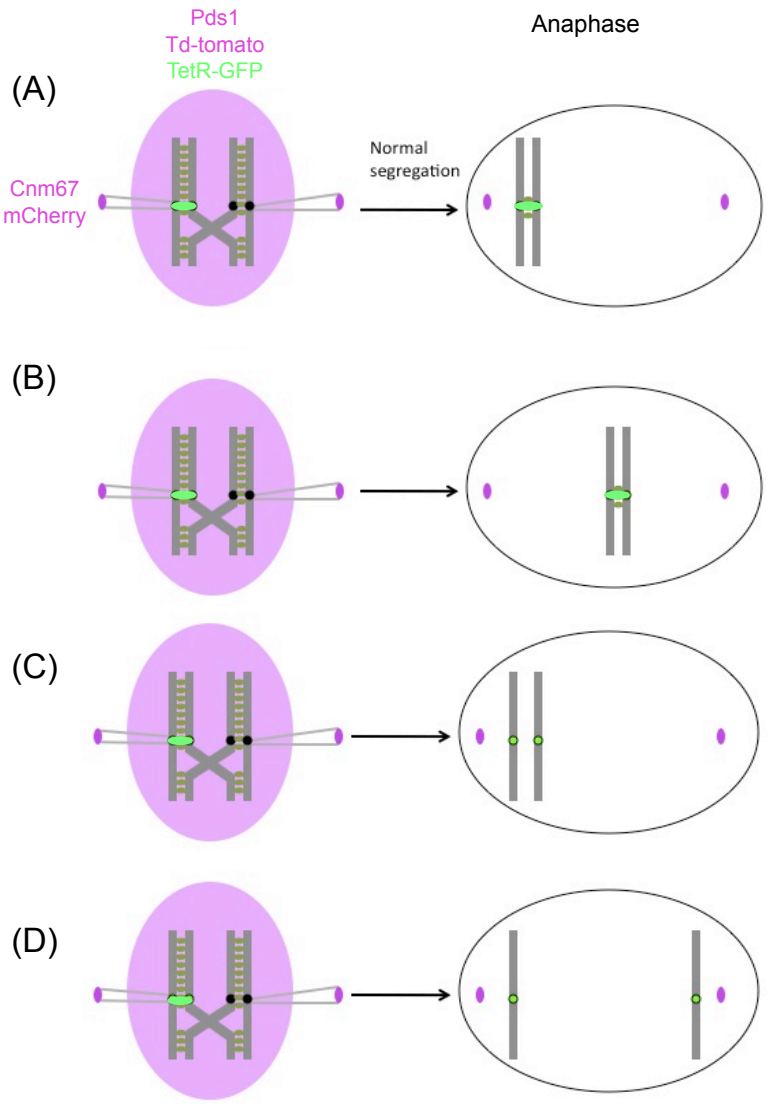
Pds1
Td-tomato
TetR-GFP
Anaphase
(A)
Cnm67
mCherry
Normal
segregation
(B)
(C)
(D)

Figure 3.11 – Cartoon of sister kinetochore separation analysis (live cell)

Cartoons demonstrating the binding of tetR-GFP to tetO repeats which are inserted 1.5kb from *CEN5*. In each case only one of the homologues contains the tetO-*CEN5* insertion and tetR is constitutively expressed.

A) Demonstrates sister chromatid co-segregation at anaphase I

B) Demonstrates sister chromatids in the middle of the Cnm67 foci at anaphase I

C) Demonstrates sisters chromatids at the same pole but displaying separated tetR-GFP at anaphase I

D) Demonstrates sister chromatids at opposite poles of the cell at anaphase I

(A)

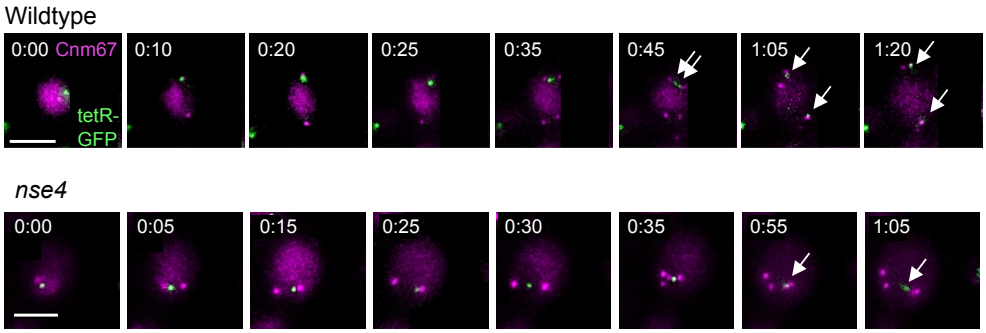
Wildtype
0:00 Cnm67
tetR-GFP
0:10
0:20
0:25
0:35
0:45
1:05
1:20
nse4
0:00
0:05
0:15
0:25
0:30
0:35
0:55
1:05

(B)

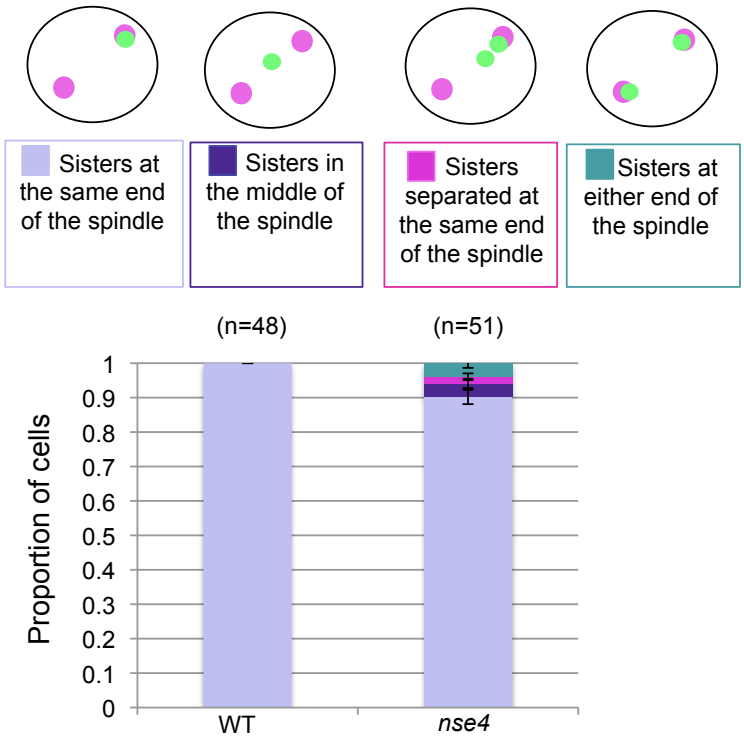
Sisters at the same end of the spindle
Sisters in the middle of the spindle
Sisters separated at the same end of the spindle
Sisters at either end of the spindle
(n=48)
(n=51)
Proportion of cells
1
0.9
0.8
0.7
0.6
0.5
0.4
0.3
0.2
0.1
0
WT
nse4

Figure 3.12 –Sister kinetochore separation is slightly increased in *nse4* mutants (live cell)

A. Live cell imaging montage of wild type (Y5398) and *nse4* (Y5399) strains containing tetR-GFP, mCherry tagged Cnm67 and td-tomato tagged Pds1 to look at precocious sister chromatid separation over real time. Scale bar 5 μm.

B. Graph demonstrating the proportion of cells that display the variety of forms of sister chromatid segregation displayed in Figure 3.11 at anaphase I. (n = No. of cells) In wild type the sister chromatids were found together at the same end of the spindle in all cells analysed. In the *nse4* mutant sister chromatids were found together at the same end of the spindle in 90% of the cells analysed ($p < 0.05$), in the middle of the spindle in 4% of the cells ($p > 0.05$), at the same end of the spindle in 2% of cells ($p > 0.05$) and at either end of the spindle in 4% of cells ($p > 0.05$). Experiments 164 and 165.

indicated that the sister chromatids had separated to the same pole but away from one another (Figure 3.11C). In this case it is unknown if the sister chromatids separated from one another before or after segregation at anaphase. If two GFP foci were observed at opposite poles of the cell then this indicated that the sister chromatids had precociously segregated at anaphase (Figure 3.11D).

I found that 100% (n = 48) of wild type cells displayed sister chromatids joined at the same end of the spindle (judged via Cnm67 maximum separation; Figure 3.12A). Precocious sister chromatid separation was significantly higher in *nse4* cells (6% - n=51, t-test $p<0.05$). 2% had separated at the same end of the spindle and 4% separated to opposite ends of the spindle (Figure 3.12B). I also observed that 4% of *nse4* cells at anaphase displayed sister chromatids joined at the centre of the spindle. This is significantly lower than what was seen in the fixed cell analysis. This indicates that many of the fixed cells analysed previously, that displayed both sister chromatids in the centre of the spindle, may not have been at late anaphase and were instead likely to have been at late metaphase. This was further supported by the observation that, in some cases, in both *smc5* and *nse4* the chromosomes did not segregate until very late anaphase despite the spindles significantly elongating prior to this.

3.3.7 Precocious sister chromatid separation levels are the same in both wild type and *nse4* when Mam1 is deleted

The percentage of cells that displayed precocious sister chromatid separation in *nse4* (6%) was found to be significantly lower than the percentage of *nse4* cells that displayed a loss of centromeric Rec8 (51%, T-test $P<0.05$). This difference was hypothesized to be due to the presence of functional Mam1 which acts to mono-orientate the sister chromatids in meiosis I (Toth et al, 2000). The finding that sister chromatids only segregated equatorially in 6% cells in which Sgo1 was depleted (when centromeric Rec8 was no longer protected from seperase) supports this hypothesis (Katis et al, 2004).

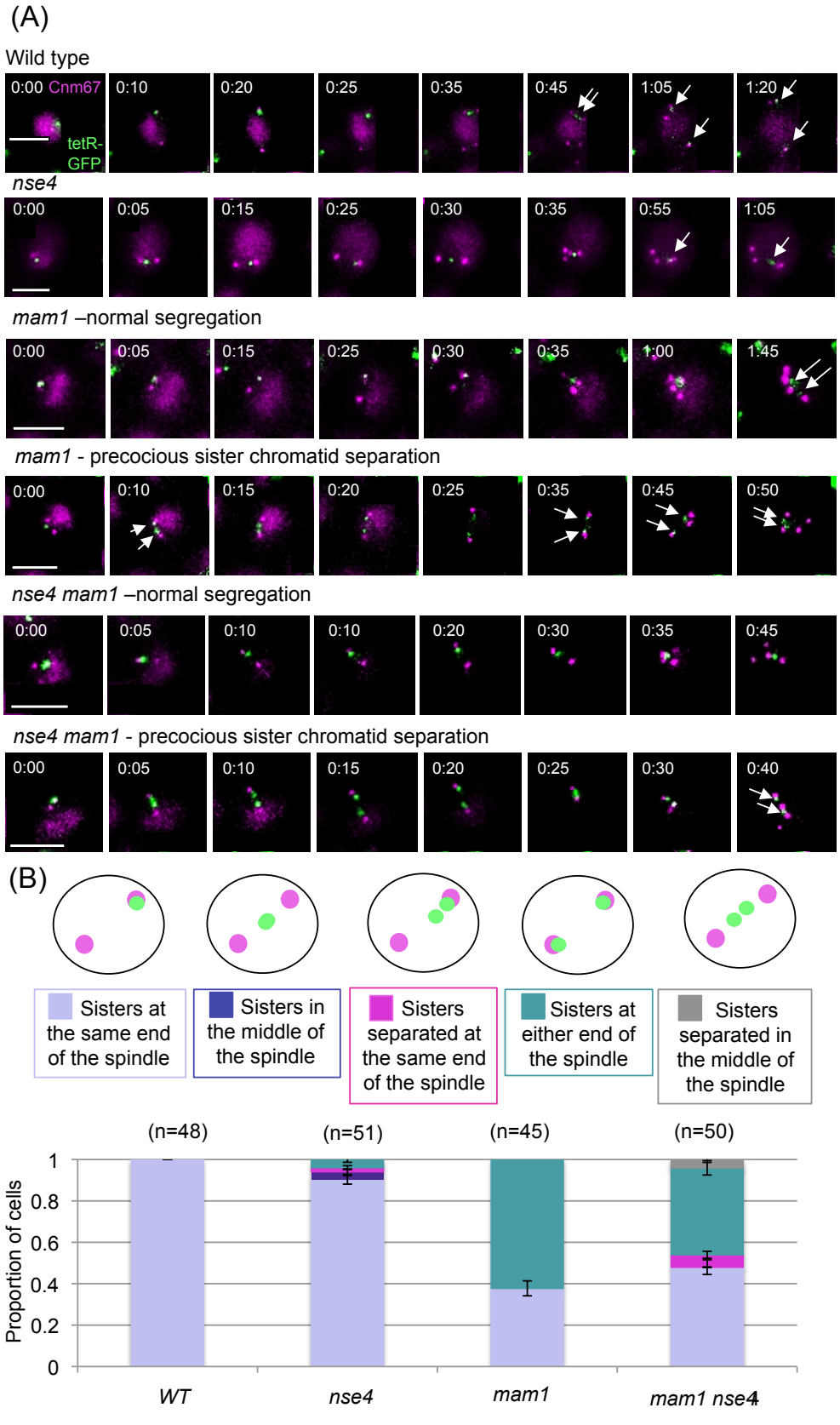
(A)
Wild type
0:00 Cnm67
tetR-GFP
0:10
0:20
0:25
0:35
0:45
1:05
1:20
nse4
0:00
0:05
0:15
0:25
0:30
0:35
0:55
1:05
mam1 –normal segregation
0:00
0:05
0:15
0:25
0:30
0:35
1:00
1:45
mam1 - precocious sister chromatid separation
0:00
0:10
0:15
0:20
0:25
0:35
0:45
0:50
nse4 mam1 –normal segregation
0:00
0:05
0:10
0:10
0:20
0:30
0:35
0:45
nse4 mam1 - precocious sister chromatid separation
0:00
0:05
0:10
0:15
0:20
0:25
0:30
0:40
(B)
Sisters at the same end of the spindle
Sisters in the middle of the spindle
Sisters separated at the same end of the spindle
Sisters at either end of the spindle
Sisters separated in the middle of the spindle
(n=48)
(n=51)
(n=45)
(n=50)
Proportion of cells
1
0.8
0.6
0.4
0.2
0
WT
nse4
mam1
mam1 nse4

Figure 3.13 – Sister kinetochore separation is not increased in *nse4 mam1* double mutants

A. Live cell imaging montage of *mam1* (Y5671) and *mam1 nse4* (Y5665) strains containing tetR-GFP, mCherry tagged Cnm67 and td-tomato tagged Pds1 to look at precocious sister chromatid separation over real time. Scale bar 5 μm. Arrows distinguish Cnm67 foci. Experiments 247 and 252.

B. Proportion of cells that display the variety of forms of sister chromatid segregation at anaphase I. (n = No. of cells). In *mam1* the sister chromatids were found at the same end of the spindle in 38% of cells analysed and at opposite ends of the spindle in 62% of cells analysed. In the *mam1 nse4* mutant sister chromatids were found together at the same end of the spindle in 46% of the cells analysed ($p > 0.05$), separated in the middle of the spindle in 4% of the cells ($p > 0.05$), separated at the same end of the spindle in 6% of cells ($p > 0.05$) and at either end of the spindle in 44% of cells ($p > 0.05$).

Toth et al (2000) found that a large proportion of the sister chromatids segregated equatorially when Mam1 was deleted (despite the presence of sister chromatid cohesion). Furthermore they found, in a strain depleted of Mam1 also containing the mitotic cohesin Scc1 under the Rec8 promoter (centromeric cohesin would not be protected), that the sister chromatids segregated equatorially rather than reductionally. If Mam1 juxtaposes the two sister kinetochores, then deletion of Mam1 should allow sister chromatids that are not connected by centromeric Rec8, in *smc5* and *nse4,* to segregate equatorially rather than reductionally. To test this prediction I deleted both Mam1 and Nse4 in a strain containing the TetO-TetR system and Cnm67-mCherry. The cells were imaged from prophase to metaphase II (Section 2.2.5.3). I found that the sister chromatids separated in 62% of *mam1* cells (all to opposite ends of the spindle) and 52% of *nse4 mam1* cells (42% at either end of the spindle, 4% separated in the middle of the spindle and 6% separated at the same pole) (T-test $p>0.05$). (Figure 3.13B) This indicated that some of the sister chromatids were being held together in the *nse4 mam1* cells. I infer that retained arm cohesin or joint molecules impede sister chromatid segregation in *nse4 mam1* mutants (Copsey et al, 2013; see Discussion).

3.4 Discussion

In this work, I set out to investigate the role of the Smc5/6 complex in meiosis, specifically how its depletion affects chromosome segregation and cohesin regulation. This was investigated in real time, through live cell imaging, in order to examine how the chromosome dynamics, spindle dynamics and cohesin regulation interact to cause meiotic catastrophe, when components of the Smc5/6 complex are depleted. Severe spindle elongation and chromosome segregation defects were observed in both *smc5* and *nse4*. Given that the defects were dependent upon the endonucleolytic activity of Spo11, I propose that the defects observed in the spindle dynamics of both the *smc5* and *nse4* strains are downstream effects of the inability to remove joint molecules. Spindle elongation has been found to be a very sensitive output for the joint molecule defect in *smc5/6* mutants (as *nse4* has a much more severe joint molecule defect than *smc5*

and corresponding shorter spindles). In the *smc5* mutant joint molecules accumulated to 4.7% of the DNA signal and in *nse4* they were found to accumulate to 10% of the DNA signal, compared to 3% seen in wild type (Copsey et al, 2013). This difference between the mutants is thought to be due to differences in the depletion levels.

I also questioned if the retention of cohesin observed in the *smc5/6* mutants was dependent on the induction of meiotic recombination. In attempt to determine this, the *spo11-Y135F* mutation was incorporated into the strains containing GFP tagged Rec8 and mCherry tagged Cnm67 and Pds1. It was found that the time of Rec8 retention could not be determined in these strains. This was due to the very high levels of Pds1 present (as Pds1 was not lost before DNA segregation as it is when spo11 is functional), which meant that the time of spindle pole body separation could not be accurately assessed. In order to accurately assess if the retention of cohesin is dependent on the induction of meiotic recombination td-tomato tagged Pds1 would need to be removed and the time from spindle pole body separation to Rec8 loss examined.

As it has been found in *S. pombe* mitosis that the defects in chromosome segregation in *smc5/6* mutants can be resolved through cleavage of arm cohesin I tested if the situation was the same in *S. cerevisiae* meiosis (Outwin et al, 2009). In order to determine this a TEV protease site was incorporated within Rec8, meaning that Rec8 could be artificially cleaved at anaphase. Interestingly the artificial cleavage of Rec8 at anaphase only provided a small improvement to chromosome segregation in both *smc5* and *nse4* (Chi-ho Chan), contrasting to what has been seen in *S. pombe* mitosis (Outwin et al, 2009; Tapia-Alveal et al, 2014; Lin et al, 2016). This indicates that the retention of cohesin only provides a small contribution towards the meiotic catastrophe observed in the *smc5/6* mutants in *S. cerevisiae*. The major contributor is likely to be the accumulation of joint molecules. In *S. pombe* it was found that over-expression of seperase was able to overcome the segregation defects observed in *smc5/6* mutants indicating that the *smc5/6* mutants specifically had defects in their prophase pathway (Outwin et al, 2009). As the potential retention of Rec8 was only found to provide

a slight contribution to the meiotic catastrophe observed in *smc5/6* mutants I hypothesise that the Smc5/6 complex plays a less central role in arm cohesin removal in *S. cerevisiae,* likely due to the absence of a prophase pathway.

I observed that there was a reduction of centromeric cohesin in both *smc5* and *nse4*. Shugoshin localisation appeared to be unaffected in both of the mutants and the levels of precocious sister chromatid separation were found to be significantly lower than would be expected if the chromosomes that displayed a loss of Rec8 were not held together. I hypothesized this was due to the presence of functional Mam1. Interestingly the levels of precocious sister chromatid separation were slightly higher in the *mam1* mutant that in the *nse4 mam1* double mutant. This is likely to be due to the presence of retained arm cohesin or joint molecules in *nse4 mam1* double mutants preventing the separation of sister chromatids that would normally segregate in *mam1*. In order to determine if mis-regulation of cohesin removal is causing the precocious sister chromatid separation in the *smc5/6* mutants, the *spo11-Y135F* mutation should be introduced into the *mam1 nse4* mutant. As meiotic recombination would not take place, in this situation the only factor holding the sister chromatids together at anaphase would be cohesin. This experiment however would not allow a distinction between retention of arm cohesin and precocious loss of centromeric cohesin. In order to investigate this further the time of centromeric cohesin loss would need to be assayed. Only loss before anaphase would be expected to cause precocious sister chromatid separation.

One possible connect between recombination and cohesin loss at centromeres is that cohesin is removed around the site of DSBs, in order to facilitate their repair. This raises the possibility that removal of cohesin associated with DSB repair near the centromere may cause the reduction of centromeric cohesin observed in *smc5* and *nse4* (McAleenan et al, 2013). In order to determine if recombination is taking place near the centromeres in *smc5* and *nse4*, DSB levels should be examined at the centromeres during prophase using ChIP-seq analysis at the centromere. Their localization could then be compared to the Rec8 binding profile. Alternatively it is possible that the Smc5/6 complex has a role in

organizing the peri- and centromeric regions so that cohesin can be loaded. In fission yeast the binding of cohesin at the pericentromere is heterochromatin dependent (Bernard et al, 2001; Nonaka et al. 2002). It is therefore possible that the Smc5/6 complex arranges the heterochromatin so that centromeric cohesin can be loaded. In chromosome spreads of *smc6-56*, analyzed through the use of light microscopy, the cohesin complex is observed to localize to the full length of the chromosomes (Lilienthal et al, 2013). Small differences in fluorescence levels are unlikely to be able to be visualized through the use of normal light microscopy. In order to accurately determine if there are defects in cohesin loading at the centromeres photo-activated light microscopy (PALM) could be used. This would provide an accurate assessment of the cohesin levels at the centromeres, compared to the chromosome arms, in the *Smc5/6* mutants. Super resolution microscopy could also be used to determine if DSB are occurring at the centromeres in budding yeast and if so if this causes a corresponding loss of centromeric Rec8.

The levels of sister chromatid separation observed in the live cell imaging here contrast to what has been seen previously in fixed cells (Copsey et al, 2013). Previously the levels of sister chromatid separation found were significantly higher (*smc5* – 38% and *nse4* – 39%, Supplementary figure 2; Copsey et al, 2013). The main difference between the previous and these studies is that previously only long spindles (4 um or longer) were assessed. Very few *smc5* and nse4 cells reach that length. In either case the studies indicate, Smc5/6 regulates the cohesin association with chromosomes, possibly in response to recombination. Furthermore, these studies suggest that there are severe implications for spindle and chromosome dynamics when joint molecules persist.

Chapter 4 – Investigating the effect of the haploinsufficiency of SMC6 on mammalian meiosis

4.1 Introduction

Much knowledge has been gained by studying the role of the Smc5/6 complex in mitosis and meiosis in the last decade from work in model organisms such as *S.cerevisiae*, *S.pombe* and *Drosophila melanogaster*; however, little is known about the role of the Smc5/6 complex in mammals. Interestingly the Smc5/6 complex has been found to be essential in fission yeast, budding yeast and mice, but is dispensable for viability in chicken DT40 cells, Drosophila, and *C. elegans* (Hirano et al, 2002; Lehmann et al, 1995; Stephan et al, 2011; Ju et al, 2013; Li et al, 2013). Most of the studies examining the role of the Smc5/6 complex in mammals have used siRNA depletion of specific subunits. Initial siRNA studies found the Smc5/6 complex was not essential in human cells (Potts and Yu, 2005; Potts et al, 2006; Potts et al, 2007). However the siRNA depletion is never 100% and therefore phenotypes caused by total loss of the protein will not be discovered using this method.

In order to assess the role of the Smc5/6 complex in a mammalian system Ju *et al* (2013) used a mouse containing a gene trap in intron 6 of *Smc6* ($Smc6^{GT}$), which disrupted the formation of functional protein after exon 6 (Ju et al, 2013, Figure 4.1A). The fragment produced was modeled using Phyre[2] and was found to contain the majority of the N-terminal lobe of Smc6 (a head domain), but not any of the exiting coiled coil (Figure 4.1B). Studies in yeast found that Smc6 binds to Nse4 via its coiled coil rather than the head domain, suggesting that the fragment produced when a gene trap is inserted in intron 6 will not bind to the Smc5/6 complex (Antony Oliver, personal communication). Depletion of Smc5 also decreases Smc6 levels, suggesting that the constituent proteins are stabilized as part of the Smc5/6 complex (Pryzhkova et al, 2016). This therefore suggests that the

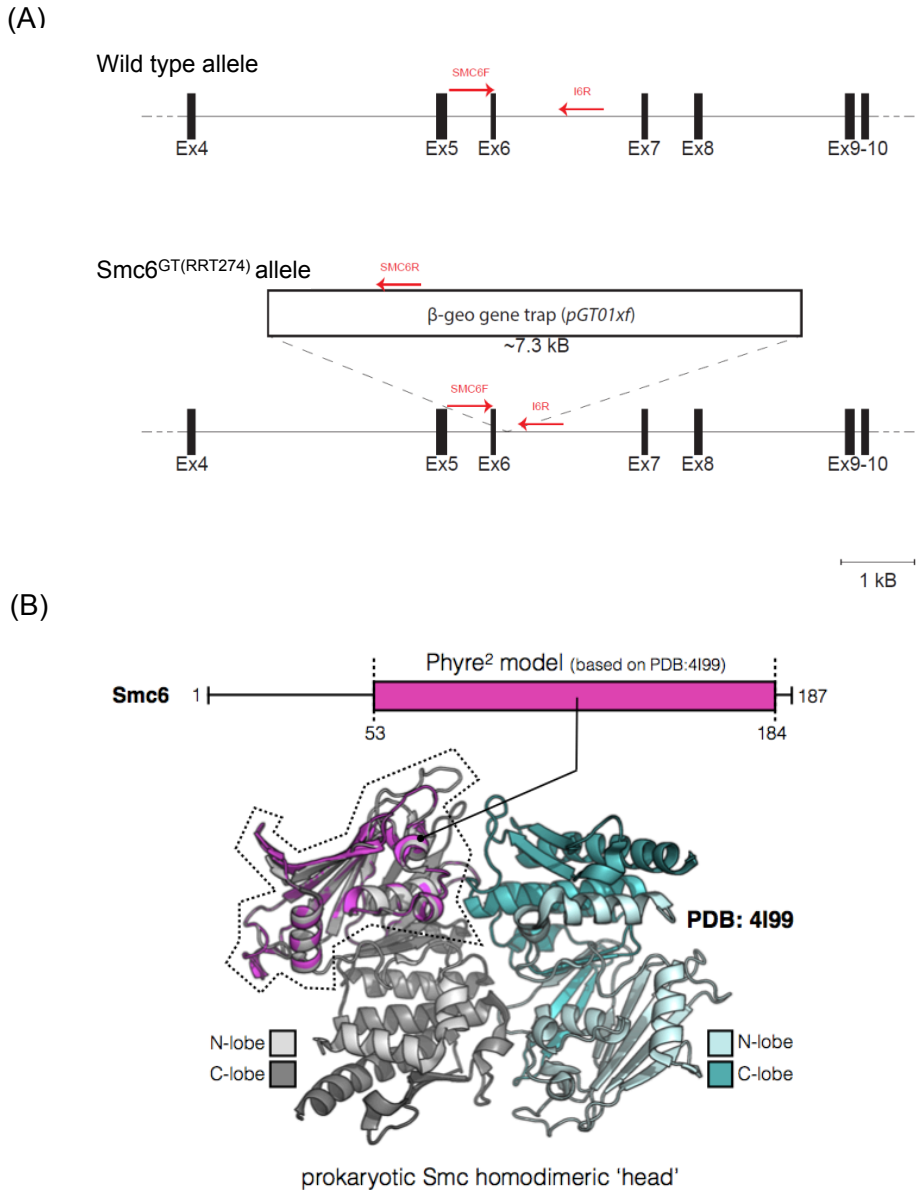

Figure 4.1 – Addition of an exon trap into intron 6 of Smc6 produces a fragment that cannot form part of the Smc5/6 complex

A. A strain was obtained from BayGenomics (SMC6$^{GT(RRT274)}$) that contained an exon trap (*pGT01xf* containing splice acceptor site, a reporter gene (β-geo) and a polyadenylation sequence) in intron 6 of Smc6. The introduction of the exon trap means that only a very small fragment of Smc6 (187 amino acids) is produced. Red arrows indicate the primers used for genotyping (Alex Widger).

B. Diagram of the Phyre2 model produced when the 187 amino acid fragment of Smc6 is modeled. Amino acid 1-187 encode most of the N-terminal load (Smc6 head domain). They do not encode any of the exiting coiled coil which has found to be the part of Smc6 that binds to Nse4 (Personal communication Antony Oliver).

truncated Smc6, generated from the gene trap, renders the Smc5/6 complex non-functional.

When heterozygous *Smc6*$^{+/GT}$ females and males were mated, no homozygotes were obtained (Figure 4.2A). From 25 matings, only 53 wild type mice and 83 heterozygous mice were obtained, which was not dissimilar from the predicted Mendelian ratio values of 45.3 and 90.6. As no *Smc6*$^{GT/GT}$ embryos were observed, this indicates that embryos homozygous for the *Smc6* gene trap fail to implant, most likely due to embryonic lethality because Smc5/6 is essential. Similar phenotypes have been observed in other Smc5/6 homozygous mutants. Homozygous mutations in both Smc5 and Nsmce2 have been reported to cause embryonic lethality (Jacome et al, 2015; Hwang et al, 2017). It is predicted that this is due to a failure of the homozygous embryos to implant.

Analysis of the embryos from the heterozygote crosses at E9.5 (around half way through mouse embryonic development) revealed that some of the embryos appeared abnormally small and poorly developed (Figure 4.2B; Ju et al, 2013). These were then often reabsorbed by day E10.5. Genotyping revealed that none of the abnormal embryos at E9.5 were homozygous *Smc6*$^{GT/GT}$, but were either wild type or *Smc6*$^{+/GT}$ (Figure 4.2A). This indicates that it is not the genotype of the embryo that caused abnormalities and embryo loss (Ju et al, 2013).

The *Smc6*$^{+/GT}$ mice showed no abnormal phenotypes. The only difference to wild type found was in the size of the litters that the mice produced. Preliminary data suggested that the heterozygous mice produced slightly reduced litter sizes compared to wild type (Figure 4.2C, Personal communication Alan Lehmann). There are several potential explanations as to why embryo loss at E9.5 and the correspondingly reduced litter sizes were observed in *Smc6*$^{+/GT}$ mice. Firstly, *Smc6*$^{GT/GT}$ embryos in the womb could affect the development of the other embryos. This however is unlikely as when an *Smc6*$^{+/GT}$ female mouse is mated with a wild type male

(A)

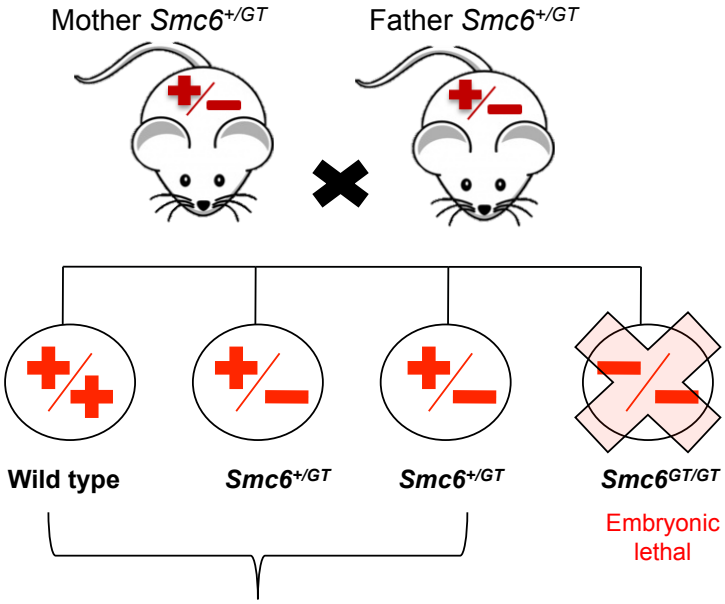

(B)

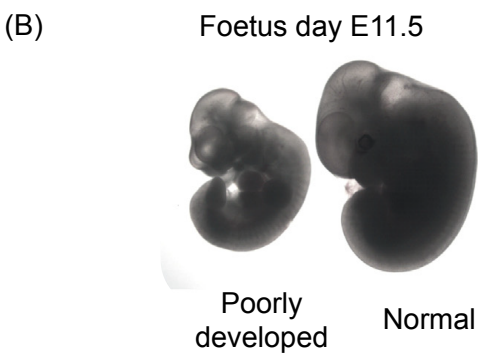

(Ju et al, 2013)

(C)

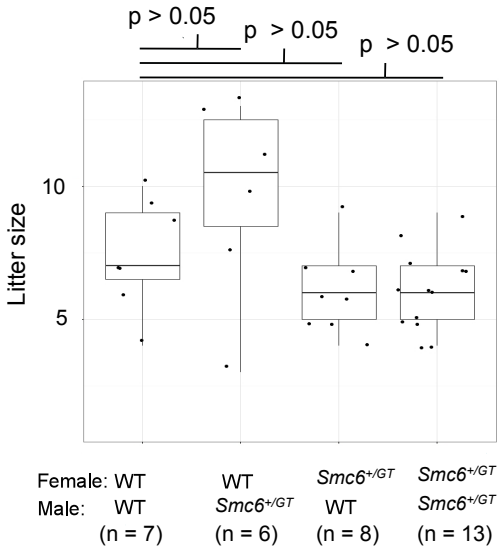

Figure 4.2 – Female meiosis is affected in the *Smc6$^{+/GT}$* mouse

A. Diagram demonstrating the reproductive outcomes when two *Smc6$^{GT/+}$* mice are crossed. Both wildtype and *Smc6$^{+/GT}$* offspring were produced. No *Smc6$^{GT/GT}$* offspring were produced indicating that mice *Smc6$^{GT/GT}$* are embryonic lethal. Some of the embryos appeared abnormal (Figure 3.1B). When genotyped it was found that the abnormal embryos were equally as likely to be either wild type or *Smc6$^{+/GT}$*.

B. Images of the poorly developed 'abnormal' mouse embryo compared to a normal mouse embryo at day E9.5. By day 10.5 these abnormal embryos were often re-absorbed (Ju et al, 2013).

C. Boxplot demonstrating the variation in litter sizes for crosses of wild type × wild type, *Smc6$^{+/GT}$* (female) × wild type (male), *Smc6$^{+/GT}$* (male) × wild type (female) and *Smc6$^{+/GT}$* × *Smc6$^{+/GT}$*. (n denotes the number of litters) (Personal communication, Alan Lehmann)

mouse reduced litter sizes were still observed and in this situation no *Smc6*$^{GT/GT}$ embryos are produced (Figure 4.2A). Secondly, embryonic development is affected in the uterus of the *Smc6*$^{+/GT}$ mother (Ju et al, 2013). Although I cannot rule out the possibilities suggested by Ju *et al* (2013) to account for the embryo loss, I considered a different possibility, namely that the *Smc6*$^{+/GT}$ mother is producing aneuploidy oocytes. I hypothesized this could be the case, because embryos were commonly lost from the *Smc6*$^{+/GT}$ mice at day E10.5, when embryos are commonly lost due to aneuploidy in mice (Inoue et al, 2007). This hypothesis is further supported by our knowledge that the Smc5/6 complex affects chromosome structure, chromosome segregation and recombination in yeast meiosis (Copsey et al, 2013). If correct, this would imply Smc5/6 is haploinsufficient for aneuploidy and may be relevant as a model for human females.

In this study, I utilized molecular and cytogenetic methodologies to determine the potential causes for embryo loss in heterozygous *Smc6*$^{+/GT}$ female mice. Metaphase II (MII) and metaphase I (MI) oocytes from these animals were spread in order to investigate aneuploidy levels and how chromosome cohesion and compaction is affected, respectively. I found that the size of the litters produced, from the *Smc6*$^{+/GT}$ mice, were reduced compared to wild type. This was only observed from *Smc6*$^{+/GT}$ X *Smc6*$^{+/+}$ crosses with a female heterozygote and not in the reciprocal cross. Subsequent analysis of MII oocyte chromosome spreads, from the *Smc6*$^{+/GT}$ mice, found they contained significantly higher levels of aneuploidy than observed in wild type. Chromosome cohesion was also observed to be reduced. I also observed that chromosome structure was significantly different in the *Smc6*$^{+/GT}$ oocytes, indicating it is possible chromosome condensation is also affected in the oocytes from the *Smc6*$^{+/GT}$ mouse.

4.2 Materials and methods

4.2.1 Ethics statement

All mice were bred at the University of Sussex under the home office license number PPL: 70 / 7007 (01-01-2010 - 21-01-2015) and PPL: 70/8300 (22-01-2015 - 28-01-2017).

4.2.2 Mouse colonies

RRT274 mice, containing an exon trap (which contained a splice acceptor site and a βgeo fusion gene) in intron 6, were originally obtained from Bay Genomics (Figure 4.1A). These were obtained as heterozygotes with a C57Bl6/129 background. Mouse mating's were carried out by Limei Ju. All mice used in experiments had been backcrossed to wildtype Black 6 six times and were four weeks of age.

4.2.3 Image J analysis

All of the images were deconvolved in order to restore out of focus light to its original position. This was carried out using SoftworX deconvolution. A mask was then made of the CREST signal. This was made by selecting the CREST channel and using the ImageJ plugin 'FindFoci GUI'. The 'FindFoci GUI' plugin identifies the peak intensity regions in the chosen image. A Gaussian blur is then adjusted in order to segment all of the CREST foci in the image. This produced an output in which every CREST focus was classified as an individual object. The plugin 'Mask Object Dimensions' was then used to identify the centre of each object in the image and calculate the distance from the centre of one object to the centre of the nearest object (Figure 4.10Aii) (Herbert et al, 2014).

4.3 Results

4.3.1 *Smc6*$^{+/GT}$ females produce reduced litter sizes compared to wild type

Smc6$^{+/GT}$ mice have been found to be healthy and have normal lifespan's. The only noticeable phenotype is that the female *Smc6*$^{+/GT}$ mice produced litters of a reduced size compared to wild type (Figure 4.2C, Alan Lehmann - personal communication). This finding was based on quite a small dataset, therefore, in order to test if the *Smc6*$^{+/GT}$ females litter sizes were significantly reduced compared to wild type the dataset was expanded. Four different mouse crosses were set up: 1 – wild type female (*Smc6*$^{+/+}$) X wild type male (*Smc6*$^{+/+}$); 2 – heterozygous female (*Smc6*$^{+/GT}$) X wild type male (*Smc6*$^{+/+}$); 3 – wild type female (*Smc6*$^{+/+}$) X heterozygous male (*Smc6*$^{+/GT}$) and 4 – heterozygous female (*Smc6*$^{+/GT}$) X heterozygous male (*Smc6*$^{+/GT}$).

Our analysis confirmed that the female *Smc6*$^{+/GT}$ X male *Smc6*$^{+/+}$ cross produced significantly reduced litter sizes compared to *Smc6*$^{+/+}$ X *Smc6*$^{+/+}$ (Wilcox test $P<0.05$, Power 1- β: 0.69; Figure 4.3). Interestingly the litter sizes were not reduced in female *Smc6*$^{+/+}$ X male *Smc6*$^{+/GT}$ crosses (Wilcox test $P>0.05$, Power 1- β: 0.2). This indicates that gene dosage only reduces the reproductive ability of females. The litter sizes were not significantly different between the female *Smc6*$^{+/GT}$ X male *Smc6*$^{+/+}$ and *Smc6*$^{+/GT}$ X *Smc6*$^{+/GT}$ crosses (Wilcox test $P> 0.05$, Power 1- β: 0.05). In *Smc6*$^{+/GT}$ X *Smc6*$^{+/GT}$ litters, homozygous offspring, which are embryonic lethal, are possible. This should lead to a reduction in the litter size compared to when only the female in the cross is *Smc6*$^{+/GT}$. However, as the litter size of the mice used in this study ranged from 1 to 12 with similar variation in litter sizes observed in both wild type and *Smc6*$^{+/GT}$, it is unlikely that this small reduction in litter size would be observed.

4.3.2 Chromosome errors are elevated in *Smc6*$^{+/GT}$ mouse MII oocytes.

Homologous chromosomes segregate during the first metaphase division of meiosis. If they segregate accurately then one homologous chromosome remains within the secondary oocyte and one is segregated to the polar body (Figure 4.4A). In some cases the homologous chromosomes do not

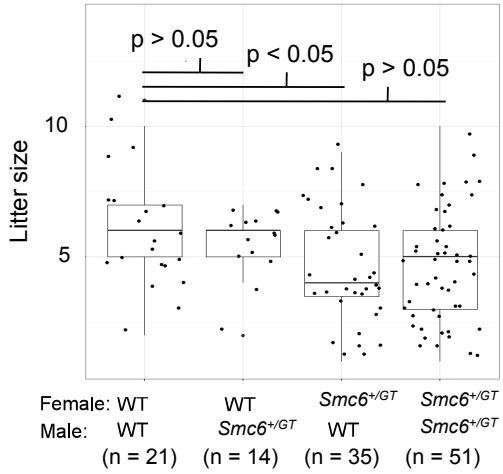

Figure 4.3 – *Smc6*$^{+/GT}$ females have reduced litter sizes compared to wild type

Continued litter size analysis from the mating's: wild type × wild type, *Smc6*$^{+/GT}$ (female) × wild type (male), *Smc6*$^{+/GT}$ (male) × wild type (female) and *Smc6*$^{+/GT}$ × *Smc6*$^{+/GT}$. The litter sizes from the wild type (male) × *Smc6*$^{+/GT}$ (female) and *Smc6*$^{+/GT}$ × *Smc6*$^{+/GT}$ were significantly reduced compared to wild type ($p<0.05$). (n denotes the number of litters) (Mouse experiments 1-20)

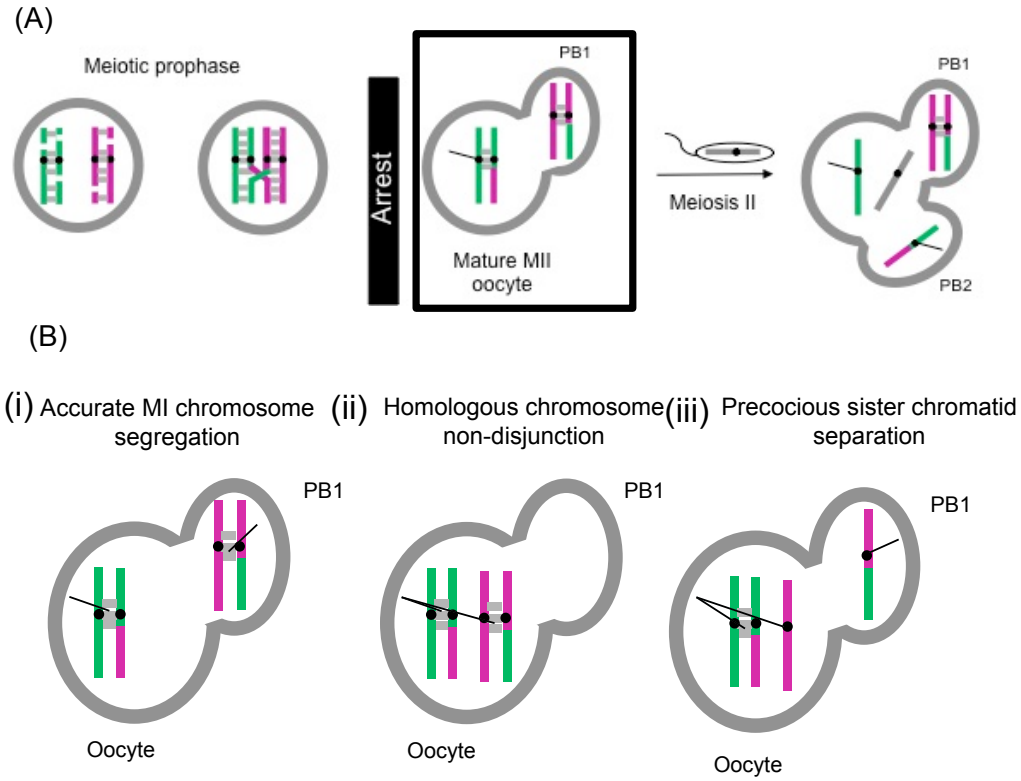

Figure 4.4 – Normal and abnormal chromosome segregation at meiosis I

A. Diagram of oogenisis where the end of meiosis I is highlighted with a box.

B. Diagrams demonstrating the different types of chromosome segregation that can take place at anaphase of meiosis I. If the chromosomes segregate accurately then one of the homologous chromosomes will be lost to the polar body and the other will remain in the secondary oocyte (i). Sometimes the homologous chromosomes do not segregate and so both end up in either the polar or the secondary oocyte (ii). This is known as homologous chromosome non- disjunction. There can also be precocious sister chromatid separation (iii). Here the sister chromatids prematurely separate and so one is lost to the polar body and the other remains in the secondary oocyte.

segregate and both remain in the secondary oocyte or are both lost to the polar body (Figure 4.4Bii), also known as meiosis I non-disjunction. There can also be instances when the sister chromatid precociously segregate at meiosis I, i.e. precocious sister chromatid separation (Figure 4.4Biii). To determine whether the oocytes from 4-week old *Smc6*$^{+/GT}$ mice were chromosomally normal, I analysed metaphase II (MII) oocytes, which have completed their first meiotic division and are arrested prior to the second meiotic division. To do this, the MII oocytes from the *Smc6*$^{+/GT}$ females were spread such that the chromosomes could be counted. The spreads were stained with DAPI to detect DNA and an antibody against CREST, which marks kinetochores before being visualised using light microscopy.

As the chromosomes in the oocyte spreads were often bunched, CREST foci rather than chromosome/chromatid number was counted. MII oocytes should contain 20 chromosomes, each consisting of two chromatids, thus each oocyte should display a total of 40 CREST foci (Figure 4.5Aii). In the wild type, 96% of the oocytes contained 40 CREST signals indicating that the chromosomes had segregated accurately. This was reduced to 67% in *Smc6*$^{+/GT}$ oocytes indicating that there was significant chromosome mis-segregation during meiosis I in the *Smc6*$^{+/GT}$ oocytes (Figure 4.5B). In the wild type, only 1% of the oocytes displayed the loss of a chromatid (39 centromere signals; Figure 4.5Aiii) and 3% of the oocytes displayed loss of a chromosome or two chromatids (38 centromere signals; Figure 4.5Aiv) (Figure 4.5C). In *Smc6*$^{+/GT}$ oocytes, 7% displayed the loss of a chromatid and 10% displayed loss of a chromosome or two chromatids. In *Smc6*$^{+/GT}$, 5% of the oocytes also displayed the loss of two chromosomes or four chromatids (36 centromere signals). A significant gain was also observed in *Smc6*$^{+/GT}$ oocytes, in which 7% displayed the gain of a chromatid (41 centromeric signals; Figure 4.5Av) and 5% displayed the gain of a chromosome or two chromatids (42 centromeric signals; Figure 4.5Avi). In one case it was also observed that there was the gain of 10 centromeric signals. In wild type, the gain of a chromosome or a chromatid was never observed.

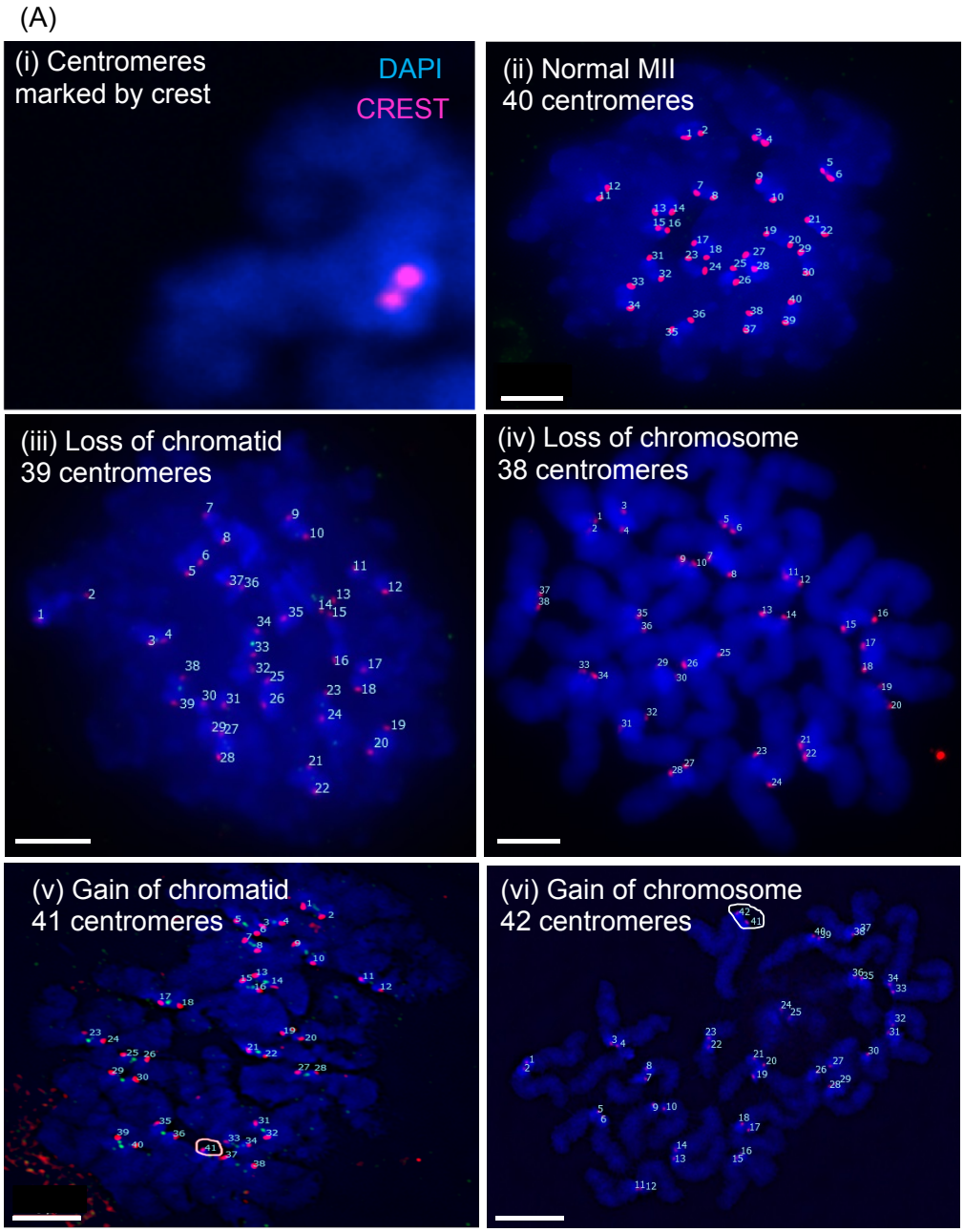
(A)
(i) Centromeres marked by crest
DAPI
CREST
(ii) Normal MII 40 centromeres
(iii) Loss of chromatid 39 centromeres
(iv) Loss of chromosome 38 centromeres
(v) Gain of chromatid 41 centromeres
(vi) Gain of chromosome 42 centromeres
(B)
Proportion of oocytes
100
80
60
40
20
0
WT
Smc6+/GT
Loss
Gain
Normal
(C)
Proportion of oocytes
25
20
15
10
5
0
WT
Smc6+/GT
Loss (-4)
Loss (-2)
Loss (-1)
Gain (+1)
Gain (+2)
Gain (+10)

Figure 4.5 – MII oocytes from the *Smc6*$^{+/GT}$ female display significant chromosome mis-segregation

A. Images of the different types of chromosome segregation observed in the oocytes from the *Smc6*$^{+/GT}$ mice. To determine the chromosome segregation that had taken place the centromeres were marked with CREST and the DNA was stained with DAPI (i). If the chromosomes have segregated accurately at meiosis I then you would expect to observe 20 chromosomes/ 40 centromeric CREST signals (ii). The loss of a centromeric CREST signal indicates that a chromatid has been lost (iii) and the loss of two centromeric CREST signals indicates that there has been the loss of a chromosome or two chromatids (iv). The gain of a centromeric CREST signal indicates that there has been the gain of a chromatid (v) and the gain of two centromeric CREST signals indicates that there has been the gain of a chromosome or two chromatids (vi).

B. Graph demonstrating the proportion of secondary oocytes from both wild type and *Smc6*$^{+/GT}$ that displayed normal or abnormal segregations at meiosis I. Here abnormal segregation was characterised as either displaying a loss (blue) or a gain (red) of centromeric CREST signals. (Mouse experiments 3, 4, 6, 9, 10, 11, 13)

C. Graph specifying the number of chromosomes lost (blue) or gained (red) in wild type and *Smc6*$^{+/GT}$ MII oocytes. (Mouse experiments 3, 4, 6, 9, 10, 11, 13)

It is possible that some of the loss observed in wild type was due to loss of chromosomes/chromatids in the spreading procedure. The finding that a significantly greater proportion of chromosomes were lost rather than gained in the oocytes from the *Smc6*$^{+/GT}$ mouse supports this hypothesis. However, the proportion of loss in *Smc6*$^{+/GT}$ was significantly higher than observed in wildtype indicating there is significant loss in *Smc6*$^{+/GT}$. This data demonstrates that there is significant mis-segregation in *Smc6*$^{+/GT}$ oocytes.

4.3.3 mFISH analysis of chromosomal content in MII oocytes from *Smc6*$^{+/GT}$ females

As I found significant aneuploidy in the MII oocytes from *Smc6*$^{+/GT}$ females, I addressed which chromosomes had mis-segregated. Were specific chromosomes such as the smaller chromosomes commonly mis-segregated or were the chromosomes that mis-segregated random? To address this mFISH was used. mFISH allows individual chromosomes in a chromosome spread to be identified by colouring each chromosome with a unique pattern of colours. mFISH staining and visualisation of the mFISH staining was initially optimised (Supplementary Figure 3 & 4; Section 2.2.5.4). The optimised staining conditions and the optimised emission settings were then used to determine which chromosomes/chromatids were lost and gained in some of the aneuploid oocyte spreads (Figure 4.6 & 4.7).

I also observed structural defects in some of the MII oocytes and employed mFISH to investigate which chromosomes were impacted. One of the MII oocytes from the *Smc6*$^{+/GT}$ mice had a gain of two lone chromatids (Figure 4.7A), which was particularly interesting, as one of did not appear to have a centromere (Figure 7Ai). I observed an extra centromere – denoted by a CREST focus surrounded by bright DNA signal (Figure 4.7Aii) – located with another chromosome on the spread, which was predicted to be its

(A)

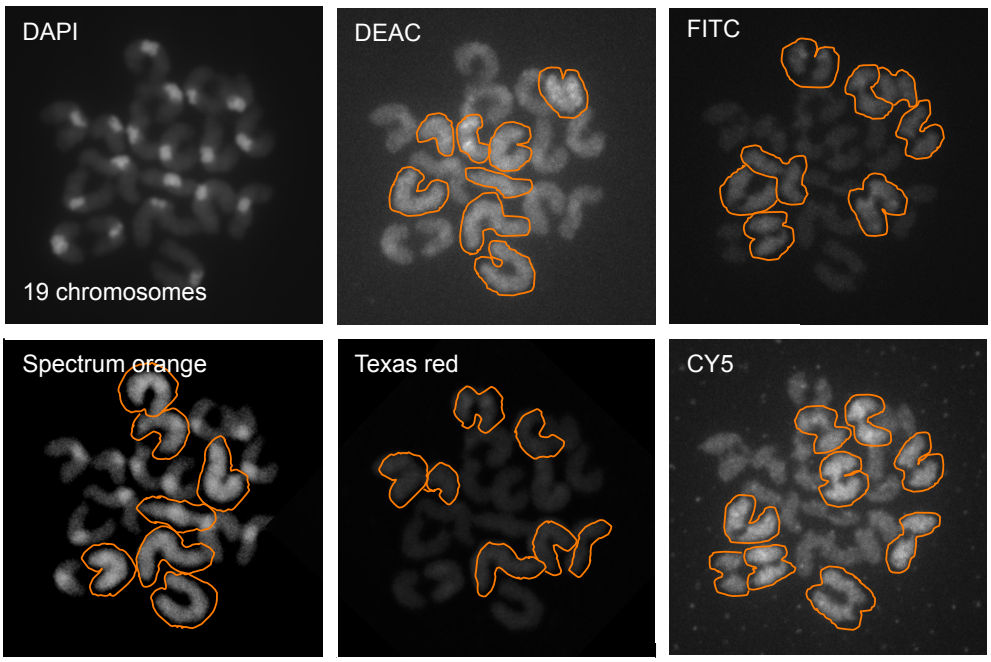

(B)

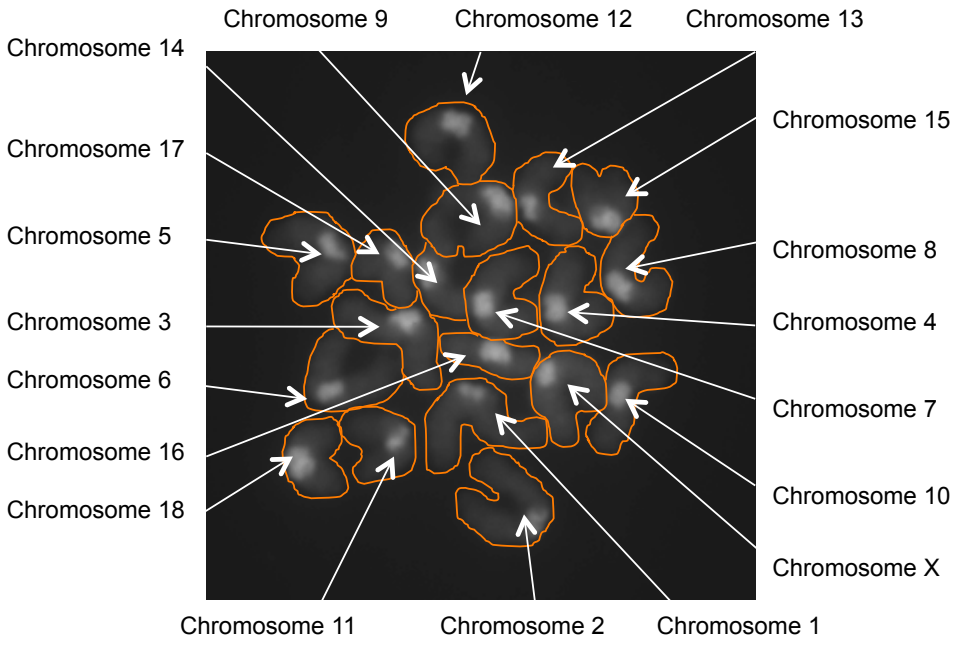

Chromosome 19 is missing

Figure 4.6 – mFISH staining of an MII oocyte spread missing a chromosome

A. Images produced on the Leica SP8 of an oocyte spread, displaying a lost chromosome, stained with Cytovision 21XMouse mFISH probes. The chromosomes that were fluorescent in each of the channels are outlined for clarity.

B. Diagram displaying the identity of each of the chromosomes in the chromosome spread. Chromosome 19 was identified as being the missing chromosome. (Experiment 210)

(A)

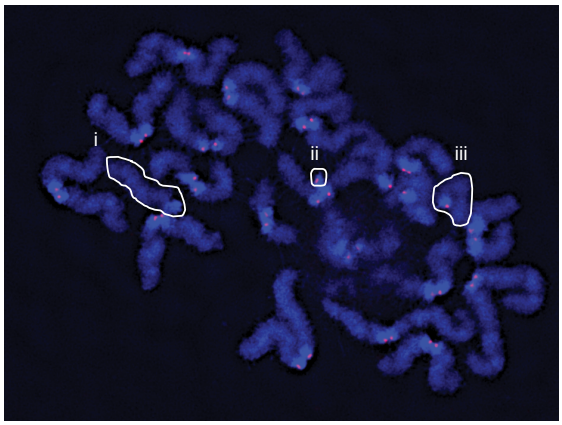

(B)

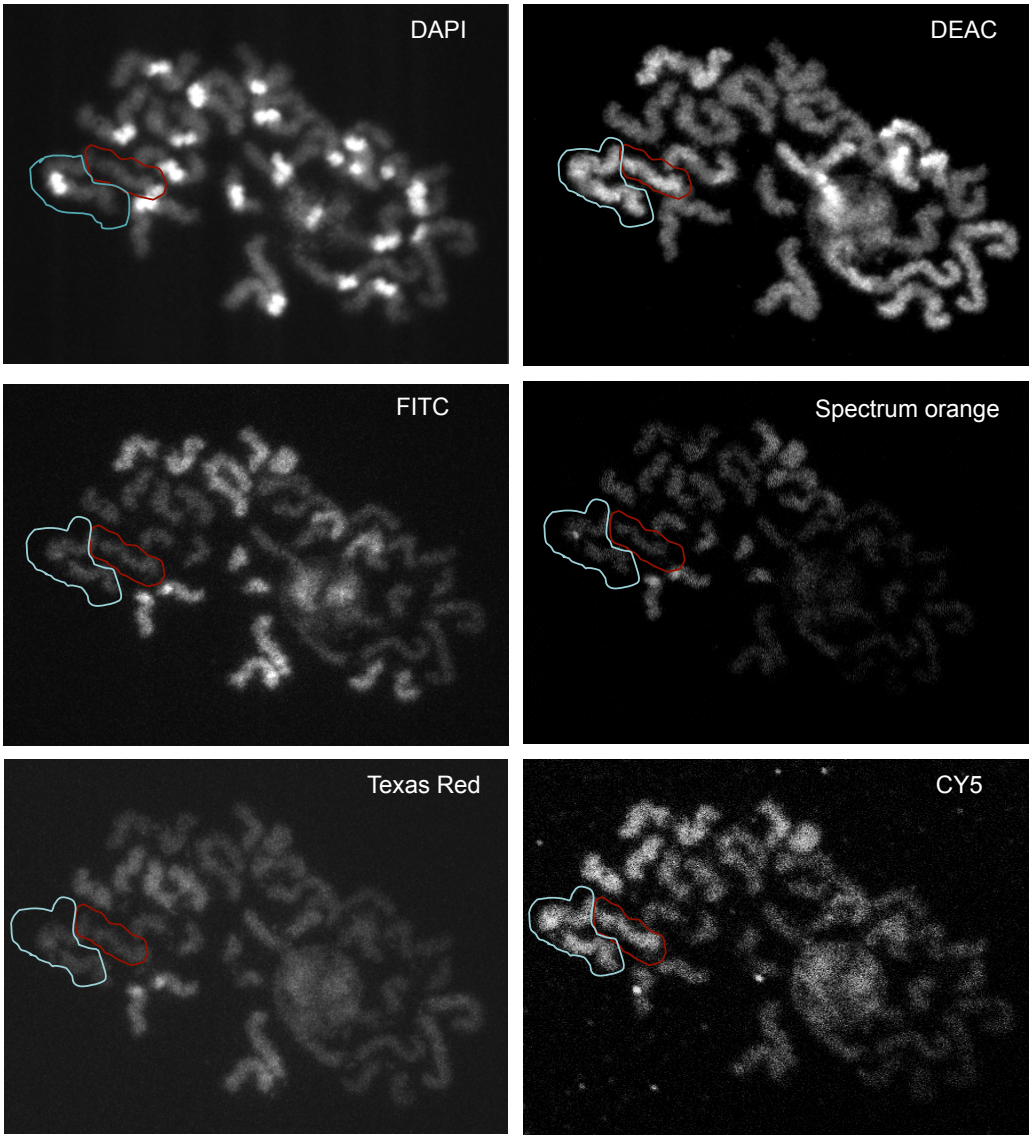

Figure 4.7 –mFISH of an MII oocyte spread containing a lone chromosome

A. Diagram outlining the lone chromosome (i) and what is predicted to be its centromere (ii) and missing chromatid (iii).

B. Images produced on the Leica SP8 of an oocyte spread, displaying a lone chromosome, stained with Cytovision 21XMouse mFISH probes. The lone chromosome is outlined in red in each of the channels and the chromosome that it appears to be joint to is outlined in light blue. It can be seen that both the chromatid and chromosome only display staining in DEAC and CY5 indicating that they are both chromosome 7. (Experiment 210)

corresponding homologous chromosome. Analysis by mFISH found that the lone chromatid was chromosome 7 and the chromosome next to it (possibly linked to the chromatid as the DAPI signals were overlapping) was also found to be chromosome 7. This indicates it is likely that there may have been an unresolved joint molecule between the homologous chromosomes that was not resolved and which lead to the chromatid breakage observed. mFISH was not able to determine if the extra centromere was in fact from chromosome 7 too. This is because the mFISH probes are not able to stain the centromeres, likely due to the high level of repetitive satellite DNA at the centromeres. It was also not possible to determine if the other lone chromatid (that appeared to lack a centromere) was also chromosome 7 due to deterioration at one end of the spread (Figure 4.7Aiii).

Many of the other chromosome spreads used in the aneuploidy analysis were very bunched and the chromosome numbers could not be assessed by distinguishing individual DAPI signals. For these spreads aneuploidy could only be assessed by counting the number of CREST foci. Additionally, individual chromosomes could not be accurately differentiated from one another using mFISH when the chromosomes were very bunched, as it was often difficult to tell how many chromosomes a fluorescent area corresponded to (Supplementary Figure 5). Due to the small sample size, and the large proportion of MII chromosome spreads that were very bunched in this study (which meant that I were not able to use mFISH) I was unable to determine which chromosomes commonly mis-segregated in the *Smc6*$^{+/GT}$ mouse oocytes.

4.3.4 *Smc6*$^{+/GT}$ oocytes display increased separation of sister kinetochores

There are several possible reasons as to why aneuploidy has been observed in the oocytes from the *Smc6*$^{+/GT}$ mice, one of which is weakened chromosome cohesion. If chromosome cohesion is weakened then this can

(A)

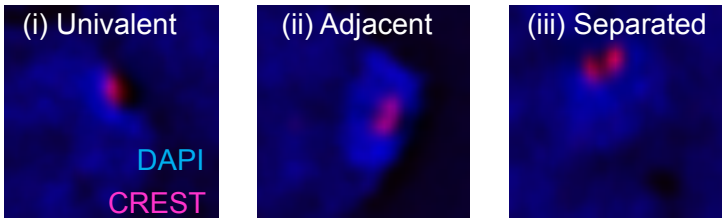
(i) Univalent
DAPI
CREST
(ii) Adjacent
(iii) Separated

(B)

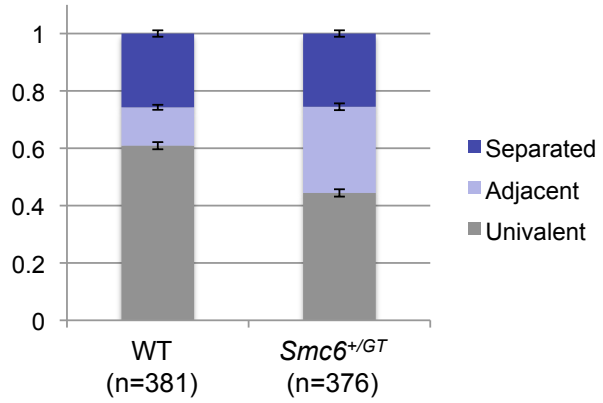
1
0.8
0.6
0.4
0.2
0
WT
(n=381)
Smc6+/GT
(n=376)
Separated
Adjacent
Univalent

(C)

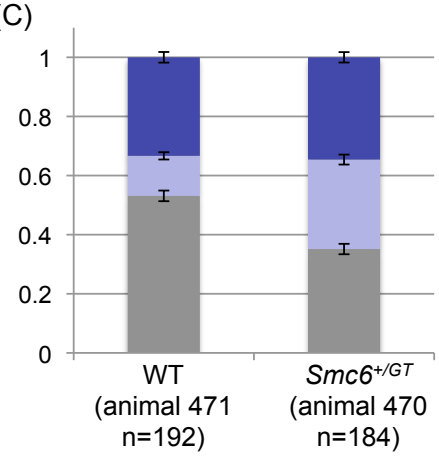
1
0.8
0.6
0.4
0.2
0
WT
(animal 471
n=192)
Smc6+/GT
(animal 470
n=184)

(D)

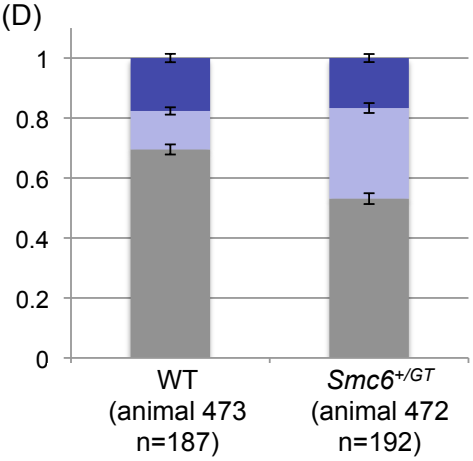
1
0.8
0.6
0.4
0.2
0
WT
(animal 473
n=187)
Smc6+/GT
(animal 472
n=192)

Figure 4.8 – The MI oocytes from the *Smc6*$^{+/GT}$ mice display significantly more adjacent kinetochores than observed in the MI oocytes from their wild type littermates

A. Examples of chromosomes where the kinetochores were classified as either univalent (i), adjacent (ii) or apart (iii). Here the DNA was stained with DAPI (displayed in blue) and the kinetochores were stained with CREST (displayed in red).

B. Graph demonstrating the percentage of chromosomes that were classified as having kinetochores that were either univalent, adjacent or apart in both wild type (animals 471 & 473, n=381 chromosomes, 10 oocyte spreads) and *Smc6*$^{+/GT}$ (animals 470 & 472, n=376 chromosomes, 10 oocyte spreads). Error bars represent the standard deviation. (n = number of chromosomes) (Mouse experiment 16)

C. Graph demonstrating the proportion of chromosomes that were classified as having kinetochores that were either univalent, adjacent or apart in both wild type (animal 471, n=192 chromosomes, 5 oocyte spreads) and *Smc6*$^{+/GT}$ (animal 470, n = 184 chromosomes, 5 oocyte spreads). Error bars represent the standard deviation.(Mouse experiment 16)

D. Graph demonstrating the proportion of chromosomes that were classified as having kinetochores that were either univalent, adjacent or apart in both wild type (animal 473, n=187 chromosomes, 5 oocyte spreads) and *Smc6*$^{+/GT}$ (animal 472, n = 192 chromosomes, 5 oocyte spreads). Error bars represent the standard deviation.(Mouse experiment 16)

lead to increased inter-kinetochore distances, chiasmata slippage and precocious sister chromatid separation (Chiang et al, 2010; Chiang et al, 2012). To investigate this, the kinetochore associations in the metaphase I (MI) oocytes from both wild type and *Smc6*$^{+/GT}$ mice were analysed. In MI oocytes from wild type, the kinetochores are held together by centromeric cohesin and appear as a single CREST focus. The sister kinetochores can also be separated, appearing as juxtaposed foci or entirely separated (Figure 4.8A).

No difference was observed in the number of separated sister kinetochores in oocytes from the *Smc6*$^{+/GT}$ mouse compared to wild type (Figure 4.8B). There however was an increase in the category where sister chromatids were separated sufficiently meaning two foci could be distinguished (*Smc6*$^{+/GT}$ mouse oocytes - 30%; 113/376 chromosomes; wild type oocytes - 13%; 51/381 chromosomes, T-test $P<0.05$) (Figure 4.8B). These data were obtained from two pairs of littermates and the same trend was observed in both pairs of littermates individually (Figure 4.8C & D). This indicates that centromeric cohesion may be affected in the MI oocytes from the *Smc6*$^{+/GT}$ mouse.

In order to obtain a more accurate assessment of kinetochore cohesion the inter-kinetochore distance was measured using Imaris (Figure 4.9A). I measured the distance from one side of the outer kinetochore to the opposite side of the sister kinetochore (Figure 4.9B). The inter-kinetochore distances were significantly longer in *Smc6*$^{+/GT}$ (animal 375) compared to the wild type littermate (animal 374) (Figure 4.9C; Wilcox test $p < 0.005$; Wild type average = 0.6 μm; *Smc6*$^{+/GT}$ average = 0.7 μm). This indicated that cohesion is affected in the oocytes from the *Smc6*$^{+/GT}$ mice.

As manual analysis of the inter-kinetochore distances using Imaris was very time consuming, I attempted a second analysis using ImageJ to increase our dataset. The plugin 'FindFoci GUI' was used to select the

(A)

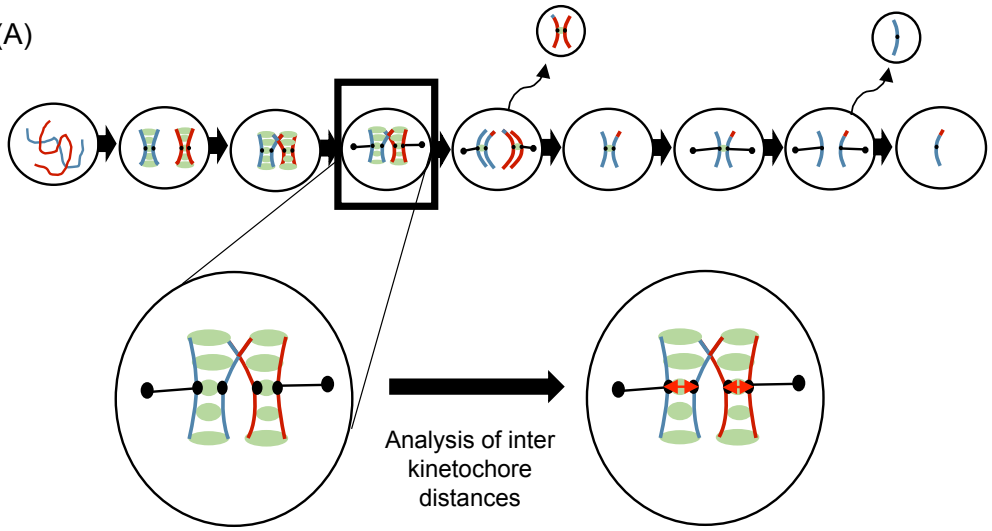
Analysis of inter
kinetochore
distances

(B)

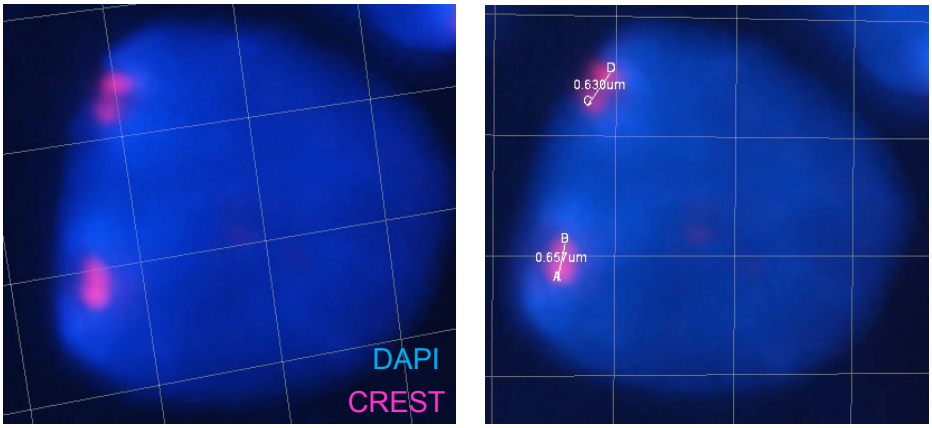
DAPI
CREST
D
0.630um
B
0.657um

(C)

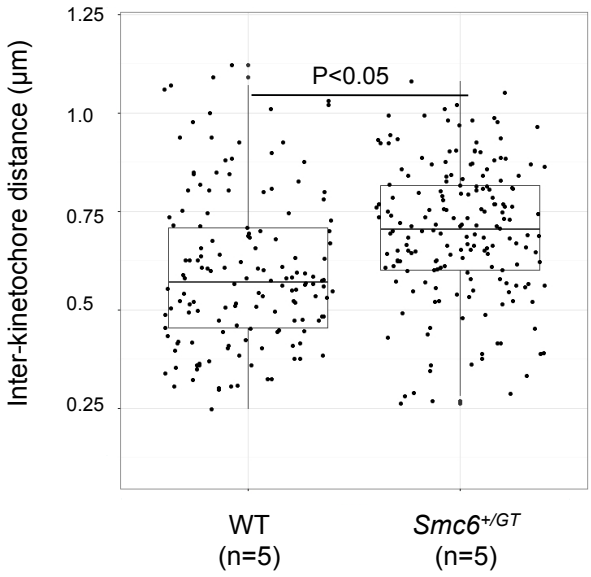
Inter-kinetochore distance (µm)
1.25
1.0
0.75
0.5
0.25
P<0.05
WT
(n=5)
Smc6+/GT
(n=5)

Figure 4.9 – Imaris analysis demonstrates that inter-kinetochore distances are increased in *Smc6*$^{+/GT}$ MI oocytes compared to MI oocytes from their wild type litter mates

A. Diagram of oogenisis in which metaphase I (MI) has been highlighted by a box. A zoomed in image more clearly shows the kinetochores (distinguished by CREST staining) on each of the chromosomes (stained with DAPI). To the right of this, on the next zoomed in image, the red arrows demonstrate how the inter-kinetochore distances are measured (from outer kinetochore to outer kinetochore).

B. Image from Imaris demonstrating how the inter-kinetochore distances are measured in 3D.

C. Boxplot demonstrating the inter-kinetochore distances measured in both wild type (animal 374, n=5) and *Smc6*$^{+/GT}$ (animal 375, n=5) oocytes. (n=number of oocytes) (Mouse experiment 12)

CREST foci in 3D in each image and the plugin 'Mask Object Dimensions' was then used to identify the distance from the centre of one object to the centre of the nearest object (Figure 4.10Aii) (Herbert et al, 2014).

Initially I tested whether ImageJ analysis would produce results comparable to those obtained from the manual Imaris analysis. Similar results were obtained from analysis of wild type (animal 374) and *Smc6*$^{+/GT}$ (animal 375). Using Imaris the wild type average kinetochore distance was 0.6μm and *Smc6*$^{+/GT}$ average kinetochore distance was 0.7 μm. Utilizing ImageJ the wild type average kinetochore distance was 0.72 μm, while the *Smc6*$^{+/GT}$ average kinetochore distance was 0.88μm. In both cases it was found that the inter-kinetochore distances were significantly greater in *Smc6*$^{+/GT}$ compared to wild type (Wilcox test, $p<0.005$; Figure 4.10B & C). The inter-kinetochore distances were slightly longer in the ImageJ analysis. A limitation of using ImageJ is that all the CREST foci need to be segmented using the same thresholding conditions. (Thresholding separates pixels within a specific intensity range from those outside the intensity range.) This was in some cases very difficult and meant that some foci were thresholded too much or too little, likely leading to the more variable results observed.

I found that the inter-kinetochore distances in wild type and *Smc6*$^{+/GT}$ were overall significantly different (Wilcox test $p < 0.005$; Figure 4.11A). However, analysis of the pairs of littermates showed that the inter-kinetochore distances were very variable (Figure 4.11B, C&D). As stated previously, I found in animals 374 and 375 that the inter-kinetochore distances were significantly longer in *Smc6*$^{+/GT}$ than wild type MI oocytes (Figure 4.11B). In contrast, in another littermate pair (animals 462 and 463) the inter-kinetochore distances were not significantly different, and that in animals 446 and 447 the inter-kinetochore distances in the wild-type oocytes were significantly longer than in the *Smc6*$^{+/GT}$ oocytes (Figure 4.11C&D).

(A)

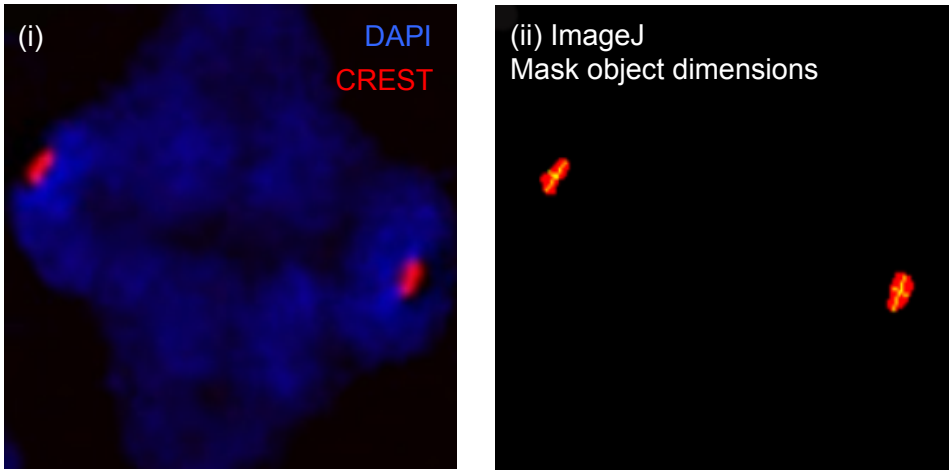
(i)
DAPI
CREST
(ii) ImageJ
Mask object dimensions

(B)

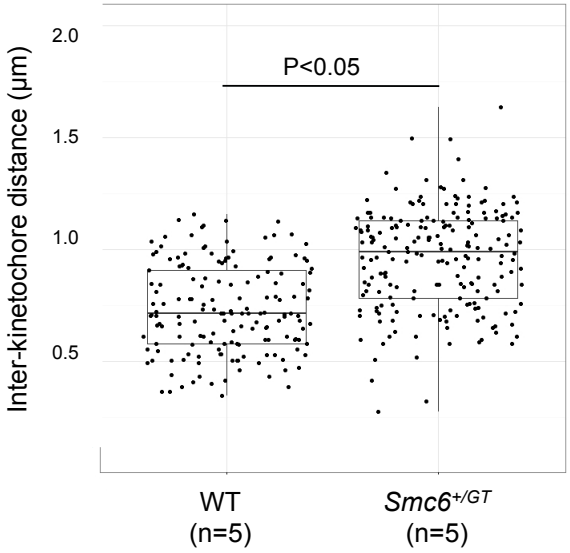
Inter-kinetochore distance (µm)
2.0
1.5
1.0
0.5
P<0.05
WT
(n=5)
Smc6+/GT
(n=5)

(C)

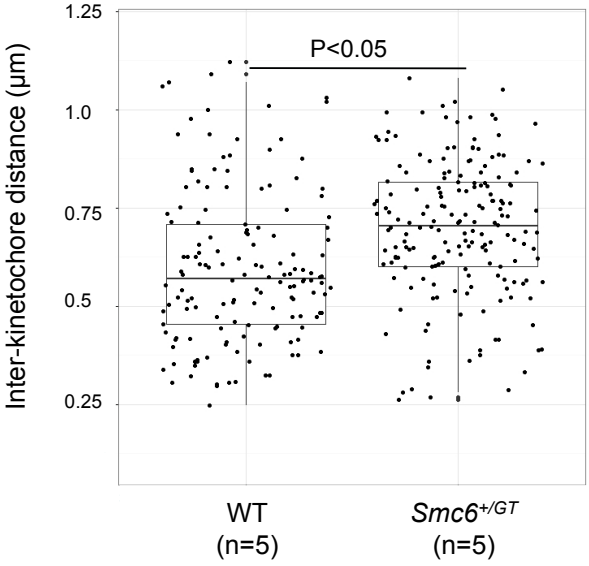
Inter-kinetochore distance (µm)
1.25
1.0
0.75
0.5
0.25
P<0.05
WT
(n=5)
Smc6+/GT
(n=5)

Figure 4.10 – Comparison of Imaris inter-kinetochore analysis with ImageJ inter-kinetochore analysis demonstrates that the two methods are comparable

A. (i) Diagram of a chromosome when the DNA has been stained with DAPI (displayed in blue) and the kinetochores stained with CREST (displayed in red). (ii) Diagram of the output from Mask object dimensions. The CREST foci are segmented and the length of the longest side determined.

B. Boxplot demonstrating the inter-kinetochore distances in wild type (animal 374) and *Smc6*$^{+/GT}$ (animal 375) MI oocytes when measured using ImageJ. Here the average inter-kinetochore distance for wild type (animal 374) was 0.73µm and *Smc6*$^{+/GT}$ (animal 375) was 0.96µm. (Wilcox test – $P < 0.05$) (n=number of oocytes) (Mouse experiment 12)

C. Boxplot demonstrating the inter-kinetochore distances in wild type (animal 374) and *Smc6*$^{+/GT}$ (animal 375) MI oocytes when measured using Imaris. Here the average inter-kinetochore distance for wild type (animal 374) was 0.6µm and for *Smc6*$^{+/GT}$ (animal 375) was 0.7µm. (Wilcox – $P < 0.05$) (n=number of oocytes) (Mouse experiment 12)

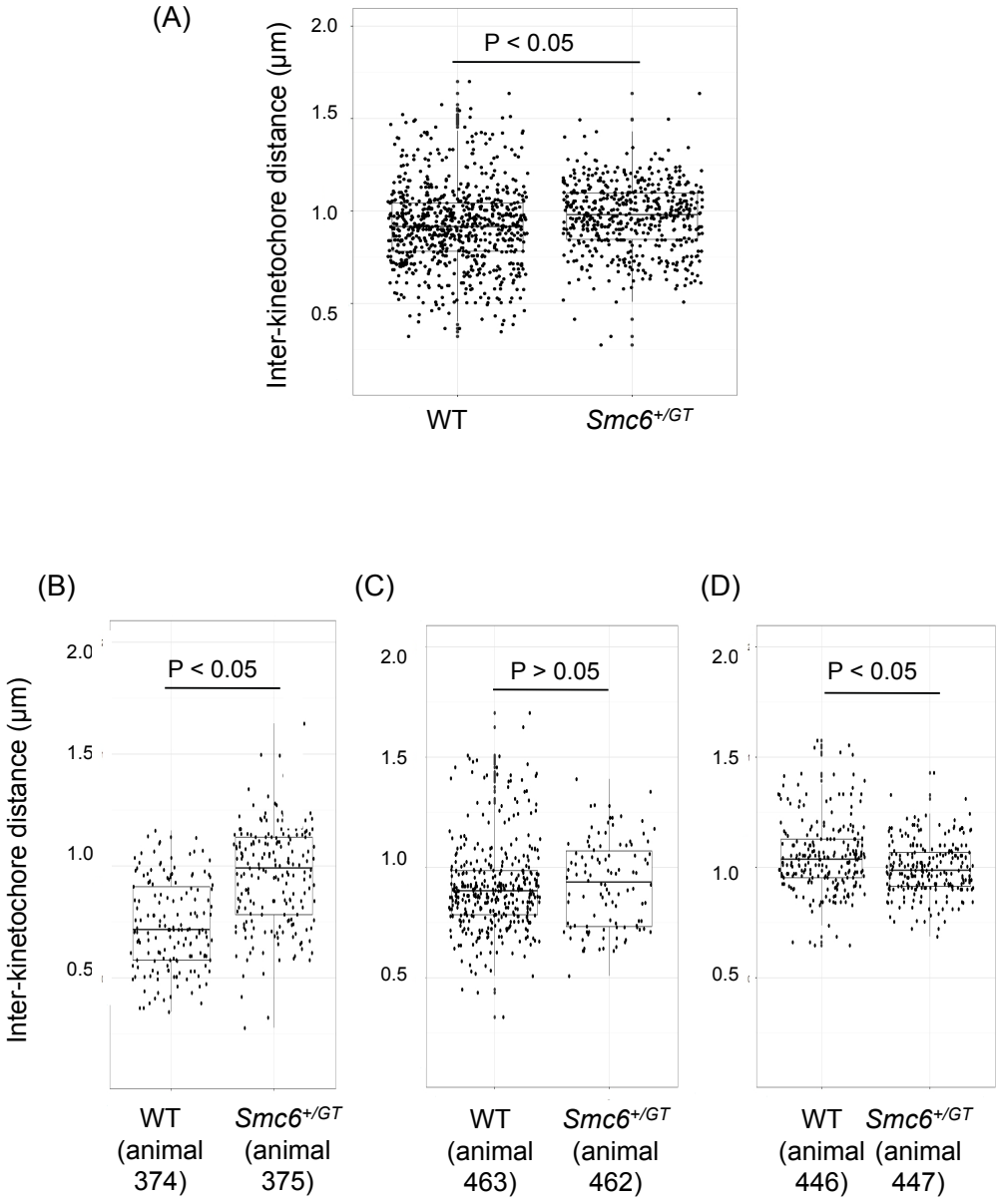
(A)
Inter-kinetochore distance (μm)
2.0
1.5
1.0
0.5
P < 0.05
WT
Smc6+/GT
(B)
(C)
(D)
P < 0.05
P > 0.05
P < 0.05
WT (animal 374)
Smc6+/GT (animal 375)
WT (animal 463)
Smc6+/GT (animal 462)
WT (animal 446)
Smc6+/GT (animal 447)

Figure 4.11 – Inter-kinetochore distances are variable in MI oocytes from the *Smc6*$^{+/GT}$ mice

A. Boxplot demonstrating the inter-kinetochore distances measured using mask object dimensions for both wild type and *Smc6*$^{+/GT}$ MI oocytes. The difference between the distribution in wild type and *Smc6*$^{+/GT}$ was found to be statistically significant ($P < 0.05$) (Mouse experiments 12, 14 & 15)

B. Boxplot demonstrating the inter-kinetochore distances measured using mask object dimensions for a pair of littermates (animal 374, wild type and animal 375, *Smc6*$^{+/GT}$). The difference between wild type (animal 374, No oocytes = 6) and *Smc6*$^{+/GT}$ (animal 375, No of oocytes = 8) was found to be statistically significant (Wilcox test $P < 0.05$). (Mouse experiment 12)

C. Boxplot demonstrating the inter-kinetochore distances measured using mask object dimensions for a pair of littermates (animal 463, wild type and animal 462, *Smc6*$^{+/GT}$). The difference between wild type (animal 463, No oocytes = 10) and *Smc6*$^{+/GT}$ (animal 462, No of oocytes = 3) was not found to be statistically significant (Wilcox test $P > 0.05$). (Mouse experiment 15)

D. Boxplot demonstrating the inter-kinetochore distances measured using mask object dimensions for a pair of littermates (animal 446, wild type and animal 447, *Smc6*$^{+/GT}$). The difference between wild type (animal 446, No oocytes = 6) and *Smc6*$^{+/GT}$ (animal 447, No of oocytes = 8) was found to be statistically significant (Wilcox test $P < 0.05$). (Mouse experiment 14)

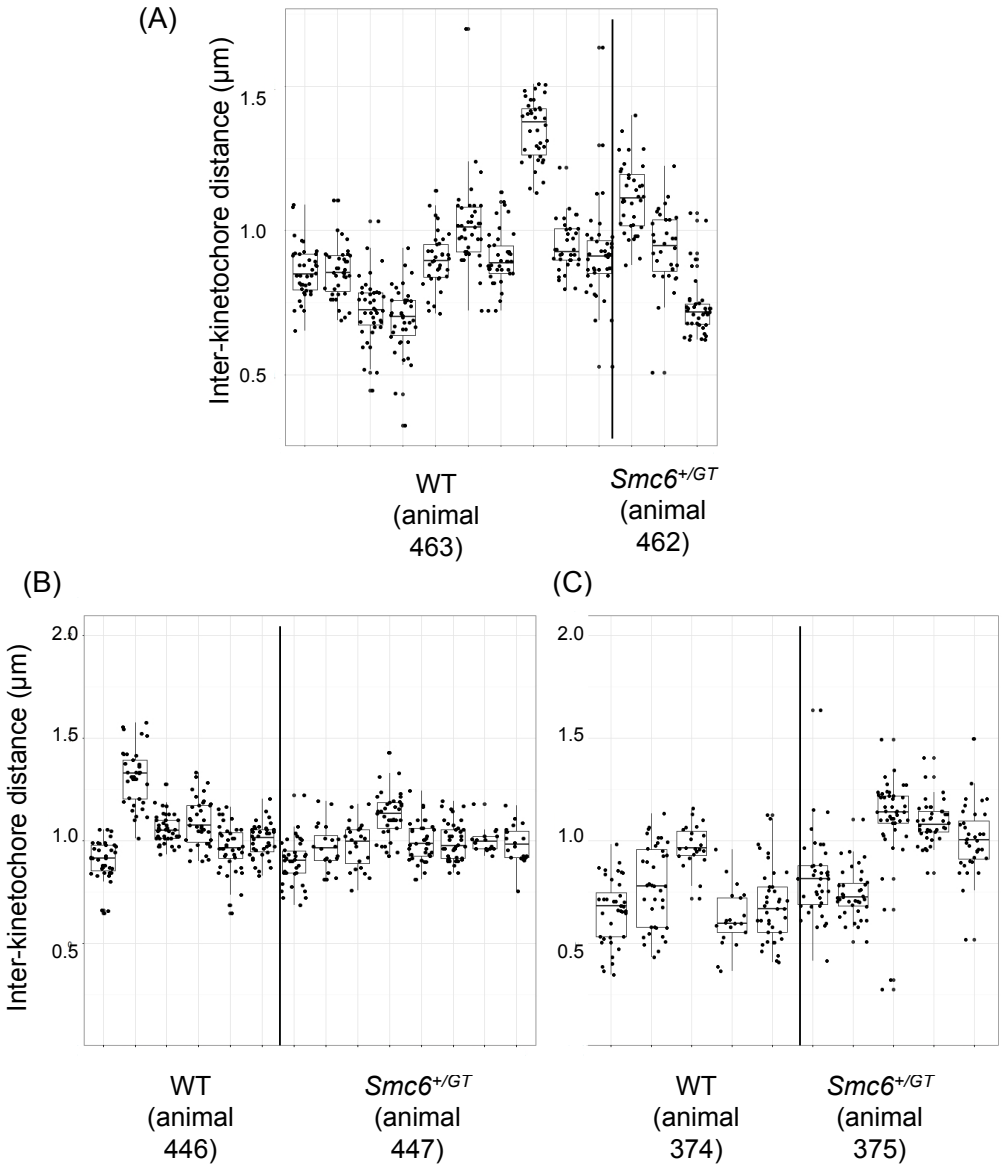

Figure 4.12 – Inter-kinetochore distances, on a per spread basis, are variable in MI oocytes from the *Smc6*$^{+/GT}$ mice

A. Boxplot demonstrating the inter-kinetochore distances measured for both wild type (animal 463) and *Smc6*$^{+/GT}$ (animal 462) littermates on a per oocyte basis. (Mouse experiment 15)

B. Boxplot demonstrating the inter-kinetochore distances measured for both wild type (animal 446) and *Smc6*$^{+/GT}$ (animal 447) littermates on a per oocyte basis. (Mouse experiment 14)

C. Boxplot demonstrating the inter-kinetochore distances measured for both wild type (animal 374) and *Smc6*$^{+/GT}$ (animal 375) littermates on a per oocyte basis. (Mouse experiment 12)

I next assessed the inter-kinetochore distances in individual spreads to see if it was specific spreads that were changing the distributions (Figure 4.12 A, B & C). Wild type animal 446 was only significantly different to *Smc6*$^{+/GT}$ animal 447 because of one oocyte containing longer inter-kinetochore distances than any of the other oocytes (Figure 4.12B). In animal 375 (*Smc6*$^{+/GT}$) however three out of the five spreads measured had significantly longer inter-kinetochore distances than seen in animal 374 (wild type) (Figure 4.12C). These results indicate that inter-kinetochore cohesion may be affected to different extents in the oocytes from the *Smc6*$^{+/GT}$ mouse. Interestingly, average kinetochore distance varied substantially in wild type (374 average = 0.73 μm; 446 average = 1.05 μm; 463 average = 0.92 μm), but not as much in *Smc6*$^{+/GT}$ (375 average = 0.96 μm; 447 average = 0.99 μm; 462 average = 0.93 μm) (Figure 4.11B, C & D). Furthermore, it was observed when the average kinetochore distance was highest in wild type (animal 446); it was also highest in the corresponding *Smc6*$^{+/GT}$ littermate (animal 447). This may indicate that oocytes from different experiments are at slightly different sub stages of metaphase I. Alternatively it is possible that the differences observed were due to technical variations in the spreading procedure (i.e. differences in the concentration of the PFA in contact with the oocyte or the humidity level) or the litter effect.

4.3.5 Chromosome orientation is affected in *Smc6*$^{+/GT}$ oocytes

To further investigate if cohesion is affected in the oocytes from the *Smc6*$^{+/GT}$ mice, MI chromosome spreads were analysed to determine chiasmata position. Chiasmata are the cytological manifestation of crossovers. The optimal position for crossovers in mice is at the centre of the chromosome, which leads to a cruciform structure (Figure 4.13Ai). If there is a loss of cohesion between homologs crossovers can slip and move to the distal end of the chromosome (Figure 4.13Aii) or be completely lost and the homologs become separated (Figure 4.13Aiii)(Lister et al, 2010). I observed no univalents in oocytes from wild type or from *Smc6*$^{+/GT}$ mice. I

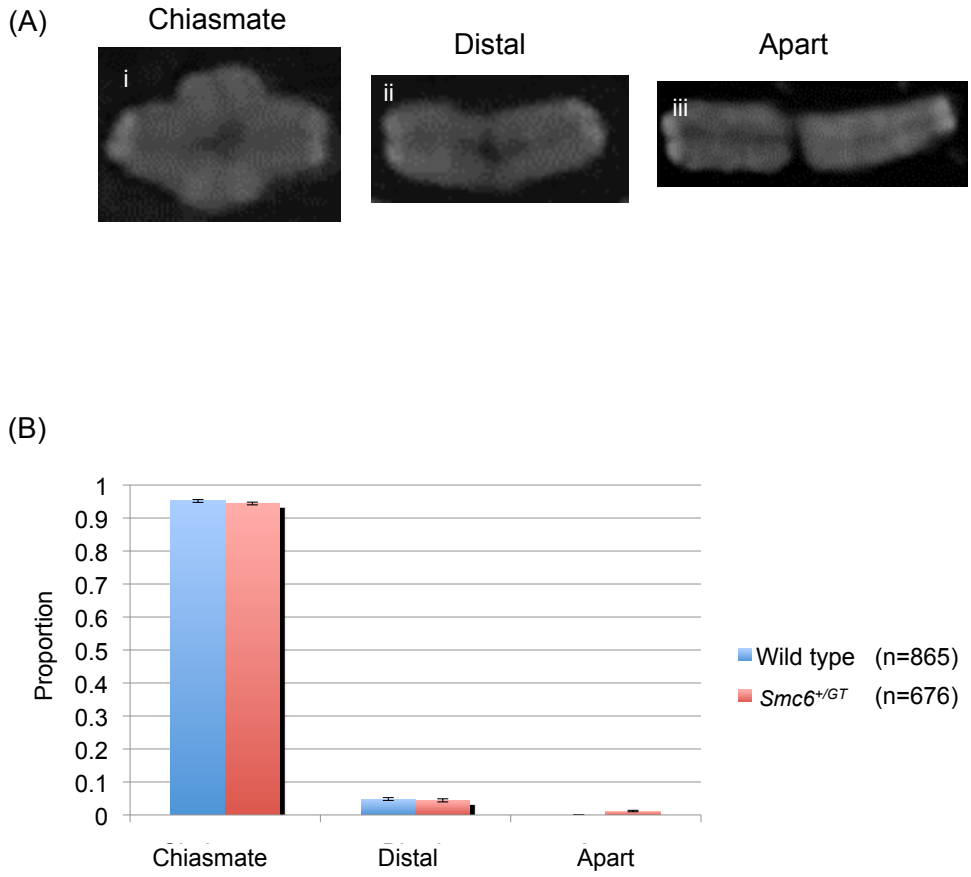

Figure 4.13 – Chromosome orientation is not affected in the MI oocytes from the *Smc6*$^{+/GT}$ mice

A. Diagrams of the different classifications of chromosome orientation; chiasmate (i), distal (ii) and apart (iii).

B. The homologous chromosomes from wild type and *Smc6*$^{+/GT}$ oocytes were classified as either chiasmate, distal or apart. (Wild type No. of chromosomes =865, No. of oocytes = 52, *Smc6*$^{+/GT}$ No. of chromosomes = 676, No. of oocytes = 39). (Mouse experiments 3, 4, 6, 8, 12, 13, 14 &15)

then compared the number of distally associated bivalents in oocytes from the *Smc6*$^{+/GT}$ mice and their wild type littermates. I found the number of distally associated chromosomes was not significantly different in *Smc6*$^{+/GT}$ compared to wild type (T-test P > 0.05; Figure 4.13B). Bivalent deterioration (in which the homologous chromosome came apart) was however observed in 13% of *Smc6*$^{+/GT}$ MI oocytes (P < 0.005, n=39). This was never observed in the wild type oocytes.

4.3.6. The size of metaphase I chromosomes is increased in *Smc6*$^{+/GT}$ oocytes.

The Smc5/6 complex is known to control many aspects of chromosome structure including chromosome compaction (Gallego-Paez et al, 2013). Studies from our laboratory found that when Smc5/6 is depleted in budding yeast, the chromosome axes are increased (unpublished data, Hoffmann lab). Similarly, during analysis of *Smc6*$^{+/GT}$ MI oocytes I observed that the chromosomes sometimes appeared larger (Figure 4.14). To accurately assess chromosome compaction in *Smc6*$^{+/GT}$ oocytes I used ImageJ to first create a mask of the DAPI staining in each oocyte to assess the total area of the chromosome spread. The total area of the spread was then divided by the number of chromosomes in the spread to determine the average area per chromosome. I found that the chromosome size was considerably more variable in oocytes from the *Smc6*$^{+/GT}$ mouse with some of them being significantly larger than those seen in wild type (Figure 4.14B). Analysis by the Wilcox test found that the two distributions were significantly different ($p < 0.05$). This indicates that chromosome compaction is affected in metaphase I in *Smc6*$^{+/GT}$ oocytes as seen in oocytes from *Smc5* cKO mice (Hwang et al, 2017).

4.3.7. Chromosome size at prophase I is reduced in *Smc6*$^{+/GT}$ oocytes

As I found that chromosome compaction was affected in the oocytes from the *Smc6*$^{+/GT}$ mouse at metaphase I, I then assessed if there were similar

(A)

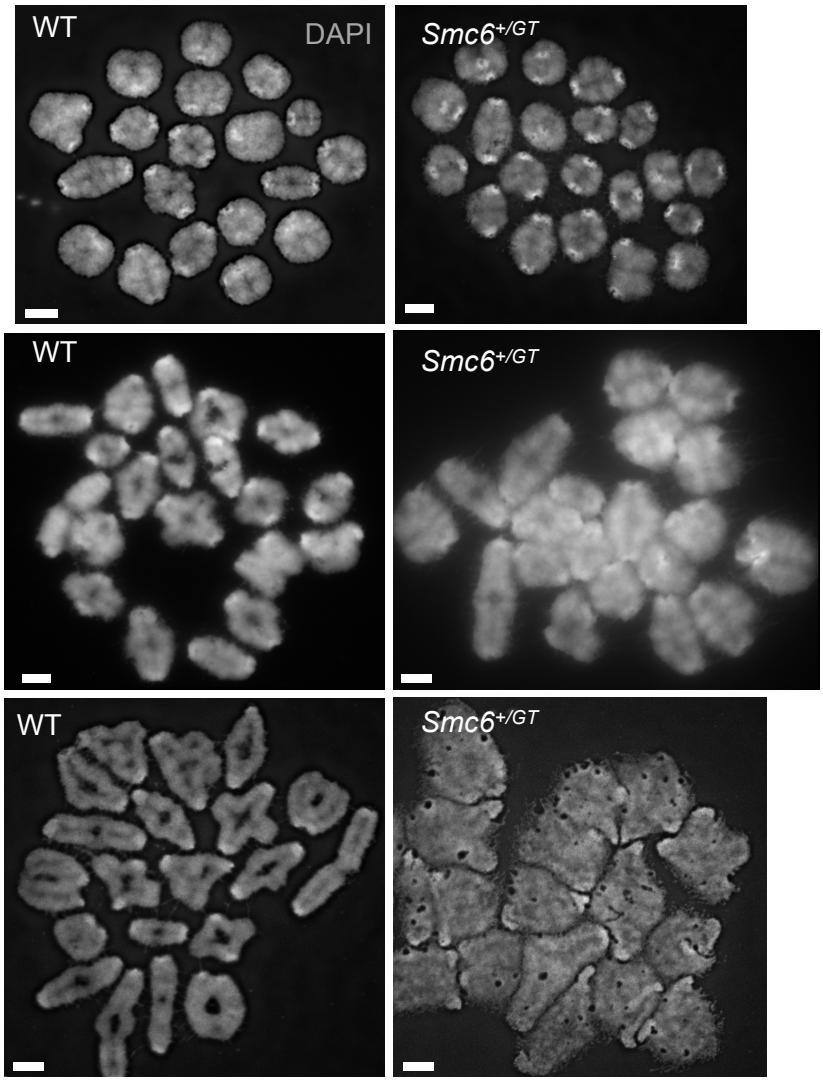
WT
DAPI
Smc6+/GT
WT
Smc6+/GT
WT
Smc6+/GT

(B)

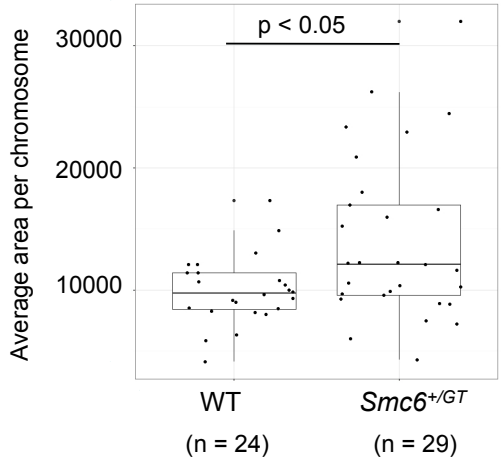
p < 0.05
30000
20000
10000
Average area per chromosome
WT
Smc6+/GT
(n = 24)
(n = 29)

Figure 4.14 – Chromosome compaction is reduced in the MI oocytes of the *Smc6*$^{+/GT}$ mice

A. Examples of compact and more diffuse chromosome spreads in both wild type and *Smc6*$^{+/GT}$

B. Boxplot demonstrating the average area per a chromosome on a per spread basis in both wild type and *Smc6*$^{+/GT}$ oocytes. (Wild type No. of oocytes = 24, *Smc6*$^{+/GT}$ No. of oocytes = 29) The distributions were found by the Wilcox test to be significantly different. ($P < 0.05$)

differences in chromosome compaction seen prior to the dictyate arrest during prophase. To do this, the length of the synaptonemal complex in both wild type and *Smc6*$^{+/GT}$ mouse fetal oocytes (Stage e18.5) was assessed (Figure 4.15). Fetal oocyte spreads (prepared by Jenny Gruhn) were stained with antibodies raised against SYCP3, a component of the lateral-axial element of the synaptonemal complex, and MLH1, a marker of crossovers, to allow for correct staging of pachytene spreads (Yuan et al, 2000; Baker et al, 1996). MLH1 staining, however, did not work and so the oocytes were judged to be at pachytene when they displayed fully synapsed SYCP3 staining (Figure 4.15A). Oocytes were not included in the analysis if they displayed even slightly dotty staining as this indicated that the SC had yet to form properly (late zygotene) or was beginning to break down (diplotene) (Figure 4.15B). The fixation of each of the spreads was verified through assessment of CREST staining. The length of the SYCP3 staining was measured in 3D using Imaris. Here the SYCP3 length was assessed on a per spread basis (Figure 4.15; Lynn et al, 2005). I did not detect increased SYCP3 lengths on a per spread basis (Wild type average – 196 μm, number of oocytes = 24, number of embryos = 3; *Smc6*$^{+/GT}$ – 187 μm, number of oocytes = 26, number of embryos = 3; Wilcox test: $p>0.05$). This indicates that chromosome axis length is not affected in the oocytes from the *Smc6*$^{+/GT}$ mouse at pachytene.

4.3.8. Structural deterioration ('fraying') of chromosomes in *Smc6*$^{+/GT}$ oocytes

Some of the MI spreads displayed frayed chromosomes or chromosome threads connecting the chromosomes (Figure 4.16). The percentage of oocytes that displayed frayed chromosomes in both wild type and *Smc6*$^{+/GT}$ oocytes were analysed and I found that frayed chromosomes were observed in significantly more *Smc6*$^{+/GT}$ oocytes (35.3%, n=7) compared to wildtype (8.3%, n=7, T-test $P<0.05$) (Figure 4.16B). Smc5/6 is known to have a role in preventing ectopic recombination and so it is possible that the threads observed may correspond to ectopic

(A)

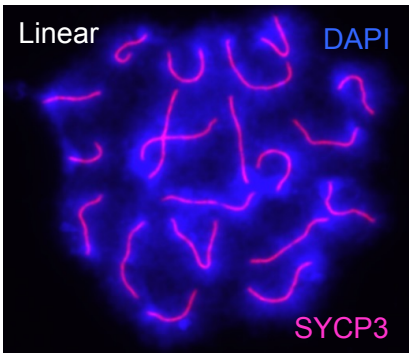
Linear
DAPI
SYCP3

(B)

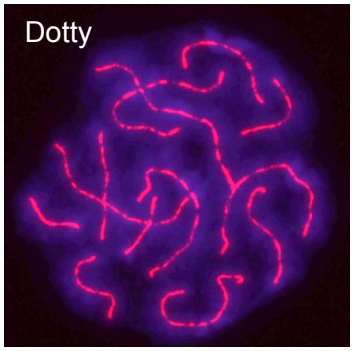
Dotty

(C)

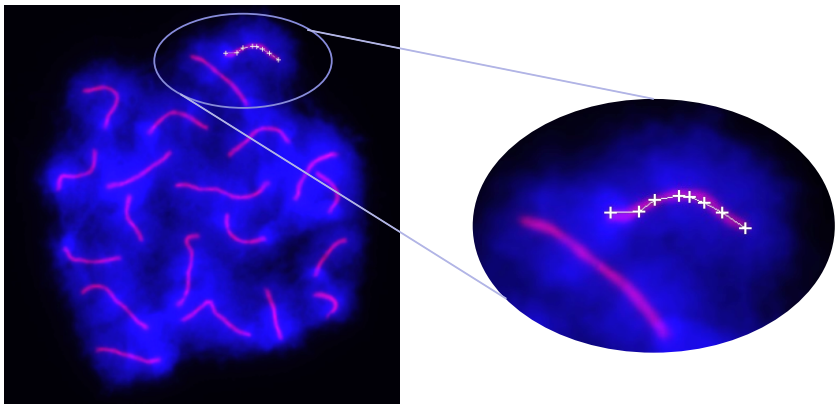

(D)

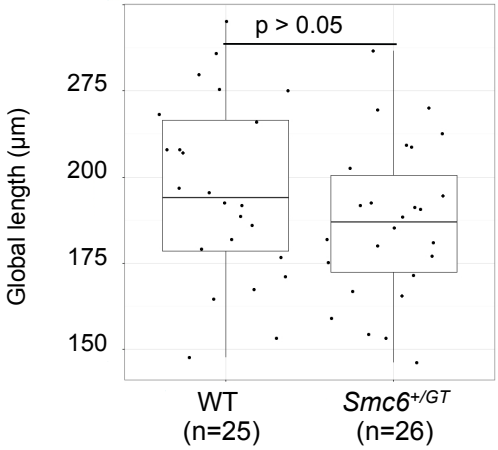
p > 0.05
Global length (µm)
275
200
175
150
WT
(n=25)
Smc6+/GT
(n=26)

Figure 4.15 –Chromosome length is not affected at Pachytene oocytes from the *Smc6*$^{+/GT}$ mice

A. Example of a Pachytene oocyte with linear SYCP3 staining.

B. Example of a Pachytene oocyte with dotty SYCP3 staining.

C. Example of how the length of SYCP3 is measured using Imaris.

D. Total length of SYCP3 on a per spread basis in both wild type (No. of spreads = 25) and *Smc6*$^{+/GT}$ (No. of spreads=26) oocytes. The difference in size was not found to be statistically significant ($p > 0.05$).

(A)

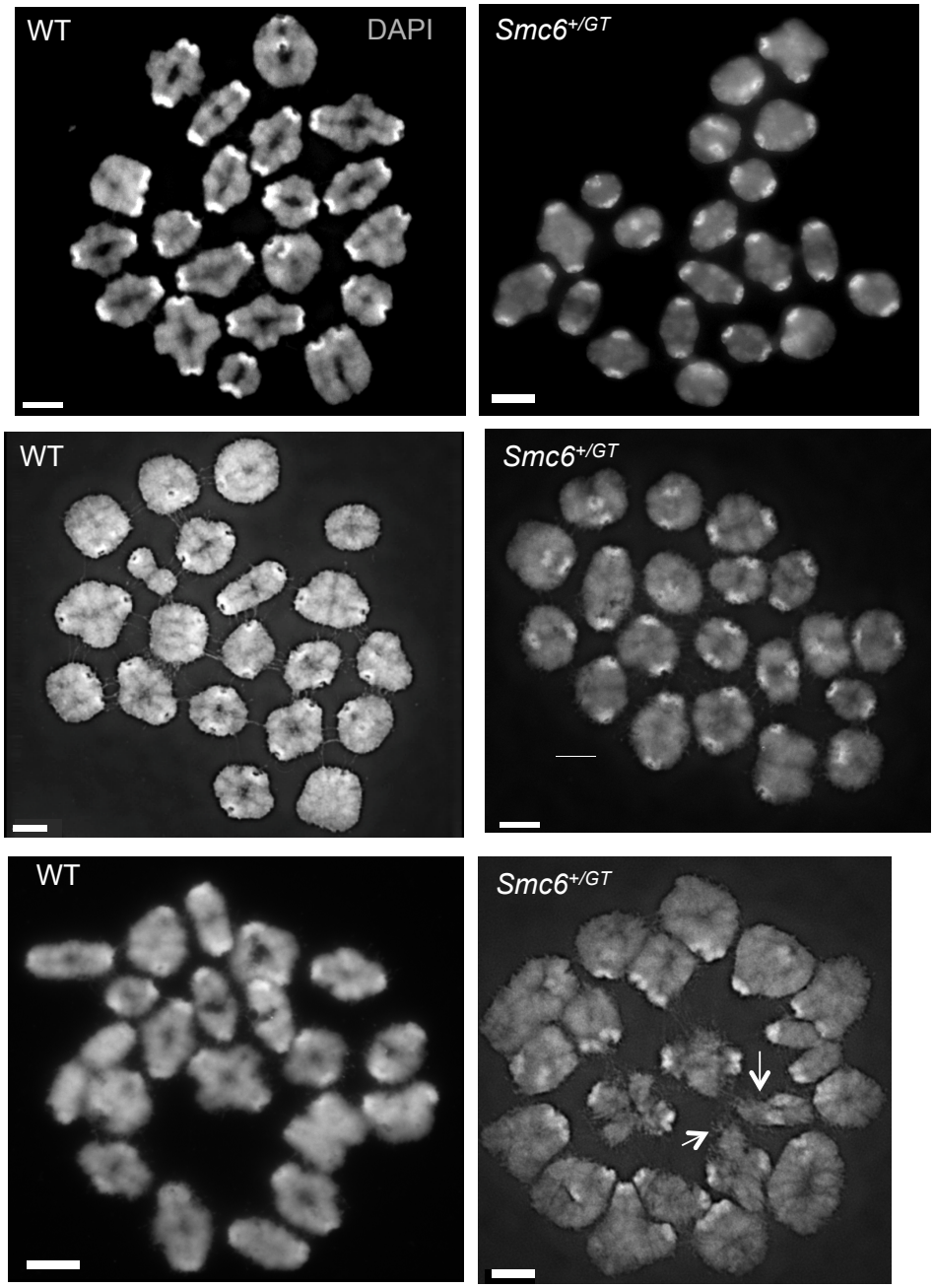

(B)

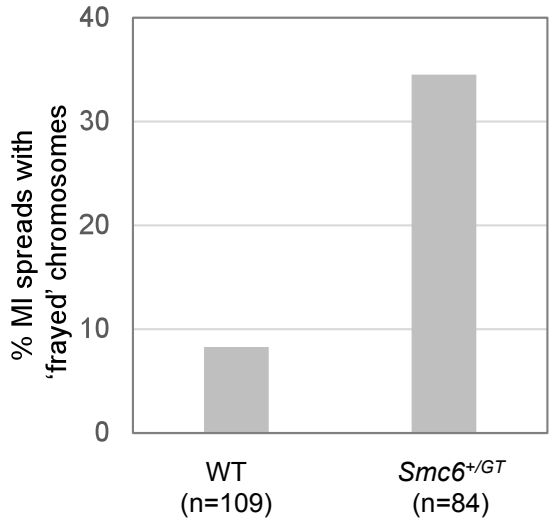

Figure 4.16 – Chromosome fraying is increased in MI oocytes from *Smc6*$^{+/GT}$ mice

A. Examples of both frayed and non-frayed chromosomes in MI oocyte spreads from both wild type and *Smc6*$^{+/GT}$

B. Graph demonstrating the percentage of MI oocyte spreads from both wild type and *Smc6*$^{+/GT}$ mice that displayed frayed chromosomes. (Wild type No. of oocytes = 109, *Smc6*$^{+/GT}$ No. of oocytes = 84) Arrows demonstrate examples of frayed chromosomes. (Mouse experiments 16, 17 & 18)

recombination between homologues of different chromosomes (Hong et al, 2016). The chromosome threads could not be quantified, as generally the chromosomes were too close to one another in the MI spreads. Reliable quantification would require that the chromosomes were more greatly spread so that the threads were clear, but not so spread that the threads would break. These results, however, indicate that overall chromosome structure is affected in the oocytes from the female *Smc6*$^{+/GT}$ mice.

4.3.9. Live-cell dynamics of chromosome segregation in *Smc6+/*^{GT} oocytes

Live cell imaging was used to further investigate chromosome segregation in oocytes from the *Smc6*$^{+/GT}$ mice. In order to visualize the chromosomes in real time the oocytes were microinjected with cDNAs of EGFP-CENPC and histone 2B-mCherry (Simon Lane, University of Southampton) and imaged throughout the first meiotic division (Supplementary figure 6). Analysis of chromosome segregation could not be carried out on these images as many of the wildtype oocytes did not extrude a polar body and generally did not appear healthy. The poor viability may have been due to the high laser power used. It is also possible that the viability of the oocytes was affected due to the oocytes initially being collected at Sussex University and then transported to Southampton University for imaging.

4.4 Discussion

In murine oocytes the cohesin complex has been found to be important for the formation of the synaptonemal complex, the establishment and maintenance of sister chromatid cohesion and for meiotic recombination (Xu et al, 2005; Tachibana-Konwalski et al, 2010; Revenkova et al, 2004). Condensin has been found to be important for chromosome rigidity, thread formation and disentaglement (Houlard et al, 2015). Despite the increasing amounts discovered about cohesin and condensin in

mammalian meiosis previously little was known about the role of the Smc5/6 complex.

This study, alongside recently published work by Hwang *et al* (2017), has provided the first real insight into the role of the Smc5/6 complex in murine meiosis. Here I found that the litter size was significantly reduced, compared to wildtype, but only in a heterozygous female (*Smc6*$^{+/GT}$) X wild type male (*Smc6*$^{+/+}$) cross, not in the reciprocal cross (Figure 4.3). Corresponding results were observed in Hwang *et al* (2017). They observed that *Smc5* cKO females, when crossed with wild type males, produced significantly less mature blastocysts than when *Smc5* cKO males were crossed with wild type females. These results together indicate that the reproductive problems, induced by depletion of the Smc5/6 complex, are female specific.

I did not find a significant difference between the litter sizes from heterozygous female (*Smc6*$^{+/GT}$) X wild type male (*Smc6*$^{+/+}$) cross and heterozygous female (*Smc6*$^{+/GT}$) X heterozygous male (*Smc6*$^{+/GT}$) cross. It is predicted in the heterozygous female (*Smc6*$^{+/GT}$) X wild type male (*Smc6*$^{+/+}$) cross that 25% of the offspring would be lost as they are *Smc6*$^{GT/GT}$. As it was found that 33.3% of the oocytes from the Smc6$^{+/GT}$ mouse were aneuploid it is predicted that some of the homozygote's produced would also be aneuploid (Figure 4.17). This therefore suggests that the difference between the litter sizes produced from when either just the female is *Smc6*$^{+/GT}$ or when both the male and female are *Smc6*$^{+/GT}$ would be less than 20%. It is unlikely that this difference would be seen as the litter sizes of the mice used in this study are quite small and because there is a large amount of general variation in the litter sizes.

I hypothesized that the reduced litter size was due to the *Smc6*$^{+/GT}$ females producing aneuploid oocytes as the embryos were lost around day 10.5, when embryos are commonly lost due to aneuploidy in mice (Inoue et al, 2007). This was confirmed through analysis of MII oocyte chromosome

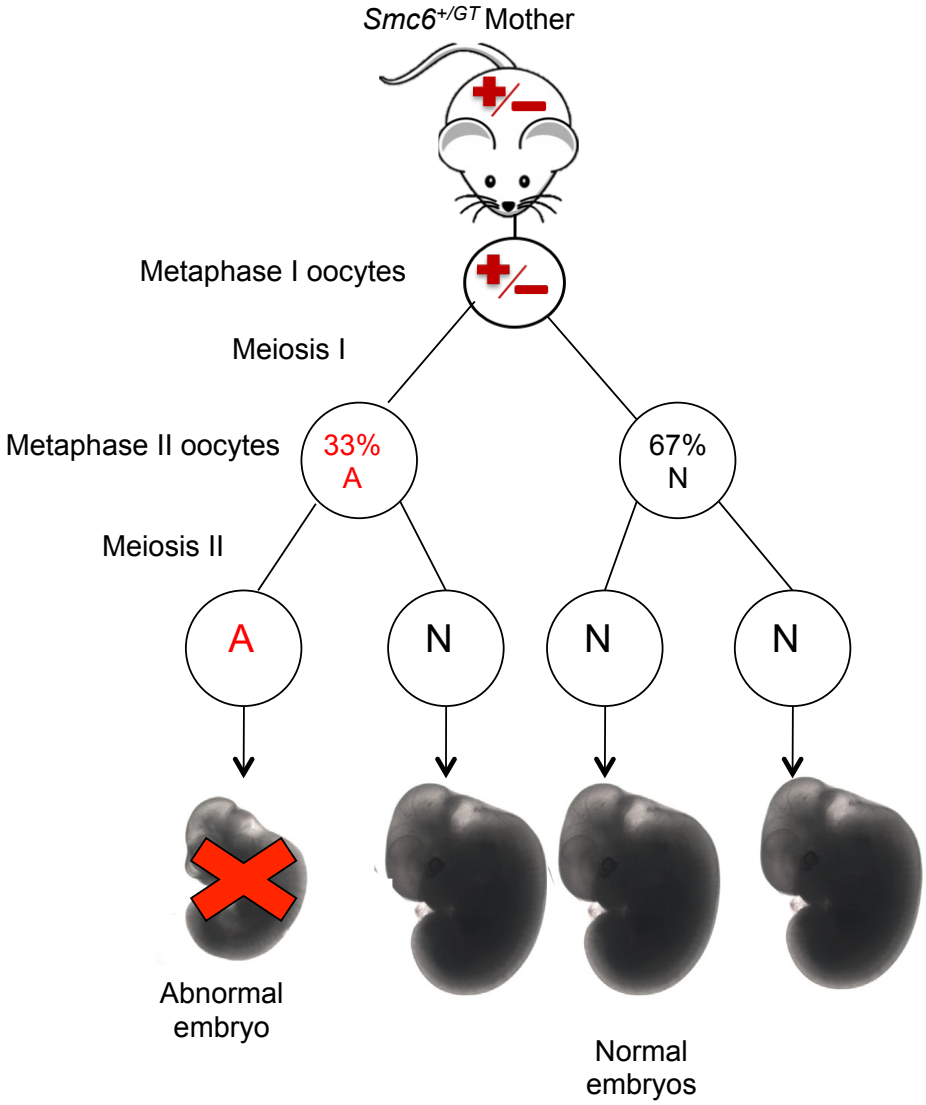

Figure 4.17 - *Smc6*$^{+/GT}$ mothers oocytes are predisposed to aneuploidy in their oocytes

Cartoon demonstrating the percentage of oocytes that mis-segregate their chromosomes in meiosis I (33% were observed to be aneuploid (A) and 67% normal (N)) in the *Smc6*$^{+/GT}$ mouse. Some of these mis-segregations will be corrected in meiosis II, some however will remain in the oocyte and lead to aneuploidy in the embryo.

spreads that showed significantly higher levels of aneuploidy in the oocytes from the *Smc6*$^{+/GT}$ mice compared to wild type (Figure 4.5). Live cell imaging was then tested in attempt to confirm the aneuploidy rates observed in the MII chromosome spreads (Supplementary figure 6, Simon Lane, Southampton University). The viability of the imaged oocytes from both wild type and *Smc6*$^{+/GT}$ was very low likely due to transporting the collected oocytes from Sussex University to Southampton University. Mice are currently in the process of being transferred to Southampton so that the imaging can be carried out straight after oocyte collection.

Inter-kinetochore chromosome cohesion was not greatly affected in the oocytes from the *Smc6*$^{+/GT}$ mouse (Figure 4.13). Analysis of the inter-kinetochore distances on a per spread basis found that the inter-kinetochore distances in both wild type and *Smc6*$^{+/GT}$ oocytes were variable and indicated that in many cases differences were only observed between litter mates due to specific spreads displaying longer inter-kinetochore distances (Figure 4.12). Work by Merriman et al (2012) also found variable inter-kinetochore distances in 1-month-old wild type mice. They proposed this indicates that as mice age the rate of cohesin loss varies from mouse to mouse and also oocyte to oocyte. This indicates that the variation in inter-kinetochore distances observed may reflect natural variation in the levels of cohesin loss between oocytes. The proportions of distally associated homologous chromosomes were also found to be the similar in both wild type and *Smc6*$^{+/GT}$ oocytes (Figure 4.13). I did, however, find that there was some precocious separation of homologous chromosomes from their bivalent configuration into univalents in the *Smc6*$^{+/GT}$ MI oocytes. Univalents are at risk of precocious sister chromatid separation at anaphase I in mouse and human oocytes (Kouznetsova et al, 2007; Zielinska et al, 2015). These were never observed in wild type. This indicates that chromosome cohesion is affected at the chromosome arms but not at the kinetochores in oocytes from the *Smc6*$^{+/GT}$ mouse.

Many of the chromosomes in the MI oocyte spreads from the *Smc6*$^{+/GT}$ mouse appeared larger than observed in wild type, indicating that chromosome compaction is affected (Figure 4.14). It was also observed that the chromosomes often appeared frayed, indicative of the presence of unresolved ectopic recombination (Hong et al, 2016). Oocytes from *Smc5* cKO mice were also found to contain chromosomes with an abnormal morphology (Hwang et al, 2017). The chromosomal abnormalities, both from the *Smc6*$^{+/GT}$ mouse and the *Smc5* cKO mice, are similar to those seen by Houlard *et al* (2015) in oocytes from *Ncaph2* cKO mice. This indicates that condensin is likely to be affected in the *Smc6*$^{+/GT}$ mouse oocytes.

Analysis of the MII spreads, using mFISH, found that one of the oocyte spreads from the *Smc6*$^{+/GT}$ mouse contained an extra chromatid next to (and potentially linked to due to overlapping DAPI signals) its homologous chromosome (Figure 4.7). This indicates it is possible a retention of joint molecules is in fact causing the high levels of aneuploidy observed in the oocytes of the *Smc6*$^{+/GT}$ mouse which is in turn causing the reduced litter sizes observed. Further FISH analysis is required to determine if this is the case.

The results indicate that the mother having a reduced level of Smc6 leads to problems in chromosome segregation in their oocytes during meiosis I. From this I hypothesise that the aneuploidy observed in the *Smc6*$^{+/GT}$ oocytes, which is not corrected in meiosis II, leads to the development of abnormal embryos that are then lost at day 10.5 (Figure 4.16). This is supported by recent work by Hwang *et al* (2017) who found that *Smc5* cKO mice have high levels of aneuploidy in their oocytes and that once fertilised, oocytes from the *Smc5* cKO mice did not form mature blastocysts. Chromosome cohesion appears to be reduced and chromosome structure was observed to be significantly different in the *Smc6*$^{+/GT}$ oocytes. This indicating it is possible condensin is affected in the *Smc6*$^{+/GT}$ mouse oocytes, as was found in Pryzhkova *et al*, (2016) and Hwang *et al* (2017).

This work indicates that the Smc5/6 complex has a role in regulating chromosome structure and compaction and also a potential role in maintaining chromosome cohesion during mouse meiosis. This indicates that the SMC complexes function together to promote chromosome segregation in mammalian meiosis. It is also possible that the Smc5/6 has a role in promoting joint molecule resolution, as seen in budding yeast meiosis (Copsey et al, 2013; Xaver et al, 2013; Lilenthal et al, 2013). Live cell imaging of the oocytes from the $Smc6^{+/GT}$ mouse should help to provide an insight into if this is the case. If an accumulation of unresolved recombination intermediates is causing the aneuploidy observed then I predict that there would be a large amount of homologous chromosome stretching at metaphase I (as observed in *Smc5* cKO mouse oocytes in Hwang *et al*, 2017). If a loss/weakening of cohesin is instead responsible for the increased levels of aneuploidy in the oocytes from the $Smc6^{+/GT}$ mouse then I predict that the chromosomes would be easily pulled apart.

In humans, aneuploidy rates have been found to be significantly higher in oocytes compared to sperm (Hassold and Hunt, 2001). This difference is likely to be linked to the extended dictyate arrest in females. Females are born with their full complement of oocytes, which remain in an arrested state from birth until ovulation, which in humans can be from 10-50 years later (Hassold and Hunt, 2001). In contrast, in males, sperm is produced post-puberty and from this time onward is produced continually. A mature sperm cell only takes 9 weeks to be generated and if not used is simply degraded. The molecular basis of human aneuploidy is largely unknown. This study suggests that heterozygosity of Smc6 may contribute to human aneuploidy.

Chapter 5: Characterization of SMC protein levels in *Smc6*$^{+/GT}$ mouse oocytes

5.1. Introduction

In the previous chapter, I found that *Smc6*$^{+/GT}$ mice have significantly reduced litter sizes compared to wild type due to aneuploidy and potentially poor chromosome quality in a subset of their oocytes. Further analysis found bivalent deterioration into univalents in MI oocytes from the *Smc6*$^{+/GT}$ mouse as well as compaction defects (Chapter 4). Deterioration of chromosome cohesin could be affected in the oocytes from the *Smc6*$^{+/GT}$ mouse. This hypothesis was supported by the work in Chapter 3, which revealed a role for Smc5/6 complex in cohesin regulation (Outwin et al., 2009; Tapia-Alveal et al., 2010, Kim et al, 2016).

Chromosomes in *Smc6*$^{+/GT}$ mouse oocytes were also observed to be more variable in size, compared to wild type, and often frayed (Chapter 4). Houlard *et al* (2015) found that depletion of condensin II lead to increased chromosome size. This indicated that condensin could also be affected in the oocytes from the *Smc6*$^{+/GT}$ mouse. Support for this idea came from Gallego-Paez et al (2014), who found that the Smc5/6 complex is required to co-ordinate condensin and TopIIα recruitment to newly replicated chromosomes in human mitosis (Gallego-Paez et al, 2014). Further support for this hypothesis comes from Pryzhkova *et al* (2016), who noted a mis-localisation of condensin, more condensin along the chromosome arms and less at the centromeres, in *Smc5* embryonic stem cells and from Hwang *et al* (2017) who observed discontinuous condensin staining along the chromosomes in oocytes from *smc5* cKO mice. In addition Hwang *et al* (2017) observed that there was an overall reduction of condensin staining in the oocytes from *smc5* cKO mice (Hwang et al, 2017).

Only some of the oocytes from *Smc6*$^{+/GT}$ mice displayed aneuploidy and precocious homologue separation, which lead us to two potential models.

The first is a deterministic model that SMC6 is reduced to the same level in all of the oocytes from the *Smc6*$^{+/GT}$ mother and therefore they are all equally predisposed to aneuploidy. Specific oocytes may become aneuploid due to the formation of increased numbers of joint molecules or potentially cohesin misregulation. The second model is a stochastic model proposing that oocytes from the *Smc6*$^{+/GT}$ mouse have different levels of SMC6, thus predisposing them to aneuploidy. In order to investigate this, oocytes need to be examined on single cell basis.

This study aims to investigate the levels of the SMC6, cohesin and condensin in a heterozygous mouse model; therefore, a very sensitive quantification method is required to detect changes in protein levels that are subtler than what you would see in a homozygous mutant. There are very few methods that can be used to look at protein levels on a per oocyte basis. Western blots are commonly used to look at protein levels in populations of cells. Recently a new method to carry out single cell western blots been developed by Hughes *et al* (2014) in order to examine cell to cell variation of protein levels (Hughes et al, 2014). However, for the analysis in this study western blots were not suitable as they were unlikely to be able to determine the very small difference in protein levels between homozygous and heterozygous animals. Western blots are also unable to distinguish between chromosomally bound protein and protein in the cell. In a study by Chiang *et al* (2010) they found no differences in the levels of cohesin in aged oocytes by western blot, but further analysis using immunofluorescence found significantly reduced levels of chromatin-associated cohesin in aged oocytes (Chiang et al, 2010). This indicates that a large amount of the cohesin picked up on the western blot must have been soluble and not associated with chromatin. There are however caveats when using antibody-based quantification to assess protein levels. For example we do not know if the relationship between protein abundance and antibody staining is linear.

In this study I used immunoflourescence to examine chromosome associated protein levels of SMC6, REC8 and SMC4. Immunofluorescence is commonly used to assess the localisation of specific proteins and to calculate distances and sizes. Immunofluorescence more recently has also be used to determine the concentration of protein present in a sample (Pryzhkova et al, 2016). Protein concentration can be calculated using immunofluorescence, as the fluorescent intensity of a pixel in an image is proportional to the number of fluorophores present in that area of the sample. In many papers that have used immunofluorescence to examine protein levels, differences are judged by eye or an area of the image is selected and the average background fluorescence is subtracted from the intensity of the area of interest (Pryzhkova et al, 2016). In this study I was looking for potentially quite subtle differences, thus a systematic approach was developed for the accurate quantification of the protein levels of subunits of the SMC proteins in the *Smc6*$^{+/GT}$ mouse.

5.2. Materials and methods

5.2.1. Determination of the optimum image exposure

As significant chromosome mis-segregation was found in oocytes from *Smc6*$^{+/GT}$ mice, I then tested to see if these errors were linked to disruption of the SMC protein levels in the mouse. In order to make comparisons between the fluorescent protein levels in the *Smc6*$^{+/GT}$ oocytes and wild type oocytes, all the images must be taken at the same exposure and using the same level of transmission. Prior to implementation of the new analysis, images were taken at several different exposures (from 0.05 – 1 second exposure, Figure 5.1). The optimum exposure was then chosen to be on the linear slope of the graph, in this case 0.25 seconds, well before the saturation level was reached at 0.5 seconds. Saturation occurs when the light intensity used to image the sample is too bright. When the camera is saturated it can no longer accurately record the signal produced and information is lost.

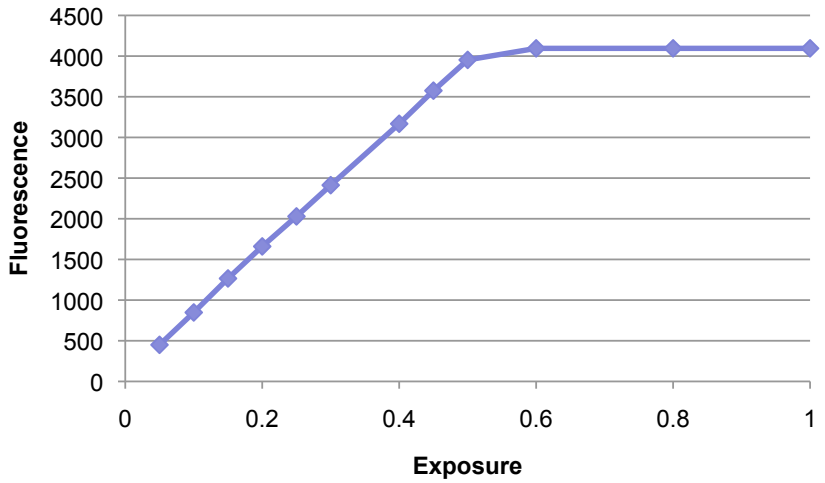

Figure 5.1 – Maximum SMC6 pixel intensity at a range of exposures

Images were taken of a spread containing SMC6 stained with a secondary antibody conjugated to FITC at a range of different exposures. The maximum pixel intensities were determined using the Find Min Max plugin in ImageJ. The graph demonstrates the maximum FITC pixel intensity at 0.05-1 second exposures. It can be seen that fluorescence is linear from 0.05 to 0.5 second exposures. At exposures of 0.55 and higher the images become saturated. From this graph it was chosen that an exposure of 0.25 would be used to image SMC6.

5.2.2. Pipeline for protein level quantification on MI spreads

Two methods were developed which used ImageJ to either determine the total protein levels over the whole spread or specifically the protein levels at the centromere (Figures 5.2 & 5.3). Initially the images were checked to ensure that there was no saturation in any of the channels. To do this the ImageJ plugin FindMaxMin was used. This plugin determines the maximum and minimum pixel intensity in any chosen image. Here any images that included values outside of the dynamic range of the camera were analysed and the reason for the saturation was determined. If it was found to be due to an accumulation of antibody on the spread (a polycomplex) or a bubble on the spread then the images were cropped. If they were saturated due to high signal from the protein of interest, as this meant that data had been lost, the dataset was not included in the analysis.

All of the images were deconvolved in order to restore out of focus light to its original position. This was carried out using SoftworX deconvolution. A mask was then made for either the DAPI signal (in order to determine the amount of protein over the whole spread) or the CREST signal (in order to specifically determine the protein concentration at the centromeres). In order to make the DAPI mask (assessing protein levels over the whole spread) the DAPI channel was selected and I used the ImageJ plugin Mask creator (GDSC ImageJ plugin, Herbert et al, 2014). This works by applying a threshold to the image, which based on the image containing a good signal to noise ratio, segments the DNA signal from the background. To accurately determine the centromeric signal I made a 3D mask of the CREST staining by selecting the CREST channel and using the ImageJ plugin FindFoci GUI. The FindFoci plugin identifies the peak intensity regions in the chosen image. A Gaussian blur is then adjusted in order to segment all of the CREST foci in the image. This produced an output in which every CREST focus was classified as an individual object. The chosen mask was then selected and the ImageJ plugin Mask Analyse Particles was used to determine the

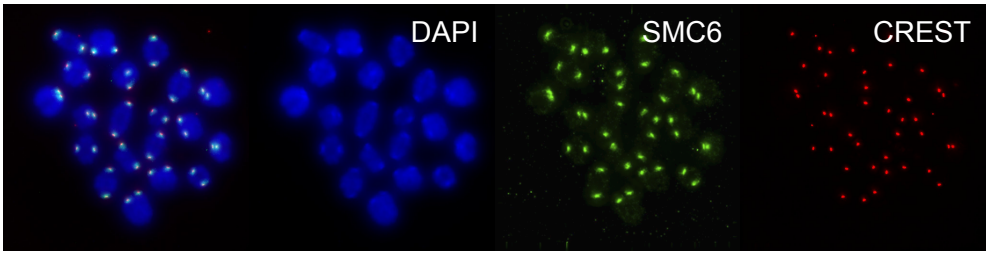

Check for pixel saturation in each of the channels using ImageJ FindMaxMin

Deconvolution

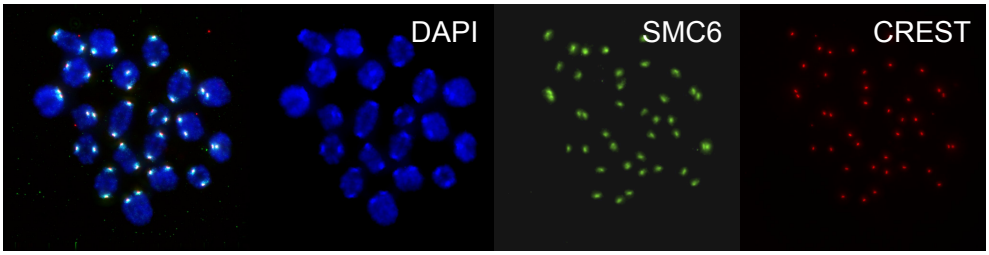

Create a mask of the DAPI staining

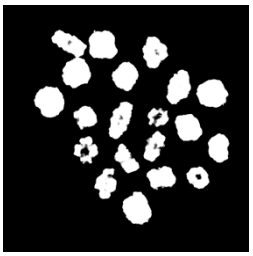

Z-project channel of interest, overlay with DAPI mask and measure the fluorescence within the mask

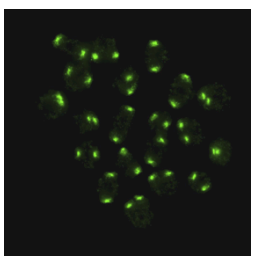

Figure 5.2 - Flow diagram demonstrating how the total fluorescence over a whole a spread is assayed

Initially the images are checked for saturation using the ImageJ plugin Find Min Max. Then each of the images are deconvolved. The DAPI channel is then selected and using the ImageJ plugin Mask Creator a mask of the DAPI channel is made. The channel of interest is then z-projected and the fluorescence of this channel within the DAPI mask is determined using the ImageJ plugin Mask Analyse Particles.

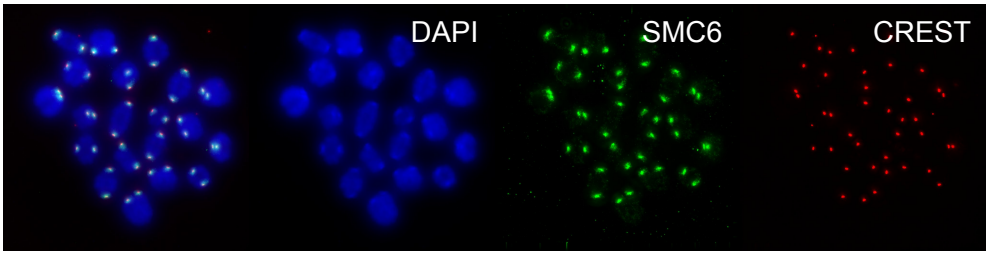

Check for pixel saturation in each of the channels using ImageJ FindMaxMin

Deconvolution

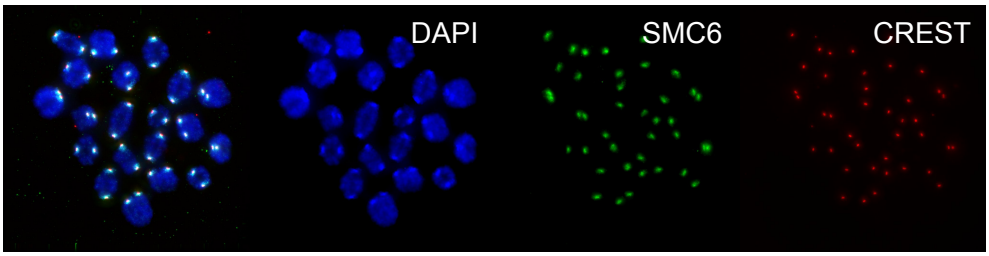

Use FindFoci GUI to identify each of the foci in the image

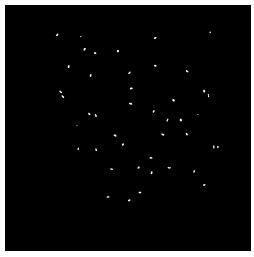

Note: Check that selected foci correspond to crest foci and not background

Z-project channel of interest and FindFoci output, overlay FindFoci output onto channel of interest and measure the fluorescence of each foci using mask analyse particles.

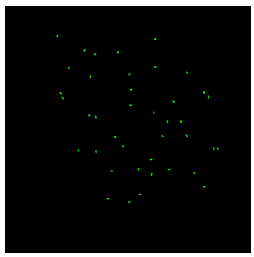

Figure 5.3 - Flow diagram demonstrating how the fluorescence at the centromeres is assessed

Initially the images are checked for saturation using the ImageJ plugin Find Min Max. Then each of the images are deconvolved. The CREST channel is selected and the plugin FindFoci GUI is used to identify each of the CREST foci in 3D in the chosen channel. (At this point it is important to check that all of the foci selected are in-fact CREST foci and not background.) The FindFoci output and the channel of interest are then z-projected and the plugin Mask Analyse Particles is used to determine the average pixel fluorescence of the channel of interest within the mask of each CREST foci.

fluorescence within each of the objects defined in either the DAPI or FindFoci output mask.

5.2.3. Controlling for microscope variation using TetraSpeck beads

In order to control for any differences with the camera/microscope over time, I utilized images of TetraSpeck beads as a control for intensity. Initially the TetraSpeck beads were imaged and the variation in bead intensity determined (Figure 5.4). Significant variation was seen between beads when analyzing the total intensity per bead and the bead intensity per a pixel. In this study, I was looking at the effects of a reduction in protein levels rather than a total knock out, which I predicted would cause very small differences in protein levels. Therefore, it was possible that if the beads are used for normalization, the large variation in bead fluorescence could overwhelm the small change in signal. Instead I chose to use oocytes from littermates from the same imaging session as part of our normalization.

5.2.4. Protein normalisation

Initial analysis of the SMC6 protein levels in wild type and *Smc6*$^{+/GT}$ oocytes found that five of the *Smc6*$^{+/GT}$ oocytes (from two separate slides) had significantly increased levels of SMC6 compared to all of the other spreads (Supplementary figure 7, spreads 15-20). Further analysis found that they also contained significantly increased levels of CREST, suggesting that antibody binding was increased. However, this could also have been due to the presence of different levels of cytoplasm from the oocyte, which could affect antibody binding, or slight differences in the concentrations of the antibodies used. The same antibody preparation was always added to slides from both wild-type and *Smc6*$^{+/GT}$ oocytes in each experiment to ensure that the same concentration of antibody was added to each of the slides, but it may be that for these slides the antibodies were not mixed thoroughly. These differences in antibody binding indicated that an internal control on

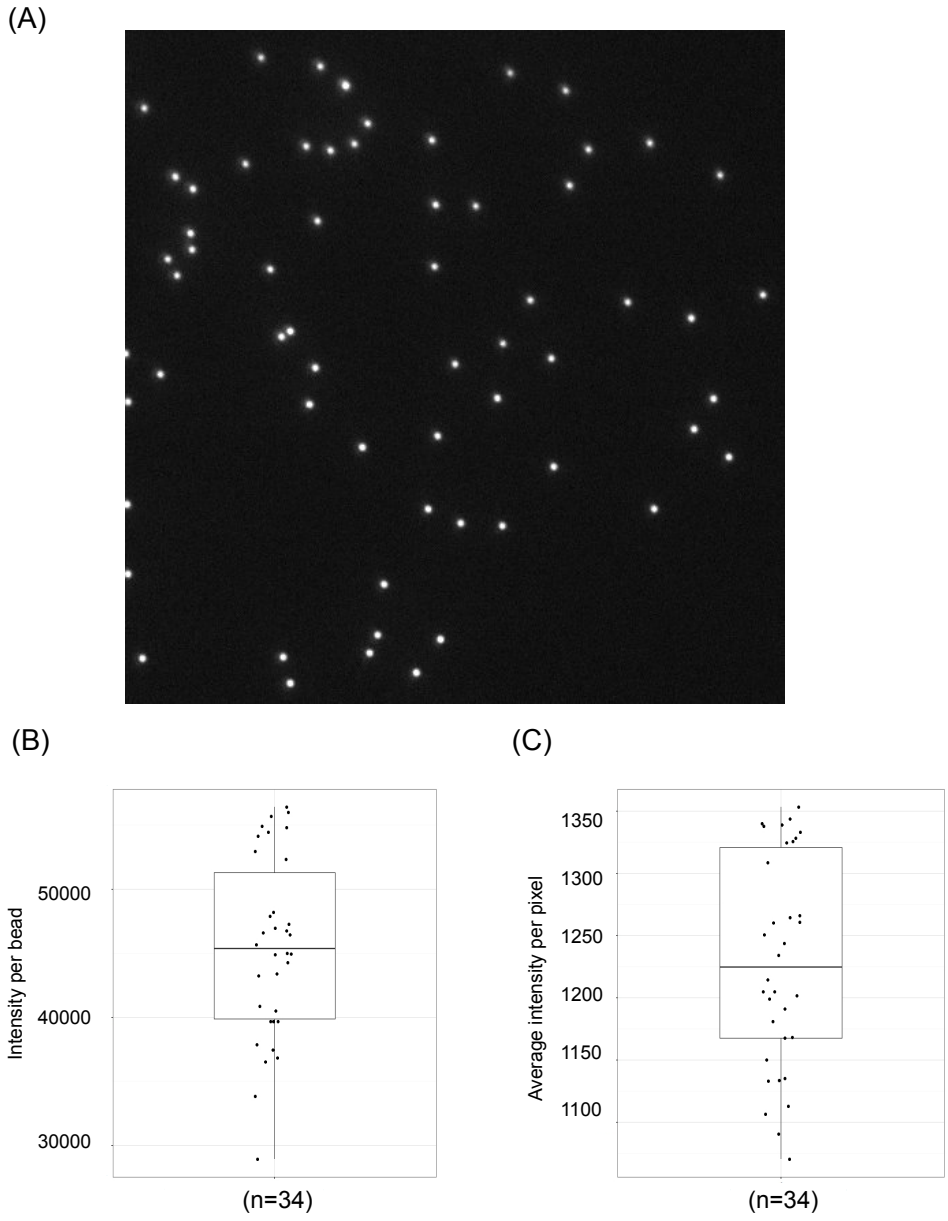

Figure 5.4 – TetraSpeck bead intensity is too variable for use in normalisation

A. Image of TetraSpeck fluorescent beads on a glass slide (100x magnification).

B. Boxplot demonstrating the variation in the total intensity of the TetraSpeck beads (n = No. of beads)

C. Boxplot demonstrating the variation in the average intensity of the TetraSpeck beads (n = No. of beads)

the slide was required. CREST was chosen to be the internal control because I observed that the oocytes with significantly increased levels of SMC6 also displayed significantly increased levels of CREST. A comparison of CREST staining to SMC6 staining was carried out on a per spread basis in wild type (Figure 5.5A). As expected, the correlation of both of the antibodies is not 100% (Figure 5.5B). This is likely due to natural variation in both SMC6 and CREST protein levels and slight variations in the amount of the antibodies added to the slides.

I was also interested in utilizing global antibody staining to compare the total amounts of the proteins between wild type and *Smc6*$^{+/GT}$, thus I tested if total SMC6 protein concentration also varied with CREST (Supplementary figure 8A). Our analysis found that there was a poor correlation between the average CREST intensity and the average total SMC6 intensity (R^2 =0.06, Supplementary figure 8B). I then tested if the average total SMC6 intensity varied more closely with the average DAPI intensity. Large amounts of variation were found in the DAPI staining between experiments and the DAPI signal did not correlate well with the total SMC6 staining (Supplementary figure 9). Therefore, I predicted that the DAPI staining did not correlate with the SMC6 staining, as DAPI is a DNA intercalating agent and so stains differently to antibodies. This indicates that antibody staining must be normalised to another factor stained by antibodies in the same cell.

5.3. Results

5.3.1. Centromeric SMC6:CREST ratio is significantly reduced in *Smc6*$^{+/GT}$ oocytes

Previously I observed that there was significant chromosome mis-segregation in the oocytes from the *Smc6*$^{+/GT}$ mouse. Interestingly mis-segregation was not observed in all of the oocytes from the *Smc6*$^{+/GT}$ mouse, only 33% displayed mis-segregation. I therefore set out to investigate why the chromosomes mis-segregated in some of the oocytes from the *Smc6*$^{+/GT}$

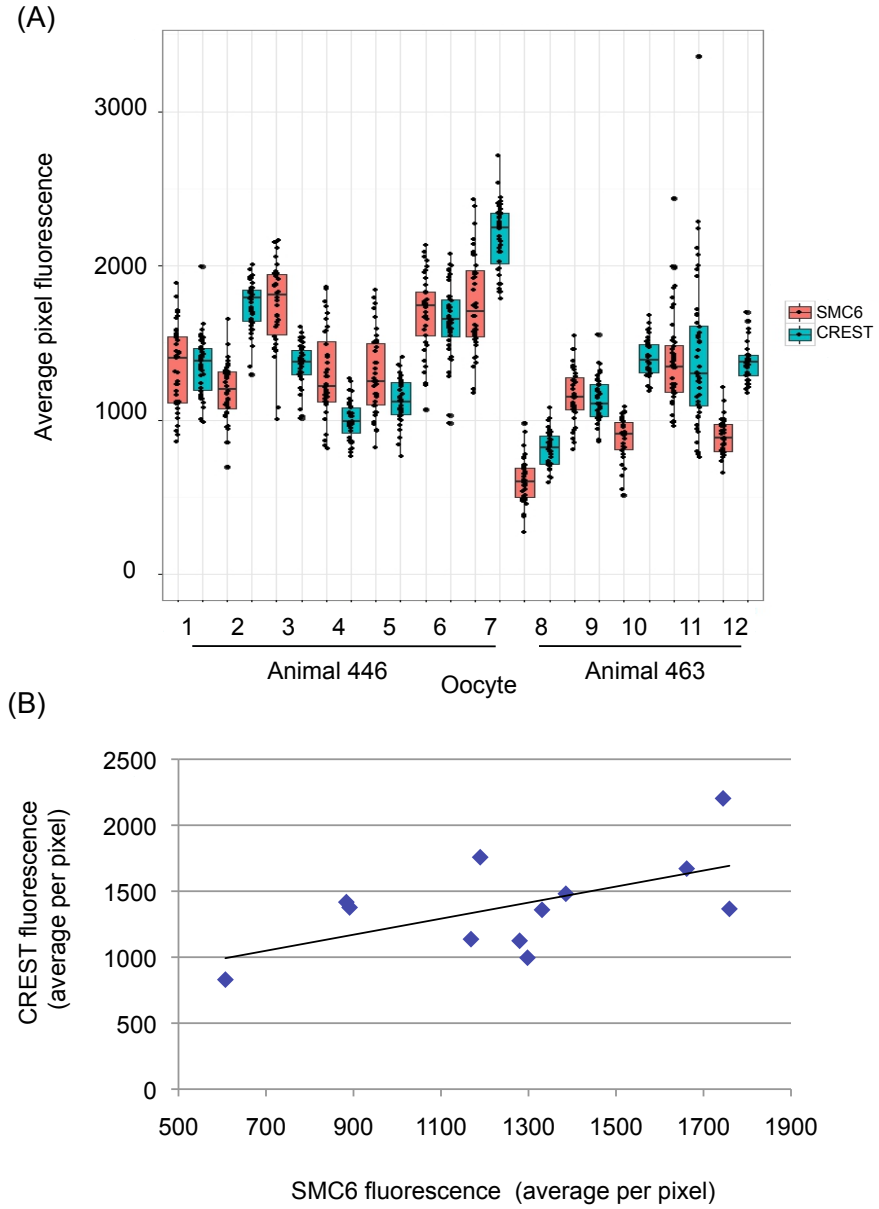

Figure 5.5 – Centromeric SMC6 signal varies with CREST signal

A. Boxplot comparing the average centromeric pixel signal from SMC6 and CREST on a per spread basis. (Jittering corresponds to individual centromeric signals.) Oocytes were all from two wild type mice (Animals 446 & 463). **(**Mouse experiments 14 & 15)

B. Graph demonstrating how the average centromeric SMC6 pixel signal correlates with the average CREST pixel signal on a per spread basis (R^2=0.3397) (Oocytes from animals 446 & 463). **(**Mouse experiments 14 & 15)

mother and not in others. Firstly I wanted to investigate if the levels of functional SMC6 were altered in the oocytes from the *Smc6*$^{+/GT}$ mouse. I hypothesized that there may be variation in the levels of SMC6 in the oocytes from the *Smc6*$^{+/GT}$ mother and that this was causing the observed chromosome mis-segregation. In order to test this, MI oocytes from both wild type and *Smc6*$^{+/GT}$ were stained using an antibody against the C-terminus of SMC6 kindly proved by Alan Lehmann (Gomez et al, 2013). The fragment produced after the addition of an exon trap to intron 6 of SMC6 will only produce a small N-terminal fragment that if present in the cell, will not be recognized by this antibody. Initially the oocytes were visually analysed to determine the localisation of SMC6 in wild type (n=53) compared to *Smc6*$^{+/GT}$ (n=73). SMC6 signal was generally observed as an accumulation at the centromeric and pericentromeric region and threadlike staining along the chromosome arms (Figure 5.6 & 5.7), as seen previously in mouse oocytes and spermatocytes (Gomez et al, 2013; Hwang et al, 2017; Verver et al, 2013). As the *Smc6*$^{+/GT}$ mouse only has reduced levels of functional SMC6 I expected differences in protein levels to be quite subtle. By eye, no clear difference in the SMC6 protein levels could be observed. The number of the oocytes from the *Smc6*$^{+/GT}$ mice displaying just centromeric and pericentromeric SMC6 staining, centromeric, pericentromeric and faint arm SMC6 staining and centromeric, pericentromeric and arm SMC6 staining were not significantly different to wild type (Figure 5.8A)

As analysis by eye is quite subjective and small differences in protein levels cannot be determined quantitative analysis was also carried out. As I previously found that the average centromeric CREST fluorescence varied with the average centromeric SMC6 fluorescence I normalised centromeric SMC6 fluorescence to CREST (Figure 5.5A). I observed that the level of SMC6 was significantly reduced at the centromeres in the oocytes from the *Smc6*$^{+/GT}$ mouse (Figure 5.8C). The centromeric SMC6 signals were then compared amongst oocytes to determine whether all of the oocytes displayed reduced levels of SMC6 or if specific oocytes were instead causing

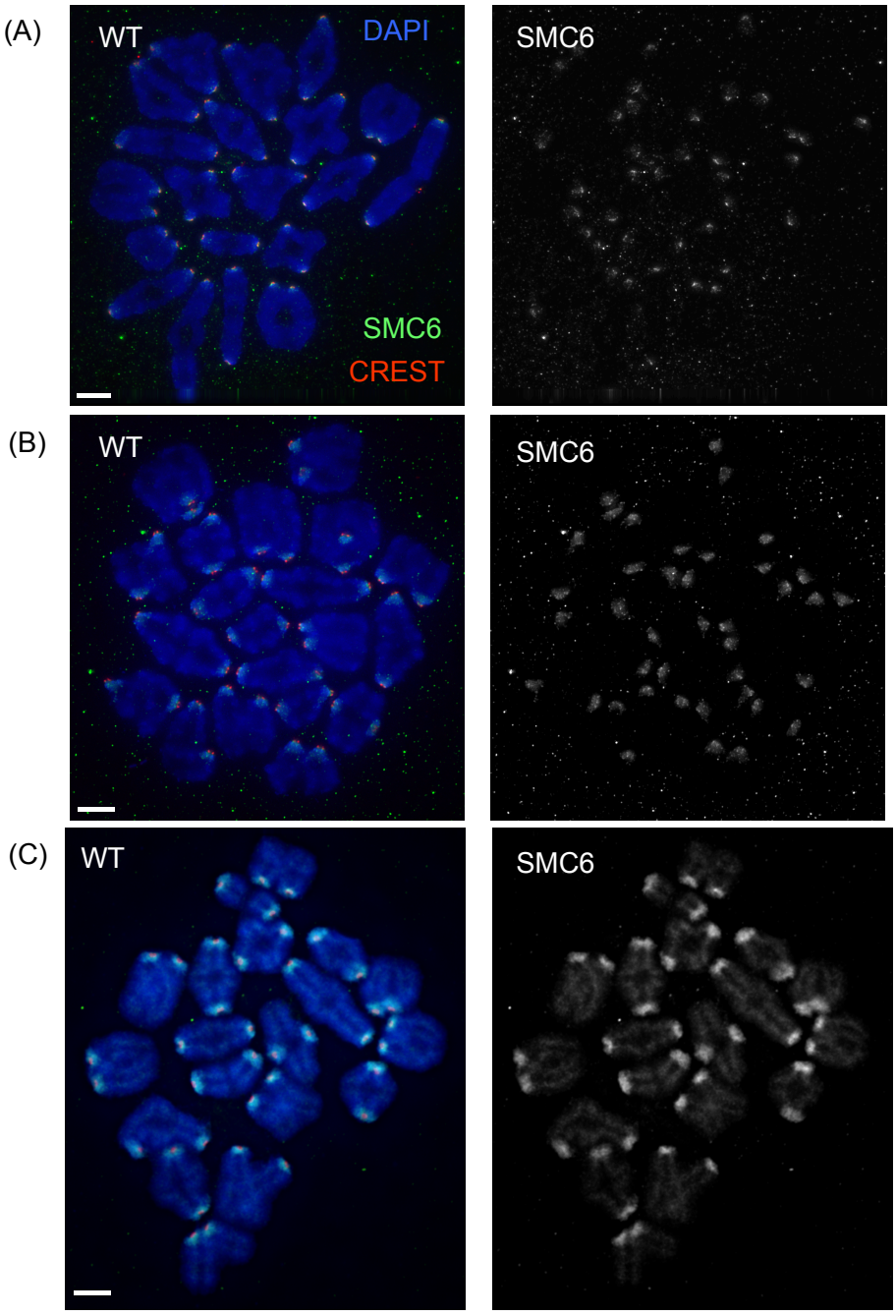

Figure 5.6 - SMC6 staining in wild type MI oocytes

Images of wild type MI oocytes stained with DAPI (blue), human anti-CREST (red) and rabbit anti-SMC6 (green). All images were taken using at 32% transmission using a 0.25 second exposure to ensure that the images were not saturated. Image (A) was classified as just having centromeric and pericentromeric SMC6 staining, Image (B) was classified as displaying centromeric, pericentromeric and faint arm SMC6 staining and Image (C) was classified as displaying centromeric, pericentromeric and arm SMC6 staining. Scale bar 5 μm. (Mouse experiments 14 & 15)

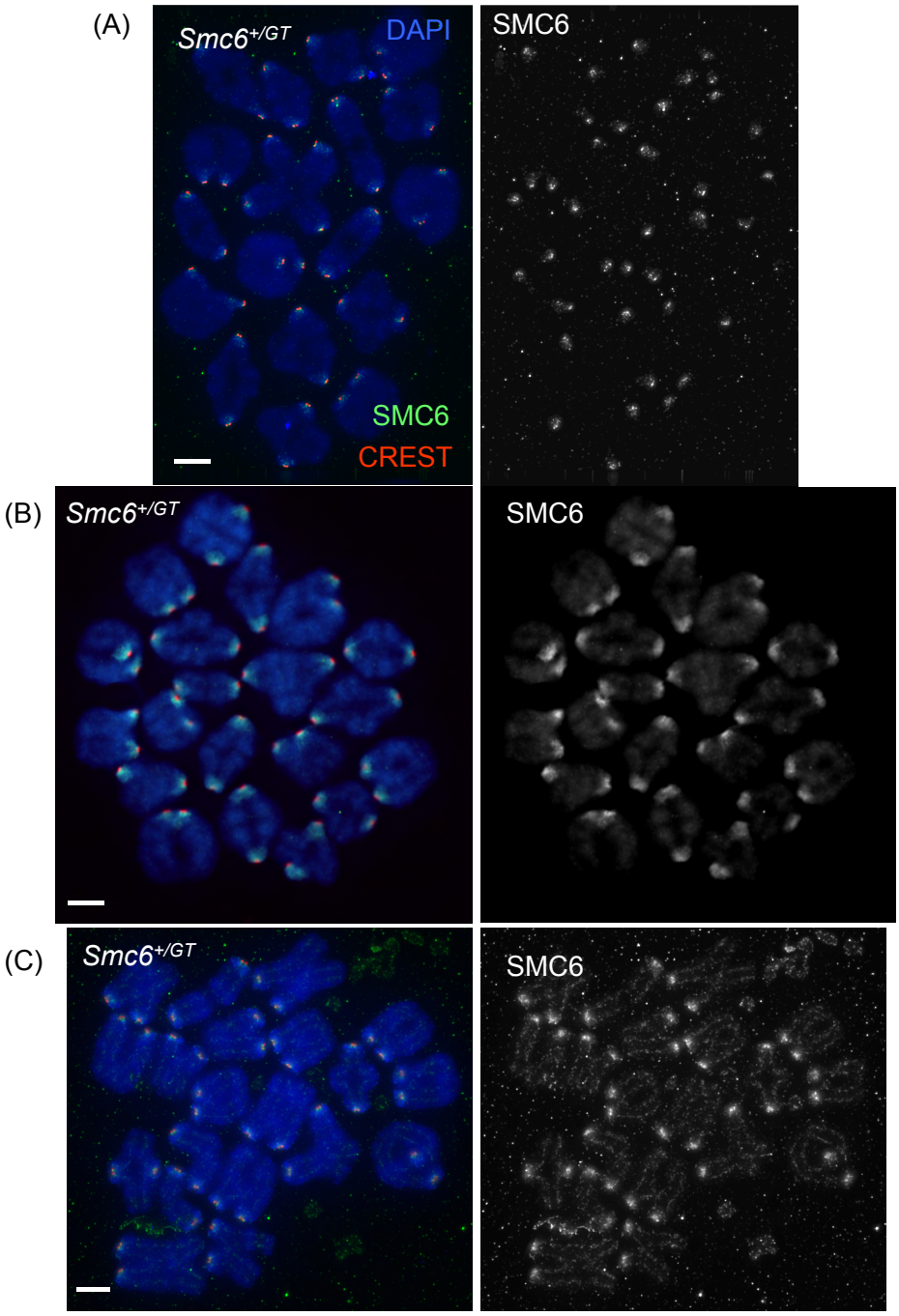

Figure 5.7 - SMC6 staining in *Smc6*$^{+/GT}$ MI oocytes

Images of *Smc6* $^{+/GT}$ MI oocytes stained with DAPI (blue), human anti-CREST (red) and rabbit anti-SMC6 (green). All images were taken using at 32% transmission using a 0.25 second exposure to ensure that the images were not saturated. Image (A) was classified as just having centromeric and pericentromeric SMC6 staining, Image (B) was classified as displaying centromeric, pericentromeric and faint arm SMC6 staining and Image (C) was classified as displaying centromeric, pericentromeric and arm SMC6 staining. Scale bar 5 µm. (Mouse experiments 14 & 15)

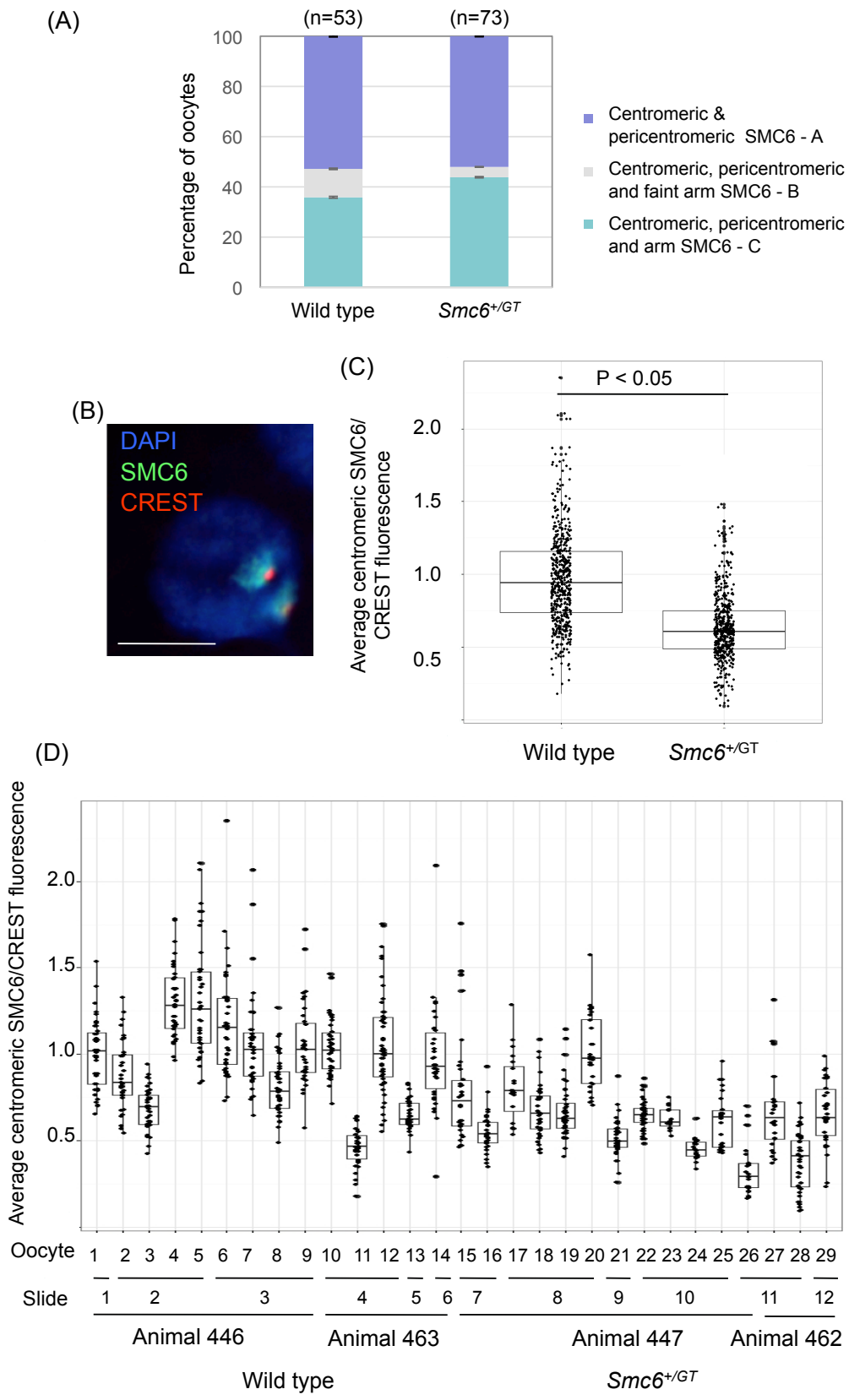
(A)
(n=53)
(n=73)
Percentage of oocytes
100
80
60
40
20
0
Wild type
Smc6+/GT
Centromeric & pericentromeric SMC6 - A
Centromeric, pericentromeric and faint arm SMC6 - B
Centromeric, pericentromeric and arm SMC6 - C
(B)
DAPI
SMC6
CREST
(C)
P < 0.05
Average centromeric SMC6/CREST fluorescence
2.0
1.5
1.0
0.5
Wild type
Smc6+/GT
(D)
Average centromeric SMC6/CREST fluorescence
2.0
1.5
1.0
0.5
Oocyte 1 2 3 4 5 6 7 8 9 10 11 12 13 14 15 16 17 18 19 20 21 22 23 24 25 26 27 28 29
Slide 1 2 3 4 5 6 7 8 9 10 11 12
Animal 446
Animal 463
Animal 447
Animal 462
Wild type
Smc6+/GT

Figure 5.8 – Centromeric SMC6:CREST ratio is significantly reduced in *Smc6*$^{+/GT}$ oocytes

A. Bar graph demonstrating the percentage of MI oocyte spreads that display either only centromeric & pericentromeric SMC6 staining (A in Figure 5.6 & 5.7), centromeric, pericentromeric and faint arm SMC6 staining (B in Figure 5.6 & 5.7) or centromeric, pericentromeric and arm SMC6 staining (C in Figure 5.6 & 5.7) in both wild type (n=53) and *Smc6*$^{+/GT}$ (n=73).

B. Image of a chromosome stained with DAPI (blue), human anti-CREST (red) and rabbit anti-SMC6 (green). Scale bar 5μm.

C. Boxplot of the average SMC6 centromeric levels normalised to CREST in both wild type (n=13) and *Smc6*$^{+/GT}$ (n=16). Here the jittering corresponds to the average pixel values of individual centromeric signals on a per spread basis. (Wilcox test $P < 0.05$) (Mouse experiments 14 & 15)

D. Boxplot showing the average centromeric SMC6 fluorescent levels normalised to CREST on a per spread basis in both wild type (animals 446 & 463) and *Smc6*$^{+/GT}$ (animals 447 & 462). Animals 446 and 447 were litter mates and so were animals 462 and 463. Here the jittering corresponds to the average pixel values of individual centromeric signals. (Mouse experiments 14 & 15)

the observed reduction in SMC6. There was substantial variation in the SMC6 fluorescence in the oocytes from the *Smc6*$^{+/GT}$ and wild type mice, however, SMC6 fluorescence was generally reduced in the oocytes from the *Smc6*$^{+/GT}$ females (Figure 5.8D). This indicates that when one of the copies of SMC6 is non-functional, the level of SMC6 at the centromeres is reduced. I propose that the variation in the levels of SMC6 staining from oocyte to oocyte may explain why some oocytes were aneuploid. It however cannot be ruled out that the differences observed are in part due to technical variations such as differences in the concentration of PFA in contact with the oocytes, differences in humidity or differences in antibody concentration.

5.3.2. Combined centromeric and pericentromeric SMC6:CREST ratio is significantly reduced in *Smc6*$^{+/GT}$ oocytes

As I observed that there was also significant SMC6 staining in the pericentromeric region, the combined centromeric and pericentromeric SMC6 staining was compared in both wild type and *Smc6*$^{+/GT}$ oocytes (Figure 5.9A.). I predicted that a greater difference would be observed in the levels of SMC6 when the combined centromeric and pericentromeric SMC6 fluorescence was compared in the oocytes from wild type and *Smc6*$^{+/GT}$ females, as this provides a readout of the majority of the SMC6 staining along the chromosomes. Thus any differences will be exacerbated compared to when staining at the centromere alone is compared (Figure 5.9B). In order to test this, I used a similar method to the method previously used to determine the centromeric SMC6 fluorescence. Here the ImageJ plugin Mask creator was used to create a mask of the area covering the centromeric and pericentromeric SMC6 fluorescence (Figure 5.9C). As the fluorescence in this region was significantly brighter than the fluorescence observed along the chromosome arms it could be easily segmented. The combined centromeric and pericentromeric SMC6 fluorescence was then compared to the CREST fluorescence, on a per spread basis, to see if CREST could again be normalised to. It was found that generally the average

(A)

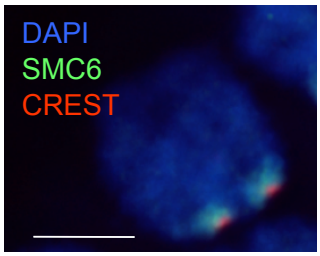
DAPI
SMC6
CREST

(B)

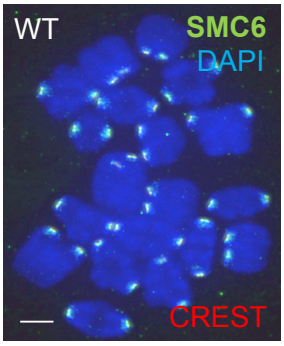
WT
SMC6
DAPI
CREST

(C)

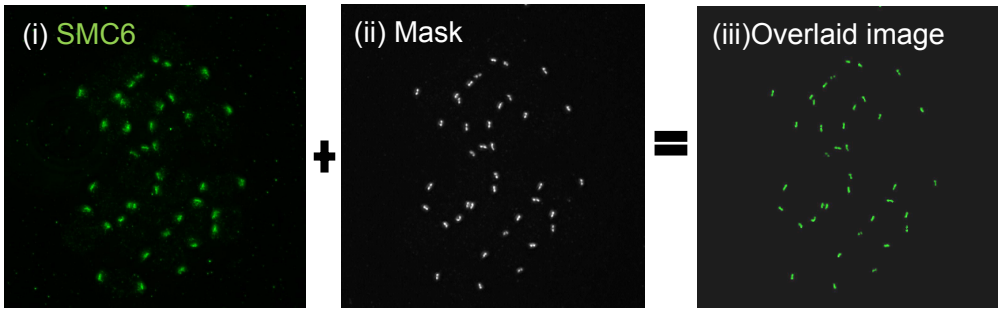
(i) SMC6
(ii) Mask
(iii)Overlaid image

(D)

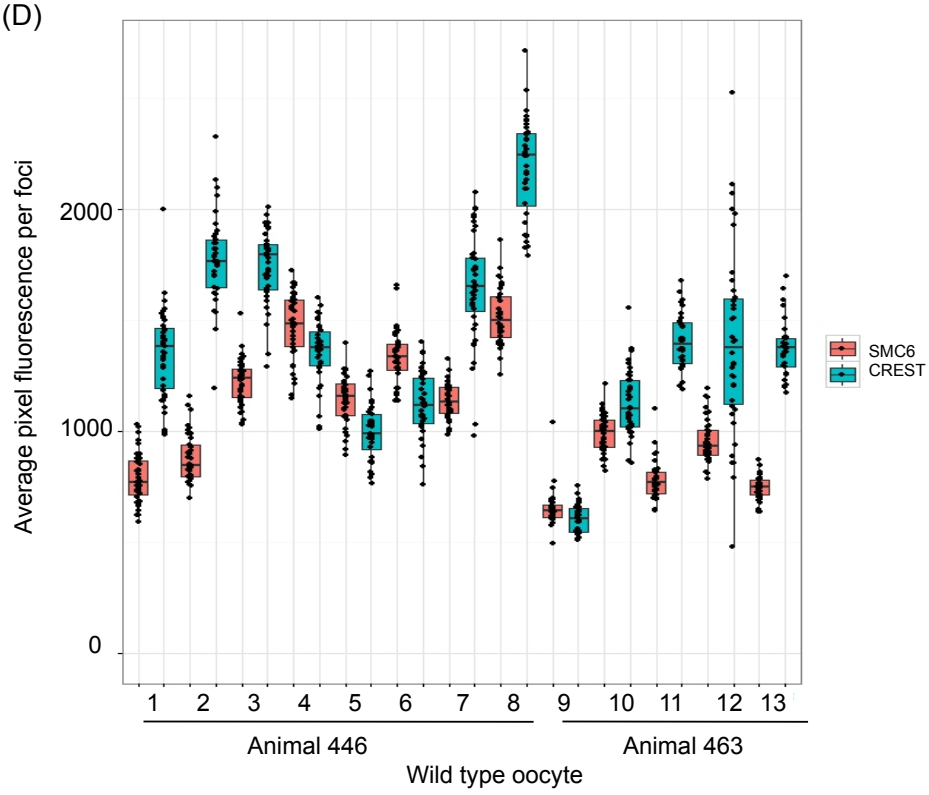
Average pixel fluorescence per foci
2000
1000
0
1
2
3
4
5
6
7
8
9
10
11
12
13
Animal 446
Animal 463
Wild type oocyte
SMC6
CREST

Figure 5.9 – Analysis of SMC6 staining in the combined centromeric and pericentromeric area compared to CREST in wild type oocytes

A. Image of a chromosome stained with DAPI (blue), human anti-CREST (red) and rabbit anti-SMC6 (green) demonstrating that there is significant pericentromeric SMC6 staining. Scale bar 5μm.

B. Image of a MI spread stained with DAPI (blue), human anti-CREST (red) and rabbit anti-SMC6 (green). Scale bar 5μm.

C. Panel demonstrating how SMC6 fluorescent levels are assessed within the combined centromeric and pericentromeric area. The SMC6 channel is selected and the plugin FindFoci GUI is used to identify each of the regions corresponding to the combined centromeric and pericentromeric SMC6 fluorescence in 3D. As the centromeric and pericentromeric SMC6 fluorescence is significantly brighter than the SMC6 arm region fluorescence the centromeric and pericentromeric regions can be accurately segmented. The FindFoci output is z-projected and the plugin Mask Analyse Particles is used to determine the SMC6 fluorescence within the area of the combined centromeric and pericentromeric mask.

D. Boxplot comparing the average pixel signal from the combined centromeric and pericentromeric SMC6 areas and CREST on a per spread basis. Jittering corresponds to individual peri-centromeric signals. Oocytes were all from two wild type mice (animals 446 & 463). **(**Mouse experiments 14 & 15)

centromeric and pericentromeric SMC6 fluorescence varied with the average CREST fluorescence (Figure 5.9D). Overall analysis found the average centromeric and pericentromeric SMC6 fluorescence was significantly reduced in *Smc6*$^{+/GT}$ oocytes ($P < 0.05$, Figure 5.10A). Analysis of the average centromeric and pericentromeric SMC6 signal on a per spread basis demonstrated that the majority of the spreads from the *Smc6*$^{+/GT}$ mice displayed lower levels of centromeric and pericentromeric SMC6 (Figure 5.10B). The difference was not as pronounced as observed in the comparison of the centromeric SMC6 fluorescence. This may indicate that the localisation of SMC6 is affected in the *Smc6*$^{+/GT}$ oocytes, meaning that there is less at the centromere but not significantly less around the centromere. Alternatively it is possible that there is more variation in SMC6 staining in the pericentromeric region. Overall a reduction was observed in the levels of SMC6 in oocytes from the Smc6$^{+/GT}$ mouse both through analysis at the centromere alone and at the area covering the centromere and the pericentromere. Variability in the SMC6 protein level was observed between the mice and between oocytes. From this it was predicted that there may also be co-variation in other regulatory proteins.

5.3.3. SMC4 signal is variable in oocytes

Since the oocytes from the *Smc6*$^{+/GT}$ mouse generally had larger chromosomes (Section 4.2.7), I hypothesized that condensin could be affected as deletion of either of the condensin complexes leads to increased chromosome size (Houlard et al, 2015). Furthermore, condensin is mis-localised in human cells depleted of Smc5 and in *Smc5* embryonic stem cells (Pryzhkova et al, 2016; Gallego-Paez et al, 2014). Condensin, like the other SMC proteins, is made up of a central heterodimer of two SMC proteins (SMC2 and SMC4) joint by a kleisin (NCAPH or NACPH2). In order to assess condensin localisation in the *Smc6*$^{+/GT}$ oocytes, MI spreads were stained with an antibody against SMC4 (Novus biological). SMC4 staining was present along the chromosome arms and at the centromeres (Figure 5.11 & 5.12) consistent with previous observations Pryzhkova *et al* (2016). The

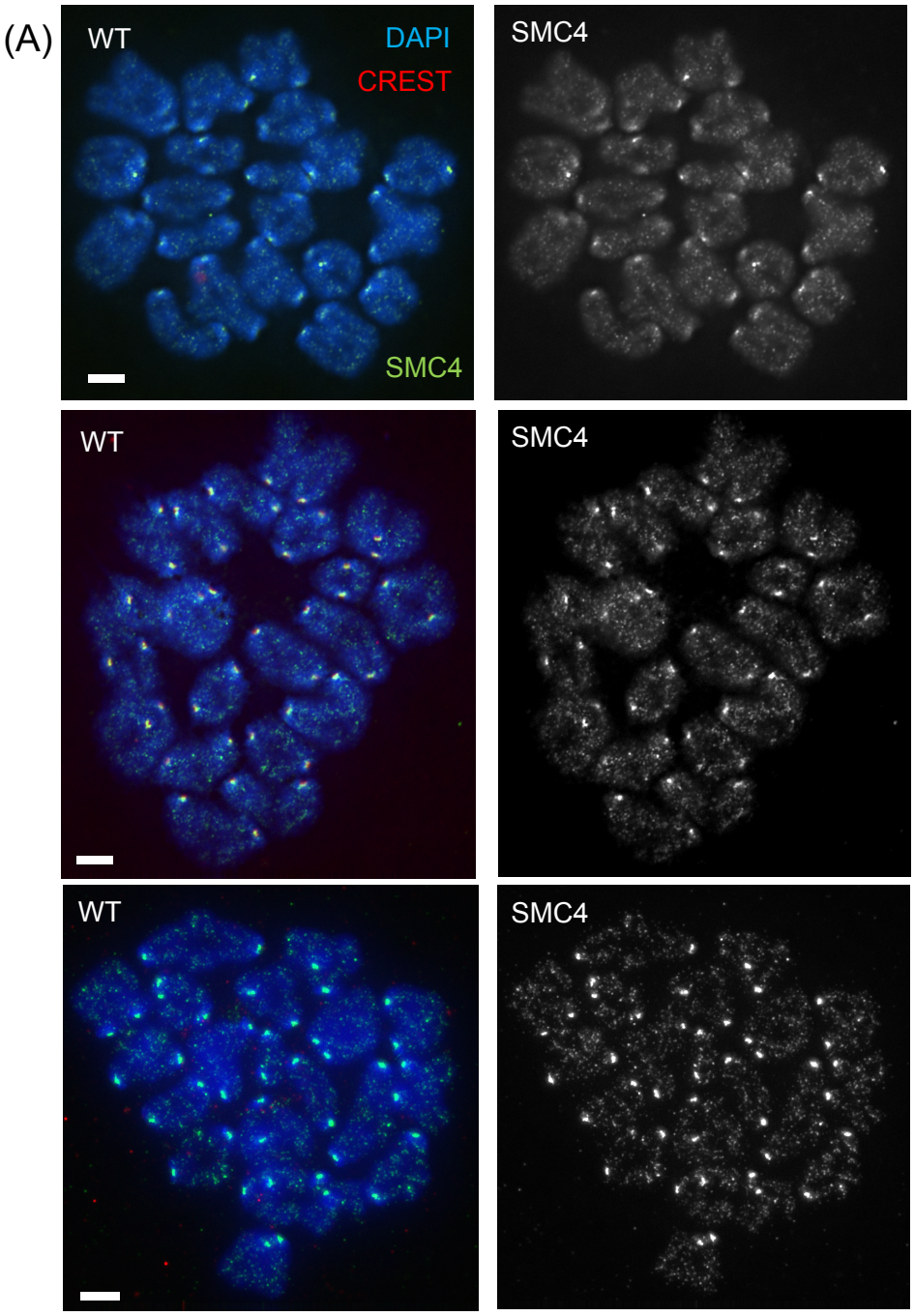

Figure 5.11 – SMC4 staining in wild type MI oocytes

Images of wild type oocytes stained with DAPI (blue), anti-human CREST (red) and anti-rabbit SMC4 (green). All images were taken using at 32% transmission using a 0.2 second exposure to ensure that the images were not saturated. Scale bar 5 μm. **(**Mouse experiments 16 & 18)

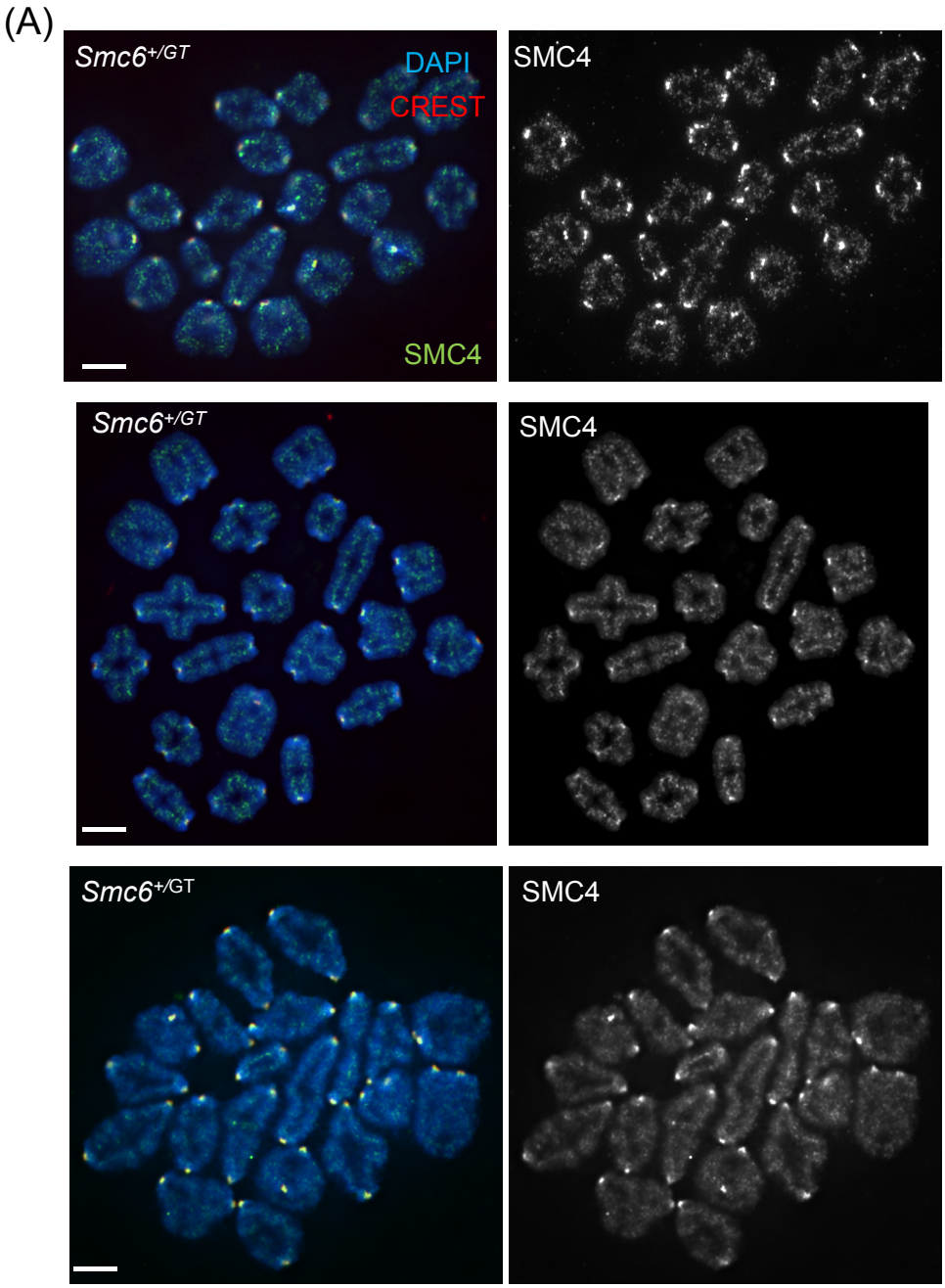

Figure 5.12 - SMC4 staining in *Smc6$^{+/GT}$* MI oocytes

Images of *Smc6$^{+/GT}$* oocytes stained with DAPI (blue), anti-human CREST (red) and anti-rabbit SMC4 (green). All images were taken using at 32% transmission using a 0.2 second exposure to ensure that the images were not saturated. Scale bar 5 μm. (Mouse experiments 16 & 18)

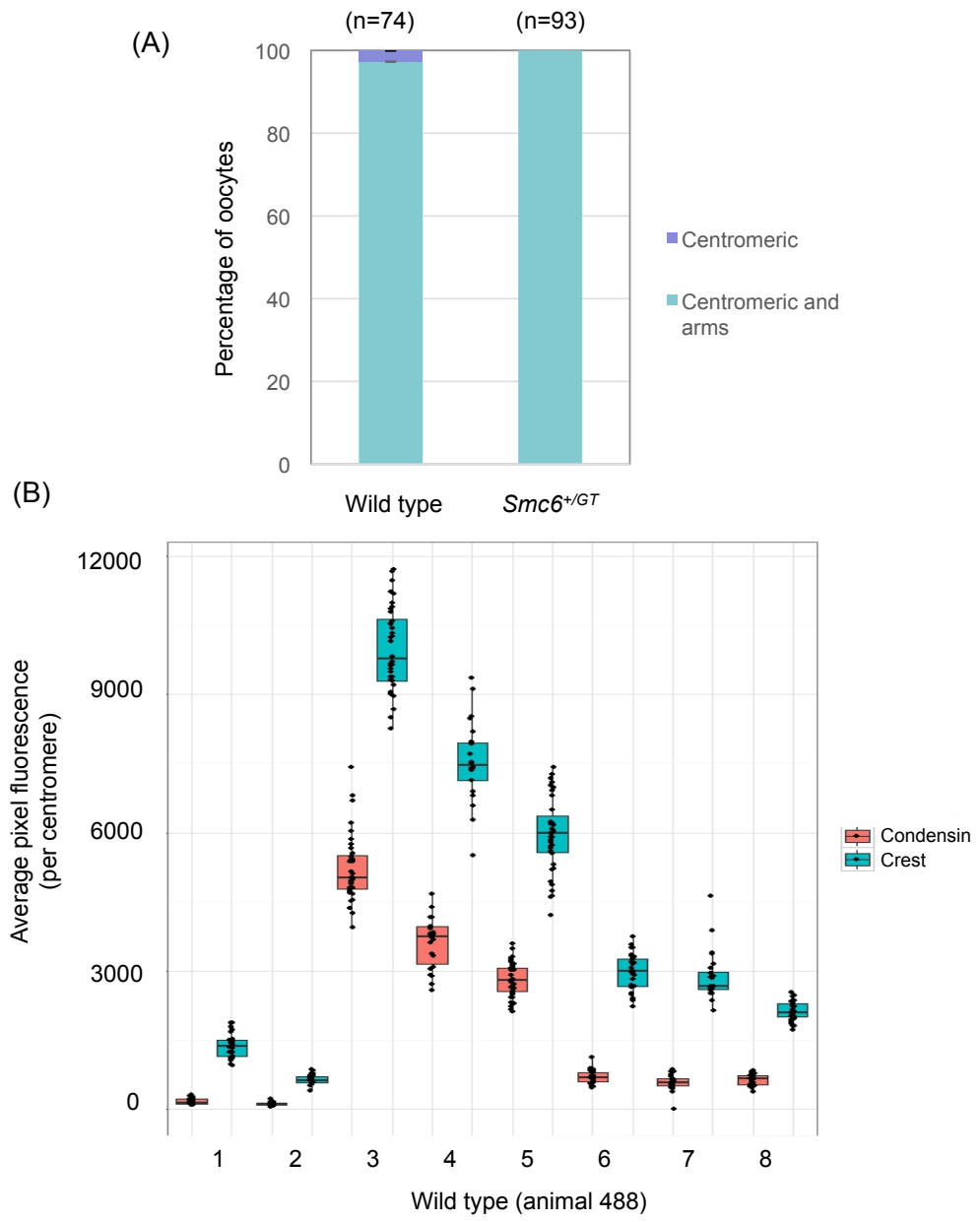

Figure 5.13 – Analysis of SMC4 fluorescence in wild type MI oocytes

A. Bar graph demonstrating the percentage of MI oocyte spreads, in both wild type (n=74) and *Smc6*$^{+/GT}$ (n=93), that display centromeric only SMC4 staining or centromeric and arm SMC4 staining. (Mouse experiment 18)

B. Graph demonstrating how the average CREST fluorescence varies with the average SMC4 fluorescence (in the area defined by CREST) on a per chromosome basis, plotted on a per spread basis in wild type (animal 488). (Mouse experiment 18)

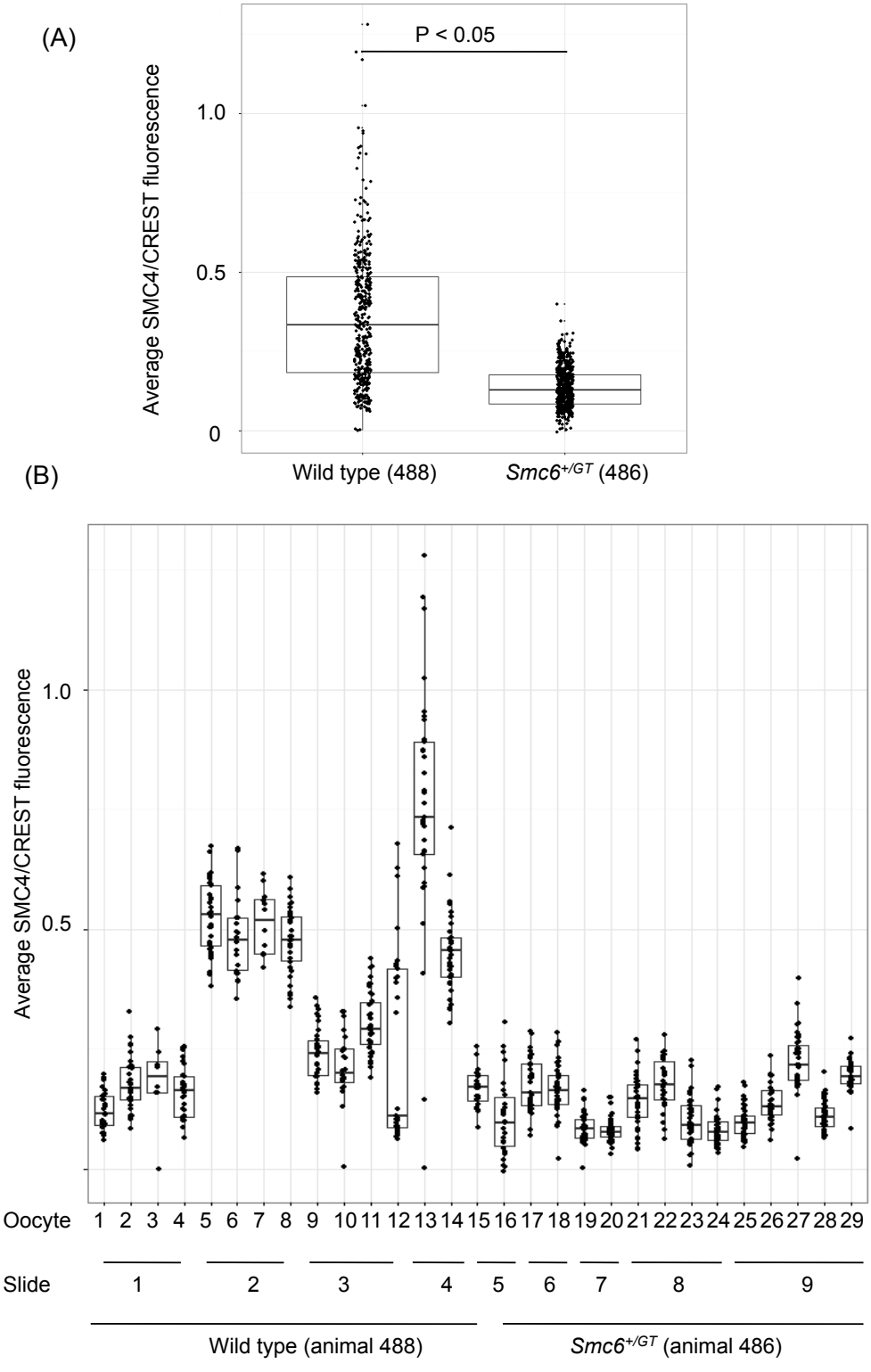
(A)
P < 0.05
Average SMC4/CREST fluorescence
1.0
0.5
0
Wild type (488)
Smc6+/GT (486)
(B)
Average SMC4/CREST fluorescence
1.0
0.5
Oocyte 1 2 3 4 5 6 7 8 9 10 11 12 13 14 15 16 17 18 19 20 21 22 23 24 25 26 27 28 29
Slide 1 2 3 4 5 6 7 8 9
Wild type (animal 488)
Smc6+/GT (animal 486)

Figure 5.14 – Centromeric SMC4:CREST ratio is significantly reduced in MI oocytes from the *Smc6$^{+/GT}$* mouse

A. Boxplot of the average centromeric SMC4 fluorescence levels normalised to average CREST fluorescence on a per chromosome basis in both wild type (animal 488, n=15) and *Smc6$^{+/GT}$* (animal 486, n=14). Here the mice were matched littermates. (Mouse experiment 18)

B. Boxplot of the average centromeric SMC4 fluorescence levels normalised to average CREST fluorescence on a per chromosome basis, plotted on a per spread basis in both wild type (animal 488) and *Smc6$^{+/GT}$* (animal 486). (Mouse experiment 18)

(A)

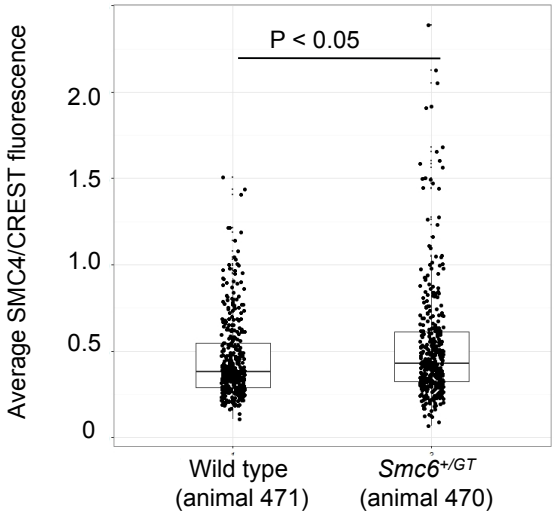
P < 0.05
Average SMC4/CREST fluorescence
2.0
1.5
1.0
0.5
0
Wild type
(animal 471)
Smc6+/GT
(animal 470)

(B)

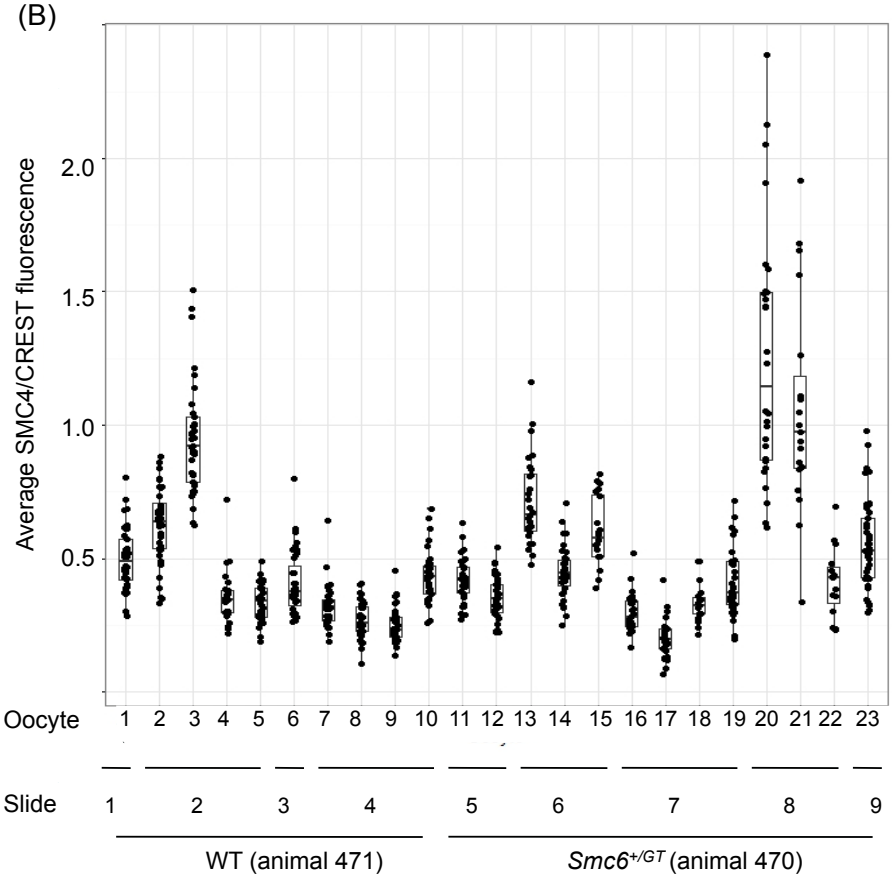
Average SMC4/CREST fluorescence
2.0
1.5
1.0
0.5
Oocyte 1 2 3 4 5 6 7 8 9 10 11 12 13 14 15 16 17 18 19 20 21 22 23
Slide 1 2 3 4 5 6 7 8 9
WT (animal 471)
Smc6+/GT (animal 470)

Figure 5.15 – SMC4:CREST ratio is variable in *Smc6*$^{+/GT}$ oocytes

A. Boxplot of the average centromeric SMC4 fluorescence levels normalised to average CREST fluorescence on a per chromosome basis in wild type (animal 471, n=11) and *Smc6*$^{+/GT}$ (animal 470, n=13). Here the mice were matched littermates. (Mouse experiment 16)

B. Boxplot of the average centromeric SMC4 fluorescence levels normalised to average CREST fluorescence on a per chromosome basis, plotted on a per spread basis in both wild type (animal 471) and *Smc6*$^{+/GT}$ (animal 470). (Mouse experiment 16)

spreads were analysed to determine the percentage of cells that displayed centromeric only SMC4 staining or centromeric and arm SMC4 staining (Figure 5.13A). It was found that all of the oocytes from the *Smc6*$^{+/GT}$ mice displayed both arm and centromeric SMC4 staining. A small proportion of wild type oocytes (3%) displayed only centromeric condensin ($P > 0.05$).

In order to examine the levels of centromeric SMC4 the average SMC4 fluorescence of each centromere was normalised to the average CREST fluorescence of that centromere. (Figure 5.13B demonstrates that SMC4 fluorescence varies with CREST fluorescence in wild type on a per spread basis.) Initially SMC4 stained spreads were compared in littermate's animal 488 (wild type) and animal 486 (*Smc6*$^{+/GT}$). It was observed overall that SMC4 levels were significantly reduced in the oocytes from the *Smc6*$^{+/GT}$ mouse ($P < 0.005$, Figure 5.14A). Analysis on a per spread basis demonstrated that that condensin was generally significantly reduced in all the oocytes from the *Smc6*$^{+/GT}$ mouse. SMC4 localisation was also assessed in another pair of littermates (animal 471 – wild type and animal 470 – *Smc6*$^{+/GT}$). Contrastingly here overall it was observed that SMC4, on a per mouse basis, was significantly increased in oocytes from the *Smc6*$^{+/GT}$ mouse. Analysis on a per spread basis however indicated that there was great variability in the staining in both the wild type and *Smc6*$^{+/GT}$ oocytes and that the significant difference between wild type and *Smc6*$^{+/GT}$ mouse oocytes observed was due to two oocytes from the *Smc6*$^{+/GT}$ mouse displaying significantly higher levels of SMC4 staining (Figure 5.15B, spreads 20 and 21). Further experiments are required to determine if condensin is affected in the oocytes from the *Smc6*$^{+/GT}$ mouse.

5.3.4. REC8 is variable in oocytes

Murine oocytes display age dependent decay of the important meiotic components such as cohesin (Lister et al, 2010). If cohesin is precociously degraded then this can lead to chiasmata slippage and chromosome mis-segregation. As both aneuploid and bivalent deterioration were observed in

oocytes from the *Smc6*$^{+/GT}$ mouse I investigated if cohesin was affected in the oocytes from the *Smc6*$^{+/GT}$ mouse. In order to look at the cohesin localisation MI spreads were stained with an antibody against REC8 (donated by Scott Keeney). It was observed, as in Garcia-Cruz *et al* (2010), that there was cohesin along the chromosome arms and at the centromeres, similar to what was seen for SMC4 (Figure 5.16 & 5.17). Initial analysis by eye found that all of the oocyte chromosome spreads, from both wild type and *Smc6*$^{+/GT}$ mice, displayed both arm and centromeric REC8. This staining pattern was also observed in oocytes from *Smc5* cKO mice in Hwang *et al* (2017).

In order to determine if CREST could be used as a normalizing factor a comparison was made between the average centromeric REC8 fluorescence and average CREST fluorescence of each spread (Figure 5.18). I found that centromeric REC8 fluorescence in the oocytes from one mouse (480) generally varied with CREST. Several of the spreads from a different mouse (374) however had significantly higher CREST intensities compared to REC8. Analysis of littermate's animal 374 (wild type) and animal 375 (*Smc6*$^{+/GT}$) revealed elevated levels of centromeric REC8 in the *Smc6*$^{+/GT}$ oocytes compared to wildtype (Figure 5.19A). Some of the spreads from 375 (*Smc6*$^{+/GT}$) displayed significantly increased levels of centromeric REC8 compared to wild type (Figure 5.24A, Wilcox test $P < 0.005$). However because of the variability observed in the CREST staining in the wild type mouse oocytes it is difficult to determine if this is variability has biological significance (Figure 5.19B).

To test this further the centromeric REC8 staining I examined a second pair of littermates (animals 480 & 481). As stated previously the centromeric REC8 fluorescence in the wild type oocytes (animal 480) varied quite consistently with the CREST fluorescence (Figure 5.18). When the average centromeric REC8 fluorescence was normalised to the average CREST staining on a per centromere basis I observed that the centromeric REC8 fluorescence appeared significantly reduced in all the *Smc6*$^{+/GT}$ mouse

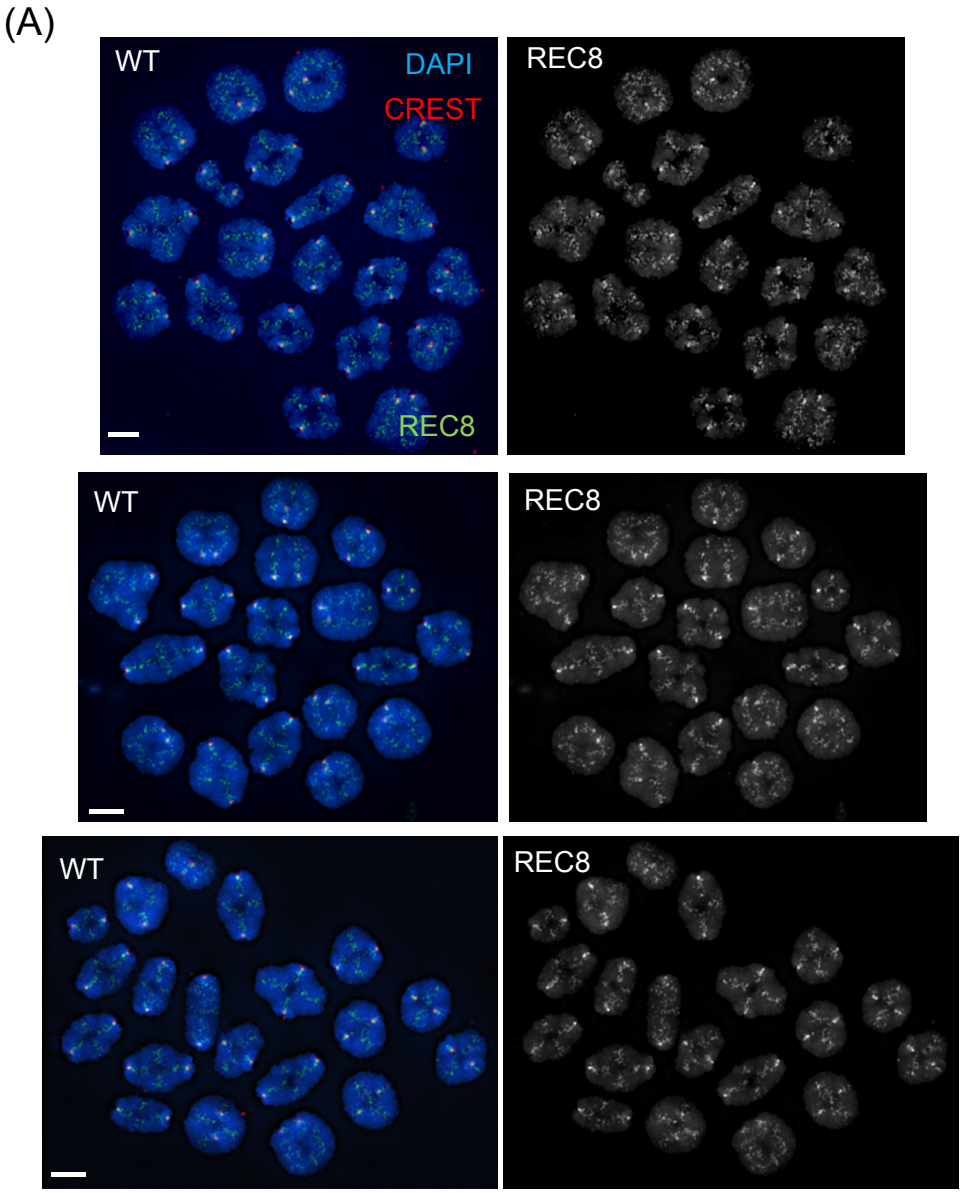

Figure 5.16 – REC8 staining in wild type MI oocytes

Images of wild type MI oocytes stained with DAPI (blue), anti-human CREST (red) and anti-rabbit REC8 (green). All images were taken using 32% transmission and 1 second exposure to image REC8 and 32% transmission and 1 second exposure to image CREST in order to ensure that the images were not saturated. Scale bar 5μm. Many of the oocytes stained with the antibody against REC8 displayed large aggregates on the spread. These were not included in the quantitative analysis. (Mouse experiments 12 & 17)

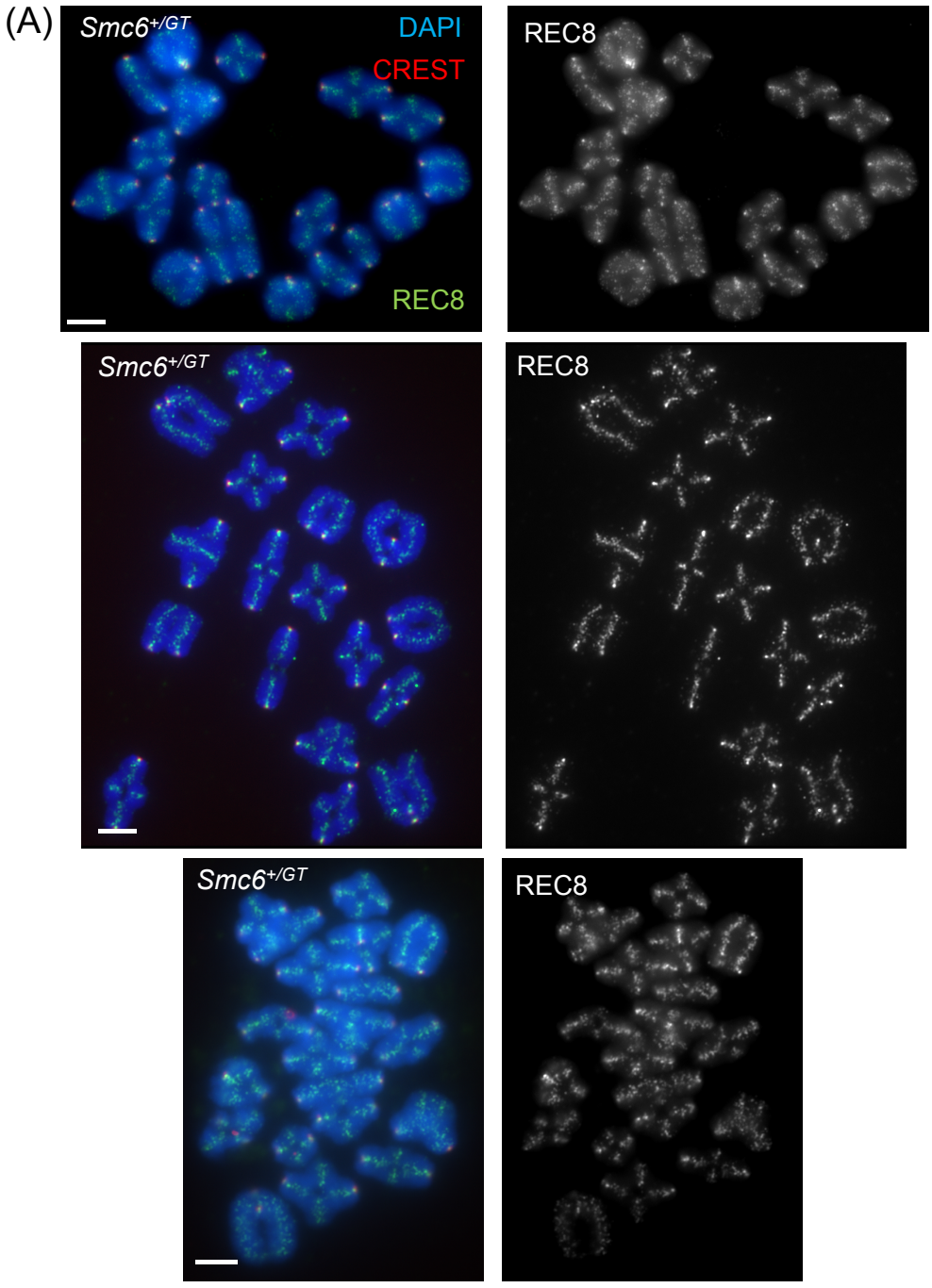

Figure 5.17 – REC8 staining in *Smc6*$^{+/GT}$ MI oocytes

Images of *Smc6*$^{+/GT}$ oocytes stained with DAPI (blue), anti-human CREST (red) and anti-rabbit REC8 (green). All images were taken using 32% transmission and 1 second exposure to image REC8 and 32% transmission and 1 second exposure to image CREST in order to ensure that the images were not saturated. Scale bar 5 μm. (Mouse experiments 12 & 17)

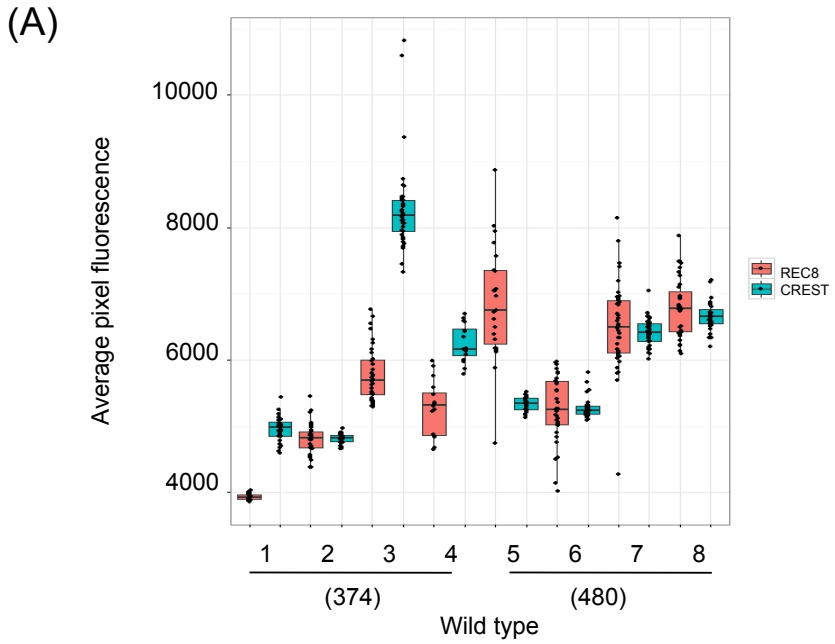

Figure 5.18 – Analysis of centromeric REC8 staining compared to CREST in wild type

Graph demonstrating how the average centromeric REC8 fluorescence (displayed in red) varies with the average CREST fluorescence (displayed in green) on a per chromosome basis, plotted on a per spread basis in wild type (animals 374 & 480). (Mouse experiments 12 & 17)

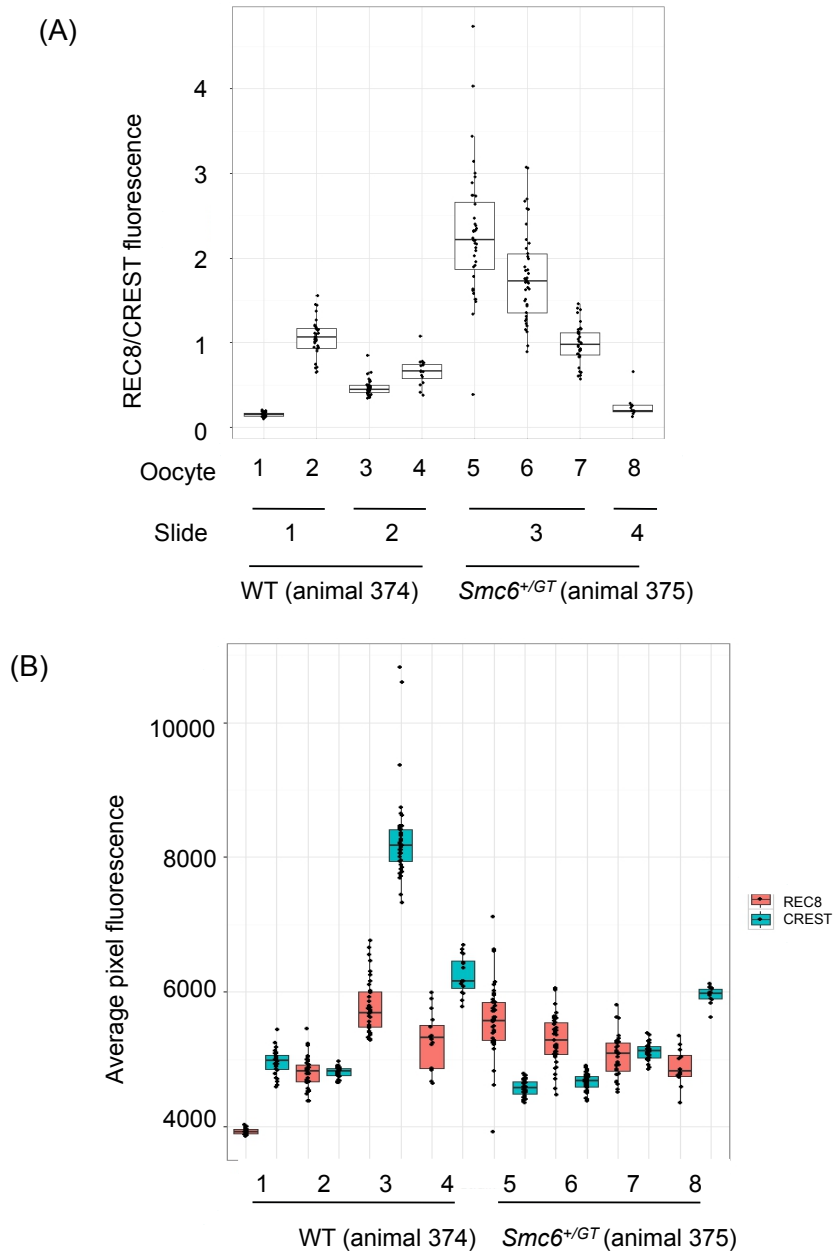

Figure 5.19 - Analysis of centromeric REC8 staining in *Smc6*$^{+/GT}$ oocytes

A. Boxplot of the average centromeric REC8 fluorescence levels normalised to average CREST fluorescence on a per chromosome basis, plotted on a per spread basis in both wild type (animal 374) and *Smc6*$^{+/GT}$ (animal 375). Here the mice were matched littermates. (Mouse experiment 12)

B. Boxplot demonstrating how the average centromeric REC8 fluorescence varies with the average CREST fluorescence on a per chromosome basis, plotted on a per spread basis in both wild type (animal 374) and *Smc6*$^{+/GT}$ (animal 375). (Mouse experiment 12)

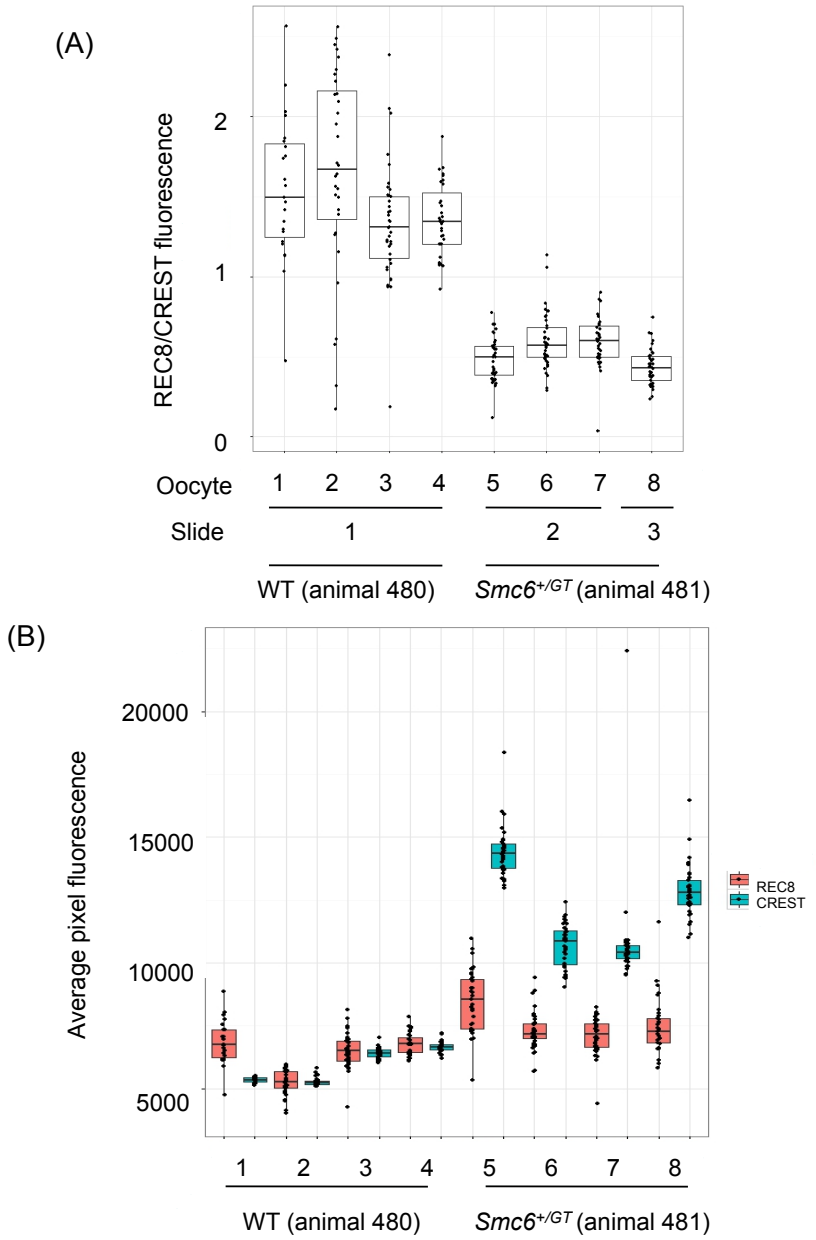

Figure 5.20 - Analysis of centromeric REC8 staining in *Smc6*$^{+/GT}$ oocytes (part two)

A. Boxplot of the average centromeric REC8 fluorescence levels normalised to average CREST fluorescence on a per chromosome basis, plotted on a per spread basis in both wild type (animal 480) and *Smc6*$^{+/GT}$ (animal 481). Here the mice were matched littermates. (Mouse experiment 17)

B. Boxplot demonstrating how the average centromeric REC8 fluorescence varies with the average CREST fluorescence on a per chromosome basis, plotted on a per spread basis in both wild type (animal 480) and *Smc6*$^{+/GT}$ (animal 481). (Mouse experiment 17)

oocytes (Figure 5.20A, Wilcox test P < 0.005). The CREST signal was however very high in all of the 481 (*Smc6*$^{+/GT}$) oocytes (Figure 5.20B), which indicates it is possible that these slides had increased levels of antibody binding. This analysis only included a very small number of the slides, as many could not be analyzed due to the presence of antibody aggregates. Therefore to determine if the cohesin level is reduced in oocytes from the *Smc6*$^{+/GT}$ mouse this experiment should be repeated again and ideally a different antibody used.

5.3.5. Acetylated SMC3 is reduced in *Smc6*$^{+/GT}$ mouse MI oocytes

Only a fraction of cohesin is cohesive in mitotic cells. I therefore questioned if the high level of chromosome mis-segregation was linked to the cohesin present along the chromosomes not being cohesive. It has been found that chromosomes can mis-segregate even if there is cohesin along their entire length (Garcia-Cruz et al, 2010). In mammals SMC3 must be acetylated at two lysine residues K105/106 in its N-terminus to ensure that the cohesin establishes cohesion between the sister chromatids (Zhang et al., 2008). I therefore looked at the levels of acetylated SMC3 in the oocytes from the *Smc6*$^{+/GT}$ mouse using a mouse monoclonal anti-acetyl-SMC3 antibody kindly donated by Katsuhiko Shirahige (Beckouet et al, 2010). Acetylated SMC3 was found to localize to the centromeres and in some cases also to the chromosome arms (Figure 5.21 & 5.22). Interestingly I saw several cases where no acetylated SMC3 staining was observed in both wild type and *Smc6*$^{+/GT}$ oocytes (Figure 5.23A). The proportion of oocytes that displayed no acetylated SMC3 staining was significantly higher in *Smc6*$^{+/GT}$ than in wild type. It was also observed that the number of oocytes that displayed dim acetylated SMC3 staining was significantly higher in *Smc6*$^{+/GT}$ than wild type. This indicated that there are significantly reduced levels of acetylated SMC3 in the oocytes from the *Smc6*$^{+/GT}$ mouse. From this I proposed that there is reduced cohesion in the oocytes from the *Smc6*$^{+/GT}$ mouse and that this contributes to the aneuploidy observed.

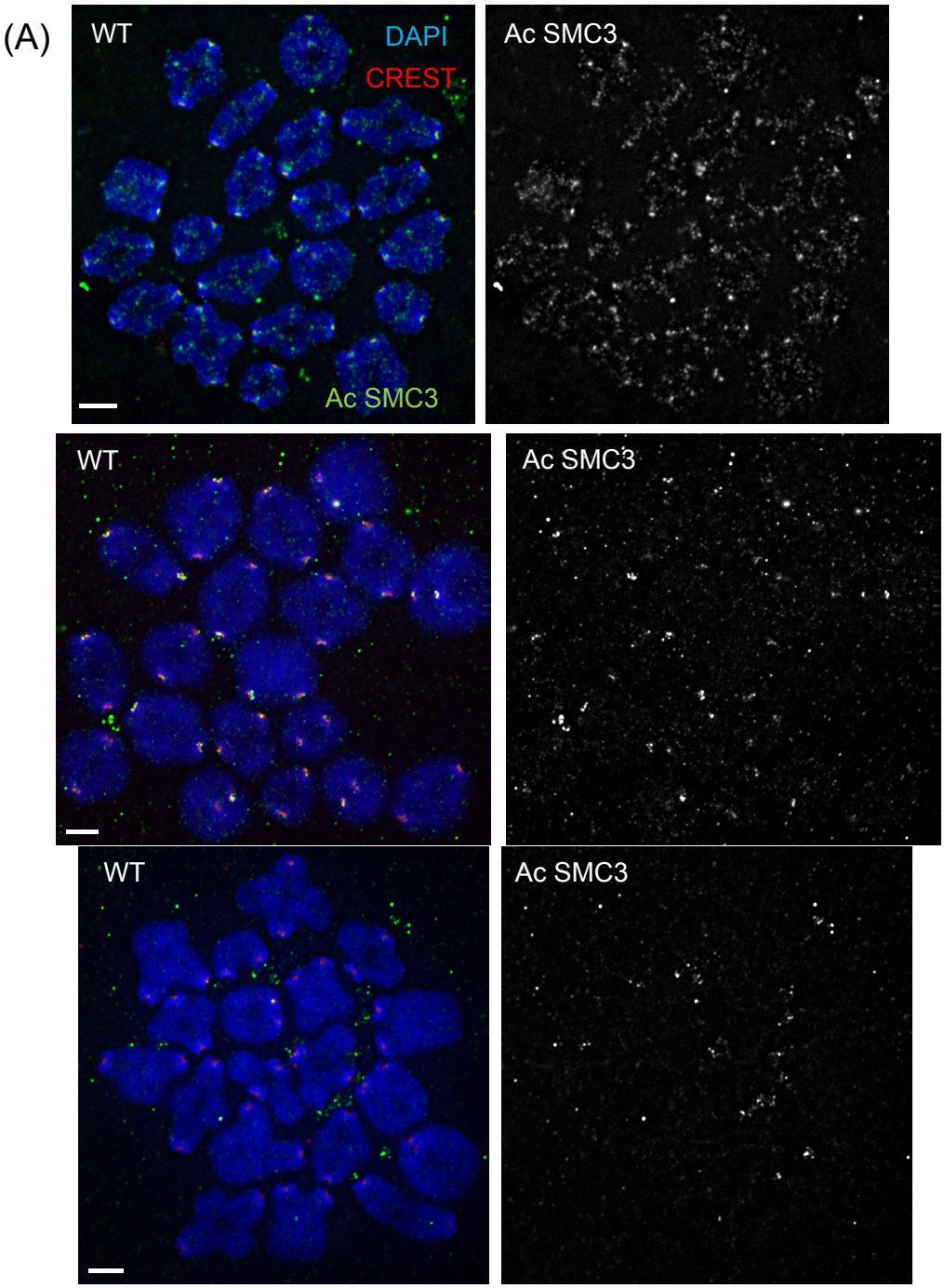

Figure 5.21 - Acetylated SMC3 staining in wild type MI oocytes

Images of wild type oocytes stained with DAPI (blue), ant-human CREST (red) and anti-mouse acetylated SMC3 (green). All images were taken using 100% transmission and 1 second exposure to image acetylated SMC3 and 32% transmission and 1 second exposure to image CREST in order to ensure that the images were not saturated. Scale bar 5 μm. (Mouse experiments 15, 16, 17 & 18)

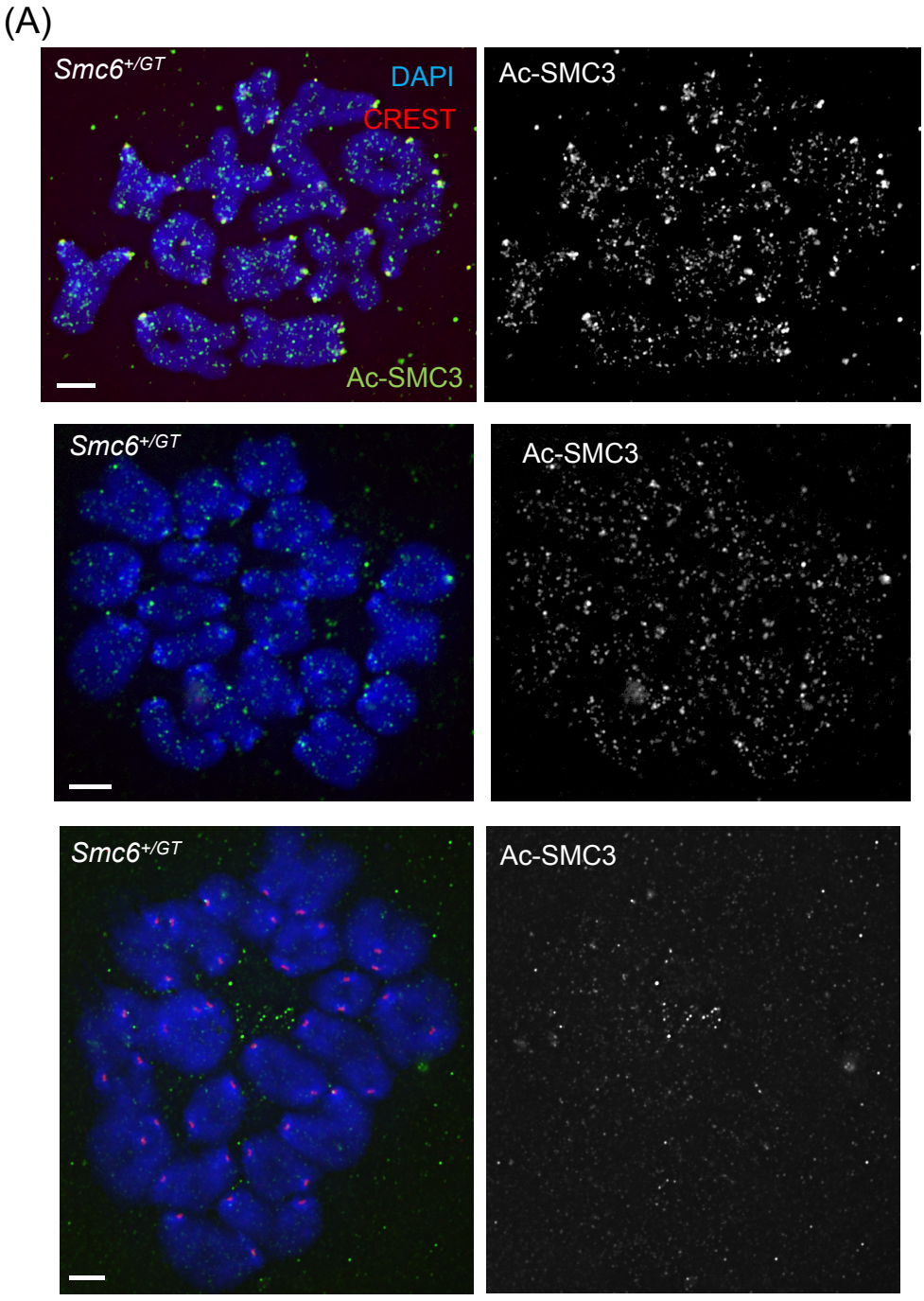

Figure 5.22 – Acetylated SMC3 staining in *Smc6*$^{+/GT}$ MI oocytes

Images of *Smc6*$^{+/GT}$ oocytes stained with DAPI (blue), ant-human CREST (red) and anti-mouse acetylated SMC3 (green). All images were taken using 100% transmission and 1 second exposure to image acetylated SMC3 and 32% transmission and 1 second exposure to image CREST in order to ensure that the images were not saturated. Scale bar 5 μm. (Mouse experiments 15, 16, 17 & 18)

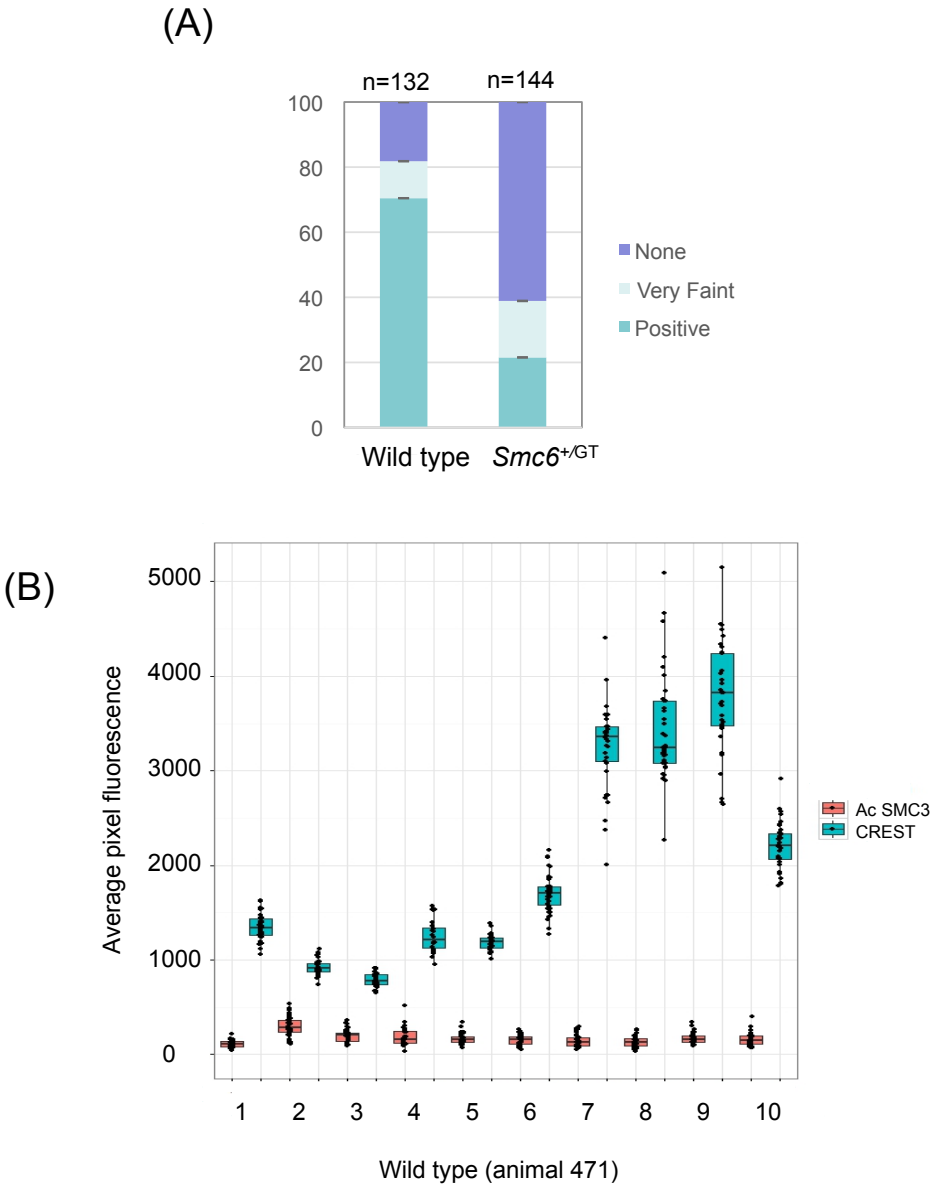

Figure 5.23 – Analysis of acetylated SMC3 staining compared to CREST staining

A. Bar graph demonstrating the percentage of MI spreads that display clear acetylated SMC3, dim acetylated SMC3 or no SMC3 staining in both wild type (n=132) and *Smc6*$^{+/GT}$ (n=144). **(**Mouse experiments 12, 16, 17 & 18)

B. Graph demonstrating how the average centromeric acetylated SMC3 fluorescence varies with the average CREST fluorescence on a chromosome basis, displayed on a per spread basis in wild type (animal 471). **(**Mouse experiments 12, 16, 17 & 18)

I attempted to quantify the level of acetylated SMC3 along the chromosomes in the oocytes from wild type and *Smc6*$^{+/GT}$ mice. However the background was very high in many of the images and even in the cases where acetylated SMC3 was present, the acetylated SMC3 signal was only elevated slightly from background (Figure 5.23B). This demonstrates that this antibody is sufficient to determine if acetylated SMC3 is present but it is not suitable for use in protein quantification.

As I found that a large proportion of the oocytes from the *Smc6*$^{+/GT}$ mother displayed a reduced level of acetylated SMC3 staining or no acetylated SMC3 staining, I tested if oocytes that had reduced levels of acetylated SMC3 also had reduced levels of SMC6 (Supplementary Figure 13). Interestingly spreads without acetylated SMC3 staining in wild type displayed high levels of SMC6 staining. I observed that the *Smc6*$^{+/GT}$ mouse oocytes spreads that contained the highest level of SMC6 staining also displayed no acetylated SMC3 staining. This could be to be linked to the difficulty in assessing the acetylated SMC3 staining in the mouse oocytes. The high background produced by the acetylated SMC3 antibody may mean that real signal acetylated SMC3 was masked on some of the chromosome spreads.

5.3.6. Acetylated SMC3 staining is reduced in *Smc6*$^{+/GT}$ pachytene oocytes

As I found that the levels of acetylated SMC3 were reduced in the MI oocytes from the *Smc6*$^{+/GT}$ mouse I investigated whether the levels of acetylated SMC3 were also reduced in their pachytene oocytes (Stage e18.5, Spreads prepared by Dr J. Grhun). This is the stage at which cohesion is established, prior to the arrest. Analysis was carried out at pachytene in order to determine if the cohesion was lost during the dictyate arrest or if cohesion was never established in some of the oocytes from the *Smc6*$^{+/GT}$ mouse. Pachytene oocytes were stained with antibodies against acetylated SMC3 and SYCP3 (the central element of the synaptonemal complex) so that the stage of the oocytes could be determined (Figures 5.24 & 5.25). Only

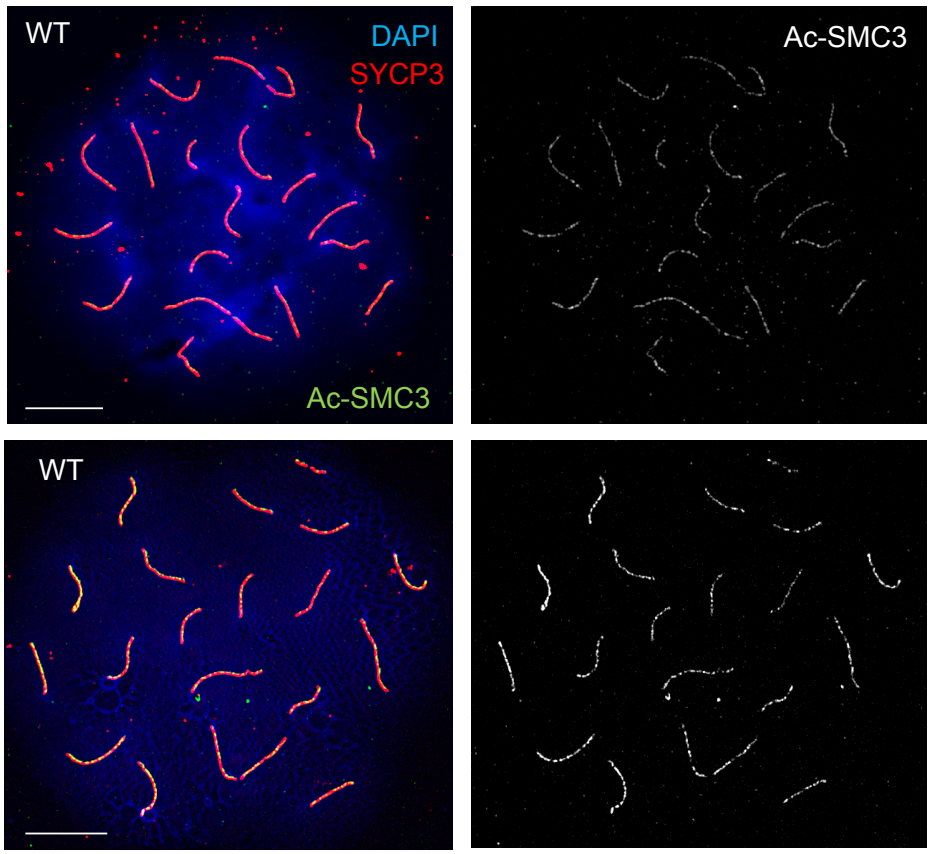

Figure 5.24 - Acetylated SMC3 staining in wild type pachytene oocytes

Images of wild type oocytes stained with DAPI (blue), SYCP3 (red) and anti-mouse acetylated SMC3 (green). All images were taken using 32% transmission and 0.2 second exposure to image acetylated SMC3 and 32% transmission and 1 second exposure to image SYCP3 in order to ensure that the images were not saturated. Scale bar 5 μm.

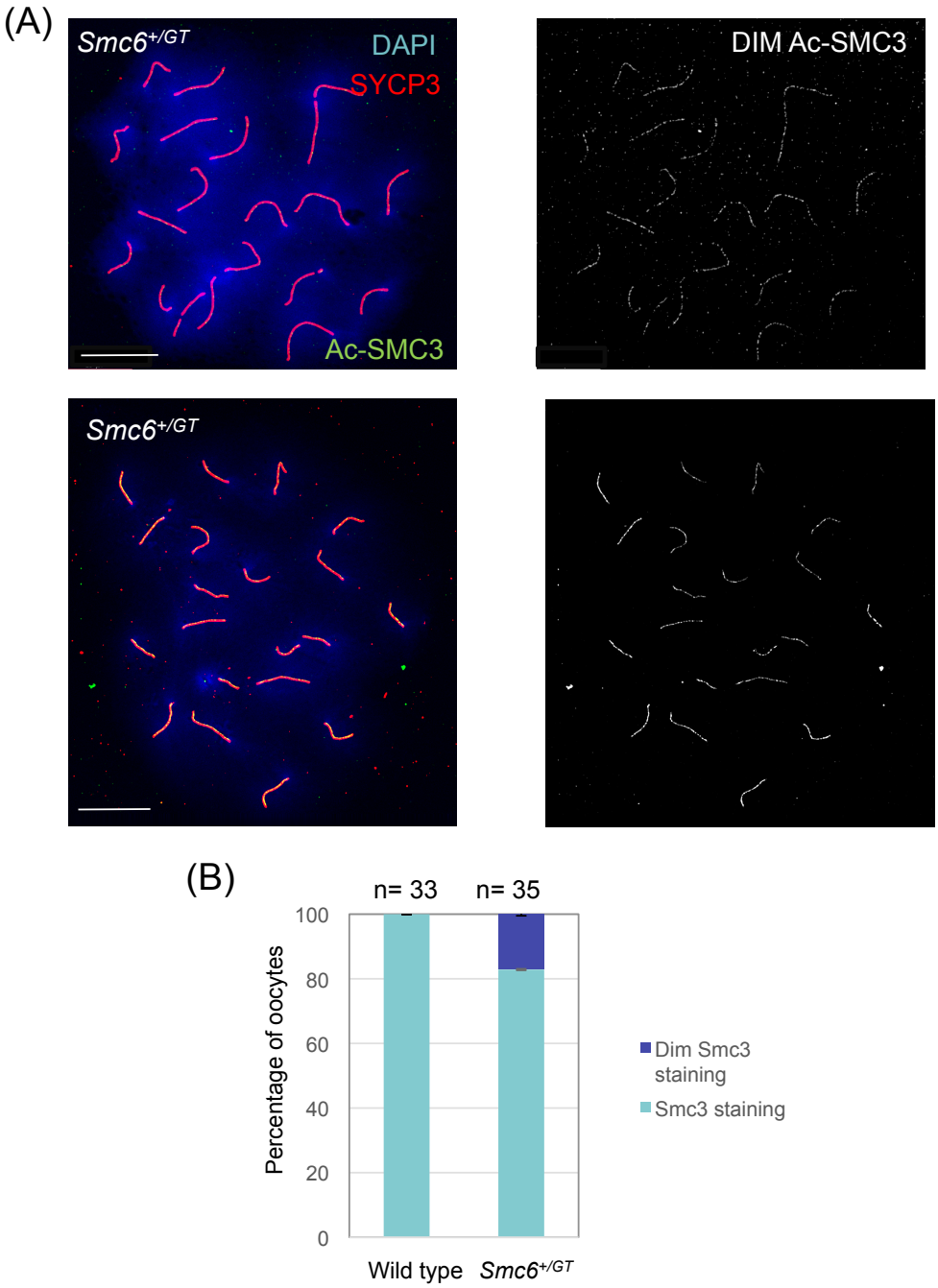

Figure 5.25 - Acetylated SMC3 staining is reduced in *Smc6*$^{+/GT}$ pachytene oocytes

A. Images of *Smc6*$^{+/GT}$ oocytes stained with DAPI (blue), SYCP3 (red) and anti-mouse acetylated SMC3 (green)**. (**Experiment 205)

B. Bar graph demonstrating the percentage of pachytene spreads that display acetylated SMC3 staining in both wild type (n=33) and *Smc6*$^{+/GT}$ (n=35). Here the mice were matched littermates.

oocytes that contained linear SYCP3 staining were analysed (as this indicated that the oocytes were at pachynema). Visual analysis found that there was acetylated SMC3 staining along the chromosomes in all of the pachytene oocytes in wild type (number of oocytes = 33, number of embryos =2) and *Smc6*$^{+/GT}$ (number of oocytes = 35, number of embryos =2) (Figure 5.25B). Approximately 20% of the oocytes from the *Smc6*$^{+/GT}$ mouse displayed dim acetylated SMC3 staining. Clear acetylated SMC3 staining was observed in all of the wild type pachytene oocytes. As the phenotype at pachytene is significantly less severe than observed at metaphase I (where 61% of the *Smc6*$^{+/GT}$ mouse oocytes displayed no acetylated SMC3 staining and a further 17% displayed dim acetylated SMC3 staining) this indicates that the *Smc6*$^{+/GT}$ mice may have defects in their cohesion maintenance during the dictyate arrest. As I observed that there was a slight reduction in the acetylated Smc3 staining at pachytene this indicates that the oocytes from the *Smc6*$^{+/GT}$ mouse may also have a defect in the establishment of chromosome cohesion, presumably during premeiotic S-phase.

5.3.7. Oocytes that display lower levels of SMC6 do not have larger chromosomes

As I previously observed that the chromosomes in the oocytes from the *Smc6*$^{+/GT}$ mouse were in many cases significantly larger than observed in wild type I questioned if the spreads that displayed reduced levels of SMC6 staining also contained larger chromosomes. To test this the levels of centromeric SMC6 in the oocytes from 446, 447, 462 and 463 were correlated with their average chromosome size (Supplementary figure 10). Chromosome spreads with larger chromosomes did not display reduced levels of centromeric SMC6. Ideally I would have liked to also investigate if the oocytes that displayed reduced levels of SMC6 staining also displayed reduced levels of condensin staining. This experiment however could not be carried out as both the SMC4 and SMC6 antibodies were raised in mouse. As a significant number of the chromosomes in the oocyte spreads from the *Smc6*$^{+/GT}$ mouse displayed frayed chromosomes I then examined if the

spreads that displayed lower levels of SMC6 staining were found previously to display frayed chromosomes. In the spreads analysed I observed no correlation between the level of SMC6 staining and the spreads, which displayed frayed chromosomes (Supplementary figure 11). As this analysis was based on a small sample, further experiments are required to investigate this if increased chromosome fraying is linked to SMC6 levels.

5.3.8. Oocytes that display lower levels of SMC6 do not display reduced chromosome cohesion

Previously it was found that there were slightly higher levels of precocious homologous chromosome segregation in the oocytes from the *Smc6*$^{+/GT}$ mouse (Section 4.2.6). I then questioned if these spreads also had reduced levels of SMC6 staining. I found that one of the spreads that contained very low levels of SMC6 also displayed distal homologous chromosomes (Supplementary figure 12). However other spreads that contained similarly low levels of SMC6 did not display distal homologous chromosomes. Furthermore distal chromosomes were also observed in a spread with higher levels of SMC6. This indicates it is unlikely that there is a link between the levels of SMC6 and the chromosomes forming a distal orientation. I also questioned if spreads that displayed lower levels of centromeric SMC6 displayed increased inter-kinetochore distances. Analysis found that there was no correlation between the average inter-kinetochore distances and average SMC6 fluorescence at the centromere on a per spread basis (R^2 = 0.02, Supplementary figure 14). This analysis was also based on a small sample. In order to more accurately determine if there is a link between SMC6 levels and inter kinetochore distances or chromosome orientations much larger sample sizes are required.

5.4 Discussion

This work has shown that the oocytes from the wild type and *Smc6*$^{+/GT}$ females contain variable levels of the SMC proteins. A high degree of

heterogeneity in the levels of protein between oocytes has also been seen in other studies (Tsutsumi et al, 2014). These variations could be due to slight differences in the rate of transcription and translation, slight variations in the stage of the oocytes or technical variations (such as variations in the oocyte spread preparation, the antibody concentration or differences in the levels of cytoplasm removed from the spreads). Despite this, I observed that the SMC6 levels were on average significantly lower in the oocytes from the *Smc6*$^{+/GT}$ mouse than seen in wild type. Again variability was observed in the protein levels from oocyte to oocyte in the oocytes from the *Smc6*$^{+/GT}$ mother with some displaying significantly less SMC6 than generally seen in wild type. From this I propose that the oocytes that contained significantly reduced levels of SMC6 were predisposed to aneuploidy.

In order to obtain an insight into why these oocytes could be predisposed to aneuploidy I examined how the levels of the other SMC complexes were affected in the oocytes from the *Smc6*$^{+/GT}$ mother. I observed that REC8 was present in all the oocytes from both wild type and *Smc6*$^{+/GT}$ females, as seen in oocytes from *Smc5* cKO mice (Hwang et al, 2017). The levels were variable. Results from Merriman *et al* (2012) and Tsutsumi *et al* (2014) also indicated that cohesin levels varied tremendously between different oocytes and between mice. They proposed that this indicated that the loss of cohesin with age is not constant in oocytes. This would mean that small differences in cohesin levels between wild type and *Smc6*$^{+/GT}$ could not be accurately characterised. As I observed that REC8 was present in all of the oocytes from wild type and *Smc6*$^{+/GT}$ I questioned if the cohesin present was cohesive. Interestingly a large proportion of the metaphase I oocytes from the *Smc6*$^{+/GT}$ mother were found to contain reduced levels of acetylated SMC3 staining (or none at all) (Figure 5.23). This indicated that, in many oocytes, the cohesin present may not be cohesive. From this I hypothesized that some of the aneuploidy observed at MII was due to a lack of cohesive cohesin holding the homologous chromosomes together. As I saw genome-wide loss of acetylated SMC3 staining but only mis-segregation of specific chromosomes this indicates it is likely that loss of chromosome cohesion

pre-disposes the oocytes to aneuploidy. Further analysis of pachytene oocytes found that the levels of acetylated SMC3 staining were also reduced at pachytene but to a much lesser extent (Figure 5.25). This indicated that the main loss of acetylated SMC3 staining, in the *Smc6*$^{+/GT}$ oocytes, occurred during the dictyate arrest. However it is also possible that there is a slight defect in the establishment of cohesion in the oocytes from the *Smc6*$^{+/GT}$ mother.

As I observed that the levels of acetylated SMC3 staining were reduced in such a high proportion of the oocytes from the *Smc6*$^{+/GT}$ mother I then questioned if the oocytes containing reduced levels of SMC6 staining also had reduced levels of acetylated SMC3 staining (Supplementary figure 13). Interestingly I did not see a correlation between the levels of SMC6 staining and the levels of acetylated SMC3 staining. Furthermore it was observed that there was no acetylated SMC3 staining present in a significantly higher proportion of the *Smc6*$^{+/GT}$ oocytes than I saw aneuploidy in. This either indicates that having a reduced level of acetylated SMC3 predisposes the oocytes to aneuploidy or that the high background observed in the acetylated SMC3 channel masked the low acetylated SMC3 signal present.

As I previously observed that many of the oocytes from the *Smc6*$^{+/GT}$ mother displayed larger and often-frayed chromosome I then examined if the oocytes that contained reduced levels of SMC6 staining also had larger or frayed chromosomes. The analysis found that there was no correlation between the SMC6 levels and the chromosome size or level of chromosome fraying. This analysis however was based on quite a small sample (18 oocytes). Larger sample sizes are required to investigate this relationship further. I also examined the levels of condensin in the oocytes from the *Smc6*$^{+/GT}$ mother. Here the results obtained were very variable. In one pair of littermates I observed no real difference in the level of condensin staining in the oocytes between wild type and *Smc6*$^{+/GT}$. However analysis of another pair of littermates found that condensin was greatly reduced in the *Smc6*$^{+/GT}$ oocytes. As both the SMC4 and SMC6 were raised in the same animal a

comparison could not be carried out to see if the oocytes that contained lower levels of condensin also contained lower levels of SMC6.

A major limitation of this study was that only the staining at the centromeres (or the centromeric and pericentromeric area) could be assessed. The total antibody staining could not be assayed, as there was no suitable factor to normalise to. It is possible that an antibody against a histone would provide a good factor to normalise total protein fluorescence too. Another limitation of this study was the variability in the antibody staining observed. As it was found that the antibodies stained more strongly on specific slides a normalizing factor was required. Here it was found that CREST varied quite well with the antibodies used in this study. However it is likely that there was some variability in the CREST antibody staining. As I was looking for quite subtle differences between the wild type and the *Smc6*$^{+/GT}$ oocytes, this variability could mean that differences were not observed. We also do not know how the oocyte chromosome spread preparation affected the antibody staining. It is possible that differences in oocyte chromosome spread preparation may have contributed to the variation observed.

As this study and other studies found such a large variability in protein levels between oocytes and between mice this indicates that small differences in protein levels, potentially expected in oocytes from the *Smc6*$^{+/GT}$ mouse, may not be decipherable. The results however do indicate that cohesion is affected in the oocytes from the *Smc6*$^{+/GT}$ mouse. This loss of cohesion is likely to contribute towards the aneuploidy observed previously. It is currently unclear if condensin is affected in the oocytes of the *Smc6*$^{+/GT}$ mouse but it seems likely as the chromosomes in the oocytes from the *Smc6*$^{+/GT}$ mother were observed to be considerably more variable in size compared to wild type and often frayed.

Chapter 6 – Discussion and future outlook

6.1 Discussion

The work outlined here provides us with more information about the role of the Smc5/6 complex in both *Saccharomyces cerevisiae* and mammalian female meiosis. In *Saccharomyces cerevisiae* I found that the Smc5/6 complex is required for accurate chromosome segregation and spindle elongation during meiosis (Chapter 3). I also found that the Smc5/6 complex is required for accurate chromosome segregation in mouse meiosis (Chapter 4). Interestingly I found that there was clear chromosome mis-segregation even though the levels of the Smc5/6 complex were only slightly reduced. I propose that oocytes that have reduced levels of Smc5/6 are predisposed to aneuploidy. The causes of the observed aneuploidy are still unclear. However since I observed a reduction in the levels of acetylated Smc3 in the oocytes from the $Smc6^{+/GT}$ mouse, I hypothesise that a loss of functional chromosome cohesion contributes towards the chromosome mis-segregation observed (Chapter 5).

The Smc5/6 complex is structurally conserved protein that is required for many aspects of both mitosis and meiosis. The role of the Smc5/6 complex has been investigated in many different model systems from budding yeast to human cell lines (Ampatzidou et al, 2006; Copsey et al, 2013; Hong et al, 2016; Hwang et al, 2017; Lehmann et al, 1995; Potts et al, 2009; Pryzhkova and Jordan, 2016; Watanabe et al, 2009). The Smc5/6 complex alongside the other SMC complexes, cohesin and condensin, is required for chromatin structure and function. Specifically, it is important for homologous recombination, maintenance of the heterochromatin and rDNA, restart of stalled replication forks and regulation of chromosome topology (Section 1.12). Defects in the SMC complexes have been linked to many developmental disorders in humans. Misregulation and mutations in cohesin lead to cohesinopthies including Cornelia de Lange syndrome (CdLS) and Roberts's syndrome (Krantz et al, 2004; Tonkin et al, 2004;

Musio et al, 2006; Deardorff et al, 2007; Vega et al, 2005). Mutations in components of the condensin complex lead to microcephaly (reduced brain size) (Martin et al, 2016). Examples of humans with defects in the Smc5/6 complex have also been found. A study by Payne et al (2014) found that patients with severely reduced levels of Nse2 displayed insulin resistance, primordial dwarfism and primary ovarian failure. Several patients with missense within Nsmce3 have also been identified (Van der Crabben et al, 2016). These patients displayed chromosome breakage syndrome, which correlated with severe lung disease early in life. As work in mice demonstrates that the Smc5/6 complex is essential (mice deficient in either Nse2 or Smc6 have been found to be embryonic lethal) this indicates that these patients likely have some functional protein present in their cells (Jacome et al, 2015; Ju et al, 2013). Furthermore it is likely that the severity of the phenotype observed is linked to the level of functional protein present.

This work, alongside the work recently published by Hwang *et al* (2017), has provided the first insight into the role of the Smc5/6 complex in female mammalian meiosis. In the work outlined here I found that a reduction in the levels of Smc6 protein caused sub-fertility in mice. Interestingly other than displaying a reduced litter size, mice that had reduced levels of Smc6 appeared healthy. Analysis of the oocytes from the $Smc6^{+/GT}$ mouse indicated that there were defects in chromosome segregation, likely to be the cause of the reduction in fertility observed. Increased levels of aneuploidy were also observed in oocytes from *Smc5* cKO mice (Hwang et al, 2017). Interestingly in the work by Hwang *et al* (2017) aneuploidy was only observed in oocytes from mice 12-16 weeks of age and not in oocytes from mice 4 weeks of age. Analysis of the SMC6 protein levels in oocytes from mice in both of these age ranges found that 85% of oocytes from mice 4 weeks of age displayed SMC6 staining but only 39% of oocytes from mice 12-16 weeks of age displayed SMC6 staining. They proposed that only in mice 12-16 weeks of age were the levels of Smc6 depleted below a level that could support meiotic segregation (Hwang et al, 2017). This indicates that

there is a threshold level of Smc5/6, below which meiotic segregation is not supported. As high levels of aneuploidy were observed in oocytes from the *Smc6*$^{+/GT}$ mouse, this indicates that they also contain SMC6 below this threshold level.

Joint molecule resolution and cohesin regulation are known to be affected in Smc5/6 yeast mutants (Copsey et al, 2013). I therefore predicted that the chromosome mis-segregation may be due to unresolved joint molecule or mis-regulation of cohesin in oocytes from heterozygous mice. Defects in chromosome cohesion were observed. The cohesin protein; REC8 was found to be present along the chromosomes but chromosome cohesion was observed to be affected as demonstrated by a loss/reduction in acetylated SMC3 staining. Our results from yeast also indicate that the Smc5/6 complex may also have a role in regulating cohesin in meiosis, specifically in the removal of cohesin at anaphase. Artificial cleavage of cohesin at anaphase interestingly only slightly improved the segregation defects observed in the Smc5/6 mutants (Copsey et al, 2013). This was contrasting to what was previously seen in *S.pombe* mitosis. In *S.pombe* it was observed that separase overexpression was able to remove the chromosome segregation defects observed, indicating the defects observed in *S.pombe* were likely to be due to problems with the prophase pathway (Outwin et al, 2009). As *S.cerevisiae* does not have a prophase pathway, and all cohesin is cleaved through the action of seperase this is could explain the difference. In support of this it was found that there was no retention of cohesin in *S.cerevisiae* mitosis when the Smc5/6 complex is depleted (Jeppsson et al., 2014).

Chromosome morphology was affected in the oocytes from the *Smc6*$^{+/GT}$ mouse, as seen in oocytes from *Smc5* cKO mice (Hwang et al, 2017). The chromosomes in the oocytes from the *Smc6*$^{+/GT}$ mouse were found to be more variable in size. I also observed that the chromosomes were often frayed and in some cases that there were threads between the chromosomes. It has been proposed by Hong *et al*, 2016 that decondensed

chromosomes have a higher rate of ectopic recombination. As the Smc5/6 complex has a role in regulating ectopic recombination this leads to the possibility that the presence of threads and the frayed appearance of some of the chromosomes in the *Smc6*$^{+/GT}$ mouse indicates the presence of increased levels of ectopic recombination.

Work by several labs has found that condensin is mis-localised when the Smc5/6 complex is depleted (Gallego-Paez et al, 2014; Hong et al, 2016; Hwang et al, 2017; Pryzhkova and Jordan, 2016). In this study I saw, when looking on a per oocyte basis, that the condensin levels in wild type and *Smc6*$^{+/GT}$ were very variable. A large amount of variability was observed between the protein levels in all of the oocytes assessed. Variability in oocyte protein levels has also been seen in several other studies including Pryzhkova and Jordan (2016), Merriman et al (2012) and Tsutsumi et al (2014). There are several potential reasons for the variation I observed. The first is that the oocytes were at slightly different stages of metaphase. This would affect both the protein levels in the oocytes and the level of chromosome condensation, which could in turn affect antibody binding. It could also be due to the level of cytoplasm remaining on the spreads. Oocytes contain a very large amount of cytoplasm. Residual cytoplasm remaining on chromosome spreads is known to affect FISH staining and so it is likely that it also affects antibody staining. The difference could also be due to differences in protein expression. Before oocytes enter the dictyate arrest there is active transcription of genes required for oocyte development including cohesin (Revenkova et al, 2010). As it is known that there are bursts in transcription and translation in many organisms it is possible that the oocytes enter the dictyate arrest with different levels of protein (Lee et al, 2005; Chubb et al, 2006; Yunger et al, 2010; Ohno et al, 2014). This could cause the stocasticity in protein expression that I observed. It however cannot be ruled out that technical differences also contribute to the variability in staining observed.

Interestingly reduced litter sizes were only observed when the female in the cross was *Smc6*$^{+/GT}$, not when the male was *Smc6*$^{+/GT}$. This alongside the finding by Hwang *et al* (2017), that *Smc5* cKO females crossed with wild type males produce significantly less mature blastocysts than observed in the reciprocal cross, indicates that the reproductive problems in mice depleted of the Smc5/6 complex are female specific. In humans aneuploidy rates have been found to be significantly higher in oocytes compared to sperm (Hassold and Hunt, 2001). This is likely to be due to the protracted dictyate arrest. Research also indicates that there are increased levels of mis-segregation in oocytes due to oocytes having a weaker SAC. A sharp rise in aneuploidy with increased maternal ages has also been found. This has been linked to recombination rates, altered crossover position and cohesin regulation.

Research indicates that a loss of cohesin may contribute to age-related aneuploidy (Jeffreys et al, 2003; Liu and Keefe, 2008; Chiang et al, 2010; Lister et al, 2010). Mouse mutants heterozygous for the cohesin components Rec8 and Smc1β have been found to display oocyte aneuploidy (Murdoch et al, 2013). As the Smc5/6 complex has been found to diminish with increased maternal age in mice, leading to an increase in chromosome mis-segregation, this leads to the possibility that heterozygosity of the Smc5/6 complex may contribute to the maternal age affect (Hwang et al, 2017).

6.2. Conclusions and future work

As it was found that both chromosome cohesion and chromosome condensation are affected in the oocytes from the *Smc6*$^{+/GT}$ mouse this indicates that the SMC complexes may work together to co-ordinate chromosome segregation in humans. This work also indicates that only carrying a single functional copy of Smc6 is an example of a carrier mutation that only affects the reproductive potential of the carrier. Humans experience high levels of miscarriage due to aneuploidy in their oocytes

(Hassold and Hunt, 2001). Despite the prevalence of miscarriage, very little is known about its genetic basis. This leads to the possibility that SMC6 is an example of a protein that when reduced could contribute towards human aneuploidy.

In this study I was only able to look at protein levels in the centromeric and pericentromeric regions, as CREST staining was normalised to. In order to look at the protein distribution along the chromosome arms an anti-histone antibody, such as an anti-histone H3, could be normalised to. This would also allow a comparison of the protein levels at the centromeres and along the arms. Pryzhkova and Jordan (2016) observed that Smc5 depleted mouse embryonic stem cells displayed slightly decreased levels of centromeric condensin staining but increased levels of condensin staining along the chromosome arms. It would be interesting to see if I see trends like this in the oocytes from the *Smc6*$^{+/GT}$ mouse.

In the last 10 years there have been great advances in the field of super resolution microscopy. The developments mean molecular distribution and interactions between individual molecules can be visualised at resolutions as low as ~10nm (Ishitsuka et al, 2014). Photoactivated localisation microscopy (PALM) overcomes the resolution limit by stochastically activating single molecules in a diffraction-limited region at different times (Betzig et al, 2006). This could be used to accurately determine the level and distribution of SMC proteins along the meiotic chromosomes.

It would also be interesting to further investigate the anaphase chromosome dynamics in the oocytes from the *Smc6*$^{+/GT}$ mouse to see if they are reminiscent of what was seen in *Smc5* cKO oocytes by Hwang *et al*, 2017. This could be investigated through live cell imaging of the oocytes from the *Smc6*$^{+/GT}$ mouse. This would provide us with an insight into if the chromosome mis-segregate, at meiosis I, due to a loss of chromosome cohesion, where it would be expected that the chromosomes are easily pulled apart, or due to an accumulation of unresolved recombination

intermediates, where I would expect to see a large amount of homologous chromosome stretching, as seen in *Smc5* cKO oocytes (Hwang et al, 2017). It would also allow us to see if there are lagging chromosomes or spindle assembly/stability defects.

Finally, it would be of great interest to investigate the prevalence of Smc5/6 mutations amongst women suffering recurrent miscarriage and/or those identified as having high levels of age-independent oocyte aneuploidy.

Chapter 7. Bibliography

Abe, S., Nagasaka, K., Hirayama, Y., Kozuka-Hata, H., Oyama, M., Aoyagi, Y., Obuse, C. and Hirota, T. (2011) 'The initial phase of chromosome condensation requires Cdk1-mediated phosphorylation of the CAP-D3 subunit of condensin II', *Genes Dev,* 25(8), pp. 863-74.

Acquaviva, L., Drogat, J., Dehé, P. M., de La Roche Saint-André, C. and Géli, V. (2013) 'Spp1 at the crossroads of H3K4me3 regulation and meiotic recombination', *Epigenetics,* 8(4), pp. 355-60.

Agmon, N., Yovel, M., Harari, Y., Liefshitz, B. and Kupiec, M. (2011) 'The role of Holliday junction resolvases in the repair of spontaneous and induced DNA damage', *Nucleic Acids Res,* 39(16), pp. 7009-19.

Agostinho, A., Manneberg, O., van Schendel, R., Hernández-Hernández, A., Kouznetsova, A., Blom, H., Brismar, H. and Höög, C. (2016) 'High density of REC8 constrains sister chromatid axes and prevents illegitimate synaptonemal complex formation', *EMBO Rep,* 17(6), pp. 901-13.

Ajimura, S., Ejiri, H., Higashi, A., Inoue, G., Iseki, Y., Kishimoto, T., Nakamura, F., Noumi, H., Ohsumi, H., Sano, H., Gill, D. R., Lee, L., Olin, A., Yen, S., Fukuda, T., Hashimoto, O., Shibata, T., Nomachi, M., Kimura, Y. and Maeda, K. (1992) 'Polarization of Lambda hyperons produced by the quasifree (pi +,K+) reaction on 12C', *Phys Rev Lett,* 68(14), pp. 2137-2140.

Alani, E., Padmore, R. and Kleckner, N. (1990) 'Analysis of wild-type and rad50 mutants of yeast suggests an intimate relationship between meiotic chromosome synapsis and recombination', *Cell,* 61(3), pp. 419-36.

Alexandru, G., Uhlmann, F., Mechtler, K., Poupart, M. A. and Nasmyth, K. (2001) 'Phosphorylation of the cohesin subunit Scc1 by Polo/Cdc5 kinase regulates sister chromatid separation in yeast', *Cell,* 105(4), pp. 459-72.

Allers, T. and Lichten, M. (2001a) 'Differential timing and control of noncrossover and crossover recombination during meiosis', *Cell,*

106(1), pp. 47-57.

Allers, T. and Lichten, M. (2001b) 'Intermediates of yeast meiotic recombination contain heteroduplex DNA', *Mol Cell,* 8(1), pp. 225-31.

Almagro, S., Riveline, D., Hirano, T., Houchmandzadeh, B. and Dimitrov, S. (2004) 'The mitotic chromosome is an assembly of rigid elastic axes organized by structural maintenance of chromosomes (SMC) proteins and surrounded by a soft chromatin envelope', *J Biol Chem,* 279(7), pp. 5118-26.

Ampatzidou, E., Irmisch, A., O'Connell, M. J. and Murray, J. M. (2006) 'Smc5/6 is required for repair at collapsed replication forks', *Mol Cell Biol,* 26(24), pp. 9387-401.

Anderson, D. E., Losada, A., Erickson, H. P. and Hirano, T. (2002) 'Condensin and cohesin display different arm conformations with characteristic hinge angles', *J Cell Biol,* 156(3), pp. 419-24.

Andrews, E. A., Palecek, J., Sergeant, J., Taylor, E., Lehmann, A. R. and Watts, F. Z. (2005) 'Nse2, a component of the Smc5-6 complex, is a SUMO ligase required for the response to DNA damage', *Mol Cell Biol,* 25(1), pp. 185-96.

Arora, C., Kee, K., Maleki, S. and Keeney, S. (2004) 'Antiviral protein Ski8 is a direct partner of Spo11 in meiotic DNA break formation, independent of its cytoplasmic role in RNA metabolism', *Mol Cell,* 13(4), pp. 549-59.

Ashton, T. M. and Hickson, I. D. (2010) 'Yeast as a model system to study RecQ helicase function', *DNA Repair (Amst),* 9(3), pp. 303-14.

Bachrati, C. Z., Borts, R. H. and Hickson, I. D. (2006) 'Mobile D-loops are a preferred substrate for the Bloom's syndrome helicase', *Nucleic Acids Res,* 34(8), pp. 2269-79.

Bachrati, C. Z. and Hickson, I. D. (2006) 'Analysis of the DNA unwinding activity of RecQ family helicases', *Methods Enzymol,* 409, pp. 86-100.

Bachvarova, R. (1985) 'Gene expression during oogenesis and oocyte development in mammals', *Dev Biol (N Y 1985),* 1, pp. 453-524.

Bachvarova, R., De Leon, V., Johnson, A., Kaplan, G. and Paynton, B. V. (1985) 'Changes in total RNA, polyadenylated RNA, and actin mRNA during meiotic maturation of mouse oocytes', *Dev Biol,* 108(2), pp. 325-31.

Baker, S. M., Plug, A. W., Prolla, T. A., Bronner, C. E., Harris, A. C., Yao, X., Christie, D. M., Monell, C., Arnheim, N., Bradley, A., Ashley, T. and Liskay, R. M. (1996) 'Involvement of mouse Mlh1 in DNA mismatch repair and meiotic crossing over', *Nat Genet,* 13(3), pp. 336-42.

Bannister, L. A., Pezza, R. J., Donaldson, J. R., de Rooij, D. G., Schimenti, K. J., Camerini-Otero, R. D. and Schimenti, J. C. (2007) 'A dominant, recombination-defective allele of Dmc1 causing male-specific sterility', *PLoS Biol,* 5(5), pp. e105.

Barlow, A. L., Benson, F. E., West, S. C. and Hultén, M. A. (1997) 'Distribution of the Rad51 recombinase in human and mouse spermatocytes', *EMBO J,* 16(17), pp. 5207-15.

Barnhart, M. C., Kuich, P. H., Stellfox, M. E., Ward, J. A., Bassett, E. A., Black, B. E. and Foltz, D. R. (2011) 'HJURP is a CENP-A chromatin assembly factor sufficient to form a functional de novo kinetochore', *J Cell Biol,* 194(2), pp. 229-43.

Baudat, F., Buard, J., Grey, C., Fledel-Alon, A., Ober, C., Przeworski, M., Coop, G. and de Massy, B. (2010) 'PRDM9 is a major determinant of meiotic recombination hotspots in humans and mice', *Science,* 327(5967), pp. 836-40.

Baudat, F. and de Massy, B. (2007) 'Regulating double-stranded DNA break repair towards crossover or non-crossover during mammalian meiosis', *Chromosome Res,* 15(5), pp. 565-77.

Baudat, F., Manova, K., Yuen, J. P., Jasin, M. and Keeney, S. (2000) 'Chromosome synapsis defects and sexually dimorphic meiotic progression in mice lacking Spo11', *Mol Cell,* 6(5), pp. 989-98.

Baxter, J. and Aragón, L. (2012) 'A model for chromosome condensation based on the interplay between condensin and topoisomerase II', *Trends Genet,* 28(3), pp. 110-7.

Baxter, J., Sen, N., Martínez, V. L., De Carandini, M. E., Schvartzman, J. B., Diffley, J. F. and Aragón, L. (2011) 'Positive supercoiling of mitotic DNA drives decatenation by topoisomerase II in eukaryotes', *Science,* 331(6022), pp. 1328-32.

Beckouët, F., Hu, B., Roig, M. B., Sutani, T., Komata, M., Uluocak, P., Katis, V.

L., Shirahige, K. and Nasmyth, K. (2010) 'An Smc3 acetylation cycle is essential for establishment of sister chromatid cohesion', *Mol Cell,* 39(5), pp. 689-99.

Beckouët, F., Srinivasan, M., Roig, M. B., Chan, K. L., Scheinost, J. C., Batty, P., Hu, B., Petela, N., Gligoris, T., Smith, A. C., Strmecki, L., Rowland, B. D. and Nasmyth, K. (2016) 'Releasing Activity Disengages Cohesin's Smc3/Scc1 Interface in a Process Blocked by Acetylation', *Mol Cell,* 61(4), pp. 563-74.

Bellani, M. A., Romanienko, P. J., Cairatti, D. A. and Camerini-Otero, R. D. (2005) 'SPO11 is required for sex-body formation, and Spo11 heterozygosity rescues the prophase arrest of Atm-/- spermatocytes', *J Cell Sci,* 118(Pt 15), pp. 3233-45.

Bennett, R. J., Noirot-Gros, M. F. and Wang, J. C. (2000) 'Interaction between yeast sgs1 helicase and DNA topoisomerase III', *J Biol Chem,* 275(35), pp. 26898-905.

Berchowitz, L. E., Francis, K. E., Bey, A. L. and Copenhaver, G. P. (2007) 'The role of AtMUS81 in interference-insensitive crossovers in A. thaliana', *PLoS Genet,* 3(8), pp. e132.

Bergerat, A., de Massy, B., Gadelle, D., Varoutas, P. C., Nicolas, A. and Forterre, P. (1997) 'An atypical topoisomerase II from Archaea with implications for meiotic recombination', *Nature,* 386(6623), pp. 414-7.

Bermudez, V. P., Maniwa, Y., Tappin, I., Ozato, K., Yokomori, K. and Hurwitz, J. (2003) 'The alternative Ctf18-Dcc1-Ctf8-replication factor C complex required for sister chromatid cohesion loads proliferating cell nuclear antigen onto DNA', *Proc Natl Acad Sci U S A,* 100(18), pp. 10237-42.

Bermúdez-López, M., Ceschia, A., de Piccoli, G., Colomina, N., Pasero, P., Aragón, L. and Torres-Rosell, J. (2010) 'The Smc5/6 complex is required for dissolution of DNA-mediated sister chromatid linkages', *Nucleic Acids Res,* 38(19), pp. 6502-12.

Bermúdez-López, M., Villoria, M. T., Esteras, M., Jarmuz, A., Torres-Rosell, J., Clemente-Blanco, A. and Aragon, L. (2016) 'Sgs1's roles in DNA end

resection, HJ dissolution, and crossover suppression require a two-step SUMO regulation dependent on Smc5/6', *Genes Dev,* 30(11), pp. 1339-56.

Bernard, P., Maure, J. F., Partridge, J. F., Genier, S., Javerzat, J. P. and Allshire, R. C. (2001) 'Requirement of heterochromatin for cohesion at centromeres', *Science,* 294(5551), pp. 2539-42.

Betzig, E., Patterson, G. H., Sougrat, R., Lindwasser, O. W., Olenych, S., Bonifacino, J. S., Davidson, M. W., Lippincott-Schwartz, J. and Hess, H. F. (2006) 'Imaging intracellular fluorescent proteins at nanometer resolution', *Science,* 313(5793), pp. 1642-5.

Bhalla, N., Biggins, S. and Murray, A. W. (2002) 'Mutation of YCS4, a budding yeast condensin subunit, affects mitotic and nonmitotic chromosome behavior', *Mol Biol Cell,* 13(2), pp. 632-45.

Bhat, M. A., Philp, A. V., Glover, D. M. and Bellen, H. J. (1996) 'Chromatid segregation at anaphase requires the barren product, a novel chromosome-associated protein that interacts with Topoisomerase II', *Cell,* 87(6), pp. 1103-14.

Bickel, J. S., Chen, L., Hayward, J., Yeap, S. L., Alkers, A. E. and Chan, R. C. (2010) 'Structural maintenance of chromosomes (SMC) proteins promote homolog-independent recombination repair in meiosis crucial for germ cell genomic stability', *PLoS Genet,* 6(7), pp. e1001028.

Bishop, D. K., Park, D., Xu, L. and Kleckner, N. (1992) 'DMC1: a meiosis-specific yeast homolog of E. coli recA required for recombination, synaptonemal complex formation, and cell cycle progression', *Cell,* 69(3), pp. 439-56.

Bishop, D. K. and Zickler, D. (2004) 'Early decision; meiotic crossover interference prior to stable strand exchange and synapsis', *Cell,* 117(1), pp. 9-15.

Black, B. E. and Bassett, E. A. (2008) 'The histone variant CENP-A and centromere specification', *Curr Opin Cell Biol,* 20(1), pp. 91-100.

Blat, Y. and Kleckner, N. (1999) 'Cohesins bind to preferential sites along yeast chromosome III, with differential regulation along arms versus

the centric region', *Cell,* 98(2), pp. 249-59.

Blat, Y., Protacio, R. U., Hunter, N. and Kleckner, N. (2002) 'Physical and functional interactions among basic chromosome organizational features govern early steps of meiotic chiasma formation', *Cell,* 111(6), pp. 791-802.

Boateng, K. A., Bellani, M. A., Gregoretti, I. V., Pratto, F. and Camerini-Otero, R. D. (2013) 'Homologous pairing preceding SPO11-mediated double-strand breaks in mice', *Dev Cell,* 24(2), pp. 196-205.

Boddy, M. N., Gaillard, P. H., McDonald, W. H., Shanahan, P., Yates, J. R. and Russell, P. (2001) 'Mus81-Eme1 are essential components of a Holliday junction resolvase', *Cell,* 107(4), pp. 537-48.

Borde, V., Goldman, A. S. and Lichten, M. (2000) 'Direct coupling between meiotic DNA replication and recombination initiation', *Science,* 290(5492), pp. 806-9.

Borde, V., Robine, N., Lin, W., Bonfils, S., Géli, V. and Nicolas, A. (2009) 'Histone H3 lysine 4 trimethylation marks meiotic recombination initiation sites', *EMBO J,* 28(2), pp. 99-111.

Bowles, J. and Koopman, P. (2010) 'Sex determination in mammalian germ cells: extrinsic versus intrinsic factors', *Reproduction,* 139(6), pp. 943-58.

Branzei, D., Sollier, J., Liberi, G., Zhao, X., Maeda, D., Seki, M., Enomoto, T., Ohta, K. and Foiani, M. (2006) 'Ubc9- and mms21-mediated sumoylation counteracts recombinogenic events at damaged replication forks', *Cell,* 127(3), pp. 509-22.

Brar, G. A., Kiburz, B. M., Zhang, Y., Kim, J. E., White, F. and Amon, A. (2006) 'Rec8 phosphorylation and recombination promote the step-wise loss of cohesins in meiosis', *Nature,* 441(7092), pp. 532-6.

Brick, K., Smagulova, F., Khil, P., Camerini-Otero, R. D. and Petukhova, G. V. (2012) 'Genetic recombination is directed away from functional genomic elements in mice', *Nature,* 485(7400), pp. 642-5.

Britton, R. A., Lin, D. C. and Grossman, A. D. (1998) 'Characterization of a prokaryotic SMC protein involved in chromosome partitioning', *Genes Dev,* 12(9), pp. 1254-9.

Brooker, A. S. and Berkowitz, K. M. (2014) 'The roles of cohesins in mitosis, meiosis, and human health and disease', *Methods Mol Biol,* 1170, pp. 229-66.

Buheitel, J. and Stemmann, O. (2013) 'Prophase pathway-dependent removal of cohesin from human chromosomes requires opening of the Smc3-Scc1 gate', *EMBO J,* 32(5), pp. 666-76.

Bullard, S. A., Kim, S., Galbraith, A. M. and Malone, R. E. (1996) 'Double strand breaks at the HIS2 recombination hot spot in Saccharomyces cerevisiae', *Proc Natl Acad Sci U S A,* 93(23), pp. 13054-9.

Buonomo, S. B., Clyne, R. K., Fuchs, J., Loidl, J., Uhlmann, F. and Nasmyth, K. (2000) 'Disjunction of homologous chromosomes in meiosis I depends on proteolytic cleavage of the meiotic cohesin Rec8 by separin', *Cell,* 103(3), pp. 387-98.

Bylund, G. O. and Burgers, P. M. (2005) 'Replication protein A-directed unloading of PCNA by the Ctf18 cohesion establishment complex', *Mol Cell Biol,* 25(13), pp. 5445-55.

Bähler, J., Wyler, T., Loidl, J. and Kohli, J. (1993) 'Unusual nuclear structures in meiotic prophase of fission yeast: a cytological analysis', *J Cell Biol,* 121(2), pp. 241-56.

Börner, G. V., Kleckner, N. and Hunter, N. (2004) 'Crossover/noncrossover differentiation, synaptonemal complex formation, and regulatory surveillance at the leptotene/zygotene transition of meiosis', *Cell,* 117(1), pp. 29-45.

Cao, L., Alani, E. and Kleckner, N. (1990) 'A pathway for generation and processing of double-strand breaks during meiotic recombination in S. cerevisiae', *Cell,* 61(6), pp. 1089-101.

Carballo, J. A., Johnson, A. L., Sedgwick, S. G. and Cha, R. S. (2008) 'Phosphorylation of the axial element protein Hop1 by Mec1/Tel1 ensures meiotic interhomolog recombination', *Cell,* 132(5), pp. 758-70.

Carramolino, L., Lee, B. C., Zaballos, A., Peled, A., Barthelemy, I., Shav-Tal, Y., Prieto, I., Carmi, P., Gothelf, Y., González de Buitrago, G., Aracil, M., Márquez, G., Barbero, J. L. and Zipori, D. (1997) 'SA-1, a nuclear

protein encoded by one member of a novel gene family: molecular cloning and detection in hemopoietic organs', *Gene,* 195(2), pp. 151-9.

Carretero, M., Ruiz-Torres, M., Rodríguez-Corsino, M., Barthelemy, I. and Losada, A. (2013) 'Pds5B is required for cohesion establishment and Aurora B accumulation at centromeres', *EMBO J,* 32(22), pp. 2938-49.

Carter, S. D. and Sjögren, C. (2012) 'The SMC complexes, DNA and chromosome topology: right or knot?', *Crit Rev Biochem Mol Biol,* 47(1), pp. 1-16.

Cejka, P., Plank, J. L., Bachrati, C. Z., Hickson, I. D. and Kowalczykowski, S. C. (2010) 'Rmi1 stimulates decatenation of double Holliday junctions during dissolution by Sgs1-Top3', *Nat Struct Mol Biol,* 17(11), pp. 1377-82.

Cha, R. S., Weiner, B. M., Keeney, S., Dekker, J. and Kleckner, N. (2000) 'Progression of meiotic DNA replication is modulated by interchromosomal interaction proteins, negatively by Spo11p and positively by Rec8p', *Genes Dev,* 14(4), pp. 493-503.

Chan, K. L., Gligoris, T., Upcher, W., Kato, Y., Shirahige, K., Nasmyth, K. and Beckouët, F. (2013) 'Pds5 promotes and protects cohesin acetylation', *Proc Natl Acad Sci U S A,* 110(32), pp. 13020-5.

Chan, K. L., Roig, M. B., Hu, B., Beckouët, F., Metson, J. and Nasmyth, K. (2012) 'Cohesin's DNA exit gate is distinct from its entrance gate and is regulated by acetylation', *Cell,* 150(5), pp. 961-74.

Chang, M., Bellaoui, M., Zhang, C., Desai, R., Morozov, P., Delgado-Cruzata, L., Rothstein, R., Freyer, G. A., Boone, C. and Brown, G. W. (2005) 'RMI1/NCE4, a suppressor of genome instability, encodes a member of the RecQ helicase/Topo III complex', *EMBO J,* 24(11), pp. 2024-33.

Cheeseman, I. M., Chappie, J. S., Wilson-Kubalek, E. M. and Desai, A. (2006) 'The conserved KMN network constitutes the core microtubule-binding site of the kinetochore', *Cell,* 127(5), pp. 983-97.

Cheeseman, I. M. and Desai, A. (2008) 'Molecular architecture of the kinetochore-microtubule interface', *Nat Rev Mol Cell Biol,* 9(1), pp. 33-46.

Chelysheva, L., Diallo, S., Vezon, D., Gendrot, G., Vrielynck, N., Belcram, K.,

Rocques, N., Márquez-Lema, A., Bhatt, A. M., Horlow, C., Mercier, R., Mézard, C. and Grelon, M. (2005) 'AtREC8 and AtSCC3 are essential to the monopolar orientation of the kinetochores during meiosis', *J Cell Sci,* 118(Pt 20), pp. 4621-32.

Chen, C. F. and Brill, S. J. (2010) 'An essential DNA strand-exchange activity is conserved in the divergent N-termini of BLM orthologs', *EMBO J,* 29(10), pp. 1713-25.

Cheng, C. H., Lo, Y. H., Liang, S. S., Ti, S. C., Lin, F. M., Yeh, C. H., Huang, H. Y. and Wang, T. F. (2006) 'SUMO modifications control assembly of synaptonemal complex and polycomplex in meiosis of Saccharomyces cerevisiae', *Genes Dev,* 20(15), pp. 2067-81.

Cheng, E. Y., Hunt, P. A., Naluai-Cecchini, T. A., Fligner, C. L., Fujimoto, V. Y., Pasternack, T. L., Schwartz, J. M., Steinauer, J. E., Woodruff, T. J., Cherry, S. M., Hansen, T. A., Vallente, R. U., Broman, K. W. and Hassold, T. J. (2009) 'Meiotic recombination in human oocytes', *PLoS Genet,* 5(9), pp. e1000661.

Chi, P., San Filippo, J., Sehorn, M. G., Petukhova, G. V. and Sung, P. (2007) 'Bipartite stimulatory action of the Hop2-Mnd1 complex on the Rad51 recombinase', *Genes Dev,* 21(14), pp. 1747-57.

Chiang, T., Duncan, F. E., Schindler, K., Schultz, R. M. and Lampson, M. A. (2010) 'Evidence that weakened centromere cohesion is a leading cause of age-related aneuploidy in oocytes', *Curr Biol,* 20(17), pp. 1522-8.

Chiang, T., Schultz, R. M. and Lampson, M. A. (2012) 'Meiotic origins of maternal age-related aneuploidy', *Biol Reprod,* 86(1), pp. 1-7.

Chikashige, Y., Kinoshita, N., Nakaseko, Y., Matsumoto, T., Murakami, S., Niwa, O. and Yanagida, M. (1989) 'Composite motifs and repeat symmetry in S. pombe centromeres: direct analysis by integration of NotI restriction sites', *Cell,* 57(5), pp. 739-51.

Chiolo, I., Minoda, A., Colmenares, S. U., Polyzos, A., Costes, S. V. and Karpen, G. H. (2011) 'Double-strand breaks in heterochromatin move outside of a dynamic HP1a domain to complete recombinational repair', *Cell,* 144(5), pp. 732-44.

Chu, S., DeRisi, J., Eisen, M., Mulholland, J., Botstein, D., Brown, P. O. and Herskowitz, I. (1998) 'The transcriptional program of sporulation in budding yeast', *Science,* 282(5389), pp. 699-705.

Chu, S. and Herskowitz, I. (1998) 'Gametogenesis in yeast is regulated by a transcriptional cascade dependent on Ndt80', *Mol Cell,* 1(5), pp. 685-96.

Chubb, J. R., Trcek, T., Shenoy, S. M. and Singer, R. H. (2006) 'Transcriptional pulsing of a developmental gene', *Curr Biol,* 16(10), pp. 1018-25.

Ciccia, A., McDonald, N. and West, S. C. (2008) 'Structural and functional relationships of the XPF/MUS81 family of proteins', *Annu Rev Biochem,* 77, pp. 259-87.

Ciosk, R., Shirayama, M., Shevchenko, A., Tanaka, T., Toth, A. and Nasmyth, K. (2000) 'Cohesin's binding to chromosomes depends on a separate complex consisting of Scc2 and Scc4 proteins', *Mol Cell,* 5(2), pp. 243-54.

Ciosk, R., Zachariae, W., Michaelis, C., Shevchenko, A., Mann, M. and Nasmyth, K. (1998) 'An ESP1/PDS1 complex regulates loss of sister chromatid cohesion at the metaphase to anaphase transition in yeast', *Cell,* 93(6), pp. 1067-76.

Clarke, L. and Carbon, J. (1980) 'Isolation of a yeast centromere and construction of functional small circular chromosomes', *Nature,* 287(5782), pp. 504-9.

Cleveland, D. W., Mao, Y. and Sullivan, K. F. (2003) 'Centromeres and kinetochores: from epigenetics to mitotic checkpoint signaling', *Cell,* 112(4), pp. 407-21.

Cloud, V., Chan, Y. L., Grubb, J., Budke, B. and Bishop, D. K. (2012) 'Rad51 is an accessory factor for Dmc1-mediated joint molecule formation during meiosis', *Science,* 337(6099), pp. 1222-5.

Clyne, R. K., Katis, V. L., Jessop, L., Benjamin, K. R., Herskowitz, I., Lichten, M. and Nasmyth, K. (2003) 'Polo-like kinase Cdc5 promotes chiasmata formation and cosegregation of sister centromeres at meiosis I', *Nat Cell Biol,* 5(5), pp. 480-5.

Cobbe, N. and Heck, M. M. (2006) 'The evolution of ATPase activity in SMC

proteins', *Proteins,* 63(3), pp. 685-96.

Cohen-Fix, O., Peters, J. M., Kirschner, M. W. and Koshland, D. (1996) 'Anaphase initiation in Saccharomyces cerevisiae is controlled by the APC-dependent degradation of the anaphase inhibitor Pds1p', *Genes Dev,* 10(24), pp. 3081-93.

Collins, J. K., Lane, S. I., Merriman, J. A. and Jones, K. T. (2015) 'DNA damage induces a meiotic arrest in mouse oocytes mediated by the spindle assembly checkpoint', *Nat Commun,* 6, pp. 8553.

Cooper, T. J., Garcia, V. and Neale, M. J. (2016) 'Meiotic DSB patterning: A multifaceted process', *Cell Cycle,* 15(1), pp. 13-21.

Copsey, A., Tang, S., Jordan, P. W., Blitzblau, H. G., Newcombe, S., Chan, A. C., Newnham, L., Li, Z., Gray, S., Herbert, A. D., Arumugam, P., Hochwagen, A., Hunter, N. and Hoffmann, E. (2013) 'Smc5/6 coordinates formation and resolution of joint molecules with chromosome morphology to ensure meiotic divisions', *PLoS Genet,* 9(12), pp. e1004071.

Corbett, K. D. and Harrison, S. C. (2012) 'Molecular architecture of the yeast monopolin complex', *Cell Rep,* 1(6), pp. 583-9.

Corbett, K. D., Yip, C. K., Ee, L. S., Walz, T., Amon, A. and Harrison, S. C. (2010) 'The monopolin complex crosslinks kinetochore components to regulate chromosome-microtubule attachments', *Cell,* 142(4), pp. 556-67.

Cost, G. J. and Cozzarelli, N. R. (2006) 'Smc5p promotes faithful chromosome transmission and DNA repair in Saccharomyces cerevisiae', *Genetics,* 172(4), pp. 2185-200.

Costa, Y., Speed, R., Ollinger, R., Alsheimer, M., Semple, C. A., Gautier, P., Maratou, K., Novak, I., Höög, C., Benavente, R. and Cooke, H. J. (2005) 'Two novel proteins recruited by synaptonemal complex protein 1 (SYCP1) are at the centre of meiosis', *J Cell Sci,* 118(Pt 12), pp. 2755-62.

Cremer, T., Lichter, P., Borden, J., Ward, D. C. and Manuelidis, L. (1988) 'Detection of chromosome aberrations in metaphase and interphase tumor cells by in situ hybridization using chromosome-specific library probes', *Hum Genet,* 80(3), pp. 235-46.

Cromie, G. A., Hyppa, R. W. and Smith, G. R. (2008) 'The fission yeast BLM homolog Rqh1 promotes meiotic recombination', *Genetics,* 179(3), pp. 1157-67.

Cromie, G. A., Hyppa, R. W., Taylor, A. F., Zakharyevich, K., Hunter, N. and Smith, G. R. (2006) 'Single Holliday junctions are intermediates of meiotic recombination', *Cell,* 127(6), pp. 1167-78.

Csankovszki, G., Collette, K., Spahl, K., Carey, J., Snyder, M., Petty, E., Patel, U., Tabuchi, T., Liu, H., McLeod, I., Thompson, J., Sarkeshik, A., Sarkesik, A., Yates, J., Meyer, B. J. and Hagstrom, K. (2009) 'Three distinct condensin complexes control C. elegans chromosome dynamics', *Curr Biol,* 19(1), pp. 9-19.

Cuylen, S., Metz, J. and Haering, C. H. (2011) 'Condensin structures chromosomal DNA through topological links', *Nat Struct Mol Biol,* 18(8), pp. 894-901.

Dai, J., Sullivan, B. A. and Higgins, J. M. (2006) 'Regulation of mitotic chromosome cohesion by Haspin and Aurora B', *Dev Cell,* 11(5), pp. 741-50.

De La Fuente, R., Viveiros, M. M., Burns, K. H., Adashi, E. Y., Matzuk, M. M. and Eppig, J. J. (2004) 'Major chromatin remodeling in the germinal vesicle (GV) of mammalian oocytes is dispensable for global transcriptional silencing but required for centromeric heterochromatin function', *Dev Biol,* 275(2), pp. 447-58.

de los Santos, T., Hunter, N., Lee, C., Larkin, B., Loidl, J. and Hollingsworth, N. M. (2003) 'The Mus81/Mms4 endonuclease acts independently of double-Holliday junction resolution to promote a distinct subset of crossovers during meiosis in budding yeast', *Genetics,* 164(1), pp. 81-94.

De Piccoli, G., Cortes-Ledesma, F., Ira, G., Torres-Rosell, J., Uhle, S., Farmer, S., Hwang, J. Y., Machin, F., Ceschia, A., McAleenan, A., Cordon-Preciado, V., Clemente-Blanco, A., Vilella-Mitjana, F., Ullal, P., Jarmuz, A., Leitao, B., Bressan, D., Dotiwala, F., Papusha, A., Zhao, X., Myung, K., Haber, J. E., Aguilera, A. and Aragón, L. (2006) 'Smc5-Smc6 mediate DNA double-strand-break repair by promoting sister-chromatid

recombination', *Nat Cell Biol,* 8(9), pp. 1032-4.

De Piccoli, G., Torres-Rosell, J. and Aragón, L. (2009) 'The unnamed complex: what do we know about Smc5-Smc6?', *Chromosome Res,* 17(2), pp. 251-63.

Deardorff, M. A., Kaur, M., Yaeger, D., Rampuria, A., Korolev, S., Pie, J., Gil-Rodríguez, C., Arnedo, M., Loeys, B., Kline, A. D., Wilson, M., Lillquist, K., Siu, V., Ramos, F. J., Musio, A., Jackson, L. S., Dorsett, D. and Krantz, I. D. (2007) 'Mutations in cohesin complex members SMC3 and SMC1A cause a mild variant of cornelia de Lange syndrome with predominant mental retardation', *Am J Hum Genet,* 80(3), pp. 485-94.

DeLuca, J. G., Gall, W. E., Ciferri, C., Cimini, D., Musacchio, A. and Salmon, E. D. (2006) 'Kinetochore microtubule dynamics and attachment stability are regulated by Hec1', *Cell,* 127(5), pp. 969-82.

Dernburg, A. F., McDonald, K., Moulder, G., Barstead, R., Dresser, M. and Villeneuve, A. M. (1998) 'Meiotic recombination in C. elegans initiates by a conserved mechanism and is dispensable for homologous chromosome synapsis', *Cell,* 94(3), pp. 387-98.

Ding, R., McDonald, K. L. and McIntosh, J. R. (1993) 'Three-dimensional reconstruction and analysis of mitotic spindles from the yeast, Schizosaccharomyces pombe', *J Cell Biol,* 120(1), pp. 141-51.

Doyle, J. M., Gao, J., Wang, J., Yang, M. and Potts, P. R. (2010) 'MAGE-RING protein complexes comprise a family of E3 ubiquitin ligases', *Mol Cell,* 39(6), pp. 963-74.

Duan, X., Sarangi, P., Liu, X., Rangi, G. K., Zhao, X. and Ye, H. (2009) 'Structural and functional insights into the roles of the Mms21 subunit of the Smc5/6 complex', *Mol Cell,* 35(5), pp. 657-68.

Dunin-Horkawicz, S., Feder, M. and Bujnicki, J. M. (2006) 'Phylogenomic analysis of the GIY-YIG nuclease superfamily', *BMC Genomics,* 7, pp. 98.

Eckert-Boulet, N. and Lisby, M. (2009) 'Regulation of rDNA stability by sumoylation', *DNA Repair (Amst),* 8(4), pp. 507-16.

Edelmann, W., Cohen, P. E., Kneitz, B., Winand, N., Lia, M., Heyer, J., Kolodner, R., Pollard, J. W. and Kucherlapati, R. (1999) 'Mammalian

MutS homologue 5 is required for chromosome pairing in meiosis', *Nat Genet,* 21(1), pp. 123-7.

Egel-Mitani, M., Olson, L. W. and Egel, R. (1982) 'Meiosis in Aspergillus nidulans: another example for lacking synaptonemal complexes in the absence of crossover interference', *Hereditas,* 97(2), pp. 179-87.

Eng, T., Guacci, V. and Koshland, D. (2015) 'Interallelic complementation provides functional evidence for cohesin-cohesin interactions on DNA', *Mol Biol Cell,* 26(23), pp. 4224-35.

Eppig, J. J. and O'Brien, M. J. (1996) 'Development in vitro of mouse oocytes from primordial follicles', *Biol Reprod,* 54(1), pp. 197-207.

Fabre, F., Chan, A., Heyer, W. D. and Gangloff, S. (2002) 'Alternate pathways involving Sgs1/Top3, Mus81/ Mms4, and Srs2 prevent formation of toxic recombination intermediates from single-stranded gaps created by DNA replication', *Proc Natl Acad Sci U S A,* 99(26), pp. 16887-92.

Farmer, S., San-Segundo, P. A. and Aragón, L. (2011) 'The Smc5-Smc6 complex is required to remove chromosome junctions in meiosis', *PLoS One,* 6(6), pp. e20948.

Fay, A., Misulovin, Z., Li, J., Schaaf, C. A., Gause, M., Gilmour, D. S. and Dorsett, D. (2011) 'Cohesin selectively binds and regulates genes with paused RNA polymerase', *Curr Biol,* 21(19), pp. 1624-34.

Foltz, D. R., Jansen, L. E., Black, B. E., Bailey, A. O., Yates, J. R. and Cleveland, D. W. (2006) 'The human CENP-A centromeric nucleosome-associated complex', *Nat Cell Biol,* 8(5), pp. 458-69.

Fousteri, M. I. and Lehmann, A. R. (2000) 'A novel SMC protein complex in Schizosaccharomyces pombe contains the Rad18 DNA repair protein', *EMBO J,* 19(7), pp. 1691-702.

Freeman, L., Aragon-Alcaide, L. and Strunnikov, A. (2000) 'The condensin complex governs chromosome condensation and mitotic transmission of rDNA', *J Cell Biol,* 149(4), pp. 811-24.

Fujioka, Y., Kimata, Y., Nomaguchi, K., Watanabe, K. and Kohno, K. (2002) 'Identification of a novel non-structural maintenance of chromosomes (SMC) component of the SMC5-SMC6 complex involved in DNA repair', *J Biol Chem,* 277(24), pp. 21585-91.

Funabiki, H., Yamano, H., Kumada, K., Nagao, K., Hunt, T. and Yanagida, M. (1996) 'Cut2 proteolysis required for sister-chromatid seperation in fission yeast', *Nature,* 381(6581), pp. 438-41.

Fung, J. C., Rockmill, B., Odell, M. and Roeder, G. S. (2004) 'Imposition of crossover interference through the nonrandom distribution of synapsis initiation complexes', *Cell,* 116(6), pp. 795-802.

Gallego-Paez, L. M., Tanaka, H., Bando, M., Takahashi, M., Nozaki, N., Nakato, R., Shirahige, K. and Hirota, T. (2014) 'Smc5/6-mediated regulation of replication progression contributes to chromosome assembly during mitosis in human cells', *Mol Biol Cell,* 25(2), pp. 302-17.

Gandhi, R., Gillespie, P. J. and Hirano, T. (2006) 'Human Wapl is a cohesin-binding protein that promotes sister-chromatid resolution in mitotic prophase', *Curr Biol,* 16(24), pp. 2406-17.

Gangloff, S., McDonald, J. P., Bendixen, C., Arthur, L. and Rothstein, R. (1994) 'The yeast type I topoisomerase Top3 interacts with Sgs1, a DNA helicase homolog: a potential eukaryotic reverse gyrase', *Mol Cell Biol,* 14(12), pp. 8391-8.

Garcia, V., Gray, S., Allison, R. M., Cooper, T. J. and Neale, M. J. (2015) 'Tel1(ATM)-mediated interference suppresses clustered meiotic double-strand-break formation', *Nature,* 520(7545), pp. 114-8.

Garcia-Cruz, R., Brieño, M. A., Roig, I., Grossmann, M., Velilla, E., Pujol, A., Cabero, L., Pessarrodona, A., Barbero, J. L. and Garcia Caldés, M. (2010) 'Dynamics of cohesin proteins REC8, STAG3, SMC1 beta and SMC3 are consistent with a role in sister chromatid cohesion during meiosis in human oocytes', *Hum Reprod,* 25(9), pp. 2316-27.

Gerlich, D., Hirota, T., Koch, B., Peters, J. M. and Ellenberg, J. (2006a) 'Condensin I stabilizes chromosomes mechanically through a dynamic interaction in live cells', *Curr Biol,* 16(4), pp. 333-44.

Gerlich, D., Koch, B., Dupeux, F., Peters, J. M. and Ellenberg, J. (2006b) 'Live-cell imaging reveals a stable cohesin-chromatin interaction after but not before DNA replication', *Curr Biol,* 16(15), pp. 1571-8.

Gerton, J. L., DeRisi, J., Shroff, R., Lichten, M., Brown, P. O. and Petes, T. D. (2000) 'Global mapping of meiotic recombination hotspots and

coldspots in the yeast Saccharomyces cerevisiae', *Proc Natl Acad Sci U S A,* 97(21), pp. 11383-90.

Gietz, R. D., Schiestl, R. H., Willems, A. R. and Woods, R. A. (1995) 'Studies on the transformation of intact yeast cells by the LiAc/SS-DNA/PEG procedure', *Yeast,* 11(4), pp. 355-60.

Giménez-Abián, J. F., Sumara, I., Hirota, T., Hauf, S., Gerlich, D., de la Torre, C., Ellenberg, J. and Peters, J. M. (2004) 'Regulation of sister chromatid cohesion between chromosome arms', *Curr Biol,* 14(13), pp. 1187-93.

Gligoris, T. G., Scheinost, J. C., Bürmann, F., Petela, N., Chan, K. L., Uluocak, P., Beckouët, F., Gruber, S., Nasmyth, K. and Löwe, J. (2014) 'Closing the cohesin ring: structure and function of its Smc3-kleisin interface', *Science,* 346(6212), pp. 963-7.

Golding, I., Paulsson, J., Zawilski, S. M. and Cox, E. C. (2005) 'Real-time kinetics of gene activity in individual bacteria', *Cell,* 123(6), pp. 1025-36.

Goldstein, L. S. (1980) 'Mechanisms of chromosome orientation revealed by two meiotic mutants in Drosophila melanogaster', *Chromosoma,* 78(1), pp. 79-111.

Goodarzi, A. A. and Jeggo, P. A. (2012) 'The heterochromatic barrier to DNA double strand break repair: how to get the entry visa', *Int J Mol Sci,* 13(9), pp. 11844-60.

Gregan, J., Riedel, C. G., Pidoux, A. L., Katou, Y., Rumpf, C., Schleiffer, A., Kearsey, S. E., Shirahige, K., Allshire, R. C. and Nasmyth, K. (2007) 'The kinetochore proteins Pcs1 and Mde4 and heterochromatin are required to prevent merotelic orientation', *Curr Biol,* 17(14), pp. 1190-200.

Grelon, M., Vezon, D., Gendrot, G. and Pelletier, G. (2001) 'AtSPO11-1 is necessary for efficient meiotic recombination in plants', *EMBO J,* 20(3), pp. 589-600.

Grey, C., Barthès, P., Chauveau-Le Friec, G., Langa, F., Baudat, F. and de Massy, B. (2011) 'Mouse PRDM9 DNA-binding specificity determines sites of histone H3 lysine 4 trimethylation for initiation of meiotic recombination', *PLoS Biol,* 9(10), pp. e1001176.

Gruber, S., Arumugam, P., Katou, Y., Kuglitsch, D., Helmhart, W., Shirahige, K. and Nasmyth, K. (2006) 'Evidence that loading of cohesin onto chromosomes involves opening of its SMC hinge', *Cell,* 127(3), pp. 523-37.

Gruber, S., Haering, C. H. and Nasmyth, K. (2003) 'Chromosomal cohesin forms a ring', *Cell,* 112(6), pp. 765-77.

Gruhn, J. R., Rubio, C., Broman, K. W., Hunt, P. A. and Hassold, T. (2013) 'Cytological studies of human meiosis: sex-specific differences in recombination originate at, or prior to, establishment of double-strand breaks', *PLoS One,* 8(12), pp. e85075.

Gui, L. and Homer, H. (2012) 'Spindle assembly checkpoint signalling is uncoupled from chromosomal position in mouse oocytes', *Development,* 139(11), pp. 1941-6.

Gyuricza, M. R., Manheimer, K. B., Apte, V., Krishnan, B., Joyce, E. F., McKee, B. D. and McKim, K. S. (2016) 'Dynamic and Stable Cohesins Regulate Synaptonemal Complex Assembly and Chromosome Segregation', *Curr Biol,* 26(13), pp. 1688-98.

Gómez, R., Jordan, P. W., Viera, A., Alsheimer, M., Fukuda, T., Jessberger, R., Llano, E., Pendás, A. M., Handel, M. A. and Suja, J. A. (2013) 'Dynamic localization of SMC5/6 complex proteins during mammalian meiosis and mitosis suggests functions in distinct chromosome processes', *J Cell Sci,* 126(Pt 18), pp. 4239-52.

Haering, C. H., Löwe, J., Hochwagen, A. and Nasmyth, K. (2002) 'Molecular architecture of SMC proteins and the yeast cohesin complex', *Mol Cell,* 9(4), pp. 773-88.

Haering, C. H., Schoffnegger, D., Nishino, T., Helmhart, W., Nasmyth, K. and Löwe, J. (2004) 'Structure and stability of cohesin's Smc1-kleisin interaction', *Mol Cell,* 15(6), pp. 951-64.

Hagstrom, K. A., Holmes, V. F., Cozzarelli, N. R. and Meyer, B. J. (2002) 'C. elegans condensin promotes mitotic chromosome architecture, centromere organization, and sister chromatid segregation during mitosis and meiosis', *Genes Dev,* 16(6), pp. 729-42.

Hamant, O., Golubovskaya, I., Meeley, R., Fiume, E., Timofejeva, L., Schleiffer,

A., Nasmyth, K. and Cande, W. Z. (2005) 'A REC8-dependent plant Shugoshin is required for maintenance of centromeric cohesion during meiosis and has no mitotic functions', *Curr Biol,* 15(10), pp. 948-54.

Hamer, G., Gell, K., Kouznetsova, A., Novak, I., Benavente, R. and Höög, C. (2006) 'Characterization of a novel meiosis-specific protein within the central element of the synaptonemal complex', *J Cell Sci,* 119(Pt 19), pp. 4025-32.

Hanna, J. S., Kroll, E. S., Lundblad, V. and Spencer, F. A. (2001) 'Saccharomyces cerevisiae CTF18 and CTF4 are required for sister chromatid cohesion', *Mol Cell Biol,* 21(9), pp. 3144-58.

Hara, K., Zheng, G., Qu, Q., Liu, H., Ouyang, Z., Chen, Z., Tomchick, D. R. and Yu, H. (2014) 'Structure of cohesin subcomplex pinpoints direct shugoshin-Wapl antagonism in centromeric cohesion', *Nat Struct Mol Biol,* 21(10), pp. 864-70.

Hardy, C. F., Dryga, O., Seematter, S., Pahl, P. M. and Sclafani, R. A. (1997) 'mcm5/cdc46-bob1 bypasses the requirement for the S phase activator Cdc7p', *Proc Natl Acad Sci U S A,* 94(7), pp. 3151-5.

Hartman, T., Stead, K., Koshland, D. and Guacci, V. (2000) 'Pds5p is an essential chromosomal protein required for both sister chromatid cohesion and condensation in Saccharomyces cerevisiae', *J Cell Biol,* 151(3), pp. 613-26.

Harvey, S. H., Sheedy, D. M., Cuddihy, A. R. and O'Connell, M. J. (2004) 'Coordination of DNA damage responses via the Smc5/Smc6 complex', *Mol Cell Biol,* 24(2), pp. 662-74.

Hassold, T., Abruzzo, M., Adkins, K., Griffin, D., Merrill, M., Millie, E., Saker, D., Shen, J. and Zaragoza, M. (1996) 'Human aneuploidy: incidence, origin, and etiology', *Environ Mol Mutagen,* 28(3), pp. 167-75.

Hassold, T. and Chiu, D. (1985) 'Maternal age-specific rates of numerical chromosome abnormalities with special reference to trisomy', *Hum Genet,* 70(1), pp. 11-7.

Hassold, T. and Hunt, P. (2001) 'To err (meiotically) is human: the genesis of human aneuploidy', *Nat Rev Genet,* 2(4), pp. 280-91.

Hassold, T., Merrill, M., Adkins, K., Freeman, S. and Sherman, S. (1995) 'Recombination and maternal age-dependent nondisjunction: molecular studies of trisomy 16', *Am J Hum Genet,* 57(4), pp. 867-74.

Hassold, T. J. (1998) 'Nondisjunction in the human male', *Curr Top Dev Biol,* 37, pp. 383-406.

Hassold, T. J. and Jacobs, P. A. (1984) 'Trisomy in man', *Annu Rev Genet,* 18, pp. 69-97.

Hauf, S., Roitinger, E., Koch, B., Dittrich, C. M., Mechtler, K. and Peters, J. M. (2005) 'Dissociation of cohesin from chromosome arms and loss of arm cohesion during early mitosis depends on phosphorylation of SA2', *PLoS Biol,* 3(3), pp. e69.

Heckmann, S., Jankowska, M., Schubert, V., Kumke, K., Ma, W. and Houben, A. (2014) 'Alternative meiotic chromatid segregation in the holocentric plant Luzula elegans', *Nat Commun,* 5, pp. 4979.

Heidinger-Pauli, J. M., Mert, O., Davenport, C., Guacci, V. and Koshland, D. (2010) 'Systematic reduction of cohesin differentially affects chromosome segregation, condensation, and DNA repair', *Curr Biol,* 20(10), pp. 957-63.

Henderson, K. A., Kee, K., Maleki, S., Santini, P. A. and Keeney, S. (2006) 'Cyclin-dependent kinase directly regulates initiation of meiotic recombination', *Cell,* 125(7), pp. 1321-32.

Henderson, K. A. and Keeney, S. (2004) 'Tying synaptonemal complex initiation to the formation and programmed repair of DNA double-strand breaks', *Proc Natl Acad Sci U S A,* 101(13), pp. 4519-24.

Herbert, A. D., Carr, A. M. and Hoffmann, E. (2014) 'FindFoci: a focus detection algorithm with automated parameter training that closely matches human assignments, reduces human inconsistencies and increases speed of analysis', *PLoS One,* 9(12), pp. e114749.

Herrán, Y., Gutiérrez-Caballero, C., Sánchez-Martín, M., Hernández, T., Viera, A., Barbero, J. L., de Álava, E., de Rooij, D. G., Suja, J., Llano, E. and Pendás, A. M. (2011) 'The cohesin subunit RAD21L functions in meiotic synapsis and exhibits sexual dimorphism in fertility', *EMBO J,* 30(15), pp. 3091-105.

Higgins, J. D., Buckling, E. F., Franklin, F. C. and Jones, G. H. (2008) 'Expression and functional analysis of AtMUS81 in Arabidopsis meiosis reveals a role in the second pathway of crossing-over', *Plant J,* 54(1), pp. 152-62.

Hirano, T. (2002) 'The ABCs of SMC proteins: two-armed ATPases for chromosome condensation, cohesion, and repair', *Genes Dev,* 16(4), pp. 399-414.

Hirano, T. (2006) 'At the heart of the chromosome: SMC proteins in action', *Nat Rev Mol Cell Biol,* 7(5), pp. 311-22.

Hirano, T. (2012) 'Condensins: universal organizers of chromosomes with diverse functions', *Genes Dev,* 26(15), pp. 1659-78.

Hirano, T., Kobayashi, R. and Hirano, M. (1997) 'Condensins, chromosome condensation protein complexes containing XCAP-C, XCAP-E and a Xenopus homolog of the Drosophila Barren protein', *Cell,* 89(4), pp. 511-21.

Hirano, T. and Mitchison, T. J. (1994) 'A heterodimeric coiled-coil protein required for mitotic chromosome condensation in vitro', *Cell,* 79(3), pp. 449-58.

Hirose, Y., Suzuki, R., Ohba, T., Hinohara, Y., Matsuhara, H., Yoshida, M., Itabashi, Y., Murakami, H. and Yamamoto, A. (2011) 'Chiasmata promote monopolar attachment of sister chromatids and their co-segregation toward the proper pole during meiosis I', *PLoS Genet,* 7(3), pp. e1001329.

Hirota, T., Gerlich, D., Koch, B., Ellenberg, J. and Peters, J. M. (2004) 'Distinct functions of condensin I and II in mitotic chromosome assembly', *J Cell Sci,* 117(Pt 26), pp. 6435-45.

Hodges, C. A. and Hunt, P. A. (2002) 'Simultaneous analysis of chromosomes and chromosome-associated proteins in mammalian oocytes and embryos', *Chromosoma,* 111(3), pp. 165-9.

Hodges, C. A., Revenkova, E., Jessberger, R., Hassold, T. J. and Hunt, P. A. (2005) 'SMC1beta-deficient female mice provide evidence that cohesins are a missing link in age-related nondisjunction', *Nat Genet,* 37(12), pp. 1351-5.

Holland, A. J., Böttger, F., Stemmann, O. and Taylor, S. S. (2007) 'Protein phosphatase 2A and separase form a complex regulated by separase autocleavage', *J Biol Chem,* 282(34), pp. 24623-32.

Holloway, J. K., Booth, J., Edelmann, W., McGowan, C. H. and Cohen, P. E. (2008) 'MUS81 generates a subset of MLH1-MLH3-independent crossovers in mammalian meiosis', *PLoS Genet,* 4(9), pp. e1000186.

Holubcová, Z., Blayney, M., Elder, K. and Schuh, M. (2015) 'Human oocytes. Error-prone chromosome-mediated spindle assembly favors chromosome segregation defects in human oocytes', *Science,* 348(6239), pp. 1143-7.

Hong, Y., Sonneville, R., Agostinho, A., Meier, B., Wang, B., Blow, J. J. and Gartner, A. (2016) 'The SMC-5/6 Complex and the HIM-6 (BLM) Helicase Synergistically Promote Meiotic Recombination Intermediate Processing and Chromosome Maturation during Caenorhabditis elegans Meiosis', *PLoS Genet,* 12(3), pp. e1005872.

Hopkins, J., Hwang, G., Jacob, J., Sapp, N., Bedigian, R., Oka, K., Overbeek, P., Murray, S. and Jordan, P. W. (2014) 'Meiosis-specific cohesin component, Stag3 is essential for maintaining centromere chromatid cohesion, and required for DNA repair and synapsis between homologous chromosomes', *PLoS Genet,* 10(7), pp. e1004413.

Hoque, M. T. and Ishikawa, F. (2002) 'Cohesin defects lead to premature sister chromatid separation, kinetochore dysfunction, and spindle-assembly checkpoint activation', *J Biol Chem,* 277(44), pp. 42306-14.

Houlard, M., Godwin, J., Metson, J., Lee, J., Hirano, T. and Nasmyth, K. (2015) 'Condensin confers the longitudinal rigidity of chromosomes', *Nat Cell Biol,* 17(6), pp. 771-81.

Hu, B., Itoh, T., Mishra, A., Katoh, Y., Chan, K. L., Upcher, W., Godlee, C., Roig, M. B., Shirahige, K. and Nasmyth, K. (2011) 'ATP hydrolysis is required for relocating cohesin from sites occupied by its Scc2/4 loading complex', *Curr Biol,* 21(1), pp. 12-24.

Hu, B., Liao, C., Millson, S. H., Mollapour, M., Prodromou, C., Pearl, L. H., Piper, P. W. and Panaretou, B. (2005) 'Qri2/Nse4, a component of the essential Smc5/6 DNA repair complex', *Mol Microbiol,* 55(6), pp.

1735-50.

Huang, C. E., Milutinovich, M. and Koshland, D. (2005) 'Rings, bracelet or snaps: fashionable alternatives for Smc complexes', *Philos Trans R Soc Lond B Biol Sci,* 360(1455), pp. 537-42.

Huang, H., Feng, J., Famulski, J., Rattner, J. B., Liu, S. T., Kao, G. D., Muschel, R., Chan, G. K. and Yen, T. J. (2007) 'Tripin/hSgo2 recruits MCAK to the inner centromere to correct defective kinetochore attachments', *J Cell Biol,* 177(3), pp. 413-24.

Huang, J., Brito, I. L., Villén, J., Gygi, S. P., Amon, A. and Moazed, D. (2006) 'Inhibition of homologous recombination by a cohesin-associated clamp complex recruited to the rDNA recombination enhancer', *Genes Dev,* 20(20), pp. 2887-901.

Hudson, D. F., Vagnarelli, P., Gassmann, R. and Earnshaw, W. C. (2003) 'Condensin is required for nonhistone protein assembly and structural integrity of vertebrate mitotic chromosomes', *Dev Cell,* 5(2), pp. 323-36.

Hughes, A. J., Spelke, D. P., Xu, Z., Kang, C. C., Schaffer, D. V. and Herr, A. E. (2014) 'Single-cell western blotting', *Nat Methods,* 11(7), pp. 749-55.

Humphryes, N., Leung, W. K., Argunhan, B., Terentyev, Y., Dvorackova, M. and Tsubouchi, H. (2013) 'The Ecm11-Gmc2 complex promotes synaptonemal complex formation through assembly of transverse filaments in budding yeast', *PLoS Genet,* 9(1), pp. e1003194.

Hunt, P. A. and Hassold, T. J. (2002) 'Sex matters in meiosis', *Science,* 296(5576), pp. 2181-3.

Hunt, P. A. and Hassold, T. J. (2008) 'Human female meiosis: what makes a good egg go bad?', *Trends Genet,* 24(2), pp. 86-93.

Hunt, P. A., Koehler, K. E., Susiarjo, M., Hodges, C. A., Ilagan, A., Voigt, R. C., Thomas, S., Thomas, B. F. and Hassold, T. J. (2003) 'Bisphenol a exposure causes meiotic aneuploidy in the female mouse', *Curr Biol,* 13(7), pp. 546-53.

Hunter, N. (2011) 'Double duty for Exo1 during meiotic recombination', *Cell Cycle,* 10(16), pp. 2607-9.

Hunter, N. and Kleckner, N. (2001) 'The single-end invasion: an asymmetric

intermediate at the double-strand break to double-holliday junction transition of meiotic recombination', *Cell,* 106(1), pp. 59-70.

Hwang, G., Sun, F., O'Brien, M., Eppig, J. J., Handel, M. A. and Jordan, P. W. (2017) 'SMC5/6 is required for the formation of segregation-competent bivalent chromosomes during meiosis I in mouse oocytes', *Development*.

Hwang, L. H., Lau, L. F., Smith, D. L., Mistrot, C. A., Hardwick, K. G., Hwang, E. S., Amon, A. and Murray, A. W. (1998) 'Budding yeast Cdc20: a target of the spindle checkpoint', *Science,* 279(5353), pp. 1041-4.

Ichijima, Y., Sin, H. S. and Namekawa, S. H. (2012) 'Sex chromosome inactivation in germ cells: emerging roles of DNA damage response pathways', *Cell Mol Life Sci,* 69(15), pp. 2559-72.

Inoue, A., Li, T., Roby, S. K., Valentine, M. B., Inoue, M., Boyd, K., Kidd, V. J. and Lahti, J. M. (2007) 'Loss of ChlR1 helicase in mouse causes lethality due to the accumulation of aneuploid cells generated by cohesion defects and placental malformation', *Cell Cycle,* 6(13), pp. 1646-54.

Ip, S. C., Rass, U., Blanco, M. G., Flynn, H. R., Skehel, J. M. and West, S. C. (2008) 'Identification of Holliday junction resolvases from humans and yeast', *Nature,* 456(7220), pp. 357-61.

Ira, G., Malkova, A., Liberi, G., Foiani, M. and Haber, J. E. (2003) 'Srs2 and Sgs1-Top3 suppress crossovers during double-strand break repair in yeast', *Cell,* 115(4), pp. 401-11.

Irmisch, A., Ampatzidou, E., Mizuno, K., O'Connell, M. J. and Murray, J. M. (2009) 'Smc5/6 maintains stalled replication forks in a recombination-competent conformation', *EMBO J,* 28(2), pp. 144-55.

Ishitsuka, Y., Nienhaus, K. and Nienhaus, G. U. (2014) 'Photoactivatable fluorescent proteins for super-resolution microscopy', *Methods Mol Biol,* 1148, pp. 239-60.

Ivanov, E. L., Korolev, V. G. and Fabre, F. (1992) 'XRS2, a DNA repair gene of Saccharomyces cerevisiae, is needed for meiotic recombination', *Genetics,* 132(3), pp. 651-64.

Jackson, S. P. and Bartek, J. (2009) 'The DNA-damage response in human

biology and disease', *Nature,* 461(7267), pp. 1071-8.

Jacobs, P. A. (1992) 'The chromosome complement of human gametes', *Oxf Rev Reprod Biol,* 14, pp. 47-72.

Jacome, A., Gutierrez-Martinez, P., Schiavoni, F., Tenaglia, E., Martinez, P., Rodríguez-Acebes, S., Lecona, E., Murga, M., Méndez, J., Blasco, M. A. and Fernandez-Capetillo, O. (2015) 'NSMCE2 suppresses cancer and aging in mice independently of its SUMO ligase activity', *EMBO J,* 34(21), pp. 2604-19.

Jeffreys, C. A., Burrage, P. S. and Bickel, S. E. (2003) 'A model system for increased meiotic nondisjunction in older oocytes', *Curr Biol,* 13(6), pp. 498-503.

Jeppsson, K., Carlborg, K. K., Nakato, R., Berta, D. G., Lilienthal, I., Kanno, T., Lindqvist, A., Brink, M. C., Dantuma, N. P., Katou, Y., Shirahige, K. and Sjögren, C. (2014a) 'The chromosomal association of the Smc5/6 complex depends on cohesion and predicts the level of sister chromatid entanglement', *PLoS Genet,* 10(10), pp. e1004680.

Jeppsson, K., Kanno, T., Shirahige, K. and Sjögren, C. (2014b) 'The maintenance of chromosome structure: positioning and functioning of SMC complexes', *Nat Rev Mol Cell Biol,* 15(9), pp. 601-14.

Jessop, L. and Lichten, M. (2008) 'Mus81/Mms4 endonuclease and Sgs1 helicase collaborate to ensure proper recombination intermediate metabolism during meiosis', *Mol Cell,* 31(3), pp. 313-23.

Jessop, L., Rockmill, B., Roeder, G. S. and Lichten, M. (2006) 'Meiotic chromosome synapsis-promoting proteins antagonize the anti-crossover activity of sgs1', *PLoS Genet,* 2(9), pp. e155.

Jiao, K., Salem, L. and Malone, R. (2003) 'Support for a meiotic recombination initiation complex: interactions among Rec102p, Rec104p, and Spo11p', *Mol Cell Biol,* 23(16), pp. 5928-38.

Jordan, P., Copsey, A., Newnham, L., Kolar, E., Lichten, M. and Hoffmann, E. (2009) 'Ipl1/Aurora B kinase coordinates synaptonemal complex disassembly with cell cycle progression and crossover formation in budding yeast meiosis', *Genes Dev,* 23(18), pp. 2237-51.

Ju, L., Wing, J., Taylor, E., Brandt, R., Slijepcevic, P., Horsch, M., Rathkolb, B.,

Rácz, I., Becker, L., Hans, W., Adler, T., Beckers, J., Rozman, J., Klingenspor, M., Wolf, E., Zimmer, A., Klopstock, T., Busch, D. H., Gailus-Durner, V., Fuchs, H., de Angelis, M. H., van der Horst, G. and Lehmann, A. R. (2013) 'SMC6 is an essential gene in mice, but a hypomorphic mutant in the ATPase domain has a mild phenotype with a range of subtle abnormalities', *DNA Repair (Amst),* 12(5), pp. 356-66.

Kagey, M. H., Newman, J. J., Bilodeau, S., Zhan, Y., Orlando, D. A., van Berkum, N. L., Ebmeier, C. C., Goossens, J., Rahl, P. B., Levine, S. S., Taatjes, D. J., Dekker, J. and Young, R. A. (2010) 'Mediator and cohesin connect gene expression and chromatin architecture', *Nature,* 467(7314), pp. 430-5.

Kanno, T., Berta, D. G. and Sjögren, C. (2015) 'The Smc5/6 Complex Is an ATP-Dependent Intermolecular DNA Linker', *Cell Rep,* 12(9), pp. 1471-82.

Katis, V. L., Galova, M., Rabitsch, K. P., Gregan, J. and Nasmyth, K. (2004) 'Maintenance of cohesin at centromeres after meiosis I in budding yeast requires a kinetochore-associated protein related to MEI-S332', *Curr Biol,* 14(7), pp. 560-72.

Katis, V. L., Lipp, J. J., Imre, R., Bogdanova, A., Okaz, E., Habermann, B., Mechtler, K., Nasmyth, K. and Zachariae, W. (2010) 'Rec8 phosphorylation by casein kinase 1 and Cdc7-Dbf4 kinase regulates cohesin cleavage by separase during meiosis', *Dev Cell,* 18(3), pp. 397-409.

Kauppi, L., Barchi, M., Lange, J., Baudat, F., Jasin, M. and Keeney, S. (2013) 'Numerical constraints and feedback control of double-strand breaks in mouse meiosis', *Genes Dev,* 27(8), pp. 873-86.

Kawashima, S. A., Yamagishi, Y., Honda, T., Ishiguro, K. and Watanabe, Y. (2010) 'Phosphorylation of H2A by Bub1 prevents chromosomal instability through localizing shugoshin', *Science,* 327(5962), pp. 172-7.

Kee, K., Protacio, R. U., Arora, C. and Keeney, S. (2004) 'Spatial organization and dynamics of the association of Rec102 and Rec104 with meiotic

chromosomes', *EMBO J,* 23(8), pp. 1815-24.

Keeney, S. and Neale, M. J. (2006) 'Initiation of meiotic recombination by formation of DNA double-strand breaks: mechanism and regulation', *Biochem Soc Trans,* 34(Pt 4), pp. 523-5.

Kegel, A., Betts-Lindroos, H., Kanno, T., Jeppsson, K., Ström, L., Katou, Y., Itoh, T., Shirahige, K. and Sjögren, C. (2011) 'Chromosome length influences replication-induced topological stress', *Nature,* 471(7338), pp. 392-6.

Khil, P. P., Smagulova, F., Brick, K. M., Camerini-Otero, R. D. and Petukhova, G. V. (2012) 'Sensitive mapping of recombination hotspots using sequencing-based detection of ssDNA', *Genome Res,* 22(5), pp. 957-65.

Kiburz, B. M., Reynolds, D. B., Megee, P. C., Marston, A. L., Lee, B. H., Lee, T. I., Levine, S. S., Young, R. A. and Amon, A. (2005) 'The core centromere and Sgo1 establish a 50-kb cohesin-protected domain around centromeres during meiosis I', *Genes Dev,* 19(24), pp. 3017-30.

Kim, J., Ishiguro, K., Nambu, A., Akiyoshi, B., Yokobayashi, S., Kagami, A., Ishiguro, T., Pendas, A. M., Takeda, N., Sakakibara, Y., Kitajima, T. S., Tanno, Y., Sakuno, T. and Watanabe, Y. (2015) 'Meikin is a conserved regulator of meiosis-I-specific kinetochore function', *Nature,* 517(7535), pp. 466-71.

Kim, S. H., Lin, D. P., Matsumoto, S., Kitazono, A. and Matsumoto, T. (1998) 'Fission yeast Slp1: an effector of the Mad2-dependent spindle checkpoint', *Science,* 279(5353), pp. 1045-7.

Kim, S. T., Xu, B. and Kastan, M. B. (2002) 'Involvement of the cohesin protein, Smc1, in Atm-dependent and independent responses to DNA damage', *Genes Dev,* 16(5), pp. 560-70.

Kimura, K. and Hirano, T. (1997) 'ATP-dependent positive supercoiling of DNA by 13S condensin: a biochemical implication for chromosome condensation', *Cell,* 90(4), pp. 625-34.

Kimura, K., Rybenkov, V. V., Crisona, N. J., Hirano, T. and Cozzarelli, N. R. (1999) '13S condensin actively reconfigures DNA by introducing global positive writhe: implications for chromosome condensation', *Cell,* 98(2), pp. 239-48.

Kitajima, T. S., Kawashima, S. A. and Watanabe, Y. (2004) 'The conserved kinetochore protein shugoshin protects centromeric cohesion during meiosis', *Nature,* 427(6974), pp. 510-7.

Kitajima, T. S., Sakuno, T., Ishiguro, K., Iemura, S., Natsume, T., Kawashima, S. A. and Watanabe, Y. (2006) 'Shugoshin collaborates with protein phosphatase 2A to protect cohesin', *Nature,* 441(7089), pp. 46-52.

Klein, F., Mahr, P., Galova, M., Buonomo, S. B., Michaelis, C., Nairz, K. and Nasmyth, K. (1999) 'A central role for cohesins in sister chromatid cohesion, formation of axial elements, and recombination during yeast meiosis', *Cell,* 98(1), pp. 91-103.

Kneitz, B., Cohen, P. E., Avdievich, E., Zhu, L., Kane, M. F., Hou, H., Kolodner, R. D., Kucherlapati, R., Pollard, J. W. and Edelmann, W. (2000) 'MutS homolog 4 localization to meiotic chromosomes is required for chromosome pairing during meiosis in male and female mice', *Genes Dev,* 14(9), pp. 1085-97.

Kobayashi, T. and Ganley, A. R. (2005) 'Recombination regulation by transcription-induced cohesin dissociation in rDNA repeats', *Science,* 309(5740), pp. 1581-4.

Kolano, A., Brunet, S., Silk, A. D., Cleveland, D. W. and Verlhac, M. H. (2012) 'Error-prone mammalian female meiosis from silencing the spindle assembly checkpoint without normal interkinetochore tension', *Proc Natl Acad Sci U S A,* 109(27), pp. E1858-67.

Kolas, N. K. and Cohen, P. E. (2004) 'Novel and diverse functions of the DNA mismatch repair family in mammalian meiosis and recombination', *Cytogenet Genome Res,* 107(3-4), pp. 216-31.

Kolas, N. K., Svetlanov, A., Lenzi, M. L., Macaluso, F. P., Lipkin, S. M., Liskay, R. M., Greally, J., Edelmann, W. and Cohen, P. E. (2005) 'Localization of MMR proteins on meiotic chromosomes in mice indicates distinct functions during prophase I', *J Cell Biol,* 171(3), pp. 447-58.

Kota, S. K. and Feil, R. (2010) 'Epigenetic transitions in germ cell development and meiosis', *Dev Cell,* 19(5), pp. 675-86.

Kouznetsova, A., Benavente, R., Pastink, A. and Höög, C. (2011) 'Meiosis in mice without a synaptonemal complex', *PLoS One,* 6(12), pp. e28255.

Kouznetsova, A., Lister, L., Nordenskjöld, M., Herbert, M. and Höög, C. (2007) 'Bi-orientation of achiasmatic chromosomes in meiosis I oocytes contributes to aneuploidy in mice', *Nat Genet,* 39(8), pp. 966-8.

Krantz, I. D., McCallum, J., DeScipio, C., Kaur, M., Gillis, L. A., Yaeger, D., Jukofsky, L., Wasserman, N., Bottani, A., Morris, C. A., Nowaczyk, M. J., Toriello, H., Bamshad, M. J., Carey, J. C., Rappaport, E., Kawauchi, S., Lander, A. D., Calof, A. L., Li, H. H., Devoto, M. and Jackson, L. G. (2004) 'Cornelia de Lange syndrome is caused by mutations in NIPBL, the human homolog of Drosophila melanogaster Nipped-B', *Nat Genet,* 36(6), pp. 631-5.

Kudo, N. R., Anger, M., Peters, A. H., Stemmann, O., Theussl, H. C., Helmhart, W., Kudo, H., Heyting, C. and Nasmyth, K. (2009) 'Role of cleavage by separase of the Rec8 kleisin subunit of cohesin during mammalian meiosis I', *J Cell Sci,* 122(Pt 15), pp. 2686-98.

Kueng, S., Hegemann, B., Peters, B. H., Lipp, J. J., Schleiffer, A., Mechtler, K. and Peters, J. M. (2006) 'Wapl controls the dynamic association of cohesin with chromatin', *Cell,* 127(5), pp. 955-67.

Kulemzina, I., Schumacher, M. R., Verma, V., Reiter, J., Metzler, J., Failla, A. V., Lanz, C., Sreedharan, V. T., Rätsch, G. and Ivanov, D. (2012) 'Cohesin rings devoid of Scc3 and Pds5 maintain their stable association with the DNA', *PLoS Genet,* 8(8), pp. e1002856.

Lake, C. M. and Hawley, R. S. (2012) 'The molecular control of meiotic chromosomal behavior: events in early meiotic prophase in Drosophila oocytes', *Annu Rev Physiol,* 74, pp. 425-51.

Lamb, N. E., Feingold, E., Savage, A., Avramopoulos, D., Freeman, S., Gu, Y., Hallberg, A., Hersey, J., Karadima, G., Pettay, D., Saker, D., Shen, J., Taft, L., Mikkelsen, M., Petersen, M. B., Hassold, T. and Sherman, S. L. (1997) 'Characterization of susceptible chiasma configurations that increase the risk for maternal nondisjunction of chromosome 21', *Hum Mol Genet,* 6(9), pp. 1391-9.

Lamb, N. E. and Hassold, T. J. (2004) 'Nondisjunction--a view from ringside', *N Engl J Med,* 351(19), pp. 1931-4.

Lane, S. I., Yun, Y. and Jones, K. T. (2012) 'Timing of anaphase-promoting complex activation in mouse oocytes is predicted by microtubule-kinetochore attachment but not by bivalent alignment or tension', *Development,* 139(11), pp. 1947-55.

Lao, J. P., Oh, S. D., Shinohara, M., Shinohara, A. and Hunter, N. (2008) 'Rad52 promotes postinvasion steps of meiotic double-strand-break repair', *Mol Cell,* 29(4), pp. 517-24.

Lavoie, B. D., Hogan, E. and Koshland, D. (2004) 'In vivo requirements for rDNA chromosome condensation reveal two cell-cycle-regulated pathways for mitotic chromosome folding', *Genes Dev,* 18(1), pp. 76-87.

Lawson, K. A. and Hage, W. J. (1994) 'Clonal analysis of the origin of primordial germ cells in the mouse', *Ciba Found Symp,* 182, pp. 68-84; discussion 84-91.

Le, T. T., Harlepp, S., Guet, C. C., Dittmar, K., Emonet, T., Pan, T. and Cluzel, P. (2005) 'Real-time RNA profiling within a single bacterium', *Proc Natl Acad Sci U S A,* 102(26), pp. 9160-4.

Lee, B. H. and Amon, A. (2003) 'Role of Polo-like kinase CDC5 in programming meiosis I chromosome segregation', *Science,* 300(5618), pp. 482-6.

Lee, D., Ezhkova, E., Li, B., Pattenden, S. G., Tansey, W. P. and Workman, J. L. (2005) 'The proteasome regulatory particle alters the SAGA coactivator to enhance its interactions with transcriptional activators', *Cell,* 123(3), pp. 423-36.

Lee, J., Iwai, T., Yokota, T. and Yamashita, M. (2003) 'Temporally and spatially selective loss of Rec8 protein from meiotic chromosomes during mammalian meiosis', *J Cell Sci,* 116(Pt 13), pp. 2781-90.

Lee, J., Kitajima, T. S., Tanno, Y., Yoshida, K., Morita, T., Miyano, T., Miyake, M. and Watanabe, Y. (2008) 'Unified mode of centromeric protection by shugoshin in mammalian oocytes and somatic cells', *Nat Cell Biol,* 10(1), pp. 42-52.

Lee, J., Ogushi, S., Saitou, M. and Hirano, T. (2011) 'Condensins I and II are essential for construction of bivalent chromosomes in mouse oocytes',

Mol Biol Cell, 22(18), pp. 3465-77.

Lee, K. M., Nizza, S., Hayes, T., Bass, K. L., Irmisch, A., Murray, J. M. and O'Connell, M. J. (2007) 'Brc1-mediated rescue of Smc5/6 deficiency: requirement for multiple nucleases and a novel Rad18 function', *Genetics,* 175(4), pp. 1585-95.

Lehmann, A. R., Walicka, M., Griffiths, D. J., Murray, J. M., Watts, F. Z., McCready, S. and Carr, A. M. (1995) 'The rad18 gene of Schizosaccharomyces pombe defines a new subgroup of the SMC superfamily involved in DNA repair', *Mol Cell Biol,* 15(12), pp. 7067-80.

Lengronne, A., Katou, Y., Mori, S., Yokobayashi, S., Kelly, G. P., Itoh, T., Watanabe, Y., Shirahige, K. and Uhlmann, F. (2004) 'Cohesin relocation from sites of chromosomal loading to places of convergent transcription', *Nature,* 430(6999), pp. 573-8.

Leu, J. Y., Chua, P. R. and Roeder, G. S. (1998) 'The meiosis-specific Hop2 protein of S. cerevisiae ensures synapsis between homologous chromosomes', *Cell,* 94(3), pp. 375-86.

Li, R. and Murray, A. W. (1991) 'Feedback control of mitosis in budding yeast', *Cell,* 66(3), pp. 519-31.

Li, X., Zhuo, R., Tiong, S., Di Cara, F., King-Jones, K., Hughes, S. C., Campbell, S. D. and Wevrick, R. (2013) 'The Smc5/Smc6/MAGE complex confers resistance to caffeine and genotoxic stress in Drosophila melanogaster', *PLoS One,* 8(3), pp. e59866.

Liberi, G., Maffioletti, G., Lucca, C., Chiolo, I., Baryshnikova, A., Cotta-Ramusino, C., Lopes, M., Pellicioli, A., Haber, J. E. and Foiani, M. (2005) 'Rad51-dependent DNA structures accumulate at damaged replication forks in sgs1 mutants defective in the yeast ortholog of BLM RecQ helicase', *Genes Dev,* 19(3), pp. 339-50.

Lichten, M. and de Massy, B. (2011) 'The impressionistic landscape of meiotic recombination', *Cell,* 147(2), pp. 267-70.

Lightfoot, J., Testori, S., Barroso, C. and Martinez-Perez, E. (2011) 'Loading of meiotic cohesin by SCC-2 is required for early processing of DSBs and for the DNA damage checkpoint', *Curr Biol,* 21(17), pp. 1421-30.

Lilienthal, I., Kanno, T. and Sjögren, C. (2013) 'Inhibition of the Smc5/6 complex during meiosis perturbs joint molecule formation and resolution without significantly changing crossover or non-crossover levels', *PLoS Genet,* 9(11), pp. e1003898.

Lin, F. M., Lai, Y. J., Shen, H. J., Cheng, Y. H. and Wang, T. F. (2010) 'Yeast axial-element protein, Red1, binds SUMO chains to promote meiotic interhomologue recombination and chromosome synapsis', *EMBO J,* 29(3), pp. 586-96.

Lin, S. J., Tapia-Alveal, C., Jabado, O. J., Germain, D. and O'Connell, M. J. (2016) 'An acetyltransferase-independent function of Eso1 regulates centromere cohesion', *Mol Biol Cell,* 27(25), pp. 4002-4010.

Lindroos, H. B., Ström, L., Itoh, T., Katou, Y., Shirahige, K. and Sjögren, C. (2006) 'Chromosomal association of the Smc5/6 complex reveals that it functions in differently regulated pathways', *Mol Cell,* 22(6), pp. 755-67.

Lipp, J. J., Hirota, T., Poser, I. and Peters, J. M. (2007) 'Aurora B controls the association of condensin I but not condensin II with mitotic chromosomes', *J Cell Sci,* 120(Pt 7), pp. 1245-55.

Lister, L. M., Kouznetsova, A., Hyslop, L. A., Kalleas, D., Pace, S. L., Barel, J. C., Nathan, A., Floros, V., Adelfalk, C., Watanabe, Y., Jessberger, R., Kirkwood, T. B., Höög, C. and Herbert, M. (2010) 'Age-related meiotic segregation errors in mammalian oocytes are preceded by depletion of cohesin and Sgo2', *Curr Biol,* 20(17), pp. 1511-21.

Liu, D., Vader, G., Vromans, M. J., Lampson, M. A. and Lens, S. M. (2009) 'Sensing chromosome bi-orientation by spatial separation of aurora B kinase from kinetochore substrates', *Science,* 323(5919), pp. 1350-3.

Liu, H., Rankin, S. and Yu, H. (2013) 'Phosphorylation-enabled binding of SGO1-PP2A to cohesin protects sororin and centromeric cohesion during mitosis', *Nat Cell Biol,* 15(1), pp. 40-9.

Liu, L. and Keefe, D. L. (2008) 'Defective cohesin is associated with age-dependent misaligned chromosomes in oocytes', *Reprod Biomed Online,* 16(1), pp. 103-12.

Llano, E., Gómez, R., Gutiérrez-Caballero, C., Herrán, Y., Sánchez-Martín, M.,

Vázquez-Quiñones, L., Hernández, T., de Alava, E., Cuadrado, A., Barbero, J. L., Suja, J. A. and Pendás, A. M. (2008) 'Shugoshin-2 is essential for the completion of meiosis but not for mitotic cell division in mice', *Genes Dev,* 22(17), pp. 2400-13.

Longtine, M. S., McKenzie, A., Demarini, D. J., Shah, N. G., Wach, A., Brachat, A., Philippsen, P. and Pringle, J. R. (1998) 'Additional modules for versatile and economical PCR-based gene deletion and modification in Saccharomyces cerevisiae', *Yeast,* 14(10), pp. 953-61.

Losada, A., Hirano, M. and Hirano, T. (1998) 'Identification of Xenopus SMC protein complexes required for sister chromatid cohesion', *Genes Dev,* 12(13), pp. 1986-97.

Losada, A. and Hirano, T. (2001a) 'Intermolecular DNA interactions stimulated by the cohesin complex in vitro: implications for sister chromatid cohesion', *Curr Biol,* 11(4), pp. 268-72.

Losada, A. and Hirano, T. (2001b) 'Shaping the metaphase chromosome: coordination of cohesion and condensation', *Bioessays,* 23(10), pp. 924-35.

Losada, A. and Hirano, T. (2005) 'Dynamic molecular linkers of the genome: the first decade of SMC proteins', *Genes Dev,* 19(11), pp. 1269-87.

Losada, A., Yokochi, T. and Hirano, T. (2005) 'Functional contribution of Pds5 to cohesin-mediated cohesion in human cells and Xenopus egg extracts', *J Cell Sci,* 118(Pt 10), pp. 2133-41.

Losada, A., Yokochi, T., Kobayashi, R. and Hirano, T. (2000) 'Identification and characterization of SA/Scc3p subunits in the Xenopus and human cohesin complexes', *J Cell Biol,* 150(3), pp. 405-16.

Lynn, A., Ashley, T. and Hassold, T. (2004) 'Variation in human meiotic recombination', *Annu Rev Genomics Hum Genet,* 5, pp. 317-49.

Lynn, A., Soucek, R. and Börner, G. V. (2007) 'ZMM proteins during meiosis: crossover artists at work', *Chromosome Res,* 15(5), pp. 591-605.

Lyons, N. A. and Morgan, D. O. (2011) 'Cdk1-dependent destruction of Eco1 prevents cohesion establishment after S phase', *Mol Cell,* 42(3), pp. 378-89.

MacQueen, A. J., Colaiácovo, M. P., McDonald, K. and Villeneuve, A. M. (2002)

'Synapsis-dependent and -independent mechanisms stabilize homolog pairing during meiotic prophase in C. elegans', *Genes Dev,* 16(18), pp. 2428-42.

MacQueen, A. J., Phillips, C. M., Bhalla, N., Weiser, P., Villeneuve, A. M. and Dernburg, A. F. (2005) 'Chromosome sites play dual roles to establish homologous synapsis during meiosis in C. elegans', *Cell,* 123(6), pp. 1037-50.

Mahadevaiah, S. K., Turner, J. M., Baudat, F., Rogakou, E. P., de Boer, P., Blanco-Rodríguez, J., Jasin, M., Keeney, S., Bonner, W. M. and Burgoyne, P. S. (2001) 'Recombinational DNA double-strand breaks in mice precede synapsis', *Nat Genet,* 27(3), pp. 271-6.

Maleki, S., Neale, M. J., Arora, C., Henderson, K. A. and Keeney, S. (2007) 'Interactions between Mei4, Rec114, and other proteins required for meiotic DNA double-strand break formation in Saccharomyces cerevisiae', *Chromosoma,* 116(5), pp. 471-86.

Mannini, L., Cucco, F., Quarantotti, V., Krantz, I. D. and Musio, A. (2013) 'Mutation spectrum and genotype-phenotype correlation in Cornelia de Lange syndrome', *Hum Mutat,* 34(12), pp. 1589-96.

Marston, A. L., Tham, W. H., Shah, H. and Amon, A. (2004) 'A genome-wide screen identifies genes required for centromeric cohesion', *Science,* 303(5662), pp. 1367-70.

Martin, C. A., Murray, J. E., Carroll, P., Leitch, A., Mackenzie, K. J., Halachev, M., Fetit, A. E., Keith, C., Bicknell, L. S., Fluteau, A., Gautier, P., Hall, E. A., Joss, S., Soares, G., Silva, J., Bober, M. B., Duker, A., Wise, C. A., Quigley, A. J., Phadke, S. R., Wood, A. J., Vagnarelli, P., Jackson, A. P. and Study, D. D. D. (2016) 'Mutations in genes encoding condensin complex proteins cause microcephaly through decatenation failure at mitosis', *Genes Dev,* 30(19), pp. 2158-2172.

Matos, J., Blanco, M. G., Maslen, S., Skehel, J. M. and West, S. C. (2011) 'Regulatory control of the resolution of DNA recombination intermediates during meiosis and mitosis', *Cell,* 147(1), pp. 158-72.

Matos, J., Lipp, J. J., Bogdanova, A., Guillot, S., Okaz, E., Junqueira, M., Shevchenko, A. and Zachariae, W. (2008) 'Dbf4-dependent CDC7

kinase links DNA replication to the segregation of homologous chromosomes in meiosis I', *Cell,* 135(4), pp. 662-78.

Mayer, M. L., Gygi, S. P., Aebersold, R. and Hieter, P. (2001) 'Identification of RFC(Ctf18p, Ctf8p, Dcc1p): an alternative RFC complex required for sister chromatid cohesion in S. cerevisiae', *Mol Cell,* 7(5), pp. 959-70.

McAleenan, A., Clemente-Blanco, A., Cordon-Preciado, V., Sen, N., Esteras, M., Jarmuz, A. and Aragón, L. (2013) 'Post-replicative repair involves separase-dependent removal of the kleisin subunit of cohesin', *Nature,* 493(7431), pp. 250-4.

McDonald, W. H., Pavlova, Y., Yates, J. R. and Boddy, M. N. (2003) 'Novel essential DNA repair proteins Nse1 and Nse2 are subunits of the fission yeast Smc5-Smc6 complex', *J Biol Chem,* 278(46), pp. 45460-7.

McMahill, M. S., Sham, C. W. and Bishop, D. K. (2007) 'Synthesis-dependent strand annealing in meiosis', *PLoS Biol,* 5(11), pp. e299.

McVey, M., Andersen, S. L., Broze, Y. and Sekelsky, J. (2007) 'Multiple functions of Drosophila BLM helicase in maintenance of genome stability', *Genetics,* 176(4), pp. 1979-92.

Megee, P. C., Mistrot, C., Guacci, V. and Koshland, D. (1999) 'The centromeric sister chromatid cohesion site directs Mcd1p binding to adjacent sequences', *Mol Cell,* 4(3), pp. 445-50.

Mendiburo, M. J., Padeken, J., Fülöp, S., Schepers, A. and Heun, P. (2011) 'Drosophila CENH3 is sufficient for centromere formation', *Science,* 334(6056), pp. 686-90.

Menees, T. M., Ross-MacDonald, P. B. and Roeder, G. S. (1992) 'MEI4, a meiosis-specific yeast gene required for chromosome synapsis', *Mol Cell Biol,* 12(3), pp. 1340-51.

Mengiste, T., Revenkova, E., Bechtold, N. and Paszkowski, J. (1999) 'An SMC-like protein is required for efficient homologous recombination in Arabidopsis', *EMBO J,* 18(16), pp. 4505-12.

Meuwissen, R. L., Offenberg, H. H., Dietrich, A. J., Riesewijk, A., van Iersel, M. and Heyting, C. (1992) 'A coiled-coil related protein specific for synapsed regions of meiotic prophase chromosomes', *EMBO J,* 11(13), pp. 5091-100.

Mimitou, E. P. and Symington, L. S. (2008) 'Sae2, Exo1 and Sgs1 collaborate in DNA double-strand break processing', *Nature,* 455(7214), pp. 770-4.

Misulovin, Z., Schwartz, Y. B., Li, X. Y., Kahn, T. G., Gause, M., MacArthur, S., Fay, J. C., Eisen, M. B., Pirrotta, V., Biggin, M. D. and Dorsett, D. (2008) 'Association of cohesin and Nipped-B with transcriptionally active regions of the Drosophila melanogaster genome', *Chromosoma,* 117(1), pp. 89-102.

Miyabe, I., Morishita, T., Hishida, T., Yonei, S. and Shinagawa, H. (2006) 'Rhp51-dependent recombination intermediates that do not generate checkpoint signal are accumulated in Schizosaccharomyces pombe rad60 and smc5/6 mutants after release from replication arrest', *Mol Cell Biol,* 26(1), pp. 343-53.

Moens, P. B., Kolas, N. K., Tarsounas, M., Marcon, E., Cohen, P. E. and Spyropoulos, B. (2002) 'The time course and chromosomal localization of recombination-related proteins at meiosis in the mouse are compatible with models that can resolve the early DNA-DNA interactions without reciprocal recombination', *J Cell Sci,* 115(Pt 8), pp. 1611-22.

Monje-Casas, F., Prabhu, V. R., Lee, B. H., Boselli, M. and Amon, A. (2007) 'Kinetochore orientation during meiosis is controlled by Aurora B and the monopolin complex', *Cell,* 128(3), pp. 477-90.

Moore, D. P. and Orr-Weaver, T. L. (1998) 'Chromosome segregation during meiosis: building an unambivalent bivalent', *Curr Top Dev Biol,* 37, pp. 263-99.

Moore, G. P. and Lintern-Moore, S. (1978) 'Transcription of the mouse oocyte genome', *Biol Reprod,* 18(5), pp. 865-70.

Morikawa, H., Morishita, T., Kawane, S., Iwasaki, H., Carr, A. M. and Shinagawa, H. (2004) 'Rad62 protein functionally and physically associates with the smc5/smc6 protein complex and is required for chromosome integrity and recombination repair in fission yeast', *Mol Cell Biol,* 24(21), pp. 9401-13.

Morishita, T., Tsutsui, Y., Iwasaki, H. and Shinagawa, H. (2002) 'The

Schizosaccharomyces pombe rad60 gene is essential for repairing double-strand DNA breaks spontaneously occurring during replication and induced by DNA-damaging agents', *Mol Cell Biol,* 22(10), pp. 3537-48.

Muir, K. W., Kschonsak, M., Li, Y., Metz, J., Haering, C. H. and Panne, D. (2016) 'Structure of the Pds5-Scc1 Complex and Implications for Cohesin Function', *Cell Rep,* 14(9), pp. 2116-26.

Mullen, J. R., Nallaseth, F. S., Lan, Y. Q., Slagle, C. E. and Brill, S. J. (2005) 'Yeast Rmi1/Nce4 controls genome stability as a subunit of the Sgs1-Top3 complex', *Mol Cell Biol,* 25(11), pp. 4476-87.

Murakami, H. and Keeney, S. (2008) 'Regulating the formation of DNA double-strand breaks in meiosis', *Genes Dev,* 22(3), pp. 286-92.

Murakami, H. and Keeney, S. (2014) 'Temporospatial coordination of meiotic DNA replication and recombination via DDK recruitment to replisomes', *Cell,* 158(4), pp. 861-73.

Murayama, Y. and Uhlmann, F. (2014) 'Biochemical reconstitution of topological DNA binding by the cohesin ring', *Nature,* 505(7483), pp. 367-71.

Murayama, Y. and Uhlmann, F. (2015) 'DNA Entry into and Exit out of the Cohesin Ring by an Interlocking Gate Mechanism', *Cell,* 163(7), pp. 1628-40.

Murray, J. M. and Carr, A. M. (2008) 'Smc5/6: a link between DNA repair and unidirectional replication?', *Nat Rev Mol Cell Biol,* 9(2), pp. 177-82.

Musacchio, A. and Salmon, E. D. (2007) 'The spindle-assembly checkpoint in space and time', *Nat Rev Mol Cell Biol,* 8(5), pp. 379-93.

Musio, A., Selicorni, A., Focarelli, M. L., Gervasini, C., Milani, D., Russo, S., Vezzoni, P. and Larizza, L. (2006) 'X-linked Cornelia de Lange syndrome owing to SMC1L1 mutations', *Nat Genet,* 38(5), pp. 528-30.

Muñoz, I. M., Hain, K., Déclais, A. C., Gardiner, M., Toh, G. W., Sanchez-Pulido, L., Heuckmann, J. M., Toth, R., Macartney, T., Eppink, B., Kanaar, R., Ponting, C. P., Lilley, D. M. and Rouse, J. (2009) 'Coordination of structure-specific nucleases by human SLX4/BTBD12 is required for

DNA repair', *Mol Cell,* 35(1), pp. 116-27.

Nagaoka, S. I., Hassold, T. J. and Hunt, P. A. (2012) 'Human aneuploidy: mechanisms and new insights into an age-old problem', *Nat Rev Genet,* 13(7), pp. 493-504.

Nakajima, M., Kumada, K., Hatakeyama, K., Noda, T., Peters, J. M. and Hirota, T. (2007) 'The complete removal of cohesin from chromosome arms depends on separase', *J Cell Sci,* 120(Pt 23), pp. 4188-96.

Nasim, A. and Smith, B. P. (1975) 'Genetic control of radiation sensitivity in Schizosaccharomyces pombe', *Genetics,* 79(4), pp. 573-82.

Nasmyth, K. (2002) 'Segregating sister genomes: the molecular biology of chromosome separation', *Science,* 297(5581), pp. 559-65.

Nasmyth, K. (2015) 'A meiotic mystery: How sister kinetochores avoid being pulled in opposite directions during the first division', *Bioessays,* 37(6), pp. 657-65.

Neale, M. J., Pan, J. and Keeney, S. (2005) 'Endonucleolytic processing of covalent protein-linked DNA double-strand breaks', *Nature,* 436(7053), pp. 1053-7.

Nerusheva, O. O., Galander, S., Fernius, J., Kelly, D. and Marston, A. L. (2014) 'Tension-dependent removal of pericentromeric shugoshin is an indicator of sister chromosome biorientation', *Genes Dev,* 28(12), pp. 1291-309.

Nicolette, M. L., Lee, K., Guo, Z., Rani, M., Chow, J. M., Lee, S. E. and Paull, T. T. (2010) 'Mre11-Rad50-Xrs2 and Sae2 promote 5' strand resection of DNA double-strand breaks', *Nat Struct Mol Biol,* 17(12), pp. 1478-85.

Nishide, K. and Hirano, T. (2014) 'Overlapping and non-overlapping functions of condensins I and II in neural stem cell divisions', *PLoS Genet,* 10(12), pp. e1004847.

Nitiss, J. L. (2009) 'Targeting DNA topoisomerase II in cancer chemotherapy', *Nat Rev Cancer,* 9(5), pp. 338-50.

Niu, H., Wan, L., Busygina, V., Kwon, Y., Allen, J. A., Li, X., Kunz, R. C., Kubota, K., Wang, B., Sung, P., Shokat, K. M., Gygi, S. P. and Hollingsworth, N. M. (2009) 'Regulation of meiotic recombination via Mek1-mediated Rad54 phosphorylation', *Mol Cell,* 36(3), pp. 393-404.

Nonaka, N., Kitajima, T., Yokobayashi, S., Xiao, G., Yamamoto, M., Grewal, S. I. and Watanabe, Y. (2002) 'Recruitment of cohesin to heterochromatic regions by Swi6/HP1 in fission yeast', *Nat Cell Biol,* 4(1), pp. 89-93.

Novak, J. E., Ross-Macdonald, P. B. and Roeder, G. S. (2001) 'The budding yeast Msh4 protein functions in chromosome synapsis and the regulation of crossover distribution', *Genetics,* 158(3), pp. 1013-25.

Novatchkova, M., Bachmair, A., Eisenhaber, B. and Eisenhaber, F. (2005) 'Proteins with two SUMO-like domains in chromatin-associated complexes: the RENi (Rad60-Esc2-NIP45) family', *BMC Bioinformatics,* 6, pp. 22.

O'Neil, N. J., Martin, J. S., Youds, J. L., Ward, J. D., Petalcorin, M. I., Rose, A. M. and Boulton, S. J. (2013) 'Joint molecule resolution requires the redundant activities of MUS-81 and XPF-1 during Caenorhabditis elegans meiosis', *PLoS Genet,* 9(7), pp. e1003582.

Oakes, M. L., Johzuka, K., Vu, L., Eliason, K. and Nomura, M. (2006) 'Expression of rRNA genes and nucleolus formation at ectopic chromosomal sites in the yeast Saccharomyces cerevisiae', *Mol Cell Biol,* 26(16), pp. 6223-38.

Oakley, T. J., Goodwin, A., Chakraverty, R. K. and Hickson, I. D. (2002) 'Inactivation of homologous recombination suppresses defects in topoisomerase III-deficient mutants', *DNA Repair (Amst),* 1(6), pp. 463-82.

Offenberg, H. H., Schalk, J. A., Meuwissen, R. L., van Aalderen, M., Kester, H. A., Dietrich, A. J. and Heyting, C. (1998) 'SCP2: a major protein component of the axial elements of synaptonemal complexes of the rat', *Nucleic Acids Res,* 26(11), pp. 2572-9.

Ohno, M., Karagiannis, P. and Taniguchi, Y. (2014) 'Protein expression analyses at the single cell level', *Molecules,* 19(9), pp. 13932-47.

Ohta, K., Nicolas, A., Furuse, M., Nabetani, A., Ogawa, H. and Shibata, T. (1998) 'Mutations in the MRE11, RAD50, XRS2, and MRE2 genes alter chromatin configuration at meiotic DNA double-stranded break sites in premeiotic and meiotic cells', *Proc Natl Acad Sci U S A,* 95(2), pp. 646-51.

Oliveira, R. A., Coelho, P. A. and Sunkel, C. E. (2005) 'The condensin I subunit Barren/CAP-H is essential for the structural integrity of centromeric heterochromatin during mitosis', *Mol Cell Biol,* 25(20), pp. 8971-84.

Oliver, T. R., Feingold, E., Yu, K., Cheung, V., Tinker, S., Yadav-Shah, M., Masse, N. and Sherman, S. L. (2008) 'New insights into human nondisjunction of chromosome 21 in oocytes', *PLoS Genet,* 4(3), pp. e1000033.

Onn, I., Aono, N., Hirano, M. and Hirano, T. (2007) 'Reconstitution and subunit geometry of human condensin complexes', *EMBO J,* 26(4), pp. 1024-34.

Ono, T., Fang, Y., Spector, D. L. and Hirano, T. (2004) 'Spatial and temporal regulation of Condensins I and II in mitotic chromosome assembly in human cells', *Mol Biol Cell,* 15(7), pp. 3296-308.

Orr-Weaver, T. (1996) 'Meiotic nondisjunction does the two-step', *Nat Genet,* 14(4), pp. 374-6.

Osman, F., Dixon, J., Doe, C. L. and Whitby, M. C. (2003) 'Generating crossovers by resolution of nicked Holliday junctions: a role for Mus81-Eme1 in meiosis', *Mol Cell,* 12(3), pp. 761-74.

Outwin, E. A., Irmisch, A., Murray, J. M. and O'Connell, M. J. (2009) 'Smc5-Smc6-dependent removal of cohesin from mitotic chromosomes', *Mol Cell Biol,* 29(16), pp. 4363-75.

Ouyang, Z., Zheng, G., Song, J., Borek, D. M., Otwinowski, Z., Brautigam, C. A., Tomchick, D. R., Rankin, S. and Yu, H. (2013) 'Structure of the human cohesin inhibitor Wapl', *Proc Natl Acad Sci U S A,* 110(28), pp. 11355-60.

Pacchierotti, F., Adler, I. D., Eichenlaub-Ritter, U. and Mailhes, J. B. (2007) 'Gender effects on the incidence of aneuploidy in mammalian germ cells', *Environ Res,* 104(1), pp. 46-69.

Page, S. L. and Hawley, R. S. (2004) 'The genetics and molecular biology of the synaptonemal complex', *Annu Rev Cell Dev Biol,* 20, pp. 525-58.

Palecek, J., Vidot, S., Feng, M., Doherty, A. J. and Lehmann, A. R. (2006) 'The Smc5-Smc6 DNA repair complex. bridging of the Smc5-Smc6 heads by the KLEISIN, Nse4, and non-Kleisin subunits', *J Biol Chem,* 281(48), pp. 36952-9.

Pan, J., Sasaki, M., Kniewel, R., Murakami, H., Blitzblau, H. G., Tischfield, S. E., Zhu, X., Neale, M. J., Jasin, M., Socci, N. D., Hochwagen, A. and Keeney, S. (2011)

'A hierarchical combination of factors shapes the genome-wide topography of yeast meiotic recombination initiation', *Cell,* 144(5), pp. 719-31.

Panizza, S., Mendoza, M. A., Berlinger, M., Huang, L., Nicolas, A., Shirahige, K. and Klein, F. (2011) 'Spo11-accessory proteins link double-strand break sites to the chromosome axis in early meiotic recombination', *Cell,* 146(3), pp. 372-83.

Panizza, S., Tanaka, T., Hochwagen, A., Eisenhaber, F. and Nasmyth, K. (2000) 'Pds5 cooperates with cohesin in maintaining sister chromatid cohesion', *Curr Biol,* 10(24), pp. 1557-64.

Pasierbek, P., Jantsch, M., Melcher, M., Schleiffer, A., Schweizer, D. and Loidl, J. (2001) 'A Caenorhabditis elegans cohesion protein with functions in meiotic chromosome pairing and disjunction', *Genes Dev,* 15(11), pp. 1349-60.

Payne, F., Colnaghi, R., Rocha, N., Seth, A., Harris, J., Carpenter, G., Bottomley, W. E., Wheeler, E., Wong, S., Saudek, V., Savage, D., O'Rahilly, S., Carel, J. C., Barroso, I., O'Driscoll, M. and Semple, R. (2014) 'Hypomorphism in human NSMCE2 linked to primordial dwarfism and insulin resistance', *J Clin Invest,* 124(9), pp. 4028-38.

Pebernard, S., McDonald, W. H., Pavlova, Y., Yates, J. R. and Boddy, M. N. (2004) 'Nse1, Nse2, and a novel subunit of the Smc5-Smc6 complex, Nse3, play a crucial role in meiosis', *Mol Biol Cell,* 15(11), pp. 4866-76.

Pebernard, S., Perry, J. J., Tainer, J. A. and Boddy, M. N. (2008) 'Nse1 RING-like domain supports functions of the Smc5-Smc6 holocomplex in genome stability', *Mol Biol Cell,* 19(10), pp. 4099-109.

Pebernard, S., Wohlschlegel, J., McDonald, W. H., Yates, J. R. and Boddy, M. N. (2006) 'The Nse5-Nse6 dimer mediates DNA repair roles of the Smc5-Smc6 complex', *Mol Cell Biol,* 26(5), pp. 1617-30.

Penrose, L. S. (2009) 'The relative effects of paternal and maternal age in mongolism. 1933', *J Genet,* 88(1), pp. 9-14.

Pepling, M. E. (2006) 'From primordial germ cell to primordial follicle: mammalian female germ cell development', *Genesis,* 44(12), pp. 622-32.

Perera, D. and Taylor, S. S. (2010) 'Sgo1 establishes the centromeric cohesion

protection mechanism in G2 before subsequent Bub1-dependent recruitment in mitosis', *J Cell Sci,* 123(Pt 5), pp. 653-9.

Petronczki, M., Matos, J., Mori, S., Gregan, J., Bogdanova, A., Schwickart, M., Mechtler, K., Shirahige, K., Zachariae, W. and Nasmyth, K. (2006) 'Monopolar attachment of sister kinetochores at meiosis I requires casein kinase 1', *Cell,* 126(6), pp. 1049-64.

Petronczki, M., Siomos, M. F. and Nasmyth, K. (2003) 'Un ménage à quatre: the molecular biology of chromosome segregation in meiosis', *Cell,* 112(4), pp. 423-40.

Petukhova, G. V., Pezza, R. J., Vanevski, F., Ploquin, M., Masson, J. Y. and Camerini-Otero, R. D. (2005) 'The Hop2 and Mnd1 proteins act in concert with Rad51 and Dmc1 in meiotic recombination', *Nat Struct Mol Biol,* 12(5), pp. 449-53.

Petukhova, G. V., Romanienko, P. J. and Camerini-Otero, R. D. (2003) 'The Hop2 protein has a direct role in promoting interhomolog interactions during mouse meiosis', *Dev Cell,* 5(6), pp. 927-36.

Pidoux, A. L. and Allshire, R. C. (2004) 'Kinetochore and heterochromatin domains of the fission yeast centromere', *Chromosome Res,* 12(6), pp. 521-34.

Potts, P. R. (2009) 'The Yin and Yang of the MMS21-SMC5/6 SUMO ligase complex in homologous recombination', *DNA Repair (Amst),* 8(4), pp. 499-506.

Potts, P. R., Porteus, M. H. and Yu, H. (2006) 'Human SMC5/6 complex promotes sister chromatid homologous recombination by recruiting the SMC1/3 cohesin complex to double-strand breaks', *EMBO J,* 25(14), pp. 3377-88.

Potts, P. R. and Yu, H. (2005) 'Human MMS21/NSE2 is a SUMO ligase required for DNA repair', *Mol Cell Biol,* 25(16), pp. 7021-32.

Potts, P. R. and Yu, H. (2007) 'The SMC5/6 complex maintains telomere length in ALT cancer cells through SUMOylation of telomere-binding proteins', *Nat Struct Mol Biol,* 14(7), pp. 581-90.

Powers, A. F., Franck, A. D., Gestaut, D. R., Cooper, J., Gracyzk, B., Wei, R. R., Wordeman, L., Davis, T. N. and Asbury, C. L. (2009) 'The Ndc80 kinetochore complex forms load-bearing attachments to dynamic

microtubule tips via biased diffusion', *Cell,* 136(5), pp. 865-75.

Prakash, R., Satory, D., Dray, E., Papusha, A., Scheller, J., Kramer, W., Krejci, L., Klein, H., Haber, J. E., Sung, P. and Ira, G. (2009) 'Yeast Mph1 helicase dissociates Rad51-made D-loops: implications for crossover control in mitotic recombination', *Genes Dev,* 23(1), pp. 67-79.

Pratto, F., Brick, K., Khil, P., Smagulova, F., Petukhova, G. V. and Camerini-Otero, R. D. (2014) 'DNA recombination. Recombination initiation maps of individual human genomes', *Science,* 346(6211), pp. 1256442.

Prieto, I., Suja, J. A., Pezzi, N., Kremer, L., Martínez-A, C., Rufas, J. S. and Barbero, J. L. (2001) 'Mammalian STAG3 is a cohesin specific to sister chromatid arms in meiosis I', *Nat Cell Biol,* 3(8), pp. 761-6.

Pryzhkova, M. V. and Jordan, P. W. (2016) 'Conditional mutation of Smc5 in mouse embryonic stem cells perturbs condensin localization and mitotic progression', *J Cell Sci,* 129(8), pp. 1619-34.

Pâques, F. and Haber, J. E. (1999) 'Multiple pathways of recombination induced by double-strand breaks in Saccharomyces cerevisiae', *Microbiol Mol Biol Rev,* 63(2), pp. 349-404.

R, W. R. a. S. 1971. The molecular architecture of the synaptonemal complex.

Rabitsch, K. P., Petronczki, M., Javerzat, J. P., Genier, S., Chwalla, B., Schleiffer, A., Tanaka, T. U. and Nasmyth, K. (2003) 'Kinetochore recruitment of two nucleolar proteins is required for homolog segregation in meiosis I', *Dev Cell,* 4(4), pp. 535-48.

Rankin, S., Ayad, N. G. and Kirschner, M. W. (2005) 'Sororin, a substrate of the anaphase-promoting complex, is required for sister chromatid cohesion in vertebrates', *Mol Cell,* 18(2), pp. 185-200.

Rankin, S. and Dawson, D. S. (2016) 'Recent advances in cohesin biology', *F1000Res,* 5.

Rass, U., Compton, S. A., Matos, J., Singleton, M. R., Ip, S. C., Blanco, M. G., Griffith, J. D. and West, S. C. (2010) 'Mechanism of Holliday junction resolution by the human GEN1 protein', *Genes Dev,* 24(14), pp. 1559-69.

Rattani, A., Wolna, M., Ploquin, M., Helmhart, W., Morrone, S., Mayer, B., Godwin, J., Xu, W., Stemmann, O., Pendas, A. and Nasmyth, K. (2013) 'Sgol2 provides a regulatory platform that coordinates essential cell cycle

processes during meiosis I in oocytes', *Elife,* 2, pp. e01133.

Revenkova, E., Eijpe, M., Heyting, C., Hodges, C. A., Hunt, P. A., Liebe, B., Scherthan, H. and Jessberger, R. (2004) 'Cohesin SMC1 beta is required for meiotic chromosome dynamics, sister chromatid cohesion and DNA recombination', *Nat Cell Biol,* 6(6), pp. 555-62.

Revenkova, E., Herrmann, K., Adelfalk, C. and Jessberger, R. (2010) 'Oocyte cohesin expression restricted to predictyate stages provides full fertility and prevents aneuploidy', *Curr Biol,* 20(17), pp. 1529-33.

Revenkova, E. and Jessberger, R. (2006) 'Shaping meiotic prophase chromosomes: cohesins and synaptonemal complex proteins', *Chromosoma,* 115(3), pp. 235-40.

Ribeiro, S. A., Gatlin, J. C., Dong, Y., Joglekar, A., Cameron, L., Hudson, D. F., Farr, C. J., McEwen, B. F., Salmon, E. D., Earnshaw, W. C. and Vagnarelli, P. (2009) 'Condensin regulates the stiffness of vertebrate centromeres', *Mol Biol Cell,* 20(9), pp. 2371-80.

Riedel, C. G., Katis, V. L., Katou, Y., Mori, S., Itoh, T., Helmhart, W., Gálová, M., Petronczki, M., Gregan, J., Cetin, B., Mudrak, I., Ogris, E., Mechtler, K., Pelletier, L., Buchholz, F., Shirahige, K. and Nasmyth, K. (2006) 'Protein phosphatase 2A protects centromeric sister chromatid cohesion during meiosis I', *Nature,* 441(7089), pp. 53-61.

Risch, N., Stein, Z., Kline, J. and Warburton, D. (1986) 'The relationship between maternal age and chromosome size in autosomal trisomy', *Am J Hum Genet,* 39(1), pp. 68-78.

Roberts, T. M., Kobor, M. S., Bastin-Shanower, S. A., Ii, M., Horte, S. A., Gin, J. W., Emili, A., Rine, J., Brill, S. J. and Brown, G. W. (2006) 'Slx4 regulates DNA damage checkpoint-dependent phosphorylation of the BRCT domain protein Rtt107/Esc4', *Mol Biol Cell,* 17(1), pp. 539-48.

Robine, N., Uematsu, N., Amiot, F., Gidrol, X., Barillot, E., Nicolas, A. and Borde, V. (2007) 'Genome-wide redistribution of meiotic double-strand breaks in Saccharomyces cerevisiae', *Mol Cell Biol,* 27(5), pp. 1868-80.

Rockmill, B., Engebrecht, J. A., Scherthan, H., Loidl, J. and Roeder, G. S. (1995) 'The yeast MER2 gene is required for chromosome synapsis and the initiation of meiotic recombination', *Genetics,* 141(1), pp. 49-59.

Roeder, G. S. and Bailis, J. M. (2000) 'The pachytene checkpoint', *Trends Genet,* 16(9), pp. 395-403.

Roig, M. B., Löwe, J., Chan, K. L., Beckouët, F., Metson, J. and Nasmyth, K. (2014) 'Structure and function of cohesin's Scc3/SA regulatory subunit', *FEBS Lett,* 588(20), pp. 3692-702.

Rolef Ben-Shahar, T., Heeger, S., Lehane, C., East, P., Flynn, H., Skehel, M. and Uhlmann, F. (2008) 'Eco1-dependent cohesin acetylation during establishment of sister chromatid cohesion', *Science,* 321(5888), pp. 563-6.

Rollins, R. A., Morcillo, P. and Dorsett, D. (1999) 'Nipped-B, a Drosophila homologue of chromosomal adherins, participates in activation by remote enhancers in the cut and Ultrabithorax genes', *Genetics,* 152(2), pp. 577-93.

Rowland, B. D., Roig, M. B., Nishino, T., Kurze, A., Uluocak, P., Mishra, A., Beckouët, F., Underwood, P., Metson, J., Imre, R., Mechtler, K., Katis, V. L. and Nasmyth, K. (2009) 'Building sister chromatid cohesion: smc3 acetylation counteracts an antiestablishment activity', *Mol Cell,* 33(6), pp. 763-74.

Roy, M. A., Siddiqui, N. and D'Amours, D. (2011) 'Dynamic and selective DNA-binding activity of Smc5, a core component of the Smc5-Smc6 complex', *Cell Cycle,* 10(4), pp. 690-700.

Ruchaud, S., Carmena, M. and Earnshaw, W. C. (2007) 'Chromosomal passengers: conducting cell division', *Nat Rev Mol Cell Biol,* 8(10), pp. 798-812.

Rudner, A. D. and Murray, A. W. (1996) 'The spindle assembly checkpoint', *Curr Opin Cell Biol,* 8(6), pp. 773-80.

Ryu, T., Spatola, B., Delabaere, L., Bowlin, K., Hopp, H., Kunitake, R., Karpen, G. H. and Chiolo, I. (2015) 'Heterochromatic breaks move to the nuclear periphery to continue recombinational repair', *Nat Cell Biol,* 17(11), pp. 1401-11.

Salic, A., Waters, J. C. and Mitchison, T. J. (2004) 'Vertebrate shugoshin links sister centromere cohesion and kinetochore microtubule stability in mitosis', *Cell,* 118(5), pp. 567-78.

Santaguida, S. and Musacchio, A. (2009) 'The life and miracles of kinetochores', *EMBO J,* 28(17), pp. 2511-31.

Sarangapani, K. K., Duro, E., Deng, Y., Alves, F. e. L., Ye, Q., Opoku, K. N., Ceto, S., Rappsilber, J., Corbett, K. D., Biggins, S., Marston, A. L. and Asbury, C. L. (2014) 'Sister kinetochores are mechanically fused during meiosis I in yeast', *Science,* 346(6206), pp. 248-51.

Sarkar, S., Shenoy, R. T., Dalgaard, J. Z., Newnham, L., Hoffmann, E., Millar, J. B. and Arumugam, P. (2013) 'Monopolin subunit Csm1 associates with MIND complex to establish monopolar attachment of sister kinetochores at meiosis I', *PLoS Genet,* 9(7), pp. e1003610.

Sasanuma, H., Hirota, K., Fukuda, T., Kakusho, N., Kugou, K., Kawasaki, Y., Shibata, T., Masai, H. and Ohta, K. (2008) 'Cdc7-dependent phosphorylation of Mer2 facilitates initiation of yeast meiotic recombination', *Genes Dev,* 22(3), pp. 398-410.

Schaaf, C. A., Misulovin, Z., Sahota, G., Siddiqui, A. M., Schwartz, Y. B., Kahn, T. G., Pirrotta, V., Gause, M. and Dorsett, D. (2009) 'Regulation of the Drosophila Enhancer of split and invected-engrailed gene complexes by sister chromatid cohesion proteins', *PLoS One,* 4(7), pp. e6202.

Schalk, J. A., Dietrich, A. J., Vink, A. C., Offenberg, H. H., van Aalderen, M. and Heyting, C. (1998) 'Localization of SCP2 and SCP3 protein molecules within synaptonemal complexes of the rat', *Chromosoma,* 107(8), pp. 540-8.

Schild, D. and Byers, B. (1978) 'Meiotic effects of DNA-defective cell division cycle mutations of Saccharomyces cerevisiae', *Chromosoma,* 70(1), pp. 109-30.

Schleiffer, A., Kaitna, S., Maurer-Stroh, S., Glotzer, M., Nasmyth, K. and Eisenhaber, F. (2003) 'Kleisins: a superfamily of bacterial and eukaryotic SMC protein partners', *Mol Cell,* 11(3), pp. 571-5.

Schramm, S., Fraune, J., Naumann, R., Hernandez-Hernandez, A., Höög, C., Cooke, H. J., Alsheimer, M. and Benavente, R. (2011) 'A novel mouse synaptonemal complex protein is essential for loading of central element proteins, recombination, and fertility', *PLoS Genet,* 7(5), pp. e1002088.

Schwacha, A. and Kleckner, N. (1995) 'Identification of double Holliday junctions as intermediates in meiotic recombination', *Cell,* 83(5), pp. 783-91.

Screpanti, E., De Antoni, A., Alushin, G. M., Petrovic, A., Melis, T., Nogales, E. and Musacchio, A. (2011) 'Direct binding of Cenp-C to the Mis12 complex joins

the inner and outer kinetochore', *Curr Biol,* 21(5), pp. 391-8.

Sebestova, J., Danylevska, A., Novakova, L., Kubelka, M. and Anger, M. (2012) 'Lack of response to unaligned chromosomes in mammalian female gametes', *Cell Cycle,* 11(16), pp. 3011-8.

Sergeant, J., Taylor, E., Palecek, J., Fousteri, M., Andrews, E. A., Sweeney, S., Shinagawa, H., Watts, F. Z. and Lehmann, A. R. (2005) 'Composition and architecture of the Schizosaccharomyces pombe Rad18 (Smc5-6) complex', *Mol Cell Biol,* 25(1), pp. 172-84.

Sharan, S. K., Pyle, A., Coppola, V., Babus, J., Swaminathan, S., Benedict, J., Swing, D., Martin, B. K., Tessarollo, L., Evans, J. P., Flaws, J. A. and Handel, M. A. (2004) 'BRCA2 deficiency in mice leads to meiotic impairment and infertility', *Development,* 131(1), pp. 131-42.

Sheedy, D. M., Dimitrova, D., Rankin, J. K., Bass, K. L., Lee, K. M., Tapia-Alveal, C., Harvey, S. H., Murray, J. M. and O'Connell, M. J. (2005) 'Brc1-mediated DNA repair and damage tolerance', *Genetics,* 171(2), pp. 457-68.

Shinohara, A., Gasior, S., Ogawa, T., Kleckner, N. and Bishop, D. K. (1997) 'Saccharomyces cerevisiae recA homologues RAD51 and DMC1 have both distinct and overlapping roles in meiotic recombination', *Genes Cells,* 2(10), pp. 615-29.

Shinohara, M., Oh, S. D., Hunter, N. and Shinohara, A. (2008) 'Crossover assurance and crossover interference are distinctly regulated by the ZMM proteins during yeast meiosis', *Nat Genet,* 40(3), pp. 299-309.

Shintomi, K. and Hirano, T. (2011) 'The relative ratio of condensin I to II determines chromosome shapes', *Genes Dev,* 25(14), pp. 1464-9.

Sjögren, C. and Nasmyth, K. (2001) 'Sister chromatid cohesion is required for postreplicative double-strand break repair in Saccharomyces cerevisiae', *Curr Biol,* 11(12), pp. 991-5.

Smagulova, F., Gregoretti, I. V., Brick, K., Khil, P., Camerini-Otero, R. D. and Petukhova, G. V. (2011) 'Genome-wide analysis reveals novel molecular features of mouse recombination hotspots', *Nature,* 472(7343), pp. 375-8.

Smith, G. R., Boddy, M. N., Shanahan, P. and Russell, P. (2003) 'Fission yeast Mus81.Eme1 Holliday junction resolvase is required for meiotic crossing over but not for gene conversion', *Genetics,* 165(4), pp. 2289-93.

Snowden, T., Acharya, S., Butz, C., Berardini, M. and Fishel, R. (2004) 'hMSH4-hMSH5 recognizes Holliday Junctions and forms a meiosis-specific sliding clamp that embraces homologous chromosomes', *Mol Cell,* 15(3), pp. 437-51.

Sommermeyer, V., Béneut, C., Chaplais, E., Serrentino, M. E. and Borde, V. (2013) 'Spp1, a member of the Set1 Complex, promotes meiotic DSB formation in promoters by tethering histone H3K4 methylation sites to chromosome axes', *Mol Cell,* 49(1), pp. 43-54.

Song, J., Lafont, A., Chen, J., Wu, F. M., Shirahige, K. and Rankin, S. (2012) 'Cohesin acetylation promotes sister chromatid cohesion only in association with the replication machinery', *J Biol Chem,* 287(41), pp. 34325-36.

Sonoda, E., Matsusaka, T., Morrison, C., Vagnarelli, P., Hoshi, O., Ushiki, T., Nojima, K., Fukagawa, T., Waizenegger, I. C., Peters, J. M., Earnshaw, W. C. and Takeda, S. (2001) 'Scc1/Rad21/Mcd1 is required for sister chromatid cohesion and kinetochore function in vertebrate cells', *Dev Cell,* 1(6), pp. 759-70.

Sourirajan, A. and Lichten, M. (2008) 'Polo-like kinase Cdc5 drives exit from pachytene during budding yeast meiosis', *Genes Dev,* 22(19), pp. 2627-32.

Spence, J. M., Phua, H. H., Mills, W., Carpenter, A. J., Porter, A. C. and Farr, C. J. (2007) 'Depletion of topoisomerase IIalpha leads to shortening of the metaphase interkinetochore distance and abnormal persistence of PICH-coated anaphase threads', *J Cell Sci,* 120(Pt 22), pp. 3952-64.

St-Pierre, J., Douziech, M., Bazile, F., Pascariu, M., Bonneil, E., Sauvé, V., Ratsima, H. and D'Amours, D. (2009) 'Polo kinase regulates mitotic chromosome condensation by hyperactivation of condensin DNA supercoiling activity', *Mol Cell,* 34(4), pp. 416-26.

Steffensen, S., Coelho, P. A., Cobbe, N., Vass, S., Costa, M., Hassan, B., Prokopenko, S. N., Bellen, H., Heck, M. M. and Sunkel, C. E. (2001) 'A role for Drosophila SMC4 in the resolution of sister chromatids in mitosis', *Curr Biol,* 11(5), pp. 295-307.

Stephan, A. K., Kliszczak, M., Dodson, H., Cooley, C. and Morrison, C. G. (2011) 'Roles of vertebrate Smc5 in sister chromatid cohesion and homologous recombinational repair', *Mol Cell Biol,* 31(7), pp. 1369-81.

Stigler, J., Çamdere, G., Koshland, D. E. and Greene, E. C. (2016) 'Single-Molecule Imaging Reveals a Collapsed Conformational State for DNA-Bound Cohesin', *Cell Rep,* 15(5), pp. 988-98.

Strunnikov, A. V., Hogan, E. and Koshland, D. (1995) 'SMC2, a Saccharomyces cerevisiae gene essential for chromosome segregation and condensation, defines a subgroup within the SMC family', *Genes Dev,* 9(5), pp. 587-99.

Ström, L., Lindroos, H. B., Shirahige, K. and Sjögren, C. (2004) 'Postreplicative recruitment of cohesin to double-strand breaks is required for DNA repair', *Mol Cell,* 16(6), pp. 1003-15.

Sugawara, N., Goldfarb, T., Studamire, B., Alani, E. and Haber, J. E. (2004) 'Heteroduplex rejection during single-strand annealing requires Sgs1 helicase and mismatch repair proteins Msh2 and Msh6 but not Pms1', *Proc Natl Acad Sci U S A,* 101(25), pp. 9315-20.

Sullivan, M. and Morgan, D. O. (2007) 'A novel destruction sequence targets the meiotic regulator Spo13 for anaphase-promoting complex-dependent degradation in anaphase I', *J Biol Chem,* 282(27), pp. 19710-5.

Sumara, I., Vorlaufer, E., Gieffers, C., Peters, B. H. and Peters, J. M. (2000) 'Characterization of vertebrate cohesin complexes and their regulation in prophase', *J Cell Biol,* 151(4), pp. 749-62.

Sumara, I., Vorlaufer, E., Stukenberg, P. T., Kelm, O., Redemann, N., Nigg, E. A. and Peters, J. M. (2002) 'The dissociation of cohesin from chromosomes in prophase is regulated by Polo-like kinase', *Mol Cell,* 9(3), pp. 515-25.

Sun, H., Treco, D. and Szostak, J. W. (1991) 'Extensive 3'-overhanging, single-stranded DNA associated with the meiosis-specific double-strand breaks at the ARG4 recombination initiation site', *Cell,* 64(6), pp. 1155-61.

Sun, J., Shi, Y., Georgescu, R. E., Yuan, Z., Chait, B. T., Li, H. and O'Donnell, M. E. (2015) 'The architecture of a eukaryotic replisome', *Nat Struct Mol Biol,* 22(12), pp. 976-82.

Sutani, T., Kawaguchi, T., Kanno, R., Itoh, T. and Shirahige, K. (2009) 'Budding yeast Wpl1(Rad61)-Pds5 complex counteracts sister chromatid cohesion-establishing reaction', *Curr Biol,* 19(6), pp. 492-7.

Sutani, T., Yuasa, T., Tomonaga, T., Dohmae, N., Takio, K. and Yanagida, M. (1999) 'Fission yeast condensin complex: essential roles of non-SMC subunits for

condensation and Cdc2 phosphorylation of Cut3/SMC4', *Genes Dev,* 13(17), pp. 2271-83.

Svendsen, J. M., Smogorzewska, A., Sowa, M. E., O'Connell, B. C., Gygi, S. P., Elledge, S. J. and Harper, J. W. (2009) 'Mammalian BTBD12/SLX4 assembles a Holliday junction resolvase and is required for DNA repair', *Cell,* 138(1), pp. 63-77.

Sym, M., Engebrecht, J. A. and Roeder, G. S. (1993) 'ZIP1 is a synaptonemal complex protein required for meiotic chromosome synapsis', *Cell,* 72(3), pp. 365-78.

Sym, M. and Roeder, G. S. (1994) 'Crossover interference is abolished in the absence of a synaptonemal complex protein', *Cell,* 79(2), pp. 283-92.

Sym, M. and Roeder, G. S. (1995) 'Zip1-induced changes in synaptonemal complex structure and polycomplex assembly', *J Cell Biol,* 128(4), pp. 455-66.

Szostak, J. W., Orr-Weaver, T. L., Rothstein, R. J. and Stahl, F. W. (1983) 'The double-strand-break repair model for recombination', *Cell,* 33(1), pp. 25-35.

Tachibana-Konwalski, K., Godwin, J., Borsos, M., Rattani, A., Adams, D. J. and Nasmyth, K. (2013) 'Spindle assembly checkpoint of oocytes depends on a kinetochore structure determined by cohesin in meiosis I', *Curr Biol,* 23(24), pp. 2534-9.

Tachibana-Konwalski, K., Godwin, J., van der Weyden, L., Champion, L., Kudo, N. R., Adams, D. J. and Nasmyth, K. (2010) 'Rec8-containing cohesin maintains bivalents without turnover during the growing phase of mouse oocytes', *Genes Dev,* 24(22), pp. 2505-16.

Tada, K., Susumu, H., Sakuno, T. and Watanabe, Y. (2011) 'Condensin association with histone H2A shapes mitotic chromosomes', *Nature,* 474(7352), pp. 477-83.

Tanaka, K., Hao, Z., Kai, M. and Okayama, H. (2001) 'Establishment and maintenance of sister chromatid cohesion in fission yeast by a unique mechanism', *EMBO J,* 20(20), pp. 5779-90.

Tanaka, T., Cosma, M. P., Wirth, K. and Nasmyth, K. (1999) 'Identification of cohesin association sites at centromeres and along chromosome arms',

Cell, 98(6), pp. 847-58.

Tanaka, T., Fuchs, J., Loidl, J. and Nasmyth, K. (2000) 'Cohesin ensures bipolar attachment of microtubules to sister centromeres and resists their precocious separation', *Nat Cell Biol,* 2(8), pp. 492-9.

Tapia-Alveal, C., Lin, S. J., Yeoh, A., Jabado, O. J. and O'Connell, M. J. (2014) 'H2A.Z-dependent regulation of cohesin dynamics on chromosome arms', *Mol Cell Biol,* 34(11), pp. 2092-104.

Tapia-Alveal, C., Outwin, E. A., Trempolec, N., Dziadkowiec, D., Murray, J. M. and O'Connell, M. J. (2010) 'SMC complexes and topoisomerase II work together so that sister chromatids can work apart', *Cell Cycle,* 9(11), pp. 2065-70.

Taylor, E. M., Copsey, A. C., Hudson, J. J., Vidot, S. and Lehmann, A. R. (2008) 'Identification of the proteins, including MAGEG1, that make up the human SMC5-6 protein complex', *Mol Cell Biol,* 28(4), pp. 1197-206.

Taylor, E. M., Moghraby, J. S., Lees, J. H., Smit, B., Moens, P. B. and Lehmann, A. R. (2001) 'Characterization of a novel human SMC heterodimer homologous to the Schizosaccharomyces pombe Rad18/Spr18 complex', *Mol Biol Cell,* 12(6), pp. 1583-94.

Taylor, S. S., Ha, E. and McKeon, F. (1998) 'The human homologue of Bub3 is required for kinetochore localization of Bub1 and a Mad3/Bub1-related protein kinase', *J Cell Biol,* 142(1), pp. 1-11.

Tinker-Kulberg, R. L. and Morgan, D. O. (1999) 'Pds1 and Esp1 control both anaphase and mitotic exit in normal cells and after DNA damage', *Genes Dev,* 13(15), pp. 1936-49.

Tischfield, S. E. and Keeney, S. (2012) 'Scale matters: the spatial correlation of yeast meiotic DNA breaks with histone H3 trimethylation is driven largely by independent colocalization at promoters', *Cell Cycle,* 11(8), pp. 1496-503.

Tonkin, E. T., Smith, M., Eichhorn, P., Jones, S., Imamwerdi, B., Lindsay, S., Jackson, M., Wang, T. J., Ireland, M., Burn, J., Krantz, I. D., Carr, P. and Strachan, T. (2004a) 'A giant novel gene undergoing extensive alternative splicing is severed by a Cornelia de Lange-associated translocation breakpoint at 3q26.3', *Hum Genet,* 115(2), pp. 139-48.

Tonkin, E. T., Wang, T. J., Lisgo, S., Bamshad, M. J. and Strachan, T. (2004b) 'NIPBL, encoding a homolog of fungal Scc2-type sister chromatid cohesion proteins and fly Nipped-B, is mutated in Cornelia de Lange syndrome', *Nat Genet,* 36(6), pp. 636-41.

Torres-Rosell, J., Machín, F., Farmer, S., Jarmuz, A., Eydmann, T., Dalgaard, J. Z. and Aragón, L. (2005) 'SMC5 and SMC6 genes are required for the segregation of repetitive chromosome regions', *Nat Cell Biol,* 7(4), pp. 412-9.

Torres-Rosell, J., Sunjevaric, I., De Piccoli, G., Sacher, M., Eckert-Boulet, N., Reid, R., Jentsch, S., Rothstein, R., Aragón, L. and Lisby, M. (2007) 'The Smc5-Smc6 complex and SUMO modification of Rad52 regulates recombinational repair at the ribosomal gene locus', *Nat Cell Biol,* 9(8), pp. 923-31.

Tsubouchi, H. and Roeder, G. S. (2002) 'The Mnd1 protein forms a complex with hop2 to promote homologous chromosome pairing and meiotic double-strand break repair', *Mol Cell Biol,* 22(9), pp. 3078-88.

Tsubouchi, T., Macqueen, A. J. and Roeder, G. S. (2008) 'Initiation of meiotic chromosome synapsis at centromeres in budding yeast', *Genes Dev,* 22(22), pp. 3217-26.

Tsukahara, T., Tanno, Y. and Watanabe, Y. (2010) 'Phosphorylation of the CPC by Cdk1 promotes chromosome bi-orientation', *Nature,* 467(7316), pp. 719-23.

Tsutsumi, M., Fujiwara, R., Nishizawa, H., Ito, M., Kogo, H., Inagaki, H., Ohye, T., Kato, T., Fujii, T. and Kurahashi, H. (2014) 'Age-related decrease of meiotic cohesins in human oocytes', *PLoS One,* 9(5), pp. e96710.

Tung, K. S., Hong, E. J. and Roeder, G. S. (2000) 'The pachytene checkpoint prevents accumulation and phosphorylation of the meiosis-specific transcription factor Ndt80', *Proc Natl Acad Sci U S A,* 97(22), pp. 12187-92.

Tóth, A., Ciosk, R., Uhlmann, F., Galova, M., Schleiffer, A. and Nasmyth, K. (1999) 'Yeast cohesin complex requires a conserved protein, Eco1p(Ctf7), to establish cohesion between sister chromatids during DNA replication', *Genes Dev,* 13(3), pp. 320-33.

Tóth, A., Rabitsch, K. P., Gálová, M., Schleiffer, A., Buonomo, S. B. and Nasmyth, K.

(2000) 'Functional genomics identifies monopolin: a kinetochore protein required for segregation of homologs during meiosis i', *Cell,* 103(7), pp. 1155-68.

Uhlmann, F. (2016) 'SMC complexes: from DNA to chromosomes', *Nat Rev Mol Cell Biol,* 17(7), pp. 399-412.

Uhlmann, F., Lottspeich, F. and Nasmyth, K. (1999) 'Sister-chromatid separation at anaphase onset is promoted by cleavage of the cohesin subunit Scc1', *Nature,* 400(6739), pp. 37-42.

Uhlmann, F., Wernic, D., Poupart, M. A., Koonin, E. V. and Nasmyth, K. (2000) 'Cleavage of cohesin by the CD clan protease separin triggers anaphase in yeast', *Cell,* 103(3), pp. 375-86.

Unal, E., Arbel-Eden, A., Sattler, U., Shroff, R., Lichten, M., Haber, J. E. and Koshland, D. (2004) 'DNA damage response pathway uses histone modification to assemble a double-strand break-specific cohesin domain', *Mol Cell,* 16(6), pp. 991-1002.

Unal, E., Heidinger-Pauli, J. M., Kim, W., Guacci, V., Onn, I., Gygi, S. P. and Koshland, D. E. (2008) 'A molecular determinant for the establishment of sister chromatid cohesion', *Science,* 321(5888), pp. 566-9.

Unal, E., Heidinger-Pauli, J. M. and Koshland, D. (2007) 'DNA double-strand breaks trigger genome-wide sister-chromatid cohesion through Eco1 (Ctf7)', *Science,* 317(5835), pp. 245-8.

Usui, T., Ohta, T., Oshiumi, H., Tomizawa, J., Ogawa, H. and Ogawa, T. (1998) 'Complex formation and functional versatility of Mre11 of budding yeast in recombination', *Cell,* 95(5), pp. 705-16.

Vagnarelli, P., Hudson, D. F., Ribeiro, S. A., Trinkle-Mulcahy, L., Spence, J. M., Lai, F., Farr, C. J., Lamond, A. I. and Earnshaw, W. C. (2006) 'Condensin and Repo-Man-PP1 co-operate in the regulation of chromosome architecture during mitosis', *Nat Cell Biol,* 8(10), pp. 1133-42.

Valentin, G., Schwob, E. and Della Seta, F. (2006) 'Dual role of the Cdc7-regulatory protein Dbf4 during yeast meiosis', *J Biol Chem,* 281(5), pp. 2828-34.

van Brabant, A. J., Ye, T., Sanz, M., German III, J. L., Ellis, N. A. and Holloman, W. K. (2000) 'Binding and melting of D-loops by the Bloom syndrome helicase', *Biochemistry,* 39(47), pp. 14617-25.

van der Crabben, S. N., Hennus, M. P., McGregor, G. A., Ritter, D. I., Nagamani, S. C., Wells, O. S., Harakalova, M., Chinn, I. K., Alt, A., Vondrova, L., Hochstenbach, R., van Montfrans, J. M., Terheggen-Lagro, S. W., van Lieshout, S., van Roosmalen, M. J., Renkens, I., Duran, K., Nijman, I. J., Kloosterman, W. P., Hennekam, E., Orange, J. S., van Hasselt, P. M., Wheeler, D. A., Palecek, J. J., Lehmann, A. R., Oliver, A. W., Pearl, L. H., Plon, S. E., Murray, J. M. and van Haaften, G. (2016) 'Destabilized SMC5/6 complex leads to chromosome breakage syndrome with severe lung disease', *J Clin Invest,* 126(8), pp. 2881-92.

Vaur, S., Feytout, A., Vazquez, S. and Javerzat, J. P. (2012) 'Pds5 promotes cohesin acetylation and stable cohesin-chromosome interaction', *EMBO Rep,* 13(7), pp. 645-52.

Vega, H., Waisfisz, Q., Gordillo, M., Sakai, N., Yanagihara, I., Yamada, M., van Gosliga, D., Kayserili, H., Xu, C., Ozono, K., Jabs, E. W., Inui, K. and Joenje, H. (2005) 'Roberts syndrome is caused by mutations in ESCO2, a human homolog of yeast ECO1 that is essential for the establishment of sister chromatid cohesion', *Nat Genet,* 37(5), pp. 468-70.

Verkade, H. M., Bugg, S. J., Lindsay, H. D., Carr, A. M. and O'Connell, M. J. (1999) 'Rad18 is required for DNA repair and checkpoint responses in fission yeast', *Mol Biol Cell,* 10(9), pp. 2905-18.

Verver, D. E., Langedijk, N. S., Jordan, P. W., Repping, S. and Hamer, G. (2014) 'The SMC5/6 complex is involved in crucial processes during human spermatogenesis', *Biol Reprod,* 91(1), pp. 22.

Verver, D. E., van Pelt, A. M., Repping, S. and Hamer, G. (2013) 'Role for rodent Smc6 in pericentromeric heterochromatin domains during spermatogonial differentiation and meiosis', *Cell Death Dis,* 4, pp. e749.

Volarcik, K., Sheean, L., Goldfarb, J., Woods, L., Abdul-Karim, F. W. and Hunt, P. (1998) 'The meiotic competence of in-vitro matured human oocytes is influenced by donor age: evidence that folliculogenesis is compromised in the reproductively aged ovary', *Hum Reprod,* 13(1), pp. 154-60.

von Wettstein, D. (1984) 'The synaptonemal complex and genetic segregation', *Symp Soc Exp Biol,* 38, pp. 195-231.

Waizenegger, I. C., Hauf, S., Meinke, A. and Peters, J. M. (2000) 'Two distinct

pathways remove mammalian cohesin from chromosome arms in prophase and from centromeres in anaphase', *Cell,* 103(3), pp. 399-410.

Wan, L., Zhang, C., Shokat, K. M. and Hollingsworth, N. M. (2006) 'Chemical inactivation of cdc7 kinase in budding yeast results in a reversible arrest that allows efficient cell synchronization prior to meiotic recombination', *Genetics,* 174(4), pp. 1767-74.

Wang, F., Yoder, J., Antoshechkin, I. and Han, M. (2003) 'Caenorhabditis elegans EVL-14/PDS-5 and SCC-3 are essential for sister chromatid cohesion in meiosis and mitosis', *Mol Cell Biol,* 23(21), pp. 7698-707.

Wang, J. C. (2002) 'Cellular roles of DNA topoisomerases: a molecular perspective', *Nat Rev Mol Cell Biol,* 3(6), pp. 430-40.

Watanabe, K., Pacher, M., Dukowic, S., Schubert, V., Puchta, H. and Schubert, I. (2009) 'The STRUCTURAL MAINTENANCE OF CHROMOSOMES 5/6 complex promotes sister chromatid alignment and homologous recombination after DNA damage in Arabidopsis thaliana', *Plant Cell,* 21(9), pp. 2688-99.

Watanabe, Y., Yokobayashi, S., Yamamoto, M. and Nurse, P. (2001) 'Pre-meiotic S phase is linked to reductional chromosome segregation and recombination', *Nature,* 409(6818), pp. 359-63.

Watrin, E., Schleiffer, A., Tanaka, K., Eisenhaber, F., Nasmyth, K. and Peters, J. M. (2006) 'Human Scc4 is required for cohesin binding to chromatin, sister-chromatid cohesion, and mitotic progression', *Curr Biol,* 16(9), pp. 863-74.

Wehrkamp-Richter, S., Hyppa, R. W., Prudden, J., Smith, G. R. and Boddy, M. N. (2012) 'Meiotic DNA joint molecule resolution depends on Nse5-Nse6 of the Smc5-Smc6 holocomplex', *Nucleic Acids Res,* 40(19), pp. 9633-46.

Wendt, K. S., Yoshida, K., Itoh, T., Bando, M., Koch, B., Schirghuber, E., Tsutsumi, S., Nagae, G., Ishihara, K., Mishiro, T., Yahata, K., Imamoto, F., Aburatani, H., Nakao, M., Imamoto, N., Maeshima, K., Shirahige, K. and Peters, J. M. (2008) 'Cohesin mediates transcriptional insulation by CCCTC-binding factor', *Nature,* 451(7180), pp. 796-801.

West, S. C. (1997) 'Processing of recombination intermediates by the RuvABC proteins', *Annu Rev Genet,* 31, pp. 213-44.

Westergaard, M. and von Wettstein, D. (1972) 'The synaptinemal complex', *Annu*

Rev Genet, 6, pp. 71-110.

Westermann, S. and Schleiffer, A. (2013) 'Family matters: structural and functional conservation of centromere-associated proteins from yeast to humans', *Trends Cell Biol,* 23(6), pp. 260-9.

Wilhelm, L., Bürmann, F., Minnen, A., Shin, H. C., Toseland, C. P., Oh, B. H. and Gruber, S. (2015) 'SMC condensin entraps chromosomal DNA by an ATP hydrolysis dependent loading mechanism in Bacillus subtilis', *Elife,* 4.

Winey, M., Mamay, C. L., O'Toole, E. T., Mastronarde, D. N., Giddings, T. H., McDonald, K. L. and McIntosh, J. R. (1995) 'Three-dimensional ultrastructural analysis of the Saccharomyces cerevisiae mitotic spindle', *J Cell Biol,* 129(6), pp. 1601-15.

Winey, M., Morgan, G. P., Straight, P. D., Giddings, T. H. and Mastronarde, D. N. (2005) 'Three-dimensional ultrastructure of Saccharomyces cerevisiae meiotic spindles', *Mol Biol Cell,* 16(3), pp. 1178-88.

Wu, N., Kong, X., Ji, Z., Zeng, W., Potts, P. R., Yokomori, K. and Yu, H. (2012) 'Scc1 sumoylation by Mms21 promotes sister chromatid recombination through counteracting Wapl', *Genes Dev,* 26(13), pp. 1473-85.

Wu, N. and Yu, H. (2012) 'The Smc complexes in DNA damage response', *Cell Biosci,* 2, pp. 5.

Wu, Y., Gause, M., Xu, D., Misulovin, Z., Schaaf, C. A., Mosarla, R. C., Mannino, E., Shannon, M., Jones, E., Shi, M., Chen, W. F., Katz, O. L., Sehgal, A., Jongens, T. A., Krantz, I. D. and Dorsett, D. (2015) 'Drosophila Nipped-B Mutants Model Cornelia de Lange Syndrome in Growth and Behavior', *PLoS Genet,* 11(11), pp. e1005655.

Xaver, M., Huang, L., Chen, D. and Klein, F. (2013) 'Smc5/6-Mms21 prevents and eliminates inappropriate recombination intermediates in meiosis', *PLoS Genet,* 9(12), pp. e1004067.

Xu, H., Beasley, M. D., Warren, W. D., van der Horst, G. T. and McKay, M. J. (2005) 'Absence of mouse REC8 cohesin promotes synapsis of sister chromatids in meiosis', *Dev Cell,* 8(6), pp. 949-61.

Xu, L., Ajimura, M., Padmore, R., Klein, C. and Kleckner, N. (1995) 'NDT80, a meiosis-specific gene required for exit from pachytene in Saccharomyces cerevisiae', *Mol Cell Biol,* 15(12), pp. 6572-81.

Xu, X., Aprelikova, O., Moens, P., Deng, C. X. and Furth, P. A. (2003) 'Impaired meiotic DNA-damage repair and lack of crossing-over during spermatogenesis in BRCA1 full-length isoform deficient mice', *Development,* 130(9), pp. 2001-12.

Xu, Z., Cetin, B., Anger, M., Cho, U. S., Helmhart, W., Nasmyth, K. and Xu, W. (2009) 'Structure and function of the PP2A-shugoshin interaction', *Mol Cell,* 35(4), pp. 426-41.

Xue, X., Choi, K., Bonner, J., Chiba, T., Kwon, Y., Xu, Y., Sanchez, H., Wyman, C., Niu, H., Zhao, X. and Sung, P. (2014) 'Restriction of replication fork regression activities by a conserved SMC complex', *Mol Cell,* 56(3), pp. 436-45.

Yokobayashi, S. and Watanabe, Y. (2005) 'The kinetochore protein Moa1 enables cohesion-mediated monopolar attachment at meiosis I', *Cell,* 123(5), pp. 803-17.

Yong-Gonzales, V., Hang, L. E., Castellucci, F., Branzei, D. and Zhao, X. (2012) 'The Smc5-Smc6 complex regulates recombination at centromeric regions and affects kinetochore protein sumoylation during normal growth', *PLoS One,* 7(12), pp. e51540.

Yu, H. G. and Koshland, D. (2007) 'The Aurora kinase Ipl1 maintains the centromeric localization of PP2A to protect cohesin during meiosis', *J Cell Biol,* 176(7), pp. 911-8.

Yuan, L., Liu, J. G., Zhao, J., Brundell, E., Daneholt, B. and Höög, C. (2000) 'The murine SCP3 gene is required for synaptonemal complex assembly, chromosome synapsis, and male fertility', *Mol Cell,* 5(1), pp. 73-83.

Yun, Y., Holt, J. E., Lane, S. I., McLaughlin, E. A., Merriman, J. A. and Jones, K. T. (2014) 'Reduced ability to recover from spindle disruption and loss of kinetochore spindle assembly checkpoint proteins in oocytes from aged mice', *Cell Cycle,* 13(12), pp. 1938-47.

Yunger, S., Rosenfeld, L., Garini, Y. and Shav-Tal, Y. (2010) 'Single-allele analysis of transcription kinetics in living mammalian cells', *Nat Methods,* 7(8), pp. 631-3.

Zabrady, K., Adamus, M., Vondrova, L., Liao, C., Skoupilova, H., Novakova, M., Jurcisinova, L., Alt, A., Oliver, A. W., Lehmann, A. R. and Palecek, J. J. (2016) 'Chromatin association of the SMC5/6 complex is dependent on binding of

its NSE3 subunit to DNA', *Nucleic Acids Res,* 44(3), pp. 1064-79.

Zachariae, W. and Nasmyth, K. (1999) 'Whose end is destruction: cell division and the anaphase-promoting complex', *Genes Dev,* 13(16), pp. 2039-58.

Zakharyevich, K., Ma, Y., Tang, S., Hwang, P. Y., Boiteux, S. and Hunter, N. (2010) 'Temporally and biochemically distinct activities of Exo1 during meiosis: double-strand break resection and resolution of double Holliday junctions', *Mol Cell,* 40(6), pp. 1001-15.

Zakharyevich, K., Tang, S., Ma, Y. and Hunter, N. (2012) 'Delineation of joint molecule resolution pathways in meiosis identifies a crossover-specific resolvase', *Cell,* 149(2), pp. 334-47.

Zetka, M. C. and Rose, A. M. (1995) 'Mutant rec-1 eliminates the meiotic pattern of crossing over in Caenorhabditis elegans', *Genetics,* 141(4), pp. 1339-49.

Zhang, B., Chang, J., Fu, M., Huang, J., Kashyap, R., Salavaggione, E., Jain, S., Kulkarni, S., Shashikant, K., Deardorff, M. A., Uzielli, M. L., Dorsett, D., Beebe, D. C., Jay, P. Y., Heuckeroth, R. O., Krantz, I. and Milbrandt, J. (2009) 'Dosage effects of cohesin regulatory factor PDS5 on mammalian development: implications for cohesinopathies', *PLoS One,* 4(5), pp. e5232.

Zhang, L., Kim, K. P., Kleckner, N. E. and Storlazzi, A. (2011) 'Meiotic double-strand breaks occur once per pair of (sister) chromatids and, via Mec1/ATR and Tel1/ATM, once per quartet of chromatids', *Proc Natl Acad Sci U S A,* 108(50), pp. 20036-41.

Zhang, N., Kuznetsov, S. G., Sharan, S. K., Li, K., Rao, P. H. and Pati, D. (2008) 'A handcuff model for the cohesin complex', *J Cell Biol,* 183(6), pp. 1019-31.

Zhao, X. and Blobel, G. (2005) 'A SUMO ligase is part of a nuclear multiprotein complex that affects DNA repair and chromosomal organization', *Proc Natl Acad Sci U S A,* 102(13), pp. 4777-82.

Zickler, D. and Kleckner, N. (1998) 'The leptotene-zygotene transition of meiosis', *Annu Rev Genet,* 32, pp. 619-97.

Zickler, D. and Kleckner, N. (1999) 'Meiotic chromosomes: integrating structure and function', *Annu Rev Genet,* 33, pp. 603-754.

Zickler, D. and Kleckner, N. (2015) 'Recombination, Pairing, and Synapsis of Homologs during Meiosis', *Cold Spring Harb Perspect Biol,* 7(6).

Zielinska, A. P., Holubcova, Z., Blayney, M., Elder, K. and Schuh, M. (2015) 'Sister kinetochore splitting and precocious disintegration of bivalents could explain the maternal age effect', *Elife,* 4, pp. e11389.

Zuin, J., Franke, V., van Ijcken, W. F., van der Sloot, A., Krantz, I. D., van der Reijden, M. I., Nakato, R., Lenhard, B. and Wendt, K. S. (2014) 'A cohesin-independent role for NIPBL at promoters provides insights in CdLS', *PLoS Genet,* 10(2), pp. e1004153.

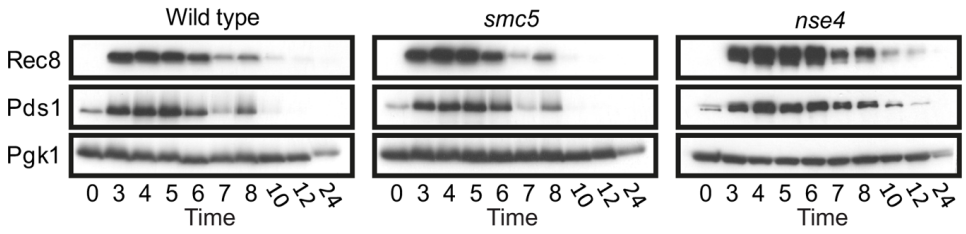

Supplementary figure 1 – Western blot analysis of Rec8 and Pds1 levels in wild type, *smc5* and *nse4* mutants

Western blot looking at the levels of Rec8, Pds1 and Pgk1 in wild type (Y2572), *smc5* (Y2673) and *nse4* (Y3653) (Copsey et al, 2013).

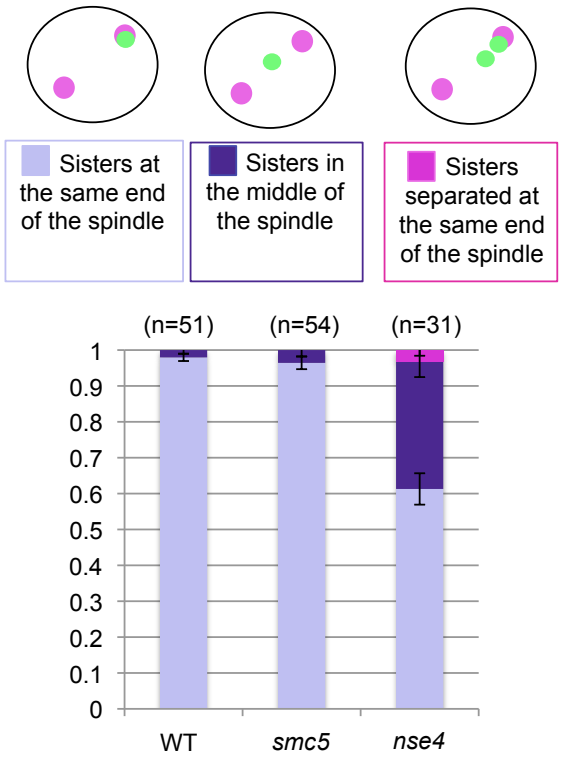

Supplementary figure 2 – Analysis of the sister chromatid separation in fixed cells containing spindles of 4 microns or longer

Proportion of cells that display the variety of forms of sister chromatid segregation (as demonstrated in Figure 3.11A) at anaphase I where the spindles were 4 micron or longer. Strains used were WT (Y5398), *smc5* (Y5419) and *nse4* (Y5399).

(A)

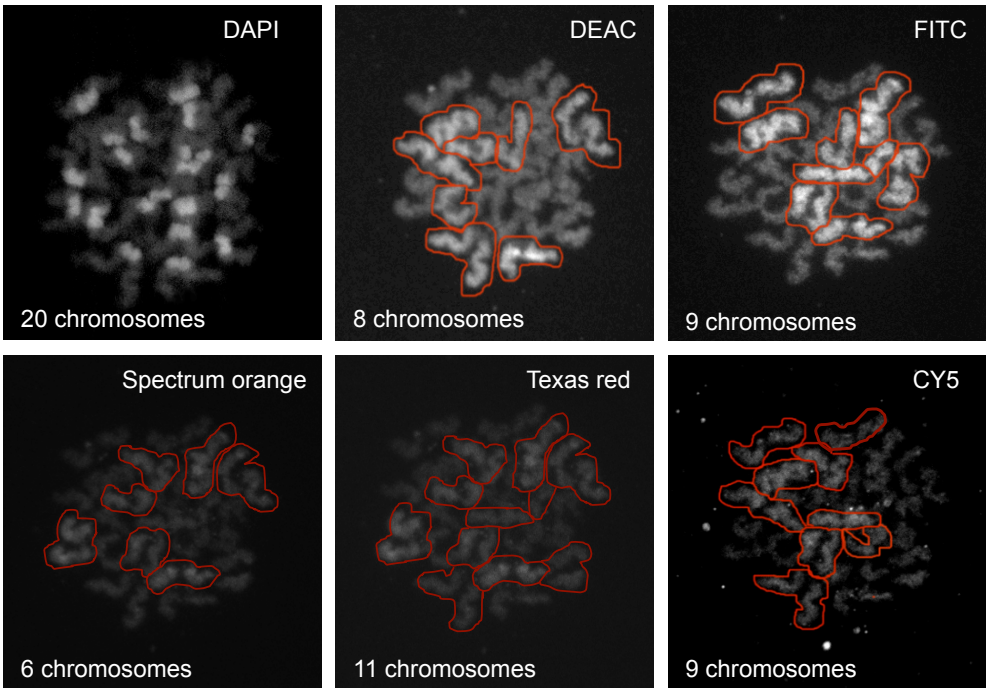

(B)

21XMouse

Chr.	aqua	green	orange	red	nir*
1					
2					
3					
4					
5					
6					
7					
8					
9					
10					
11					
12					
13					
14					
15					
16					
17					
18					
19					
X					

http://www.metasystems-international.com

Supplementary figure 3 - mFISH analysis of MII oocyte spreads using the pDV

A. Images produced on the personal Delta Vision of an oocyte stained with cytovision 21XMouse mFISH probes. The chromosomes that were fluorescent in each of the channels are outlined for clarity.

B. Table demonstrating the colour that each of the chromosomes are meant to be stained when using the 21Xmouse mFISH kit.

(A)

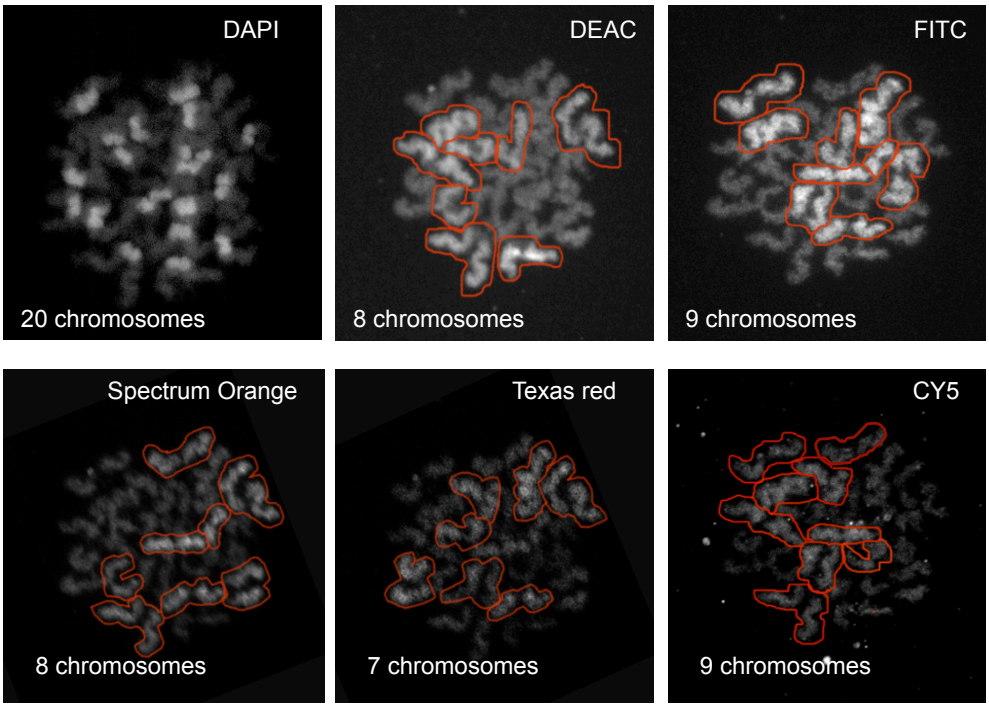
DAPI
20 chromosomes
DEAC
8 chromosomes
FITC
9 chromosomes
Spectrum Orange
8 chromosomes
Texas red
7 chromosomes
CY5
9 chromosomes

(B)

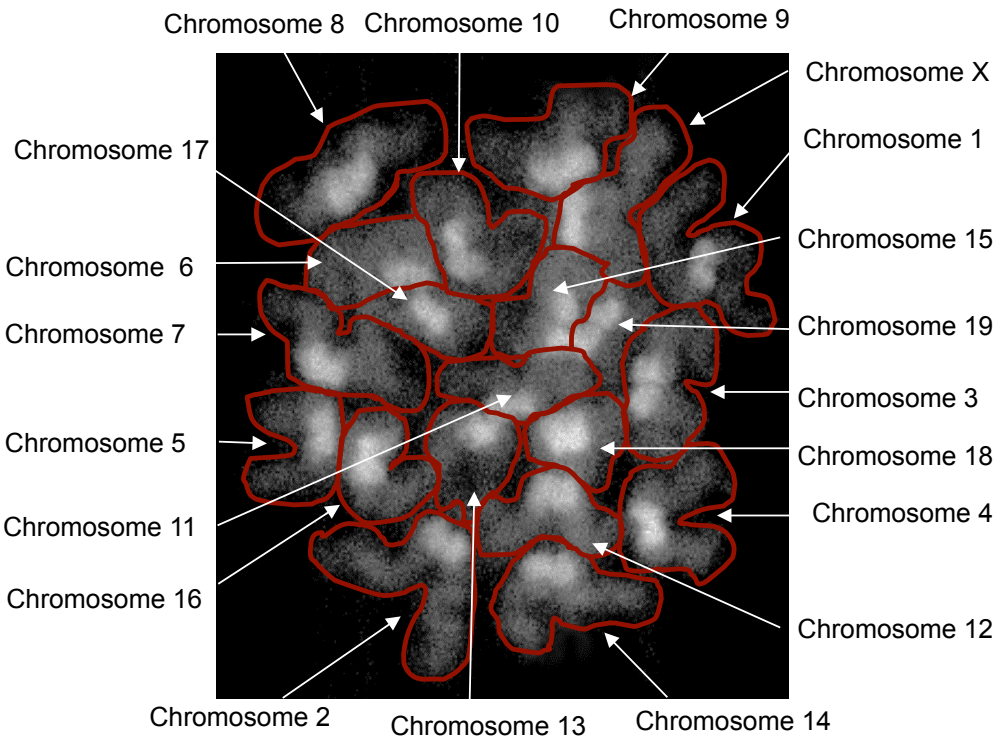
Chromosome 8
Chromosome 10
Chromosome 9
Chromosome X
Chromosome 17
Chromosome 1
Chromosome 15
Chromosome 6
Chromosome 7
Chromosome 19
Chromosome 3
Chromosome 5
Chromosome 18
Chromosome 11
Chromosome 4
Chromosome 16
Chromosome 12
Chromosome 2
Chromosome 13
Chromosome 14

Supplementary figure 4 – mFISH of an MII oocyte spread containing 20 chromosomes using a Leica SP8

A. Images produced on the Leica SP8 of an oocyte stained with Cytovision 21XMouse mFISH probes. The chromosomes that were fluorescent in each of the channels are outlined for clarity.

B. Diagram displaying the identity of each of the chromosomes in the chromosome spread. These were allocated using the table in Figure 4.3B.

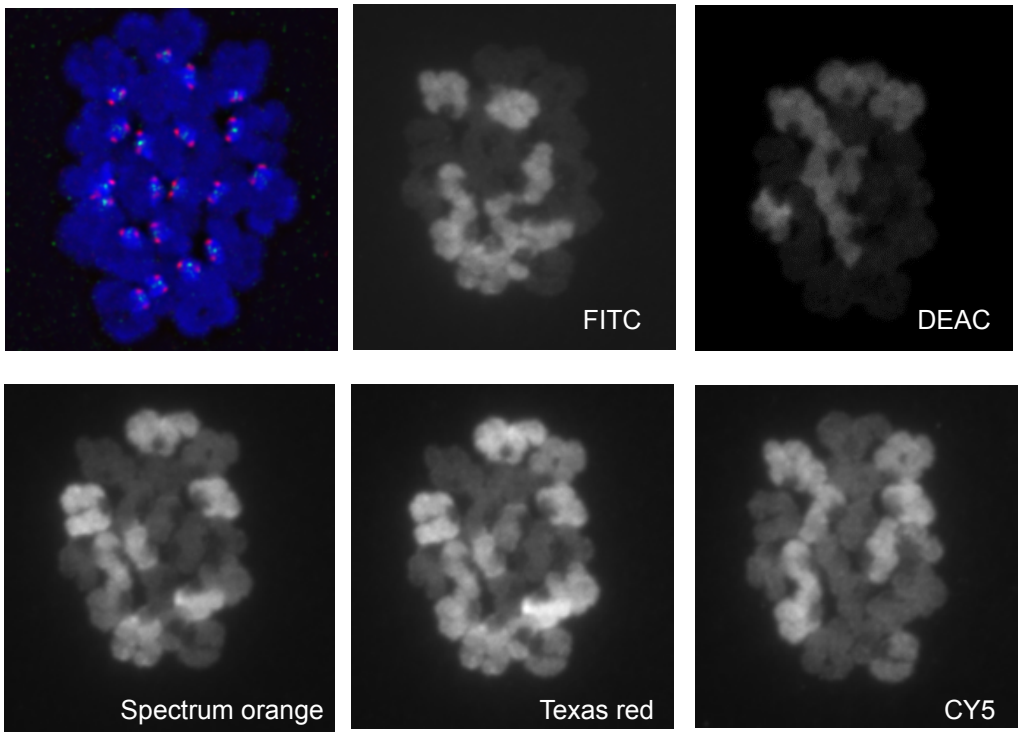

Supplementary figure 5 – mFISH on bunched MII oocyte spread

mFISH on a bunched chromosome spread. Here specific chromosomes could not be accurately distinguished from one another.

(A) Wild Type

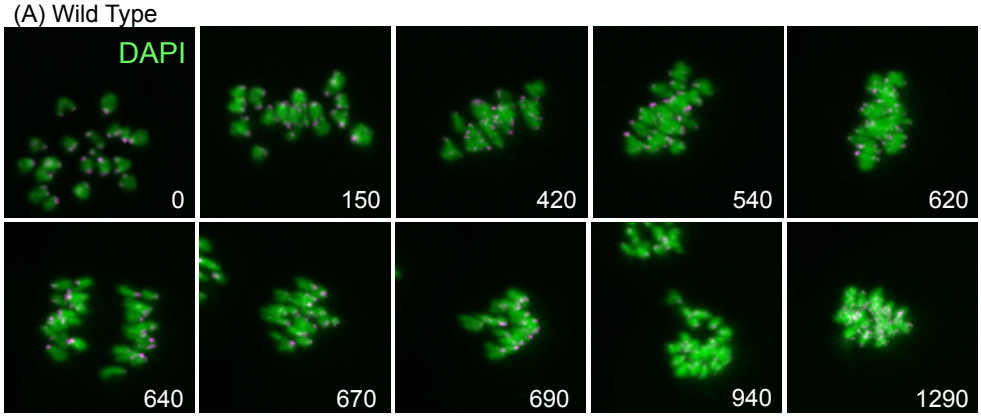

(B) *Smc6* $^{+/GT}$ (normal anaphase)

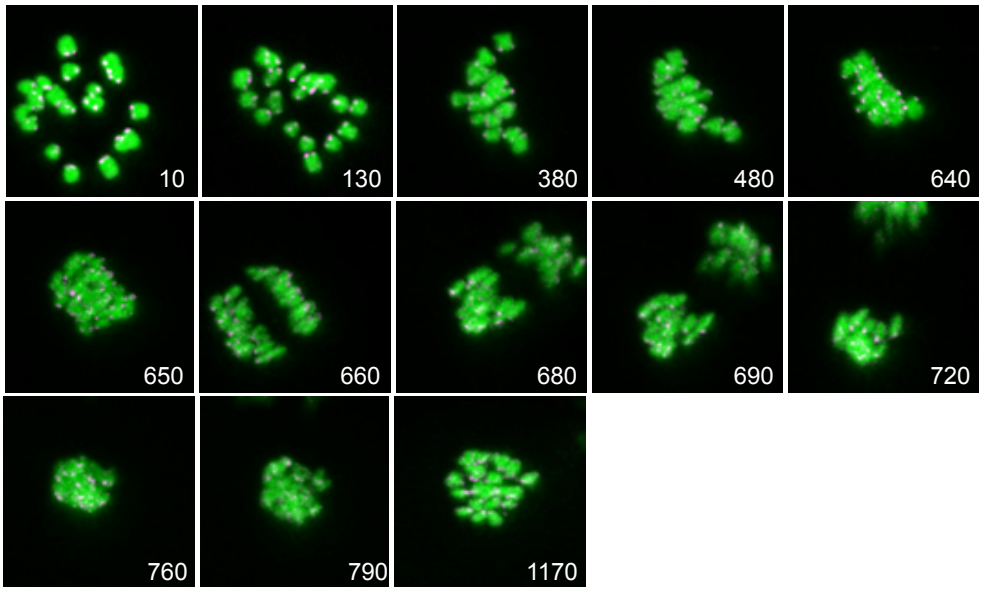

(C) *Smc6* $^{+/GT}$ (abnormal anaphase)

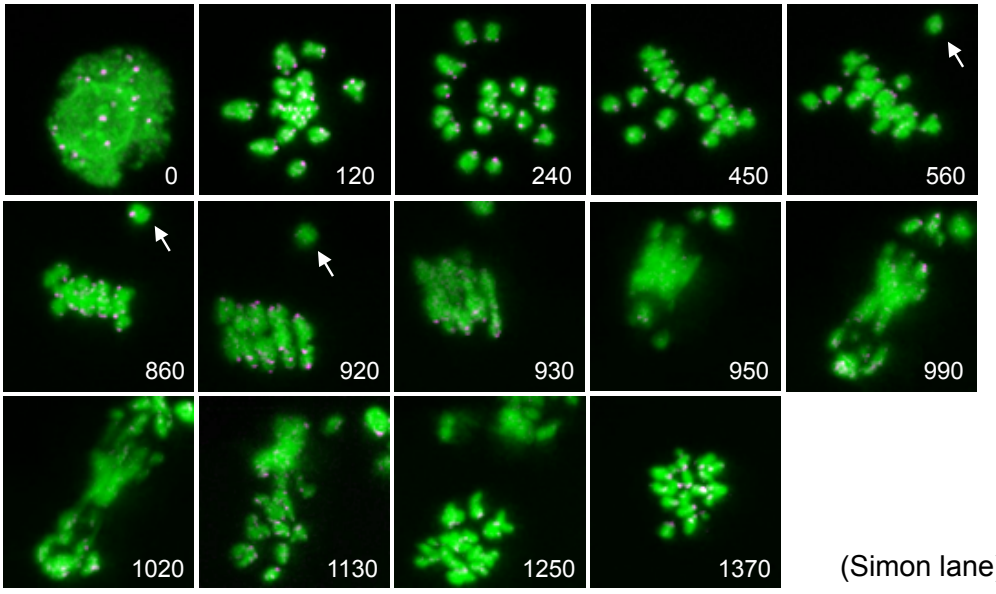

(Simon lane)

Supplementary figure 6 – Live cell imaging of oocytes from both wildtype and *Smc6*$^{+/GT}$ mice

A. Example of live cell imaging in a wildtype oocyte from pachytene to anaphase. Here the chromosomes accurately congress to the metaphase plane and then at the end of anaphase loose half the chromosomes to the polar body.

B. Example of a normal chromosome segregation in a *Smc6*$^{+/GT}$ mouse oocyte.

C. Example of a abnormal chromosome segregation in a *Smc6*$^{+/GT}$ mouse oocyte. Here the chromosomes do not congress properly at metaphase (as demonstrated by the arrow pointing towards the lone chromosome). Then at anaphase the chromosomes do not segregate properly and in the end appear to be ripped apart.

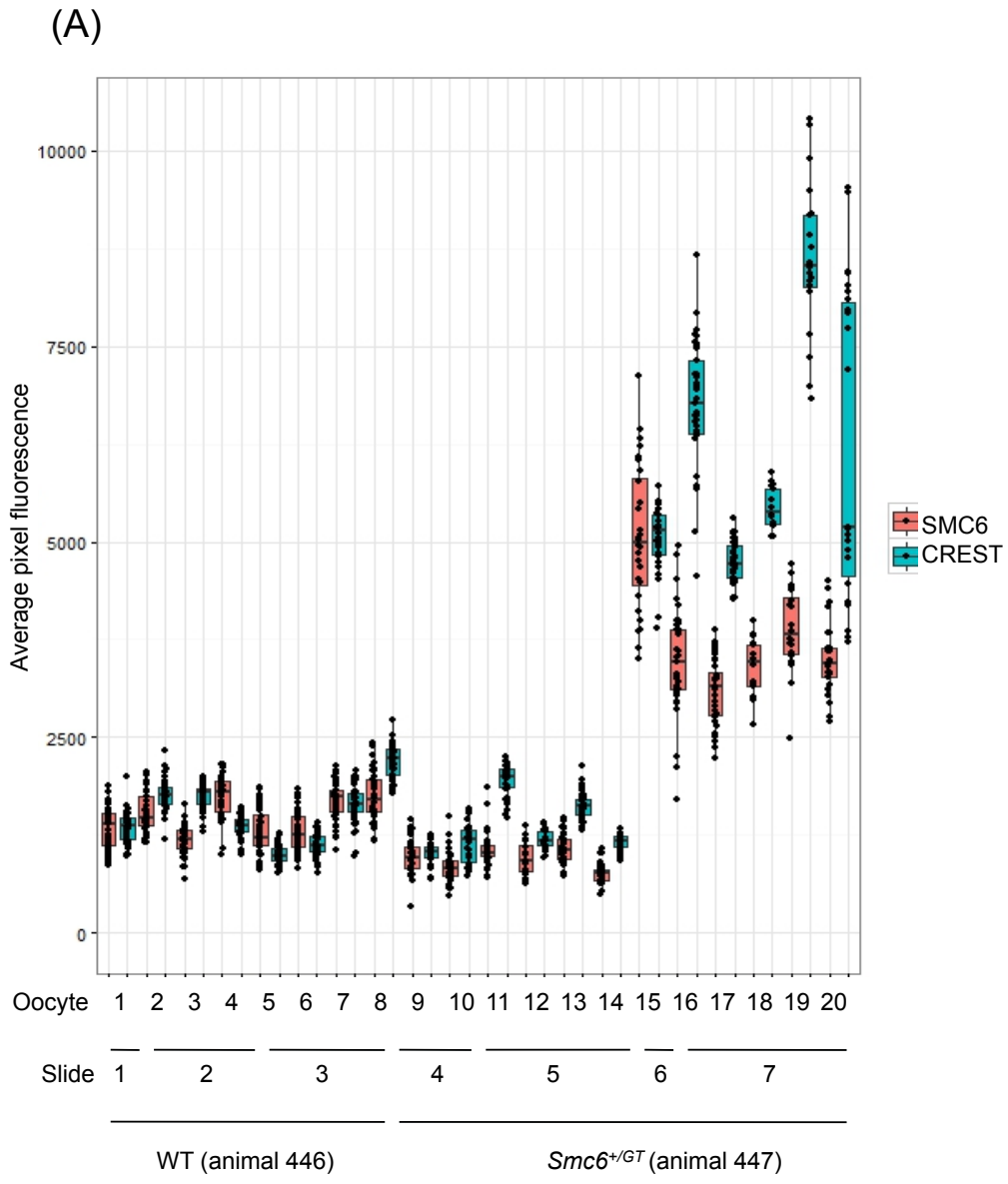

Supplementary figure 7 – Centromeric SMC6 signal varies with CREST signal

Box plots demonstrating how centromeric SMC6 staining varies with CREST staining on a per chromosome basis, plotted on a per oocyte basis in both wild type (animal 446) and $Smc6^{+/GT}$ (animal 447). Spreads 15-20 stained to a much greater extent for both antibodies. (Mouse experiments 14)

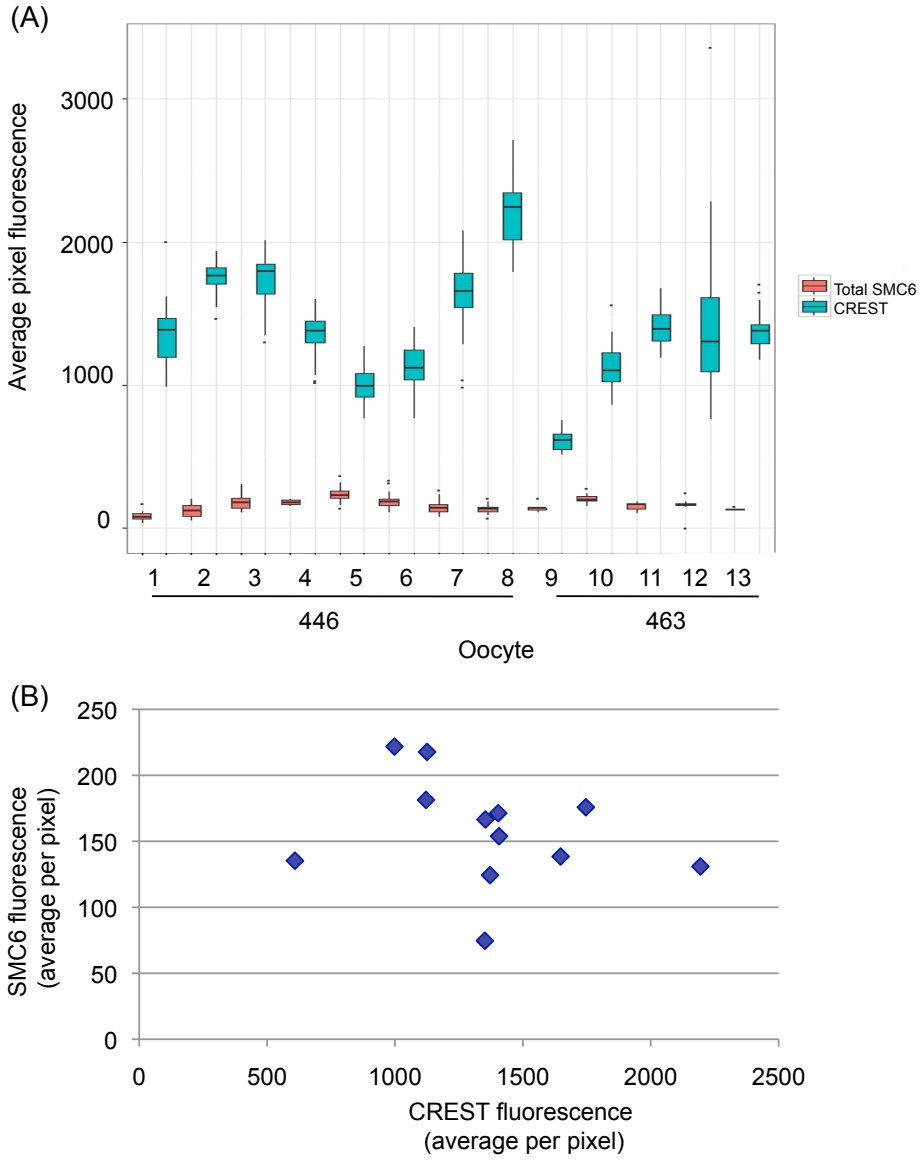

Supplementary figure 8 – CREST fluorescence does not vary with average total SMC6 fluorescence

A. Boxplot comparing the average total SMC6 pixel signal and the average CREST pixel signals on a per spread basis. Oocytes were all from two wild type mice (animals 446 & 463). **(**Mouse experiments 14 & 15)

B. Graph demonstrating how the average total SMC6 pixel signal correlates with the average CREST pixel signal on a per spread basis (R^2=0.06) (Oocytes from animals 446 & 463). **(**Mouse experiments 14 & 15)

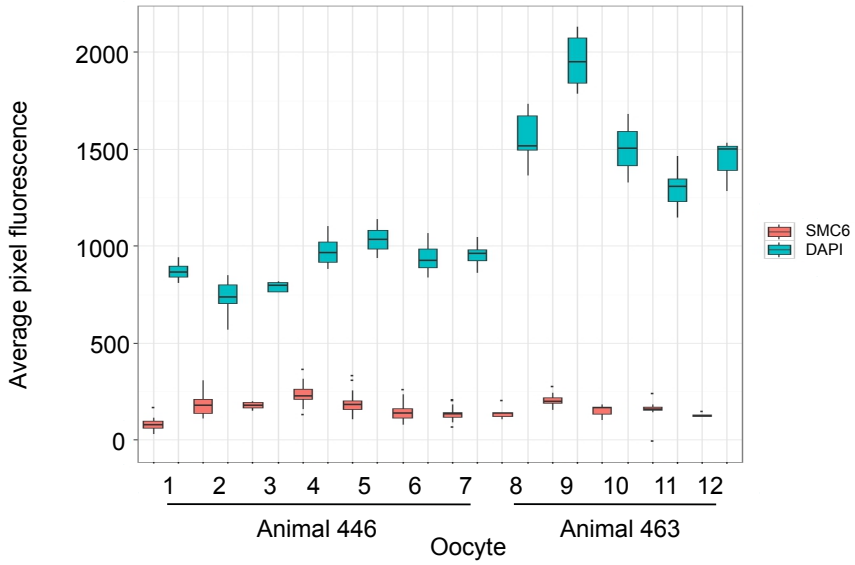

Supplementary figure 9 – Total SMC6 signal does not vary with DAPI signal

Boxplot comparing the average pixel signal from the total SMC6 and DAPI on a per spread basis. Oocytes were all from two wild type mice (wild type animals 446 & 463). (Mouse experiments 14 & 15)

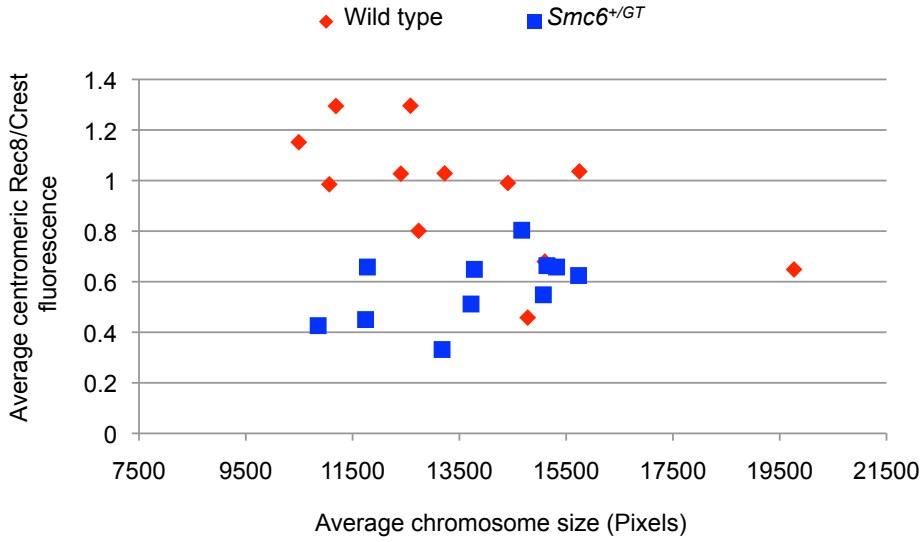

Supplementary figure 10 – Oocytes with reduced levels of centromeric SMC6 do not have larger chromosomes

Plot of the average crest fluorescence (normalised to crest) against the average chromosome size of the spread. Wildtype data from 2 mice, 12 spreads. *Smc6*$^{+/GT}$ 2 mice, 11 spreads. (animals 446,447,462 & 463). (Mouse experiments 14 & 15)

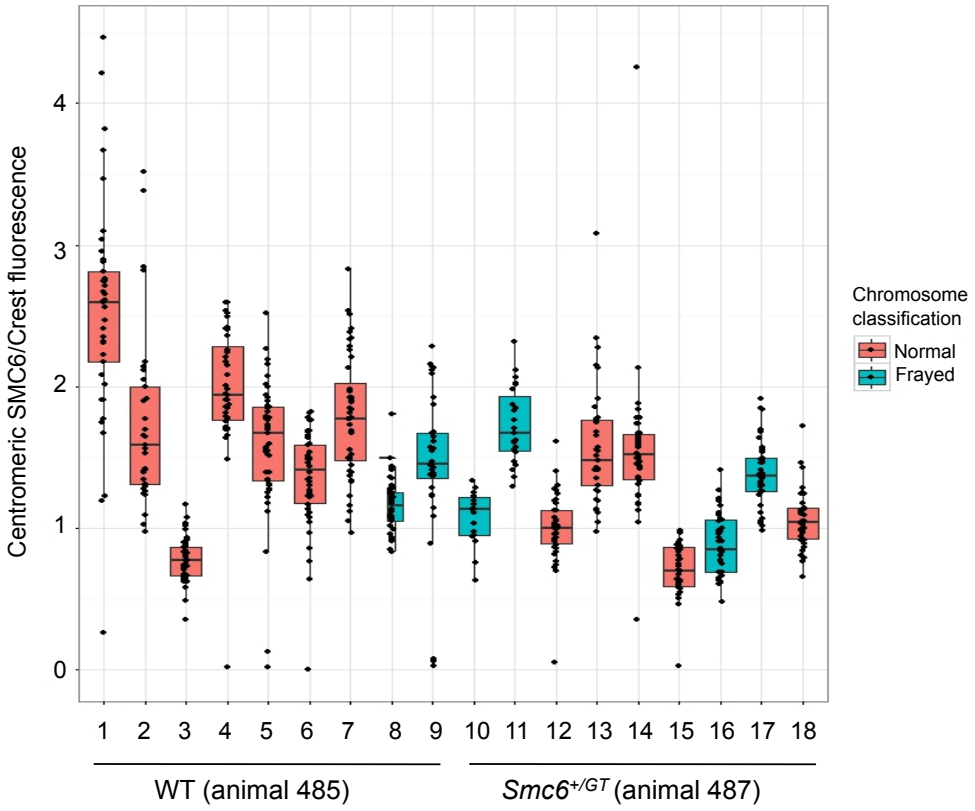

Supplementary figure 11 – Low SMC6 staining does not correlate with chromosome fraying

Plot demonstrating the normalised centromeric SMC6 fluorescence. Spreads classified as normal are coloured red and spreads classified as displaying frayed chromosomes are coloured green. (Mouse experiment 18)

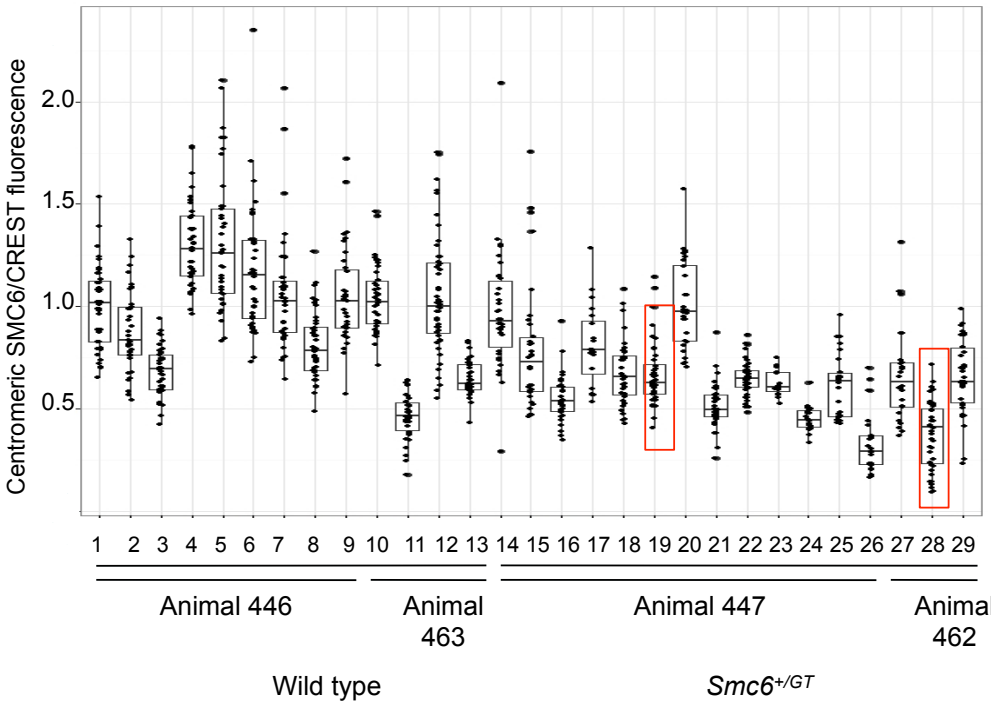

Supplementary figure 12 – Low levels of SMC6 fluorescence may not be linked with increased chance of the spread displaying distal chromosomes

Boxplot showing the average centromeric SMC6 fluorescent levels normalised to crest on a per spread basis in both wild type (animals 446 & 463) and Smc6$^{+/GT}$ (animals 447 & 462). Here the jittering corresponds to the average pixel values from individual centromeric signals. The spreads that contained distal chromosomes are outlined in red. (Mouse experiments 14 & 15)

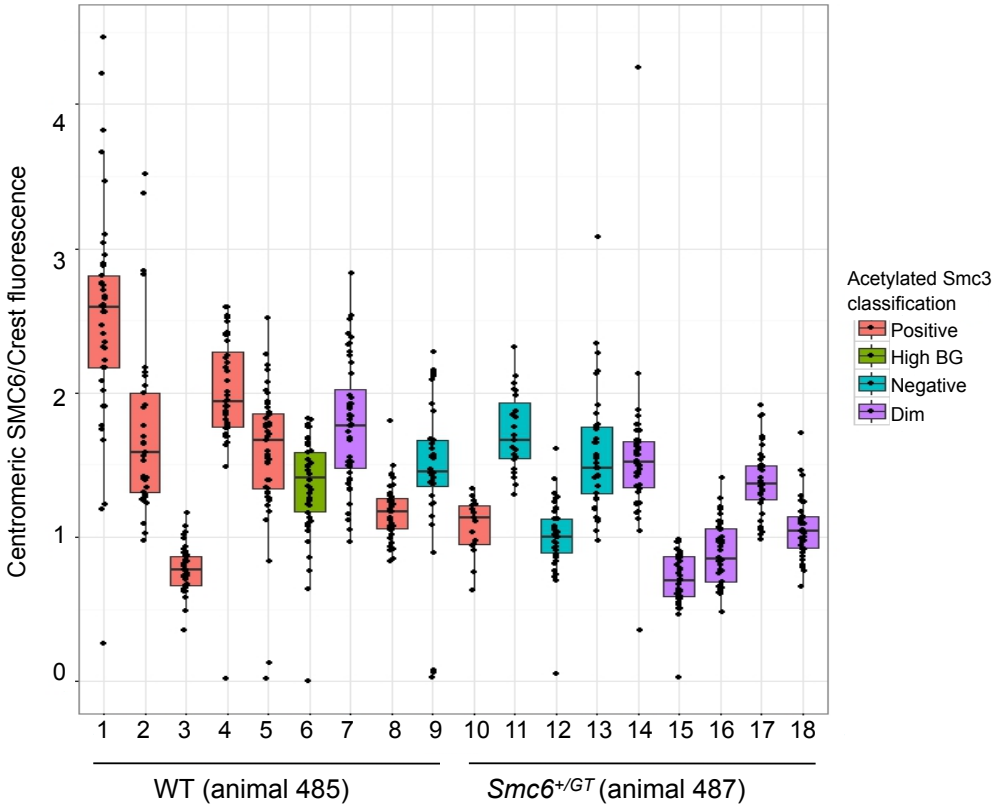

Supplementary figure 13 – Low levels of SMC6 staining may not be linked with reduced acetylated SMC3 staining

Boxplot showing the average centromeric SMC6 fluorescent levels normalised to CREST on a per spread basis in both wild type (animal 485) and *Smc6*$^{+/GT}$ (animal 487). The jittering corresponds to the average pixel values from individual centromeric signals. The spreads that displayed positive SMC3 staining are coloured red, the spreads that displayed a high background are coloured green, the spreads that were negative for SMC3 staining are coloured blue and those that displayed dim SMC3 staining are coloured purple. (Mouse experiments 18)

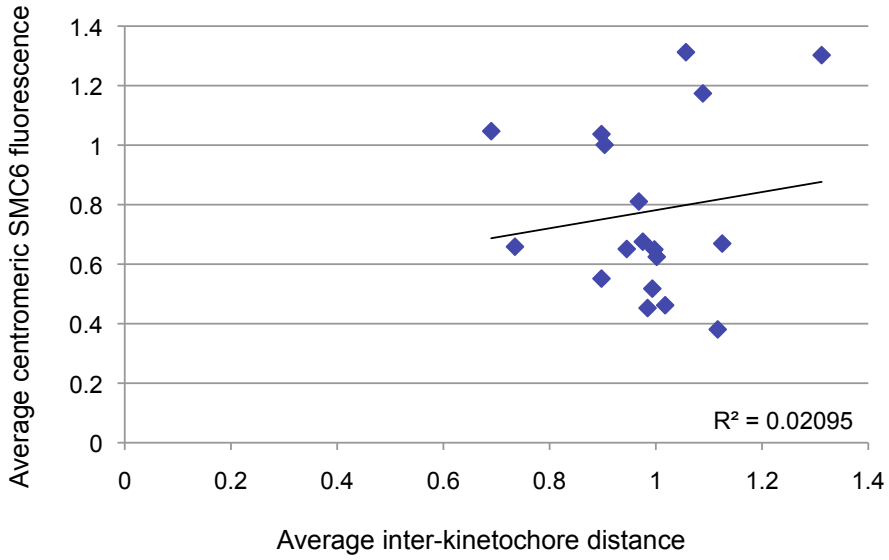

Supplementary figure 14 - Low levels of SMC6 staining do not correlate with increased inter-kinetochore distances

Plot of the average centromeric SMC6 fluorescence (normalised to CREST) against the average inter-kinetochore distance (on a per spread basis) (R^2=0.029). Wildtype data from 2 mice, 8 spreads. *Smc6*$^{+/GT}$ data from 2 mice, 10 spreads (animals 446, 447, 462 & 463). (Mouse experiments 14 & 15)

8.2 Published work

OPEN ACCESS Freely available online

PLOS | GENETICS

Smc5/6 Coordinates Formation and Resolution of Joint Molecules with Chromosome Morphology to Ensure Meiotic Divisions

Alice Copsey[1☯], Shangming Tang[2,3☯], Philip W. Jordan[1☯¤], Hannah G. Blitzblau[4], Sonya Newcombe[1], Andrew Chi-ho Chan[1], Louise Newnham[1], Zhaobo Li[1], Stephen Gray[1], Alex D. Herbert[1], Prakash Arumugam[5], Andreas Hochwagen[4,6], Neil Hunter[2,3,6,7,8], Eva Hoffmann[1]*

1 MRC Genome Damage and Stability Centre, University of Sussex, Brighton, United Kingdom, **2** Howard Hughes Medical Institute, University of California, Davis, Davis, California, United States of America, **3** Department of Microbiology & Molecular Genetics, University of California, Davis, Davis, California, United States of America, **4** Whitehead Institute for Biomedical Research, Cambridge, Massachusetts, United States of America, **5** Department of Life Sciences, University of Warwick, Coventry, United Kingdom, **6** Department of Biology, New York University, New York, New York, United States of America, **7** Department of Molecular & Cellular Biology, University of California, Davis, Davis, California, United States of America, **8** Department of Cell Biology & Human Anatomy, University of California, Davis, Davis, California, United States of America

Abstract

During meiosis, Structural Maintenance of Chromosome (SMC) complexes underpin two fundamental features of meiosis: homologous recombination and chromosome segregation. While meiotic functions of the cohesin and condensin complexes have been delineated, the role of the third SMC complex, Smc5/6, remains enigmatic. Here we identify specific, essential meiotic functions for the Smc5/6 complex in homologous recombination and the regulation of cohesin. We show that Smc5/6 is enriched at centromeres and cohesin-association sites where it regulates sister-chromatid cohesion and the timely removal of cohesin from chromosomal arms, respectively. Smc5/6 also localizes to recombination hotspots, where it promotes normal formation and resolution of a subset of joint-molecule intermediates. In this regard, Smc5/6 functions independently of the major crossover pathway defined by the MutLγ complex. Furthermore, we show that Smc5/6 is required for stable chromosomal localization of the XPF-family endonuclease, Mus81-Mms4^{Eme1}. Our data suggest that the Smc5/6 complex is required for specific recombination and chromosomal processes throughout meiosis and that in its absence, attempts at cell division with unresolved joint molecules and residual cohesin lead to severe recombination-induced meiotic catastrophe.

Citation: Copsey A, Tang S, Jordan PW, Blitzblau HG, Newcombe S, et al. (2013) Smc5/6 Coordinates Formation and Resolution of Joint Molecules with Chromosome Morphology to Ensure Meiotic Divisions. PLoS Genet 9(12): e1004071. doi:10.1371/journal.pgen.1004071

Editor: Michael Lichten, National Cancer Institute, United States of America

Received June 21, 2013; **Accepted** November 8, 2013; **Published** December 26, 2013

Funding: ST was supported by a National Institute of Environmental Health Sciences funded training program in Environmental Health Sciences (T32 ES007058-33). PWJ was funded by BBSRC grant (BB/G00353X/1). HGB was supported by a Charles A. King Trust award. SG was supported by a MRC Centenary Award. NH is an Investigator of the Howard Hughes Medical Institute. This work was supported by NIH NIGMS grant GM084955 to NH. AH was supported by NIH grant R01 GM088248. EH is an EMBO Young Investigator and MRC Senior Non-clinical Research Fellow. The funders had no role in study design, data collection and analysis, decision to publish, or preparation of the manuscript.

Competing Interests: The authors have declared that no competing interests exist.

* E-mail: eh58@sussex.ac.uk

¤ Current address: Biochemistry and Molecular Biology Department, Johns Hopkins School of Public Health, Baltimore, Maryland, United States of America.

☯ These authors contributed equally to this work.

Introduction

Sexually reproducing organisms reduce their genomic content by half in the gametes such that the normal chromosome copy number is restored in the zygote. To achieve this, homologous chromosomes (homologs) have to pair and then segregate to opposite spindle poles at the first division of meiosis. In many organisms, homolog pairing and segregation depends upon the developmental induction of hundreds of double-strand breaks (DSBs) throughout the genome (150–300 DSBs in yeasts and mammals) [1]. High levels of DSBs are necessary for homologs to pair efficiently along their entire lengths [2]. Moreover, a subset of DSB repair events lead to crossover formation. These reciprocal exchanges between homologs combine with sister-chromatid cohesion to form chiasmata, the physical connections that aid bi-orientation of homologs on the meiosis I spindle. Homolog separation at anaphase I thus requires the release of sister chromatid cohesion between chromosome arms. However, centromere cohesion is specifically protected to allow biorientation and accurate segregation of sister chromatids on the meiosis-II spindles [3–5].

Meiotic recombination is highly regulated and temporally coordinated with the meiotic cell cycle. Crossover-specific joint molecule intermediates (JMs) are formed during midprophase I of meiosis ('thick threads', pachytene), when homologous chromosomes are highly compacted and paired along their entire length by the synaptonemal complex. JMs are resolved into crossovers upon pachytene exit when a dedicated resolving process becomes

Author Summary

Meiosis is a specialized cell division that exactly halves the number of chromosomes transmitted from each parent to their offspring via gamete cells (such as sperm and eggs). This requires that matching ('homologous') chromosomes associate and then separate into different cells such that each gamete contains exactly one complete set of chromosomes. In many organisms, this sequence of events is facilitated by the induction and repair of chromosome breaks via a process called homologous recombination. As homologous chromosomes engage in recombination, matching DNA strands between broken and intact template chromosomes become intertwined in repair intermediates called Joint Molecules. In this study, we show that a highly conserved protein complex called the Structural Maintenance of Chromosomes 5/6 (Smc5/6) complex is important for regulating the choice of recombination template as well as for the resolution of Joint Molecules that is required for chromosomes to separate. Even though Joint Molecules remain unresolved in mutants that lack normal Smc5/6 function, cells still attempt to separate chromosomes and meiosis becomes catastrophic. Thus, Smc5/6 mutants have a two-fold defect: accumulation of unresolved Joint Molecules and a failure to stall meiosis in order to remove these structures.

activated by polo-like kinase [6–8]. In contrast, most noncrossovers arise during prophase I, independently of known resolving nucleases via a process termed synthesis-dependent single-strand annealing [8,9].

The formation of JMs is guided by the RecQ-family DNA helicase Sgs1/BLM, which limits the formation of aberrant JM structures, such as those that interconnect 3 or 4 chromatids instead of the normal two [10,11]. Resolution of aberrant JMs requires the activities of structure-selective nucleases, Mus81-Mms4, Slx1-Slx4 and Yen1 [11–14]. Sgs1 together with type-I topoisomerase, Top3, and accessory factor, Rmi1, defines a potent double Holliday junction (dHJ) "dissolving" enzyme that specifically promotes noncrossover formation [15,16]. At pre-crossover sites, this dissolution activity must be attenuated in order to ensure efficient crossing over.

In budding yeast, a majority of crossovers are formed via a dedicated pathway defined by the conserved, meiosis-specific MutS complex, MutSγ (Msh4–Msh5) that is predicted to encircle and thereby stabilize JMs [17–20]. From extensive studies, we know that components of the MutSγ pathway promote the formation of stable JMs, Single End Invasions (SEIs) and dHJs, and protect them from being dissociated by Sgs1 [10,20,21]. Subsequent resolution of dHJs into crossovers requires the DNA mismatch repair factors, Exo1 and the predicted endonuclease activity of MutLγ, a complex of the MutL homologs Mlh1 and Mlh3 [22,23].

In *C. elegans*, MutSγ promotes all crossovers [24]. However, other organisms, such as fission yeast and *Drosophila*, lack MutSγ. In *Drosophila*, an analogous function in protecting JMs from Sgs1/BLM anti-crossover activity has been inferred for two MCM-like proteins (mei-MCM). JM resolution in *Drosophila* occurs by the XPF-family endonuclease, MEI9-ERCC1 [25,26]. In fission yeast, essentially all crossovers are generated by Mus81-Eme1, another XPF-family endonuclease [27–29]. In budding yeast, plants and mammals MutSγ-MutLγ is the predominant pathway of crossover formation, although Mus81-Eme1 (Mus81-Mms4 in budding yeast) also promotes a subset of crossovers [30–32]. Although Exo1-MutLγ, Mus81-Mms4, and Sgs1 are the major JM processing activities during budding yeast meiosis, at least two additional endonucleases can also facilitate resolution in budding yeast and metazoans. Yen1 can act as a backup resolvase in the absence of Mus81-Mms4 [13,14,33]. Similarly, Slx1–Slx4 is essential for resolution of a subset of JMs, specifically when Sgs1 is absent [13,14,34–36]. Collectively, the JM resolution and dissolution activities establish two essential conditions for efficient homolog disjunction at meiosis I: formation of crossovers to facilitate homolog biorientation and the efficient removal of all JMs that would otherwise impede chromosome separation.

Meiotic recombination is coordinated with global changes in chromosome morphology, including sister-chromatid cohesion and condensation. These processes are mediated by Structural Maintenance of Chromosome (SMC) complexes, large clamp or ring-like structures that include cohesin, condensin and Smc5/6. Whereas cohesin and condensin have wide-ranging effects on global chromosome morphology as well as DNA repair [37], the Smc5/6 complex appears to operate locally to attenuate recombination [38–43]. During mitotic growth, the Smc5/6 has been proposed to stabilize stalled replication forks and prevent recombination at the fork [43,44]. However, if recombinational repair ensues, Smc5/6 also regulates late steps, promoting the resolution of recombination structures [38,45]. The core Smc5/6 complex does not contain any DNA repair activities, raising the question of how it facilitates replication and recombination. One model posits that Smc5/6 regulates effector proteins via an intrinsic SUMO E3 ligase activity, catalysed by the associated non-SMC element Nse2/Mms21 [46–48]. This SUMO-mediated process has been inferred for regulation of telomeric and kinetochore proteins, and the establishment of cohesion around DSB sites (in mitotically cycling cells) [49–52]. However, this emerging paradigm has not been extended to enzymes involved in JM resolution. Genetic or physical interactions between Smc5/6 and JM resolving enzymes have not been established.

Based upon the findings that chromosome segregation appeared worse in *smc6* mutants that also lacked Sgs1 or Mus81, the Smc5/6 complex has been suggested to work in parallel with both Sgs1 and Mus81-Mms4 during mitotic DNA repair [40]. However, the severity of *smc5/6* mutants in combination with *mus81* or *sgs1* could equally reflect both separate as well as collaborative functions. The only physical interaction described to date is with the Mph1/FANCM DNA helicase, whose interaction with Smc5/6 does not depend upon sumoylation [53].

Despite the central role of Smc5/6 in orchestrating responses to DNA damage in mitotic cells, the role of Smc5/6 in meiotic recombination remains equivocal. In one study, a critical role for budding yeast Smc5/6 was inferred to occur during premeiotic S-phase, since abolition of meiotic DSBs by mutation of Spo11 did not improve the block to chromosome separation caused by *smc5/6* mutation [54]. In fission yeast, deletion of Nse5 or Nse6 is epistatic with the Mus81-Eme1 resolvase with regards to crossover generation suggesting that Smc5/6 regulates Mus81-dependent crossovers [55]. However, Mus81-Eme1 appears to be the sole resolvase acting during meiosis in fission yeast [56,57], so it is unknown whether this paradigm extends to organisms that employ multiple resolvases; or whether Smc5/6 influences all resolution activities via global changes in chromosome structure. In contrast to fission yeast, in *C. elegans* animals depleted for Smc5/6, crossover formation appears normal but meiocytes contain excess RAD-51 foci indicative of unrepaired DSBs [58]. From these phenotypes, a specific defect in meiotic DSB-repair between sister-chromatids was inferred [58]. This raises the possibility that the

Smc5/6 complex regulates a subset of recombination events and their resolution via specific resolvase activities.

A possible explanation for these apparently contradictory phenotypes is the extent to which different organisms employ the different JM resolution/dissolution activities [59]. In this study, we demonstrate that budding yeast Smc5/6 has essential roles during meiotic recombination in regulating the ordered formation of interhomolog joint molecules as well as their resolution. In *smc5/6* mutants, intersister dHJs as well as multichromatid joint molecules accumulate and fail to be resolved. For the latter, we show that Smc5/6 regulates Mus81-Mms4 activity in joint molecule resolution and localization to meiotic chromosomes. In contrast, the main resolvase activity during meiosis (MutLγ) appears to function independently of the Smc5/6 complex.

Results

Smc5/6 accumulates at centromeres, cohesion-binding sites, and double-strand breaks (DSBs)

Affinity-tagged Smc5-13myc and Nse4-TAP proteins were expressed throughout meiosis (Figure S1A). A subset of Smc5-13myc migrated as a highly molecular weight band that likely corresponds to the sumoylated species (Figure S1A). Smc5-13myc displayed linear or punctate immuno-staining patterns along meiotic chromosomes, during prophase I, that became undetectable at diplonema and metaphase I (Figure S1B). The punctate localization of Smc5-13myc was dependent upon Cdc6 (which is required for meiotic DNA replication) and to a lesser extent on the type-II topoisomerase Top2 (Figure S1). In contrast, chromosomal staining of Smc5/6 did not require Spo11 (required for DSB formation), Rec8 (cohesion), or the type-I topisomerases, Top1 and Top3 (Figure S1C and data not shown).

To obtain a higher resolution picture of Smc5/6 association with meiotic chromosomes, we carried out genome-wide ChIP-on-chip localization analysis for Smc5 tagged at its C-terminus with three V5 or 13 myc epitopes. Smc5 binds to many of the same chromosomal axis-associated sites as the meiosis-specific cohesin component, Rec8, and is similarly enriched at centromeres (Figure 1A, 1B). A similar, perhaps even more pronounced, enrichment at cohesin binding sites was also observed when a tagged Smc5-13myc protein was analyzed (Pearson's correlation coefficient (PCC) for Smc5-3V5 vs. Rec8 = 0.22, $p<10^{-15}$; Smc5-13myc vs. Rec8 = 0.43, $p<10^{-15}$; Figure S2). The enrichment of Smc5 at cohesin binding sites, centromeres, and telomeres is similar to the localization pattern previously described for Smc5/6 in vegetative cells [60]. However, in contrast to the mitotic distribution [60], neither we nor Xaver et al. [61] observed an increased density of Smc5/6 association sites along longer chromosomes during meiosis.

To determine whether the association of Smc5 with meiotic chromosomes depended upon DSB formation, we determined the binding profile in the absence of Spo11 (Figure 1B). Aside from a small overall reduction in binding, we observed no gross changes in the Smc5-3V5 distribution either at or between core sites in a *spo11Δ* strain (Figure 1B). This result is consistent with our observation that Smc5 immuno-staining on individual, spread meiotic nuclei is largely unaffected in the absence of Spo11 (Figure S1C), similar to that seen for Smc6 [54].

Some weaker binding sites also occurred in between the axis association sites defined by Rec8 (Figure 1A, lower panel). DSBs tend to occur in between the Rec8 axis association sites [62,63], and Smc5/6 is recruited to DSBs in mitotic cells [60,64]. Thus, we explored the idea that a fraction of Smc5/6 binds meiotic DSB sites. The locations of non-axis Smc5 association sites were determined by normalizing the Smc5 binding signal to the Rec8 signal (Figure 1C). This analysis revealed several additional binding sites along each chromosome (Figures 1C, S2). These weaker binding sites showed significant overlap with DSB sites (PCC = 0.28, $p<10^{-15}$; Figure 1C), mapped by single-stranded DNA that accumulates at DSB sites in *dmc1Δ* mutants [65,66]. Thus, Smc5/6 displays both a strong localization to chromosomal core sites and a weaker (perhaps more transient) localization to DSB sites. Several proteins involved in the formation and processing of meiotic DSBs localize to DSB hotspots even in the absence of DSB formation. Indeed, the Smc5 pattern, including DSB-correlated sites, is essentially unchanged in a *spo11* mutant (Figure 1C). This pattern is reminiscent of the binding profiles of Rec114 and other factors required for DSB formation, which are inferred to result from interaction of the DSB sites with the chromosome axes at the time of DSB formation [62,63]. We conclude that Smc5/6 associates with cohesin association sites, centromeres, as well as DSB hotspots, and that this association occurs mostly independently of DSB formation.

The strong enrichment of Smc5/6 at centromeres (the strongest cohesin binding sites in the genome) as well as DSBs were also observed for the Smc6 subunit in independent experiments by Xaver *et al.* (2013). Using ChIP-seq, they observed a small enrichment at cohesin association sites as well. The differences in the magnitude with which Smc5 (our study) or Smc6 (Xaver et al.) binds cohesin associated sites is likely due to the affinity tags being placed on different subunits of the complex. These may be differentially accessible to the antibodies and/or local DNA. It is unlikely that the enrichment of Smc5/6 that we observe in the ChIP experiments is non-specific, because the patterns are similar for both Smc5-3V5 and Smc5-13myc, which were immunoprecipitated with different antibodies and resins. Moreover, other DSB factors tagged with 13myc did not show any significant enrichment to cohesion binding sites by ChIP-chip (data not shown). Finally, consistent with a fraction of Smc5/6 binding to chromosomal axes, more than 50% of Smc5-13myc foci localize to the synaptonemal complex (central element component, Zip1) in our experiments (Figure S1B). This makes it highly unlikely that non-specific association of the antibodies with proteins or sequences at cohesin binding sites gives rise to false peaks.

Smc5/6 is required for chromosome separation following meiotic DSB formation

Smc5 localization at sites of meiotic DSBs, cohesin binding, and centromeres suggests possible roles for the Smc5/6 complex in meiotic recombination and chromosome morphogenesis. Since Smc5/6 is essential, its meiotic functions were studied by depleting the core component, Smc5, and the kleisin (Nse4) using the *CLB2* promoter, which is strongly repressed in meiosis [67] (Figure 2A). Meiosis-specific depletion circumvents the need for temperature-sensitive conditional alleles that require temperature-shift protocols, which may be complicated by the fact that several chromosomal processes are affected by temperature [20,68].

Strains carrying the P_{CLB2}-*SMC5* or P_{CLB2}-*NSE4* alleles (hereafter, *smc5* and *nse4*) had normal vegetative growth and were not sensitive to DNA damaging agents (data not shown). In meiosis, although bulk DNA replication and spindle pole body separation were essentially normal (Figure 2B,C), nuclear divisions were severely defective (Figure 2D). Time-lapse studies revealed that although nuclear divisions were attempted at both anaphase I and II, as soon as spindles disassembled, DNA bodies retracted into a single mass that subsequently failed to be encapsulated in the spores (Figure 2F,H; Movie S1, S2, S3). None of 30 randomly-selected cells imaged for either the *smc5* or *nse4* mutant managed to

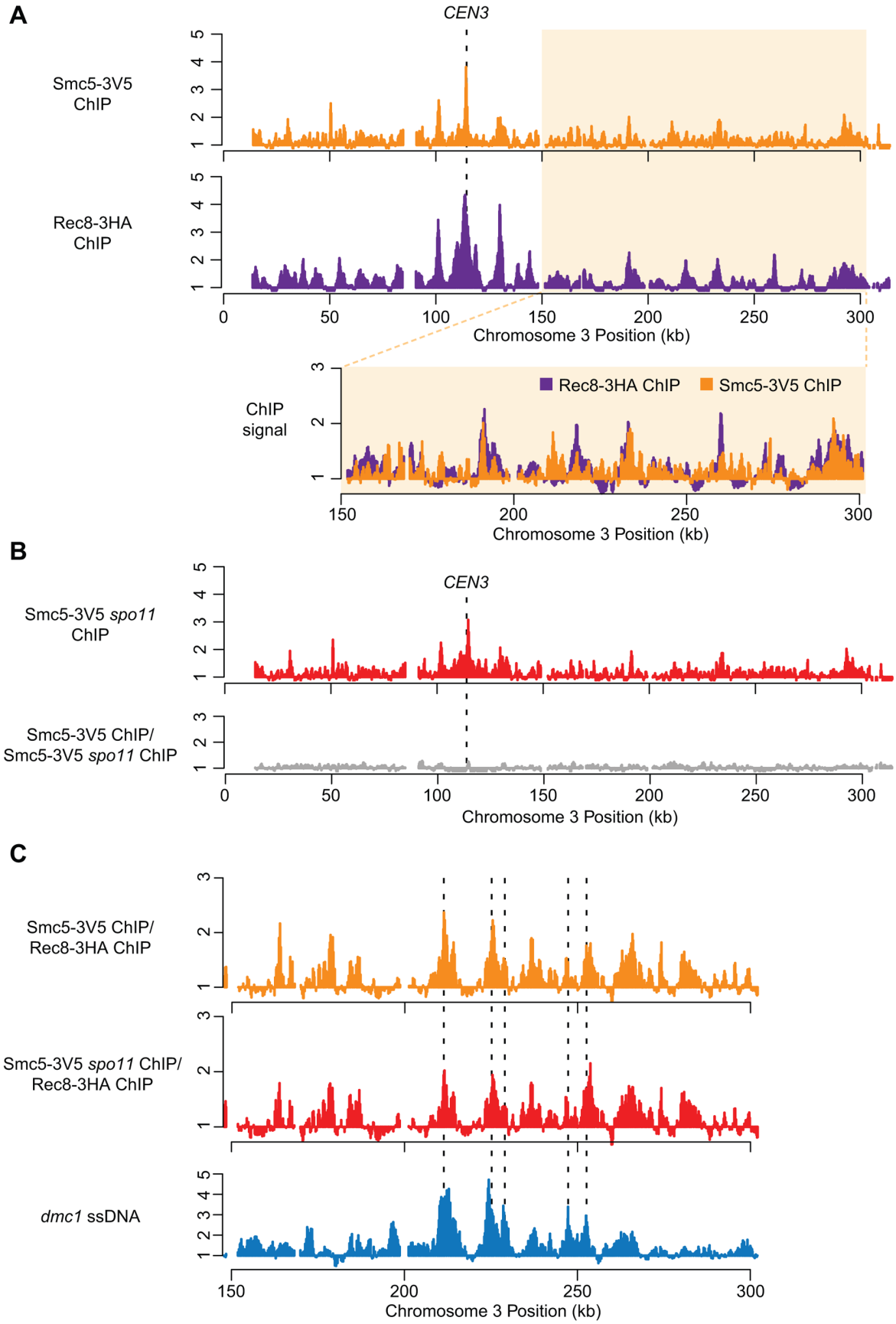
A
CEN3
Smc5-3V5 ChIP
Rec8-3HA ChIP
Chromosome 3 Position (kb)
ChIP signal
Rec8-3HA ChIP
Smc5-3V5 ChIP
B
CEN3
Smc5-3V5 spo11 ChIP
Smc5-3V5 ChIP/ Smc5-3V5 spo11 ChIP
Chromosome 3 Position (kb)
C
Smc5-3V5 ChIP/ Rec8-3HA ChIP
Smc5-3V5 spo11 ChIP/ Rec8-3HA ChIP
dmc1 ssDNA
Chromosome 3 Position (kb)

Figure 1. Smc5 associates with cohesin binding sites, centromeres, and DSBs. (A) DNA binding profiles for Smc5-3V5 (orange, H6671) and Rec8-3HA (purple, H4471, [65]) plotted for Chromosome III. Lower panel shows overlay of the right arm (150–300 kb) of Chromosome III. (B) DNA binding profiles for Smc5-3V5 in a *spo11Δ* strain (top panel, H6674) and the normalized DNA binding of Smc5-3V5 in *spo11Δ* strain versus Smc5-3V5 in the *SPO11* strain from (A) on Chromosome III. (C) The binding profile of Smc5-3V5 (orange) was normalized to Rec8-3HA binding using the data shown in (A) to reveal weaker, non-core binding regions. DSB sites mapped by ssDNA enrichment in the *dmc1*Δ mutant are indicated below (blue, H118, [100]). All ChIP experiments were carried out at 3 hours after transfer to SPM. Spindles reached their max. peak at 4 hours.
doi:10.1371/journal.pgen.1004071.g001

stably separate their DNA at the completion of meiosis I or II (Figure 2E). Micronuclei or fragmented nuclei as well as aberrant chromosomal morphologies were also observed (Figure 2E, arrows). Despite the severe nuclear separation defect, both the *smc5* and *nse4* mutants went on to complete meiosis and form asci with similar efficiencies to wild type (Figure 2F,G, ~90%). However, the failure to separate the DNA at meiosis I and II, prevented encapsulation of DNA into the spores (Figure 2H). This "meiotic catastrophe" was more pronounced for the *nse4* mutant compared to the *smc5*. This is likely due to more efficient depletion of Nse4, because when Smc5 was further depleted using an auxin-inducible degron fusion (P_{CLB2}-*SMC5-AID*, [69]), the nuclear separation defect became more severe and analogous to that seen in *nse4* cells (Figure 2F–H). We could not determine unequivocally that the P_{CLB2}-*SMC5-AID* was more depleted than P_{CLB2}-*SMC5*, since the depletion by P_{CLB2}-*SMC5* alone rendered Smc5 undetectable by Western blot (Figure 2A, data not shown). However, analysis of *SMC5-AID* (without *CLB2* depletion) demonstrated that auxin-induced degradation of Smc5 does occur, even when Smc5 is expressed at normal levels from its native promoter (Figure S3). Together, these experiments support the notion that the less severe meiotic catastrophe seen in the P_{CLB2}-*SMC5* cells relative to P_{CLB2}-*NSE4* is due to less efficient depletion of Smc5. However, they do not rule out the possibility that Nse4 has a function distinct from Smc5, perhaps acting as part of the Nse1-Nse3-Nse4 subcomplex [70].

To determine whether meiotic catastrophe required the initiation of recombination, we abolished the DSB activity of Spo11, using the catalytically-dead *spo11-Y135F* allele. This suppressed the nuclear separation defects of both *smc5* and *nse4* (Figure 3A). To address whether DNA damage or replication intermediates accumulated during pre-meiotic S-phase contribute to the nuclear separation defects of *smc5* and *nse4*, we converted meiosis I into a single mitosis-like division by de-protecting centromeric cohesin at anaphase I (*spo13*Δ), while simultaneously inactivating recombination (*spo11*Δ). No effect of *smc5* or *nse4* mutation on either dyad formation or spore viability was observed (Figure 3B,C). This experiment rules out the possibility that gross S-phase defects alone are responsible for the meiotic chromosome segregation failure in *smc5* and *nse4* mutants. Thus, depletion of Smc5/6 causes severe recombination-dependent meiotic catastrophe. This is in sharp contrast to the *smc6–9* temperature sensitive allele, which was previously shown to cause meiotic catastrophe independently of Spo11 [54].

Joint molecule metabolism is severely defective in *smc5/6* mutants

To investigate possible roles of Smc5/6 in meiotic DSB repair, we analysed meiotic recombination at the well-characterized *HIS4LEU2* recombination hotspot construct using a series of Southern blot assays [71,72] (Figure 4). Restriction site polymorphisms combined with 1D or 2D gel electrophoresis and Southern analysis allow formation of DSBs, crossovers, noncrossovers and several different species of joint molecules to be monitored at *HIS4LEU2*. Joint molecules include single-end invasions, double Holliday Junctions (formed between homologs or between sister chromatids) and multichromatid joint molecules (involving 3 or 4 chromatids) [10,71,72].

In wild-type cells, joint molecule levels peaked around 4.5 hours, at ~3% of hybridizing DNA, and disappeared by 8 hrs, when the majority of cells had completed the meiotic divisions (Figure 5A, C). In contrast, joint molecules in the *smc5* mutant appeared with normal timing but persisted at high levels (4.7%) until at least 9 hrs. The *nse4* mutant had a much more severe defect in joint molecule resolution, with very high levels of joint molecules (10%) persisting at 13 hrs (Figure 5C), when wild type cells have completed the meiotic divisions (Figure 2D). The level of unresolved joint molecules detected in the *nse4* mutant is at least 3-fold higher than any other single mutant analyzed to date and is reminiscent of mutants that simultaneously lack multiple joint molecule resolution or dissolution activities [13,14,33].

Closer inspection of both the intersister- and interhomolog-dHJ signals revealed additional spots or smears (Figure 5B). In the 1st dimension, these new signals migrated ahead of the main dHJ spots, suggesting a lower molecular weight. In contrast, the signals were retarded in the 2nd dimension relative to the main dHJ spots. It is currently unclear whether these JM species are extreme variants of dHJs (e.g. with very widely spaced Holliday junctions) or aberrant structures that are never formed in wild type. Regardless, their existence indicates that JM formation as well as resolution is altered in *smc5* and *nse4* mutants.

In contrast to joint molecules, the appearance, disappearance, and resection of DSBs in *smc5* and *nse4* mutants occurred with largely wild-type kinetics (Figure 5D, Figure S4, S5). These observations suggest that the initiation of recombination occurs without any significant defects and that *smc5/6*-depleted cells are specifically defective in steps leading to the formation and resolution of joint molecules.

Crossover formation was delayed and final levels were reduced by 20–30% in *smc5* and *nse4* mutants. Crossovers accumulated to 22% of the DNA signal in wild type, while *nse4* and *smc5* mutants formed, respectively, 15% and 17% (Figure 5D and E, S4B). The double mutant (*smc5 nse4*) was indistinguishable from the *nse4* single mutant (Figure S4).

smc5 and *nse4* mutants accumulate joint molecules between homologs, sister chromatids, and multiple chromatids

To understand whether *smc5/6* mutants accumulate a specific class of joint molecules, we separately quantified the levels of single-end invasions (SEIs), double Holliday Junctions (dHJs), and multi-chromatid joint molecules (mcJMs) using 2D gels (Figure 5C). Compared to the wild type, the *smc5* mutant showed slightly elevated levels of all joint molecule species and delayed disappearance. In the *nse4* mutant, all classes of joint molecule accumulated to higher levels than wild type and remained elevated throughout the meiotic time course (Figure 5C). We infer that Smc5/6 plays a general role in joint molecule metabolism.

Homolog bias is decreased in the *smc5* and *nse4* mutants

Our observations that *smc5* and *nse4* mutants accumulate unresolved joint molecules while still forming high levels of

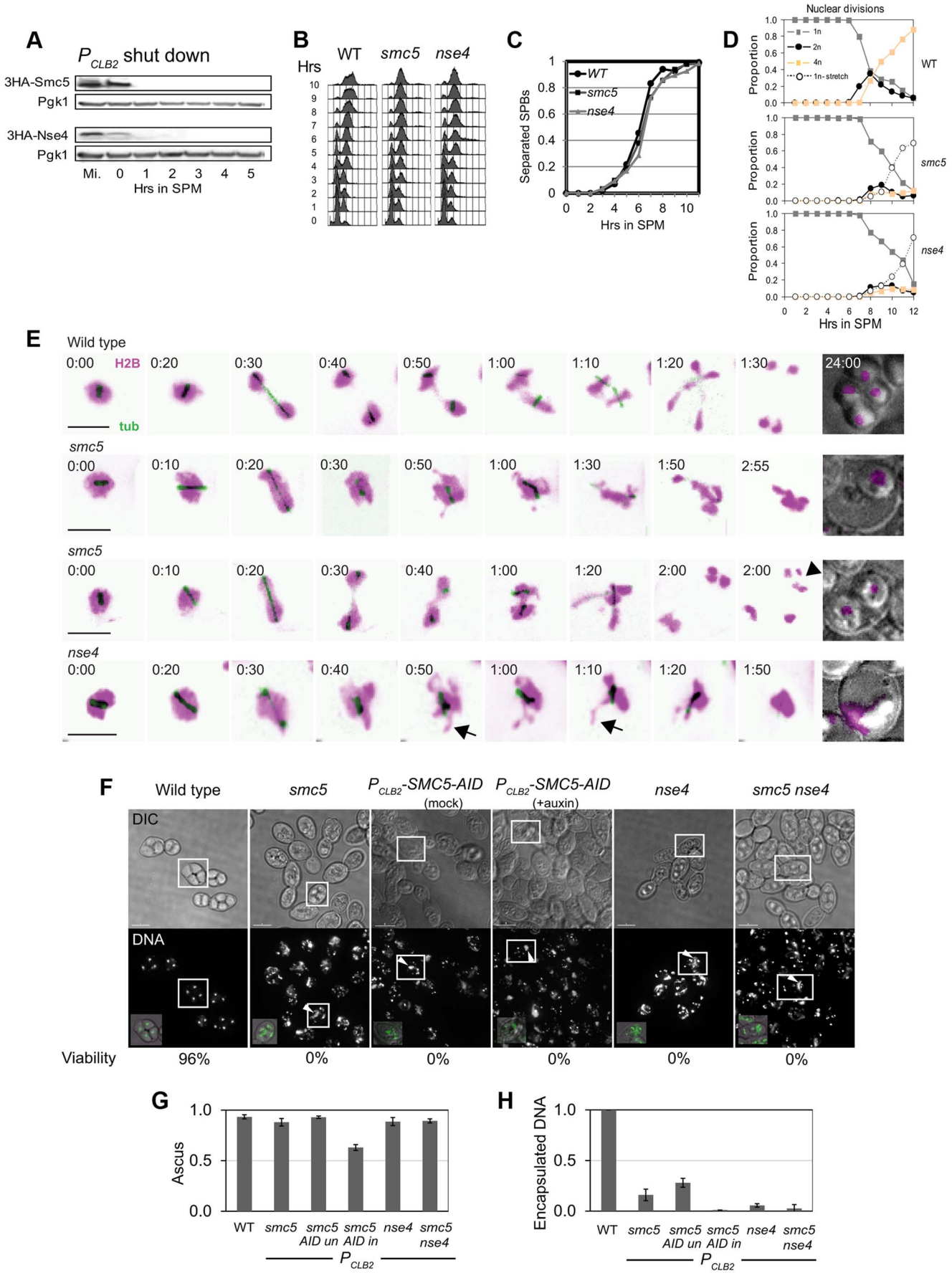
A
P_{CLB2} shut down
3HA-Smc5
Pgk1
3HA-Nse4
Pgk1
Mi. 0 1 2 3 4 5
Hrs in SPM
B
Hrs
WT smc5 nse4
C
Separated SPBs
WT
smc5
nse4
Hrs in SPM
D
Nuclear divisions
1n
2n
4n
1n-stretch
Proportion
WT
smc5
nse4
Hrs in SPM
E
Wild type
H2B
tub
smc5
smc5
nse4
F
Wild type
smc5
P_{CLB2}-SMC5-AID (mock)
P_{CLB2}-SMC5-AID (+auxin)
nse4
smc5 nse4
DIC
DNA
Viability
96% 0% 0% 0% 0% 0%
G
Ascus
WT smc5 smc5 AID un smc5 AID in nse4 smc5 nse4
P_{CLB2}
H
Encapsulated DNA
WT smc5 smc5 AID un smc5 AID in nse4 smc5 nse4
P_{CLB2}

Figure 2. Meiotic depletion of Smc5 or Nse4 leads to meiotic catastrophe. (A) Western blot of depletion of 3HA-Smc5 (Y941) and 3HA-Nse4 (Y942) protein levels under the P_{CLB2} promoter. Mutants are referred to as *smc5* and *nse4* throughout. (B) FACS analysis of S-phase progression in wild type (Y940), *smc5* (Y941) and *nse4* (Y942) mutants. (C) Population kinetics of spindle pole body separation (n = 200 *per* time point). (D) Population kinetics of nuclear divisions (n = 200 *per* time point). (E) Montage of time series of nuclear divisions and spindle dynamics from representative time-lapse movies. H2B-mCherry and Tub1-GFP are pseudo-coloured in magenta and green, respectively. Maximum projections are shown. Bars: 4 μm. Full movies are available as Supplemental Movies S1 to S4. Arrows indicate examples of nuclear spikes and arrowheads show fragmentation/micronuclei. Strains: WT (Y3606), *smc5* (Y3627), *nse4* (Y3630). (F) DNA encapsulation failure in *smc5* and *nse4* mutants. Upper panel DIC, lower panel, DAPI (DNA). The boxed asci are shown with DNA (green) overlaid in the insets in the lower panel, bottom left. Note that the samples are taken from different time points in the various strains. Bars, 5 μm. (G) Proportion of cells completing meiosis and forming an ascus (di-tyrosine fluorescence). (H) Proportion of asci with encapsulated DNA (bottom). All data were collected after 24 hours in liquid sporulation medium. Three independent diploids were assessed for each genotype (standard deviations are shown). Strains: WT (Y1381), *smc5* (Y2705), P_{CLB2}-*SMC5-AID* (Y3252), *nse4* (Y2704), *smc5 nse4* (Y3185).
doi:10.1371/journal.pgen.1004071.g002

crossovers raise the possibility that more total joint molecules are made in these mutants. To address this question, we used the resolution-defective *ndt80*Δ mutant to quantify joint molecule formation independently of changes in the efficiency of resolution [6,8]. In both *ndt80*Δ and *ndt80*Δ *nse4*, total accumulated joint molecules plateaued at similar levels and with essentially identical kinetics (~15%, Figure 5C, lower panel *ndt80*). However, intersister dHJs and multichromatid JMs were increased at the expense of interhomolog dHJs when compared to the *ndt80*Δ mutant alone (Figure 5C; lower panel *ndt80*). Consistently, the ratio of interhomolog dHJs to intersister dHJs ("interhomolog bias") was decreased from 4:1 (4.1±0.5) in the *ndt80*Δ strain, to 2:1 in both mutants (1.9±0.3 and 1.7±0.2 in *smc5 ndt80*Δ and *nse4 ndt80*Δ, respectively; Figure 5C and data shown not). Similarly, when *NDT80* was present, the IH:IS dHJs ratio was also decreased from a steady-state ratio of ~3.5±0.4 in wild type to 2.1±0.2 in *smc5* and 2.1±0.2 in *nse4* ($P<0.01$; Figure 5C). We conclude that overall JM levels are not significantly altered by depletion of Smc5/6, but the spectrum of JMs is altered such that intersister and multichromatid joint molecules are increased at the expense of interhomolog dHJs. Similar conclusions have been reached by two other labs [61,73].

Combined depletion of *sgs1* and *smc5/nse4* synergistically increases joint molecule accumulation

In budding yeast meiosis, Sgs1 helicase is a central regulator of meiotic recombination intermediates during meiotic prophase [10–14]. Similar to *smc5* and *nse4* strains, *sgs1* mutants form more multichromatid and intersister JMs, but fewer interhomolog dHJs [10]. However, unlike *smc5* and *nse4*, joint molecule resolution and chromosome segregation occur efficiently in *sgs1* cells. To examine the relationship between Smc5/6 and Sgs1, we combined *smc5* or *nse4* depletion mutants with meiosis-specific depletion of Sgs1 (P_{CLB2}-*3HA-SGS1*, hereafter *sgs1*). Both crossover and noncrossover formation were synergistically decreased in the *smc5 sgs1* and *nse4 sgs1* double mutants (Figure 6A and data not shown). On their own, *smc5*, *nse4*, and *sgs1* single mutants exhibited, respectively, 1.5%, 13%, and 0.6% joint molecules at time points when cells had completed meiosis (13 h; Figure 6A and data not shown). In both the *smc5 sgs1* and *nse4 sgs1* double mutants, we observed synergistic increases in all species of joint molecules, which accumulated to 14% and 20%, respectively (Figure 6A and data not shown). This level of accumulation of joint molecules is similar to that seen when both Sgs1 helicase and structure-specific endonucleases (Mus81-Mms, Slx1–Slx4, and Yen1) are lacking (~20%, [13,14]). Given that crossover and noncrossover levels are high in the *smc5* and *nse4* strains (Figure 5E, 6B), we infer that Sgs1 can still function proficiently to promote crossovers and noncrossovers when Smc5/6 is depleted.

Absence of MutLγ diminishes crossing over in the *nse4* mutant

MutLγ is inferred to be an endonuclease that specifically promotes the resolution of dHJs into crossovers along the MutSγ pathway for crossing over [17,22,23,74]. To test whether the crossovers formed in *smc5/6* mutants are formed via this pathway, we deleted *MLH3* in the *smc5* and *nse4* mutants. Although the *mlh3*Δ mutation alone caused a substantial decrease in crossovers (compare 18%±0.5% in wild type to 8.2%±0.2% in the *mlh3*Δ; Figure 6D), crossing-over in the double mutants was further decreased (4.5±0.5% for *smc5 mlh3*Δ and 4.4%±0.2% for *nse4 mlh3*Δ; Figure 6D; data not shown for *smc5*). Importantly, noncrossovers were unaffected, consistent with the notion that MutLγ predominantly yields crossovers [23,75]. We infer that MutLγ is active and responsible for most crossovers in *smc5/6* mutants.

Zip3 foci are increased in *smc5* and *nse4* mutants and synapsis occurs with wild-type kinetics

MutLγ promotes crossovers in conjunction with MutSγ, which in turn interacts with and requires Zip3, for its association with meiotic chromosomes (reviewed in [76]). Zip3 associates in a punctate pattern with meiotic chromosomes at axial association sites, where homolog synapsis initiates and where crossovers will form [2,77]. We reasoned that if MutLγ and MutSγ are active in the *smc5* and *nse4* mutants, then Zip3 localization along meiotic chromosomes as well as synapsis should occur with normal proficiency. To assess whether this was the case, we detected a GFP-tagged Zip3 and co-stained for the synaptonemal complex protein, Zip1 (Figure 6E). In the wild type, we observed ~30 Zip3-GFP foci in pachytene nuclei; this number was increased 1.2–1.3-fold in the *smc5* and *nse4* mutants (Figure 6F). This increase was similar in magnitude to that observed in an Sgs1-depleted strain (Figure 6F) [78].

Zip3 promotes the assembly of the synaptonemal complexes (SC). No significant differences were observed in the kinetics of SC assembly and disassembly, including turnover of Zip1 protein, in the *smc5* and *nse4* when compared to the wild type (Figure S6). Thus, early steps in MutSγ-dependent crossover formation and initiation of synapsis are not adversely affected by depletion of Smc5/6.

Smc5/6 affects Mus81-Mms4-dependent joint molecule resolution

Our results further distinguish phenotypes observed for Smc5/6 from those of Sgs1: Smc5/6 depletion does not suppress the crossover defect of MutLγ, unlike that seen in *sgs1 mlh3*Δ mutants [10]. These phenotypes could be explained if Smc5/6 has additional roles in joint molecule resolution via the Mus81-Mms4 endonuclease, which becomes essential for resolution in *sgs1* mutants [11,12].

To determine whether Smc5/6 affects the functions of structure-selective endonucleases during meiosis, we deleted *MMS4* (*mms4*), the regulatory subunit of Mus81, and also the two cryptic endonucleases Yen1 and Slx1–Slx4 [79]. Yen1 and

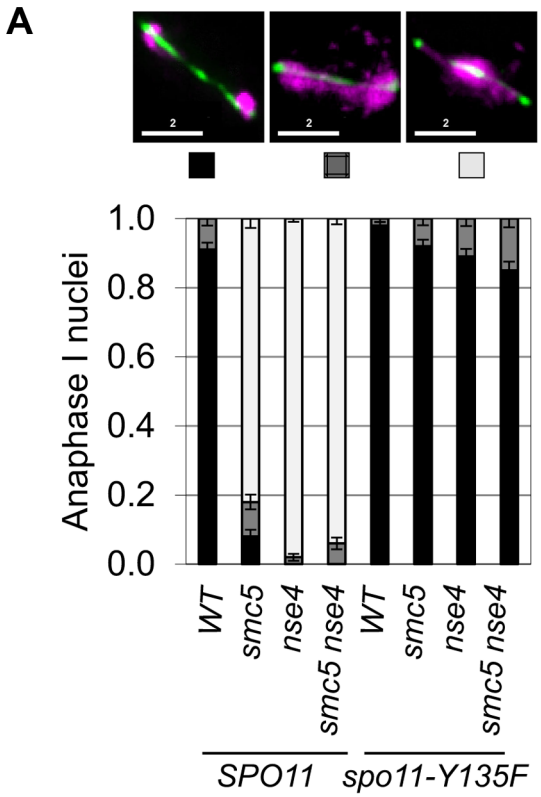

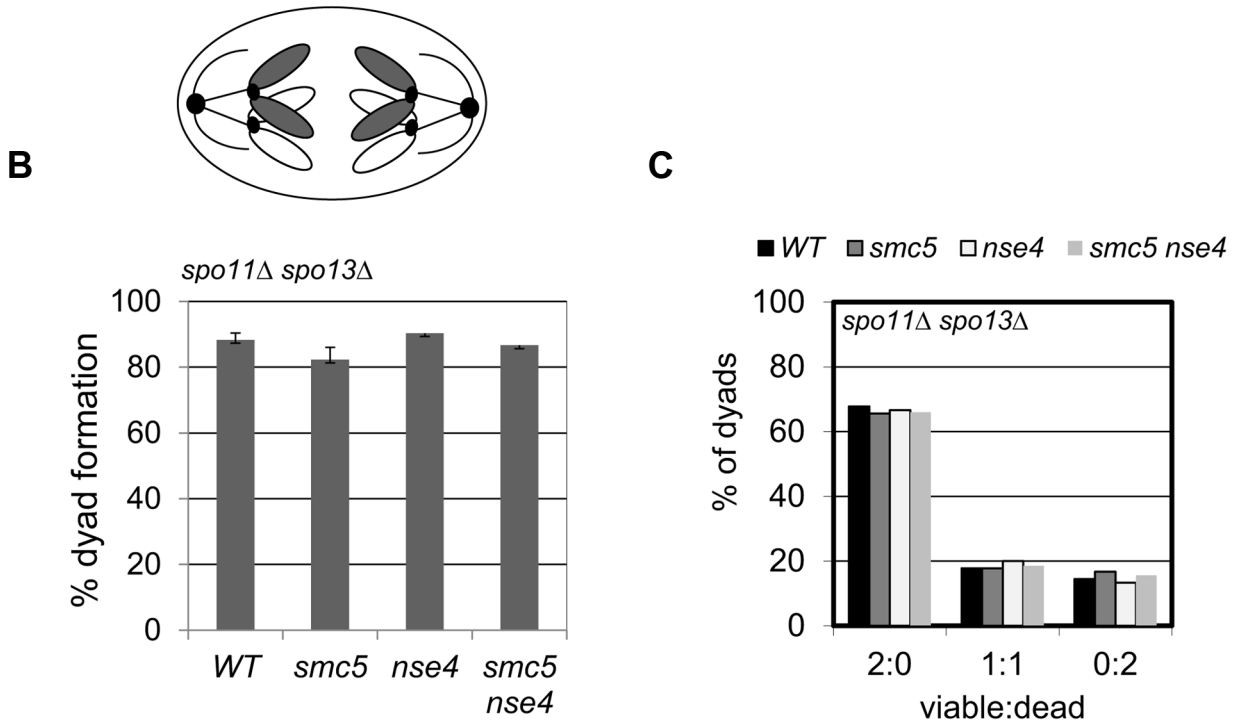

Figure 3. Meiotic depletion of Smc5 and Nse4 leads to Spo11-dependent nuclear separation defects in meiosis. (A) Catalytic-dead Spo11 mutation rescues nuclear separation at anaphase I in the Smc5/6 mutants (n≥100). Bars indicate standard error bars for a proportion. Strains: WT (Y1381), *smc5* (Y2705), *nse4* (Y2704), *smc5 nse4* (Y3185), *spo11-Y135F* (Y3147), *spo11-Y135F smc5* (Y3150), *spo11-Y135F nse4* (Y3153), *spo11-Y135F smc5 nse4* (Y4202). (B and C) Schematic of sister chromatid segregation at meiosis I in *spo11*Δ *spo13*Δ mutants. Dyad formation and viability after 24 hours in sporulation medium of Smc5/6 mutants in conjunction with the *spo11*Δ *spo13*Δ bypass. Strains: *spo11*Δ *spo13*Δ (Y2816), *spo11*Δ *spo13*Δ *smc5* (Y2846), and *spo11*Δ *spo13*Δ *nse4* (Y2848).
doi:10.1371/journal.pgen.1004071.g003

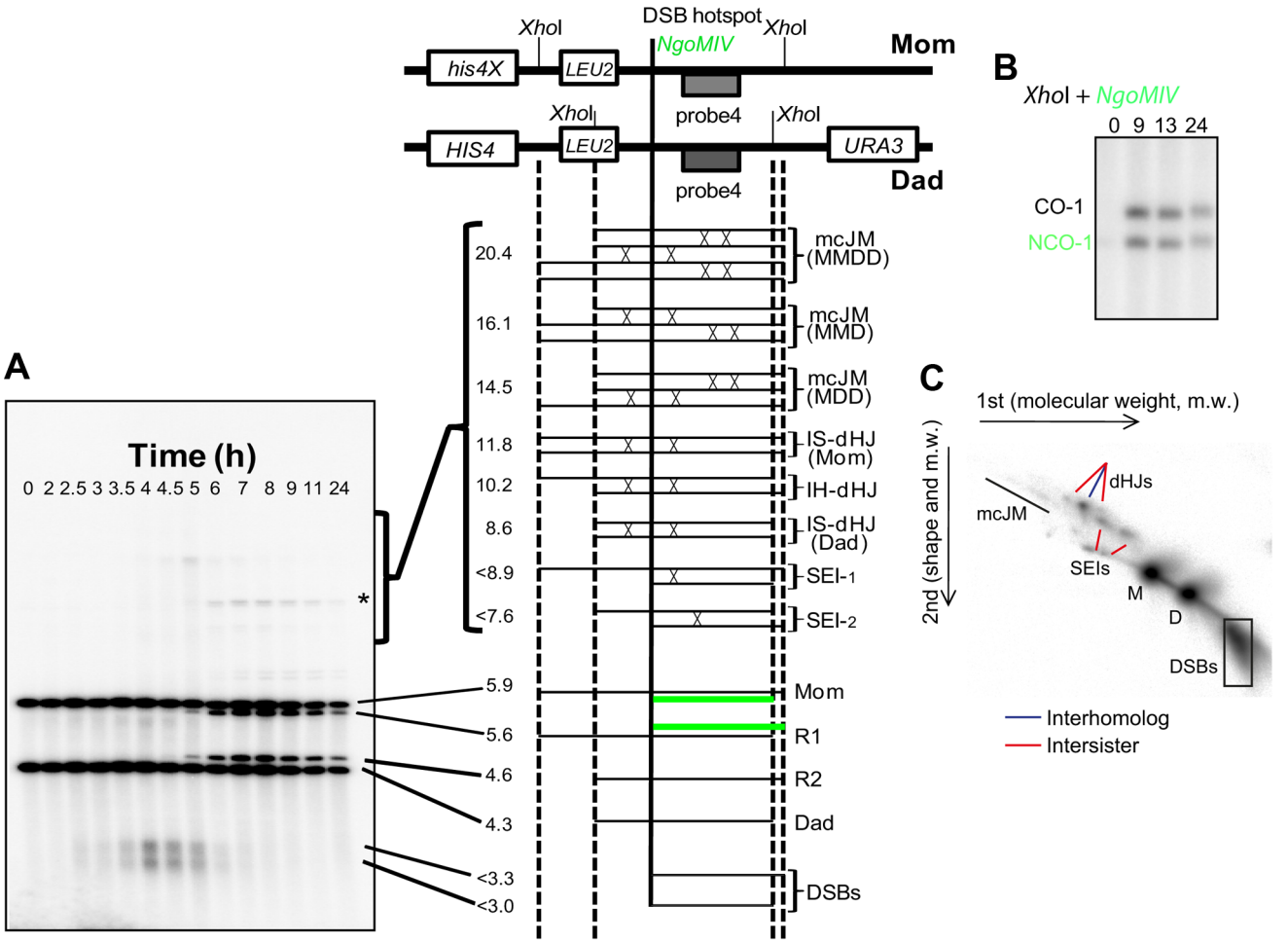

Figure 4. Assessment of meiotic recombination at the *HIS4LEU2* hotspot. (A–C) The *HIS4LEU2* hotspot. mcJM: multichromatid joint molecules (abbreviations: M-Mom, D-Dad), IS-dHJ intersister double Holliday Junctions, IH-dHJ interhomolog double Holliday Junctions, SEI- single-end invasions, DSBs- double strand breaks. Digesting with *Xho*I gives diagnostic band sizes from parental molecules, Mom and Dad, as well as recombinant fragment lengths (R1 and R2). These are predominantly crossovers. The different molecules can be separated on 1D (A) and shape-dependent separation on 2D gels (C). Further digestion with *NgoMIV* differentiates noncrossovers from parental molecules (B). The * indicates a non-specific signal.
doi:10.1371/journal.pgen.1004071.g004

Slxl–Slx4 have only minor, if any, roles in joint molecule resolution in otherwise wild-type cells [13,14,33].

Crossover levels were roughly similar in the *mms4 yen1 slx4* mutant (11±0.4%), *smc5* (12%±0.7%) and *nse4* (14.5±1.7%) mutants (Figure 7A,B and data not shown). The *nse4 mms4 yen1 slx4* quadruple mutant had a further reduction in the levels of crossovers (7.4±0.7%; Figure 7A,B). Noncrossovers were also further decreased in the *nse4 mms4 yen1 slx4* quadruple mutant. In the wild type, the noncrossover signal contributed 2.4±0.1%, compared to 2.1±0.1% in the *nse4* mutant, 1.6±0.3% in the *mms4 yen1 slx4* mutant and 1.3±0.1% in *nse4 mms4 yen1 slx4* quadruple mutant (Figure 7A,B).

At least two reasons could account for the further loss of crossover and noncrossover products in the *nse4 mms4 yen1 slx4* quadruple mutant. Smc5/6 could promote joint molecule resolution in parallel with one or more of the three endonucleases. Alternatively, the formation of joint molecules leading to crossovers and noncrossovers could be perturbed. Analysis of joint molecules in the *nse4 mms4 yen1 slx4* cells lends support to the latter possibility (Figure 7C). The *nse4 mms4 yen1 slx4* mutant displayed a further decrease in the IH:IS dHJ ratio (1:1) compared to the *nse4* single and *mms4 yen1 slx4* triple mutants (2:1). This indicates that Smc5/6 operates in parallel with the resolvases to promote interhomolog template bias (Figure 7C). Assuming a direct relationship between interhomolog-dHJs and the generation of interhomolog products (crossover and noncrossover), the decreased IH:IS bias (50%) in the *nse4 mms4 yen1 slx4* mutant would be predicted to lead to a loss of half the crossovers (predicted 7.3% crossover products based on the 14.5% crossovers seen in the *nse4* mutant). The observed value of 7.4% crossovers (Figure 7B) is in good agreement with this. The additive reduction of interhomolog bias in the *nse4* and *mms4 yen1 slx4* mutants is therefore sufficient to explain the further decreases in crossover and noncrossover levels seen in the *nse4 mms4 yen1 slx4* quadruple mutant.

To further address which endonuclease was affected by Smc5/6, we focussed upon analysing the genetic interaction with Mus81-Mms4 (Figure 7D, E). Crossover levels (Figure 7E) as well as the IH:IS dHJ ratios (Figure 7D) were similar in the *mms4*, *nse4*, and *nse4 mms4* mutants. These observations show that abolishing Mus81-Mms4 activity has little consequence for joint molecule resolution at least when Smc5/6 is depleted. Moreover, crossover

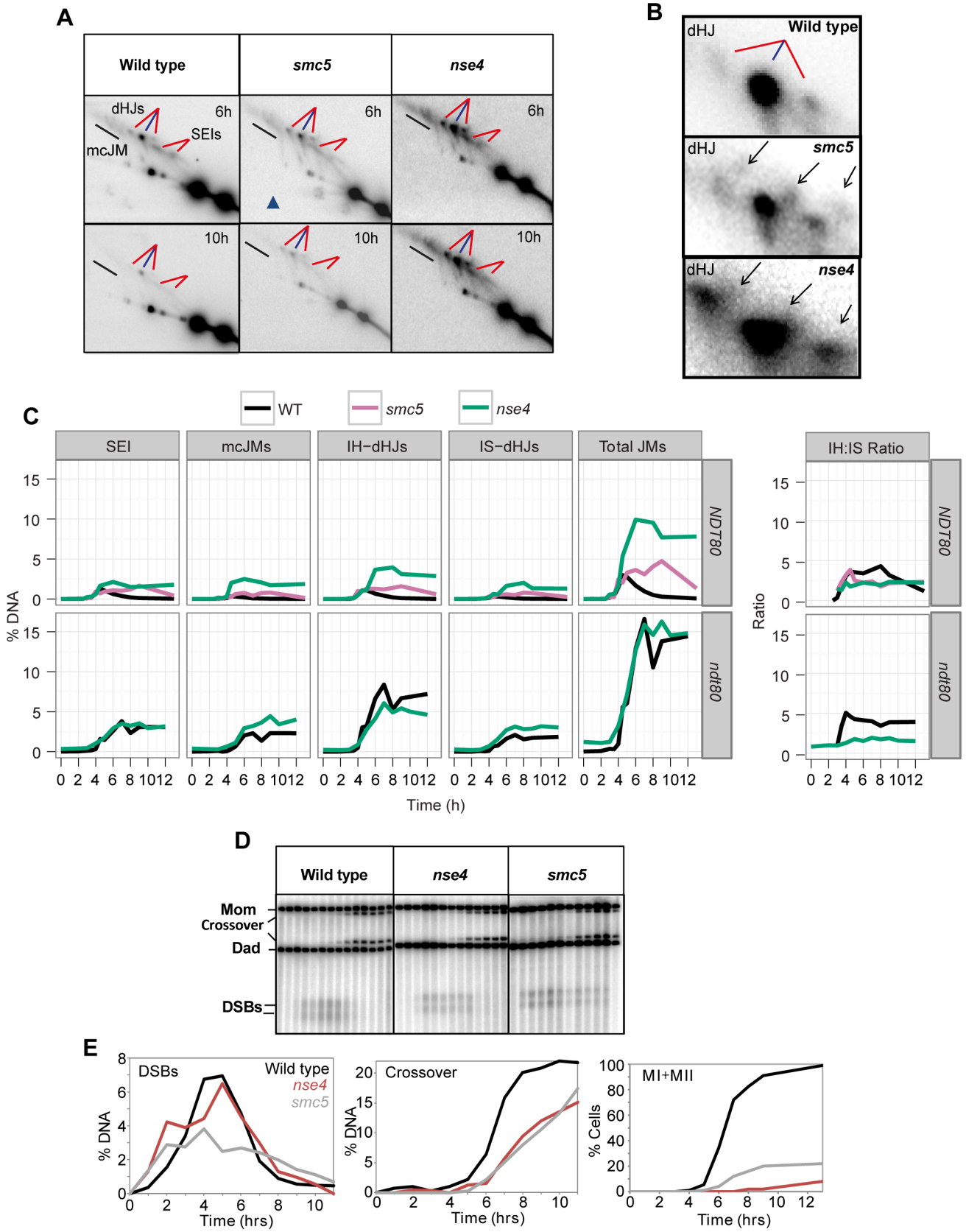

Figure 5. Aberrant joint molecules accumulate in *smc5* and *nse4* mutants. (A) Examples of time courses from 2D gels. Blue lines point at joint molecules formed between homologous chromosomes (interhomolog, IH) and red lines indicate joint molecules composed of sister chromatids (intersister, IS). Strains: WT (Y2976), *smc5* (Y1211), *nse4* (Y1212). (B) Enlarged dHJ spots from wild type, *smc5*, and *nse4*. (C) Smoothed levels of single

end invasions (SEIs), multichromatid joint molecules (mcJMs), interhomolog-double Holliday Junctions (IH-dHJs), intersister-double Holliday Junctions (IS-dHJs), IH-dHJ to IS-dHJ (IH:IS) ratio, and total joint molecules (Total JMs). Cumulative levels of recombination were assessed in the *ndt80*Δ background (lower panel). Strains: *ndt80* (Y3025), *ndt80 nse4* (Y3843). (D) Examples of time course analyses of double-strand break and crossover formation. (E) Quantification of DSB, crossover, MI+MII nuclear divisions.
doi:10.1371/journal.pgen.1004071.g005

levels were substantially higher in the *nse4 mms4* mutant compared to the *nse4 mms4 yen1 slx4* quadruple mutant, which suggests that Yen1, or more likely, Slx1–Slx4 promotes a significant amount of crossing over, presumably via a function that promotes inter-homolog bias (Figure 7C).

In contrast to the effect of depleting Sgs1 in the *nse4* mutant background, the level of unresolved joint molecules did not increase in the *nse4 mms4 yen1 slx4* quadruple mutant, but instead decreased (compare 4.3±0.6% to 12.9±2.4% in the *nse4* single mutant; Figure 7B). This was also the case for the *nse4 mms4* mutant (6.6% unresolved joint molecules; Figure 7E). We interpret there results to mean that when Smc5/6 is depleted, the Mus81-Mms4 endonuclease renders a significant proportion of joint molecules non-cleavable by Sgs1 and/or MutLγ.

Association of Mus81 with meiotic chromosomes is defective in *smc5* and *nse4* mutants

To investigate whether chromosomal localization of Mus81-Mms4 was affected in the *smc5* and *nse4* mutants, we assessed the ability of Mus81-9myc to form foci on spread, meiotic chromosomes at pachytene, when joint molecules reach their highest levels. Pachytene-stage nuclei were selected by virtue of linear staining of the synaptonemal complex component, Zip1, and the numbers of Mus81 foci were counted. In the wild type, the majority of pachytene nuclei contained more than 20 distinct foci of Mus81. In contrast, the majority of nuclei from the *smc5* and *nse4* mutants had no distinct Mus81 foci (Figure 7F,G). We ruled out that this was due to reduced levels of Mus81-Mms4 protein or failure to hyperactivate Mus81-Mms4 upon exit from pachytene (Figure S7). These observations imply that the ability of Mus81 to associate with or be stabilized on meiotic chromosomes is diminished when Smc5/6 complexes are depleted.

Smc5/6 mutants progress into the meiotic divisions with high levels of γH2A foci

Our observations imply that unresolved joint molecules in the *smc5* and *nse4* cells cause severe failure of chromosome segregation during anaphase I and II and, ultimately, meiotic catastrophe (Figure 2). This recombination-dependent meiotic catastrophe hypothesis makes at least two predictions. First, the cell cycle should occur with similar timing in the mutant and wild-type strains and, second, individual meiotic nuclei should show increased DNA damage at anaphase I and anaphase II, when cells are attempting to divide their nuclei.

To test these predictions, we monitored markers for early prophase I, exit from prophase I, and entry into meiosis II, which allowed us to calculate and thus compare transit times in the wild type to Smc5/6-depleted cells. Induction of the meiotic DNA damage response (DDR), monitored by the Mec1/ATR-dependent phosphorylation of HORMA-domain protein, Hop1, and γH2A [80,81] occurred with similar timing, 3–4 hours after transfer to sporulation medium (Figure 8A). Spindle pole body separation, a marker for pachytene exit, and indeed spindle formation both occurred with relatively normal timing in the two mutants compared to wild type (Figure 8A). Consistent with this, the timing of Cdc5 and Clb1 expression, both under the regulation of the Ndt80 transcription factor that facilitates pachytene exit [67], were also similar in all three strains. These results suggest that exit from pachytene occurred with similar timing in the *smc5* and *nse4* mutants compared to the wild type strain.

To follow M-phase events, we assessed steady-state levels of Rec8 and Pds1, the securin orthologue in budding yeast. Degradation of both occur at the onset of anaphase I and anaphase II. Rec8 and Pds1 degradation occurred around 7 hours in all three strains and the second wave of Pds1 degradation (anaphase II onset) was observed in both wild type and *smc5* (Figure 8B). The *nse4* time course was presumably less synchronous such that the second wave of Pds1 and Rec8 degradation was not detected [82]. To assess meiosis II entry, we used the B-type cyclin, Clb3. In all three strains, Clb3 expression appeared at similar times (Figure 8A). Collectively, these observations strongly support the notion that the meiotic progression is not significantly delayed or arrested in Smc5/6-depleted cells.

The population kinetics of γH2A suggest that *smc5* and *nse4* mutants undergo meiotic catastrophe with damaged DNA. In the wild-type, γH2A disappeared by 7–8 hours, whereas it remained high in the two mutant strains, even at 12 hours when meiosis was completed (Figure 8A, and data not shown). Consistent with this analysis, immunostaining for γH2A foci in combination with tubulin revealed meiosis I and meiosis II cells that also contained an increased number of γH2A foci (Figure 8C,D). In the wild type, cells with anaphase I spindles showed confluent, low intensity background γH2A staining as well as a few punctate foci (median: 3 foci). In contrast, analogous nuclei from both *smc5* and *nse4* mutants contained large numbers of γH2A foci, many of which were located off the main body of DNA (Figure 8C), suggestive of perturbed DNA/chromatin structure. Furthermore, in nuclei with meiosis II spindles, 5% of *smc5* and 42% of *nse4* nuclei (n = 50) contained punctate γH2A staining (Figure 8D). The lower number of γH2A-positive staining anaphase II nuclei in the *smc5* mutant presumably reflects the lower level of unresolved joint molecules relative to *nse4* (Figure 5). Collectively, these data indicate that *smc5/smc6* mutants progress through the meiotic divisions with elevated levels of γH2A.

Finally, we investigated whether *smc5* and *nse4* mutants are deficient in maintaining the DDR-induced meiotic arrest that occur in mutants, where high levels of single-stranded DNA accumulate (*dmc1Δ*, *rec8Δ*, and *hop2Δ*) [83]. Depletion of Smc5 or Nse4 had no effect on the meiotic progression in any of these mutants (Figure 8E). Combining the *dmc1Δ nse4* or *hop2Δ nse4* mutants with *fpr3Δ*, which is required for checkpoint maintenance [84], resulted in high levels of checkpoint bypass (Figure 8E). These data demonstrate that *smc5* and *nse4* mutants are checkpoint proficient and that the progression into the meiotic nuclear divisions with unresolved joint molecules is unlikely to be caused by defective DDR maintenance.

Meiotic cohesin is mis-regulated in *smc5* and *nse4* mutants

Unresolved joint molecules are inferred to impede chromosome separation in cells undergoing the meiotic divisions [11,12]. However, cleavage of cohesin by separase is also essential for chromosome disjunction [85]. Smc5/6 localizes to cohesin-binding sites (Figure 1) and in *S. pombe*, *smc5/6* mutants show increased retention of cohesin during mitosis that contributes to chromosome segregation defects [86,87]. These considerations led

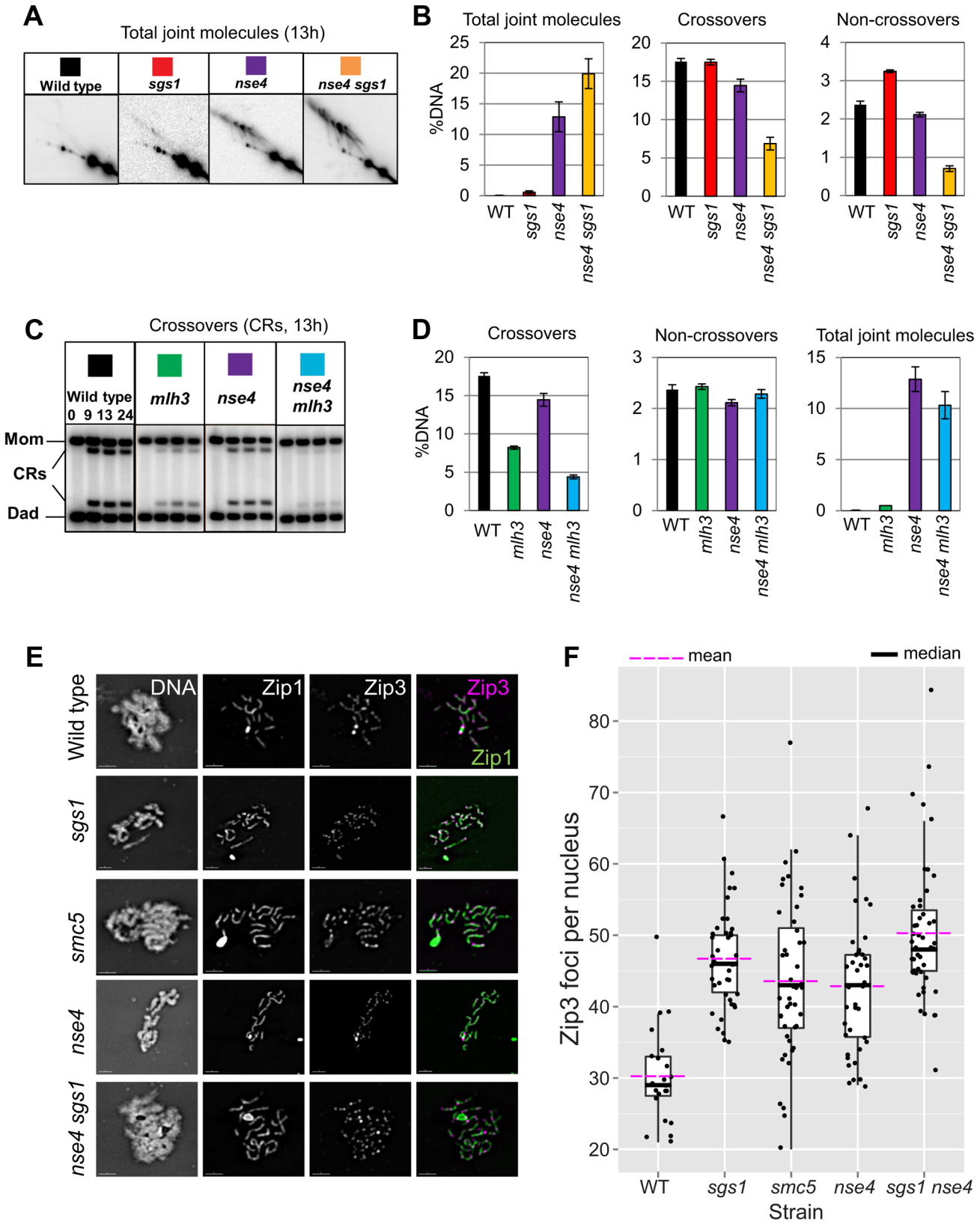

Figure 6. Sgs1 and MutLγ are functional in *smc5/6*. (A) Representative images of 2D analysis from *sgs1* mutant (P_{CLB2}-*3HA-SGS1*) in combination with *nse4*. (B) Quantification of total joint molecules, crossovers and non-crossovers, and total joint molecule levels at meiotic endpoints (13 hours). Quantification from three independent diploids; error bars represent the standard deviation. (C) Representative images of crossover formation in *mlh3*Δ mutants, in combination with *nse4*. (D) Quantification of crossovers, noncrossovers, and total joint molecules levels from three independent diploids (13 hours). (E,F) Analysis of Zip3 foci. Representative images and Tukey-Kramer box-and-whisker plot of 30 nuclei from each strain (boxes

represent the 25th–75th percentile; the median value is denoted by the horizontal bar, and the whiskers are 1.5× the 25–75th percentile or max or min. values- whichever are the lowest). Fold increase in Zip3-GFP foci relative to wild type was calculated based on the arithmetic mean (horizontal bar, magenta). Note that the Zip3-GFP causes some polycomplex formation of Zip1 predominantly in the mutants but also in the wild type. The distributions of all four mutant strains were significantly different from wild type ($p<0.01$, Kruskall-Wallace). Strains: WT (Y1435), *sgs1* (Y3591), *smc5* (Y3514), *nse4* (Y3511), *sgs1 nse4* (Y3636).
doi:10.1371/journal.pgen.1004071.g006

us to evaluate whether cohesin was mis-regulated in meiosis. To this end, we analysed Rec8-GFP dynamics in time-lapse studies [88]. Using Pds1-tdTomato as a marker for anaphase I entry (Figure 9A), cohesin removal along chromosome arms was completed in 14.2 (±5.7) minutes in wild type (n = 30; Figure 9A & B, Movies S4, S5, S6, S7). There was little or no delay in the *smc5* cells and a slight but significant delay in the *nse4* mutant (Figure 9C, Mann-Whitney $p<0.01$). Assessment of retention of cohesin in spread nuclei confirmed that the cohesin was associated with meiotic chromosomes (Figure S8). Moreover, we also observed *smc5* nuclei at anaphase II with significant cohesin staining (Figure S8B). It is likely that this residual cohesin that we detect with antibodies but not live cell imaging in the *smc5* mutant, reflect relatively low levels of retained cohesin that cannot be detected due to the decreased sensitivity of live cell imaging.

To address whether the delayed removal of cohesin relative to the nuclear divisions contributed towards the severe chromosome segregation defects of the *smc5/6* mutants, we engineered a TEV protease cleavage site into Rec8 (in addition to the two separase cleavage sites) and expressed TEV protease around anaphase I onset (Figure 10A–D). We observed small improvements in chromosome segregation at anaphase I in both strains, with a more pronounced effect in *smc5* (Figure 10F, G). However, the contribution of the persistent cohesin towards the severe meiotic catastrophe is likely relatively small compared to the failure to remove joint molecules prior to the meiotic divisions, especially in the *nse4* strain.

Finally, we noticed that the retention of centromeric cohesin was severely defective in the two mutants (Figure 9, S8A, C). This premature loss of centromeric cohesin correlated with the precocious separation of sister centromeres (Figure 9E) and indicates that *smc5/6* mutants experience problems with the establishment and/or retention of cohesion. We conclude that the mis-regulation of cohesin is two-fold in the Smc5/6-depleted cells: removal of arm cohesin is delayed while the protection of centromeric cohesin is compromised as well.

Discussion

The Smc5/6 complex is essential for chromosome segregation in following the induction of DSBs in meiosis

SMC complexes regulate a vast array of chromosomal processes, including DNA repair, during mitosis and meiosis [37]. In this study, we set out to determine whether the third, highly conserved SMC complex, Smc5/6, has roles in meiotic recombination. We were particularly interested in determining whether depletion of Smc5/6 leads to general recombination defects, like cohesin or condensin [89,90], or whether specific pathways would be perturbed in its absence (Figure S9).

Despite its central role in mitotic cells in mediating resolution and separation of chromosomes in response to DNA damage, the role of the Smc5/6 complex in meiotic recombination has remained enigmatic. Previous findings suggested that Smc5/6 mediated its critical role during premeiotic S-phase, since deletion of *SPO11* did not alleviate the chromosome separation defect of *smc6* temperature-sensitive mutants [54]. In this work, we show clearly that the budding yeast Smc5/6 complex is required for chromosome resolution following induction of meiotic recombination (Figure 3). Similar findings are reported by two independent studies in budding yeast [61,73]. Collectively, they firmly support the notion that across a range of species, Smc5/6 has essential functions in mediating chromosome resolution in response to induction of meiotic recombination [55,58,61,73,91].

Recombination-induced meiotic catastrophe in *smc5/6* mutants is caused by a combination of three factors

During meiosis, Smc5/6 localizes to centromeres, cohesin-binding sites and sites of meiotic DSBs (Figure 1). However, the chromosome-length dependent increase in the density of Smc5/6 binding sites reported in vegetative cells [60] is not observed in meiosis. We identified at least three factors that contribute to the general failure of chromosome separation seen in *smc5*/6 mutants. First, high levels of joint molecules, both between homologs and sister chromatids, remain unresolved, especially in the *nse4* mutant (Figure 5). Second, cells enter the meiotic nuclear divisions without a delay that might otherwise allow time for joint molecules to be resolved (Figure 8). Third, mis-regulation of cohesin also partly contributes to the delayed chromosome separation at anaphase I, especially in the *smc5* mutant (Figure 10). Moreover, a combination of unresolved joint molecules between sister chromatids and precocious separation of sister kinetochores (Figure 9) could also contribute to chromosomal entanglement (Figure 11B).

Time-lapse imaging of single cells delineates the sequence of severe chromosome segregation defects and meiotic catastrophe caused by unresolved joint molecules. Meiotic catastrophe was preceded by failure to separate the nuclear mass (*nse4*) or by failure to keep the nuclear masses separated upon spindle disassembly (*smc5*). Spindle formation and elongation were associated with aberrant chromosome morphology such as micronuclei and chromosome spikes (Figure 2).

It has been suggested that even low levels of unresolved joint molecules may block chromosome separation in meiotic cells [11,12]. In the *nse4* mutant, the 10% of chromosomes trapped in joint molecules at *HIS4LEU2* (Figure 5) translates to 20% of cells with an unresolved joint molecule at this recombination hotspot. Assuming that naturally occurring hotspots display a similar dependency on Smc5/6, each cell will undergo nuclear divisions with 20%, or roughly 30–40 joint molecules, unresolved (based on DSB levels of 150–200 per cell [92]). In the *smc5* mutant, the 1.8% unresolved joint molecules at 13 hours would equate to ~5–7 persistent joint molecules per cell. These considerations raise the possibility that a small number of unresolved joint molecules (less than one per chromosome) can cause a pan-nuclear segregation defect.

Smc5/6 is critical for joint molecule metabolism at meiotic DSB hotspots

Physical monitoring of joint molecules indicates that Smc5/6 regulates both the formation of recombination intermediates as well as their resolution (Figure 5) [61]. In accompanying studies the hypomorphic *smc6–56* allele and the SUMO E3 ligase-dead *mms21-11* alleles also accumulate joint molecules [61,73]. Therefore, inactivation or depletion of four distinct components of the core budding yeast Smc5/6 complex leads to defective joint

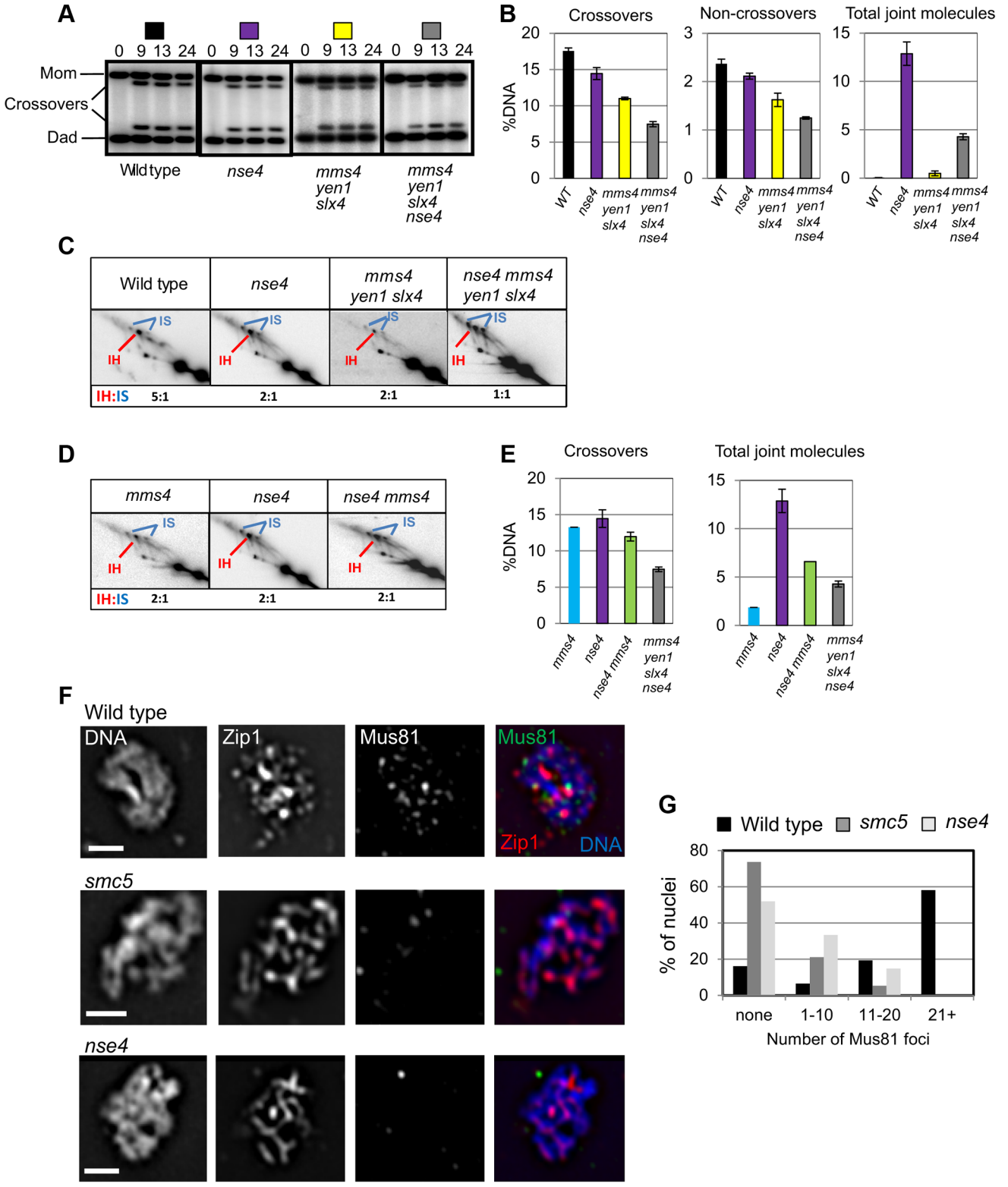

Figure 7. Smc5/6 regulates joint molecule resolution by Mus81-Mms4. (A) Representative images of 1D analysis of crossover levels. (B) Quantification of crossovers, non-crossovers, and total joint molecule levels at meiotic endpoints (13 hours). Quantification from three independent diploids; error bars represent the standard deviation. (C) Representative images of 2D analysis of IH:IS ratio in *nse4* and *nse4 mms4 yen1 slx4* quadruple mutants in the *ndt80*Δ background (13 hours). Data from three independent diploids. (D) Representative images of 2D analysis of IH:IS ratio in *nse4* and *nse4 mms4* mutants the *ndt80*Δ background (13 hours). Data from three independent diploids. (E) Quantification of crossovers and total joint molecules in *nse4 mms4* mutants compared to individual single mutants and the *nse4 mms4 yen1 slx4* quadruple mutant. (F,G) Representative images of Mus81 foci on spread, meiotic nuclei and quantification of Mus81-9myc foci. Nuclei were selected on the basis of linear Zip1 structures (pachynema). 100 nuclei were assessed for each strain. For the *mms4* single strain, we ran only one diploid in parallel with the *nse4* mutants. These data were similar to those described previously [14]. Strains: WT (Y3137), *smc5* (Y3135), and *nse4* (Y3144).
doi:10.1371/journal.pgen.1004071.g007

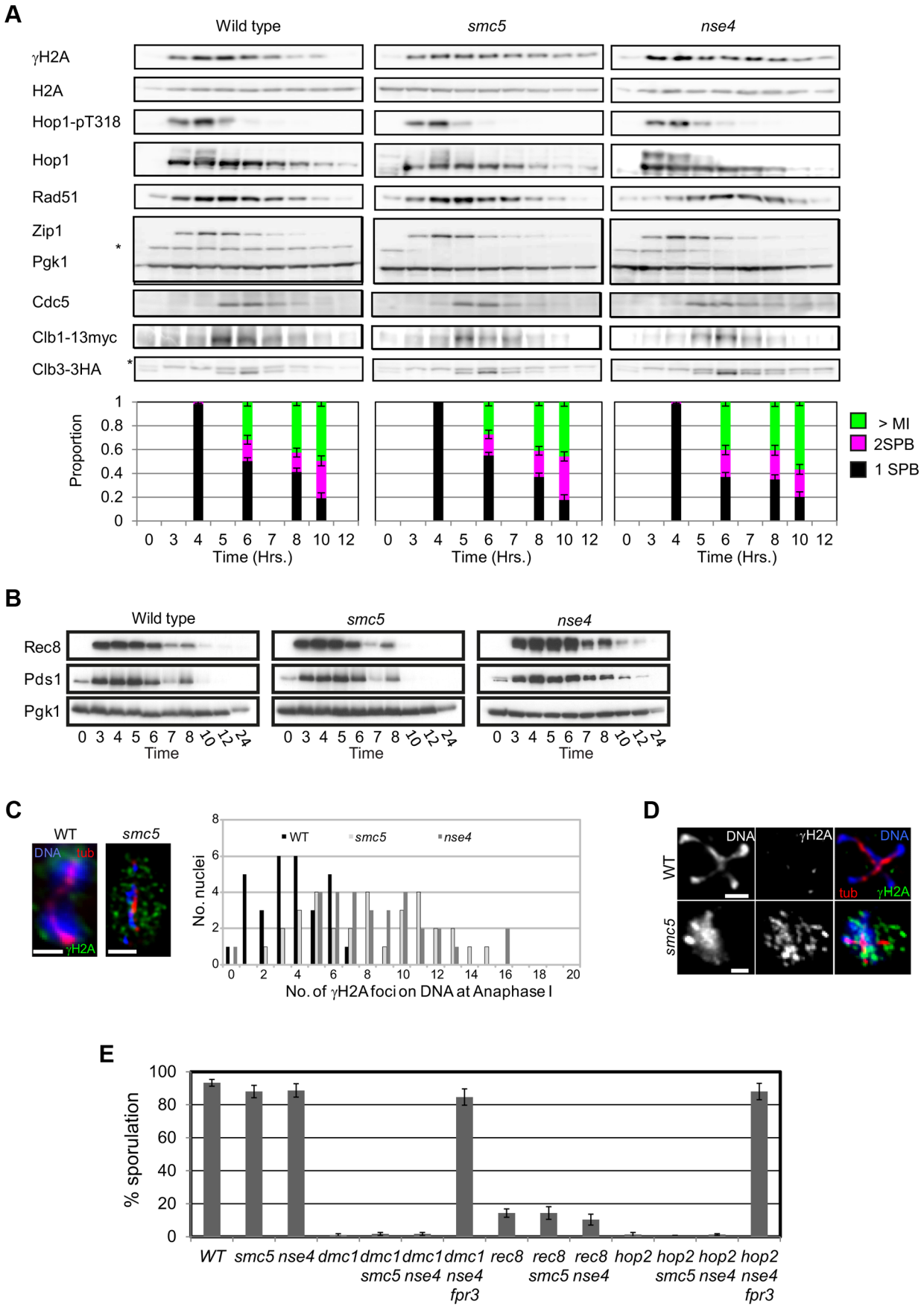
A
Wild type
smc5
nse4
γH2A
H2A
Hop1-pT318
Hop1
Rad51
Zip1
Pgk1
Cdc5
Clb1-13myc
Clb3-3HA
Proportion
Time (Hrs.)
> MI
2SPB
1 SPB
B
Wild type
smc5
nse4
Rec8
Pds1
Pgk1
Time
C
WT
smc5
DNA
tub
γH2A
No. nuclei
No. of γH2A foci on DNA at Anaphase I
D
DNA
γH2A
tub
E
% sporulation
WT
smc5
nse4
dmc1
dmc1 smc5
dmc1 nse4
dmc1 nse4 fpr3
rec8
rec8 smc5
rec8 nse4
hop2
hop2 smc5
hop2 nse4
hop2 nse4 fpr3

Figure 8. Smc5/6-depleted cells progress relatively normally through meiotic prophase I and enter nuclear divisions with damaged DNA. (A) Western blot analysis of Mec1 substrates, Hop1 (pT318) and H2A (pS129, γH2A). Clb1 and Clb3 are meiosis I- and meiosis II-specific B-type cyclins, respectively [101]. Pgk1 is a loading control. Strains: WT (Y4567), *smc5* (Y4570), and *nse4* (Y4573). Spindle pole body separation was used as a marker of cell cycle progression. (B) Western blot of Rec8-GFP and Pds1-13Myc. Strains: WT (Y2572), *smc5* (Y2673), and *nse4* (Y3653). (C) Typical examples of immunofluorescence images of γH2A at anaphase I from wild type and the two mutants. Bars: 2 μm. Right: quantification of the number of γH2A foci directly localized to the DNA. WT (Y1381), *smc5* (Y2704), and *nse4* (Y2705). (D) Typical examples of immunofluorescence images from wild type and *smc5* undergoing meiosis II. Bars: 2 μm. (E) Sporulation frequencies at 24 hours in *smc5* and *nse4* mutants in combination with mutants that show robust prophase I arrest. Strains: WT (Y1381), *smc5* (Y2704), and *nse4* (Y2705), *dmc1* (Y2045), *dmc1 smc5* (Y3491), *dmc1 nse4* (Y3488), *dmc1 nse4 fpr3* (Y4606), *rec8* (Y4607), *rec8 smc5* (Y2856), *rec8 nse4* (Y2855), *hop2* (Y2489), *hop2 smc5* (Y4610), *hop2 nse4* (Y4613), *hop2 nse4 fpr3* (Y4616).
doi:10.1371/journal.pgen.1004071.g008

molecule metabolism during meiosis. Similarly, in *S. pombe*, *nse5* and *nse6* mutants show accumulation of Rec12/Spo11-dependent joint molecules [55]. Thus, Smc5/6 has a critical and conserved role in the completion of meiotic DSB repair in both yeasts by facilitating the removal of joint molecules.

Smc5/6 has critical roles in regulating the orderly formation of recombination intermediates during meiotic prophase I

We have identified three aberrations in the joint molecules that accumulate in the *smc5/6* mutants from which we infer that Smc5/6 is critical for directing not only the removal of joint molecules upon prophase I exit ('late prophase I'', Figure 11), but also their proper formation during DSB repair (Figure 11). Smc5/6 depletion increases the fraction of joint molecules between sister chromatids that involve three and four chromatids (multi-chromatid JMs), while decreasing the levels of interhomolog dHJs. A similar conclusion is reached by Xaver *et al.* (2013), who analyzed joint molecules at a second hotspot. Since single-end invasions formed relatively normally in *smc5/6* mutants (Figure 5), these observations suggest that Smc5/6 may be important for coordinating the two DSB ends or to limit secondary strand invasions between sister chromatids (Figure 11A). Smc5/6 could also redirect multi-chromatid JMs and intersister dHJs to the interhomolog fate, perhaps via regulation of DNA helicases and/or endonucleases during early prophase I (Figure 11A). Such a redirection process was previously envisioned for Sgs1 [10].

Mus81-Mms4 was previously shown to play a small but significant role in inter-homolog bias, primarily by enhancing formation of inter-homolog dHJs [12,30]. Since inactivation of Mus81-Mms4 did not cause a further decrease in inter-homolog bias in the *nse4* mutant (Figure 7), it is possible that Smc5/6 regulates this function of Mus81-Mms4 during the formation of interhomolog dHJs. However, Mus81-Mms4 also somehow increases the final level of unresolved joint molecules in *nse4* cells (Figure 7E). Perhaps, in the absence of Smc5/6 function, Mus81-Mms4 creates structures that cannot be resolved. Alternatively, the decreased accumulation of JMs in the *nse4 mms4* and *nse4 mus81* mutants may suggest functions of Mus81-Mms4 in processing DSB repair intermediates that do not lead to crossovers (see below).

Aberrant joint molecules species accumulate in *smc5/6*

Inspection of the JM spots revealed additional spots and smears of the main dHJ molecules, suggestive of altered structure of the JMs that accumulate in *smc5/6* mutants (Figure 5B). In *S. pombe*, JMs that accumulate in *mus81* mutants can be resolved *in vivo* by expression of RusA and by RuvC after extraction from gels. In *nse5/6* mutants, however, the JMs appeared partially refractory to both RusA and RuvC treatment [55], although they migrated in similar spots of JMs in *mus81* mutants. Our observations suggest that the JMs that are formed in *smc5/6* mutants are not normal and this, together with the mislocalization of Mus81-Mms4 on the meiotic chromosomes, could contribute to the lack of resolution by Mus81-Mms4, despite its normal activation by Cdc5.

Smc5/6 regulates Mus81-Mms4-dependent resolution of joint molecules, whilst MutLγ remains active

In *S. pombe*, Mus81-Eme1 promotes most or all crossovers and deletion of Nse5 or Nse6 diminishes crossing over [27,28,55,57]. Our findings show that Smc5/6 may be specifically required for resolution mediated by structure-specific endonucleases such as Mus81-Mms4 (and possibly also Yen1 and Slx1–Slx4) in organisms with alternative resolving pathways. Specifically, we found that crossover levels and inter-homolog bias in *nse4* mutant were not further reduced when Mus81-Mms4 was also mutated (Figure 7D,E). In contrast, mutation of Sgs1 or Mlh3 synergistically reduced crossover levels in *nse4* cells (Figure 6). These observations suggest that Smc5/6 coordinates resolution of joint molecules that form independently of the major, MutSγ-dependent pathway. It is possible that Smc5/6 affects resolution of all non-Msh4/5 joint molecules. We infer that it is unlikely that Smc5/6 depletion leads to gross, general chromosomal defects that generally affect recombination, as seen in condensin mutants, where Cdc5/Polo-like kinase fails to associate with meiotic chromosomes and recombination is perturbed [90,93].

How might Smc5/6 regulate joint molecule resolution? In the case of Mus81-Mms4, hyperphosphorylation and presumably hyperactivation of endonuclease activity still occurs in in the *smc5* and *nse4* mutants (Figure S7). However, association of Mus81 with meiotic chromosomes is diminished (Figure 7F,G), even during early prophase I, consistent with observed defects during the formation of joint molecules (Figure 7D,E). Although we do not know whether the Mus81 foci we observe reflect catalytically active Mus81-Mms4 complexes, our data support the idea that Smc5/6 mediates chromosomal association of Mus81-Mms4.

Smc5/6 has been reported to have low affinity interactions with single stranded DNA [94]. It is possible that the complex targets Mus81-Mms4 to substrates containing single-stranded regions. However, no direct interaction between Mus81-Mms4 and the Smc5/6 complex has been reported. Another possibility is that Smc5/6 holds joint molecules (or their precursors) in a conformation that ultimately allows resolution by Mus81-Mms4. In this regard, the novel joint molecule species that we detect in the *smc5* and *nse4* mutants may represent structures that cannot be resolved by Mus81-Mms4 or other resolving endonucleases. EM studies have revealed aberrant JM structures in *sgs1* and *mms4 sgs1* mutants that might represent hard-to-resolve structures [12]. Finally, Smc5/6 may also regulate local chromosome structure around a subset of DSBs and this could impact on recombination [86]. For example, mis-regulation of cohesin could indirectly influence inter-homolog bias, as seen in *rec8Δ* mutants [89].

Materials and Methods

The SI contains Movie S1, S2, S3, S4, S5, S6, S7; nine additional Figures (S1, S2, S3, S4, S5, S6, S7, S8, S9); and one Table (S1).

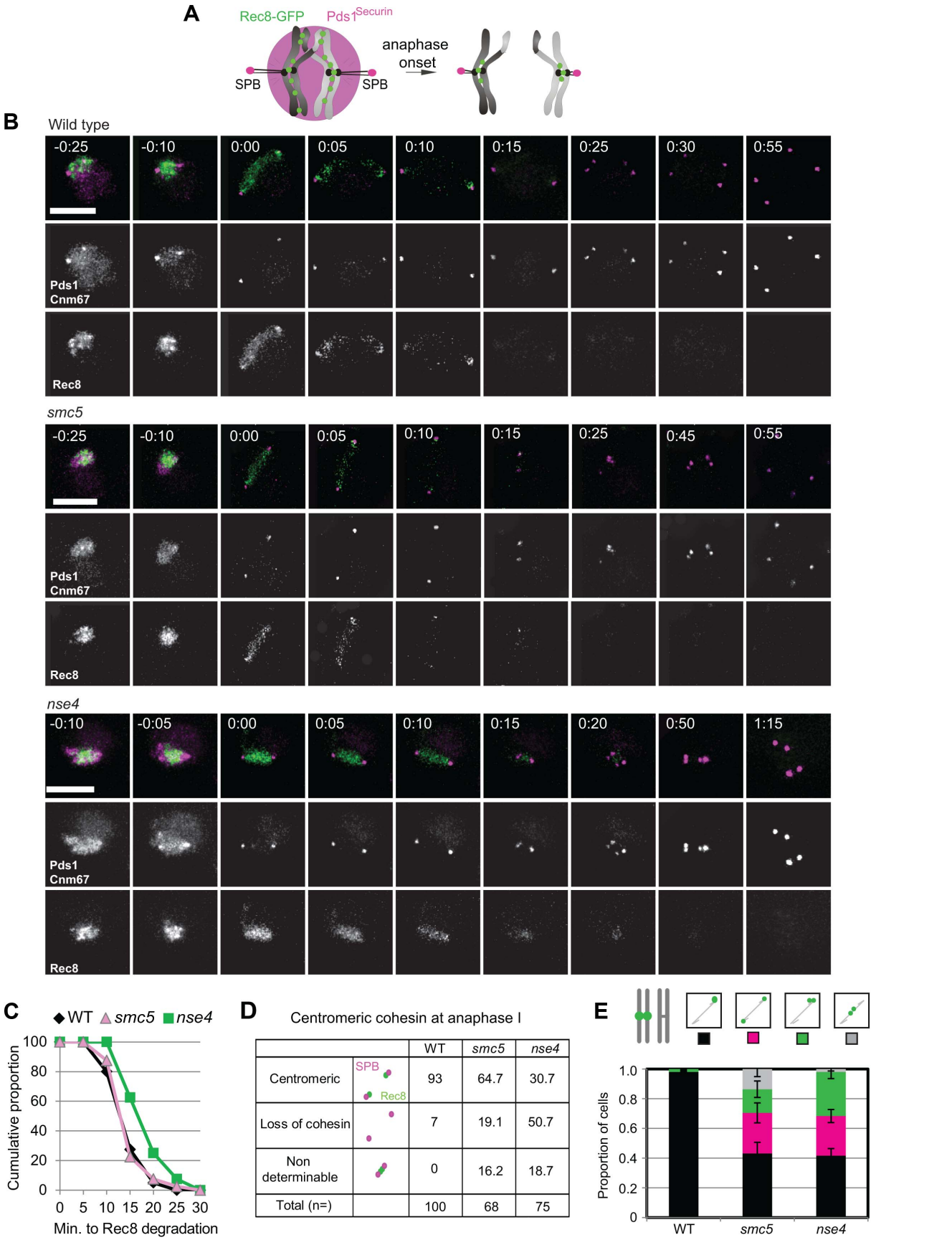
A
Rec8-GFP
Pds1Securin
SPB
SPB
anaphase onset
B
Wild type
-0:25
-0:10
0:00
0:05
0:10
0:15
0:25
0:30
0:55
Pds1 Cnm67
Rec8
smc5
-0:25
-0:10
0:00
0:05
0:10
0:15
0:25
0:45
0:55
Pds1 Cnm67
Rec8
nse4
-0:10
-0:05
0:00
0:05
0:10
0:15
0:20
0:50
1:15
Pds1 Cnm67
Rec8
C
WT smc5 nse4
Cumulative proportion
100
80
60
40
20
0
0 5 10 15 20 25 30
Min. to Rec8 degradation
D
Centromeric cohesin at anaphase I
WT smc5 nse4
Centromeric SPB Rec8 93 64.7 30.7
Loss of cohesin 7 19.1 50.7
Non determinable 0 16.2 18.7
Total (n=) 100 68 75
E
Proportion of cells
1.0
0.8
0.6
0.4
0.2
0
WT
smc5
nse4

Figure 9. Misregulation of cohesin in *smc5/6*-depleted cells. (A) Experimental set up: Spindle pole body component CNM67-mCherry and $Pds1^{Securin}$-tdTomato were used to assess spindle length and the onset of anaphase I, respectively. Rec8 is tagged with GFP. Upon anaphase I onset, $Pds1^{Securin}$-tdTomato is degraded, the distance between CNM67-mCherry foci increase, and Rec8-GFP is degraded along arm regions until only centric and pericentromeric cohesin is left (right hand diagram). (B) Typical examples of time lapse images from wild type and the two mutants. Bars: 4 μm. Arrows indicate loss of centromeric cohesin signal. Note that the temporal resolution of kinetics is limited to 5 min. Strains: WT (Y2572), *smc5* (Y2673), and *nse4* (Y3047). Full movies are available in the Supplemental Information (Movies S5, S6, S7). (C) The cumulative proportion of cells with arm cohesin has been degraded at the given time after anaphase I onset ($n \geq 40$ per strain). Significance tests for Kruskall-Wallis ($P < 0.01$) show *nse4* is delayed compared to wild type and *smc5*. (D) Proportions of nuclei with centromeric cohesin at anaphase I from live-cell imaging experiments. Anaphase I was staged by loss of Pds1 signal. (E) Analysis of sister kinetochore separation. tetO repeats are inserted 1.5 kb from *CEN5* and tetR-GFP expressed constitutively. Only one homolog contains the tetO-*CEN5* insertions, which allows analysis of sister kinetochore behaviour. Bars represent standard error ($n > 100$ for each strain). Anaphase I was staged by spindles being greater than 4 μm in length. At this length, all spindles from *smc5* and *nse4* were Pds1 negative (data not shown). WT (Y2708), *smc5* (Y2709), and *nse4* (Y3071).
doi:10.1371/journal.pgen.1004071.g009

Yeast strains and meiotic time courses

Strains are described in Table S1. They are all derived from SK1.

Diploid cells were grown to saturation in YEPD (1% yeast extract, 2% bactopeptone, 2% dextrose, pH 6.5), then inoculated at 5×10^6 cells per ml in SPS (0.05% yeast extract, 1% peptone, 0.17% YNB, 1% potassium acetate, 0.5% ammonium sulphate, 0.05 M potassium hydrogen pthalate at pH 5.5) and grown to a cell density of 5×10^7 cells per ml. To induce meiosis, cells were resuspended in SPM (pH 7.0) consisting of 1% potassium acetate, 0.02% raffinose, 0.02% antifoam (Sigma, A8311), 2% histidine, 1.5% lysine, 2% arginine, 1% leusine and 0.2% uracil.

Genome-wide Smc5 DNA binding and microarray analysis

Genome-wide Smc5 association was measured as previously published [95]. Briefly, Smc5 crosslinked chromatin was immunoprecipitated with 2 μl anti-myc 9E11 (Abcam) or 20 μl anti-V5 beads (Sigma-Aldrich). Immunoprecipitated and input DNA samples were cohybridized to a custom DNA microarray (Agilent) and data were normalized as previously described. Every 3 points along the chromosome were averaged to produce the smoothed profiles in Figure 1. The relative enrichment of Smc5 to Rec8 and Smc5 in *spo11* versus *SPO11* is the ratio of the values in each of the two datasets indicated. The raw data and log ratios from this study are available from the NCBI Gene Expression Omnibus (http://www.ncbi.nlm.nih.gov/geo/), accession number GSE44852.

Molecular assays

Molecular assays were carried out as described previously [72], with the modification that we used the Phase Lock Gel for phenol extraction. We analysed three independent diploids for each strain.

CHEF analysis of chromosome breakage

To measure genome wide DSB signal, chromosome-length DNA captured in agarose plugs [96] was separated by pulsed field gel electrophoresis under the following conditions: 1.3% agarose in 0.5×TBE; 14°C; 6 V/cm; switch angle 120°, ramped switch time of 15–25 seconds over 30 hours (Biorad CHEF DRIII). Following a denaturing transfer to nylon membrane, a radioactive DNA telomeric probe for the left side of chromosomes III (*CHA1*) was hybridized to the membrane. Radioactive signal was collected on phospho-screens, imaged using a Fuji FLA5100 and quantified using FujiFilm ImageGauge software. DSB signal was measured as a percentage of the total lane signal [97]. DSB molecules occurring further from the probe are underestimated due to DSBs occurring closer to the probe on the same molecule. To correct for this, the estimated DSB frequency was calculated using Poisson correction: Percentage broken chromosomes (Poisson corrected) = −ln(1−measured DSB signal). To produce lane profiles, 900 lane slices were exported from ImageGauge and combined from 6–10 hours and each slice plotted as a percent of total lane signal.

Yeast protein extraction & protein analysis

Cells from meiotic cultures (OD_{600} 1.2–1.5, 2 ml) were disrupted using glass beads in 200 μl of ice cold 20% TCA. Precipitates were collected by centrifugation and washed in 400 μl of ice cold 5% TCA. Precipitates were resuspended in 100 μl of SDS-PAGE sample buffer (4% SDS, 5% β-mercaptoethanol, 0.15 M DTT, 20% glycerol, 0.01% bromophenol blue); boiled for 5 minutes at 95°C, centrifuged, and the supernatant containing protein was collected.

Proteins were separated by SDS-PAGE, transferred to nitrocellulose membranes, and probed with the appropriate antibodies followed by HRP-conjugated secondary antibodies (DAKO, 1:2000). HRP activity was detected using Pierce ECL Western Blotting Substrate followed by exposure to Amersham Hyperfilm ECL or using the Image Quant LAS 4000 imaging system.

Antibodies used for western blotting

Cdc5 (Santa Cruz sc-6732, 1:2000), HA (12CA5, CRUK, 1:1000 or Abcam Ab9110, 1:1000), γH2A (J. Downs, 1:1000), H2A (1:5000, J. Downs), Rad51 (1:2000, S. Roeder), PAP (Sigma P1291, 1:2000), Pgk1 (Invitrogen 459250, 1:200 000), Myc (9E10, CRUK, 1:2000), V5 (AbDSerotec MCA1360, 1:2000), Zip1 (Santa Cruz sc-48716, 1:2000), Hop1 (F. Klein, 1:1000), pHop1-T318 (Cambridge Research Biochemicals, 1:500), and Clb3 (Santa Cruz sc-7167, 1:500).

TEV protease induction

Meiotic cultures were arrested at pachynema after 6 hours in SPM. TEV protease and Ndt80 were induced by the addition of 1 μM β-estradiol.

Protein synthesis block

Protein synthesis was blocked by the addition of cyclohexamide to meiotic cultures to a final concentration of 200 μg/ml. Cyclohexamide was added to meiotic cultures 1 hour after Ndt80 induction.

Auxin-dependent degradation of Smc5

The P_{CLB2}-*SMC5* was C-terminally-tagged with the AID [69]. To induce degradation of Smc5, we added 150 μl of 500 mM auxin (3-indoleacetic acid; Sigma I375-0), resuspended in 1N NaOH, to 50 ml meiotic cell cultures. This was added at 1 hour after transfer to SPM. Addition of auxin at earlier time points

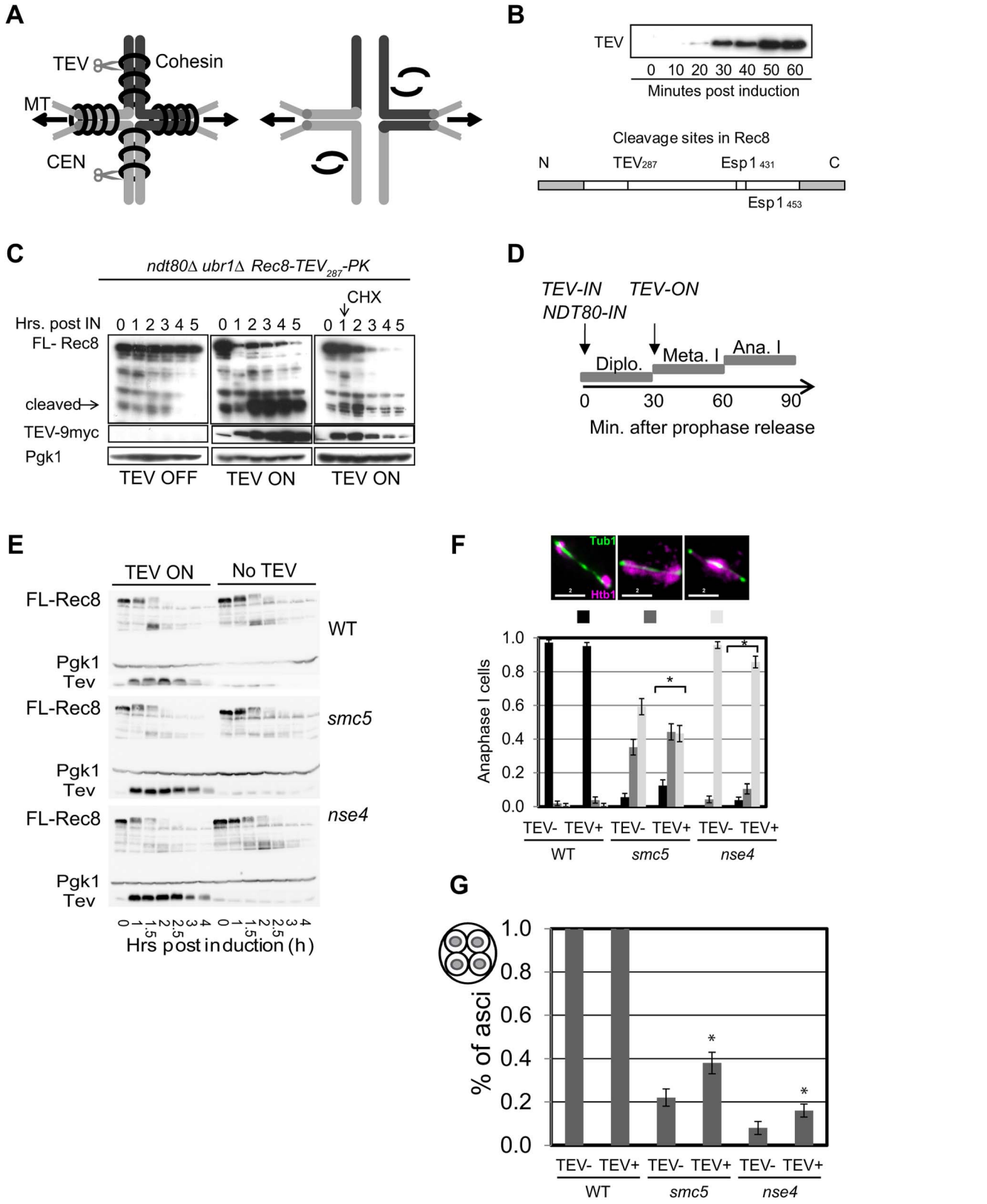

Figure 10. Retained arm cohesin at anaphase I contributes to the chromosome resolution defect in the *smc5* and *nse4* mutants. (A) Diagram of bivalent resolution by cohesin (Rec8) cleavage along arms regions Abbreviations: MT-microtubules, CEN-centromeres, scissors depict TEV protease. (B) TEV-9Myc expression after induction during a meiotic time course and the TEV cleavage site introduced into Rec8. Note that Rec8-TEV287-PK retains its two separase (Esp1) cleavage sites. (C) Rec8-TEV287-PK cleavage by TEV protease in *ndt80Δ ubr1Δ* cells. TEV protease was induced 6 hours into meiosis when >80% are arrested in pachynema. FL-full length Rec8-TEV287-PK. Left panel shows no TEV induction; the middle

panels shows TEV induction; and the right panel shows TEV induction and cyclohexamide treatment (CHX) 1.15 hours after induction. Pgk1 was used as a loading control. Strain: Y3380. (D) Experimental set up of TEV protease induction after meiotic prophase by simultaneous induction of TEV protease and prophase exit (*NDT80-IN*). (E) Analysis of protein levels of Rec8-TEV_{287}-PK in arrested and released (*NDT80-IN*) cells. (F) Nuclear separation at anaphase I. Bar graph shows proportion of tetrads with fully separated, 'stretched' or compacted nuclear appearance. The *denotes statistically significant differences ($p<0.01$, G-test) in the distribution of classes. (G) DNA encapsulation into spores. Bar graph shows proportion of tetrads with fully encapsulated DNA. The *denotes statistically significant differences ($p<0.05$, G-test) in the distribution of classes. Strains: WT (Y3264- no TEV and Y3299), *smc5* (Y3261- no TEV and Y3237), and *nse4* (Y3258- no TEV and Y3240).
doi:10.1371/journal.pgen.1004071.g010

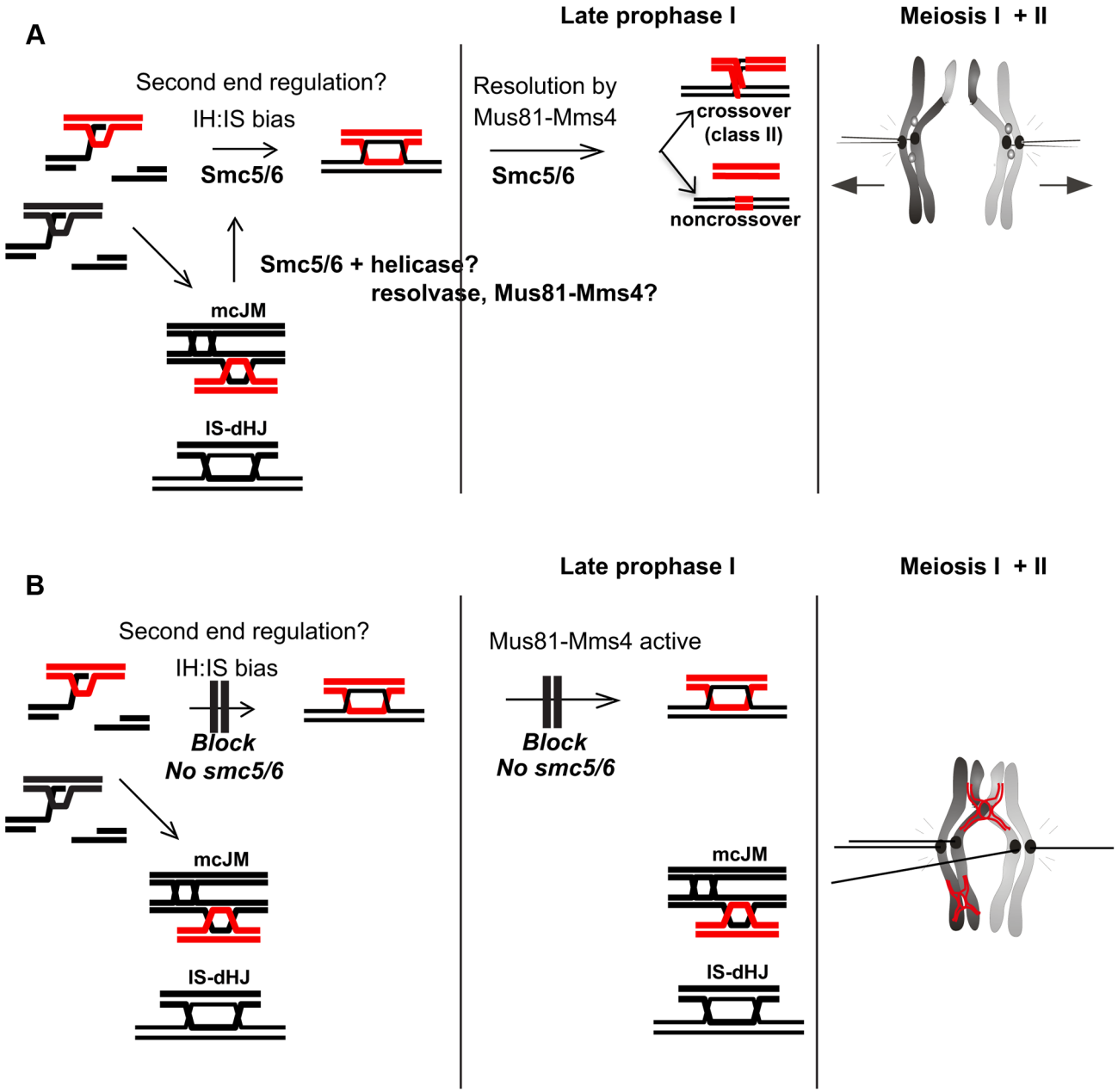

Figure 11. Model for Smc5/6 function during meiosis. (A) In wild type cells, Smc5/6 is present and ensures the formation of IH-dHJs either directly or perhaps by removing mcJMs and IS-dHJs, returning them to an interhomolog fate. This could be done in co-operation with helicases and resolvases, potentially Mus81-Mms4. (B) In the absence of Smc5/6, second end regulation is aberrant and cells enter late prophase with increased mcJMs and IS-dHJs. These are not cleaved by Mus81-Mms4, which is hyperphosphorylated by Cdc5, because it requires Smc5/6. Since the joint molecules do not appear to trigger a prophase I checkpoint, *smc5/6* mutants enter the nuclear divisions with joint molecules as well as precociously separated sister kinetochores that prevent chromosome segregation, leading to meiotic catastrophe.
doi:10.1371/journal.pgen.1004071.g011

resulted in arrest during the preceding mitotic divisions when cells underwent premeiotic growth in pre-sporulation medium (SPS).

Meiotic nuclear spreading, immunofluorescence, and antibodies

Nuclear spreading and antibodies have been described elsewhere [98,99], except that we treated cells with both zymolyase 100T and glusulase in order to generate spheroblasts for some strains. Fixation followed by indirect immunofluorescence was carried out by fixing cells in 4% formaldehyde for 15–45 minutes at room temperature.

When assessing Mus81-Mms4 foci, we carefully controlled for the extent of spreading, because we noted that even in the wild type, a small proportion of nuclei did not contain Mus81-Mms4^{Eme1} foci. When we applied more extreme spreading techniques, all Mus81-Mms4^{Eme1} staining (but not Zip1) was abolished in the wild type (data not shown). This suggests that the Mus81-Mms4^{Eme1} interaction with meiotic chromosomes is less stable than Zip1.

Live cell imaging

Cells were initially incubated in sporulation media for 6–8 hours. 20 µl of cells were added to a Y04D CellASIC plate (CellASIC ONIX microfluidic perfusion system) and imaged inside an environmental chamber set at 30°C. A flow rate of 8 psi was used to load the cells and a steady-state flow rate of 2 psi was used for the duration of the time course.

Time-lapse microscopy was carried out using a Personal DeltaVision (Applied Precision) with xenon or solid-state illumination, using associated proprietary software (SoftWoRx software; version 4.0.0, Applied Precision). Images were captured using an UPLS Apochromat 1.4 numerical aperture, ×100 magnification oil immersion objective (Olympus), auxiliary magnification to prevent undersampling, standard DeltaVision filter sets FITC (ex 490, em 525 nm) and TRIC (ex 555, em 605), yielding approximate resolutions (Rayleigh's d) of ~229 nm and 264 nm in the xy, respectively, whereas axial resolutions were approximately 811 and 935 nm. Photon detection was carried out using a Cascade2 1 K EMCCD camera (Photometrics) using a gain of 230 and no binning. Images were taken using exposure times of 0.025 sec. and 32% transmission (FITC) and 32% transmission and 0.1 sec. exposure (TRITC). 6–7 z-stacks at 1 µm were collected. Final images for sporulation were carried out with DIC, 32% transmission and 0.05 sec. exposure. Images were recorded every 5 minutes for the first 90 minutes, every 20 minutes for the next 80 minutes and then every 45 minutes for the last 90 minutes. Around 12 hours after imaging the sporulation of the cells at each point of imaging was assessed. Only cells that sporulated were included in the analyses.

Image analysis and manipulation

Images were deconvolved using SoftWoRx software (version 4.0.0, Applied Precision). Subsequent 3D analysis to measure spindle length was carried out using Imaris (version 7.0.0, Bitplane).

3D images are presented as maximum projections, rendered in Softworx or Imaris. Some images were manipulated in Adobe Photoshop CS5.1 using the following procedure. Images were converted to .psd files from *Softworx* files before being opened in Adobe Photoshop. Only the max/min input levels of each channel were adjusted manually to adjust differences in the imaging intensities. Images were cropped preserving the relative ratios, and the size bar copied to a second layer of the image. For aesthetic reasons, a broader bar covering the size and the out-of-focus number was added on top of the original. Analysis of foci numbers was carried out manually and with the 'Find Peaks algorithm' (ImageJ plugin is available from: http://www.sussex.ac.uk/gdsc/intranet/microscopy/imagej/plugins and documentation: http://www.sussex.ac.uk/gdsc/intranet/microscopy/imagej/findpeaks). Peaks were identified above a background level using non-maximal suppression. An allowance was made for peak regions covering multiple pixels with the same intensity (plateau maxima). A watershed algorithm was used to assign all non-maxima pixels to the appropriate peak by following the maximum gradient. Peak expansion was restricted using the height above background. Following identification the boundaries between peaks were calculated and the highest boundary point between touching peaks stored as saddles. A peak merge algorithm was used to join insignificant smaller peaks into their neighbour peak defined using the highest saddle point. Peaks were identified as insignificant using height and area criteria.

Noisy data were smoothed using a Gaussian blur prior to peak identification. Reported peak statistics always use the intensity values from the original unsmoothed image. The algorithm can be applied to 2D or 3D images and is available as a plugin for ImageJ. The plugin allows setting parameters to control the background identification, search method, merge criteria and the results output. The plugin is scriptable via the ImageJ macro facility and provides a GUI that allows the parameters to be adjusted with real-time results update. The plugin will be published separately elsewhere.

Statistics

We used various statistical tests in R (www.r-project.org), as indicated throughout the text. P-values were adjusted for multiple pair-wise comparisons according to Dunn-Sidak to reflect $\alpha<0.05$. Standard error bars around proportions were calculated as $\sqrt{[p(1-p)/n]}$, where p is the proportion of the specific class ($n>100$ for each strain). For the Pearson product-moment correlation, the cor.test uses the t-statistics to calculate the p-value and the Fisher z transform to generate an asymptotic confidence interval (95%).

Supporting Information

Figure S1 Smc5-13myc localization on meiotic chromosomes. (A) Expression of Smc5-13myc and Nse4-TAP during meiosis. Note the Smc5-13myc band travelling with lower electrophoretic mobility (indicated by the arrow); likely the sumoylated species of Smc5. Strain: Smc5-13myc (Y2824), and Nse4-TAP (Y2826). (B) Localization of Smc5-13myc and Zip1. Note the lack of apparent colocalization during leptonema and zygonema. (C) Localization of Smc5-13myc in *rec8Δ* and *spo11Δ* mutants. Strains: *rec8Δ* (Y2837) and *spo11Δ* (Y2836). (D) Depletion of Cdc6 expressed under the *SCC1* promoter (left) and expression of Smc5-13myc. Strain: (Y2891). (E) Lack of localization of Smc5-13myc to chromosomes in P_{SCC1}-*CDC6* strain. (F) Depletion of Top2 expressed under the *CLB2* promoter (left) and expression of Smc5-13myc. Note, this strain arrests at pachynema. Strain: (Y2851). (G) Diminished localization of Smc5-13myc to chromosomes in P_{CLB2}-*TOP2* strain. Smc5-13myc foci numbers remained normal in *top1-mn*, *top3-mn*, *sgs1-mn*, *rad50S*, *dmc1*Δ, *zip1*Δ, *zip2*Δ, *zip3*Δ, *mer3*Δ, *pch2*Δ, *fpr3*Δ (data not shown).
(PDF)

Figure S2 Association of myc-tagged Smc5 with cohesin binding sites, centromeres, and DSBs. (A) DNA binding profiles for and Smc5-13myc (red, H5492) and Rec8-3HA (purple, H4471, [65]) plotted for Chromosome III. Lower panel shows enlarged, overlay

on the right arm of Chromosome III (150–300 kb). (B) Overlay of the Rec8-3HA and Smc5-3V5 (Figure 1) or Smc5-13myc (A) binding profiles near *CEN3*. (C) The binding of Smc5-13myc was normalized to Rec8-3HA binding using the data shown in (A) to reveal weaker, non-core regions (red). DSB sites mapped by ssDNA enrichment are indicated below (blue, H118, [100]).
(EPS)

Figure S3 Auxin-induced degradation of Smc5-AID. (A) Western blot analysis of Smc5-AID-V5 after mock treatment or treatment with 1.5 mM auxin at 1 hour after transfer to sporulation medium. Strain: (Y4540). (B) Quantification of DNA encapsulation in Smc5-AID depleted cells. Note that continuous treatment with auxin leads to better depletion and a more severe phenotype, but that the mock-treatment with solvent (NaOH) alone (but not solvent+auxin) causes sporulation defects.
(PDF)

Figure S4 Meiotic recombination and crossing over in the *smc5 nse4* mutant is similar to the *nse4* single mutant. (A) Example of 1D analysis of crossover recombination. (B) Quantification of crossover levels from three independent diploids (24 hours). Strains: WT (Y2976), *smc5* (Y1211), *nse4* (Y1212), *smc5 nse4* (Y4179).
(PDF)

Figure S5 Smc5- or Nse4-depletion does not increase DSB levels in *RAD50S* or *dmc1*Δ mutants. (A) Representative CHEF gel followed by Southern blotting using the *CHA1* probe (chromosome III, left end) in *dmc1*Δ strain background. Percentage total lane signal was calculated by smoothing the histogram of signals from 900 bins in each lane. Strains: *dmc1*Δ (SG492), *nse4 dmc1*Δ (SG481), and *smc5 dmc1*Δ (SG478). (B) Quantification of DSBs (non-parentally sized fragments) are presented as raw data (left) or Poisson corrected (right, see materials and methods) for each time point. (C) Representative CHEF gel followed by Southern blotting using the *CHA1* probe (chromosome III, left end) in *RAD50S* strain background. Strains: *RAD50S* (SG488), *nse4 RAD50S* (SG484), and *smc5 RAD50S* (SG491). (D) Quantification of DSBs are presented as raw data (left) or Poisson corrected (right).
(PDF)

Figure S6 SC formation and disassembly occurs with normal kinetics in the *smc5* and *nse4* mutants. (A) Examples of Zip1 staining at pachynema in the wild type, *nse4* and *smc5* mutants. Strains: WT (Y967), *smc5* (Y3080) and *nse4* (Y2729). (B,C) Kinetics of Zip1 staining patterns and polycomplex formation (PC) in wild type and the *nse4* mutant. Left: Examples of Zip1 behaviour as 'dotty', 'dot-linear' and 'linear' staining, representative of leptonema, zygonema, and pachynema, respectively in nuclei from the *nse4* mutant (these are similar to those seen in wild type). The arrow indicates an aggregate of Zip1, likely a polycomplex (PC). Bars, 2 μm. Right: Proportion of nuclei with no Zip1, dotty, dot-linear, or fully linear Zip1 staining (upper panel) and the proportion containing a PC (lower panel). At least 100 nuclei were inspected for each time point. We chose a time course where spindle formation kinetics indicated similar synchrony in the two strains to allow direct comparison (not shown). The arrow denotes the time at which cells were released from prophase I arrest by induction of *NDT80* expression (*NDT80-IN*) allowing SC disassembly and Zip1 degradation (C) to be followed.
(PDF)

Figure S7 Steady-state levels and hyperphosphorylation of Mus81-9Myc and Mms4-9myc are not decreased in the Smc5- and Nse4-depleted strains. (A,B) Western blot of Mus81-9myc and Mms4-9myc. Loading factor Pgk1 was analysed on the same Western blot. Strains: WT (Y3618- Mus81-9myc, Y3683- Mms4-9myc), *smc5* (Y3621- Mus81-9myc, Y3689- Mms4-9myc) and *nse4* (Y3624-Mus81-9myc, Y3686- Mms4-9myc). (C) Mms4-9myc hyperphosphorylation occurs concomitantly with Cdc5 expression in wild type as well as the *smc5* and *nse4* strains. Pgk1 was used as loading factor.
(PDF)

Figure S8 (A) Immunostaining of fixed, semi-spread nuclei at anaphase I. Examples of anaphase I nuclei with associated Rec8-GFP along arms ('arm retention') as well as precocious loss of centromeric cohesin. Quantification is shown below. Anaphase I nuclei were staged by length; imaging with Pds1-tdTomato showed that all anaphase I spindles >4 μm were at anaphase I in wild type as well as the two mutants. (B) Representative images of Rec8-GFP of anaphase II nuclei in the wild type and *smc5* mutant. (C) Overexposure of the FITC (Rec8-GFP) channel to illustrate that the centromeric Rec8 is indeed not detected at anaphase I in *smc5* and *nse4* mutants. Box illustrates an anaphase I spindle (>4 μm). Overexposed GFP signals are from prophase I nuclei.
(TIF)

Figure S9 Integration of proposed Smc5/6 function within other JM regulatory mechanisms. The main crossover-generating mechanism is meiosis-specific and depends upon the preferential stabilization of recombination-intermediates by the ZMM proteins (green). Smc5/6 stabilizes other recombination intermediates and promote their resolution into both crossovers (class II) and noncrossovers by Mus81-Mms4 (grey box).
(EPS)

Movie S1 Time lapse imaging of nuclear divisions and spindle dynamics for wild type (Y3606). H2B is pseudocoloured in magenta and tubulin in green. This movie corresponds to panel 1 (upper panel) in Figure 2E.
(WMV)

Movie S2 Time lapse imaging of nuclear divisions and spindle dynamics for *smc5* (Y3627). H2B is pseudocoloured in magenta and tubulin in green. This movie corresponds to panel 2 in Figure 2E.
(WMV)

Movie S3 Time lapse imaging of nuclear divisions and spindle dynamics for *smc5* (Y3627). H2B is pseudocoloured in magenta and tubulin in green. This movie corresponds to panel 3 in Figure 2E.
(WMV)

Movie S4 Time lapse imaging of nuclear divisions and spindle dynamics for *nse4* (Y3630). H2B is pseudocoloured in magenta and tubulin in green. This movie corresponds to panel 4 in Figure 2E.
(WMV)

Movie S5 Time-lapse imaging of Rec8-GFP degradation in wild type (Y2572). Rec8-GFP is pseudocoloured in green; CNM67-mCherry and Pds1-tdTomato is shown in magenta. This movie corresponds to panel 1 in Figure 9B.
(WMV)

Movie S6 Time-lapse imaging of Rec8-GFP degradation in *smc5* (Y2673). Rec8-GFP is pseudocoloured in green; CNM67-mCherry and Pds1-tdTomato is shown in magenta. This movie corresponds to panel 2 in Figure 9B.
(WMV)

Movie S7 Time-lapse imaging of Rec8-GFP degradation in *nse4* (Y3047). Rec8-GFP is pseudocoloured in green;

CNM67-mCherry and Pds1-tdTomato is shown in magenta. This movie corresponds to panel 3 in Figure 9B.
(WMV)

Table S1 List of strains used in this study. Individual strains used for the experiments are listed in the relevant figure legend.
(DOCX)

Acknowledgments

We thank Joao Matos, Wolfgang Zachariae, Kim Nasmyth and Steve West for strains, some of which were prior to publication; Jo Murray, Alan Lehmann, Helfrid Hochegger, Alessandro Bianchi, Xavi Aran, and Jacob Kirk for stimulating discussions and comments on the manuscript; and Nils Lambacher for technical assistance with molecular assays. We are grateful to the open source R project (www.r-project.org), ImageJ, and the Wellcome Trust for the pDV equipment.

Author Contributions

Conceived and designed the experiments: EH NH AH HGB AC SN LN SG PWJ ST. Performed the experiments: AC ST PWJ HGB SN ACC LN ZL EH AH SG. Analyzed the data: EH AH HGB LN SN ST ACC AC NH SG PWJ. Contributed reagents/materials/analysis tools: ADH PA. Wrote the manuscript: EH AH NH HGB.

References

1. Neale MJ, Keeney S (2006) Clarifying the mechanics of DNA strand exchange in meiotic recombination. Nature 442: 153–158.
2. Henderson KA, Keeney S (2004) Tying synaptonemal complex initiation to the formation and programmed repair of DNA double-strand breaks. Proc Natl Acad Sci U S A 101: 4519–4524.
3. Kitajima TS, Kawashima SA, Watanabe Y (2004) The conserved kinetochore protein shugoshin protects centromeric cohesion during meiosis. Nature 427: 510–517.
4. Marston AL, Tham WH, Shah H, Amon A (2004) A genome-wide screen identifies genes required for centromeric cohesion. Science 303: 1367–1370.
5. Gregan J, Rabitsch PK, Sakem B, Csutak O, Latypov V, et al. (2005) Novel genes required for meiotic chromosome segregation are identified by a high-throughput knockout screen in fission yeast. Curr Biol 15: 1663–1669.
6. Xu L, Ajimura M, Padmore R, Klein C, Kleckner N (1995) *NDT80*, a meiosis-specific gene required for exit from pachytene in *Saccharomyces cerevisiae*. Mol Cell Biol 15: 6572–6581.
7. Clyne RK, Katis VL, Jessop L, Benjamin KR, Herskowitz I, et al. (2003) Polo-like kinase Cdc5 promotes chiasmata formation and cosegregation of sister centromeres at meiosis I. Nat Cell Biol 5: 480–485.
8. Sourirajan A, Lichten M (2008) Polo-like kinase Cdc5 drives exit from pachytene during budding yeast meiosis. Genes Dev 22: 2627–2632.
9. McMahill MS, Sham CW, Bishop DK (2007) Synthesis-dependent strand annealing in meiosis. PLoS Biol 5: e299.
10. Oh SD, Lao JP, Hwang PY, Taylor AF, Smith GR, et al. (2007) BLM ortholog, Sgs1, prevents aberrant crossing-over by suppressing formation of multichromatid joint molecules. Cell 130: 259–272.
11. Jessop L, Lichten M (2008) Mus81/Mms4 endonuclease and Sgs1 helicase collaborate to ensure proper recombination intermediate metabolism during meiosis. Mol Cell 31: 313–323.
12. Oh SD, Lao JP, Taylor AF, Smith GR, Hunter N (2008) RecQ helicase, Sgs1, and XPF family endonuclease, Mus81-Mms4, resolve aberrant joint molecules during meiotic recombination. Mol Cell 31: 324–336.
13. De Muyt A, Jessop L, Kolar E, Sourirajan A, Chen J, et al. (2012) BLM helicase ortholog Sgs1 Is a central regulator of meiotic recombination intermediate metabolism. Mol Cell 46: 43–53.
14. Zakharyevich K, Tang S, Ma Y, Hunter N (2012) Delineation of joint molecule resolution pathways in meiosis identifies a crossover-specific resolvase. Cell 149: 334–347.
15. Mullen JR, Nallaseth FS, Lan YQ, Slagle CE, Brill SJ (2005) Yeast Rmi1/Nce4 controls genome stability as a subunit of the Sgs1-Top3 complex. Mol Cell Biol 25: 4476–4487.
16. Wu L, Bachrati CZ, Ou J, Xu C, Yin J, et al. (2006) BLAP75/RMI1 promotes the BLM-dependent dissolution of homologous recombination intermediates. Proc Natl Acad Sci U S A 103: 4068–4073.
17. Hoffmann ER, Borts RH (2004) Meiotic recombination intermediates and mismatch repair proteins. Cytogenet Genome Res 107: 232–248.
18. Kolas NK, Cohen PE (2004) Novel and diverse functions of the DNA mismatch repair family in mammalian meiosis and recombination. Cytogenet Genome Res 107: 216–231.
19. Snowden T, Acharya S, Butz C, Berardini M, Fishel R (2004) hMSH4-hMSH5 recognizes Holliday Junctions and forms a meiosis-specific sliding clamp that embraces homologous chromosomes. Mol Cell 15: 437–451.
20. Borner GV, Kleckner N, Hunter N (2004) Crossover/noncrossover differentiation, synaptonemal complex formation, and regulatory surveillance at the leptotene/zygotene transition of meiosis. Cell 117: 29–45.
21. Jessop L, Rockmill B, Roeder GS, Lichten M (2006) Meiotic chromosome synapsis-promoting proteins antagonize the anti-crossover activity of Sgs1. PLoS Genet 2: e155.
22. Nishant KT, Plys AJ, Alani E (2008) A mutation in the putative *MLH3* endonuclease domain confers a defect in both mismatch repair and meiosis in *Saccharomyces cerevisiae*. Genetics 179: 747–755.
23. Zakharyevich K, Ma Y, Tang S, Hwang PY, Boiteux S, et al. (2010) Temporally and biochemically distinct activities of Exo1 during meiosis: double-strand break resection and resolution of double Holliday junctions. Mol Cell 40: 1001–1015.
24. Zalevsky J, MacQueen AJ, Duffy JB, Kemphues KJ, Villeneuve AM (1999) Crossing over during *Caenorhabditis elegans* meiosis requires a conserved MutS-based pathway that is partially dispensable in budding yeast. Genetics 153: 1271–1283.
25. Kohl KP, Jones CD, Sekelsky J (2012) Evolution of an MCM complex in flies that promotes meiotic crossovers by blocking BLM helicase. Science 338: 1363–1365.
26. Yildiz O, Majumder S, Kramer B, Sekelsky JJ (2002) *Drosophila* MUS312 interacts with the nucleotide excision repair endonuclease MEI-9 to generate meiotic crossovers. Mol Cell 10: 1503–1509.
27. Smith GR, Boddy MN, Shanahan P, Russell P (2003) Fission yeast Mus81-Eme1 Holliday junction resolvase is required for meiotic crossing over but not for gene conversion. Genetics 165: 2289–2293.
28. Osman F, Dixon J, Doe CL, Whitby MC (2003) Generating crossovers by resolution of nicked Holliday junctions: a role for Mus81-Eme1 in meiosis. Mol Cell 12: 761–774.
29. Boddy MN, Gaillard PH, McDonald WH, Shanahan P, Yates JR, 3rd, et al. (2001) Mus81-Eme1 are essential components of a Holliday junction resolvase. Cell 107: 537–548.
30. de los Santos T, Hunter N, Lee C, Larkin B, Loidl J, et al. (2003) The Mus81/Mms4 endonuclease acts independently of double-Holliday junction resolution to promote a distinct subset of crossovers during meiosis in budding yeast. Genetics 164: 81–94.
31. Berchowitz LE, Francis KE, Bey AL, Copenhaver GP (2007) The role of *AtMUS81* in interference-insensitive crossovers in *A. thaliana*. PLoS Genet 3: e132.
32. Holloway JK, Booth J, Edelmann W, McGowan CH, Cohen PE (2008) MUS81 generates a subset of MLH1-MLH3-independent crossovers in mammalian meiosis. PLoS Genet 4: e1000186.
33. Matos J, Blanco MG, Maslen S, Skehel JM, West SC (2011) Regulatory control of the resolution of DNA recombination intermediates during meiosis and mitosis. Cell 147: 158–172.
34. Fricke WM, Brill SJ (2003) Slx1–Slx4 is a second structure-specific endonuclease functionally redundant with Sgs1-Top3. Genes Dev 17: 1768–1778.
35. Mullen JR, Kaliraman V, Ibrahim SS, Brill SJ (2001) Requirement for three novel protein complexes in the absence of the Sgs1 DNA Helicase in *Saccharomyces cerevisiae*. Genetics 157: 103–118.
36. Wechsler T, Newman S, West SC (2011) Aberrant chromosome morphology in human cells defective for Holliday junction resolution. Nature 471: 642–646.
37. Wood AJ, Severson AF, Meyer BJ (2010) Condensin and cohesin complexity: the expanding repertoire of functions. Nat Rev Genet 11: 391–404.
38. Ampatzidou E, Irmisch A, O'Connell MJ, Murray JM (2006) Smc5/6 is required for repair at collapsed replication forks. Mol Cell Biol 26: 9387–9401.
39. Sheedy DM, Dimitrova D, Rankin JK, Bass KL, Lee KM, et al. (2005) Brc1-mediated DNA repair and damage tolerance. Genetics 171: 457–468.
40. Torres-Rosell J, Machin F, Farmer S, Jarmuz A, Eydmann T, et al. (2005) *SMC5* and *SMC6* genes are required for the segregation of repetitive chromosome regions. Nat Cell Biol 7: 412–419.
41. Chen YH, Choi K, Szakal B, Arenz J, Duan X, et al. (2009) Interplay between the Smc5/6 complex and the Mph1 helicase in recombinational repair. Proc Natl Acad Sci U S A 106: 21252–21257.
42. Chavez A, Agrawal V, Johnson FB (2011) Homologous recombination-dependent rescue of deficiency in the structural maintenance of chromosomes (Smc) 5/6 complex. J Biol Chem 286: 5119–5125.
43. Murray JM, Carr AM (2008) Smc5/6: a link between DNA repair and unidirectional replication? Nat Rev Mol Cell Biol 9: 177–182.
44. Irmisch A, Ampatzidou E, Mizuno K, O'Connell MJ, Murray JM (2009) Smc5/6 maintains stalled replication forks in a recombination-competent conformation. EMBO J 28: 144–155.
45. Bermudez-Lopez M, Ceschia A, de Piccoli G, Colomina N, Pasero P, et al. (2010) The Smc5/6 complex is required for dissolution of DNA-mediated sister chromatid linkages. Nucleic Acids Res 38: 6502–6512.

46. Zhao X, Blobel G (2005) A SUMO ligase is part of a nuclear multiprotein complex that affects DNA repair and chromosomal organization. Proc Natl Acad Sci U S A 102: 4777–4782.
47. Andrews EA, Palecek J, Sergeant J, Taylor E, Lehmann AR, et al. (2005) Nse2, a component of the Smc5–6 complex, is a SUMO ligase required for the response to DNA damage. Mol Cell Biol 25: 185–196.
48. Potts PR, Yu H (2005) Human MMS21/NSE2 is a SUMO ligase required for DNA repair. Mol Cell Biol 25: 7021–7032.
49. Potts PR, Yu H (2007) The SMC5/6 complex maintains telomere length in ALT cancer cells through sumoylation of telomere-binding proteins. Nat Struct Mol Biol 14: 581–590.
50. McAleenan A, Cordon-Preciado V, Clemente-Blanco A, Liu IC, Sen N, et al. (2012) Sumoylation of the alpha-kleisin subunit of cohesin is required for DNA damage-induced cohesion. Curr Biol: CB 22: 1564–1575.
51. Wu N, Kong X, Ji Z, Zeng W, Potts PR, et al. (2012) Scc1 sumoylation by Mms21 promotes sister chromatid recombination through counteracting Wapl. Genes Dev 26: 1473–1485.
52. Hang LE, Liu X, Cheung I, Yang Y, Zhao X (2011) SUMOylation regulates telomere length homeostasis by targeting Cdc13. Nat Struct Mol Biol 18: 920–926.
53. Chen YH, Choi K, Szakal B, Arenz J, Duan X, et al. (2009) Interplay between the Smc5/6 complex and the Mph1 helicase in recombinational repair. Proc Natl Acad Sci U S A 106: 21252–21257.
54. Farmer S, San-Segundo PA, Aragon L (2011) The Smc5–Smc6 complex is required to remove chromosome junctions in meiosis. PLoS One 6: e20948.
55. Wehrkamp-Richter S, Hyppa RW, Prudden J, Smith GR, Boddy MN (2012) Meiotic DNA joint molecule resolution depends on Nse5–Nse6 of the Smc5–Smc6 holocomplex. Nucleic Acids Res 40: 9633–9646.
56. Cromie GA, Hyppa RW, Taylor AF, Zakharyevich K, Hunter N, et al. (2006) Single Holliday junctions are intermediates of meiotic recombination. Cell 127: 1167–1178.
57. Gaskell LJ, Osman F, Gilbert RJ, Whitby MC (2007) Mus81 cleavage of Holliday junctions: a failsafe for processing meiotic recombination intermediates? EMBO J 26: 1891–1901.
58. Bickel JS, Chen L, Hayward J, Yeap SL, Alkers AE, et al. (2010) Structural maintenance of chromosomes (SMC) proteins promote homolog-independent recombination repair in meiosis crucial for germ cell genomic stability. PLoS Genet 6: e1001028.
59. Andersen SL, Sekelsky J (2010) Meiotic versus mitotic recombination: two different routes for double-strand break repair: the different functions of meiotic versus mitotic DSB repair are reflected in different pathway usage and different outcomes. BioEssays 32: 1058–1066.
60. Lindroos HB, Strom L, Itoh T, Katou Y, Shirahige K, et al. (2006) Chromosomal association of the Smc5/6 complex reveals that it functions in differently regulated pathways. Mol Cell 22: 755–767.
61. Xaver M, Huang L, Cheng D, Klein F (2013) Smc5/6-Mms21 prevents and eliminates inappropriate recombination intermediates in meiosis. PLoS Genet 10: e1004067
62. Blat Y, Kleckner N (1999) Cohesins bind to preferential sites along yeast chromosome III, with differential regulation along arms versus the centric region. Cell 98: 249–259.
63. Panizza S, Mendoza MA, Berlinger M, Huang L, Nicolas A, et al. (2011) Spo11-accessory proteins link double-strand break sites to the chromosome axis in early meiotic recombination. Cell 146: 372–383.
64. De Piccoli G, Cortes-Ledesma F, Ira G, Torres-Rosell J, Uhle S, et al. (2006) Smc5–Smc6 mediate DNA double-strand-break repair by promoting sister-chromatid recombination. Nat Cell Biol 8: 1032–1034.
65. Blitzblau HG, Bell GW, Rodriguez J, Bell SP, Hochwagen A (2007) Mapping of meiotic single-stranded DNA reveals double-stranded-break hotspots near centromeres and telomeres. Curr Biol 17: 2003–2012.
66. Buhler C, Borde V, Lichten M (2007) Mapping meiotic single-strand DNA reveals a new landscape of DNA double-strand breaks in *Saccharomyces cerevisiae*. PLoS Biol 5: e324.
67. Chu S, DeRisi J, Eisen M, Mulholland J, Botstein D, et al. (1998) The transcriptional program of sporulation in budding yeast. Science 282: 699–705.
68. Chan AC, Borts RH, Hoffmann E (2009) Temperature-dependent modulation of chromosome segregation in *msh4* mutants of budding yeast. PLoS One 4: e7284.
69. Nishimura K, Fukagawa T, Takisawa H, Kakimoto T, Kanemaki M (2009) An auxin-based degron system for the rapid depletion of proteins in nonplant cells. Nat Methods 6: 917–922.
70. Palecek J, Vidot S, Feng M, Doherty AJ, Lehmann AR (2006) The Smc5–Smc6 DNA repair complex. bridging of the Smc5–Smc6 heads by the kleisin, Nse4, and non-Kleisin subunits. J Biol Chem 281: 36952–36959.
71. Schwacha A, Kleckner N (1994) Identification of joint molecules that form frequently between homologs but rarely between sister chromatids during yeast meiosis. Cell 76: 51–63.
72. Hunter N, Kleckner N (2001) The single-end invasion: an asymmetric intermediate at the double- strand break to double-holliday junction transition of meiotic recombination. Cell 106: 59–70.
73. Lilienthal I, Kanno T, Sjögren C (2013) Inhibition of the Smc5/6 complex during meiosis perturbs joint molecule formation and resolution without significantly changing crossover or non-crossover levels. PLoS Genet 9: e1003898.
74. Svetlanov A, Cohen PE (2004) Mismatch repair proteins, meiosis, and mice: understanding the complexities of mammalian meiosis. Exp Cell Res 296: 71–79.
75. Hunter N, Borts RH (1997) Mlh1p is unique among mismatch repair proteins in its ability to promote crossing-over during meiosis. Genes Dev 11: 1573–1582.
76. Watts FZ, Hoffmann E (2011) SUMO meets meiosis: an encounter at the synaptonemal complex. Bioessays 33: 529–537.
77. Agarwal S, Roeder GS (2000) Zip3 provides a link between recombination enzymes and synaptonemal complex proteins. Cell 102: 245–255.
78. Rockmill B, Fung JC, Branda SS, Roeder GS (2003) The Sgs1 helicase regulates chromosome synapsis and meiotic crossing over. Curr Biol 13: 1954–1962.
79. Kaliraman V, Mullen JR, Fricke WM, Bastin-Shanower SA, Brill SJ (2001) Functional overlap between Sgs1-Top3 and the Mms4-Mus81 endonuclease. Genes Dev 15: 2730–2740.
80. Downs JA, Lowndes NF, Jackson SP (2000) A role for *Saccharomyces cerevisiae* histone H2A in DNA repair. Nature 408: 1001–1004.
81. Carballo JA, Johnson AL, Sedgwick SG, Cha RS (2008) Phosphorylation of the axial element protein Hop1 by Mec1/Tel1 ensures meiotic interhomolog recombination. Cell 132: 758–770.
82. Lee BH, Amon A (2003) Role of Polo-like kinase *CDC5* in programming meiosis I chromosome segregation. Science 300: 482–486.
83. Hochwagen A, Amon A (2006) Checking your breaks: surveillance mechanisms of meiotic recombination. Curr Biol 16: R217–228.
84. Hochwagen A, Tham WH, Brar GA, Amon A (2005) The FK506 binding protein Fpr3 counteracts protein phosphatase 1 to maintain meiotic recombination checkpoint activity. Cell 122: 861–873.
85. Buonomo SB, Clyne RK, Fuchs J, Loidl J, Uhlmann F, et al. (2000) Disjunction of homologous chromosomes in meiosis I depends on proteolytic cleavage of the meiotic cohesin Rec8 by separin. Cell 103: 387–398.
86. Tapia-Alveal C, Outwin EA, Trempolec N, Dziadkowiec D, Murray JM, et al. (2010) SMC complexes and topoisomerase II work together so that sister chromatids can work apart. Cell Cycle 9: 2065–2070.
87. Outwin EA, Irmisch A, Murray JM, O'Connell MJ (2009) Smc5–Smc6-dependent removal of cohesin from mitotic chromosomes. Mol Cell Biol 29: 4363–4375.
88. Matos J, Lipp JJ, Bogdanova A, Guillot S, Okaz E, et al. (2008) Dbf4-dependent CDC7 kinase links DNA replication to the segregation of homologous chromosomes in meiosis I. Cell 135: 662–678.
89. Kim KP, Weiner BM, Zhang L, Jordan A, Dekker J, et al. (2010) Sister cohesion and structural axis components mediate homolog bias of meiotic recombination. Cell 143: 924–937.
90. Yu HG, Koshland DE (2003) Meiotic condensin is required for proper chromosome compaction, SC assembly, and resolution of recombination-dependent chromosome linkages. J Cell Biol 163: 937–947.
91. Pebernard S, McDonald WH, Pavlova Y, Yates JR, 3rd, Boddy MN (2004) Nse1, Nse2, and a novel subunit of the Smc5–Smc6 complex, Nse3, play a crucial role in meiosis. Mol Biol Cell 15: 4866–4876.
92. Pan J, Keeney S (2007) Molecular cartography: mapping the landscape of meiotic recombination. PLoS Biol 5: e333.
93. Yu HG, Koshland D (2005) Chromosome morphogenesis: condensin-dependent cohesin removal during meiosis. Cell 123: 397–407.
94. Roy MA, Siddiqui N, D'Amours D (2011) Dynamic and selective DNA-binding activity of Smc5, a core component of the Smc5–Smc6 complex. Cell Cycle 10: 690–700.
95. Blitzblau HG, Chan CS, Hochwagen A, Bell SP (2012) Separation of DNA replication from the assembly of break-competent meiotic chromosomes. PLoS Genet 8: e1002643.
96. Murakami H, Borde V, Nicolas A, Keeney S (2009) Gel electrophoresis assays for analyzing DNA double-strand breaks in *Saccharomyces cerevisiae* at various spatial resolutions. Methods Mol Biol 557: 117–142.
97. Gray S, Allison RM, Garcia V, Goldman AS, Neale MJ (2013) Positive regulation of meiotic DNA double-strand break formation by activation of the DNA damage checkpoint kinase Mec1(ATR). Open biology 3: 130019.
98. Newnham L, Jordan P, Rockmill B, Roeder GS, Hoffmann E (2010) The synaptonemal complex protein, Zip1, promotes the segregation of nonexchange chromosomes at meiosis I. Proc Natl Acad Sci U S A 107: 781–785.
99. Jordan P, Copsey A, Newnham L, Kolar E, Lichten M, et al. (2009) Ipl1/Aurora B kinase coordinates synaptonemal complex disassembly with cell cycle progression and crossover formation in budding yeast meiosis. Genes Dev 23: 2237–2251.
100. Vader G, Blitzblau HG, Tame MA, Falk JE, Curtin L, et al. (2011) Protection of repetitive DNA borders from self-induced meiotic instability. Nature 477: 115–119.
101. Carlile TM, Amon A (2008) Meiosis I is established through division-specific translational control of a cyclin. Cell 133: 280–291.

OPEN ACCESS Freely available online

PLOS ONE

Ipl1/Aurora Kinase Suppresses S-CDK-Driven Spindle Formation during Prophase I to Ensure Chromosome Integrity during Meiosis

Louise Newnham[◔], **Philip W. Jordan**[◔¤], **Jesus A. Carballo, Sonya Newcombe, Eva Hoffmann***

MRC Genome Damage and Stability Centre, University of Sussex, Brighton, United Kingdom

Abstract

Cells coordinate spindle formation with DNA repair and morphological modifications to chromosomes prior to their segregation to prevent cell division with damaged chromosomes. Here we uncover a novel and unexpected role for Aurora kinase in preventing the formation of spindles by Clb5-CDK (S-CDK) during meiotic prophase I and when the DDR is active in budding yeast. This is critical since S-CDK is essential for replication during premeiotic S-phase as well as double-strand break induction that facilitates meiotic recombination and, ultimately, chromosome segregation. Furthermore, we find that depletion of Cdc5 polo kinase activity delays spindle formation in DDR-arrested cells and that ectopic expression of Cdc5 in prophase I enhances spindle formation, when Ipl1 is depleted. Our findings establish a new paradigm for Aurora kinase function in both negative and positive regulation of spindle dynamics.

Citation: Newnham L, Jordan PW, Carballo JA, Newcombe S, Hoffmann E (2013) Ipl1/Aurora Kinase Suppresses S-CDK-Driven Spindle Formation during Prophase I to Ensure Chromosome Integrity during Meiosis. PLoS ONE 8(12): e83982. doi:10.1371/journal.pone.0083982

Editor: Dean S. Dawson, Oklahoma Medical Research Foundation, United States of America

Received October 14, 2013; **Accepted** October 29, 2013; **Published** December 27, 2013

Funding: EH is a MRC Senior Research Fellowship and an EMBO Young Investigator. SG was funded by a MRC Centenary Award. PJ was funded by BBSCR (BB/E000614/1). The funders had no role in study design, data collection and analysis, decision to publish, or preparation of the manuscript.

Competing Interests: The authors have declared that no competing interests exist.

* E-mail: eh58@sussex.ac.uk

¤ Current address: Biochemistry and Molecular Biology Department, Johns Hopkins School of Public Health, Baltimore, Maryland, United States of America

◔ These authors contributed equally to this work.

Introduction

The DNA damage response (DDR) prolongs the G2/M or prophase arrest when cells are challenged with DNA damage. This is important to prevent attempts at chromosome segregation in the presence of DNA damage that would compromise the genomic integrity of cells. In meiosis, the importance of DNA repair and cell cycle progression has recently been demonstrated in human oocytes, where decreased capacity for DNA repair correlates with reduced ovarian reserve [1]. Even without DNA damage, there are several examples where prophase I is extended, most notably the decades-long prophase I/dictyate arrest in human oocytes. In budding yeast, meiotic prophase I is extended ~ 10-fold compared to mitotic cell cycle [2]. This allows the induction of 150–200 double-strand breaks (DSBs), whose repair by homologous recombination facilitate efficient homolog pairing and crossing over prior to the two nuclear divisions [3,4]. Modifications to chromosome morphology and behaviour are also required to set up the two consecutive segregations of first homologous chromosomes (meiosis I), followed by sister chromatids (meiosis II).

In budding yeast, a single cyclin-dependent kinase (CDK/Cdc28) drives the cell cycle together with six B-type cyclins (Clb1-6). Clb5,6-Cdc28 (S-CDK) promotes DNA replication and spindle pole body maturation (the yeast microtubule organizing centers), whereas mitotic and meiotic divisions are promoted by Clb1,2,3,4-CDK (M-CDK) [5,6,7]. Clb2 is tightly repressed throughout meiosis [8,9]. After meiotic entry, Clb5 and Clb6 are present at low levels throughout meiosis and Clb5 is required for DNA synthesis as well as DSB induction by Spo11 [10,11,12]. Clb5 mutants display low sporulation efficiency, whereas Clb6 has no detectable defects [10]. This is consistent with the notion that Clb5 is the main facilitator of S-CDK activity during meiotic prophase I.

Onset of M-phase is regulated by the meiosis-specific Ndt80 transcription factor that induces expression of the M-phase cyclins, Clb1 and Clb4 [9,10,13]. Ndt80 is negatively regulated by the meiotic DDR and when active, drives cells from mid-prophase I (pachytene) into the meiotic divisions [14,15]. Ndt80 is essential for extending prophase I and coupling prophase I exit to the DDR. Its mitotic counterpart, Ndd1, is actively degraded during meiosis and its stabilization causes a contraction in prophase and precocious expression of M-CDK and polo kinase, leading to meiotic catastrophe [16] (Fig. 1A). High levels of expression of Clb1, Clb3, or Clb4 can drive spindle formation, even when ectopically expressed in meiotic prophase I [17,18]. This is consistent with the requirement for active CDK in SPB separation and spindle formation [19,20]. In contrast, ectopic expression of Cdc5 polo kinase, which is up-regulated by Ndt80, leads to chromosome restructuring, but not SPB separation [20], although Cdc5 polo kinase activity is important for the timely separation of SPBs [21]. Thus, Cdc5 promotes the efficiency of, but is not sufficient to drive spindle formation. Combined, high levels of Cdc5 and M-CDK activity are thought to be required for spindle formation upon exit from pachytene.

Although the transcriptional activation of M-CDK is the main driver of spindle formation, S-CDK is active during all of meiotic

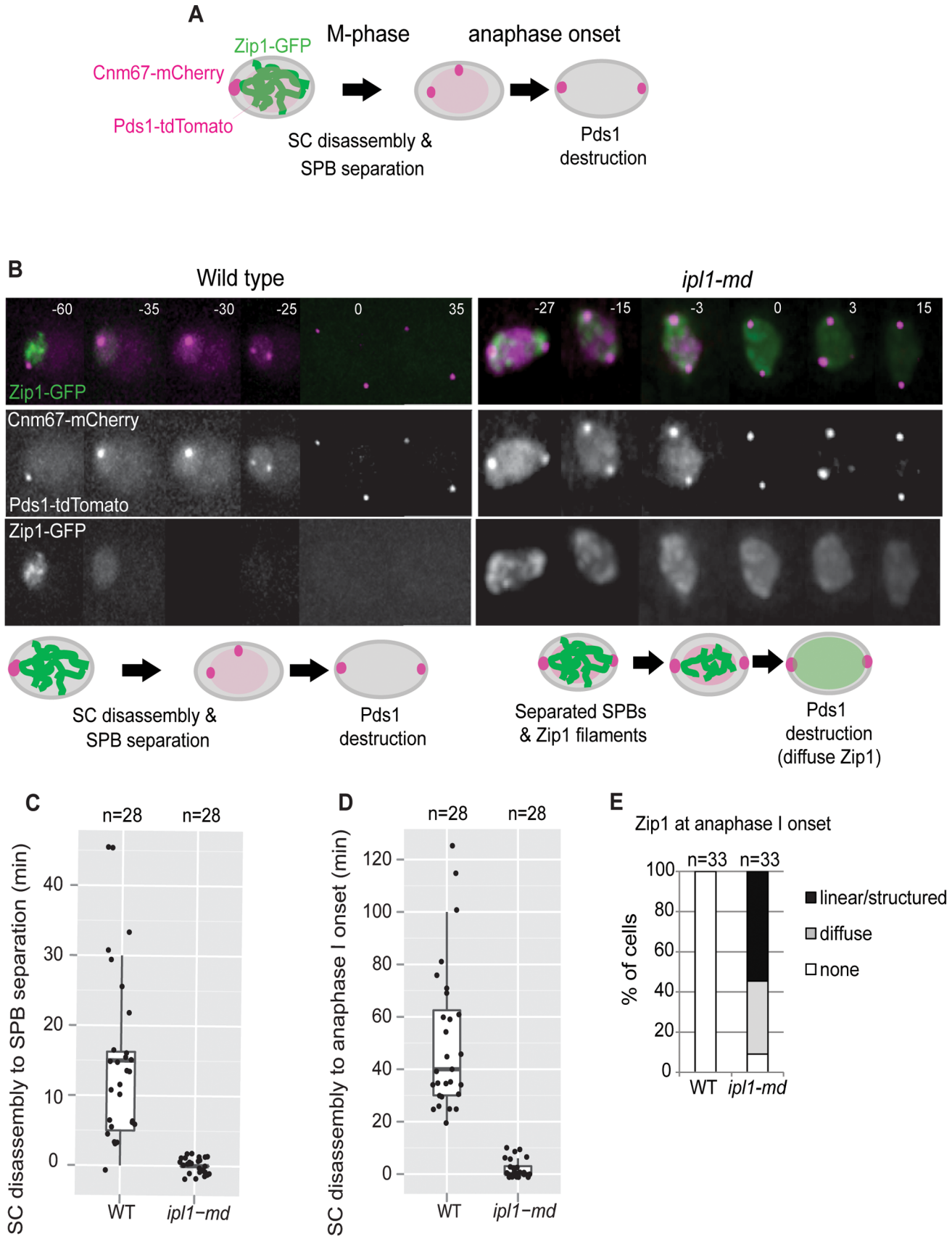

Figure 1. Zip1 disappearance is delayed in *ipl1-mn* mutants. (A) Experimental set up. SCs are followed by Zip1-GFP; SPBs by Cnm67-mCherry, and anaphase I onset by Pds1-tdTomato (confluent staining). (B) Representative montages of SC disassembly (loss of Zip1-GFP), SPB separation

(CNM67-mCherry), and anaphase I onset (degradation of Pds1-tdTomato) in wild type (Movie S1) and *ipl1-mn* (Movie S2). Bars: 2 μm. (C) The proportion of cells with linear Zip1-GFP structures, diffuse Zip1-GFP staining or no Zip1-GFP signal at anaphase I onset (Pds1 degradation). (D) Time from SC disassembly (Zip1-GFP signal loss) to separation of the SPBs. (E) Time from SC disassembly to anaphase I onset (Pds1 degradation). Strains: WT, Y4044 and *ipl1-mn*, Y4047.
doi:10.1371/journal.pone.0083982.g001

prophase I [13]. In mitotically-dividing cells, S-CDK can drive spindle formation, albeit less efficiently than M-CDK [22]. This raises the intriguing question of how cells prevent S-CDK from promoting spindle formation during prolonged prophase I arrest in meiotic cells. Indeed, it has been reported that in *ndt80*Δ-arrested cells, Ipl1 depletion leads to spindle formation, including multipolar spindles [23,24]. Here, we show that in cells in which Ipl1 is inhibited or depleted, S-CDK is both sufficient and necessary to promote spindle formation during meiotic prophase I, whereas Cdc5 Polo kinase assists in the efficiency of spindle formation. We infer that Ipl1 prevents precocious spindle formation by S-CDK and Cdc5. Consistent with the notion that precocious spindle formation is detrimental to establishing appropriate chromosome structure, the spindles that are formed in the absence of Ipl1 are highly dynamic and capable of triggering chromosome segregation and nuclear deformation [25].

Results and Discussion

Ipl1 Decouples Chromosome Restructuring and Bipolar Spindle Formation in Part by Preventing Spindle Formation during Meiotic Prophase I

In budding yeast, spindle formation normally occurs after disassembly of the synaptonemal complex (SCs), which is characteristic of pachytene/mid-prophase I. We previously demonstrated that cells depleted for the Aurora kinase orthologue, Ipl1 (*ipl1-meiotic depletion*), contained spindles in cells that displayed full SCs. Synaptonemal complexes (SCs) normally disassemble upon Ndt80-mediated exit from pachytene and entry into M-phase. However, in the Ipl1-depleted cells, the SCs were retained at later time points, despite the M-phase cyclins (Clb1 and Clb3) being expressed with wild-type timing [26,27]. This led us to suggest that Ipl1 couples SC disassembly to cell cycle progression [27]. Recent observations suggest, however, that inactivation of Ipl1 causes a contraction in metaphase I [28], consistent with an earlier timing of the appearance of spindles in Ipl1-depleted cells. This, together with the observation that cells depleted for Ipl1 show precocious spindle formation, when held in *ndt80*Δ prophase I arrest [23], raises the distinct possibility that Ipl1 could also suppress precocious spindle formation in pachytene cells.

To investigate whether chromosome restructuring was delayed and/or spindle formation premature, when Ipl1 was depleted, we took advantage of developments in time-lapse imaging of the synaptonemal complex protein, Zip1-GFP [29], whose disassembly from the SC and degradation occur concurrently [27]. Spindle poles bodies (SPB) were marked by CNM67-mCherry, and anaphase I onset was monitored by Pds1-tdTomato degradation (Fig. 1, Movie S1). In the wild type, Zip1-GFP disappeared 15 min. (median time; n = 28) prior to SPB separation and 40 min. (median time; n = 28) prior to anaphase I onset (loss of securin/Pds1 signal, Fig. 1C). In contrast, virtually all of the *ipl1-md* cells contained a strong Zip1-GFP signal at the time of SPB separation as well as anaphase I onset (Fig. 1C–D, Movie S2). By anaphase I onset (Pds1 degradation), more than half of the cells still contained significant Zip1-GFP staining (Fig. 1E), including linear structures (Fig. 1E). We assessed fixed, spread meiotic nuclei as well to ascertain that the SCs observed were indeed associated with meiotic chromosomes (Fig. 2). Using fixed cells, we observed a delayed removal of SCs from the meiotic chromosomes after release from pachytene arrest (Fig. 2), as previously reported [27]. Collectively, our observations are consistent with those made previously in fixed, spread nuclei [27], and suggest that Ipl1 promotes coupling of chromosome restructuring with cell cycle progression. Since SCs eventually disassemble in metaphase-arrested Ipl1 mutants, Ipl1 promotes the efficiency [27], as opposed to being absolutely required, for chromosome restructuring. It is possible that the chromosome restructuring defects could be due to the contraction in the cell cycle *per se*, since metaphase I is shortened in *ipl1* mutants [24]. This would imply that cell cycle progression into M-phase of meiosis I occurs in parallel with SC disassembly and that cells have a limited window for chromosome restructuring. Moreover, the nature of cell cycle contraction clearly matters, since SC disassembly is not delayed relative to spindle formation in *mad3* mutants [27], where the meiotic cell cycle is also contracted [30].

ipl1-md Mutants Display Spindle Formation in ndt80 and Efficient Spindle Formation after Entry into Meiosis I

If Ipl1 suppresses the formation of spindles during meiotic prophase I, then one would expect *ipl1-md* mutants to form spindles when cells are arrested in prophase I (*ndt80*, Fig. 3). To determine whether this was the case, we followed spindle dynamics (Tub1-GFP) and nuclear separation (H2B-mCherry) during time lapse studies. In agreement with previous observations [23], we observed spindle formation in *ndt80*Δ cells, when Ipl1 was depleted (Fig. 3A,B, Movie S3–S4) or when its kinase activity was inhibited using the *ipl1-as5* allele [31] that renders the kinase sensitive to the ATP analogue, 1-NA-PP1 (Fig. 4). Intriguingly, these spindles appeared to be highly dynamic (Fig. 3C, Movie S5), undergoing several cycles of elongation-collapse. Moreover, spindle elongation and collapse were coordinated with attempts at nuclear separation and relapse (Fig. 3C) suggesting that the spindles are capable of force generation.

We next addressed whether *ipl1-md* mutants are capable of forming spindles when released into M-phase. To do so, we released *ipl1-md* cells from Ndt80-arrest using the *ndt80-IN* ('*IN*ducible') allele. In this system, transcription of Ndt80 has been placed under the regulation of the $P_{GAL1/10}$ promoter. Addition of β-estradiol causes the translocation of Gal4-estrogen receptor fusion protein to the nucleus and induces transcription of genes under the regulation of the $P_{GAL1/10}$ promoter, including $P_{GAL1/10}$-*NDT80* [13]. In this set up, Clb1 and Clb3 are induced with normal levels and kinetics in the *ipl1-md* mutant relative to wild type [27].

Release from Ndt80 arrest revealed that proficient spindle formation occurred ~ 15 min after release in the *ipl1-md NDT80-IN* cells, whereas control *NDT80-IN* cells took ~ 1 hour to display spindles, the time at which Clb1 becomes visible on Western blots [13,27] (Fig. 3D). Moreover, by 60 min. after Ndt80 induction, when Clb1-CDK is expressed and becomes active [13,27], nearly 80% of cells had formed spindles in the *ipl1-md NDT80-IN* strain, compared to 10% in the wild type *NDT80-IN* strain (Fig. 3D). Therefore, the efficiency of spindle formation is enhanced after progression into M-phase in the absence of Ipl1. Given the low levels of SPB separation at 30–45 minutes in the *NDT80-IN* wild

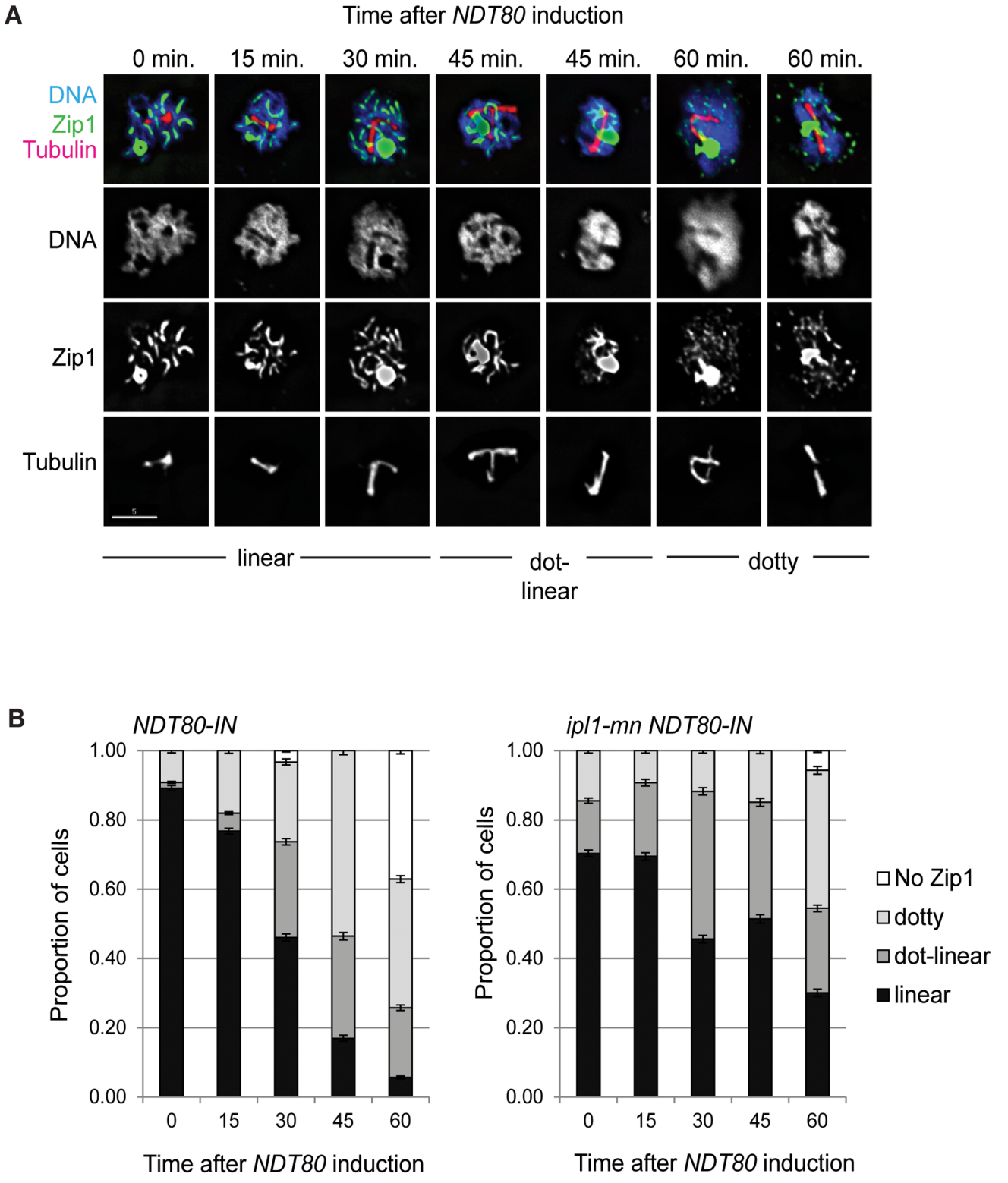

Figure 2. SC disassembly is delayed in *ipl1-mn* after release from Ndt80/mid-prophase arrest. (A) Examples of SCs, their classification and typical Zip1 staining patterns in the *ipl1-mn NDT80-IN* mutant during arrest (t = 0 min.) and after release from *ndt80* arrest. (B) Proportion of spread, meiotic nuclei with linear, dot-linear, dotty, or no Zip1 staining in *NDT80-IN* and *ipl1-mn NDT80-IN*. n >100 cells were assessed for each time point.
doi:10.1371/journal.pone.0083982.g002

type control (~ 5%, Fig. 3D), the enhanced efficiency of spindle formation in the *ipl1-md* strain may be due to the precocious separation of SPBs during the preceding prophase I. This would imply that SPB separation may be a rate-limiting step in spindle formation in meiosis. Alternatively, spindle elongation may be more proficient in *ipl1-md* mutants.

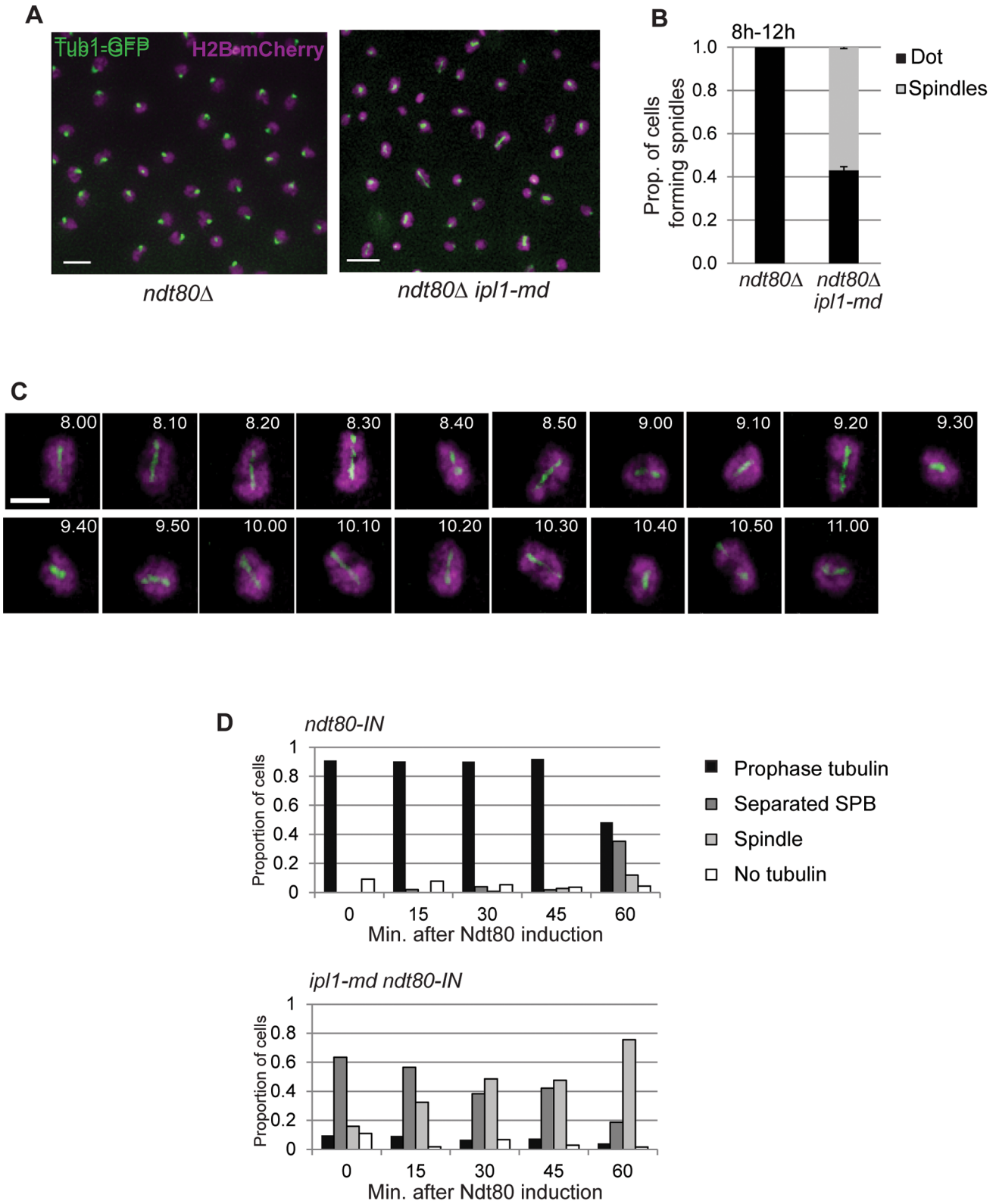

Figure 3. Ipl1 depletion causes precocious formation of spindles in prophase I-arrested *ndt80* mutants. (A) Representative examples of SPB and spindle configurations in *ndt80*Δ and *ndt80*Δ *ipl1-md* mutants. (B) The proportion of cells that formed spindles during the four hours of time-lapse imaging. A small number multipolar spindles were observed; these were added to the 'spindle' category. (C) Representative example dynamic behaviour of tubulin during time-lapse imaging of the *ndt80*Δ *ipl1-md* mutant. (D) Spindle formation in *ipl1-md* cells arrested in prophase I (t = 0; 6 hours in sporulation medium), and after release using the *ndt80-IN* system (WT: Y967 and *ipl1-mn* :Y1169). The spindle and SPB conformation were assessed in >100 cells every 15 min. after release from *NDT80* arrest.
doi:10.1371/journal.pone.0083982.g003

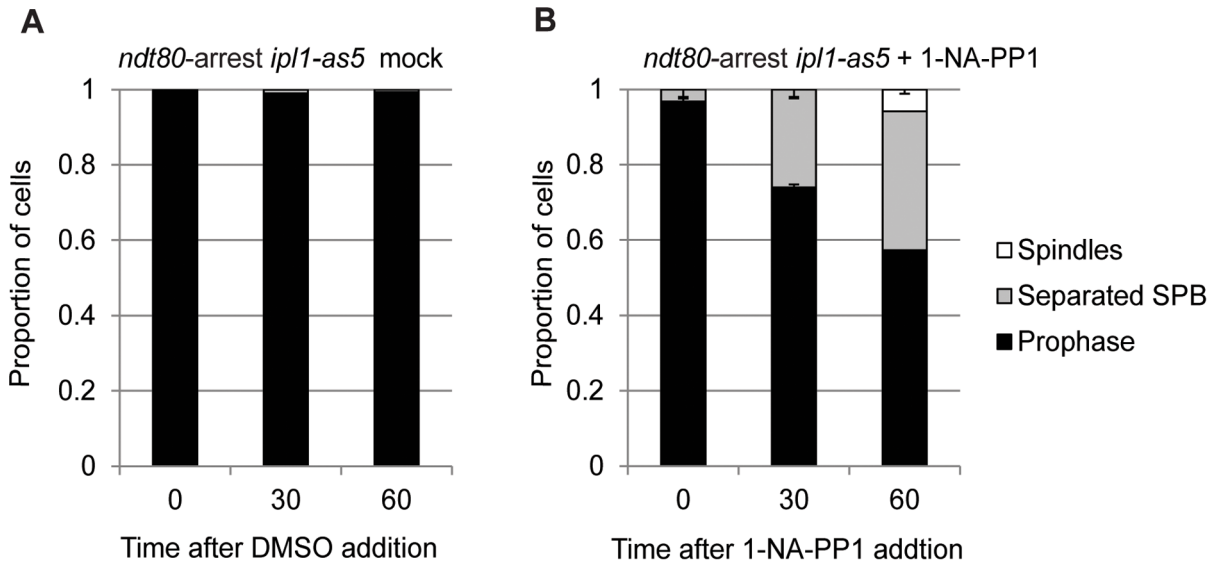

Figure 4. Spindle formation in enhanced when *ipl1-as5* is inhibited during meiotic prophase I arrest (*ndt80*). (A, B) Proportion of *ndt80*-arrested cells carrying the ATP-analogue sensitive *ipl1-as5* allele with separated SPBs or spindles after mock-treatment with DMSO (A) or 50 μM 1-NA-PP1 (B).
doi:10.1371/journal.pone.0083982.g004

Ipl1 Suppresses the Formation of Bipolar Spindles in DDR-arrested Cells

The DDR induces cell cycle arrest and delays the meiotic divisions in response to the accumulation of single-stranded DNA of unrepaired double-strand breaks [15]. We therefore addressed whether Ipl1 is required to prevent spindle formation when cells are arrested by the DDR. To test directly whether Ipl1 inhibits formation of spindles during prophase I arrest, cells were depleted for Ipl1 in three different mutants (*dmc1*Δ, *rec8*Δ, and *hop2*Δ) where the DDR is robustly induced [32,33,34]. Ipl1 depletion caused a significant population of *ipl1-md dmc1*Δ and *ipl1-md hop2*Δ cells to separate their SPBs (>80%, Fig. 5A). Even in the *rec8*Δ mutant, where SPBs reduplicate or fragment after prolonged arrest (Fig. 5A, inset), *ipl1-md* significantly shifted the timing and efficiency of SPB separation. We infer that Ipl1 is important in preventing premature SPB separation under DDR-induced arrest.

To determine whether SPB separation was accompanied by spindle formation despite DDR induction in the *ipl1-md* mutant, we examined spindle structures in fixed and live cells using GFP-tagged Tub1 (Fig. 5B–D). Nearly 60% of the *ipl1-md dmc1*Δ cells contained separated SPBs and a third of these (30% overall) contained spindle structures in fixed cells (Fig. 5B,C). Time-lapse imaging revealed that this proportion is a static assessment, which is an underestimate. During a 3 hour time-lapse imaging period, none of the control *dmc1*Δ cells displayed spindle structures (n = 424, Movie S6), whereas >80% of *ipl1-md dmc1*Δ cells (n = 1175) formed at least one spindle structure (Fig. 5D, E, Movie S7) that appeared to display dynamic phases of elongation-collapse (example shown in Fig. 5F, Movie S8). The elongation of the meiotic spindles in *ipl1-md dmc1*Δ cells occurred in concert with attempts at nuclear separation (Fig. 5F).

The spindle dynamics in the *ipl1-md dmc1*Δ cells (Fig. 5F) were reminiscent of that observed in the *ipl1-md ndt80*-arrested cells (Fig. 3C). If these spindles are formed during prophase I, their instability may be due to the lack of anaphase-dependent stabilizing factors [35], inefficient interactions between kinetochores and microtubules [18], or the presence of unresolved joint molecules that prevent chromosome segregation and may cause spindle collapse. Collectively, our data demonstrate that Ipl1 suppresses precocious SPB separation and spindle formation during prophase I, both when cells are repair-proficient (*ndt80*) and when the DDR is induced (*dmc1*, *rec8*, or *hop2*).

Ipl1 Depletion does not Display Classical Transcriptional or Cell Cycle Bypass of the DDR

At least two explanations could account for the observations that Ipl1 depletion causes the formation of spindles in DDR-arrested recombination mutants (Fig. 5A). *ipl1-md* cells could bypass or fail to initiate the DDR, which would imply a role for Ipl1 in the DDR. Alternatively, Ipl1 may prevent the precocious spindle formation in DDR-arrested cells.

To determine whether *ipl1-md* mutant cells were defective in the activation and maintenance of the DDR, we assessed γH2A and Hop1 phosphorylation, which are regulated by Mec1/ATR and the 9-1-1 clamp [14,36]. During a meiotic time course, both γH2A and Hop1 phosphorylation appeared and disappeared in wild type cells. In contrast, both γH2A and Hop1 phosphorylation remained high in the *dmc1*Δ mutant as well as in the *ipl1-md dmc1*Δ cells (Fig. 6A). These observations demonstrate that the DDR is activated in the *ipl1-md dmc1*Δ strain, from which we infer that Ipl1 is not required for the initiation of the DDR.

To assess whether the DDR was maintained similarly in the *ipl1-md dmc1*Δ and the *dmc1*Δ strains, we assessed the expression of Cdc5 polo kinase and the M-CDK cyclins, Clb1 and Clb3, which are meiosis I and II-specific, respectively (Fig. 6A, B) [10,13]. These key cell cycle genes are under the regulation of Ndt80. In both the *dmc1*Δ and *ipl1-md dmc1*Δ cells, only very low levels of Cdc5 and Clb1 appeared at late time points (10–12 hours) compared to wild type. The lack of strong induction of Cdc5 and the Clb1 is not consistent with a classical bypass of DDR maintenance, where the Ndt80-regulon and other M-phase proteins get expressed at high, wild-type levels at early time points [16,37]. Consistent with this, depletion of the mitotic M-phase transcription factor, Ndd1, did not affect spindle formation in the *ipl1-mn ndt80*Δ strain (Fig. 6F). This rules out that a switch from

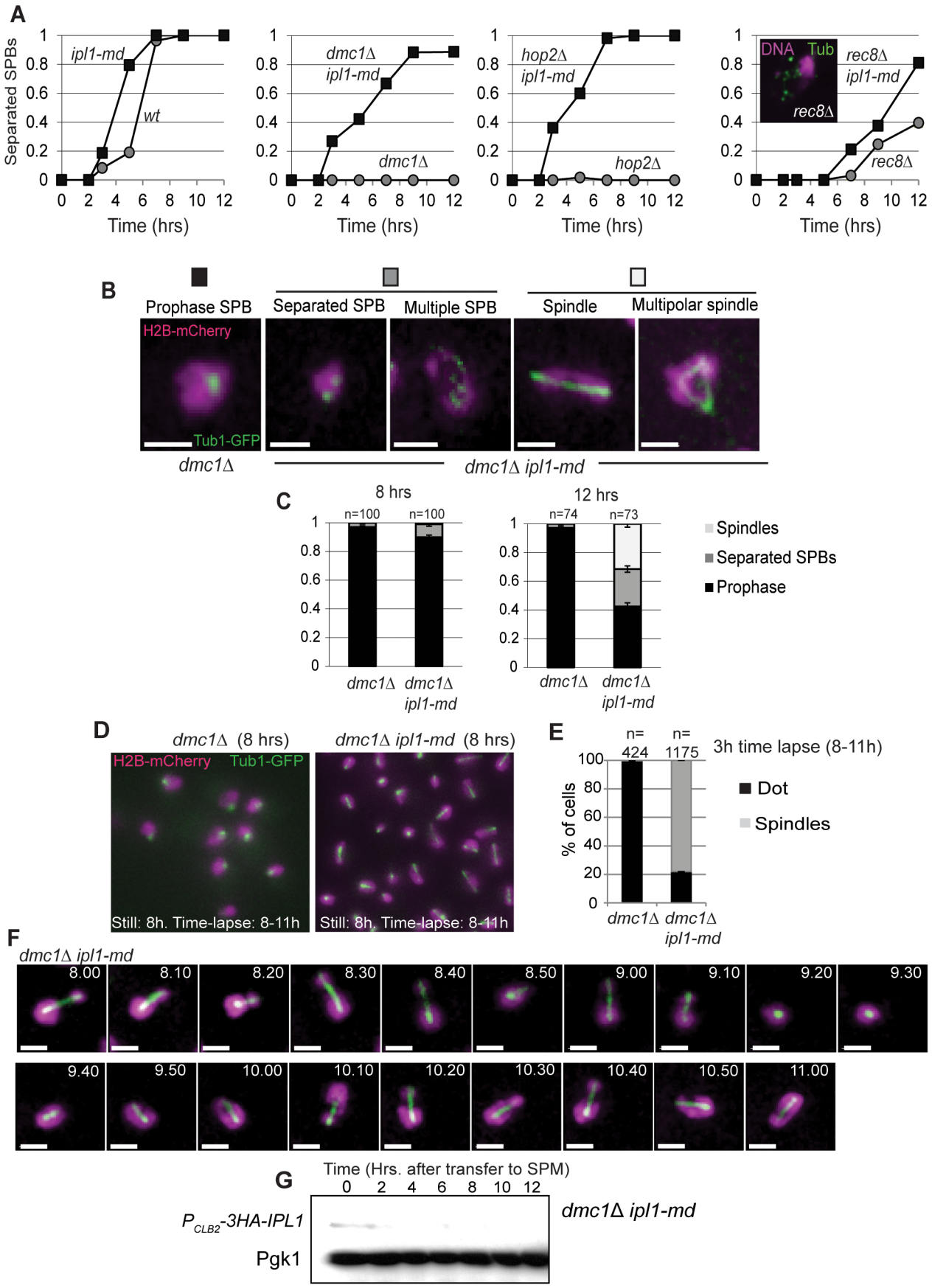
A
Separated SPBs
ipl1-md
wt
Time (hrs)
dmc1Δ
ipl1-md
dmc1Δ
hop2Δ
ipl1-md
hop2Δ
DNA Tub
rec8Δ
rec8Δ
ipl1-md
rec8Δ
B
Prophase SPB
Separated SPB
Multiple SPB
Spindle
Multipolar spindle
H2B-mCherry
Tub1-GFP
dmc1Δ
dmc1Δ ipl1-md
C
8 hrs
12 hrs
n=100
n=100
n=74
n=73
dmc1Δ
dmc1Δ ipl1-md
Spindles
Separated SPBs
Prophase
D
dmc1Δ (8 hrs)
dmc1Δ ipl1-md (8 hrs)
H2B-mCherry Tub1-GFP
Still: 8h. Time-lapse: 8-11h
Still: 8h. Time-lapse: 8-11h
E
n= 424
n= 1175
3h time lapse (8-11h)
% of cells
Dot
Spindles
dmc1Δ
dmc1Δ ipl1-md
F
dmc1Δ ipl1-md
8.00
8.10
8.20
8.30
8.40
8.50
9.00
9.10
9.20
9.30
9.40
9.50
10.00
10.10
10.20
10.30
10.40
10.50
11.00
G
Time (Hrs. after transfer to SPM)
0 2 4 6 8 10 12
P CLB2 -3HA-IPL1
Pgk1
dmc1Δ ipl1-md

Figure 5. Ipl1 prevents formation of spindles in DDR-arrested cells. (A) Proportion of cells with separated spindle-pole bodies as a function of time. Strains: Wild type (Y940), *ipl1-md* (Y1206), *dmc1*Δ (Y2266), *ipl1-md dmc1*Δ (Y2268), *hop2*Δ (Y2489), *hop2*Δ *ip1-mn* (Y2491) *rec8*Δ (Y2404), *rec8*Δ *ipl1-md* (Y2457). Three independent diploids were assessed, a representative time course is shown for each strain. (B, C) Tubulin configurations observed in *dmc1*Δ *ipl1-md* mutants and their prevalence (C). (D) Representative examples of spindle configurations from a single frame (maximum intensity projection) from time lapse imaging in *dmc1*Δ and *dmc1*Δ *ipl1-md* mutants. (E) The cumulative proportion of cells that formed spindles during the three hours of time-lapse imaging (8–11 h). (F) Representative example dynamic behaviour of tubulin (Tub1-GFP) and DNA (H2B-mCherry) during time-lapse imaging of the *dmc1*Δ *ipl1-md* mutant. (G) Western blot showing that Ipl1 is efficiently depleted in *dmc1*Δ *ipl1-md* cells.
doi:10.1371/journal.pone.0083982.g005

Ndt80-driven to Ndd1-promoted M-phase transcription occurs in Ipl1-depleted cells.

Ipl1 Prevents Formation of Spindles in Nuclei with Hop1 Phosphorylation

If Ipl1 suppresses spindle formation in DDR-activated cells, then one should observe spindles or separated SPBs in cells where the DDR is activated. This would predict the existence of meiotic nuclei stained positively for phosphorylated Hop1 and that also contain separated SPBs or spindles. To test whether this was the case, we spread meiotic nuclei and stained with a phospho-specific antibody against Hop1 [38] as well as tubulin (Fig. 6B) in order to determine DDR checkpoint activity on a single-cell basis. In the wild type, 63% (n = 110) of cells were positive for phospho-Hop1 at 4 hours and this decreased to 13% (n = 106) by 8 hours (Fig. 6C), consistent with the progression of cells in meiosis I (100% of cells had separated their SPBs). 63% (n = 110) of cells with a single SPB focus stained positive for phospho-Hop1, whereas only 2% (n = 112) of the cells with separated SPBs were positive for Hop1 phosphorylation (Fig. 6D), demonstrating that Hop1 phosphorylation normally disappears by the time of Ndt80-driven exit from meiotic prophase I. This is consistent with the DDR becoming inactivated prior to transition into M-phase. Conversely, of 71 phospho-Hop1 positive cells, 99% contained un-separated SPBs and only 1% displayed separated SPBs. These observations support the conclusion that progression into M-phase (separation of SPBs) normally occurs concomitantly with the inactivation of the DDR.

In contrast, in the *dmc1*Δ mutant, 97% (n = 200) and 95% (n = 102) of nuclei were positive for Hop1 phosphorylation at 4 and 8 hours, respectively (Fig. 6C). This is consistent with persistent DDR signalling due to the accumulation of extensive single-stranded DNA. All of these nuclei contained un-separated SPBs (Fig. 6E).

In the *ipl1-md dmc1*Δ mutant, despite the slight decrease in phospho-Hop1 positive cells from 4 hours (78%) to 8 hours (54%; Fig. 6C), more than half of the cells (54%, n = 35) with separated SPBs were positive for phospho-Hop1 (Fig. 6D). Moreover, more than a third of nuclei selected for phospho-Hop1 staining (37%, n = 52, Fig. 6E) contained separated SPBs. This demonstrates that spindles can form despite DDR activation when Ipl1 is depleted. Collectively, our data support the conclusion that Ipl1 suppresses the formation of spindles during meiotic prophase I and when the meiotic DDR is active.

S-CDK is Required and Sufficient to Drive Spindle Formation in the ipl1-md Mutant

The hypothesis that Ipl1 suppresses spindle formation during meiotic prophase I when the meiotic DDR is intact makes three clear predictions. First, if spindle formation occurs in cells that are biochemically in meiotic prophase I, then S-CDK would be expected to drive the formation of the spindles, since M-CDK is presumably inactive. This predicts that deleting S-CDK activity (*clb5*Δ *clb6*Δ) should abrogate spindle formation in *ipl1-md dmc1*Δ cells. To test this prediction, we generated an *ipl1-md dmc1*Δ *clb5*Δ *clb6*Δ quadruple mutant and assessed spindle formation (Fig. 7A,B). Without S-CDK activity, none of the cells displayed spindles and only a very minor fraction (<1%) showed a doublet of SPBs (e.g. middle image in Fig. 7A). This strongly suggests that the spindle formation in the *ipl1-md* mutant is dependent upon S-CDK activity, when the meiotic DDR is active.

Second, if S-CDK drives spindle formation, then S-CDK activity should be sufficient to cause spindle formation in the *ipl1-md dmc1*Δ mutant. To test whether this was the case, we assessed spindle formation in this mutant when the M-CDKs were deleted (*clb1*Δ *clb3*Δ *clb4*Δ *clb6*Δ). In this strain where Clb5-CDK drives meiosis and M-CDK is absent (*ipl1-md dmc1*Δ *clb1*Δ *clb3*Δ *clb4*Δ *clb6*Δ *CLB5*$^{+}$), spindle formation occurred with similar efficiency compared to the *ipl1-md dmc1*Δ strain that contained intact M-CDK (Fig. 7A, B). These observations support the notion that Clb5-CDK is sufficient to drive spindle formation, when Ipl1 is depleted.

Finally, if S-CDK promotes the formation of spindles in normal, DNA repair proficient cells (*DMC1*), then inhibiting CDK activity should abolish spindle formation during meiotic prophase (*ndt80*) in Ipl1-depleted cells. To test whether the spindle formation depended upon CDK activity, we inhibited the single cell cycle CDK in budding yeast (Cdc28) in prophase I arrested cells (*ndt80*). To this end, we used the bio-orthogonal approach of modifying the ATP binding site of Cdc28 (*cdc28-as1*) and challenging cells with a modified ATP analogue (1-NM-PP1) that specifically inhibits Cdc28-as1, but not other ATPases [39]. In the mock-treated *ipl1-md ndt80*Δ *cdc28-as1* strain, we observed 21% (±3.7%) of cells with spindles at 8 hours (fixed cells; Fig. 7C, D). In contrast, when cells were treated with the ATP analogue to inhibit Cdc28/CDK activity, the percentage of cells with spindles was reduced to 3% (±2.1%; Fig. 7C,D). This is consistent with CDK activity being critical for spindle formation during meiotic prophase I. Moreover, since the inhibitor was added after spindle formation had initiated in the *ipl1-md ndt80*Δ cells, continuous CDK activity appears to be important for spindle formation. One possibility is that CDK activity is required continuously due to the cycles of elongation-collapse that the *ipl1-md* spindles undergo (Fig. 3C, 5F).

Collectively, our data show that S-CDK is sufficient and necessary to drive spindle formation during prophase I arrest in budding yeast meiosis, when Ipl1 is depleted. From this we infer that Ipl1 is required to suppress S-CDK-mediated spindle formation during meiotic prophase I in arrested cells (*ndt80*Δ) and during DDR-mediated arrest, when double-strand break repair is defective (*dmc1*Δ).

Efficiency of Spindle Formation in Ipl1-depleted Cells is Enhanced by Cdc5 Polo Kinase

Cdc5 polo kinase is important for the timely separation of SPBs in both mitosis and meiosis of budding yeast [21,40]. In meiotic prophase I, Cdc5 levels are kept low due to degradation by the APC^{Ama1} [16], until Ndt80 induction, upon which Cdc5 levels accumulate (Fig. 6A) [10]. Depletion of Cdc5 during prophase I leads to defects in Ndt80 production [41]. To understand the requirement for polo kinase in meiotic spindle formation when

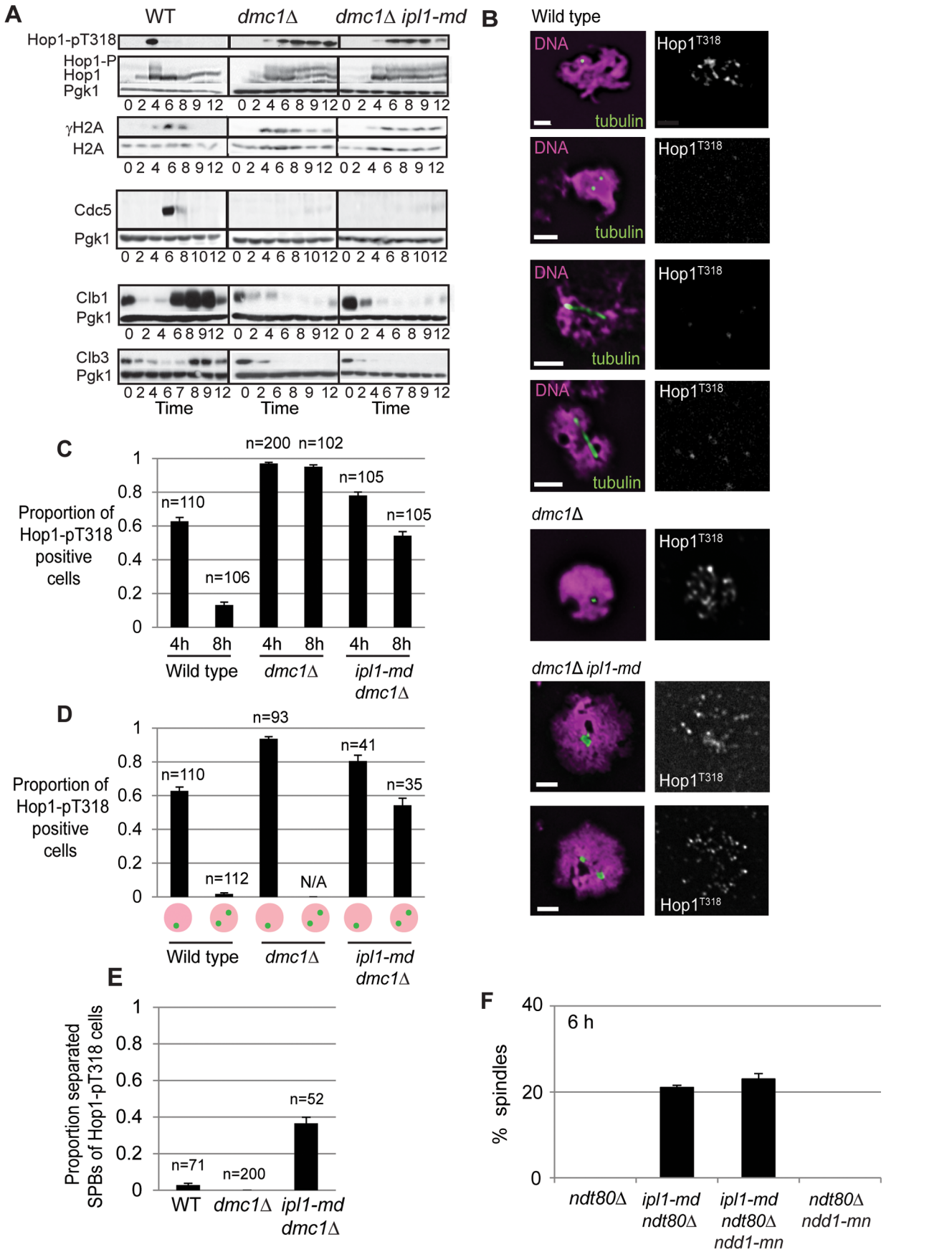
A
WT
dmc1Δ
dmc1Δ ipl1-md
Hop1-pT318
Hop1-P
Hop1
Pgk1
γH2A
H2A
Cdc5
Clb1
Clb3
Time
B
Wild type
DNA
tubulin
Hop1T318
dmc1Δ
dmc1Δ ipl1-md
C
Proportion of Hop1-pT318 positive cells
n=110
n=106
n=200
n=102
n=105
n=105
4h
8h
Wild type
dmc1Δ
ipl1-md dmc1Δ
D
Proportion of Hop1-pT318 positive cells
n=110
n=112
n=93
N/A
n=41
n=35
E
Proportion separated SPBs of Hop1-pT318 cells
n=71
n=200
n=52
WT
F
% spindles
6 h
ndt80Δ
ipl1-md ndt80Δ
ipl1-md ndt80Δ ndd1-mn
ndt80Δ ndd1-mn

Figure 6. Ipl1 mutants do not bypass the DDR at early time points or display defective regulation of Ndd1. (A) Western blot analysis of Hop1 and γH2A phosphorylation and expression of Cdc5 (MI), Clb1 (MI) and Clb3 (MII) under the regulation of Ndt80. Pgk1 is used as a loading control. Strains: Y4489–Y4494. (B) Examples of phosphorylated Hop1 localization to meiotic chromosomes in wild type, *dmc1*Δ, and *dmc1*Δ *ipl1-md* nuclei. (C) Proportion of nuclei with phospho-Hop1 (T318) staining at 4 h and 8 h. (D) Proportion of nuclei with phospho-Hop1 (T318) staining amongst nuclei with un-separated versus separated SPBs. (E) Proportion of phospho-Hop1 positive nuclei with separated SPBs. (F) Examples of spindle formation in *ipl1-md ndt80*Δ mutant and the % of cells that display spindles in *ndt80*Δ (Y2241), *ipl1-md ndt80*Δ (Y2575), *ipl1-md ndt80*Δ *ndd1-mn* (Y4499), and *ndt80*Δ *ndd1-mn* (Y2646) at 8 hours.
doi:10.1371/journal.pone.0083982.g006

Ipl1 is depleted, we assessed SPB dynamics in *ipl1-md* mutants that also lacked polo kinase activity (*cdc5-meiotic depletion*). In the *ipl1-md dmc1*Δ mutant, the cumulative proportion of cells that formed a spindle during 3 hours of time-lapse imaging was ~ 80% (Fig. 8B, Movie S7). In contrast, when Cdc5 was depleted in this background, SPB separation and spindle appearance was significantly reduced (5% of cells; Fig. 8C,D, Movie S9–S10). Only from 12 hours onwards, after a 4 hour delay, did a significant proportion of *ipl1-md dmc1*Δ *cdc5-mn* cells form spindles (Fig. 8E,F, Movie S11–S12). This delay is similar to that reported in ensemble population studies of *cdc5* alone [21]. Unlike the prophase I spindles formed in the *ipl1-md dmc1*Δ of *ipl1-md nt80* mutants, these spindles were not dynamic, but appeared to elongate before disassembling with separated DNA masses (Movie S13). From these observations, we infer that although even low levels of Cdc5 may be sufficient to promote SPB separation, when Ipl1 activity is low or suppressed.

If Cdc5 promotes the efficiency of spindle formation during meiotic prophase I in *ipl1-md* cells, then ectopic expression of Cdc5 in *ndt80*-arrested prophase cells should enhance spindle formation in *ipl1-md* mutant. Ectopic overexpression of Cdc5 on its own is insufficient to drive spindle formation in *ndt80* arrested cells

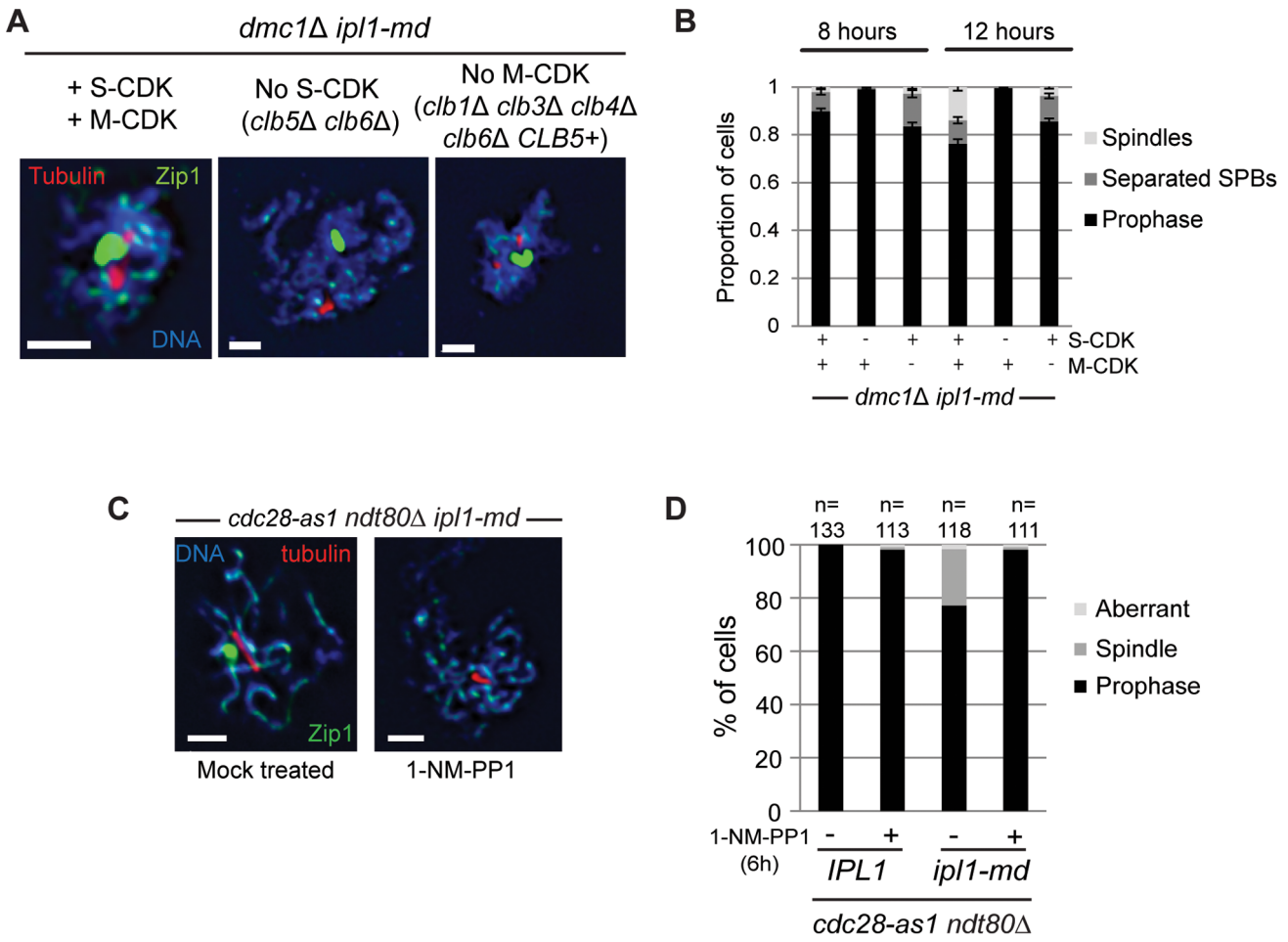

Figure 7. S-CDK is required and sufficient to drive SPB separation and spindle formation during prophase I in *ipl1-md* cells. (A)Images for tubulin and Zip1 staining in *dmc1*Δ *ipl1-md* strains with normal S-CDK and M-CDK (left image), lacking S-CDK activity (*clb5*Δ *clb6*Δ; middle image), or without M-CDK proficient for Clb5 only (*clb1*Δ, *clb3*Δ, *clb4*Δ, *clb6*Δ *CLB5*$^{+}$; right panel). Strains: Y4495, Y4435, and Y4496, respectively. Bars, 2 μm. (B) Quantification on the proportion of fixed cells with spindles and separated SPBs at 8 hours and 12 hours. (C, D) *ipl1-md ndt80*Δ *cdc28-as1* (Y2577) cells were treated with either 50 μM 1-NM-PP1 (+) or solvent only (DMSO) (−) to inhibit Cdc28/CDK kinase activity at 6 hours, when spindles have formed in at least 20% of *ipl1-md ndt80*Δ cells. Examples of spread, meiotic nuclei are shown to the left. Note that there was no effect on inhibiting Cdc28-as1 in *ndt80*Δ alone bars, 2 μm. The graph shows that Quantification of prophase spreads with spindles or aberrant spindle pole structures (*e.g.* multipolar spindles).
doi:10.1371/journal.pone.0083982.g007

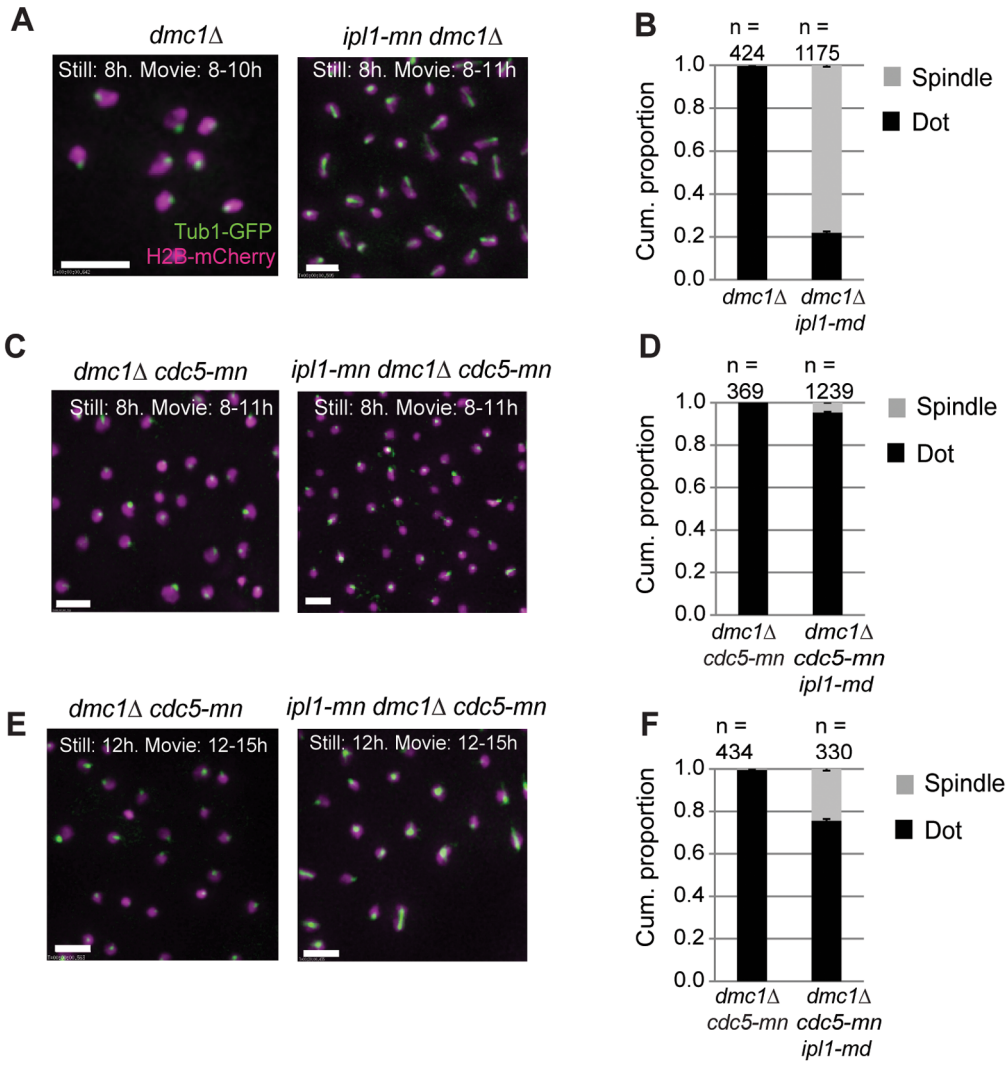
A
dmc1Δ
ipl1-mn dmc1Δ
Still: 8h. Movie: 8-10h
Still: 8h. Movie: 8-11h
Tub1-GFP
H2B-mCherry
B
n = 424
n = 1175
Cum. proportion
Spindle
Dot
dmc1Δ
dmc1Δ ipl1-md
C
dmc1Δ cdc5-mn
ipl1-mn dmc1Δ cdc5-mn
Still: 8h. Movie: 8-11h
Still: 8h. Movie: 8-11h
D
n = 369
n = 1239
dmc1Δ cdc5-mn
dmc1Δ cdc5-mn ipl1-md
E
dmc1Δ cdc5-mn
ipl1-mn dmc1Δ cdc5-mn
Still: 12h. Movie: 12-15h
Still: 12h. Movie: 12-15h
F
n = 434
n = 330

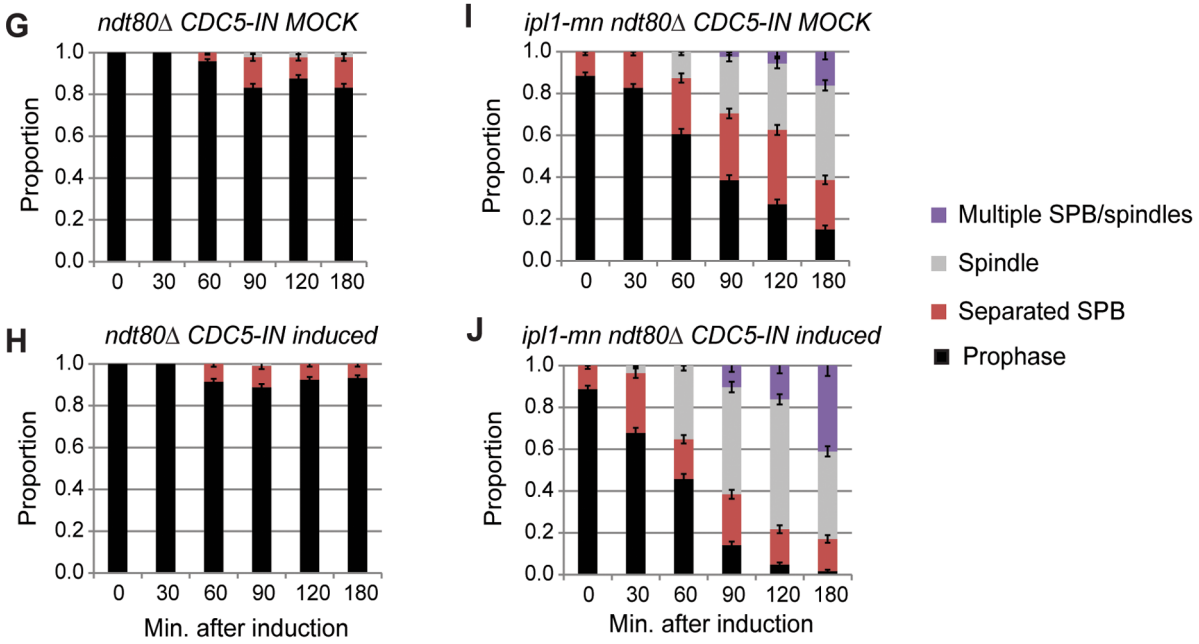
G
ndt80Δ CDC5-IN MOCK
I
ipl1-mn ndt80Δ CDC5-IN MOCK
H
ndt80Δ CDC5-IN induced
J
ipl1-mn ndt80Δ CDC5-IN induced
Proportion
0 30 60 90 120 180
Min. after induction
Multiple SPB/spindles
Spindle
Separated SPB
Prophase

Figure 8. Meiotic depletion of Cdc5 causes delayed spindle formation in *ipl1-md* cells. (A,B) Examples of spindle formation (Tub1-GFP) and nuclear dynamics (H2B-mCherry) in *dmc1*Δ (Y4301), *ipl1-mn dmc1*Δ (Y4304). Bar: 5 μm. The cumulative proportion of cells forming spindle structures during the time lapse are shown in the graph to the right (B). (C,D) Examples of spindle formation (Tub1-GFP) and nuclear dynamics (H2B-mCherry) *dmc1*Δ *cdc5-mn* (Y4405; Movie S6), and *ipl1-mn dmc1*Δ *cdc5-mn* (Y4398; Movie S9–10). The cumulative proportion of cells forming spindle structures during the time lapse from 8–11 hours are shown in the graph (D). (E,F) Examples of spindle formation (Tub1-GFP) and nuclear dynamics (H2B-mCherry) *dmc1*Δ *cdc5-mn* (Y4405; Movie S11), and *ipl1-mn dmc1*Δ *cdc5-mn* (Y4398; Movie S11–12). The cumulative proportion of cells forming spindle structures during the time lapse from 12–15 hours is shown in the graph (F). (G, H) Population dynamics of SPB separation and spindle formation in prophase I arrested cells (*ndt80*), where mock-treatment (K) or induction of *CDC5* (L) occurred. *CDC5-IN* ($P_{GAL1/10}$-*CDC5 GAL4.ER*) has been described previously (Souranajan and Lichten, 2008; Jordan et al. 2009) and strains also carried a wild-type copy of *CDC5*. (I, J) Population dynamics of SPB separation and spindle formation in prophase I arrested cells with Ipl1 depleted (*ipl1-md ndt80*), where mock-treatment (D) or induction of *CDC5* (E) occurred, as in (K,L).
doi:10.1371/journal.pone.0083982.g008

(Sourirajan and Lichten 2008, and Fig. 8H). However, when Cdc5 was induced in the Ipl1-depleted cells (*ndt80*Δ *ipl1-md CDC5-IN*), enhanced efficiency of SPB separation and spindle formation was observed compared to mock induction (Fig. 8J versus I, respectively; $P<0.01$, G-test). These experiments demonstrates that Cdc5 contributes towards the efficient formation of spindles when Ipl1 is depleted. Furthermore, they show that, at least in part, induction of Cdc5 has no effect due to the presence of Ipl1.

Coordination of spindle formation and chromosome restructuring in preparation for chromosome segregation is essential during meiosis. In this work, we have identified a novel and unexpected role for Ipl1 during meiotic prophase I in suppressing spindle formation in both prophase I-arrested (*ndt80*Δ) and DDR-arrested (*dmc1*Δ) cells. Specifically, Ipl1 activity is required to suppress or counteract spindle formation by S-CDK and when Cdc5 activity is low. Repressing the formation of spindles by S-CDK during meiotic prophase I is essential, because S-CDK is active and indeed required for the initiation of meiotic recombination [12]. Many studies of Aurora kinases to date have revealed critical functions in the formation and stabilization of spindles. Our findings and those of Kim *et al.* [24] reveal another function in the suppression of precocious spindle formation. Ipl1 is also important for the disassembly of the outer kinetochores during early stages of meiotic prophase I, which prevents ends-on chromosomal attachments to microtubules [28]. Thus, Ipl1 has a dual function in suppressing inappropriate attachment of immature meiotic chromosomes to spindles during meiotic prophase I. Our data show that Ipl1 prevents spindle formation facilitated by S-CDK and to lesser extent, Cdc5, during prophase I. The active suppression of S-CDK-mediated and Cdc5 polo kinase-driven spindle formation during meiotic prophase I, or when the DDR is active (illustrated in Figure 9), is consistent with findings that ectopic expression of Cdc5 or Clb5 during prophase I is not sufficient to cause spindle formation [18,20]. In particular, Clb5 overexpression in prophase I leads to an enhancement of CDK activity that is similar in magnitude to that observed for the meiosis II specific M-phase cyclin, Clb3 [18]. However, unlike Clb3, overexpression of Clb5 does not induce spindle formation [18], presumably due to the presence of Ipl1.

Our findings that CDK and polo kinase can drive or enhance spindle formation in prophase I (when Ipl1 is depleted or inactivated) is analogous to recent reports that CDK- and polo kinase promote centrosome separation during interphase in higher eukaryotes (mitotic cell cycle) [42,43,44]. Our data further demonstrate that M-CDK and high protein levels of Cdc5 (both induced by Ndt80 upon entry into M-phase) are not a *de facto* requirement for spindle formation in budding yeast meiosis. Instead, S-CDK and low levels of Cdc5 are sufficient to drive spindle elongation, but only in the absence of Ipl1. In a separate study, Kim *et al.* [24] showed that Ipl1 may prevent precocious spindle formation by blocking Clb4 localisation at spindle pole bodies. This raises the intriguing possibility that Ipl1 functions directly at SPBs in a localized manner to prevent SPB separation and spindle formation by S-CDK (Clb5) during meiotic prophase I. Another possibility is that Ipl1's role in SPB cohesion in itself [23] prevents Cdc5- and S-CDK-mediated spindle formation. For example, if SPB separation is the rate limiting step during spindle formation in budding yeast, then loss of SPB cohesion might be sufficient to trigger spindle formation by S-CDK and Cdc5.

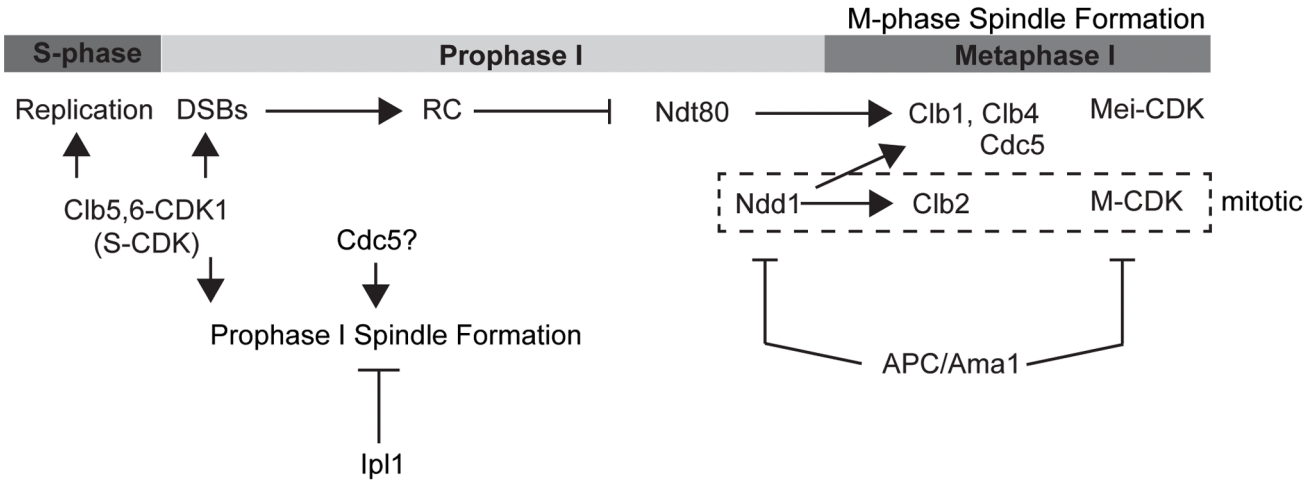

Figure 9. Model of entry into meiosis I, which is regulated by M-CDK (Clb1, Clb3, and Clb4). S-CDK (Clb5, Clb6) is required for induction of meiotic recombination.
doi:10.1371/journal.pone.0083982.g009

Materials and Methods

Strains and Meiotic Time Course Experiments

All strains were generated in the SK1 background and are shown in Table S1. Diploid strains were generated from freshly mated haploids, individual diploid colonies were then incubated in 5 ml of liquid rich medium and transferred to pre-sporulation medium (SPS). Cells were subsequently resuspended in 2% liquid potassium acetate medium (KAC) to induce meiosis [27]. All experiments were performed at 30°C. We observed day-to-day variation on time courses and therefore carried out all wild-type versus mutant analyses on the same day.

Time-lapse Imaging, Image Rendering, and Image Analysis

All time-lapse imaging took place in CellAsics Y0D microfluidics chambers, with conditions on a pDV with solid-state illumination and detection by the Cascade 1K EMCCD. All conditions were optimized for Nyquist sampling and illumination times were tested on wild type cells to ensure sporulation. Specific conditions for imaging are being published elsewhere. The movies were all rendered in Softworx. 3D measurements of spindle lengths were carried out in Imaris. All images of the live cells are maximum intensity projections. For meiotic spreads, images were prepared from.dv files in Adobe Photoshop files in Softworx and rendered in Photoshop CS5. Only total brightness/contrast levels were altered (not alpha).

Protein Extraction, Western Blot Analysis and Antibodies

Protein extraction by TCA and Western blot analysis were carried out as described previously [27]. For Western blot analysis, blots were probed with the appropriate antibodies followed by HRP-conjugated secondary antibodies (DAKO, 1:2000). HRP activity was detected using Pierce ECL Western Blotting Substrate followed by exposure to Amersham Hyperfilm ^{TM}ECL or using the Image Quant^{TM} LAS 4000 imaging system. Antibodies used for Western blot analysis were as follows:

Mouse (monoclonal) anti-HA (12CA5), 1:1000, S. Ley, NIMR, UK. Rabbit (polyclonal) anti-Hop1, 1:1500, F. Klein, MFPL, Vienna, Austria. Rabbit (polyclonal) anti-phosphoT318-Hop1, 1:500, Cambridge Research Biomedicals. Mouse (monoclonal) anti-Myc (9E10), 1:1000, S. Ley, NIMR, UK. Goat (polyclonal) anti-Cdc5 (YN019), 1:1000, Santa Cruz Biotech (sc-6732). Rabbit Anti-γH2A (Dr. Jessica Downs, 1:1000). Rabbit Anti-H2A (Dr. Jessica Downs, 1:1000). Mouse Anti-Pgk1 (Invitrogen 459250, 1:20,000). Rat anti-tubulin (YOL034W (1:400, Novus Biologicals).

Rabbit (polyclonal) anti-Zip1, 1:100, Hoffmann lab [45,46]. Antibodies used for immunofluorescence were as follows:

Guinea pig anti-phosphoT298-Hop1, 1:100, Cambridge Research Biomedicals.

Rabbit (polyclonal) anti-phosphoT318-Hop1, 1:500, Cambridge Research Biomedicals. Secondary antibodies were used as described previously, all from Jackson Immunoresearch [45,46].

Statistics

Box-and-whisker plots were rendered in R (www.r-project.org) and the vertical bar denotes the median value. Error bars around proportions were calculated as $\sqrt{p \times [1-p]/n}$, where n the number of observations.

Supporting Information

Table S1 Strain list.
(PDF)

Movie S1 SC disassembly in wild type, matching the stills in Fig. 1B.
(MOV)

Movie S2 SC disassembly in *ipl1-mn*, matching the stills in Fig. 1B.
(MOV)

Movie S3 Tub1-GFP and H2B-mCherry dynamics in *ndt80*Δ, matching stills in Fig. 1B.
(MOV)

Movie S4 Tub1-GFP and H2B-mCherry dynamics in *ndt80*Δ *ipl1-md*, matching stills in Fig. 1B.
(MOV)

Movie S5 Tub1-GFP and H2B-mCherry dynamics of a single cell *ndt80*Δ *ipl1-md*, matching stills in Fig. 1E.
(MOV)

Movie S6 Tub1-GFP and H2B-mCherry dynamics in *dmc1*Δ, matching stills in Fig. 2D.
(MOV)

Movie S7 Tub1-GFP and H2B-mCherry dynamics in *ipl1-mn dmc1*Δ, matching stills in Fig. 2D.
(MOV)

Movie S8 Tub1-GFP and H2B-mCherry dynamics of a *ipl1-mn dmc1*Δ single cell, matching stills in Fig. 2F.
(MOV)

Movie S9 Tub1-GFP and H2B-mCherry dynamics *dmc1*Δ *cdc5-mn* at 8 h, matching stills in Fig. 5B.
(MOV)

Movie S10 Tub1-GFP and H2B-mCherry dynamics *ipl1-mn dmc1*Δ *cdc5-mn* at 8 h, matching stills in Fig. 5B.
(MOV)

Movie S11 Tub1-GFP and H2B-mCherry dynamics *dmc1*Δ *cdc5-mn* at 12 h, matching stills in Fig. 5C.
(MOV)

Movie S12 Tub1-GFP and H2B-mCherry dynamics *ipl1-mn dmc1*Δ *cdc5-mn* at 12 h, matching stills in Fig. 5C.
(MOV)

Movie S13 Close up of a single cell displaying nuclear separation and multipolar spindles in the *ipl1-mn dmc1*Δ *cdc5-mn* at 12 h.
(MOV)

Acknowledgments

We thank Angelika Amon, Sue Biggins, David Kaback, Wolfgang Zachariae, Michael Lichten, and Andreas Hochwagen for strains; Dean Dawson for communicating findings prior to publication; and Tony Carr and Helfrid Hochegger for discussions and critical reading of the manuscript.

Author Contributions

Conceived and designed the experiments: LN PJ EH. Performed the experiments: LN PJ JC SN. Analyzed the data: LN PJ JC SN EH. Wrote the paper: LN EH.

References

1. Titus S, Li F, Stobezki R, Akula K, Unsal E, et al. (2013) Impairment of BRCA1-related DNA double-strand break repair leads to ovarian aging in mice and humans. Science translational medicine 5: 172ra121.
2. Padmore R, Cao L, Kleckner N (1991) Temporal comparison of recombination and synaptonemal complex formation during meiosis in *S. cerevisiae*. Cell 66: 1239–1256.
3. Pan J, Sasaki M, Kniewel R, Murakami H, Blitzblau HG, et al. (2011) A Hierarchical Combination of Factors Shapes the Genome-wide Topography of Yeast Meiotic Recombination Initiation. Cell 144: 719–731.
4. Henderson KA, Keeney S (2004) Tying synaptonemal complex initiation to the formation and programmed repair of DNA double-strand breaks. Proc Natl Acad Sci U S A 101: 4519–4524.
5. Stuart D, Wittenberg C (1998) CLB5 and CLB6 are required for premeiotic DNA replication and activation of the meiotic S/M checkpoint. Genes Dev 12: 2698–2710.
6. Nasmyth K (1996) Viewpoint: putting the cell cycle in order. Science 274: 1643–1645.
7. Grandin N, Reed SI (1993) Differential function and expression of *Saccharomyces cerevisiae* B-type cyclins in mitosis and meiosis. Mol Cell Biol 13: 2113–2125.
8. Fitch I, Dahmann C, Surana U, Amon A, Nasmyth K, et al. (1992) Characterization of four B-type cyclin genes of the budding yeast *Saccharomyces cerevisiae*. Mol Biol Cell 3: 805–818.
9. Chu S, DeRisi J, Eisen M, Mulholland J, Botstein D, et al. (1998) The transcriptional program of sporulation in budding yeast. Science 282: 699–705.
10. Chu S, Herskowitz I (1998) Gametogenesis in yeast is regulated by a transcriptional cascade dependent on Ndt80. Mol Cell 1: 685–696.
11. Smith KN, Penkner A, Ohta K, Klein F, Nicolas A (2001) B-type cyclins *CLB5* and *CLB6* control the initiation of recombination and synaptonemal complex formation in yeast meiosis. Current biology: CB 11: 88–97.
12. Henderson KA, Kee K, Maleki S, Santini PA, Keeney S (2006) Cyclin-dependent kinase directly regulates initiation of meiotic recombination. Cell 125: 1321–1332.
13. Carlile TM, Amon A (2008) Meiosis I is established through division-specific translational control of a cyclin. Cell 133: 280–291.
14. Lydall D, Nikolsky Y, Bishop DK, Weinert T (1996) A meiotic recombination checkpoint controlled by mitotic checkpoint genes. Nature 383: 840–843.
15. MacQueen AJ, Hochwagen A (2011) Checkpoint mechanisms: the puppet masters of meiotic prophase. Trends in cell biology 21: 393–400.
16. Okaz E, Arguello-Miranda O, Bogdanova A, Vinod PK, Lipp JJ, et al. (2012) Meiotic Prophase Requires Proteolysis of M Phase Regulators Mediated by the Meiosis-Specific APC/C(Ama1). Cell 151: 603–618.
17. Dahmann C, Futcher B (1995) Specialization of B-type cyclins for mitosis or meiosis in *S. cerevisiae*. Genetics 140: 957–963.
18. Miller MP, Unal E, Brar GA, Amon A (2012) Meiosis I chromosome segregation is established through regulation of microtubule-kinetochore interactions. elife 1: e00117.
19. Shuster EO, Byers B (1989) Pachytene arrest and other meiotic effects of the start mutations in *Saccharomyces cerevisiae*. Genetics 123: 29–43.
20. Sourirajan A, Lichten M (2008) Polo-like kinase Cdc5 drives exit from pachytene during budding yeast meiosis. Genes Dev 22: 2627–2632.
21. Clyne RK, Katis VL, Jessop L, Benjamin KR, Herskowitz I, et al. (2003) Polo-like kinase Cdc5 promotes chiasmata formation and cosegregation of sister centromeres at meiosis I. Nat Cell Biol 5: 480–485.
22. Haase SB, Winey M, Reed SI (2001) Multi-step control of spindle pole body duplication by cyclin-dependent kinase. Nat Cell Biol 3: 38–42.
23. Shirk K, Jin H, Giddings TH Jr, Winey M, Yu HG (2011) The Aurora kinase Ipl1 is necessary for spindle pole body cohesion during budding yeast meiosis. J Cell Sci 124: 2891–2896.
24. Kim S, Meyer R, Chuong H, Dawson DS (2013) Dual mechanisms prevent premature chromosome segregation during meiosis. Genes Dev 27: 2139–2146.
25. Hochegger H, Hegarat N, Pereira-Leal JB (2013) Aurora at the pole and equator: overlapping functions of Aurora kinases in the mitotic spindle. Open biology 3: 120185.
26. Monje-Casas F, Prabhu VR, Lee BH, Boselli M, Amon A (2007) Kinetochore orientation during meiosis is controlled by Aurora B and the Monopolin Complex. Cell 128: 477–490.
27. Jordan P, Copsey A, Newnham L, Kolar E, Lichten M, et al. (2009) Ipl1/Aurora B kinase coordinates synaptonemal complex disassembly with cell cycle progression and crossover formation in budding yeast meiosis. Genes Dev 23: 2237–2251.
28. Meyer RE, Kim S, Obeso D, Straight PD, Winey M, et al. (2013) Mps1 and Ipl1/Aurora B act sequentially to correctly orient chromosomes on the meiotic spindle of budding yeast. Science 339: 1071–1074.
29. Scherthan H, Wang H, Adelfalk C, White EJ, Cowan C, et al. (2007) Chromosome mobility during meiotic prophase in *Saccharomyces cerevisiae*. Proc Natl Acad Sci U S A 104: 16934–16939.
30. Cheslock PS, Kemp BJ, Boumil RM, Dawson DS (2005) The roles of *MAD1*, *MAD2* and *MAD3* in meiotic progression and the segregation of nonexchange chromosomes. Nat Genet 37: 756–760.
31. Pinsky BA, Kung C, Shokat KM, Biggins S (2006) The Ipl1-Aurora protein kinase activates the spindle checkpoint by creating unattached kinetochores. Nat Cell Biol 8: 78–83.
32. Bishop DK, Park L, Xu L, Kleckner N (1992) *DMC1*: a meiosis-specific yeast homolog of *E. coli recA* required for recombination, synaptonemal complex formation, and cell cycle progression. Cell 69: 439–456.
33. Klein F, Mahr P, Galova M, Buonomo SB, Michaelis C, et al. (1999) A central role for cohesins in sister chromatid cohesion, formation of axial elements, and recombination during yeast meiosis. Cell 98: 91–103.
34. Leu JY, Chua PR, Roeder GS (1998) The meiosis-specific Hop2 protein of *S. cerevisiae* ensures synapsis between homologous chromosomes. Cell 94: 375–386.
35. Woodbury EL, Morgan DO (2007) Cdk and APC activities limit the spindle-stabilizing function of Fin1 to anaphase. Nat Cell Biol 9: 106–112.
36. Carballo JA, Johnson AL, Sedgwick SG, Cha RS (2008) Phosphorylation of the axial element protein Hop1 by Mec1/Tel1 ensures meiotic interhomolog recombination. Cell 132: 758–770.
37. Hochwagen A, Tham WH, Brar GA, Amon A (2005) The FK506 binding protein Fpr3 counteracts protein phosphatase 1 to maintain meiotic recombination checkpoint activity. Cell 122: 861–873.
38. Chuang CN, Cheng YH, Wang TF (2012) Mek1 stabilizes Hop1-Thr318 phosphorylation to promote interhomolog recombination and checkpoint responses during yeast meiosis. Nucleic acids research 40: 11416–11427.
39. Bishop AC, Ubersax JA, Petsch DT, Matheos DP, Gray NS, et al. (2000) A chemical switch for inhibitor-sensitive alleles of any protein kinase. Nature 407: 395–401.
40. Crasta K, Lim HH, Giddings TH Jr, Winey M, Surana U (2008) Inactivation of Cdh1 by synergistic action of Cdk1 and polo kinase is necessary for proper assembly of the mitotic spindle. Nat Cell Biol 10: 665–675.
41. Acosta I, Ontoso D, San-Segundo PA (2011) The budding yeast polo-like kinase Cdc5 regulates the Ndt80 branch of the meiotic recombination checkpoint pathway. Mol Biol Cell 22: 3478–3490.
42. Smith E, Hegarat N, Vesely C, Roseboom I, Larch C, et al. (2011) Differential control of Eg5-dependent centrosome separation by Plk1 and Cdk1. The EMBO J 30: 2233–2245.
43. Mardin BR, Agircan FG, Lange C, Schiebel E (2011) Plk1 controls the Nek2A-PP1gamma antagonism in centrosome disjunction. Current biology: CB 21: 1145–1151.
44. Bertran MT, Sdelci S, Regue L, Avruch J, Caelles C, et al. (2011) Nek9 is a Plk1-activated kinase that controls early centrosome separation through Nek6/7 and Eg5. The EMBO J 30: 2634–2647.
45. Jordan P, Karppinen J, Handel M (2012) Polo-like kinase is required for synaptonemal complex disassembly and phosphorylation in mouse spermatocytes. J Cell Sci 125: 5061–5072.
46. Newnham L, Jordan P, Rockmill B, Roeder GS, Hoffmann E (2010) The synaptonemal complex protein, Zip1, promotes the segregation of nonexchange chromosomes at meiosis I. Proc Natl Acad Sci U S A 107: 781–785.